

ІНСТИТУТ ТЕОРЕТИЧНОЇ ФІЗИКИ ІМЕНІ О. І. АХІЄЗЕРА  
НАЦІОНАЛЬНИЙ НАУКОВИЙ ЦЕНТР  
“ХАРКІВСЬКИЙ ФІЗИКО-ТЕХНІЧНИЙ ІНСТИТУТ”  
НАЦІОНАЛЬНА АКАДЕМІЯ НАУК УКРАЇНИ

Кваліфікаційна наукова  
праця на правах рукопису

**Абизов Олександр Сергійович**

УДК 538.9, 539.2, 536.421.48, 532.787, 532.782

**ДИСЕРТАЦІЯ**

**УЗАГАЛЬНЕНИЙ ПІДХІД ГІББСА У ТЕОРІЇ НУКЛЕАЦІЇ**

01.04.02 – Теоретична фізика

Фізико-математичні науки

Подається на здобуття наукового ступеня доктора фізико-математичних наук.  
Дисертація містить результати власних досліджень. Використання ідей,  
результатів і текстів інших авторів мають посилання на відповідне джерело

---

О. С. Абизов

Науковий консультант **Бакай Олександр Степанович**, доктор  
фізико-математичних наук, професор, академік НАН України

Харків – 2021

## АНОТАЦІЯ

*Абизов О. С. Узагальнений підхід Гіббса у теорії нуклеації. – Кваліфікаційна наукова праця на правах рукопису.*

Дисертація на здобуття наукового ступеня доктора фізико-математичних наук за спеціальністю 01.04.02 «Теоретична фізика» (104 – Фізика та астрономія). – Інститут теоретичної фізики ім. О. І. Ахієзера, Національний науковий центр “Харківський фізико-технічний інститут” НАН України, Харків, 2021.

При інтерпретації експериментальних результатів з динаміки фазових переходів першого порядку, починаючи з метастабільних початкових станів, досі застосовується переважно класична теорія нуклеації що трактує відповідний процес з точки зору формування та зростання кластерів. Також часто припускається, що об’ємні властивості кластерів дуже схожі з властивостями макрофаз. Це або подібні припущення, що лежать в основі класичного підходу, підтримуються (принаймні, якщо аналізуються процеси формування конденсованих фаз) результатами класичної теорії Гіббса гетерогенних систем, яка застосовується до процесів формування критичного кластера. Розглядаючи кластери як дрібні частинки з властивостями нової макроскопічної фази, вважається, що процес росту і розчинення кластера відбувається в основному за рахунок додавання або випромінювання окремих одиниць (атомів, молекул). Як друге додаткове термодинамічне припущення передбачається, що в першому наближенні міжфазна енергія критичних кластерів дорівнює відповідному значенню для рівноважного співіснування обох фаз з плоскою границею. Альтернативна континуальна концепція опису термодинаміки гетерогенних систем, розроблена ван дер Ваальсом, вперше була застосована до аналізу процесів нуклеації-росту Хілертом, Каном і Хілліардом, як і прийшли, зокрема, до висновку, що параметри об’ємного стану критичних кластерів можуть значно відрізнятись від відповідних значень макрофаз що передбачаються у теорії Гіббса. Крім того,

згадані автори також розробили альтернативу теоретичному опису нуклеації – модель спінодального розпаду. Загально визнано (маючи в основі класичний аналіз Гіббса), що модель нуклеації-росту описує формування фаз, починаючи з метастабільних початкових станів, тоді як модель спінодального розпаду описує термодинамічно нестійкі стани. Як наслідок, виникає проблема, як один режим (нуклеація-рост) переходить в альтернативний (спінодальний розпад), якщо стан фази навколишнього середовища безперервно змінюється від метастабільних до нестабільних станів, тобто поблизу класичної спінодальної кривої. Класичний підхід Гіббса тут передбачає певну сингулярну поведінку, яка, однак, не підтверджується описом Кана–Хілліарда, статистико-механічним аналізом моделі, та експериментом. Це протиріччя в прогнозах двох усталених теорій вирішується за допомогою узагальнення класичного термодинамічного методу Гіббса. Результати такого узагальнення представлені у дисертаційній роботі для гомогенної (розділи 1-4, 9, 10) та гетерогенної (розділи 6-8) нуклеації нової фази на прикладі бінарного регулярного розчину (розділи 1-4, 6, 8), рідини ван дер Ваальса (розділи 5, 7), рідкої ртуті при адсорбуванні протонного пучка (розділ 9) та створення пори у розтягнутому розплаві діопсиду (розділ 10).

1. У першому розділі узагальнений метод Гіббса розвинений для нуклеації нової фази у простій моделі регулярного бінарного розчину. Шлях еволюції кластера за розміром та складом визначається *методом найшвидшого спуску* на гіперповерхні термодинамічного потенціалу з урахуванням термодинамічних та кінетичних факторів. Відповідно до цього аналізу зміна розміру та складу кластерів нової фази якісно відрізняються порівняно з класичною картиною. Показано, що нуклеація, тобто перша стадія формування кластера, починаючи з метастабільних початкових станів, виявляє властивості, що нагадують спінодальний розпад: спочатку розмір кластера залишається майже постійним, а його склад змінюється, хоча наявність активаційного бар'єра відрізняє процес нуклеації від справжнього спінодального розпаду. Крім того, показано, що утво-

рення фаз як у метастабільних, так і нестабільних початкових станах поблизу класичної спінодалі, може протікати через проходження хребта термодинамічного потенціалу, тобто через деякий активаційний бар'єр, незважаючи на те, що для нестабільних початкових станів значення роботи формування критичного кластера, що відповідає сідловій точці термодинамічного потенціалу, дорівнює нулю. Таким чином, показано, що концепція нуклеації – в модифікованій формі порівняно з класичною картиною – може також бути придатною для аналізу процесу утворення нової фази у нестабільному початковому стані, тобто, на відміну від класичного підходу Гіббса, узагальнений метод Гіббса дає опис формування нової фази як для бінодальної, так і для спінодальної ділянок фазової діаграми. *Основним результатом*, що має практичне значення, є те, що робота утворення кластера критичного розміру в узагальненому методі Гіббса менша, ніж у класичній теорії нуклеації у капілярному наближенні, і зменшується до нуля на спінодалі.

2. У другому розділі основні особливості спінодального розпаду, з одного боку, та нуклеації, з іншого, та перехід між обома механізмами аналізуються в рамках термодинамічної кластерної моделі на основі узагальненого методу Гіббса у моделі регулярного бінарного розчину. При цьому кластери нової фази можуть змінюватися з часом як за розмірами, так і за своїми інтенсивними параметрами стану, наприклад, густиною або складом. Аналізується також вплив зміни параметрів стану навколишнього середовища на еволюцію кластера. Наслідки такої зміни мають важливе значення як для аналізу фазоутворення в обмежених (нанорозмірних) системах, так і для розуміння еволюції ансамблів кластерів у великих (необмежених) системах. Показано, що процеси нуклеації, починаючи з термодинамічно метастабільних початкових станів, протікають якісно значною мірою аналогічно процесу утворення нової фази за механізмом спінодального розпаду. Ця схожість особливо помітна, якщо розглядати нестабільну систему малого розміру. У цьому випадку еволюція системи

починається за механізмом спінодального розпаду, але через зростання кластерів пересичення зменшується, система стає метастабільною. Нарешті, пересичення зменшується настільки, що розчинення кластерів з меншими розмірами стає необхідною умовою для зростання кластерів більшого розміру, і починається стадія коалесценції. Таким чином, підхід дозволяє описати еволюцію системи від спінодального розпаду до стадії коалесценції.

3. У першому та другому розділах аналіз було проведено методом найшвидшого спуску на гіперповерхні термодинамічного потенціалу, який дає тільки основний шлях еволюції кластера за розміром та складом. У третьому розділі проведено більш детальний аналіз за допомогою чисельного моделювання на основі кінетичної теорії нуклеації, термодинаміка формування кластерів аналізується на основі узагальненого методу Гіббса для моделі регулярного бінарного розчину. У результаті проаналізовано *еволюцію функції розподілу кластерів* за розміром та складом як для метастабільних (нуклеація), так і для нестабільних (спінодальний розпад) початкових станів. Розраховано потік кластерів нової фази в просторі розмірів, показано, що максимум потоку може проходити не тільки через сідлову точку, але також і через гребінь гіперповерхні термодинамічного потенціалу.

4. У четвертому розділі за допомогою чисельного моделювання на основі кінетичної теорії нуклеації у бінарному регулярному розчині визначається найбільш вірогідний потік кластерів нової фази в просторі розмірів, залежно від початкового пересичення. Показано, що можна виділити три області залежно від ступеня нестабільності системи. У першій області, при малому значенні пересичення, результати класичної теорії нуклеації на основі капілярного наближення та узагальненого методу Гіббса майже ідентичні, максимум потоку кластерів нової фази в просторі розмірів проходить через сідлову точку. В другій області, при більшому значенні пересичення, робота створення кластера нової фази помітно менша, ніж в класичній теорії нуклеації, що призводить до істотно

більш високого значення швидкості нуклеації. Максимум потоку в просторі розмірів, як і в першій області, проходить переважно через сідло. У першій і другій областях можна використовувати для розрахунку швидкості нуклеації прості аналітичні вирази через активаційний бар'єр. У третій області, поблизу спінодалі, нуклеація відбуватиметься не через сідлову точку, але траєкторією, що проходить через гребінь гіперповерхні термодинамічного потенціалу. Розрахунок швидкості нуклеації у третій області можливий тільки на основі чисельного моделювання на основі кластерної динаміки.

5. У п'ятому розділі досліджено гетерогенна нуклеація кластерів нової фази (конденсація та кипіння) на плоских твердих поверхнях з урахуванням зміни параметрів стану критичних кластерів (крапельок або бульбашок) залежно від пересичення в рамках узагальненого підходу Гіббса. Однокомпонентна рідина ван дер Ваальса обрана як модель для аналізу основних характеристик процесу. Показано, що у випадку утворення крапельки в перенасиченій парі на гідрофобній поверхні та утворення бульбашок у рідині на гідрофільній поверхні ефект гетерогенності незначний. В альтернативних випадках конденсації крапельки на гідрофільній поверхні та утворення бульбашок у рідині на гідрофобній поверхні нуклеація значно посилюється. Фактично, у цьому випадку існування твердої поверхні призводить до значного зміщення спінодалі до менших значень пересичення порівняно з гомогенною нуклеацією, тобто гетерогенна спінодаль наближається до бінодалі, а область метастабільності звужується за рахунок розширення області нестабільності.

6. У шостому розділі досліджено гетерогенна нуклеація у *регулярному бінарному розчині* на плоских твердих поверхнях. Показано, що контактний кут та каталітичний фактор для гетерогенної нуклеації стають залежними від ступеня метастабільності (пересичення) розчину. У випадку утворення кластерів нової фази на поверхні з низькою змочуваністю (контактний кут більше  $90^\circ$ ) каталітична активність твердої поверхні мала. В альтернативному випадку

високої змочуваності (контактний кут менше  $90^\circ$ ) інтенсивність нуклеації значно посилюється твердою поверхнею. Таким чином, у цьому випадку, як і у рідині ван дер Ваальса, гетерогенна спінодаль наближається до бінодалі, а область метастабільності звужується за рахунок розширення області нестабільності.

7. У сьомому розділі досліджено гетерогенна нуклеація (конденсація) крапель рідини з пари (газу) на дефектній твердій поверхні. Пара описується *рівнянням стану ван дер Ваальса*, як поверхневий дефект обрана конічна пора. Показано, що контактний кут та каталітичний фактор для нуклеації на дефектній поверхні залежать від ступеня переохолодження пари. У разі утворення крапель на гідрофільній поверхні конічної пори швидкість нуклеації значно збільшується порівняно з конденсацією на планарній поверхні. Наявність дефекту на гідрофільній поверхні призводить до значного зсуву спінодалі порівняно з гетерогенною нуклеацією на планарній поверхні. Зі зменшенням кута конуса пори гетерогенна спінодаль наближається до бінодалі, і область метастабільності звужується за рахунок розширення області нестабільності, показано також, що існує граничний кут конуса пори, менше якого формування нової фази проходить безбар'єрно.

8. У восьмому розділі досліджена гетерогенна нуклеація кластерів нової фази в *регулярному бінарному розчині* на дефектній твердій поверхні, і так, як і в попередньому розділі, як дефект поверхні обрана конічна пора. Розрахована швидкість нуклеації кластера нової фази у залежності від кута конуса пори і ступеня пересичення розчину.

9. У дев'ятому розділі теоретично досліджено процес закипання ртуті у імпульсних джерелах нейтронів, що працюють на реакції сколювання (Spallation Neutron Source). При адсорбуванні протонного пучка ртуть піддається великим термічним ударам та ударам тиску. Ці локальні зміни стану ртуті можуть спричинити утворення в рідині нестабільних бульбашок, які можуть пошкодити при їх кавітації конструкційні матеріали (стінка труби). У даному розділі

обчислена робота формування критичних кластерів (мікробульбашок пари ртуті) та швидкість їх зародження. Показано, що швидкість гомогенного зародження дуже низька при розглянутих умовах процесу навіть після адсорбції декількох імпульсів протонів, тому ймовірність кавітаційних процесів незначна.

10. У десятому розділі проведено теоретичний аналіз процесу зародження пори у малих зразках переохолодженої діюксидної рідини у процесі кристалізації поверхневого шару зразка. Обчислена робота формування пори критичного розміру в залежності від негативного тиску та час очікування першого критичного зародка (пори) в процесі зростання кристалічного шару на поверхні зразка. Аналіз цього процесу з точки зору класичної теорії нуклеації дає якісно правильний результат, однак кількісно теоретичні оцінки та експериментальні дані відрізняються. Показано, що узагальнений підхід Гіббса приводить до кількісно правильного опису процесу зародження пори у переохолодженої діюксидної рідини і дозволив пояснити походження внутрігранулярних пір, що утворюються при спіканні кераміки.

Результати досліджень доповнюють і розширюють наявні уявлення про механізми фазових переходів першого роду. Вони визначають кінетику процесів самоструктурування речовини від нанорозмірних до галактичних розмірів із широким спектром застосувань як у фундаментальних, так і в прикладних дослідженнях (фізика, астрономія, хімія, біологія, метеорологія, медицина, матеріалознавство) та технології – конденсація та кипіння, сегрегація у твердих та рідких розчинах, або кристалізація та плавлення. Дослідження, проведені в дисертації, є актуальними та мають як фундаментальне, так і прикладне значення.

*Ключові слова:* Нуклеація; Теорія Гіббса; Гетерогенна нуклеація; Термодинаміка нуклеації; Спінодальний розпад; Загальна теорія та комп'ютерне моделювання нуклеації; Загальна теорія фазових переходів; Шорстка поверхня; Поверхневий натяг.

## СПИСОК ПУБЛІКАЦІЙ ЗДОБУВАЧА ЗА ТЕМОЮ ДИСЕРТАЦІЇ

### Наукові праці, в яких опубліковані основні наукові результати дисертації:

1. Schmelzer J., Abyzov A. S. and Möller J. Nucleation versus spinodal decomposition in phase formation processes in multicomponent solutions. *J. Chem. Physics*. 2004. Vol. 121. P. 6900-6917. [Квартиль Q1](#) (2004).
2. Abyzov A. S., Schmelzer J. Nucleation versus spinodal decomposition in confined binary solutions. *J. Chem. Physics*. 2007. Vol. 127. P. 114504. [Квартиль Q1](#) (2007).
3. Abyzov A. S., Schmelzer J., Kovalchuk A. A. and Slezov V. V. Evolution of cluster size-distributions in nucleation-growth and spinodal decomposition processes in a regular solution. *J. Non-Cryst. Solids*. 2010. Vol. 356. P. 2915-2955. [Квартиль Q1-Q2](#) (2010).
4. Abyzov A. S., Schmelzer J. Kinetics of segregation processes in solutions: Saddle point versus ridge crossing of the thermodynamic potential barrier. *J. Non-Cryst. Solids*. 2014. Vol. 384. P. 8-14. [Квартиль Q1-Q2](#) (2014).
5. Abyzov A. S., Schmelzer J. Generalized Gibbs' approach in heterogeneous nucleation. *J. Chem. Physics*. 2013. Vol. 138, P. 164504. [Квартиль Q1](#) (2013).
6. Abyzov A. S., Schmelzer J. Heterogeneous nucleation in solutions: Generalized Gibbs' approach. *J. Chem. Physics*. 2014. Vol. 140. P. 244706. [Квартиль Q1](#) (2014).
7. Abyzov A. S., Schmelzer J. and Davydov L. N. Heterogeneous nucleation on rough surfaces: Generalized Gibbs' approach. *J. Chem. Physics*. 2017. Vol. 147. P. 214705. [Квартиль Q1](#) (2017).
8. Abyzov A. S., Davydov L. N. and Schmelzer J. Heterogeneous nucleation in solutions on rough solid surfaces: Generalized Gibbs Approach. *Entropy*. 2019. Vol. 21. P. 782. [Квартиль Q2](#) (2019).
9. Imre A. R., Abyzov A. S., Barna I. F. and Schmelzer J. Homogeneous bubble nucleation limit of mercury under the normal working conditions of the planned

European Spallation Neutron Source. *Eur. Phys. J. B.* 2011. Vol. 79. P. 101-113.  
 Квартиль Q1 (2011).

10. Abyzov A. S., Schmelzer J. and Fokin V. M. Theory of pore formation in glass under tensile stress: Generalized Gibbs approach. *J. Non-Cryst. Solids.* 2011. Vol. 357. P. 3474–3479. Квартиль Q1-Q2 (2011).

**Наукові праці, які засвідчують апробацію матеріалів дисертації:**

11. Abyzov A. S., Schmelzer J. Nucleation versus spinodal decomposition in confined binary solutions. *17th International Conference “Nucleation and Atmospheric Aerosols”*: Book of abstracts (August 13-17, 2007, National University of Ireland. Editors C. D. O’Dowd and P. Wagner). Galway, Ireland, 2007. P. 278-281.

12. Abyzov A. S., Kovalchuk A. A., Schmelzer J., Slezov V. V. Evolution of cluster size distributions in phase formation processes in multi-component solutions: nucleation and spinodal decomposition. *XIIIth Research Workshop Nucleation Theory and Applications* (JINR, April 1 – 30, 2009). Dubna, Russia, 2009.

13. Abyzov A. S., Schmelzer J., Kovalchuk A. A. and Slezov V. V. Evolution of cluster size-distributions in nucleation and spinodal decomposition in regular solutions. *9-th International Symposium on Crystallization in Glasses and Liquids* (September 10 – 13, 2009, Foz do Iguaçu, PR). Brazil, 2009.

14. Abyzov A. S., Schmelzer J. Kinetics of Segregation Processes: Classical versus generalized Gibbs approaches. *XVIth Research Workshop Nucleation Theory and Applications* (JINR, April 1 – 30, 2012). Dubna, Russia, 2012.

15. Abyzov A. S., Schmelzer J. Kinetics of segregation processes: Classical versus generalized Gibbs approaches. *Diffusion and diffusional phase transformations (DSSR-2012)* (1-7 June, 2012). Cherkassy, Ukraine, 2012.

16. Abyzov A. S., Schmelzer J. Kinetics of nucleation: Classical versus generalized Gibbs approaches. *11th Lahnwitzseminar on Calorimetry 2012 in Rostock.* Germany, 2012.

17. Schmelzer J., Abyzov A. S. Some comments on the thermodynamic analysis of nucleation in confined spaces. *Crystallization 2012. 10th International*

*Symposium on Crystallization in Glasses and Liquids* (September 23 – 26, 2012). Goslar, Germany, 2012.

18. Abyzov A. S., Schmelzer J. Kinetics of segregation processes: Classical versus generalized Gibbs approaches. *Crystallization 2012. 10th International Symposium on Crystallization in Glasses and Liquids* (September 23 – 26, 2012). Goslar, Germany, 2012.

19. Abyzov A. S., Schmelzer J. Generalized Gibbs's approach in heterogeneous nucleation. *XVIIth Research Workshop Nucleation Theory and Applications* (JINR, April 1 – 30, 2013). Dubna, Russia, 2013.

20. Schmelzer J., Abyzov A. S. Kinetics of phase transitions: some new results. *Polymer Group Seminar; University of Rostock, Institute of Physics* (February 12). Rostock, Germany, 2013.

21. Abyzov A. S., Schmelzer J. Generalized Gibbs' approach in nucleation: Application to heterogeneous nucleation. *The Eighth International Conference on Material Technologies and Modeling (MMT-2014)* (Ariel University. July 28 - August 01, 2014) Ariel, Israel, 2014.

22. Schmelzer J., Abyzov A. S. Generalized Gibbs approach in nucleation: Basic ideas and results. *The Eighth International Conference on Material Technologies and Modeling (MMT-2014)* (Ariel University. July 28 - August 01, 2014) Ariel, Israel, 2014.

**Наукові праці, які додатково відображають наукові результати дисертації:**

23. Schmelzer J., Slezov V. V. and Abyzov A. S. A new method of determination of the coefficients of emission in nucleation theory. *Nucleation Theory and Applications* (Editor J. Schmelzer, Wiley-VCH). 2006. P. 39-73.

24. Schmelzer J., Abyzov A. S. Generalized Gibbs' Approach to the thermodynamics of heterogeneous systems and the kinetics of first-order phase transitions. *J. Engineering Thermophysics*. 2007. Vol. 16. P. 119-129.

25. Schmelzer J., Abyzov A. S. Thermodynamic analysis of nucleation in

confined space: Generalized Gibbs approach. *J. Chem. Physics*. 2011. Vol. 134. P. 054511. [Квартиль Q1](#) (2011).

26. Schmelzer J., Abyzov A. S. Comment on “Minimum free-energy pathway of nucleation” [J. Chem. Phys. 135, 134508 (2011)] *J. Chem. Physics*. 2012. Vol. 136. P. 107101. [Квартиль Q1](#) (2011).

27. Schmelzer J., Abyzov A. S. Comments on the thermodynamic analysis of nucleation in confined space. *J. Non-Cryst. Solids*. 2014. Vol. 384. P. 2-7. [Квартиль Q1-Q2](#) (2014).

28. Schmelzer J., Fokin V. M., Abyzov A. S., Zanutto E. and Gutzow I. S. How do crystals form and grow in glass-forming liquids: Ostwald’s rule of stages and beyond. *Int. J. Appl. Glass Sci.* 2010. Vol. 1. P. 16-26. [Квартиль Q2](#) (2011).

29. Schmelzer J., Abyzov A. S. Crystallization of glass-forming liquids: Thermodynamic driving force. *J. Non-Cryst. Solids*. 2016. Vol. 449. P. 41-49. [Квартиль Q1-Q2](#) (2016).

30. Schmelzer J., Abyzov A. S. How do crystals nucleate and grow: Ostwald’s rule of stages and beyond. *Thermal Physics and Thermal Analysis* (Editors: J. Šesták, P. Hubík, J. Mareš, Springer). 2017. P. 195-211.

31. Schmelzer J., Abyzov A. S. Crystallization of glass-forming melts: New answers to old questions. *J. Non-Cryst. Solids*. 2018. Vol. 501. P. 11-20. [Квартиль Q1-Q2](#) (2018).

32. Fokin V. M., Karamanov A., Abyzov A. S., Schmelzer J. and Zanutto E. D. Stress-induced pore formation and phase selection in a crystallizing stretched glass. *Glass. Selected Properties and Crystallization* (Editor J. Schmelzer, De Gruyter). 2014. P. 441–479.

33. Abyzov A. S., Schmelzer J., Davydov L. N. and Slezov V. V. Homogeneous bubble nucleation limit of lead. *Problems of atomic science and technology. Series: Nuclear Physics Investigations*. 2012. Vol. 57. P. 283-287. [Квартиль Q3](#) (2012).

## ABSTRACT

*Abyzov A. S.* Generalised Gibbs' approach in nucleation theory. – Qualification scientific paper, manuscript.

Thesis for a Doctoral Degree in Physics and Mathematics: Speciality 01.04.02 “Theoretical physics” (104 – Physics and Astronomy). – A. I. Akhiezer Institute for Theoretical Physics, National Science Center “Kharkiv Institute of Physics and Technology” NAS of Ukraine, Kharkiv, 2021.

In the interpretation of experimental results on the dynamics of first-order phase transitions starting from metastable initial states, up to now, predominantly the classical nucleation theory is employed treating the respective processes in terms of cluster formation and growth. As a simplifying assumption, it is assumed frequently that the bulk properties of the clusters are widely similar to the properties of the newly evolving macroscopic phases. This or similar assumptions, underlying the classical approach, are supported (at least, as far as processes of formation of condensed phases are analyzed) by the results of Gibbs' classical theory of heterogeneous systems applied to processes of critical cluster formation. Treating the clusters as small particles with properties of the newly evolving macroscopic phase, the process of cluster growth and dissolution is considered to proceed basically via addition or emission of single units (atoms, molecules). As a second additional thermodynamic assumption, the interfacial specific energy of critical clusters is supposed in a first approximation to be equal to the respective value for an equilibrium coexistence of both phases at planar interfaces. The alternative continuum's concept of the description of the thermodynamics of heterogeneous systems, as developed by van der Waals, has been applied for the first time to an analysis of nucleation by Hillert, Cahn and Hilliard. They came, in particular, to the conclusion that the bulk state parameters of the critical clusters may deviate considerably from the respective values of the evolving macrophases and from the predictions of Gibbs' theory.

Moreover, the mentioned authors developed also as the alternative to the theoretical description of nucleation – the model of spinodal decomposition. According to the common belief (having again its origin in the classical analysis due to Gibbs), the nucleation-growth model works for the description of phase formation starting from metastable initial states, while thermodynamically unstable states are believed to decay via spinodal decomposition. As one consequence, the problem arises as to how one mode of transition (nucleation-growth) goes over into the alternative one (spinodal decomposition) if the state of the ambient phase is changed continuously from metastable to unstable states, i.e., how the transition proceeds in the vicinity of the classical spinodal curve. The classical Gibbs' approach predicts here some kind of singular behavior, which is, however, not confirmed by the Cahn-Hilliard description, statistical-mechanical model analyses and experiment. The resolution of this contradiction is performed following a generalization of Gibbs' classical thermodynamic method. The results of this generalization are presented in the dissertation for homogeneous (sections 1-4, 9, 10) and heterogeneous (sections 6-8) nucleation of a new phase on the example of binary regular solution (sections 1-4, 6, 8), van der Waals fluid (sections 5, 7), liquid mercury during proton beam adsorption (section 9) and pore formation in the stretched diopside melt (section 10).

1. In the first section, the generalized Gibbs method is developed for the nucleation of a new phase in a simple model of a regular binary solution. The evolution path of the cluster in terms of size and composition is determined by the *method of the fastest descent* on the hypersurface of the thermodynamic potential, taking into account thermodynamic and kinetic factors. According to this analysis, the change in the size and composition of the clusters of the new phase are qualitatively different compared to the classical picture. It is shown that nucleation, i.e. the first stage of cluster formation, starting from metastable initial states, exhibits properties resembling spinodal decay: initially the cluster size remains almost constant, and its composition changes, although the presence of an activation barrier distinguishes

the nucleation process from true spinodal decay. In addition, it is shown that the formation of phases in both metastable and unstable initial states near the classical spinodal can occur through the passage of the ridge of thermodynamic potential, i.e. through some activation barrier, despite the fact that for unstable initial states the value of critical cluster formation, which corresponds to the saddle point of the thermodynamic potential, is zero. Thus, it is shown that the concept of nucleation – in a modified form compared to the classical picture – may also be suitable for analyzing the process of formation of a new phase in an unstable initial state, i.e., in contrast to the classical Gibbs approach, the generalized Gibbs method describes the formation of a new phases for both binodal and spinodal regions of the phase diagram. The main result, which is of practical importance, is that the work of formation of a cluster of critical size in the generalized Gibbs approach is smaller than in the classical theory of nucleation in the capillary approximation, and decreases to zero on the spinodal.

2. In the second section, the main features of spinodal decay, on the one hand, and nucleation, on the other, and the transition between the two mechanisms are analyzed in a thermodynamic cluster model based on the generalized Gibbs approach in the model of regular binary solution. In this case, the clusters of the new phase can change over time, both in size and in their intensive state parameters – for example, density or composition. The first part of the analysis considers the processes of formation of a new phase depending on the initial state of the system for the case when the change of environmental parameters due to the evolution of clusters can be neglected (this is possible if the fraction of the new phase is small). The next step analyzes the impact of changes in environmental parameters on the evolution of the cluster. The consequences of such a change are important both for the analysis of phase formation in limited (nanoscale) systems and for understanding the evolution of cluster ensembles in large (infinite) systems. It is shown that nucleation processes, starting from thermodynamically metastable initial states, proceed qualitatively to a large extent similar to the process of formation of a new phase by the mechanism of

spinodal decay. This similarity is especially noticeable when considering an unstable system of small size. In this case, the evolution of the system begins by the mechanism of spinodal decay, but due to the growth of clusters, the supersaturation decreases, the system becomes metastable. Finally, supersaturation decreases to such an extent that the dissolution of clusters with smaller sizes becomes a necessary condition for the growth of larger clusters, and the coalescence stage begins. Thus, the approach allows us to describe the evolution of the system from spinodal decay to the stage of coalescence.

3. In the first and second sections, the analysis was performed by the method of the fastest descent on the hypersurface of the thermodynamic potential, which gives only the main path of evolution of the cluster in size and composition. In the third section, a more detailed analysis is performed using numerical simulations based on the kinetic model of nucleation, the thermodynamics of cluster formation is analyzed based on the generalized Gibbs method for the regular binary solution model. As a result, we analyzed the *evolution of the cluster distribution function* by size and composition for both metastable (nucleation) and unstable (spinodal decay) initial states. The calculated flux of new phase clusters in the space of size shows that the maximum flux can pass not only through the saddle point, but also through the ridge of the hypersurface of the thermodynamic potential.

4. In the fourth section, using the numerical simulation based on cluster dynamics in binary regular solution, the most probable flux of clusters of the new phase in the size space is determined, depending on the initial supersaturation. It is shown that three regions can be distinguished depending on the degree of system instability. In the first region, with a small value of supersaturation, the results of the classical nucleation theory based on the capillary approximation and the generalized Gibbs approach are almost identical, the maximum flux of new phase clusters in the size space passes through the saddle point. In the second region, with a higher value of supersaturation, the work of a cluster of a new phase formation is significantly

less than in the classical theory of nucleation, which leads to a significantly higher value of the nucleation rate. The maximum flux in the size space, as well as in the first area, passes mainly through a saddle. In the first and second regions, simple analytical expressions can be used to calculate the nucleation rate through the activation barrier. In the third region, near the spinodal, nucleation will take place not through the saddle point, but through a trajectory passing through the ridge of the hypersurface of thermodynamic potential. The calculation of the nucleation rate in the third region is possible only via numerical simulations based on cluster dynamics.

5. The fifth section the heterogeneous nucleation of new phase clusters (condensation and boiling) on flat solid surfaces taking into account the change in the state parameters of critical clusters (droplets or bubbles) depending on supersaturation within the framework of the generalized Gibbs approach is analysed. The one-component van der Waals fluid was chosen as a model for the analysis of the main characteristics of the process. It is shown, that in the case of the formation of a droplet in supersaturated vapor on a hydrophobic surface and the formation of bubbles in a liquid on a hydrophilic surface, the effect of heterogeneity is insignificant. In alternative cases of droplet condensation on the hydrophilic surface and the formation of bubbles in the liquid on the hydrophobic surface, the nucleation is significantly increased. In fact, in this case, the existence of a solid surface leads to a significant shift of the spinodal to smaller saturation values compared to homogeneous nucleation, i.e. heterogeneous spinodal approaches the binodal, and the metastability region shrinks due to the expansion of the instability region.

6. In the sixth section, heterogeneous nucleation in a regular binary solution on flat solid surfaces is investigated. It is shown that the contact angle and the catalytic factor for heterogeneous nucleation become dependent on the degree of metastability (supersaturation) of the solution. In the case of the formation of new phase clusters on a surface with low wettability (contact angle greater than  $90^\circ$ ), the catalytic activity of the solid surface was low. In the alternative case of high wettability (contact angle

less than  $90^\circ$ ), the intensity of nucleation is significantly increased by a solid surface. Thus, in this case, as in the case of van der Waals fluid, the heterogeneous spinodal approaches the binodal, and the region of metastability narrows due to the expansion of the region of instability.

7. In the seventh section, heterogeneous nucleation (condensation) of liquid droplets from vapor (gas) on a defective solid surface is considered. The vapor is described by the van der Waals equation of state, as a surface defect, a conic void is taken. It is shown that contact angle and catalytic factor for heterogeneous nucleation on a rough surface depend on the degree of vapor overcooling. In case of droplet formation on a hydrophilic surface of a conic void the nucleation rate considerably increases in comparison with the condensation on a planar interface. The presence of a defect on the hydrophilic surface leads to a considerable shift of the spinodal towards lower supersaturation in comparison with heterogeneous nucleation on a planar interface. With the decrease in the void cone angle the heterogeneous spinodal approaches the binodal, and the region of metastability is diminished at the expense of the instability region.

8. In the eighth section the heterogeneous nucleation of new phase clusters in regular solution on a defective solid surface is investigated, as in the previous section, a conical pore is selected as a surface defect. The nucleation rate of the new phase cluster is calculated depending on the angle of the pore cone and the degree of supersaturation of the solution.

9. The ninth section theoretically investigates the boiling process of liquid mercury in pulsed neutron sources operating on the spallation reaction (Spallation Neutron Source). During the adsorption of a proton beam, liquid mercury is subjected to large thermal and pressure shocks. These local changes in the state of mercury can cause the formation of unstable bubbles in the liquid, which can damage the cavitation structural materials (pipe wall). The work of critical clusters formation (microbubbles of mercury vapor) and their nucleation rate are calculated. It is shown that the rate

of homogeneous nucleation is very low under the considered process conditions even after adsorption of several proton pulses, so the probability of cavitation processes is insignificant.

10. In the tenth section, a theoretical analysis is performed of the process of nucleation of a pore in small samples of an under-cooled diopside liquid, enclosed by a solid crystalline surface layer growing from the melt. Analysis of this process from the point of view of the classical theory of nucleation gives a qualitatively correct result, however, quantitatively, theoretical estimates performed in the framework of classical nucleation theory and experimental data differ. It is shown here that the generalized Gibbs approach results in a more adequate quantitatively correct description of the process of pore nucleation and explains the formation of intragranular residual pores during ceramic sintering.

The results of the research complement and expand the existing ideas about the mechanisms of the first-order phase transitions. They determine the kinetics of the processes of self-structuring of matter from nanoscale to galactic size with a wide range of applications in both basic and applied research (physics, astronomy, chemistry, biology, meteorology, medicine, materials science) and technology – condensation and boiling, segregation in solids and liquid solutions, or crystallization and melting. The research performed in the dissertation is relevant and has both fundamental and applied significance.

*Key words:* Nucleation; Gibbs theory; Heterogeneous nucleation; Thermodynamics of nucleation; Spinodal decomposition; General theory and computer simulations of nucleation; General theory of phase transitions; Rough surface; Surface tension.

## ЗМІСТ

ЗМІСТ . . . . .	20
ВСТУП . . . . .	27
Список використаних джерел . . . . .	37
<b>РОЗДІЛ 1</b> <b>НУКЛЕАЦІЯ АБО СПІНОДАЛЬНИЙ РОЗПАД В ПРО-</b> <b>ЦЕСАХ ФАЗОУТВОРЕННЯ В БАГАТОКОМПОНЕНТНИХ РОЗЧИ-</b> <b>НАХ (Nucleation versus spinodal decomposition in phase formation</b> <b>processes in multi-component solutions) . . . . .</b>	<b>44</b>
1.1. Introduction . . . . .	45
1.2. The Trajectory of Cluster Evolution in the Space of Thermodynamic State Parameters . . . . .	51
1.2.1. Thermodynamic Determination . . . . .	51
1.2.1.1. Segregation in Multi-Component Solutions: General Case .	51
1.2.1.2. The Case of an Incompressible Cluster Phase . . . . .	53
1.2.2. Incorporation of the Kinetics of Cluster Evolution on the Determi- nation of the Trajectory . . . . .	54
1.2.2.1. Some Special Cases . . . . .	54
1.2.2.2. General Method of Determination of the Cluster Trajectory	55
1.2.2.3. Discussion . . . . .	56
1.3. An Example: Binary Regular Solutions . . . . .	57
1.4. On Some Intrinsic Similarity of Nucleation and Spinodal Decomposition	63
1.5. Nucleation, Spinodal Decomposition and the Kinetics of Phase Transformations in the Vicinity of the Spinodal Curve . . . . .	67
1.5.1. Predictions of the Classical Gibbs' and the Cahn-Hilliard Approaches . . . . .	67
1.5.2. Predictions of the Generalized Gibbs Approach . . . . .	73
1.5.2.1. Critical Cluster Properties Near the Spinodal Curve . . . . .	73

1.5.2.2. Nucleation near the Spinodal Curve By-Passing the Saddle Point . . . . .	78
1.5.2.3. Application of Nucleation Concepts to Thermodynamically Unstable States Beyond the Spinodal Curve . . . . .	81
1.6. Discussion . . . . .	84
References . . . . .	91
1.7. Висновки до розділу 1 . . . . .	93
РОЗДІЛ 2 НУКЛЕАЦІЯ АБО СПІНОДАЛЬНИЙ РОЗПАД В ОБМЕЖЕНИХ БІНАРНИХ РОЗЧИНАХ (Nucleation versus spinodal decomposition in confined binary solutions) . . . . .	95
2.1. Introduction . . . . .	96
2.2. The model system . . . . .	100
2.3. Phase separation in infinite domains . . . . .	104
2.3.1. Thermodynamic analysis . . . . .	104
2.3.2. Kinetics versus thermodynamics in phase separation . . . . .	112
2.4. Phase separation in finite domains . . . . .	114
2.4.1. Thermodynamic analysis . . . . .	114
2.4.2. Kinetics . . . . .	122
2.4.3. Transition from independent cluster growth to coarsening . . . . .	132
2.5. Results and discussion . . . . .	137
2.6. Acknowledgments . . . . .	140
References . . . . .	140
2.7. Висновки до розділу 2 . . . . .	143
РОЗДІЛ 3 ЕВОЛЮЦІЯ РОЗПОДІЛУ КЛАСТЕРІВ ЗА РОЗМІРОМ У ПРОЦЕСАХ ЗАРОДЖЕННЯ-ЗРОСТАННЯ ТА СПІНОДАЛЬНОГО РОЗПАДУ В РЕГУЛЯРНОМУ РОЗЧИНІ (Evolution of cluster size-distributions in nucleation-growth and spinodal decomposition processes in a regular solution) . . . . .	144

3.1. Introduction . . . . .	145
3.2. Model system . . . . .	146
3.3. Results and discussion . . . . .	157
3.4. Acknowledgments . . . . .	164
References . . . . .	164
3.5. Висновки до розділу 3 . . . . .	165
<b>РОЗДІЛ 4 КІНЕТИКА ПРОЦЕСІВ СЕГРЕГАЦІЇ У РОЗЧИНАХ: ЕВО-</b> <b>ЛЮЦІЯ ЧЕРЕЗ СІДЛОВУ ТОЧКУ АБО ЧЕРЕЗ ГРЕБІНЬ ТЕРМО-</b> <b>ДИНАМІЧНОГО ПОТЕНЦІАЛУ (Kinetics of segregation processes</b> <b>in solutions: Saddle point versus ridge crossing of the thermodynamic</b> <b>potential barrier) . . . . .</b>	<b>167</b>
4.1. Introduction . . . . .	168
4.2. Brief description of the methodology and the model system . . . . .	171
4.3. Results and discussion . . . . .	176
4.4. Conclusions . . . . .	185
References . . . . .	186
4.5. Висновки до розділу 4 . . . . .	188
<b>РОЗДІЛ 5 УЗАГАЛЬНЕНИЙ МЕТОД ГІББСА ДЛЯ ГЕТЕРОГЕННОЇ</b> <b>НУКЛЕАЦІЇ (Generalized Gibbs' approach in heterogeneous nucleation)</b>	<b>190</b>
5.1. Introduction . . . . .	191
5.2. Basic equations . . . . .	195
5.2.1. Bulk properties of ambient and newly evolving phases, binodal and spinodal curves . . . . .	195
5.2.2. Work of critical cluster formation: General expression . . . . .	197
5.3. Contact angle and catalytic activity factor for nucleation at a planar surface . . . . .	202
5.3.1. Contact angle . . . . .	202
5.3.2. Catalytic factor for nucleation: Limiting cases . . . . .	206

5.4. Heterogeneous condensation on planar solid surfaces: Results . . . . .	208
5.4.1. Vapor condensation on a hydrophilic surface . . . . .	208
5.4.2. Vapor condensation on a hydrophobic surface . . . . .	212
5.4.3. Boiling on a hydrophobic surface . . . . .	214
5.4.4. Boiling on hydrophilic surface . . . . .	216
5.4.5. Saddle-point versus ridge crossing . . . . .	217
5.5. Discussion and conclusions . . . . .	217
References . . . . .	219
5.6. Висновки до розділу 5 . . . . .	222
РОЗДІЛ 6    ГЕТЕРОГЕННА НУКЛЕАЦІЯ В РОЗЧИНАХ: УЗАГАЛЬ-	
НЕНИЙ ПІДХІД ГІББСА (Heterogeneous nucleation in solutions:	
Generalized Gibbs' approach) . . . . .	223
6.1. Introduction . . . . .	224
6.2. Basic equations . . . . .	227
6.2.1. Bulk properties of ambient and newly evolving phases, binodal	
and spinodal curves . . . . .	227
6.2.2. Work of critical cluster formation: General expression . . . . .	229
6.3. Contact angle in heterogeneous nucleation at a planar solid surface . . .	239
6.3.1. Contact angle . . . . .	239
6.3.2. Specific energy of the solid-liquid interface . . . . .	240
6.3.3. Some first consequences . . . . .	242
6.4. Nucleation activity and heterogeneous nucleation on planar solid	
interfaces: Results . . . . .	244
6.4.1. Case of high wettability . . . . .	244
6.4.2. Case of low wettability . . . . .	252
6.4.3. Segregation in thermodynamically unstable initial states . . . . .	254
6.4.4. Alternative case: Segregation at solute concentrations $x > 0.5$ . .	259
6.4.5. Effect on the steady-state nucleation rate . . . . .	261

6.5. Discussion and conclusions . . . . .	262
References . . . . .	263
6.6. Висновки до розділу 6 . . . . .	265
РОЗДІЛ 7 ГЕТЕРОГЕННА НУКЛЕАЦІЯ НА ДЕФЕКТНИХ ПОВЕРХ- НЯХ: УЗАГАЛЬНЕНИЙ ПІДХІД ГІББСА (Heterogeneous nucleation on rough surfaces: Generalized Gibbs' approach) . . . . .	267
7.1. Introduction . . . . .	268
7.2. Work of the formation of a critical cluster in the generalized Gibbs approach . . . . .	271
7.3. Vapor condensation on a hydrophilic surface . . . . .	283
7.4. Conclusion . . . . .	287
References . . . . .	288
7.5. Висновки до розділу 7 . . . . .	292
РОЗДІЛ 8 ГЕТЕРОГЕННА НУКЛЕАЦІЯ У РОЗЧИНАХ НА ДЕФЕ- КТНИХ ТВЕРДИХ ПОВЕРХНЯХ: УЗАГАЛЬНЕНИЙ ПІДХІД ГІББ- СА (Heterogeneous Nucleation in Solutions on Rough Solid Surfaces: Generalized Gibbs Approach) . . . . .	293
8.1. Introduction . . . . .	294
8.2. Basic Equations . . . . .	296
8.3. Determination of the Contact Angle . . . . .	306
8.4. Heterogeneous Nucleation in a Conic Pore: Results . . . . .	310
8.5. Conclusions . . . . .	316
References . . . . .	317
8.6. Висновки до розділу 8 . . . . .	319

РОЗДІЛ 9	МЕЖА ГОМОГЕННОЇ НУКЛЕАЦІЇ БУЛЬБАШОК РТУТІ ЗА НОРМАЛЬНИХ УМОВ РОБОТИ ЗАПЛАНОВАНОГО ЄВРО- ПЕЙСЬКОГО ДЖЕРЕЛА НЕЙТРОНІВ, ЩО ПРАЦЮЄ НА РЕАКЦІЇ СКОЛЮВАННЯ (Homogeneous bubble nucleation limit of mercury under the normal working conditions of the planned European spallation neutron source) . . . . .	321
9.1.	Introduction . . . . .	322
9.2.	Model system . . . . .	323
9.2.1.	Location of binodal and spinodal curves . . . . .	323
9.2.2.	Determination of the chemical potential and the interfacial tension	328
9.3.	Determination of the pressure and temperature change after proton adsorption . . . . .	331
9.4.	Determination of the work of critical cluster formation . . . . .	332
9.5.	Conclusions . . . . .	338
References	. . . . .	339
9.6.	Висновки до розділу 9 . . . . .	341
РОЗДІЛ 10	ТЕОРІЯ УТВОРЕННЯ ПОРИ В РОЗТЯГНУТОМУ СКЛІ: УЗАГАЛЬНЕНИЙ ПІДХІД ГІББСА (Theory of pore formation in glass under tensile stress: Generalized Gibbs approach) . . . . .	342
10.1.	Introduction . . . . .	343
10.2.	Experimental data and their analysis . . . . .	344
10.3.	Theory of pore formation . . . . .	348
10.3.1.	Equation of state for stretched diopside glass . . . . .	348
10.3.2.	Determination of the work of critical pore formation and of the nucleation rate . . . . .	351
10.4.	Summary of results and discussion . . . . .	357
10.5.	Conclusions . . . . .	358
References	. . . . .	358

10.6. Висновки до розділу 10 . . . . .	360
ВИСНОВКИ . . . . .	361
Подяки . . . . .	364
ДОДАТОК А. СПИСОК ПУБЛІКАЦІЙ ЗДОБУВАЧА ЗА ТЕМОЮ ДИСЕР- ТАЦІЇ . . . . .	365

## ВСТУП

**Обґрунтування вибору теми дослідження.** Процеси нуклеації-росту та спінодального розпаду є двома основними механізмами фазових переходів першого роду, таких як конденсація та кипіння, сегрегація у твердих та рідких розчинах, або кристалізація та плавлення. Вони визначають кінетику процесів самоструктурування речовини від нанорозмірних до галактичних розмірів із широким спектром застосувань як у фундаментальних, так і в прикладних дослідженнях (фізика, астрономія, хімія, біологія, метеорологія, медицина, матеріалознавство) та технології.

При інтерпретації експериментальних результатів по динаміці фазових переходів першого порядку, починаючи з метастабільних початкових станів, досі застосовується переважно класична теорія нуклеації що трактує відповідний процес з точки зору формування та росту кластерів [1–10]. Як ще одне спрощення як правило припускається, що об'ємні властивості кластерів схожі з властивостями макрофаз [11]. Це або подібні припущення, що лежать в основі класичного підходу, підтримуються (принаймні, якщо аналізуються процеси формування конденсованих фаз) результатами класичної теорії Гіббса гетерогенних систем, яка застосовується до процесів формування критичного кластера. Розглядаючи кластери як дрібні частинки з властивостями нової макроскопічної фази, вважається, що процес росту і розчинення кластера відбувається в основному за рахунок додавання або випромінювання окремих одиниць (атомів, молекул) [1, 3, 8, 9]. Як друге додаткове термодинамічне припущення передбачається, що в першому наближенні міжфазна енергія критичних кластерів дорівнює відповідному значенню для рівноважного співіснування обох фаз із плоскою границею [8].

Альтернативна континуальна концепція опису термодинаміки гетерогенних систем, розроблена ван дер Ваальсом [12], вперше була застосована до

аналізу процесів нуклеації-росту Хілертом, Каном і Хілліардом [13–15], які дійшли висновку, що параметри об'ємного стану критичних кластерів можуть значно відрізнятись від відповідних значень макрофаз, що передбачаються у теорії Гіббса (ці результати підходу ван дер Ваальса були підтверджені згодом більш досконалим методом функціонала густини [16]). Крім того, згадані автори також розробили альтернативу теоретичному опису нуклеації – модель спінодального розпаду.

Загально визнано (маючи в основі класичний аналіз Гіббса), що модель нуклеації-росту описує формування фаз, починаючи з метастабільних початкових станів, тоді як модель спінодального розпаду описує термодинамічно нестійкі стани. Як наслідок, виникає проблема, як один режим (нуклеація-рост) переходить в альтернативний (спінодальний розпад), якщо стан фази навколишнього середовища безперервно змінюється від метастабільних до нестабільних станів, тобто поблизу класичної спінодальної кривої. Класичний підхід Гіббса тут передбачає певну сингулярну поведінку, яка, однак, не підтверджується описом Кана–Хілліарда, аналізом у статистико-механічній моделі [17, 18] та експериментом [19].

Перша спроба усунути протиріччя в прогнозах двох усталених теорій була зроблена в моделі Шайла-Хобстеттера [20, 21] 1948-1952 років (дивись також [22]), яка, однак, не отримала розвитку в результаті появи незабаром теорії спінодального розпаду Кана–Хілліарда [14, 15]).

Значно пізніше ідеї моделі Шайла-Хобстеттера були відкриті заново за допомогою узагальнення класичного термодинамічного методу Гіббса в роботах [23–26] та були значно розвинені в публікаціях здобувача [27–36], що становлять основу дисертаційної роботи. Зокрема, результати такого узагальнення представлені для гомогенної та гетерогенної нуклеації нової фази на прикладі бінарного регулярного розчину, рідини ван дер Ваальса, рідкої ртуті при адсорбуванні протонного пучка та створення пори при кристалізації

розплаві діопсиду. Показано, що зародження, тобто перша стадія формування кластера, починаючи з метастабільних початкових станів, виявляє властивості, що нагадують спінодальний розпад: спочатку розмір кластера залишається майже постійним, а його склад змінюється, і тільки після того, як склад кластера досягне деякого критичного значення, його розмір починає зростати, хоча наявність активаційного бар'єру відрізняє процес зародження від справжнього спінодального розпаду. Крім того, показано, що утворення фаз як у метастабільних, так і нестабільних початкових станах поблизу класичної спінодалі може протікати через проходження хребта термодинамічного потенціалу, тобто через деякий активаційний бар'єр, незважаючи на те, що для нестабільних початкових станів значення роботи формування критичного кластера, що відповідає сідлової точці термодинамічного потенціалу, дорівнює нулю. Таким чином, показано, що концепція нуклеації – в модифікованій формі порівняно з класичною картиною – може також бути придатною для аналізу процесу утворення нової фази у нестабільному початковому стані, тобто, на відміну від класичного підходу Гіббса, узагальнений метод Гіббса дає опис формування нової фази як для бінодальної, так і для спінодальної ділянок фазової діаграми. Також показано, що при аналізі гетерогенній нуклеації нової фази в узагальненому підході Гіббса контактний кут і каталітичний фактор (фактор зменшення роботи утворення кластера критичного розміру за рахунок твердої поверхні) стають залежними від ступеня метастабільності (пересичення, переохолодження або перегрівання) системи. Саме це коло досліджень, яке вже відоме у світовій літературі [37–39] як **узагальнений підхід Гіббса** (Generalized Gibbs Approach, GGA), робить тему дисертації **актуальною**.

**Мета і завдання дослідження.** Основна мета дисертаційної праці полягає у виявленні специфічних особливостей процесів формування нової фази в *узагальненому підході Гіббса*.

Для досягнення поставленої мети було сформульовано такі завдання:

- побудувати *теорію нуклеації* в узагальненому підході Гіббса з урахуванням *різних коефіцієнтів дифузії* компонентів регулярного розчину, провести аналіз еволюції кластера нової фази за розміром та складом з урахуванням термодинамічних та кінетичних факторів;
- дослідити особливості та зв'язок між механізмами *нуклеації*, з одного боку, та *спінодального розпаду*, з іншого, на основі узагальненого методу Гіббса у моделі регулярного бінарного розчину;
- побудувати кінетичну теорію нуклеації для регулярного бінарного розчину, де термодинаміка утворення кластерів формулюється на основі узагальненого методу Гіббса;
- побудувати теорію *гетерогенної нуклеації* на плоскій твердій поверхні у моделях однокомпонентної рідини ван дер Ваальса та регулярного бінарного розчину з урахуванням залежності кута змочування від параметрів кластера;
- побудувати теорію *гетерогенної нуклеації на дефектах* твердої поверхні у моделях однокомпонентної рідини ван дер Ваальса та регулярного бінарного розчину з урахуванням залежності кута змочування від параметрів кластера;
- дослідити процес закипання ртуті в імпульсних джерелах нейтронів, що працюють на реакції сколювання (Spallation Neutron Source), при адсорбуванні протонного пучка на основі узагальненого методу Гіббса;
- провести теоретичний аналіз процесу зародження пори в малих зразках переохолодженої діопсидної рідини у процесі кристалізації поверхневого шару зразка на основі узагальненого методу Гіббса.

*Об'єктом дослідження* є процес формування нової фази у метастабільній або нестабільній (пересиченої, переохолодженої або перегрітої) системі.

*Предметом дослідження* є параметри процесу нуклеації нової фази: швидкість нуклеації, робота створювання, розмір та склад (густина) кластера критичного розміру, функція розподілу кластерів нової фази за розміром.

*Метод дослідження.* Для вирішення поставлених у дисертації задач були

використані загальноприйняті та добре перевірені методи теоретичної фізики: методи аналітичного та чисельного рішення нелінійних диференціальних рівнянь, метод найшвидшого спуску, чисельне рішення системи кінетичних рівнянь кластерної динаміки для функції розподілу кластерів за розміром.

### **Наукова новизна отриманих результатів**

Побудована нова теорія нуклеації, *узагальнений метод Гіббса*, яка, на відміну від класичної теорії нуклеації, дає можливість аналізу процесу утворення нової фази у нестабільному початковому стані поблизу *класичної спінодали*, в рамках якої здобуто наступні результати:

- показано, що зародження, тобто перша стадія формування кластера, починаючи з метастабільних початкових станів, виявляє властивості, що нагадують спінодальний розпад, хоча наявність активаційного бар'єру відрізняє процес зародження від справжнього спінодального розпаду;

- показано, що утворення фаз у нестабільних початкових станах поблизу *класичної спінодали* може протікати через деякий *активаційний бар'єр*, незважаючи на те, що у цьому випадку значення роботи формування критичного кластера, що відповідає сідловій точці термодинамічного потенціалу, дорівнює нулю;

- передбачено *ефект зменшення кута змочування*, і, таким чином, збільшення каталітичної активності поверхні у випадку *гетерогенної нуклеації* на плоскій твердій поверхні у моделях однокомпонентної рідини ван дер Ваальса та регулярного бінарного розчину; розвинуто теоретичний опис цього ефекту у випадку утворення кластерів нової фази на поверхні з низькою (контактний кут більше  $90^\circ$ ) та високою змочуваністю (контактний кут менше  $90^\circ$ ), показано, що гетерогенна спінодаль наближається до бінодали, а область метастабільності звужується за рахунок розширення області нестабільності;

- вперше розглянуто ефекти *гетерогенної нуклеації на дефектах* твердої поверхні у моделях однокомпонентної рідини ван дер Ваальса та регулярного

бінарного розчину, проведено порівняння результатів класичної теорії нуклеації із *узагальненим методом Гіббса*, отримано залежність параметрів критичного кластера та швидкості нуклеації від ступеня дефектності поверхні;

- вперше теоретично досліджено процес закипання рідкої у імпульсних джерелах нейтронів, що працюють на реакції сколювання (Spallation Neutron Source), при адсорбуванні протонного пучка, отримано залежність швидкості нуклеації від температури та тиску ртуті;

- вперше проведено теоретичний аналіз процесу зародження пори у малих зразках переохолодженої діюксидної рідини у процесі кристалізації поверхневого шару зразка, який дозволив пояснити походження внутрішньогранулярних пір, що утворюються при спіканні кераміки.

**Практичне і наукове значення отриманих результатів** полягає в тому, що результати досліджень доповнюють і розширюють існуючі уявлення про механізми фазових переходів першого роду. Вони визначають кінетику процесів самоструктурування речовини від нанорозмірних до галактичних розмірів із широким спектром застосувань як у фундаментальних, так і в прикладних дослідженнях (фізика, астрономія, хімія, біологія, метеорологія, медицина, матеріалознавство) та технології – конденсація та кипіння, сегрегація у твердих та рідких розчинах, або кристалізація та плавлення.

**Особистий внесок здобувача.** Наукові результати опубліковані у статтях [27–36], які становлять основу дисертації, також результати дисертації додатково відображені у статтях [40–50] і доповідалися на наукових конференціях [51–62]. Постановка більшості задач, вирішених у дисертації, формулюванні основних ідей та методів дослідження належить здобувачеві, а також він виконував усі розрахунки і брав участь у аналізі результатів.

У статті [27] здобувачем було запропоновано *метод найшвидшого спуску* на гіперповерхні термодинамічного потенціалу з урахуванням кінетичних факторів для дослідження нуклеації нової фази у моделі регулярного бінарного

розчину. У [28] здобувачем було запропоновано і проведено аналіз впливу зміни параметрів стану навколишнього середовища на еволюцію кластера. У статтях [29] і [30] здобувачем було проведено чисельне моделювання на основі кінетичної теорії нуклеації для регулярного бінарного розчину, де термодинаміка утворення кластерів формулюється на основі узагальненого методу Гіббса. Здобувачем була запропонована гіпотеза, що в узагальненому методі Гіббса контактний кут і каталітичний фактор (фактор зменшення роботи утворення кластера нової фази критичного розміру на твердій поверхні) гетерогенної нуклеації стають залежними від ступеня метастабільності рідини, яку було підтверджено у статті [31] для рідини ван дер Ваальса та у статті [32] для моделі регулярного бінарного розчину. У статтях [33] і [34] здобувачем було виконано теоретичні розрахунки гетерогенного зародження нової фази на дефектній твердій поверхні. У статті [35] здобувачем було теоретично досліджено процес закипання рідкої ртуті у імпульсних джерелах нейтронів, що працюють на реакції сколювання (Spallation Neutron Source). В статті [36] здобувачем було проведено теоретичний аналіз процесу зародження пори у малих зразках переохолодженої діюксидної рідини у процесі кристалізації поверхневого шару зразка.

**Апробація результатів дисертації.** Результати дисертаційної роботи доповідалися та обговорювалися на семінарах Інституту теоретичної фізики імені О. І. Ахієзера Національного наукового центру «Харківський фізико-технічний інститут» НАН України, а також на таких Міжнародних наукових конференціях та семінарах:

- Nucleation and Atmospheric Aerosols. 17th International Conference (August 13 – 17, 2007, National University of Ireland, Galway, Ireland),
- 4th international workshop “Diffusion and diffusional phase transformations in alloys (DIFTRANS-07)” (July 16-21, 2007, Sofiyivka (Uman) Cherkasy region, Ukraine).
- XIII.th, XVI.th, XVII.th and XVIII.th Research Workshop Nucleation

Theory and Applications (Joint Institute of Nuclear Researches, April 1 – 30, 2009, 2012, 2013 and 2014, Dubna, Russia),

- 9-th International Symposium on Crystallization in Glasses and Liquids (September 10 – 13, 2009, Foz do Iguacu, PR, Brazil),

- 3rd International Conference on Quantum Electrodynamics and Statistical Physics (QEDSP2011) (August 29 – September 2, 2011, Kharkov, Ukraine),

- 11th Lahnwitzseminar on Calorimetry 2012 (June 11 – 14, Rostock-Warnemünde, Germany, 2012),

- Crystallization 2012. 10th International Symposium on Crystallization in Glasses and Liquids (September 23 – 26, 2012, Goslar, Germany),

- Polymer Group Seminar, Institute of Physics, University of Rostock (February 12, 2013, Germany, Rostock),

- The Eighth International Conference on Material Technologies and Modeling (MMT-2014) (July 28 – August 01, 2014, Ariel University, Ariel, Israel).

**Зв'язок праці з науковими програмами, планами, темами.** Дисертація виконана у відділі теорії конденсованих середовищ і ядерної матерії Інституту теоретичної фізики імені О. І. Ахієзера Національного наукового центру «Харківський фізико-технічний інститут» НАН України. Вона є невід'ємною складовою таких проєктів:

- базова програма «Відомче замовлення НАН України на проведення наукових досліджень з атомної науки і техніки Національного наукового центру «Харківський фізико-технічний інститут» на 2006-2010 рр. за темою: «Дифузійні процеси й електронні властивості конденсованих середовищ» (номер держреєстрації 080906UP0010, виконавець);

- базова програма «Відомче замовлення НАН України на проведення наукових досліджень з атомної науки і техніки Національного наукового центру «Харківський фізико-технічний інститут» на 2011-2015 рр. за темою: «Фазові

перетворення, явища переносу і електромагнітні процеси в гетерогенних конденсованих системах» (номер держреєстрації 0111U009545, виконавець);

- базова програма «Відомче замовлення НАН України на проведення наукових досліджень з атомної науки і техніки Національного наукового центру «Харківський фізико-технічний інститут» на 2016-2020 рр. за темою: «Електрон-фононні процеси і фазові перетворення в класичних і квантових конденсованих середовищах» (номер держреєстрації 0116U007068, виконавець);

- цільова комплексна програма НАН України «Науково-технічний супровід розвитку ядерної енергетики та застосування радіаційних технологій у галузях економіки» за темою: “Моделювання кінетичних процесів в U-Pu паливі та в конструкційних матеріалах активної зони перспективних ядерних реакторів на швидких нейтронах” (номер державної реєстрації 0111U009547, термін виконання 2011 – 2012 рр., виконавець);

- цільова комплексна програма НАН України «Науково-технічний супровід розвитку ядерної енергетики та застосування радіаційних технологій у галузях економіки» за темою: “Розробка перехідних процесів у перспективному швидкому реакторі з хвилею ядерного горіння та в матеріалах активної зони реакторів четвертого покоління” (номер державної реєстрації 0113U003968, термін виконання 2013 – 2015 рр., виконавець);

- цільова комплексна програма НАН України «Наукове забезпечення розвитку ядерно-енергетичного комплексу та перспективних ядерних технологій» за темою: “Розвиток методів пасивного контролю та керування потужністю перспективного швидкого ядерного реактора з хвилею ядерного горіння та дослідження реакторних матеріалів перспективних ядерних установок” (номер державної реєстрації 0116U007071, термін виконання 2016 – 2018 рр., виконавець);

- цільова комплексна програма НАН України «Ядерні та радіаційні технології для енергетичного сектору і суспільних потреб» за темою: “Розробка

методів регулювання потужності перспективного швидкого реактора з хвилею ядерного горіння та моделювання матеріалів для ядерної енергетики наступного покоління” (номер державної реєстрації 0119U101826, термін виконання 2019 – 2021 рр., виконавець);

- проект німецького науково-дослідницького співтовариства (Deutsche Forschungsgemeinschaft) “Nucleation-growth processes in multicomponent systems” (University of Rostock, Germany, 2002, 2003, 2005 – 2009);

- проект німецької служби академічних обмінів (DAAD) “First-order phase transformation in multicomponent finite domains” (Section 322, Code number A/05/24752, University of Rostock, Germany, 2005);

- спільний проект фундаментальних досліджень “ДФФД – БРФФД – 2009” “Кінетичні аспекти формування ансамблів наночастинок при піролізі краплі розчинів при зниженому тиску” (номер державної реєстрації Ф29/377 – 2009, термін виконання 2009 – 2010 рр.);

- проект німецької служби академічних обмінів (DAAD) “Generalized Gibbs’ approach to the thermodynamics of heterogeneous systems: applications to crystallization and cavitation processes in confined systems with non-conserved order parameter” (Section 322, Code number A/11/05260, University of Rostock, Germany, 2011).

**Публікації.** Основні результати дисертації опубліковані у 10 наукових статтях у фахових міжнародних виданнях першого та другого квартілю <sup>1</sup>, процитовані понад 230 разів, додаткові результати опубліковані у 8 наукових працях та у 3 главах в монографіях (процитовані понад 140 разів). Результати дисертації доповідалися на вітчизняних і міжнародних наукових конференціях та семінарах.

---

<sup>1</sup>The Journal of Chemical Physics (2004, 2007, 2013, 2014, 2017),  
Journal of Non-Crystalline Solids (2010, 2011, 2014),  
European Physical Journal B (2011),  
Entropy (2019)

**Структура і обсяг дисертації.** Дисертація складається з вступу, десяти розділів, висновків, та одного додатку. Загальний обсяг дисертаційної роботи складає 369 сторінок, обсяг основної частини складає 344 сторінки, з яких додаток займає 5 сторінок. Робота містить 120 рисунків, з яких 13 повністю займають площу сторінки, та 363 найменування використаних джерел. Дисертаційна робота підготовлена для захисту в формі *наукової доповіді*. Відповідно Наказу Міністерства освіти і науки України № 1220 від 23.09.2019, “за наявності не менше ніж десять публікацій, які розкривають основні наукові результати дисертації, у виданнях, віднесених до першого і другого кuartилів (Q1 і Q2) відповідно до класифікації SCImago Journal and Country Rank або Journal Citation Reports, захист може відбуватися у формі наукової доповіді. Під науковою доповіддю розуміють дисертацію, оформлену відповідно розділу II Вимог до оформлення дисертації, затверджених наказом Міністерства освіти і науки України 12 січня 2017 року № 40, зареєстрованих в Міністерстві юстиції України від 03 лютого 2017 року за № 155/30023. Розділами дисертації є публікації здобувача наукового ступеня” [63].

### **Список використаних джерел**

1. Volmer M. Kinetik der Phasenbildung. Dresden, Leipzig: Th. Steinkopff, 1939. 232 p.
2. Hirth J. P. and Pound G. M. Condensation and evaporation. Oxford-London-Paris-Frankfurt: Pergamon Press, 1963. 190 p.
3. Skripov V. P. Metastable liquids. New York: Wiley, 1974. 284 p.
4. Nielsen A. E., Kinetics of precipitation. Oxford: Pergamon, 1964.
5. Christian J. W. The Theory of transformations in metals and alloys. Oxford: Oxford University Press, 1975. 1200 p.
6. Gutzow I. S., Schmelzer J. W. P. [The vitreous state: thermodynamics, structure, rheology, and crystallization](#) (1st ed.). Berlin: Springer, 1995, Second enlarged

edition, Springer, Heidelberg, 2013. 553 p.

7. Stanley H. A. Introduction to phase transitions and critical phenomena, Oxford: Clarendon, 1971. 336 p.
8. Kelton K. F., Greer A. L. Nucleation in condensed matter. Applications in Materials and Biology. Pergamon Materials Series, 2010, 756 p.
9. Wu D. T. Nucleation theory. *Solid State Physics: Advances in Research and Applications* (Editors Ehrenreich, H. and Spaepen, F.). New York: Academic Press, 1997, Vol. 50. P. 37–91.
10. Skripov V. P. and Faizullin M. Z. Crystal-liquid-gas phase transitions and thermodynamic similarity, Berlin-Weinheim: Wiley-VCH, 2006. 183 p.
11. Gibbs J. W. The collected works, vol. 1, Thermodynamics. New York: Longmans Green, 1928. XXVIII + 434 p.
12. van der Waals J. D. and Kohnstamm Ph. Lehrbuch der Thermodynamik. Leipzig und Amsterdam: Johann-Ambrosius-Barth Verlag, 1908. XII+287 p.
13. Hillert M. A Theory of nucleation of solid metallic solutions, Sc.D. Thesis, Mass. In. Tech. (1956).
14. Cahn J. W. and Hilliard J. E. Free energy of a non-uniform system. I. Interfacial free energy. *J. Chem. Phys.* 1958. Vol. 28. P. 258–267.
15. Cahn J. W. and Hilliard J. E. Energy of a non-uniform system. III. Nucleation in a two-component incompressible fluid. *J. Chem. Phys.* 1959. Vol. 31. P. 688–699.
16. Oxtoby D. W. Nucleation at first-order phase transitions. *Accounts Chem. Res.* 1998. Vol. 31. P. 91–97.
17. Gunton J. D., San Miguel M. and Sahni P.S. The dynamics of first-order phase transitions. *Phase Transitions and Critical Phenomena* (Editors Domb C. and Lebowitz J.L.). London-New York: Academic Press, 1983. Vol. 8. P. 85–187.
18. Binder K. Theory of first-order phase transitions. *Rep. Progr. Phys.* 1987. Vol. 50. P. 783–860.

19. Shah M., Galkin O. and Vekilov P. Smooth transition from metastability to instability in phase separating protein solutions. *J. Chem. Phys.* 2004. Vol. 121. P. 7505–7512.
20. Hobstetter J. N. Copper and copper alloys - stable transformation nuclei in solids. *Metals Tech.* 1948. TP 2447.
21. Scheil E. Bemerkung die Konzentration von Keimen bei ihrer Ausscheidung aus überstättigen Mischkristallen. *Z. Metallk.* 1952. Vol. 43. P. 40.
22. Burke J. The kinetics of phase transformations in metals. Pergamon Press: New York, 1965. 226 p.
23. Schmelzer J. W. P., Schmelzer J., Jr., and Gutzow I. Reconciling Gibbs and van der Waals: A new approach to nucleation theory. *J. Chem. Phys.* 2000. Vol. 112. P. 3820–3831.
24. Schmelzer J. W. P. and Baidakov V. G. Nucleation versus spinodal decomposition in phase formation processes in multicomponent solutions. *J. Phys. Chem.* 2001. Vol. 105. P. 11595.
25. Schmelzer J. W. P., Baidakov V. G. and Boltachev G. Sh. Kinetics of boiling in binary liquid–gas solutions: Comparison of different approaches. *J. Chem. Phys.* 2003. Vol. 119. P. 6166.
26. Schmelzer J. W. P., Gokhman A. R., and Fokin V. M. Dynamics of first-order phase transitions in multicomponent systems: a new theoretical approach. *J. Colloid Interface Science.* 2004. Vol. 272. P. 109.
27. Schmelzer J., Abyzov A. S. and Möller J. Nucleation versus spinodal decomposition in phase formation processes in multicomponent solutions. *J. Chem. Physics.* 2004. Vol. 121. P. 6900-6917.
28. Abyzov A. S., Schmelzer J. Nucleation versus spinodal decomposition in confined binary solutions. *J. Chem. Physics.* 2007. Vol. 127. P. 114504.

29. Abyzov A. S., Schmelzer J., Kovalchuk A. A. and Slezov V. V. Evolution of cluster size-distributions in nucleation-growth and spinodal decomposition processes in a regular solution. *J. Non-Cryst. Solids*. 2010. Vol. 356. P. 2915-2955.
30. Abyzov A. S., Schmelzer J. Kinetics of segregation processes in solutions: Saddle point versus ridge crossing of the thermodynamic potential barrier. *J. Non-Cryst. Solids*. 2014. Vol. 384. P. 8-14.
31. Abyzov A. S., Schmelzer J. Generalized Gibbs' approach in heterogeneous nucleation. *J. Chem. Physics*. 2013. Vol. 138, P. 164504.
32. Abyzov A. S., Schmelzer J. Heterogeneous nucleation in solutions: Generalized Gibbs' approach. *J. Chem. Physics*. 2014. Vol. 140. P. 244706.
33. Abyzov A. S., Schmelzer J. and Davydov L. N. Heterogeneous nucleation on rough surfaces: Generalized Gibbs' approach. *J. Chem. Physics*. 2017. Vol. 147. P. 214705.
34. Abyzov A. S., Davydov L. N. and Schmelzer J. Heterogeneous nucleation in solutions on rough solid surfaces: Generalized Gibbs Approach. *Entropy*. 2019. Vol. 21. P. 782.
35. Imre A. R., Abyzov A. S., Barna I. F. and Schmelzer J. Homogeneous bubble nucleation limit of mercury under the normal working conditions of the planned European Spallation Neutron Source. *Eur. Phys. J. B*. 2011. Vol. 79. P. 101-113.
36. Abyzov A. S., Schmelzer J. and Fokin V. M. Theory of pore formation in glass under tensile stress: Generalized Gibbs approach. *J. Non-Cryst. Solids*. 2011. Vol. 357. P. 3474–3479. Квартиль Q1-Q2 (2011).
37. Cormier L. Nucleation in Glasses – Nucleation in glasses – new experimental findings and recent theories. *Procedia Materials Science*. 2004. Vol. 7. P. 60–71 (2nd International Summer School on Nuclear Glass Wasteform: Structure, Properties and Long-Term Behavior, SumGLASS 2013).

38. Allix M., Cormier L. Crystallization and glass-ceramics. *Springer Handbook of Glass. Springer Handbooks* (Editors Musgraves J.D., Hu J., Calvez L.). Springer, Cham. 2019. P. 113-167.
39. Minji Ha et al. Multicomponent plasmonic nanoparticles: from heterostructured nanoparticles to colloidal composite nanostructures. *Chemical Reviews*. 2021. Vol. 119. P. 12208–12278.
40. Schmelzer J., Slezov V. V. and Abyzov A. S. A new method of determination of the coefficients of emission in nucleation theory. *Nucleation Theory and Applications* (Editor J. Schmelzer, Wiley-VCH). 2006. P. 39-73.
41. Schmelzer J., Abyzov A. S. Generalized Gibbs' approach to the thermodynamics of heterogeneous systems and the kinetics of first-order phase transitions. *J. Engineering Thermophysics*. 2007. Vol. 16. P. 119-129.
42. Schmelzer J., Abyzov A. S. Thermodynamic analysis of nucleation in confined space: Generalized Gibbs approach. *J. Chem. Physics*. 2011. Vol. 134. P. 054511.
43. Schmelzer J., Abyzov A. S. Comment on "Minimum free-energy pathway of nucleation" [J. Chem. Phys. 135, 134508 (2011)] *J. Chem. Physics*. 2012. Vol. 136. P. 107101.
44. Schmelzer J., Abyzov A. S. Comments on the thermodynamic analysis of nucleation in confined space. *J. Non-Cryst. Solids*. 2014. Vol. 384. P. 2-7.
45. Schmelzer J., Fokin V. M., Abyzov A. S., Zanotto E. and Gutzow I. S. How do crystals form and grow in glass-forming liquids: Ostwald's rule of stages and beyond. *Int. J. Appl. Glass Sci*. 2010. Vol. 1. P. 16-26.
46. Schmelzer J., Abyzov A. S. Crystallization of glass-forming liquids: Thermodynamic driving force. *J. Non-Cryst. Solids*. 2016. Vol. 449. P. 41-49.
47. Schmelzer J., Abyzov A. S. How do crystals nucleate and grow: Ostwald's rule of stages and beyond. *Thermal Physics and Thermal Analysis* (Editors: J. Šesták, P. Hubík, J. Mareš, Springer). 2017. P. 195-211.

48. Schmelzer J., Abyzov A. S. Crystallization of glass-forming melts: New answers to old questions. *J. Non-Cryst. Solids*. 2018. Vol. 501. P. 11-20.
49. Fokin V. M., Karamanov A., Abyzov A. S., Schmelzer J. and Zanotto E. D. Stress-induced pore formation and phase selection in a crystallizing stretched glass. *Glass. Selected Properties and Crystallization* (Editor J. Schmelzer, De Gruyter). 2014. P. 441–479.
50. Abyzov A. S., Schmelzer J., Davydov L. N. and Slezov V. V. Homogeneous bubble nucleation limit of lead. *Problems of atomic science and technology. Series: Nuclear Physics Investigations*. 2012. Vol. 57. P. 283-287.
51. Abyzov A. S., Schmelzer J. Nucleation versus spinodal decomposition in confined binary solutions. *17th International Conference “Nucleation and Atmospheric Aerosols”*: Book of abstracts (August 13-17, 2007, National University of Ireland. Editors C. D. O’Dowd and P. Wagner). Galway, Ireland, 2007. P. 278-281.
52. Abyzov A. S., Kovalchuk A. A., Schmelzer J., Slezov V. V. Evolution of cluster size distributions in phase formation processes in multi-component solutions: nucleation and spinodal decomposition. *XIIIth Research Workshop Nucleation Theory and Applications* (JINR, April 1 – 30, 2009). Dubna, Russia, 2009.
53. Abyzov A. S., Schmelzer J., Kovalchuk A. A. and Slezov V. V. Evolution of cluster size-distributions in nucleation and spinodal decomposition in regular solutions. *9-th International Symposium on Crystallization in Glasses and Liquids* (September 10 – 13, 2009, Foz do Iguaçu, PR). Brazil, 2009.
54. Abyzov A. S., Schmelzer J. Kinetics of Segregation Processes: Classical versus generalized Gibbs approaches. *XVIth Research Workshop Nucleation Theory and Applications* (JINR, April 1 – 30, 2012). Dubna, Russia, 2012.
55. Abyzov A. S., Schmelzer J. Kinetics of segregation processes: Classical versus generalized Gibbs approaches. *Diffusion and diffusional phase transformations (DSSR-2012)* (1-7 June, 2012). Cherkassy, Ukraine, 2012.

56. Abyzov A. S., Schmelzer J. Kinetics of nucleation: Classical versus generalized Gibbs approaches. *11th Lahnwitzseminar on Calorimetry 2012 in Rostock*. Germany, 2012.
57. Schmelzer J., Abyzov A. S. Some comments on the thermodynamic analysis of nucleation in confined spaces. *Crystallization 2012. 10th International Symposium on Crystallization in Glasses and Liquids* (September 23 – 26, 2012). Goslar, Germany, 2012.
58. Abyzov A. S., Schmelzer J. Kinetics of segregation processes: Classical versus generalized Gibbs approaches.. *Crystallization 2012. 10th International Symposium on Crystallization in Glasses and Liquids* (September 23 – 26, 2012). Goslar, Germany, 2012.
59. Abyzov A. S., Schmelzer J. Generalized Gibbs's approach in heterogeneous nucleation. *XVIIth Research Workshop Nucleation Theory and Applications* (JINR, April 1 – 30, 2013). Dubna, Russia, 2013.
60. Schmelzer J., Abyzov A. S. Kinetics of phase transitions: some new results. *Polymer Group Seminar, University of Rostock, Institute of Physics* (February 12). Rostock, Germany, 2013.
61. Abyzov A. S., Schmelzer J. Generalized Gibbs' approach in nucleation: Application to heterogeneous nucleation. *The Eighth International Conference on Material Technologies and Modeling (MMT-2014)* (Ariel University. July 28 - August 01, 2014) Ariel, Israel, 2014.
62. Schmelzer J., Abyzov A. S. Generalized Gibbs approach in nucleation: Basic ideas and results. *The Eighth International Conference on Material Technologies and Modeling (MMT-2014)* (Ariel University. July 28 - August 01, 2014) Ariel, Israel, 2014.
63. Наказ Міністерства освіти і науки України № 1220 від 23.09.2019.

## РОЗДІЛ 1

**НУКЛЕАЦІЯ АБО СПІНОДАЛЬНИЙ РОЗПАД В ПРОЦЕСАХ  
ФАЗОУТВОРЕННЯ В БАГАТОКОМПОНЕНТНИХ РОЗЧИНАХ**

У першому розділі узагальнений метод Гіббса розвинений для нуклеації нової фази у простій моделі регулярного бінарного розчину. Шлях еволюції кластера за розміром та складом визначається *методом найшвидшого спуску* на гіперповерхні термодинамічного потенціалу з урахуванням термодинамічних та кінетичних факторів.

JOURNAL OF CHEMICAL PHYSICS

VOLUME 121, NUMBER 14

8 OCTOBER 2004

**Nucleation versus spinodal decomposition in phase formation processes in multi-component solutions**

Jörn W. P. Schmelzer

*Fachbereich Physik der Universität Rostock, Universitätsplatz, 18051 Rostock, Germany and  
Universidade Federal de São Carlos, Vitreous Materials Laboratory, 13.565-905 São Carlos - SP - Brazil*

Alexander S. Abyzov

*Kharkov Institute of Physics and Technology, Academician Street 1, 61108 Kharkov, Ukraine*

Jörg Möller

*Technische Universität Dresden, Institut für Werkstoffwissenschaften Hallwachstr. 3, 01062 Dresden, Germany*

(Received 27 April 2004; accepted 6 July 2004)

In the present paper, some further results of application of the generalized Gibbs' approach (J. W. P. Schmelzer *et al.*, J. Chem. Phys. **112**, 3820 (2000); **114**, 5180 (2001); **119**, 6166 (2003)) to describing new-phase formation processes are outlined. The path of cluster evolution in size and composition space is determined taking into account both thermodynamic and kinetic factors. The basic features of these paths of evolution are discussed in detail for a simple model of a binary mixture. According to this analysis,

size and composition of the clusters of the newly evolving phase change in an unexpected way which is qualitatively different as compared to the classical picture of nucleation-growth processes. As shown, nucleation (i.e., the first stage of cluster formation starting from metastable initial states) exhibits properties resembling spinodal decomposition (the size remains nearly constant while the composition changes) although the presence of an activation barrier distinguishes the nucleation process from true spinodal decomposition. In addition, it is shown that phase formation both in metastable and unstable initial states near the classical spinodal may proceed via a passage of a ridge of the thermodynamic potential with a finite work of the activation barrier even though (for unstable initial states) the value of the work of critical cluster formation (corresponding to the saddle point of the thermodynamic potential) is zero. This way, it turns out that nucleation concepts – in a modified form as compared with the classical picture – may govern also phase formation processes starting from unstable initial states. In contrast to the classical Gibbs' approach, the generalized Gibbs' method provides a description of phase changes both in binodal and spinodal regions of the phase diagram and confirms the point of view assuming a continuity of the basic features of the phase transformation kinetics in the vicinity of the classical spinodal curve. ©2004 American Institute of Physics. [DOI: 10.1063/1.1786914]

## 1.1. Introduction

In the interpretation of experimental results on the dynamics of first-order phase transitions starting from metastable initial states, up to now predominantly the classical nucleation theory is employed [1–5] treating the respective process in terms of cluster formation and growth. As one additional simplifying assumption

it is assumed hereby frequently that the bulk properties of the clusters are widely similar to the properties of the newly evolving macrophases [6]. This or similar assumptions (cf. [7]), underlying the classical approach, are supported (at least, as far as processes of formation of condensed phases are analyzed) by the results of Gibbs' classical theory of heterogeneous systems [8] applied to processes of critical cluster formation. Treating the clusters as small particles with properties of the newly evolving macroscopic phase, the process of cluster growth and dissolution is considered to proceed basically via addition or emission of single units (atoms, molecules) with the same properties.

As a second additional thermodynamic assumption, the interfacial specific energy of critical clusters is supposed in a first approximation to be equal to the respective value for an equilibrium coexistence of both phases at planar interfaces. In order to come to an agreement between experimental and theoretical results, this second assumption often has to be released by introducing a curvature dependence of the surface tension. However, such assumption leads to other internal contradictions in the theory [9–11].

The alternative continuum's concept of the description of the thermodynamics of heterogeneous systems, as developed by van der Waals [12, 13], has been applied for the first time to an analysis of nucleation by Cahn and Hilliard [14]. In application to nucleation-growth processes (phase transformations originating from metastable initial states), Cahn and Hilliard came, in particular, to the conclusion that the bulk state parameters of the critical clusters may deviate considerably from the respective values of the evolving macrophases and from the predictions of Gibbs' theory. These results of the van der Waals' approach were reconfirmed later-on by more advanced density functional computations (cf. e.g. [15]).

Moreover, mentioned authors developed also the alternative to the nucleation-growth model theoretical description of spinodal decomposition. According to the common believe (having again its origin in the classical analysis due to Gibbs [8]),

the nucleation-growth model works for the description of phase formation starting from metastable initial states, while thermodynamically unstable states are believed to decay via spinodal decomposition. As one consequence, the problem arises how one mode of transition (nucleation-growth) goes over into the alternative one (spinodal decomposition) if the state of the ambient phase is changed continuously from metastable to unstable states, i.e., how the transition proceeds in the vicinity of the classical spinodal curve. The classical Gibbs' approach predicts here some kind of singular behavior, which is, however, not confirmed by the Cahn-Hilliard description, statistical-mechanical model analyses (cf. e.g. [4, 16, 17]) and experiment [18]. From a more general point of view, we are confronted here with an internal contradiction in the predictions of two well-established theories which has to be, hopefully, resolved. The resolution of this contradiction is one of the aims of the present analysis, it is performed here following a generalization of Gibbs' classical thermodynamic method developed by us in recent years [19–26].

In the mentioned series of recent publications it was demonstrated [19–22] that, by developing a generalization of Gibbs' thermodynamic approach, Gibbs' and van der Waals' methods of description of critical cluster formation can be reconciled. The generalized Gibbs' approach was shown to lead for model systems to qualitatively and partly even quantitatively similar results as compared with density functional approaches [23–26]. In particular, it leads to a significant dependence of the properties of the critical clusters on supersaturation and to a vanishing of the work of critical cluster formation for initial states in the vicinity of the spinodal curve.

The generalized Gibbs' approach has, however, one additional advantage as compared with existing approaches to the description of cluster formation. Both the classical Gibbs' and van der Waals' methods of description of heterogeneous systems, as well as modern density functional analyses, have one common limitation. They are restricted in their applicability to thermodynamic equilibrium states exclusively. As a consequence, the mentioned theories can supply us with information on the properties

of critical clusters, governing nucleation (cf. e.g. [15]). However, they cannot supply us with any theoretically founded description of the properties of single clusters or ensembles of clusters being not in equilibrium with the ambient phase. By this reason, in order to describe the evolution of ensembles of clusters in first-order phase transitions, evolving either as the result of nucleation or of spinodal decomposition, additional assumptions have to be made concerning their properties and the evolution of their properties with the changes in cluster size and supersaturation in the system (cf. e.g. [7]). However, as far as one remains inside mentioned approaches, one has no theoretical tool to check the degree of validity of these assumptions.

The generalization of Gibbs' approach, described in its basic premises in detail in [10, 11, 25, 26], allows us to overcome this deficiency. It gives a tool for the determination of the thermodynamic functions of a cluster or ensembles of clusters in the ambient phase both for thermodynamic equilibrium and well-defined non-equilibrium states. In order to allow the determination of the state parameters of the clusters in dependence on their sizes, one has to formulate then merely criteria determining the most probable path of evolution of the clusters in the space of independent thermodynamic variables.

As the simplest possible prescription and in order to demonstrate the principal consequences, recently we put forward the criterion [10, 11] that the evolution of a cluster in a first-order phase transition proceeds along a valley of the appropriate thermodynamic potential. This valley connects the metastable initial state of the system with the newly evolving macrophase, passing in its course the saddle point of the appropriate thermodynamic function. As well-known, latter state corresponds to the critical cluster. As the result of such analysis, the dependence of the state parameters of the cluster on their size was established. Moreover, it was shown that a number of other thermodynamic and kinetic parameters, determining processes of cluster formation and growth, become cluster-size dependent as well [10].

It was already mentioned in the preceding analysis [10] that, in general, both

thermodynamic and kinetic properties of the system under consideration will have an effect on the most probable path of evolution of the cluster or ensembles of clusters in a first-order phase transformation. However, in [10] the possible effect, connected with the peculiarities of cluster growth kinetics, was neglected in the search for the preferred trajectory of evolution of the clusters in the space of thermodynamic state parameters. It is the first aim of the present paper, to extend the studies made in [10] to account for both mentioned factors. As in the previous investigation [10], the analysis will be performed for the case of phase formation in multi-component solutions. The method is applicable, however, for any (or, at least, for a huge variety of) other cases of first-order phase transformations as well.

Having at our disposal these results, we will go over then to an analysis of a second problem, the transition from the nucleation-growth model of the phase transition to spinodal decomposition in passing the classical spinodal curve of the system under consideration. A comparison of the classical treatment of nucleation, based on Gibbs' thermodynamic approach, and the Cahn-Hilliard theory of spinodal decomposition leads to the consequence that near the spinodal a discontinuity in the kinetic mechanisms of formation of the new phase has to be expected. Moreover, the mentioned approaches lead to different results concerning the properties of the critical clusters near the spinodal curve. As will be shown, the generalized Gibbs' approach utilized here, predicts, in agreement with computer simulations [4, 16, 17] and experimental results [18], a continuous transition from thermodynamic metastable to thermodynamic unstable initial states in the course of passing the classical spinodal curve. Even more, as it turns out from the analysis, the scenario of the initial stages of nucleation-growth processes starting from metastable initial states is shown to resemble widely the behavior well-known from the Cahn-Hilliard picture of spinodal decomposition. In addition, the basic mechanism of nucleation – the transition via a potential barrier in the evolution to the newly evolving phase – is shown to retain (in a modified form as compared with the classical picture) its importance for unstable

initial states near the spinodal curve as well.

The paper is organized as follows. In Section 1.2, a more precise formulation of a recently proposed criterion [10] is given determining the trajectory of evolution of the cluster or cluster ensembles in the space of thermodynamic state parameters. The general results are illustrated then for the model of binary regular solutions in Section 1.3. In Sections 1.4 and 1.5, the typical features of the dynamics of the phase transition starting both from metastable and unstable initial states are specified as derived in the framework of the generalized Gibbs' approach and compared with the classical models of nucleation-growth and spinodal decomposition processes. It is shown, in particular, that [i.] the classical model of cluster formation and growth is, in general, not valid for the description of segregation in solutions; [ii.] the properties of the clusters change significantly as a function of their sizes, this change proceeds most dramatically at sizes near to the critical cluster size; [iii.] the formation of the critical clusters starting from metastable initial states proceeds via a scenario widely similar to the Cahn-Hilliard picture of spinodal decomposition; [iv.] the nucleation concept – passage of some activation barrier in the evolution to the new phase – retains its importance also for new phase evolution in unstable initial states near the spinodal curve; [v.] an interpretation of the size of the region with highest amplification of density fluctuations – as derived in the Cahn-Hilliard theory of spinodal decomposition – can be given as being uniquely correlated with the critical cluster size in thermodynamically unstable initial states (with zero values of the work of critical cluster formation) computed via the generalized Gibbs' approach. A summary of the results and a discussion, performed in Section 1.6, completes the paper.

## 1.2. The Trajectory of Cluster Evolution in the Space of Thermodynamic State Parameters

### 1.2.1. Thermodynamic Determination

#### 1.2.1.1. Segregation in Multi-Component Solutions: General Case

Considering nucleation at isothermal ( $T = \text{constant}$ ) and isobaric ( $p = \text{constant}$ ) conditions, the change of the Gibbs free energy, due to the formation of one cluster in the ambient phase, is given – according to the generalized Gibbs approach [10,25,26] – in the most general form as

$$\Delta G = (p - p_\alpha)V_\alpha + \sum_{j=1}^k n_{j\alpha} [\mu_{j\alpha}(p_\alpha, T, \{x_\alpha\}) - \mu_{j\beta}(p, T, \{x_\beta\})] + \sigma A. \quad (1.1)$$

The parameters  $n_{j\alpha}$  are the numbers of particles of the different components in the cluster,  $V_\alpha$  is the volume and  $A$  the surface area,  $\sigma$  the interfacial free energy and  $\mu_j$  the chemical potential referred to one particle either in the cluster ( $\alpha$ ) or the ambient phases ( $\beta$ ). For convenience of the notations, we will omit the subscripts  $\alpha$  and  $\beta$  as far as such omission cannot lead to confusion.

For metastable initial states, we always have a critical cluster volume  $V_c$  with a corresponding value of  $\Delta G$  equal to  $\Delta G_c$ . This way, Eq. (1.1) can be brought into a dimensionless form with  $\Phi = (\Delta G/\Delta G_c)$ . The set of ( $f = k + 1$ ) independent dimensionless variables is given then by

$$q_j = n_{j\alpha}, \quad j = 1, 2, \dots, k; \quad q_{k+1} = \frac{V_\alpha}{V_c}. \quad (1.2)$$

In this representation, we have a length scale, the radius of the critical cluster size. This way, such length unit is to be preferred on physical grounds.

In Eq. (1.1), the intensive parameters of the cluster phase are not defined so far, they can have, in general, any arbitrary reasonable values. This way, as soon as

we would like to determine the states of the clusters in dependence on their sizes in the course of their evolution, we have to advance some criterion allowing to make the respective predictions. The basic postulate, formulated in [10] in order to resolve this problem, consists in the following statement: *the evolution of the cluster has to proceed along a valley of the characteristic thermodynamic potential following the path of the steepest descent from the saddle point.*

In some sense, this postulate can be considered as a generalization of the approach employed by H. Reiss in the early paper of 1950 where the generalization of classical nucleation theory to binary systems is developed [27]. Above postulate represents an extension of this approach allowing to describe the state of the clusters in the whole course of its evolution from sub-critical up to macroscopic sizes.

The mentioned valley is determined by the following considerations: The different independent kinetic mechanisms a cluster can change its size and composition consist in the change of the volume and the number of particles of the different components in the cluster. Following the basis assumptions of the thermodynamics of irreversible processes, the driving force for such changes of the state of the system are proportional to  $(\partial\Phi/\partial q_i)$ . The thermodynamically favored path of the evolution should be given thus by the set of equations (see Appendix)

$$\frac{d\Phi}{dl} = \sum_{j=1}^f \frac{\partial\Phi}{\partial q_j} \frac{dq_j}{dl}, \quad (1.3)$$

$$\frac{dq_i}{dl} = -\frac{\partial\Phi}{\partial q_i} \quad \text{with} \quad \Phi = \frac{\Delta G}{\Delta G_c}. \quad (1.4)$$

Here  $l$  is a scalar parameter determining the trajectory of the evolution in the given space of thermodynamic variables and  $dl$  is the distance between two points on the trajectory. This way, Eqs. (1.3) and (1.4) describe the trajectory of steepest descent of the thermodynamic potential with starting points in the immediate vicinity of the saddle point of the Gibbs' free energy. In dependence on the choice of these

starting points, we can determine in this way either the part of the trajectory from the saddle point to the newly evolving macroscopic phase or, alternatively, the path to the metastable ambient phase. Based on this basic set of equations, the trajectory describing the evolution can be determined also in any other appropriate set  $\{Q\}$  of thermodynamic state parameters (see Appendix).

### 1.2.1.2. The Case of an Incompressible Cluster Phase

Let us now go over to the limit of an incompressible cluster phase. In this case, the change of the thermodynamic potential due to the formation of a cluster is given by the more simple expression [10]

$$\Delta G = \sum_{j=1}^k n_{j\alpha} [\mu_{j\alpha}(p, T, \{x_\alpha\}) - \mu_{j\beta}(p, T, \{x_\beta\})] + \sigma A. \quad (1.5)$$

The number of degrees of freedom is reduced here by one and the volume of the cluster can be expressed directly via the specific volumes of the different components in the cluster phase,  $\omega_{j\alpha}$ , and the number of particles of the different components in the cluster,  $n_{j\alpha}$ , as

$$V_\alpha = \sum_{j=1}^k \omega_{j\alpha} n_{j\alpha}. \quad (1.6)$$

For this particular situation, the basic set of coordinates are exclusively dimensionless numbers.

Eq. (1.5) can be transformed into a dimensionless form, again, where the independent coordinates are given now by  $(n_{1\alpha}, n_{2\alpha}, \dots, n_{k\alpha})$ . Such choice corresponds, in this particular case, to the physically distinguished coordinate system for which Eq. (1.4) holds (the correctness of this statement will become even more

obvious in the forthcoming section, when the set of kinetic equations for cluster growth in solid solutions will be considered). This way, we may determine now either the trajectory in the distinguished set of coordinates and perform, if required, afterwards the necessary computations allowing to determine other parameters of the clusters in dependence on their sizes as well. Alternatively, we can also omit the first step and go over directly to alternative sets of coordinates (see Appendix).

## 1.2.2. Incorporation of the Kinetics of Cluster Evolution on the Determination of the Trajectory

### 1.2.2.1. Some Special Cases

For the description of phase separation processes in solutions, the deterministic growth equations can be written in most applications of interest as (cf. [28–30] and references cited therein)

$$\frac{dn_{i\alpha}}{dt} = -w_i(n_{1\alpha}, n_{2\alpha}, \dots, n_{k\alpha}) \frac{\partial \Phi}{\partial n_{i\alpha}}. \quad (1.7)$$

In the both particularly important cases of diffusion or kinetic limited growth modes, the coefficients of aggregation  $w_i(n_{1\alpha}, n_{2\alpha}, \dots, n_{k\alpha})$  are of the form

$$w_i(n_{1\alpha}, n_{2\alpha}, \dots, n_{k\alpha}) = D_i x_i \Theta(n_{1\alpha}, n_{2\alpha}, \dots, n_{k\alpha}) \quad (1.8)$$

with slightly different specific expressions for the function  $\Theta(n_{1\alpha}, n_{2\alpha}, \dots, n_{k\alpha})$  in dependence on the mode of cluster growth. Here  $D_i$  is the partial diffusion coefficient of the  $i$ -th component and  $x_i$  its molar fraction in the ambient phase. In both limiting cases, we can introduce therefore the new variables

$$dl = \Theta(n_{1\alpha}, n_{2\alpha}, \dots, n_{k\alpha}) dt, \quad m_{i\alpha} = \frac{n_{i\alpha}}{\sqrt{D_i x_i}}, \quad (1.9)$$

and rewrite Eq. (1.7) in the form of Eq. (1.4) as

$$\frac{dm_{i\alpha}}{dl} = -\frac{\partial\Phi}{\partial m_{i\alpha}}. \quad (1.10)$$

In mentioned and similar cases (when a transformation like Eq. (1.8) is possible), the evolution in the space of the independent state parameters of the clusters is given by relations similar to those (cf. Eq. (1.4)) determining the valley of the respective thermodynamic potential. However, in the expressions for  $\Phi$  a transformation of the variables  $m_{i\alpha} = (\sqrt{D_i x_i}) n_{i\alpha}$  has to be performed. Consequently, the path of cluster evolution will depend not only on thermodynamic factors but on the set of diffusion coefficients of the different components as well. This way, in the considered cases the kinetics of cluster growth affects the most probable trajectory of evolution of the cluster via the products of the values of the diffusion coefficients and the molar fractions of the different component in the ambient phase. Earlier obtained results will be reestablished if the product  $D_i x_i$  has nearly the same values for all components in the solution.

Note that this generalization is to some extent similar to Stauffer's proposal in the determination of the direction of the nucleation fluxes in the vicinity of the saddle point [31] and to generalizations of this approach by introducing so-called generalized nucleation potentials [32]. But here these ideas are extended, again, to the whole course of evolution of the clusters of the newly evolving phase.

### 1.2.2.2. General Method of Determination of the Cluster Trajectory

Let us assume, now, that the state of the thermodynamic system consisting of a cluster in the otherwise homogeneous ambient phase is determined by the set of variables  $\{q\}$  and the deterministic equations of motion are given or can be brought

into the form

$$\frac{dq_i}{dt} = \varphi_i(q_1, q_2, \dots, q_f), \quad i = 1, 2, \dots, f. \quad (1.11)$$

Here  $\{q\}$  can be given by any set of state parameters allowing to determine in a uniquely defined way the deterministic cluster trajectory.

The set of equations Eq. (1.11) can be solved then starting from initial states in the immediate vicinity of the saddle point of the thermodynamic potential. In this way, we can determine the deterministic trajectory of the cluster in the space of thermodynamic variables. In generalization of the purely thermodynamic evolution criterion proposed in [10, 11] and discussed here before, we postulate that *this deterministic trajectory gives the most probable path of evolution of the cluster from the initial ambient phase to the newly evolving macroscopic phase*. By this postulate, the task of determination of the change of the cluster properties in the course of their evolution is solved.

As evident from the determination of the most probable path, we assume here that the evolution of the clusters proceeds along a trajectory passing states near the saddle point of the appropriate thermodynamic potential. In most cases of practical interest, this assumption is fulfilled. Nevertheless, it was noted from time to time that situations may exist where this assumption does not hold (see e.g. [16, 32–35]). For these cases, a separate analysis is required. We will return to this problem shortly.

### 1.2.2.3. Discussion

In generalization of the purely thermodynamic criterion for the evolution of the state of the cluster in the course of their growth, advanced earlier [10, 11], now both thermodynamic and kinetic factors are incorporated adequately. Some consequences and differences as compared with the case of a purely thermodynamic determination

of the path of evolution will be analyzed for the case of segregation in regular solutions in the next section.

As will be demonstrated here for the case of cluster formation in solutions, the analysis of the most probable path of evolution of the clusters allows immediately to understand the basic qualitative features of the process of cluster formation and growth for the considered kind of phase formation. As it will turn out for the considered here case of phase formation in solutions, the classical picture of this process does not represent an adequate description of the real situation. In the analysis, we will consider again phase formation in binary regular solutions allowing to demonstrate the basic results for a relatively simple model system.

### 1.3. An Example: Binary Regular Solutions

For a binary regular solution, we can start the analysis with Eq. (1.5) and result at the following particular expression for  $\Delta G$  (cf. [10, 19])

$$\Delta G = -n_\alpha \Delta\mu + \sigma A, \quad \Delta\mu = -k_B T f(x, x_\alpha) \quad (1.12)$$

with

$$f(x, x_\alpha) = (1 - x_\alpha) \left[ \ln \left( \frac{1 - x_\alpha}{1 - x} \right) + 2 \left( \frac{T_c}{T} \right) (x_\alpha^2 - x^2) \right] + \quad (1.13) \\ + x_\alpha \left\{ \ln \left( \frac{x_\alpha}{x} \right) + 2 \left( \frac{T_c}{T} \right) \left[ (1 - x_\alpha)^2 - (1 - x)^2 \right] \right\},$$

$$\sigma = \tilde{\sigma} (x_\alpha - x)^2. \quad (1.14)$$

In above equations,  $k_B$  is the Boltzmann constant,  $T_c$  is the critical temperature

of the solution,  $\tilde{\sigma}$  is a parameter depending on temperature, only, and  $x_\alpha$  and  $x$  are the molar fractions of the second component in the cluster and the ambient phase, respectively. We will assume in the subsequent computations that the temperature in the system is fixed to  $T = 0.7 T_c$ . The left hand side branches of the binodal ( $x_b$ ) and the spinodal ( $x_{sp}$ ) curves are located for this temperature at  $x_b \cong 0.0857$  and  $x_{sp} \cong 0.2261$ , respectively [10, 19]. The respective right hand side values of the molar fractions for the binodal and spinodal curves are given by  $x_b^{(r)} = 1 - x_b$  and  $x_{sp}^{(r)} = 1 - x_{sp}$ . We will assume here first that the initial concentrations in the ambient phase have values in the range  $x_b \cong 0.0857 \leq x \leq x_{sp} \cong 0.2261$  extending the analysis later to unstable initial states with  $x \geq x_{sp} = 0.2261$ .

Having at our disposal the expression for the thermodynamic potential or, more generally, the deterministic equations describing cluster growth and decay, we can now determine the most probable path of evolution of the cluster and the dependence of the state parameters of the clusters on their sizes. First we show the results employing the purely thermodynamic criterion [10, 11] (i.e. we suppose that the evolution proceeds along the valley of the thermodynamic potential passing the saddle point [Eqs. (1.3) and (1.4)]). The results are presented in Figs. 1.1 – 1.2.

In the right hand side of Fig. 1.1, the shape of the Gibbs free energy surface and the path of the cluster evolution is shown in the  $(n_1/n_c, n_2/n_c)$ -space. Here  $n_1$  and  $n_2$  are the numbers of particles of the different components in the cluster,  $n_c$  is the total number of particles in the critical cluster (the subscript  $\alpha$  is omitted for convenience of the notations). The molar fraction of the ambient phase was chosen here to be equal to  $x = 0.19$ . The left hand side of Fig. 1.1 gives a similar dependence but this time in the size-composition space ( $r = R/R_c$ ,  $x_\alpha = n_{2\alpha}/(n_{1\alpha} + n_{2\alpha})$ ), where  $R_c$  is the critical cluster size in nucleation.

The whole path of evolution of the clusters can be divided into three different parts. In the first part of the trajectory ( $A-B$  in Fig. 1.1), the composition of the clusters remains the same as the composition of the ambient phase. This way, along

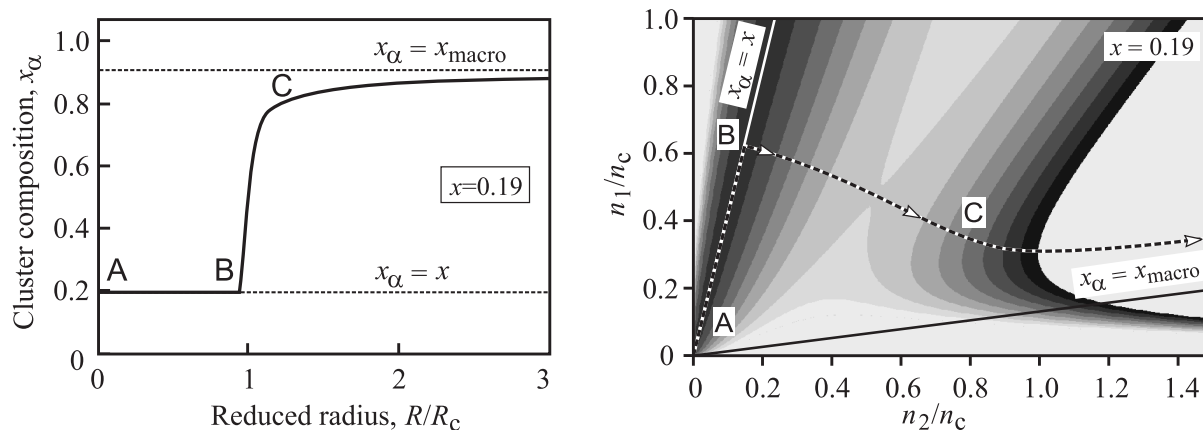


Fig. 1.1. *Left*: Path of the cluster evolution in the  $(r, x_\alpha)$ -space. *Right*: Shape of the Gibbs free energy surface and trajectory of cluster evolution in the  $(n_1/n_c, n_2/n_c)$ -space (for a regular solution with a molar fraction of the segregating component in the ambient phase equal to  $x = 0.19$ ). Here  $n_1$  and  $n_2$  are the numbers of particles of the different components in the cluster. The respective values are divided by the total number of particles in the cluster of critical size,  $n_c$

this part,  $\Delta G$  remains equal to zero. This result is easily understandable taking into account that in this range the cluster cannot be distinguished from the ambient mother phase. Consequently, the real cluster evolution begins at the point  $B$ , where the cluster composition starts to change. The size of the region in the ambient phase, specified by  $B$ , we will denote as  $R_s$ . For the example considered,  $R_s$  is nearly equal to the critical cluster size,  $R_c$ . In the next stage, in the part of the trajectory of cluster evolution  $B$ - $C$ , the cluster composition varies dramatically without significant changes in the cluster size. At the point  $C$  the cluster composition corresponds almost to the composition of the newly evolving macroscopic phase. In the third part of evolution, starting with the point  $C$ , the cluster grows further in size with an already nearly constant composition.

In Fig. 1.2, the dependence of the cluster composition,  $x_\alpha$ , on the reduced radius,  $r = R/R_c$ , is shown for different values of the molar fraction,  $x$ , of the second component in the ambient phase. Here the following cases are illustrated:  $x = 0.086$ ,  $x = 0.09$ ,  $x = 0.11$ ,  $x = 0.13$ ,  $x = 0.15$ ,  $x = 0.17$ ,  $x = 0.19$  and  $x = 0.22$ . It is evident that the basic qualitative features of the phase transformation kinetics do not depend on supersaturation in the considered range of metastable initial

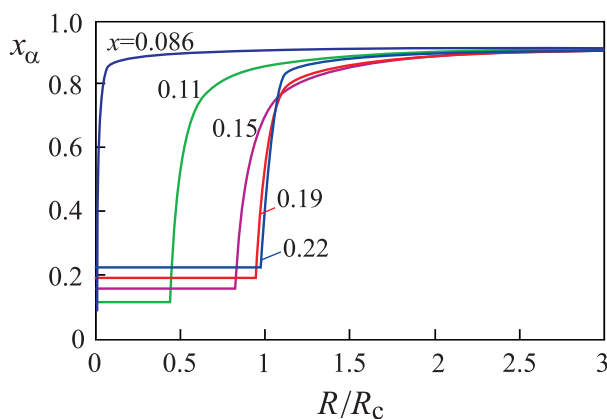


Fig. 1.2. Dependence of the cluster composition,  $x_\alpha$ , on the reduced radius,  $r = R/R_c$ , for different values of the concentration in the ambient phase:  $x = 0.086$ ,  $x = 0.09$ ,  $x = 0.11$ ,  $x = 0.13$ ,  $x = 0.15$ ,  $x = 0.17$ ,  $x = 0.19$  and  $x = 0.22$ .

states. However, the size,  $R_s$ , a cluster starts its evolution with, varies with a change in the supersaturation. For small values of the initial supersaturation, the ratio  $R_s/R_c$  tends to zero. However, in absolute units,  $R_s$  shows a behavior as presented in Fig. 1.3 (the parameter  $\Omega_2$  depends on particular properties of the system under consideration, an estimate yields  $\Omega_2 \cong 1$  nm (cf. [23])).

The size parameter  $R_s$  diverges for small supersaturations similarly to the size of the critical cluster. This way, independent on the value of the supersaturation, the classical picture of the nucleation-growth process does not give a correct description of the real situation. The cluster evolution does not proceed via a growth in size of initially very small units with properties of the newly evolving phase. In contrast, in some region in the ambient phase with spatial dimensions of the order  $2R_s$ , the concentration increases and only after this process is completed to a large extent, a further increase in cluster size occurs. An illustration of these differences – the classical model of nucleation-growth processes and the scenario based on the analysis presented here – is given in Figs. 1.4 (and somewhat later also in Figs. 1.7a and c).

So far, we have analyzed the most probable path of evolution of the cluster in cluster size space, if the motion is determined by purely thermodynamic considerations. However, as mentioned already in [10] and discussed in detail in Section 1.2.2, in general, both thermodynamic and kinetic properties will determine

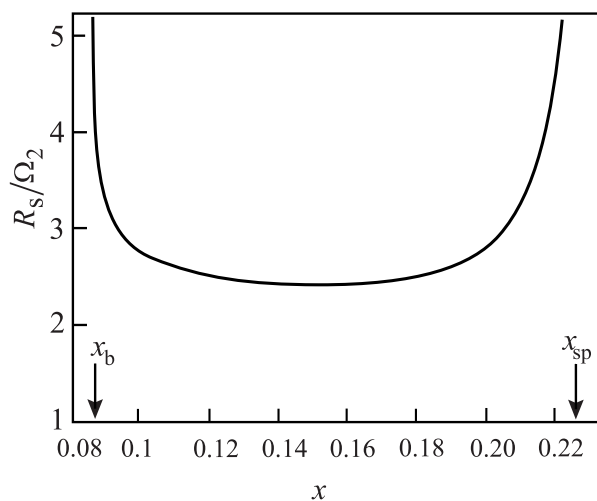


Fig. 1.3. Characteristic size,  $R_s$ , of the part of the ambient phase, where processes of amplification of the concentration occur. It is supposed here that the evolution proceeds via the most probable path in the space of thermodynamic state parameters of the clusters as determined thermodynamically. This size parameter,  $R_s$ , is determined as a multiple of a parameter  $\Omega_2$  depending on the particular properties of the solution considered (cf. Eq. (1.24)). The parameter  $\Omega_2$  has values of the order of one nanometer [23].

the most probable path of evolution of the clusters. Here we would like to study in detail the effect of kinetic factors on the evolution of the state of the clusters in the course of their growth for the limiting cases of diffusion and kinetic limited growth. As shown in detail in Section 1.2.2, for these cases we can proceed as earlier but have to replace in the final expressions  $n_{i\alpha}$  by  $m_{i\alpha}$ . The results are independent on the particular kind of growth kinetics – diffusion or kinetic limited growth – considered. Indeed, for the both considered growth modes, we get, from Eqs. (1.7) and (1.8), the same equation for the determination of the cluster trajectory in the parameter space, i.e.,

$$\frac{dn_{1\alpha}}{dn_{2\alpha}} = \frac{D_1 x_1}{D_2 x_2} \frac{\partial \Phi(n_{1\alpha}, n_{2\alpha})}{\partial n_{1\alpha}} \left( \frac{\partial \Phi(n_{1\alpha}, n_{2\alpha})}{\partial n_{2\alpha}} \right)^{-1}. \quad (1.15)$$

The results of the computations are illustrated in Figs. 1.5.

In the left hand sides of Figs. 1.5, the results of such computations are given for

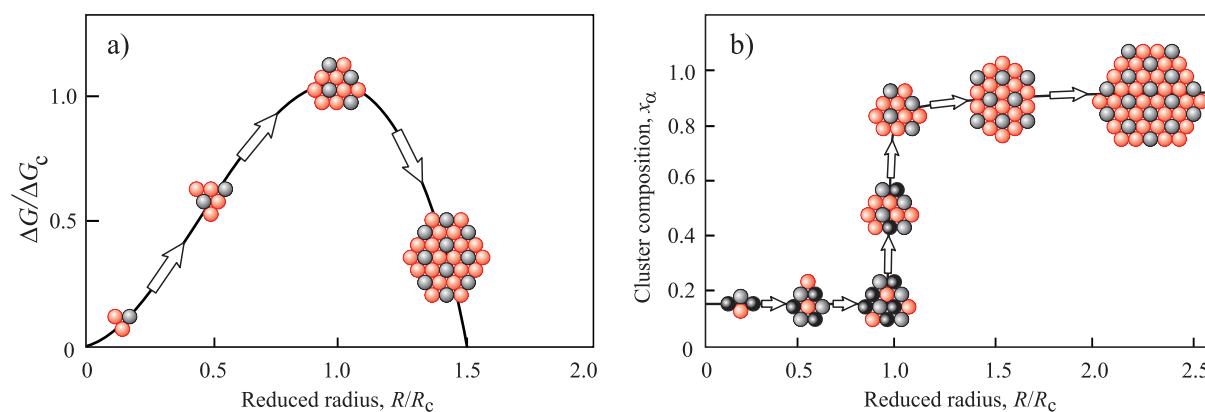


Fig. 1.4. Illustration of the differences in the classical picture of nucleation-growth processes in solutions ((a): growth in size of clusters with nearly the same composition as the newly evolving macroscopic phase) as compared with the results obtained via the generalized Gibbs' approach and the basic postulate as formulated in Section 1.2 ((b), see text). The lower curve is drawn here for a molar fraction  $x = 0.19$  (cf. Fig. 1.1).

the dependence of the cluster composition,  $x_\alpha$ , on the reduced radius,  $r$ , for different values of the molar fraction,  $x$ , of the second component (i.e.  $x_2 = x$ ,  $x_1 = 1 - x$ ) in the ambient phase ( $x = 0.11$ ,  $x = 0.15$ ,  $x = 0.19$ ,  $x = 0.22$  from top to bottom). For different values of the kinetic coefficients, different dependencies  $x_\alpha = x_\alpha(r)$  are obtained. The following values of  $D_1/D_2$  are chosen:  $D_1/D_2 = 0.1$  (1),  $D_1/D_2 = 1$  (2), and  $D_1/D_2 = 10$  (3). In the right hand side of Figs. 1.5, the shape of the Gibbs free energy surface and the path of the cluster evolution are shown in the  $(n_1/n_c, n_2/n_c)$ -space, again. With an increase of the ratio  $D_1/D_2$ , the position of the point  $B$  in the cluster trajectory (cf. Fig. 1.1) in the space of its state variables is shifted to higher values of the ratio  $R/R_c$  and  $R_s$  may even exceed  $R_c$ .

In Fig. 1.6, the situation is shown once again for the whole range of possible values of the parameters  $D_1/D_2$  and an initial concentration of the ambient phase equal to  $x = 0.17$ . Here, again, the curves, corresponding to ratios  $D_1/D_2 = 0.1$  (2),  $D_1/D_2 = 1$  (3) and  $D_1/D_2 = 10$  (4) are given. However, they are supplemented by the limiting curves  $D_1/D_2 \rightarrow 0$  (1) and  $D_1/D_2 \rightarrow \infty$  (5). As evident from Figs. 1.5 and 1.6, qualitatively the picture remains the same as in the case when the trajectory

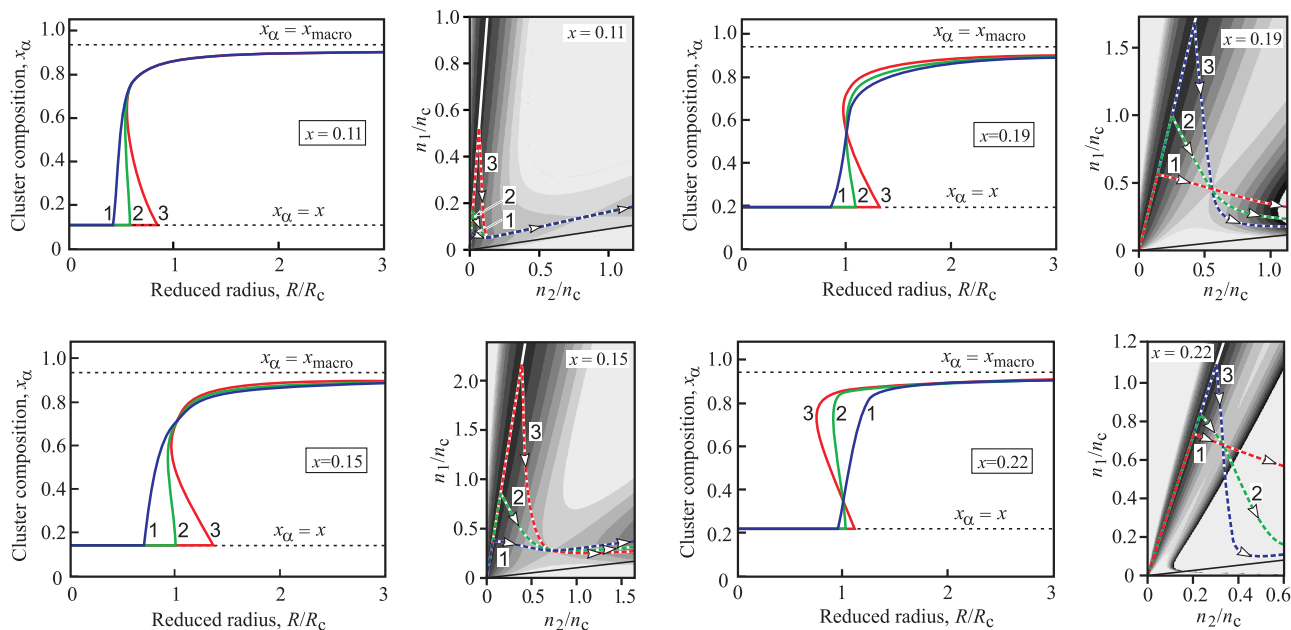


Fig. 1.5. *Left:* Path of the cluster evolution in the  $(r, x_\alpha)$ -space. *Right:* Shape of the Gibbs free energy surface and path of the cluster evolution in the  $(n_1/n_c, n_2/n_c)$ -space. The computations are made for a regular solution with molar fractions  $x = 0.11$ ,  $x = 0.15$ ,  $x = 0.19$  and  $x = 0.22$  of the second component in the ambient phase for different values of the ratio  $D_1/D_2$ :  $D_1/D_2 = 0.1$  (1),  $D_1/D_2 = 1$  (2),  $D_1/D_2 = 10$  (3). In generalization of the results shown in Fig. 1.2, here the trajectory describing the evolution of the cluster is determined taking into account both thermodynamic and kinetic factors.

of evolution is determined by purely thermodynamic criteria. Quantitatively, the most probable path is shifted in the space of cluster state variables.

#### 1.4. On Some Intrinsic Similarity of Nucleation and Spinodal Decomposition

According to the classical theory of nucleation and cluster growth, nucleation proceeds by addition and/or emission of monomers (atoms, molecules etc.) starting from monomers and leading to the formation of dimers, trimers etc. Hereby the state of the clusters is assumed to be widely independent on cluster size. As already mentioned, this feature of the theory is an additional assumption not

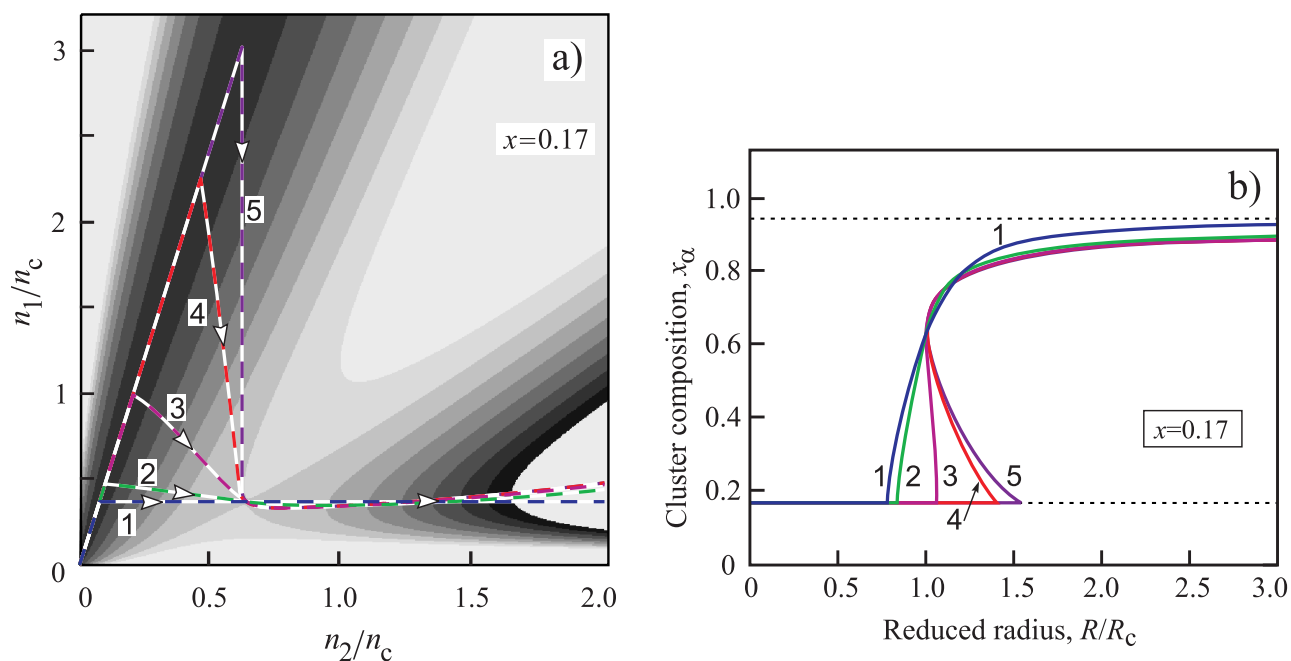


Fig. 1.6. Path of the cluster evolution for a molar fraction of the initial state equal to  $x = 0.17$  for the whole range of possible ratios of the diffusion coefficients  $D_1/D_2$ :  $D_1/D_2 \rightarrow 0$  (1),  $D_1/D_2 = 0.1$  (2),  $D_1/D_2 = 1$  (3),  $D_1/D_2 = 10$  (4),  $D_1/D_2 \rightarrow \infty$  (5).

founded theoretically. Remember that Gibbs' classical approach [8] is restricted in its applicability exclusively to *equilibria of heterogeneous substances*, it cannot give any information on thermodynamic non-equilibrium states, in general, and the state of sub- and supercritical clusters, in particular.

In the generalization of Gibbs' approach, underlying our analysis, we start with the formulation of appropriate expressions for the thermodynamic potentials (and the development of the theoretical basis underlying this approach) for clusters of arbitrary sizes in the ambient phase [10, 11, 25, 26]. This procedure allows us to give a theoretically founded prescription on the course of evolution of the clusters in the transformation as it was outlined in preceding sections. Now, let us analyze in more detail whether the results confirm the classical model of nucleation processes or not. As it will turn out, the answer is, in general, no.

In order to prove this statement, let us return to an analysis of the results shown in Figs. 1.1–1.3 and 1.5. It follows immediately from these results that the evolution

of the critical cluster does not proceed via the classical picture as sketched in Fig. 1.4a and 1.7a.

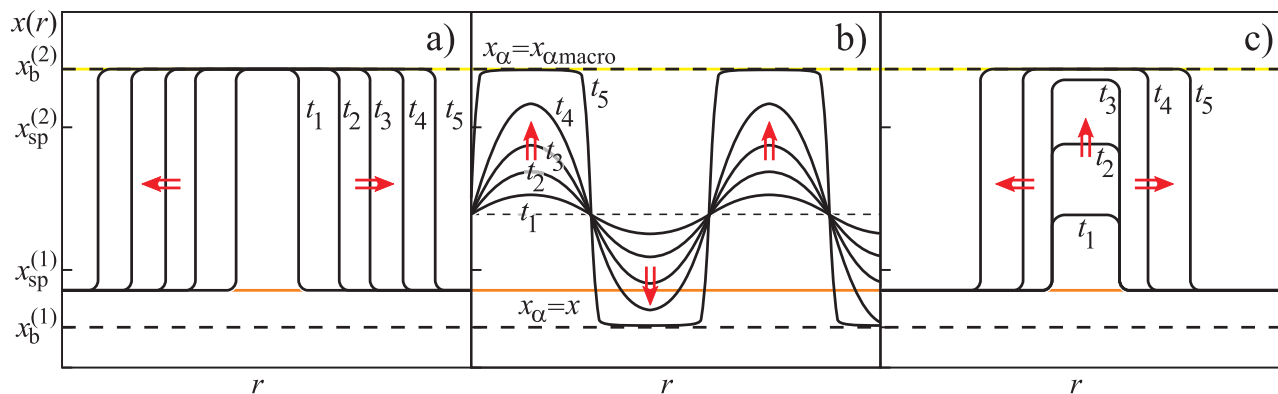


Fig. 1.7. Illustration of the basic features of (a) the classical nucleation-growth scenario, (b) the Cahn-Hilliard spinodal decomposition model and (c) the model for the description of phase formation in solutions as developed here based on the generalized Gibbs' approach (see text).

According to the classical picture of this process, aggregates having nearly the composition and structure of the newly evolving macroscopic phase grow by incorporation of additional units with similar properties. In contrast, the analysis performed here leads to the following picture of the process: in some certain region of the ambient phase with a typical size,  $2R_s$ , the molar fraction of the segregating component is increased. This increase of the concentration proceeds without significant changes in the size of the region representing the precursor of the new phase remaining comparable with the critical cluster size. As it turns out the size of this region in the ambient phase, where the concentration amplification takes place, may even decrease again in the course of increase of the molar fraction of the second component in it (cf. Figs. 1.5). In such cases, when the cluster size is reduced with the evolution to the critical size, the driving force of the initial stage of the cluster evolution consists in the change of the composition, but not of the size. Only after the change of the composition is widely completed, the cluster starts to grow, again (see Figs. 1.6b and 1.7c). The further evolution follows widely the classical model.

The dependence of the characteristic size parameter,  $R_s$ , both in absolute (as multiples of the parameter  $\Omega_2$ ) and relative units ( $r_s = R_s/R_c$ ) on supersaturation for different values of the ratio  $D_1/D_2$  is shown in Figs. 1.8 (*dotted curve*:  $D_1/D_2 = 0.1$ , *dashed curve*:  $D_1/D_2 = 1$ , *full curve*:  $D_1/D_2 = 10$ ). As evident, for most values of

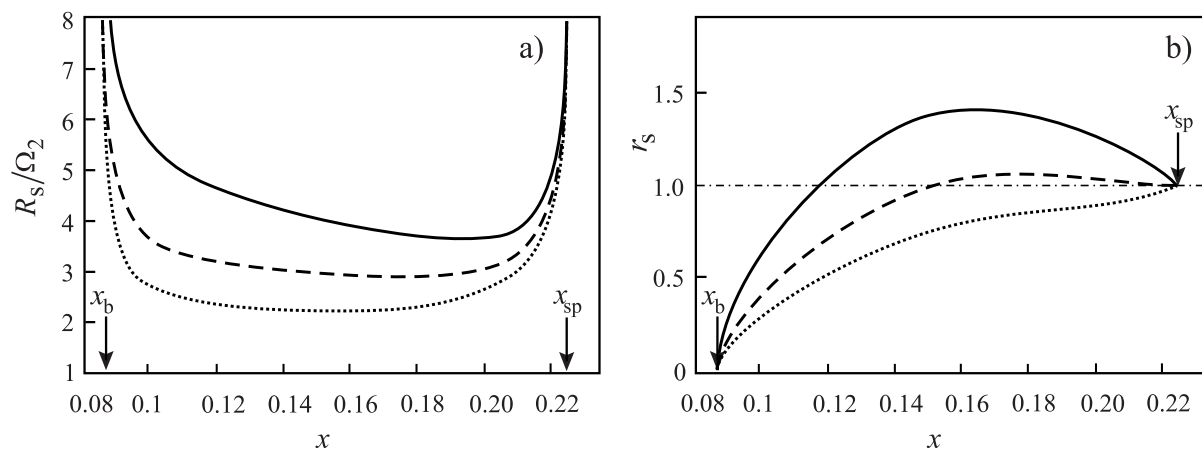


Fig. 1.8. Dependence of the size of the precursor of the newly evolving phase on supersaturation for different values of the ratio  $D_1/D_2$  (*dotted curve*:  $D_1/D_2 = 0.1$ , *dashed curve*:  $D_1/D_2 = 1$ , and *full curve*:  $D_1/D_2 = 10$ ). The respective dependencies are given both in absolute (as multiples of the parameter  $\Omega_2$ , cf. Eq. (1.24)) and in relative units as  $r_s = R_s/R_c$ .

the initial supersaturation the size parameter  $R_s$  is of the same order of magnitude as the critical cluster size and may even exceed it. Such possibility is excluded if the path of evolution is determined thermodynamically (as shown in Figs. 1.1 - 1.3), it is a consequence of kinetic effects. Indeed, if the mobility of the second component is small as compared with the first one ( $D_1 \gg D_2$ ), then its molar fraction in the cluster is increased mainly by reducing the content of the rapidly moving first component, i.e., by reducing the size of the cluster.

Summarizing above results, we find a very different picture of the scenario of the phase formation process in solutions as compared with the classical model. It is illustrated in Fig. 1.7c. In some part of space of the ambient phase with a characteristic size  $2R_s$ , the state of the ambient phase is changed continuously. In this process, the size of the evolving cluster is varied only slightly. The relative width of the range of sizes of the precursor of the new phase, where this transition proceeds, decreases

with increasing supersaturation, and a characteristic size  $R_s$ , where the cluster begins to change its composition, tends to the critical radius  $R_c$  at  $x = x_{sp}$ .

Note that the picture described is in its nature very similar to the Cahn-Hilliard picture of the initial stages of spinodal decomposition illustrated in Fig. 1.7b. Here also an amplification of density fluctuations is found in a certain stage of the transformation. The typical size of these precursors of the new phase depends on the state of the ambient phase. It is of the order of  $R_{max} \cong \lambda_{max}/2$  (cf. Eq. (1.19) and the discussion to it). This way, following the approach to nucleation as described here, we conclude that nucleation and spinodal decomposition are not complementary and different but in its nature very similar mechanisms of the phase transformation. In both cases, the driving force of the process is connected with the change of the concentration in some given region of the ambient phase. Only after the change of the composition is widely completed, the subsequent evolution is determined by factors known from classical theory, where the driving force is connected with the change of the size of the clusters. On the other hand, some distinction remains, since processes of phase formation commonly denoted as nucleation – i.e. evolving from metastable initial states - have to overcome a potential barrier, while processes of spinodal decomposition - starting from unstable initial states – have not. We will see, in addition, shortly that nucleation (i.e., processes of phase formation involving a potential barrier) may be the governing mechanism of evolution of the new phase also for initial states in the unstable region near the spinodal curve.

## **1.5. Nucleation, Spinodal Decomposition and the Kinetics of Phase Transformations in the Vicinity of the Spinodal Curve**

### **1.5.1. Predictions of the Classical Gibbs' and the Cahn-Hilliard Approaches**

The basic differences in the two classical mechanisms of first-order phase transitions – nucleation-growth and spinodal decomposition – discussed are illustrated

in Fig. 1.7a-b (cf. also [16]). According to the model, underlying the classical description of nucleation processes, in relatively small-scale parts of the ambient phase fluctuations are formed with state parameters (density, composition) widely similar in its properties to the newly evolving macroscopic phase. These initially small clusters grow then in their spatial extensions without significant changes in their properties (see Figs. 1.4b and 1.7a). In particular, in application to the considered example of segregation in a regular solution, the molar fraction of the segregating component in the critical cluster is – following the classical Gibbs' method of determination – widely identical (somewhat larger) as compared with the respective value  $x_{macro} = x_b^{(r)}$  in the newly evolving macroscopic phase [19,23]. The radius of the critical cluster (expressed in terms of Gibbs' surface of tension) is given as

$$R_c^{(Gibbs)} = \frac{2\sigma}{(p_\alpha - p_\beta)} \cong \frac{2\sigma}{c_\alpha \Delta\mu} . \quad (1.16)$$

In order to determine  $\Delta\mu$  in this expression, one has to substitute into Eq. (1.12) and (1.13) a value of  $x_\alpha$  equal (somewhat larger) than  $x_\alpha = x_{macro} = x_b^{(r)}$ .

Remaining inside the framework of the classical Gibbs' approach, one can determine uniquely the reference states for the description of the bulk properties of the critical clusters (they are determined in Gibbs' classical approach via identity of temperature and chemical potentials in both coexisting phases, cf. Fig. 1.9). However, one has no tool at the disposal allowing us to determine the dependence of the surface tension on supersaturation or, in other terms, on the size of the critical clusters. If one employs the capillarity approximation (i.e. identifies the value of  $\sigma$  with the respective value for an equilibrium coexistence of both phases at planar interfaces, i.e.,  $\sigma = \tilde{\sigma} \left( x_b^{(r)} - x_b \right)^2$ ), then  $R_c$  decreases monotonically with decreasing supersaturation (cf. Fig. 1.10). However, both  $R_c$  and the work of critical cluster formation (cf. Fig. 1.11) remain finite at the spinodal curve. However, by the physical meaning of the spinodal curve (being the boundary between thermodynamically metastable and unstable states of the homogeneous ambient phase), the work of critical cluster

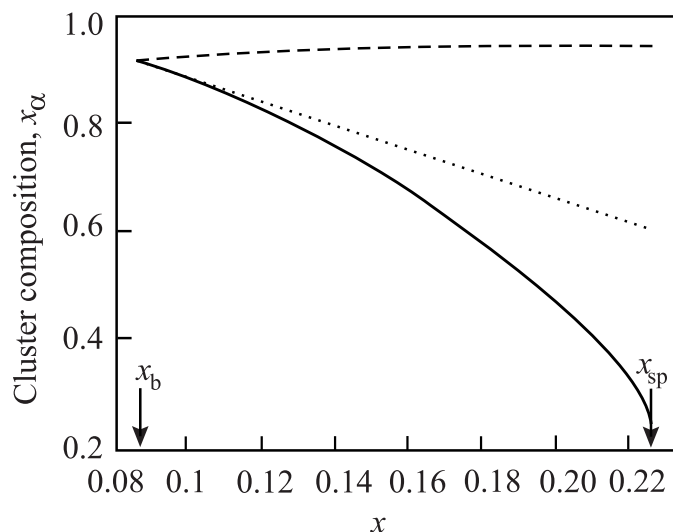


Fig. 1.9. Composition of the critical cluster for nucleation in a binary regular solution as determined via the generalized Gibbs' approach (full curve), Gibbs' classical approach (dashed curve) and the composition of the particular ridge cluster (dotted curve) having widely the same cluster size as determined via the classical Gibbs' approach (see text).

formation has to tend to zero here. Provided the surface of tension is chosen as the dividing surface, the work of critical cluster formation can be written in Gibbs' classical theory generally as

$$\Delta G_c = \frac{4\pi}{3} \sigma \left[ R_c^{(Gibbs)} \right]^2 \tag{1.17}$$

or as

$$\Delta G_c = \frac{16\pi}{3} \frac{\sigma^3}{(p_\alpha - p)^2} \cong \frac{16\pi}{3} \frac{\sigma^3}{(c_\alpha \Delta\mu)^2} . \tag{1.18}$$

In order to allow a correct description of the behavior of the system near the spinodal curve, the surface tension has to depend on supersaturation or on the size of the critical cluster. It has to vanish at the spinodal curve. As a consequence (cf. Eq. (1.16)), the radius of the critical cluster vanishes as well. Note that these conclusions do not follow directly from Gibbs' classical theory but are a consequence

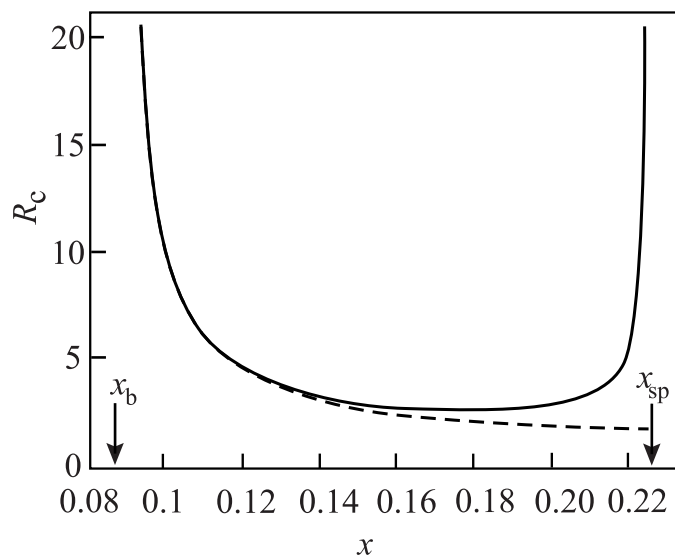


Fig. 1.10. Radius of the critical cluster for nucleation in a binary regular solution as determined via the generalized Gibbs' approach (full curve) and the classical Gibbs' approach utilizing, in addition, the capillarity approximation (dashed curve). The radius  $R_c$  is given as multiples of the parameter  $\Omega_2$  (cf. Eq. (1.24)). This parameter has a value of the order of one nanometer [23].

from above given or similar additional considerations.

Following Gibbs' classical approach, alternatively to the radius of the surface of tension also other size parameters may be introduced like the equimolecular dividing surface or their multi-component generalizations. These size parameters behave, in general, quite differently near the spinodal, they may even diverge here [23–25]. The bulk properties of the critical clusters do not depend on the choice of the dividing surface, however.

This way, taking the radii of the equimolecular or similar dividing surfaces as the size parameter for the description of the critical clusters, latter ones become near the spinodal very large with bulk properties of the clusters similar to the properties of the evolving macrophases. Obviously, such model critical clusters cannot be considered as an appropriate description of the properties of the real critical clusters. By this reason, in the search for an appropriate description of these real properties in terms of Gibbs' classical theory commonly the radius of the surface of tension is chosen as the more appropriate size parameter.

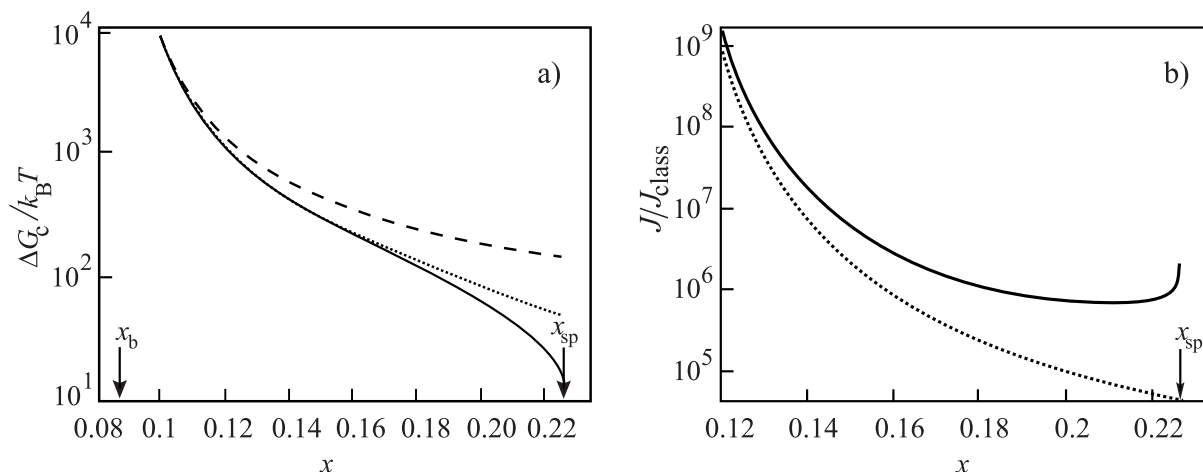


Fig. 1.11. Work of formation of the critical clusters (a) for nucleation in a binary regular solution as determined via the generalized Gibbs' approach (full curve) and the classical Gibbs' approach utilizing, in addition, the capillarity approximation (dashed curve). In the computations, the parameter  $\Omega_1$  was set equal to ten (cf. Eq. (1.23)). By a dotted curve the value of the work of formation of a cluster passing the ridge of the thermodynamic potential is specified having essentially the same size but a different composition as compared with the critical cluster in Gibbs' classical approach. The right curves (b) give an illustration of the resulting differences in the steady-state nucleation rates. Here the ratio of the nucleation rates,  $J/J_{class}$ , are shown, when  $J$  is expressed through the value of the work of critical cluster formation computed via the generalized Gibbs' approach (evolution proceeding via the saddle point (full curve)) and via the work required to evolve via the particular ridge path discussed (dotted curve).  $J_{class}$  is the steady-state nucleation rate determined via the classical Gibbs' approach and involving the capillarity approximation.

Summarizing, based on Gibbs' classical theory of heterogeneous systems [8] we come, in particular, to the following conclusions: (i.) the size of the critical cluster is not uniquely defined, it depends on the definition of the size parameter. Near the spinodal curve, different size parameters behave differently, they may, for example, tend to zero or to infinity. (ii.) The properties of the critical clusters are widely equivalent to the properties of the newly evolving macrophases. This condition is fulfilled independently of the choice of the dividing surface and an inherent consequence of the classical Gibbs' approach.

In contrast, if the van der Waals – Cahn and Hilliard method is employed for the

description of nucleation processes (i.e. for phase formation starting from metastable initial states), then directly and without the necessity of additional postulates or assumptions the following conclusions can be drawn [12–14]: For low values of the supersaturation, the results of the classical Gibbs' theory are reestablished. However, with increasing supersaturation, the bulk state parameters of the critical clusters change and approach near the spinodal the respective values of the metastable initial states. As one consequence, the work of critical cluster formation tends to zero then. In addition, the characteristic size parameter describing the spatial extension of the critical clusters tends to infinity. These results are reconfirmed by more advanced density functional computations of the properties of critical clusters [15]. This way, the predictions of the classical Gibbs' and the van der Waals-type approaches are in contradiction for metastable initial states near the spinodal curve.

In addition, according to the Cahn-Hilliard picture of spinodal decomposition (phase formation processes starting from unstable initial states), the first stages of the phase transformation starting from unstable initial states are characterized by long wave-length fluctuations with initially small changes in the state parameters of the precursor of the new phase as compared with the ambient phase (see Fig. 1.7b). Hereby the wave-number with the highest rate of amplification of the density fluctuation depends on the molar fraction of the segregating component in the unstable initial state. It diverges near the spinodal curve (e.g. [36]). For regular solutions, we get, in particular, the following expression for the wave number with the highest amplification rate

$$k_{max} \propto \left\{ 1 - \left( \frac{T}{4T_c} \right) \left( \frac{1}{x(1-x)} \right) \right\}_{p,T} . \quad (1.19)$$

For initial states near the spinodal curve,  $k_{max}$  becomes equal to zero [19, 23]. Denoting by a characteristic size parameter,  $R_{max}$ , the value of the wave-length divided by two ( $k_{max} = 2\pi/\lambda_{max}$ ,  $R_{max} = \lambda_{max}/2$ ), we come to the conclusion

that the size of the new phase precursor with the highest rate of amplification of the composition differences tends to infinity for initial states approaching the spinodal curve from the side of the unstable initial states as

$$R_{max} \propto \left\{ 1 - \left( \frac{T}{4T_c} \right) \left( \frac{1}{x(1-x)} \right) \right\}_{p,T}^{-1} . \quad (1.20)$$

This way, the van der Waals – Cahn and Hilliard approach is free of internal contradictions, in the framework of this approach, the nucleation-growth model and the model of spinodal decomposition lead, near the spinodal curve, to equivalent results. However, the picture of the nucleation process, as derived via the van der Waals or similar methods, is in contradiction with the conclusions derived based on Gibbs' classical theory: the state parameters of the critical clusters are quite different and the sizes of the critical clusters behave differently (in particular, if in Gibbs' approach the surface of tension is chosen as the dividing surface). This way, only one of both theories (if any) can be correct.

## 1.5.2. Predictions of the Generalized Gibbs Approach

### 1.5.2.1. Critical Cluster Properties Near the Spinodal Curve

Having in mind above mentioned and additional problems of Gibbs' classical approach to the description of heterogeneous systems, in a number of recent publications a generalization of Gibbs' method was developed (see e.g. [10, 11, 22, 25, 26]) and employed for the determination of the work of critical cluster formation for a variety of different processes of phase formation [19–21]. In application to segregation processes in binary regular solutions, the work of critical cluster formation and the size of the critical cluster (determined in a similar form as the surface of tension in

Gibbs' classical approach) are given via [10,19,23]

$$R_c = \frac{2\sigma}{c_\alpha \Delta\mu}, \quad \Delta G_c = \frac{16\pi}{3} \frac{\sigma^3}{(c_\alpha \Delta\mu)^2}. \quad (1.21)$$

For the considered case, these equations look similar to the classical expressions as derived via Gibbs' classical approach (cf. Eqs. (1.16)–(1.18)). However, the generalization of Gibbs' theory, as outlined in cited papers, leads to a different equation for the determination of the state parameters of the critical clusters. For the considered particular case, we get

$$3f(x, x_\alpha) + (x - x_\alpha) \frac{\partial f(x, x_\alpha)}{\partial x_\alpha} = 0. \quad (1.22)$$

The derivation of the respective equations is given in detail in [10,19,23]. Here we reproduce the final results as far as they are required for the subsequent analysis performed.

In Fig. 1.9, the composition of the critical clusters (determined via Eq. (1.22), full curve) is shown in dependence on the composition of the ambient phase in the range between the left hand side branches of the binodal and spinodal curves. For small values of the supersaturation, the composition of the critical cluster coincides with the composition of the newly evolving macroscopic phase ( $x_\alpha = x_b^{(r)}$  for  $x \rightarrow x_b$ ). It approaches the composition of the ambient phase for initial states near the spinodal curve ( $x_\alpha \rightarrow x_{sp}$  for  $x \rightarrow x_{sp}$ ). These results are widely identical to those obtained via van der Waals – Cahn and Hilliard and more sophisticated density functional approaches. By a dashed curve, the composition of the critical cluster is shown determined via Gibbs' classical method (cf. [19,23]).

It is often stated that the classical theory of nucleation describes processes of phase formation correctly for initial states in the vicinity of the binodal curve. This statement is true but only to some extent. Indeed, for initial states in the vicinity of the binodal curve both density functional computations and the generalized Gibbs'

approach come to a similar conclusion as the classical Gibbs' theory: the state parameters of the critical clusters are, in this range of supersaturations, widely similar to the respective properties of the newly evolving macroscopic phase (cf. e.g. Fig. 1.9 and [23–25]). However, as shown, for example, in Figs. 1.3 and 1.8, even in this range of supersaturations the formation of the critical clusters does not proceed via the classical model but via amplification of concentration differences in finite regions of the ambient phase. This way, the classical model is not an appropriate description of cluster formation processes in solid and liquid solutions even for low supersaturations.

Once the composition of the critical cluster is known in dependence on supersaturation, immediately other parameters like the radius and the work of formation of critical clusters may be calculated. For such purposes, we express Eqs. (1.21) in the form

$$\frac{\Delta G_c}{k_B T} = \Omega_1 \frac{g^3(x, x_\alpha)}{f^2(x, x_\alpha)}, \quad \Omega_1 = \frac{16\pi}{3} \frac{\tilde{\sigma}^3}{c_\alpha^2 (k_B T)^3}, \quad g(x, x_\alpha) = (x - x_\alpha)^2, \quad (1.23)$$

$$R_c = -\Omega_2 \frac{g(x, x_\alpha)}{f(x, x_\alpha)}, \quad \Omega_2 = \frac{2\tilde{\sigma}}{c_\alpha k_B T}. \quad (1.24)$$

These dependencies of critical cluster size and work of critical cluster formation on supersaturation, as determined via the generalized Gibbs' approach, are shown on Figs. 1.10 and 1.11a by full curves. The respective curves, obtained via the classical Gibbs' approach (corresponding to critical cluster compositions as given by the dashed curve in Fig. 1.9 and employing the capillarity approximation  $\sigma = \tilde{\sigma} \left( x_b^{(r)} - x_b \right)^2$ ) are shown for comparison by dashed curves, again. Since we are mainly interested here in qualitative results, we set the parameters  $\Omega_1$  equal to ten and  $\Omega_2$  equal to one for convenience ( $\Omega_1 = 10$ ,  $\Omega_2 = 1$  nm). Such assumption is also employed in the computations for the size parameter  $R_s$  shown in Figs. 1.3 and 1.8. More detailed estimates of these parameters for a model system are given in [23] resulting in  $\Omega_1 = 13.6$  and  $\Omega_2 = 1.2$  nm.

As evident the results of the generalized Gibbs' approach are in full agreement with the results of density functional computations of the respective parameters, again, the work of critical cluster formation tends to zero and the size of the cluster tends to infinity. This way, the generalized Gibbs' approach gives a picture of the critical clusters which is in agreement with van der Waals' and similar methods of determination and in contrast to the classical Gibbs' method of determination of the respective properties.

In Fig. 1.11b, changes in the values of the nucleation rate are shown, if the different methods are employed for the determination of the work of critical cluster formation. As evident, in the range, where intensive nucleation processes may occur, the generalized Gibbs' approach leads – provided the pre-exponential terms are taken to be of the same order of magnitude – to nucleation rates by 6–9 decimal orders larger as compared with the results of classical nucleation theory. This way, the classical Gibbs' approach, involving the capillarity approximation, underestimates the values of the steady-state nucleation rates for phase separation in solutions significantly.

Note an highly interesting feature of the curve shown in Fig. 1.10 representing the dependence of the cluster size on supersaturation in the generalized Gibbs' approach. As evident, except in the immediate vicinity of the binodal curve (where nucleation cannot occur due to large values of the work of critical cluster formation) and the vicinity of the spinodal curve (which cannot be reached commonly), there exists a broad range of supersaturations in between these limits where the cluster size remains nearly constant. Consequently, in almost any experiment, where homogeneous nucleation is observed, the critical nuclei may be expected to be always of nearly the same size.

In Fig. 1.12 another important new consequence of the generalized Gibbs' approach in comparison with the classical Gibbs' method of description is illustrated. In Fig. 1.12a, the dependence of the thermodynamic driving force,  $(\Delta\mu/k_B T) = |f(x, x_\alpha)|$ , for critical cluster formation is given both for the classical Gibbs' method

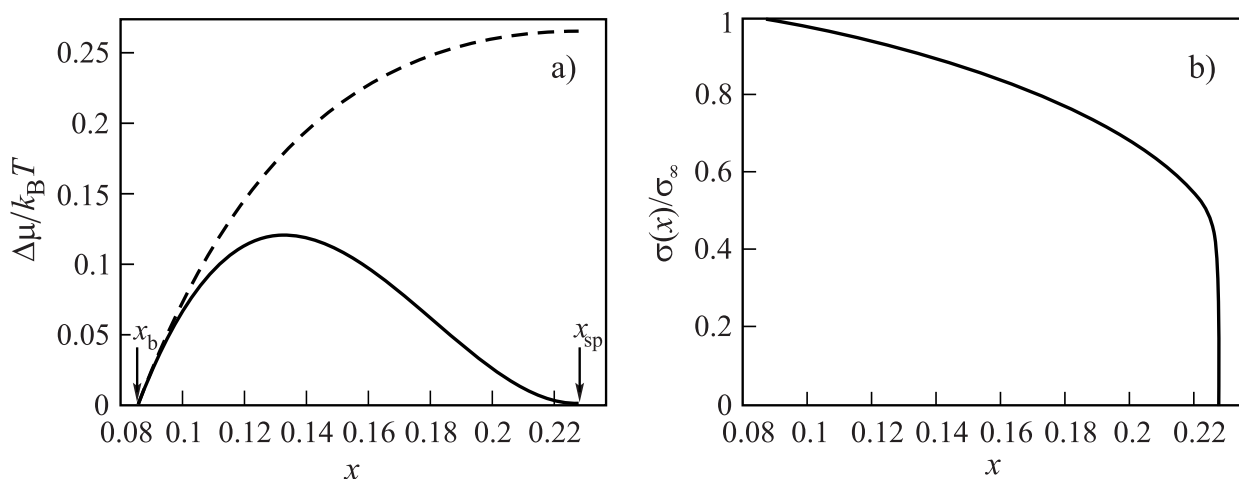


Fig. 1.12. (a) Thermodynamic driving force of critical cluster formation ( $\Delta\mu/k_B T = |f(x, x_\alpha)|$ ) and (b) surface tension ( $\sigma(x)/\sigma_\infty$ ), referred to the appropriately defined surfaces of tension, as determined via the classical (dashed curve) and generalized (full curves) Gibbs' approaches.

(dashed curve) and the generalized Gibbs' approach (full curve). While the classical Gibbs' approach (in agreement with common expectations) results in a monotonous increase of the driving force of cluster formation with increasing molar fraction of the segregating component in the metastable ambient phase, the generalized Gibbs' approach predicts a non-monotonic behavior. This way, the change of the properties of the critical clusters reduces the driving force of cluster formation as compared with the predictions of Gibbs' classical method. However, this reduction of the driving force is overcompensated by the decrease of the surface tension. The respective curves (in reduced units ( $\sigma(x)/\sigma_\infty$ ),  $\sigma_\infty = \tilde{\sigma} \left( x_b^{(r)} - x_b \right)^2$ ) are shown in Fig. 1.12b.

A similar behavior as discussed above was found also for a variety of other specific forms of phase transformations (condensation and boiling in one-component systems [20, 21, 24], boiling in binary liquid-gas solutions [25]). This way, the basic features obtained from above given analysis can be expected to be of quite general nature.

### 1.5.2.2. Nucleation near the Spinodal Curve By-Passing the Saddle Point

In the preceding analysis, we always assumed that the flux of the clusters to the new phase passes the saddle point of the characteristic thermodynamic potential. Such scenario can be considered as the rule, but exceptions from this general rule are possible as well (see e.g. [32–35]). Such exceptions correspond to situations when the main flux to the new phase passes not the saddle but some ridge point of the thermodynamic potential. General expectations and detailed analyses [37, 38] allow to conclude that ridge crossing will be the preferred channel of the transformation in cases, when the thermodynamic barrier is relatively low. In such situations, not the thermodynamic but kinetic factors will govern the process. A precondition of such change in the kinetics is obviously that the ridge crossing is characterized by relatively low values of the activation energy as well. The determination of the location of the particular ridge point of the thermodynamic potential, determining the kinetics of the transformation, is a highly complicated task [32] and will be discussed in the framework of the approach outlined in more detail in a future analysis. Here we will merely show that in the vicinity of the spinodal curve ridge points with relatively low activation barriers exists, which are kinetically favored as compared with the passage via the saddle point of the thermodynamic potential.

As already mentioned, in Figs. 1.10 and 1.11a the radius of the critical cluster and the work of critical cluster formation are shown also for the case that Gibbs' classical approach is employed for the determination of these quantities and the capillarity approximation is used, in addition (dashed curves; cf. [19, 23]). As evident from Fig. 1.10, both curves for the critical cluster size coincide widely except in the immediate vicinity of the spinodal curve.

The question now is, whether nucleation in the vicinity of the spinodal proceeds necessarily via passing the saddle point of the Gibbs free energy surface or not. On one side, the saddle point corresponds to the lowest value of the work of cluster formation

allowing – after the respective barrier is overcome – the cluster to evolve to the new phase. Indeed, by taking the derivative of the work of critical cluster formation with respect to the cluster composition,  $x_\alpha$ , for fixed values of the composition of the ambient phase, we arrive at Eq. (1.22). On the other side, in order to evolve into the new phase via the saddle point near the spinodal curve very large clusters have to be formed which is unfavorable from a kinetic point of view.

Near the spinodal curve (we restrict ourselves here to values of  $x$  larger than 0.2), the work of critical clusters is small and also other channels of the transformation may be effective. Such other channels are the formation of clusters passing not the saddle but the ridge of the thermodynamic potential, i.e., by-passing the saddle point. The cluster sizes along this ridge are given by the mechanical equilibrium conditions, which are expressed for the considered system via Eq. (1.24). This way, utilizing this expression, we can compute for any value of the composition of the ambient phase and for any value of the cluster size along the ridge the value of the concentration in this particular cluster. Then, utilizing Eq. (1.23), we can obtain the value of the work of cluster formation for this particular channel of evolution to the new phase.

In order to estimate the possible magnitude of the work of cluster formation for clusters located at the ridge, we suppose the cluster size to be determined via

$$R_c = -\Omega_2 \frac{g(x, x_b^{(r)})}{f(x, x_b^{(r)})}, \quad \Omega_2 = \frac{2\tilde{\sigma}}{c_\alpha k_B T}. \quad (1.25)$$

This expression is widely identical to the radius of the surface of tension in the classical Gibbs approach employing the capillarity approximation. The composition of the cluster at the ridge of the thermodynamic potential is determined then via the generalized Gibbs' approach as

$$\frac{g(x, x_b^{(r)})}{f(x, x_b^{(r)})} = \frac{g(x, x_\alpha)}{f(x, x_\alpha)}. \quad (1.26)$$

One of the possible solutions of this equation is obviously  $x_\alpha = x_b^{(r)}$ . This solution corresponds to the classical Gibbs' approach utilizing the capillarity approximation. As it turns out the classical Gibbs' result corresponds – interpreted in terms of the generalized Gibbs' approach – not to a saddle point path of evolution but to one of the ridge channels of evolution to the new phase.

There exists, however, also another solution of Eq. (1.26) different from the classical limiting case, i.e., there exists a ridge path of evolution to the newly evolving phase with the following properties: (i.) The size of the cluster at the ridge is widely identical to the radius of the surface of tension determined via Gibbs' classical method. (ii.) The composition of this cluster is different from the compositions of the critical clusters as determined via Gibbs' classical and the generalized Gibbs' approaches. The respective dependence of the composition of this particular ridge cluster on the molar fraction of the segregating component in the ambient phase is shown in Fig. 1.9 by a dotted curve. (iii.) The value of the work of formation of this particular cluster – located at the ridge of the thermodynamic potential – is shown in dependence on the composition of the ambient phase in Fig. 1.11a. The work of formation of a cluster on the particular ridge point is higher as compared with the saddle point, when the generalized Gibbs' method is employed for its determination, but significantly lower as compared with the value obtained via the classical Gibbs' approach employing the capillarity approximation. As the result, the considered ridge path results in an increase of the nucleation rate as compared with the classical estimate by 5-9 decimal orders (cf. Fig. 1.11b).

We have shown in this way that near the spinodal curve, at least, one channel of evolution to the new phase exists, which has values of the work of ridge cluster formation considerably lower as compared with the work of critical cluster formation according to the classical Gibbs' results, but is of the same size as the critical cluster size in Gibbs' classical approach. The system has got, in this way, at least, one additional channel of evolution to the new phase with values of the activation

barrier much less as compared with the results of the classical Gibbs' approach but much lower values of the cluster sizes as compared with the saddle point parameters computed via the generalized Gibbs' approach (or by density functional computations). This way, in metastable initial states near the spinodal curve nucleation will not proceed, in general, via the saddle point but in trajectories of evolution bypassing the saddle point of the thermodynamic potential. Hereby the mechanism of cluster evolution can be determined similarly as it is done before for the case of critical clusters in the generalized Gibbs' approach (i.e., by determining the most probable path over the particular point on the ridge of the thermodynamic potential).

### 1.5.2.3. Application of Nucleation Concepts to Thermodynamically Unstable States Beyond the Spinodal Curve

It is well-known that the classical Gibbs' approach to the determination of the work of critical cluster formation – utilizing the capillarity approximation – does not show any peculiar features for initial states approaching the spinodal curve from the side of metastable states (cf. Figs. 1.9-1.11). As mentioned, this property is one of the severe disadvantages of this approach. In this connection the question arises, what the predictions of the generalized Gibbs' approach are for unstable initial states on the right hand side of the spinodal curve.

In Fig. 1.13a, the composition of the critical cluster is given as a function of the supersaturation, but now in the range  $0 \leq x \leq 0.5$ , as obtained by the classical (dashed curve) and the generalized Gibbs' approaches (full curves). The composition of the cluster phase determined via the generalized Gibbs' approach (Eq.(1.22)) has, in general, two solutions,  $x_\alpha = x$  and  $x_\alpha > x$  (cf. Fig. 1.9). However, for values of the initial supersaturation  $x < x_{sp}$ , only one of these solutions ( $x_\alpha > x$ ) leads to physically reasonable results. The solution  $x_\alpha = x$  would result in this range of compositions in negative values of the critical cluster size (see also [19,23] and the subsequent analysis;  $x_{sp}$  is here the concentration at the left branch of the spinodal

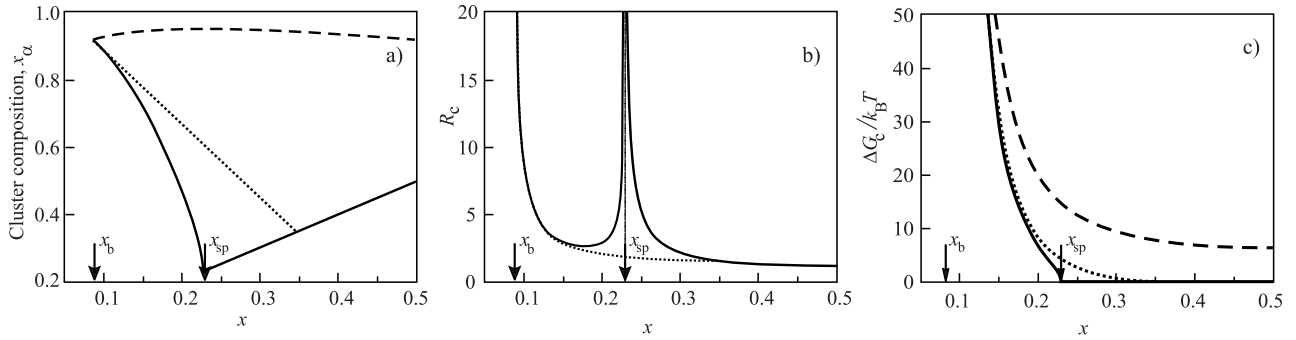


Fig. 1.13. Parameters of the critical and the ridge clusters for metastable and unstable initial states: (a) Composition of the critical cluster as determined via the classical Gibbs approach employing the capillarity approximation (dashed curve), via the generalized Gibbs approach (full curves, see text) and the composition of the ridge cluster having the same size as the critical cluster in the classical Gibbs approach (dotted curve); (b) Size of the critical cluster determined via the generalized Gibbs’ approach (full curve) and size of the ridge cluster (dotted curve; this curve gives also the size of the radius of the surface of tension in dependence on supersaturation computed in the framework of the classical Gibbs’ approach employing the capillarity approximation); (c-d) Work of formation of the the critical cluster as obtained via Gibbs’ classical approach employing the capillarity approximation (dashed curve), work of formation of the critical cluster in the generalized Gibbs’ approach (full curve) and of the particular ridge cluster (dotted curve) as specified in the text ((a)-(d): left top to right bottom).

curve, again). In contrast, for  $x \geq x_{sp}$  there exists only one solution  $x_\alpha = x$ , i.e., the concentration in the critical cluster equals the concentration in the ambient phase. For this solution, the equation for the critical cluster size Eq. (1.21) leads to an indeterminacy of the order 0/0. However, it can be resolved easily to give

$$R_c = -\Omega_2 \lim_{x_\alpha \rightarrow x} \left( \frac{g(x, x_\alpha)}{f(x, x_\alpha)} \right) = -\frac{2\Omega_2}{\left( \frac{\partial^2 f}{\partial x_\alpha^2} \Big|_{x_\alpha \rightarrow x} \right)_{p,T}} \propto \left\{ 1 - \left( \frac{T}{4T_c} \right) \left( \frac{1}{x(1-x)} \right) \right\}_{p,T}^{-1}. \tag{1.27}$$

This expression has negative values for initial states in the range  $x < x_{sp}$  (this is one of the reasons, why this solution is physically meaningless in this range), it has positive values for  $x > x_{sp}$ .

The dependence of the critical cluster size  $R_c$  on supersaturation is shown in Fig. 1.13b by a full curve. Note that the behavior of this size parameter is, in the range of unstable initial states, widely identical to the radius  $R_{max}$  determined via Eq. (1.20). This way, the generalized Gibbs' approach allows, when applied to unstable initial states, to determine the characteristic sizes of the regions in space with the highest rate of amplification of density fluctuations as predicted in the framework of the Cahn-Hilliard theory of spinodal decomposition. This way, the size parameter  $R_c$  retains a well-defined physical meaning of a characteristic size where density amplifications occur preferentially from a thermodynamic point of view.

The expression for the work of critical cluster formation Eq. (1.23), when applied to unstable initial states, results (after the resolution of the indeterminacy) in  $\Delta G_c/k_B T = 0$ . As it has to be the case, for unstable initial states the activation energy for the transition to the new phase equals zero. The work of critical cluster formation, as determined via Eq.(1.23), is shown by a full curve in Fig. 1.13c-d for the whole range of initial supersaturations considered.

Finally, let us consider also the parameters of the particular ridge pass of transition of the system, considered earlier, into the new phase when extended to unstable initial states. As defined earlier, we consider a path over the ridge of the potential hypersurface having nearly the same size as the critical cluster determined via Gibbs' classical approach (cf. the dotted curve in Fig. 1.13b). The composition of the ridge cluster is shown by a dotted curve in Fig. 1.13a, the work of formation of this particular ridge cluster in Fig. 1.13c-d by dotted curves as well.

It turns out that the evolution to the new phase can proceed easily via the formation of such types of ridge clusters having values of the activation energy of the order  $10^1 - 10^0 k_B T$  and relative small values of their characteristic sizes. This way, this channel of evolution can compete with the thermodynamically preferred channel of formation of critical clusters with zero work of critical cluster formation or, equivalently, the Cahn-Hilliard scenario of spinodal decomposition.

## 1.6. Discussion

In the present paper, the new approach to the description of nucleation-growth processes in multi-component systems, developed in its basic premises in [10,11,25] and accompanying papers, was extended to account for both thermodynamic and kinetic factors in the determination of the preferred trajectory of the clusters in the space of thermodynamic state parameters. This trajectory determines the change of the properties of the clusters in the course of their evolution. As it turns out the resulting picture of the process of the phase transition in solid solutions is quite different as compared with the classical picture. Moreover, as shown, there is no qualitative difference between nucleation and spinodal decomposition with respect to the basic mechanism of cluster evolution. Nucleation processes, starting from thermodynamically metastable initial states, proceed qualitatively widely similar as compared with processes of phase formation governed by spinodal decomposition. As one of the consequences the problem arises how the classical kinetic description of nucleation-growth processes (cf. e.g. [4–7]) has to be modified to account appropriately for the scenario of the transformation as developed here. Some first analyses in this direction are outlined in [10,30].

At part, similar consequences as developed here were drawn some time ago based on the statistical mechanical analysis of model systems (e.g. [4,16]). We come therefore to the conclusion that the generalized Gibbs' approach leads – for the model systems studied – to, at least, qualitatively equivalent results as mentioned statistical mechanical model analyses. This coincidence is considered as an additional confirmation of the validity of the generalized Gibbs' approach, utilized basically in our analysis. Moreover, since in our approach only the knowledge of macroscopic properties of the ambient and the newly evolving phases is required in order to determine the properties of the clusters in dependence on their sizes, the approach presented here seems, to our opinion, to be preferable in the analysis of experimental

results on phase formation processes. The application of the methods and results obtained to the interpretation of experimental data will be addressed in future publications.

The results of the analysis, as performed above, were obtained for the analysis of regular solutions. They can be quantitatively modified by modifications of the thermodynamic properties of the real in comparison to the model system, by peculiarities of the process of diffusion not accounted for here or additional thermodynamic factors like elastic stresses which have to be taken into consideration in a number of cases as well. Nevertheless, we believe that the scenario outlined will be valid generally for processes of segregation in solid or liquid solutions.

The question arises also immediately, whether the general scenario found for phase separation in solutions is applicable to other processes of phase formation – like condensation of gases, bubble formation in liquids, crystallization of melts – as well or not. The answer to this question requires a detailed separate analysis which can be performed straightforwardly based on the basic ideas and method as outlined here. The respective work is in progress and the results will be reported in future communications.

### **Acknowledgments**

The authors would like to express their gratitude to the Deutsche Forschungsgemeinschaft (DFG) and to the Brazilian Science Foundation FAPESP (Grant 03/12617-0) for financial support.

## Appendix

According to the basic premises of thermodynamics, the thermodynamic potential  $\Phi$  of some given system can be expressed as a function of  $f$  independent macroscopic state parameters  $\{q\} = (q_1, q_2, \dots, q_f)$ , i.e.,  $\Phi = \Phi(q_1, q_2, \dots, q_f)$ . For the analysis of nucleation processes, we can always express the thermodynamic potential referred to its value at the critical cluster size. Consequently,  $\Phi$  can be considered as a dimensionless function. We will assume that the set of variables  $\{q\}$  is given in a dimensionless form as well.

Let us assume we consider two points ( $\{q\}$  and  $\{q + dq\}$ ) on the surface  $\Phi$  located in the immediate vicinity of each other. The change of the thermodynamic potential in the transition from  $\{q\}$  to  $\{q + dq\}$  can be expressed then as

$$\Phi(\{q + dq\}) - \Phi(\{q\}) = \sum_{i=1}^f \frac{\partial \Phi}{\partial q_i} dq_i \quad \text{or} \quad d\Phi = \sum_{i=1}^f \frac{\partial \Phi}{\partial q_i} dq_i. \quad (1.28)$$

Now, let us consider some trajectory on the hypersurface  $\Phi(\{q\})$ . Along the given trajectory, the coordinates can be expressed in a parametric form via a scalar variable  $l$ . If we denote the distance between the two considered points by  $\Delta l$ , we can then introduce the derivative along some given trajectory as

$$\frac{d\Phi}{dl} = \sum_{i=1}^f \frac{\partial \Phi}{\partial q_i} \frac{dq_i}{dl}. \quad (1.29)$$

Now, based on Eqs. (1.28) or (1.29), we can introduce an  $f$ -dimensional Cartesian system of coordinates with the set of unit vectors  $\{\vec{e}_q\}$ . Then we can write

$$d\vec{q} = \sum_{i=1}^f \vec{e}_{q_i} dq_i, \quad (1.30)$$

and define a gradient in the respective system via

$$\nabla\Phi = \sum_{i=1}^f \vec{e}_{q_i} \frac{\partial\Phi}{\partial q_i} . \quad (1.31)$$

With these notations, we have

$$d\Phi = (\nabla\Phi)d\vec{q} \quad \text{or} \quad d\Phi = |\nabla\Phi||d\vec{q}| \cos(\nabla\Phi \wedge d\vec{q}) . \quad (1.32)$$

The absolute value of  $\nabla\Phi$  does not depend on the chosen direction. Consequently, the absolute value of  $d\Phi$  has its maximum (for a given value of  $|d\vec{q}|$ ), if  $d\vec{q}$  is directed parallel or antiparallel to  $\nabla\Phi$ . This way, searching for the trajectory with the steepest descent of the thermodynamic potential, we can demand

$$\frac{dq_i}{dl} = -\frac{\partial\Phi}{\partial q_i} . \quad (1.33)$$

Instead of  $\{q\}$ , we may employ also alternative sets of variables  $\{Q\}$  for the description of the thermodynamic state of the system. So, we have to have some one-to-one transformation of the form

$$Q_j = Q_j(q_1, q_2, \dots, q_f) , \quad j = 1, 2, \dots, f , \quad (1.34)$$

and the inverse transformation

$$q_j = q_j(Q_1, Q_2, \dots, Q_f) , \quad j = 1, 2, \dots, f . \quad (1.35)$$

Since the variables in each of the sets of parameters  $\{q\}$  and  $\{Q\}$  are independent

from each other, we have

$$\frac{\partial Q_j}{\partial Q_k} = \sum_{l=1}^f \frac{\partial Q_j}{\partial q_l} \frac{\partial q_l}{\partial Q_k} = \delta_{jk}, \quad \frac{\partial q_j}{\partial q_k} = \sum_{l=1}^f \frac{\partial q_j}{\partial Q_l} \frac{\partial Q_l}{\partial q_k} = \delta_{jk}. \quad (1.36)$$

With the new variables, we can carry out the same procedure as earlier and arrive, similarly to Eq. (1.28), at

$$d\Phi = \sum_{i=1}^f \frac{\partial \Phi}{\partial Q_i} dQ_i. \quad (1.37)$$

The validity of this relation can be shown also directly. Going over in Eq. (1.28) to new coordinates, we may write

$$\frac{\partial \Phi}{\partial q_i} = \sum_{j=1}^f \frac{\partial \Phi}{\partial Q_j} \frac{\partial Q_j}{\partial q_i}, \quad dq_i = \sum_{k=1}^f \frac{\partial q_i}{\partial Q_k} dQ_k. \quad (1.38)$$

A substitution into Eq. (1.28) employing Eq. (1.36) results immediately into Eq. (1.37).

Starting with Eq. (1.33) and going over to the new variables, we have

$$\sum_{j=1}^f \frac{\partial \Phi}{\partial Q_j} \frac{\partial Q_j}{\partial q_i} = - \sum_{j=1}^f \frac{\partial q_i}{\partial Q_j} \frac{dQ_j}{dl}, \quad i = 1, 2, \dots, f. \quad (1.39)$$

This set of relations allows one to determine the dependencies  $(dQ_j/dl)$  which give the direction of motion in the new system of coordinates. Now, by multiplying this relation with  $(\partial Q_k/\partial q_i)$  and taking the sum over  $i$ , we arrive with Eq. (1.36) at

$$\frac{dQ_k}{dl} = - \sum_{j=1}^f \frac{\partial \Phi}{\partial Q_j} \sum_{i=1}^f \frac{\partial Q_j}{\partial q_i} \frac{\partial Q_k}{\partial q_i}. \quad (1.40)$$

This way, in the new system of coordinates  $\{Q\}$ , a relation similar to Eq. (1.33) holds then and only then, if the conditions

$$\sum_{i=1}^f \frac{\partial Q_j}{\partial q_i} \frac{\partial Q_k}{\partial q_i} = \delta_{jk} \quad (1.41)$$

are fulfilled for any allowed values of  $j$  and  $k$ . In general, we have to employ Eq. (1.40) or equivalent expressions.

One of the sets of coordinates of particular importance for the analysis performed in the present paper is  $(r, x_{2\alpha}, x_{3\alpha}, \dots, x_{k\alpha})$  determining the evolution in the size-composition space. It is connected with the original one  $(n_{1\alpha}, n_{2\alpha}, \dots, n_{k\alpha})$  by Eq. (1.6) and the following transformations

$$r = \frac{R}{R_c}, \quad x_{i\alpha} = \frac{n_{i\alpha}}{n_\alpha}, \quad n_\alpha = \sum_{j=1}^k n_{j\alpha}. \quad (1.42)$$

Here  $R$  and  $R_c$  are the radius of the cluster and the critical cluster radius, respectively. From Eqs. (1.6) and (1.42), we obtain then

$$\frac{\partial r}{\partial n_{i\alpha}} = \frac{\omega_{i\alpha}}{4\pi R_c^3 r^2}, \quad \frac{\partial x_{j\alpha}}{\partial n_{i\alpha}} = \frac{1}{n_\alpha} (\delta_{ij} - x_{j\alpha}). \quad (1.43)$$

The path of evolution in the new space of variables is determined by the general set of equations Eq. (1.40). In the particular case considered, we arrive with Eqs. (1.6) and (1.42) also directly at

$$\frac{dr}{dl} = \frac{1}{4\pi R_c^3 r^2} \sum_{j=1}^k \omega_{j\alpha} \frac{dn_{j\alpha}}{dl}. \quad (1.44)$$

According to Eq. (1.4), we can replace now the derivatives  $(dn_{i\alpha}/dl)$  by

$-(\partial\Phi/\partial n_{i\alpha})$ , i.e.

$$\frac{dr}{dl} = -\frac{1}{4\pi R_c^3 r^2} \sum_{j=1}^k \omega_{j\alpha} \frac{\partial\Phi}{\partial n_{j\alpha}}. \quad (1.45)$$

Going over then to the description in size-composition space, we arrive at

$$\frac{dr}{dl} = -\frac{1}{4\pi R_c^3 r^2} \sum_{j=1}^k \omega_{j\alpha} \left\{ \frac{\partial\Phi}{\partial r} \frac{\partial r}{\partial n_{j\alpha}} + \sum_{l=2}^k \frac{\partial\Phi}{\partial x_{l\alpha}} \frac{\partial x_{l\alpha}}{\partial n_{j\alpha}} \right\}. \quad (1.46)$$

In the evaluation of Eq. (1.46), Eqs. (1.43) have to be utilized.

Similarly to above given considerations, we obtain from Eq. (1.42)

$$\frac{dx_{i\alpha}}{dl} = \frac{1}{n_\alpha} \left\{ \frac{dn_{i\alpha}}{dl} - x_{i\alpha} \sum_{j=1}^k \frac{dn_{j\alpha}}{dl} \right\}. \quad (1.47)$$

A substitution of Eq. (1.4) into Eq. (1.47) yields

$$\frac{dx_{i\alpha}}{dl} = -\frac{1}{n_\alpha} \left\{ \frac{\partial\Phi}{\partial n_{i\alpha}} - x_{i\alpha} \sum_{j=1}^k \frac{\partial\Phi}{\partial n_{j\alpha}} \right\}. \quad (1.48)$$

After some straightforward transformations we arrive finally at

$$\begin{aligned} \frac{dx_{i\alpha}}{dl} = & -\frac{1}{n_\alpha} \left\{ \left( \frac{\partial r}{\partial n_{i\alpha}} - x_{i\alpha} \sum_{j=1}^k \frac{\partial r}{\partial n_{j\alpha}} \right) \frac{\partial\Phi}{\partial r} + \right. \\ & \left. + \sum_{l=2}^k \frac{\partial\Phi}{\partial x_{l\alpha}} \left[ \frac{\partial x_{l\alpha}}{\partial n_{i\alpha}} - x_{i\alpha} \sum_{j=1}^k \frac{\partial x_{l\alpha}}{\partial n_{j\alpha}} \right] \right\}. \end{aligned} \quad (1.49)$$

For phase formation in a two-component system, we obtain as a special case

$$\frac{dr}{dl} = \frac{r}{3} \frac{1}{(n_{1\alpha} + n_{2\alpha})^2} \left[ \frac{2r}{3} \frac{\partial\Phi}{\partial r} + (1 - 2x_\alpha) \frac{\partial\Phi}{\partial x_\alpha} \right], \quad (1.50)$$

$$\frac{dx_\alpha}{dl} = \frac{1}{(n_{1\alpha} + n_{2\alpha})^2} \left\{ \frac{r}{3} (1 - 2x_\alpha) \frac{\partial \Phi}{\partial r} + [x_\alpha^2 + (1 - x_\alpha)^2] \frac{\partial \Phi}{\partial x_\alpha} \right\}, \quad (1.51)$$

where  $x_\alpha \equiv x_{2\alpha}$  holds.

## References

1. M. Volmer, *Kinetik der Phasenbildung* (Th. Steinkopff, Dresden, Leipzig, 1939).
2. Ya. I. Frenkel, *Kinetic Theory of Liquids* (Oxford University Press, Oxford, 1946).
3. *Nucleation*, edited by A. C. Zettlemoyer (Marcel Decker, New York, 1969); *Nucleation Phenomena*, Adv. Colloid Interface Science **7**, (1977).
4. J. D. Gunton, M. San Miguel, and P. S. Sahni, *The Dynamics of First-Order Phase Transitions*, in: *Phase Transitions and Critical Phenomena*, vol. 8, edited by C. Domb and J. L. Lebowitz (Academic Press, London - New York, 1983).
5. I. Gutzow and J. W. P. Schmelzer, *The Vitreous State: Thermodynamics, Structure, Rheology, and Crystallization* (Springer, Berlin, 1995).
6. D. T. Wu, *Nucleation theory*. In: *Solid State Physics: Advances in Research and Applications* **50**, 37 (1997).
7. K. F. Kelton, *Crystal nucleation in liquids and glasses*. In: *Solid State Physics* **45**, 75 (1991).
8. J. W. Gibbs, *Trans. Connecticut Acad. Sci.* **3**, 108, 343 (1875-78); see also: J. W. Gibbs, *The Collected Works*, vol.1 (Longmans & Green, New York - London - Toronto, 1928).
9. E. D. Zanotto and V. M. Fokin, *Phil. Trans. Royal Soc. A* **361**, 591 (2003).
10. J. W. P. Schmelzer, A. R. Gokhman, and V. M. Fokin, *J. Colloid Interface Science* **272**, 109 (2004).
11. J. W. P. Schmelzer, *Physics and Chemistry of Glasses* **45**, No. 2, 116 (2004).

12. J. D. van der Waals and Ph. Kohnstamm, *Lehrbuch der Thermodynamik* (Johann-Ambrosius-Barth Verlag, Leipzig und Amsterdam, 1908).
13. J. S. Rowlinson, Translation of J. D. van der Waals' *The thermodynamic theory of capillarity under the hypothesis of a continuous variation of density.*, J. Stat. Phys. **20**, 197 (1979); German version: J. D. van der Waals, Z. Phys. Chemie **13**, 657 (1893).
14. J. W. Cahn and J. E. Hilliard, J. Chem. Phys. **28**, 258 (1959); **31**, 688 (1959).
15. D. W. Oxtoby, Acc. Chem. Res. **31**, 91 (1998).
16. K. Binder, Rep. Progr. Phys. **50**, 783 (1987).
17. K. Binder, *Spinodal decomposition*. In: *Materials Science and Technology*, vol. 5, Eds. R. W. Cahn, P. Haasen, E. J. Kramer (VCH-Publishers, Weinheim, 1991, pgs. 405).
18. M. Shah, O. Galkin, and P. G. Vekilov, *Smooth transition from metastability to instability in phase separating protein solutions*, submitted for publication.
19. J. W. P. Schmelzer, J. Schmelzer, Jr., and I. Gutzow, J. Chem. Phys. **112**, 3820 (2000).
20. J. W. P. Schmelzer and J. Schmelzer, Jr., J. Chem. Phys. **114**, 5180 (2001).
21. J. W. P. Schmelzer and J. Schmelzer, Jr., J. Atmospheric Research **65**, 303 (2003).
22. J. W. P. Schmelzer, G. Röpke, and V. B. Priezhev (Eds.), *Nucleation Theory and Applications*, Joint Institute for Nuclear Research Publishing House, Dubna, Russia, 1999, 2002 (copies can be ordered via [juern-w.schmelzer@physik.uni-rostock.de](mailto:juern-w.schmelzer@physik.uni-rostock.de)).
23. V. G. Baidakov, G. Sh. Boltachev, and J. W. P. Schmelzer, J. Colloid Interface Sci. **231**, 312 (2000).
24. J. W. P. Schmelzer and V. G. Baidakov, J. Phys. Chem. **105**, 11595 (2001).
25. J. W. P. Schmelzer, V. G. Baidakov, and G. Sh. Boltachev, J. Chem. Phys. **119**, 6166 (2003).

26. J. W. P. Schmelzer, V. G. Baidakov, and G. Sh. Boltachev, *J. Chem. Phys.*, to be submitted for publication.
27. H. Reiss, *J. Chem. Phys.* **18**, 840 (1950).
28. V. V. Slezov and J. W. P. Schmelzer, *Kinetics of Nucleation-Growth Processes: The First Stages*, in [22], 1999, pgs. 6 - 81.
29. V. V. Slezov and J. W. P. Schmelzer, *Phys. Rev. E* **65**, 031506 (2002).
30. V. V. Slezov, J. W. P. Schmelzer, and A. S. Abyzov, *A new method of determination of the coefficients of emission in nucleation theory*. In: J. W. P. Schmelzer (Ed.): *Nucleation Theory and Applications*, WILEY-VCH, in press.
31. D. Stauffer, *J. Aerosol Science* **7**, 319 (1976).
32. Jin-Song Li, I. L. Maksimov, and G. Wilemski, *Phys. Rev. E* **61**, R4710 (2000) and cited there references.
33. H. Trinkaus, *Phys. Rev. B* **27**, 7372 (1983).
34. Z. Kozisek and P. Demo, *J. Cryst. Growth* **132**, 491 (1993).
35. B. E. Wyslouzil and G. Wilemski, *J. Chem. Phys.* **103**, 1137 (1995) and references cited therein.
36. J. W. P. Schmelzer and A. Milchev, *Physics Letters A* **158**, 307 (1991).
37. M. Sanada, I. L. Maksimov, and K. Nishioka, *J. Crystal Growth* **199**, 67 (1999).
38. I. L. Maksimov and K. Nishioka, *Phys. Lett. A* **264**, 51 (1999).

### 1.7. Висновки до розділу 1

Результати досліджень, представлених у даному розділі, опубліковано в статті [1] (Додаток А. Список публікацій здобувача за темою дисертації). Серед основних результатів у якості висновків можна виділити наступні:

- В узагальненому методі Гіббса зміна розміру та складу кластерів нової фази в процесі зародження якісно відрізняються порівняно з класичною картиною. Показано, що зародження, тобто перша стадія формування кластера, починаючи з метастабільних початкових станів, виявляє властивості, що нагадують спінодальний розпад: спочатку розмір кластера залишається майже постійним, а його склад змінюється, хоча наявність активаційного бар'єра відрізняє процес зародження від справжнього спінодального розпаду.

- Утворення фаз як у метастабільних, так і нестабільних початкових станах поблизу класичної спінодалі, може протікати через проходження хребта термодинамічного потенціалу, тобто через деякий активаційний бар'єр, незважаючи на те, що для нестабільних початкових станів значення роботи формування критичного кластера, що відповідає сідлової точці термодинамічного потенціалу, дорівнює нулю. Таким чином, показано, що концепція нуклеації – в модифікованій формі порівняно з класичною картиною – може також бути придатною для аналізу процесу утворення нової фази у нестабільному початковому стані, тобто, на відміну від класичного підходу Гіббса, узагальнений метод Гіббса дає опис формування нової фази як для бінодальної, так і для спінодальної ділянок фазової діаграми.

- Основним результатом, що має практичне значення, є те, що робота утворення кластера критичного розміру в узагальненому методі Гіббса менша, ніж у класичній теорії нуклеації у капілярному наближенні, і зменшується до нуля на спінодалі.

## РОЗДІЛ 2

### НУКЛЕАЦІЯ АБО СПІНОДАЛЬНИЙ РОЗПАД В ОБМЕЖЕНИХ БІНАРНИХ РОЗЧИНАХ

У другому розділі основні особливості спінодального розпаду, з одного боку, та нуклеації, з іншого, та перехід між обома механізмами аналізуються в рамках термодинамічної кластерної моделі на основі узагальненого методу Гіббса у моделі регулярного бінарного розчину. При цьому кластери нової фази можуть змінюватися з часом як за розмірами, так і за своїми інтенсивними параметрами стану, наприклад, густиною або складом. Аналізується також вплив зміни параметрів стану навколишнього середовища на еволюцію кластера. Наслідки такої зміни мають важливе значення як для аналізу фазоутворення в обмежених (нанорозмірних) системах, так і для розуміння еволюції ансамблів кластерів у великих (необмежених) системах.

THE JOURNAL OF CHEMICAL PHYSICS 127, 114504 2007

#### **Nucleation versus spinodal decomposition in confined binary solutions**

Alexander S. Abyzov

*Kharkov Institute of Physics and Technology, Academician Street 1, 61108 Kharkov, Ukraine*

Jörn W. P. Schmelzer

*Institut für Physik der Universität Rostock, Universitätsplatz, 18051 Rostock, Germany*

(Received 26 April 2007; accepted 31 July 2007; published online 19 September 2007)

Basic features of spinodal decomposition, on one side, and nucleation, on the other side, and the transition between both mechanisms are analyzed within the framework of a generalized thermodynamic cluster model based on the generalized Gibbs approach. Hereby the clusters, representing the density or composition variations in the system, may change with time both in size and

in their intensive state parameters (density and composition, for example). In the first part of the analysis, we consider phase separation processes in dependence on the initial state of the system for the case when changes of the state parameters of the ambient system due to the evolution of the clusters can be neglected as this is the case for cluster formation in an infinite system. As a next step, the effect of changes of the state parameters on cluster evolution is analyzed. Such depletion effects are of importance both for the analysis of phase formation in confined systems as well as for the understanding of the evolution of ensembles of clusters in large (in the limit infinite) systems. The results of the thermodynamic analysis are employed in both cases to exhibit the effect of thermodynamic constraints on the dynamics of phase separation processes. ©2004 American Institute of Physics. [DOI: 10.1063/1.2774989]

## 2.1. Introduction

Nucleation and spinodal decomposition are two major mechanisms how first-order phase transitions may proceed in a variety of systems [1–10]. Which one of the mentioned mechanisms dominates in the decomposition process is commonly assumed to depend on the degree of instability of the initial state of a phase-separating system. The phase transition is supposed to proceed via nucleation and growth for metastable systems [1, 2], while for thermodynamically unstable systems the mechanism of spinodal decomposition is expected to govern the process [3, 4, 9, 10].

Following the basic ideas anticipated in its basic premises already by Gibbs [11], in nucleation a nucleus of initially small size is supposed to be formed stochastically with state parameters widely similar to the properties of the newly evolving macroscopic phases. In contrast, spinodal decomposition is characterized by initially smooth changes of the state parameters of the system (composition, density, etc.) extended, in general, over large regions in space. These differences in the

basic models lead to essentially different theoretical approaches to the description of nucleation-growth and spinodal decomposition processes, respectively. In the simplest formulation, spinodal decomposition is treated as a process of spontaneous growth of a set of long-wavelength fluctuations of the density or composition of the initial state [9, 10]. In such description, the growth increment of these fluctuations is determined in dependence on the wave numbers of the respective modes as performed for the first time by Cahn and Hilliard [9, 10]. In the decay of initially metastable states via nucleation, the bulk properties of the clusters are supposed to be widely similar to the properties of the respective macroscopic phases [11] and the process of stochastic formation, the further growth and shrinkage of such clusters is analyzed. Briefly speaking, in the initial stages of spinodal decomposition the change of density and/or composition is determined for a more or less fixed size of the new phase regions, while nucleation-growth models draw the attention to a change of the size of the clusters at given values of their intensive state parameters.

Historically, the mentioned different approaches have been developed employing (or reinventing) two different thermodynamic methods of description of thermodynamically heterogeneous systems developed by Gibbs [11] (nucleation) and van der Waals [12, 13] (spinodal decomposition), respectively. The classical Gibbs' theory was and is employed till now as the most frequently used tool basically for the determination of the properties of critical clusters determining the rate of cluster formation in metastable systems and, employing more or less explicitly expressed additional assumptions, to cluster growth and shrinkage processes (cf. [14–16]). Gibbs' classical approach cannot give any predictions about phase formation processes evolving in unstable initial states. In contrast, the van der Waals & Cahn-Hilliard approach allows one to determine the properties of critical clusters for metastable systems and the modes of highest density amplification for phase separation in unstable initial states.

Both Gibbs' and van der Waals' methods of description of heterogeneous

systems are considered hereby conventionally as essentially correct and equivalent. However, as shown already long ago by Cahn and Hilliard [9], the predictions concerning the properties of critical clusters in metastable systems derived via the Gibbs' and van der Waals' methods are in deep contradiction to each other (for more details see [15, 16]). These contradictions are especially significant in the vicinity of the classical spinodal curve separating metastable from unstable initial states. In addition, mentioned above comparison of similarities and differences of nucleation and spinodal decomposition processes is somewhat oversimplified. Modern theories both of spinodal decomposition and nucleation exhibit more complicated features in comparison to the models as described briefly above (see, for example, [3–5, 16–20]). Moreover, in contrast to the classical picture a smooth transition from metastability to instability has been observed both in computer models of phase separating systems [3, 5, 18, 20] and in experiment [21].

In preceding papers [15, 16], it was shown that the contradictions between Gibbs' and van der Waals' methods of description of thermodynamically heterogeneous systems in application to phase formation processes can be resolved by generalizing Gibbs' approach. In this generalization (for the details see [22, 23]), Gibbs' idealized cluster model is employed again for the theoretical treatment of density or composition fluctuations, however, the basic equations are generalized allowing one to consider, in contrast to Gibbs' classical approach, the interfacial tension, in general, as a function of the state parameters of both ambient and cluster phases. It was shown that this generalization of Gibbs' approach leads, in addition to a variety of other consequences, to the reconciliation of both mentioned thermodynamic methods of description of heterogeneous systems. Moreover, the generalized Gibbs' method is shown to allow one to arrive also at an understanding of basic features of the kinetics of spinodal decomposition [16].

In the present paper we extend the analyses performed in [15, 16]. Basic features of spinodal decomposition, on one side, and nucleation, on the other side,

and the transition between both mechanisms are analyzed within the framework of described above generalized thermodynamic cluster model based on the generalized Gibbs approach [22,23]. Hereby the clusters, representing the density or composition variations in the system, may change with time both in size and in their intensive state parameters (density and composition, for example). In the first part of the analysis, we consider phase separation processes in dependence on the initial state of the system for the case when changes of the state parameters of the ambient system due to the evolution of the clusters can be neglected as this is the case for cluster formation in an infinite system. As a next step, the effect of changes of the state parameters on cluster evolution is analyzed. Such depletion effects are of importance both for the analysis of phase formation in confined systems [3,25–31] as well as for the understanding of the evolution of ensembles of clusters in large (in the limit infinite) systems [25,32–35]. The results of the thermodynamic analysis are employed in both cases to exhibit the effect of thermodynamic constraints on the dynamics of phase separation processes. As a model system for the analysis, we consider phase separation in a binary regular solution, again (see also [15,16,36]).

The paper is organized as follows. In Section 9.2, basic equations employed for the thermodynamic analysis of phase separation in solutions are summarized. In Section 9.4, these results are applied to the analysis of phase formation in infinite domains in the sense as specified above. In Section 8.4, finite size effects in the kinetics are studied both in application to phase separation in systems of finite size and with respect to the understanding of the evolution in macroscopic systems described in terms of formation and competitive growth of ensembles of clusters [25,37]. A discussion of the results and possible further developments in Section 8.5 completes the paper.

## 2.2. The model system

We consider thermodynamic aspects of new phase formation in a binary solid or liquid solution in domains both of finite and infinite sizes. Since here we are mainly interested in the discussion of the basic principles and consequences of the newly developed generalized Gibbs' approach in application to phase separation, the solution is considered as a regular one representing one of the simplest models of a system consisting of two kinds of interacting molecules. The domain, where the processes of nucleation and/or spinodal decomposition are assumed to proceed, is considered similarly to [29] as a sphere of radius  $R_0$ . The limiting situation of an infinite system is thus reached for  $R_0 \rightarrow \infty$ , while finite-size effects take place for finite values of  $R_0$  (see Fig. 2.1).

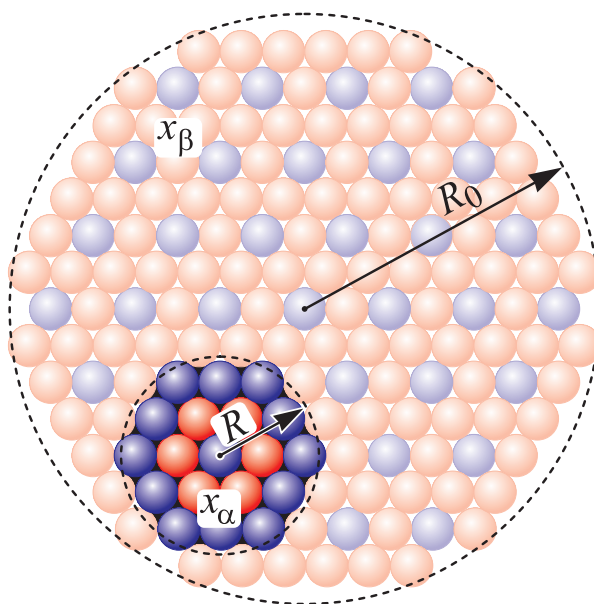


Fig. 2.1. Model employed in the analysis: A cluster of size,  $R$ , and molar fraction,  $x_\alpha$ , is formed in a volume,  $V = 4\pi R_0^3/3$ , of an initially homogeneous binary solid or liquid solution with a composition given by the molar fraction,  $x_\beta$ . The initial composition of the ambient solution we denote by  $x$ .

Cluster formation in a binary solution results from a redistribution of molecules. Following Gibbs' model approach, we consider a cluster as a spatially homogeneous part of the domain volume with a composition different from the ambient phase. Both

size and composition of the cluster may vary in a wide range. As the dividing surface, separating the cluster from the ambient phase in the thermodynamic description underlying the method of analysis, we always employ here the surface of tension [11, 22, 23]. As in our previous analyses [26, 27] performed in terms of the classical Gibbs' approach and more recent investigations of related problems by several authors employing different methods [29–31], the effect of the finite size is taken into account only by the conservation laws for the numbers of particles of the different components in the cluster (specified by the subscript  $\alpha$ ) and in the ambient phase (specified by  $\beta$ ). We may write then

$$\begin{aligned} n_j &= n_{j\alpha} + n_{j\beta} = \text{const.} , & j &= 1, 2 , \\ n &= n_\alpha + n_\beta = \text{const.} , & & \\ n_\alpha &= n_{1\alpha} + n_{2\alpha} , & n_\beta &= n_{1\beta} + n_{2\beta} . \end{aligned} \quad (2.1)$$

The molar fractions of the second component in the ambient phase ( $x_\beta$ ) and the cluster ( $x_\alpha$ ) are defined as

$$x_\beta = \frac{n_{2\beta}}{n_{1\beta} + n_{2\beta}} , \quad x_\alpha = \frac{n_{2\alpha}}{n_{1\alpha} + n_{2\alpha}} . \quad (2.2)$$

The initial state is either a metastable or unstable homogeneous state, characterized by  $x_\alpha(0) = x_\beta(0) \equiv x$ .

In line with the basic assumptions underlying the model of regular solutions [36] and for simplicity of the notations, the volume per particle,  $\omega$ , is assumed to be the same for both components and independent on composition ( $\omega_\alpha = \omega_\beta \equiv \omega$ ). Cluster size and particle number in a cluster are related then by the following simple expression

$$\frac{4\pi}{3}R^3 = n_\alpha\omega . \quad (2.3)$$

Assuming further that a cluster of radius,  $R$ , and composition,  $x_\alpha$ , is formed in a spherical domain of radius,  $R_0$ , and initial composition  $x$ , Eqs. (2.1), (2.2) and (2.3)

yield

$$x_\beta = \frac{nx - n_\alpha x_\alpha}{n - n_\alpha} = \frac{x - x_\alpha (R/R_0)^3}{1 - (R/R_0)^3}. \quad (2.4)$$

The change of the Gibbs free energy,  $\Delta G$ , connected with the formation of one cluster in the initially homogeneous ambient phase can be written in a commonly good approximation as [14–16]

$$\Delta G = \sigma A + \sum_j n_{j\alpha} (\mu_{j\alpha} - \mu_{j\beta}) + \sum_j n_j (\mu_{j\beta} - \mu_{j0}). \quad (2.5)$$

The first term in the right hand side of Eq. (2.5) reflects cluster surface effects ( $\sigma$  is the interfacial tension, and  $A$  is the surface area of the cluster) and the second term cluster bulk contributions to the change of the Gibbs' free energy. The third term describes the influence of depletion effects (change of the composition of the ambient phase due to cluster formation) resulting in differences of the chemical potentials per particle in the initial state ( $\mu_{j0}$ ) and the state of the ambient phase once a cluster has been formed ( $\mu_{j\beta}$ ).

For the binary regular solution the chemical potentials of the different components in the cluster,  $\mu_{j\alpha}$ , and ambient solution,  $\mu_{j\beta}$ , are defined by [36]

$$\begin{aligned} \mu_{1\alpha/\beta} &= \mu_{1\alpha/\beta}^* + k_B T \ln(1 - x_{\alpha/\beta}) + \Omega x_{\alpha/\beta}^2, \\ \mu_{2\alpha/\beta} &= \mu_{2\alpha/\beta}^* + k_B T \ln x_{\alpha/\beta} + \Omega (1 - x_{\alpha/\beta})^2, \end{aligned} \quad (2.6)$$

where  $k_B$  is the Boltzmann constant,  $T$  the absolute temperature, and  $\Omega$  is an interaction parameter describing specific properties of the considered system. The parameter,  $\Omega$ , can be expressed via the critical temperature,  $T_c$ , of the system (cf. also Fig. 2.2) as

$$T_c = \frac{\Omega}{2k_B}. \quad (2.7)$$

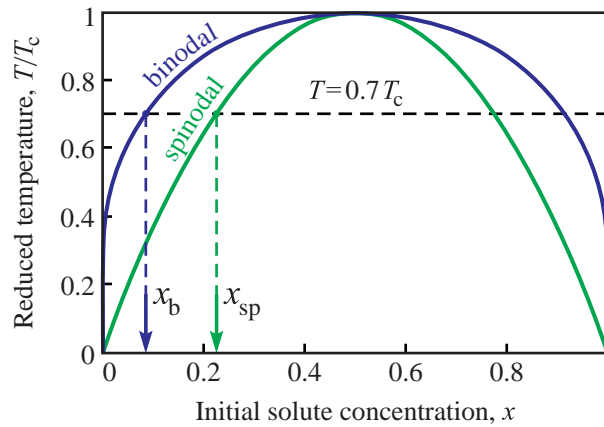


Fig. 2.2. Phase diagram of a binary regular solution with binodal and spinodal curves. The spinodal curve separates thermodynamically stable from thermodynamically unstable states of the homogeneous ambient phase. In the present analysis, we assume that the temperature is equal to  $T = 0.7T_c$  and vary the driving force of the phase transformation process by changing the initial composition of the ambient phase,  $x$ .

The surface tension between two macroscopic phases with compositions  $x_\alpha$  and  $x_\beta$ , respectively, is given, according to Becker ([36], see also [38]) by

$$\sigma = \tilde{\sigma} (x_\alpha - x_\beta)^2 . \tag{2.8}$$

From Eqs. (2.5), (2.6), (2.7) and (2.8), we have

$$\frac{\Delta G}{k_B T} = \frac{3}{2} n_\sigma^{1/3} n_\alpha^{2/3} (x_\alpha - x_\beta)^2 + n_\alpha f(x_\beta, x_\alpha) - n f(x_\beta, x) , \tag{2.9}$$

where

$$f(x_\beta, x_\alpha) = (1 - x_\alpha) \left\{ \ln \frac{1 - x_\alpha}{1 - x_\beta} + 2 \frac{T_c}{T} (x_\alpha^2 - x_\beta^2) \right\} + x_\alpha \left\{ \ln \frac{x_\alpha}{x_\beta} + 2 \frac{T_c}{T} [(1 - x_\alpha)^2 - (1 - x_\beta)^2] \right\} \tag{2.10}$$

holds and the scaling parameter,  $n_\sigma$ , for the particle number in the cluster is specified

as

$$n_{\sigma}^{1/3} = \frac{2\tilde{\sigma}}{k_B T} \left( \frac{4\pi}{3} \right)^{1/3} \omega^{2/3}. \quad (2.11)$$

In addition, we introduce via Eqs. (2.3) and (2.11) also a scaling parameter,  $R_{\sigma}$ , for the cluster radius as

$$R_{\sigma} = \left( \frac{3n_{\sigma}\omega}{4\pi} \right)^{1/3} = \frac{2\tilde{\sigma}\omega}{k_B T}. \quad (2.12)$$

In the further analysis, we will always assume for an illustration of the results that the temperature in the system is equal to  $T = 0.7T_c$ . The concentration of the solute in the initially homogeneous system is varied in the range from  $x = x_b \cong 0.086$  (left branch of the binodal curve) to  $x = x_{sp} \cong 0.226$  (left branch of the spinodal curve) covering metastable initial states and  $x_{sp} < x \leq 0.5$  covering unstable initial states (see Fig. 2.2). Since the phase diagram of a regular solution is symmetric [16], we may restrict the analysis to initial states in the considered range with initial concentrations,  $x \leq 0.5$ . A specification of further parameters like  $\tilde{\sigma}$  and  $\omega$  is not required, since we compute reduced characteristics, so that such system parameters enter the description only via the scaling quantities (see also [16]).

## 2.3. Phase separation in infinite domains

### 2.3.1. Thermodynamic analysis

Above given equations allow us to determine the thermodynamic potential surface as a function of the number of particles,  $n_{1\alpha}$  and  $n_{2\alpha}$ , in the cluster. The results are shown for different values of the initial supersaturation in Fig. 2.3 both for metastable ((a):  $x = 0.15$ , (b):  $x = 0.19$ , (c):  $x = 0.22$ ) and unstable ((d):  $x = 0.3$ ,

(e):  $x = 0.4$ , (f):  $x = 0.5$ ) initial states. Depletion effects are neglected so far (we consider infinite systems), so we set  $R_0 \rightarrow \infty$ . As far as we are interested mainly in the demonstration of the basic qualitative features, like in Fig. 2.3 and similar ones, the numbers are omitted at the axes.

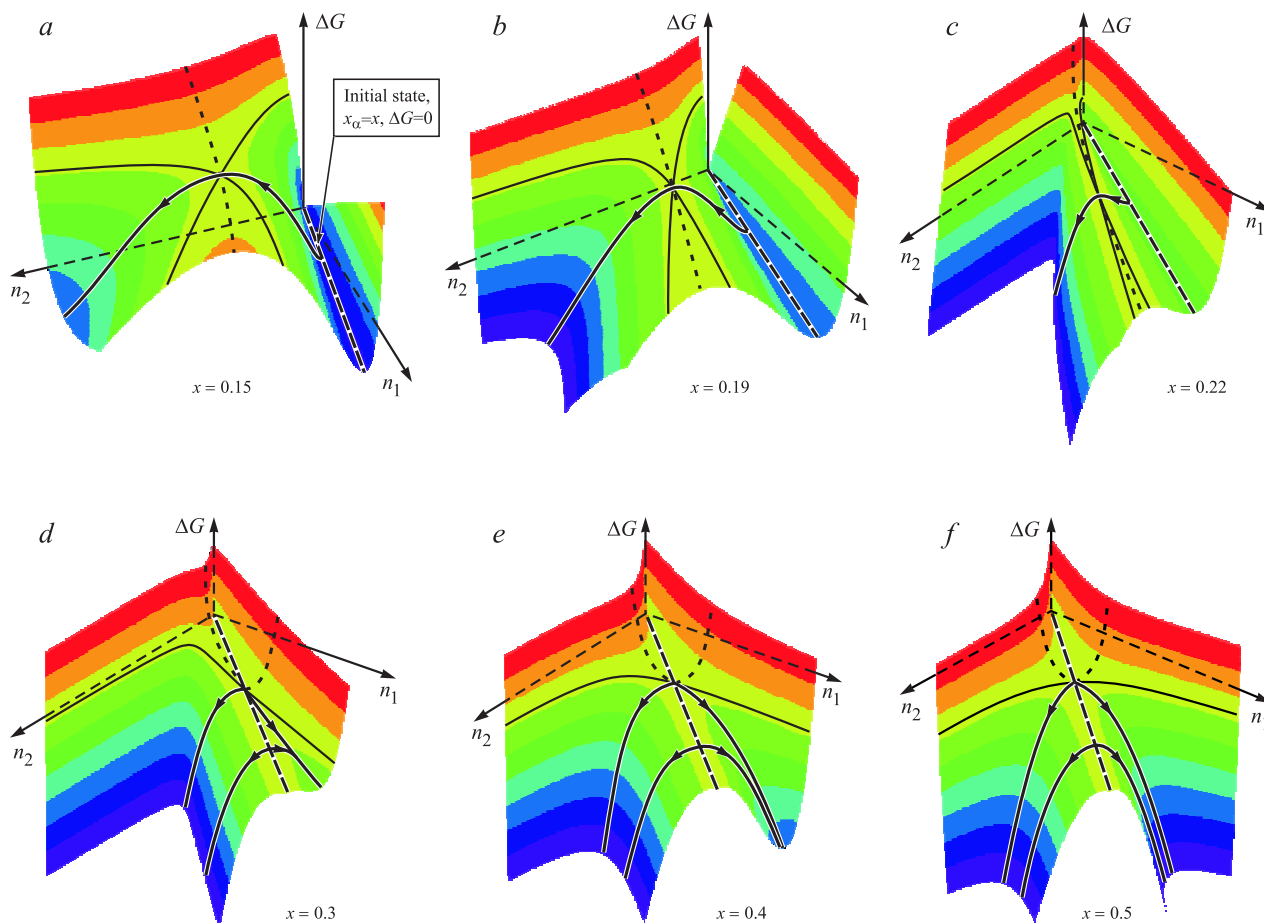


Fig. 2.3. Shape of the Gibbs free energy surface for metastable ( $x = 0.15$ ,  $x = 0.19$ , and  $x = 0.22$ ; Figs. 2.3a-c) and unstable initial states ( $x = 0.3$ ,  $x = 0.4$ , and  $x = 0.5$ ; Figs. 2.3d-f). As mentioned, the temperature is chosen equal to  $T/T_c = 0.7$  (for further details, see text).

For each of the metastable initial states, the thermodynamic potential surface has, in the vicinity of the critical cluster coordinates, a typical saddle-shape. The position of this saddle-point is determined by the set of equations

$$\frac{\partial \Delta G(n_{1\alpha}, n_{2\alpha})}{\partial n_{1\alpha}} = 0, \quad \frac{\partial \Delta G(n_{1\alpha}, n_{2\alpha})}{\partial n_{2\alpha}} = 0, \quad (2.13)$$

if we employ Eq. (2.5) for the description of the thermodynamic potential surface. In an alternative approach utilizing Eq. (2.9), we may determine first the size of the cluster for any fixed value of  $x_\alpha$  via

$$\frac{\partial \Delta G(n_\alpha, x_\alpha)}{\partial n_\alpha} = 0 \quad \Longrightarrow \quad n_\alpha^{1/3}(x_\alpha) = -n_\sigma^{1/3} \frac{(x_\alpha - x)^2}{f(x, x_\alpha)}. \quad (2.14)$$

A substitution of the expression for  $n_\alpha$  into Eq. (2.9) yields (cf. also Eq. (2.11))

$$\frac{\Delta G(n_\alpha(x_\alpha), x_\alpha)}{k_B T} = \frac{1}{2} n_\sigma \frac{(x_\alpha - x)^6}{f^2(x, x_\alpha)}, \quad n_\sigma = \frac{32\pi}{3} \frac{\tilde{\sigma}^3 \omega^2}{(k_B T)^3}. \quad (2.15)$$

The composition of the critical cluster and the work of critical cluster formation is obtained then by searching for the minimum of  $\Delta G(n_\alpha(x_\alpha), x_\alpha)$  with respect to the cluster composition,  $x_\alpha$ , [14–16, 23] as

$$\frac{d\Delta G(n_\alpha(x_\alpha), x_\alpha)}{dx_\alpha} = 0. \quad (2.16)$$

In order to allow us a better understanding of the shape of the thermodynamic potential surface, contour lines through the saddle are included in the figures by full curves and the curve of steepest increase of the potential surface starting from the critical cluster coordinates by dotted curves. The full curve with arrows describes the most probable trajectory of cluster evolution. It starts at some point along the dashed curve determined by the initial conditions  $x_\alpha = x$  and  $\Delta G = 0$  (in the initial state, the composition of the cluster is the same as in the ambient phase). Then it passes the saddle point and follows further the trajectory of macroscopic growth with an initial cluster size slightly above the critical size. As discussed in detail in [16], the trajectory of evolution from the initial state to the saddle point can be assumed to coincide, in general, with the path of cluster dissolution starting with initial states slightly below the critical cluster size.

The most probable trajectory of evolution is determined thus for both regions

by the macroscopic growth equations. For segregation in solutions, these equations can be written in the form

$$\begin{aligned}\frac{dn_{1\alpha}}{dt} &= -D_1(1 - x_\beta)\Theta(n_{1\alpha}, n_{2\alpha})\frac{d\Delta G}{dn_{1\alpha}}, \\ \frac{dn_{2\alpha}}{dt} &= -D_2x_\beta\Theta(n_{1\alpha}, n_{2\alpha})\frac{d\Delta G}{dn_{2\alpha}},\end{aligned}\tag{2.17}$$

where  $D_1$  and  $D_2$  are the partial diffusion coefficients of the different components in the ambient phase, and the notation

$$\Theta(n_{1\alpha}, n_{2\alpha}) = \Theta_0 n_\alpha^\kappa\tag{2.18}$$

is utilized. The parameter  $\kappa$  has the value  $\kappa = 2/3$  for kinetic-limited growth, and  $\kappa = 1/3$  for diffusion-limited growth and  $\Theta_0$  is a parameter depending only on temperature (we set, as mentioned, the temperature equal to  $T = 0.7T_c$ ). As evident from above considerations and the structure of Eqs. (2.17), the path of cluster evolution depends on the partial diffusion coefficients of both components of the solution (see for the details [16]), however, qualitatively the picture remains always the same. On Fig. 2.3, the trajectories are shown for  $D_1(1 - x_\beta) = D_2x_\beta$ . In this case, the kinetic prefactors to the partial derivatives of  $\Delta G$  with respect to  $n_{j\alpha}$  in Eqs. (2.17) are the same and the evolution proceeds along the valley of the thermodynamic potential surface,  $\Delta G(n_{1\alpha}, n_{2\alpha})$ , passing the saddle point.

The analysis of Eqs. (2.14) and (2.16) shows [14–16] that the composition of the critical cluster decreases with increasing supersaturation and approaches the value of the composition of the ambient phase for initial states near to the spinodal curve (cf. Fig. 2.4). The work of critical cluster formation decreases monotonously with increasing supersaturation and tends to zero at the spinodal curve (Fig. 2.5). Taking

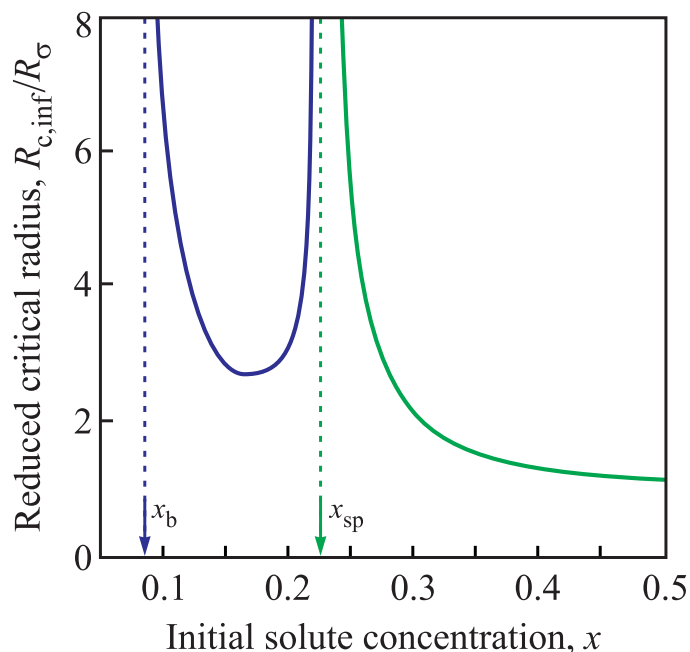


Fig. 2.4. Dependence of the composition of the critical cluster,  $x_{\alpha,c}$ , on the initial solute concentration. For  $x > x_{sp}$ , always the identity  $x_{\alpha,c} = x$  holds [16].

into account Eq. (2.10) and the relations

$$\begin{aligned} \frac{\partial f(x, x_{\alpha})}{\partial x_{\alpha}} &= \ln\left(\frac{x_{\alpha}}{x}\right) - \ln\left(\frac{1-x_{\alpha}}{1-x}\right) + 4\left(\frac{T_c}{T}\right)(x-x_{\alpha}), \\ \frac{\partial^2 f(x, x_{\alpha})}{\partial x_{\alpha}^2} &= \frac{1}{x_{\alpha}} + \frac{1}{1-x_{\alpha}} - 4\left(\frac{T_c}{T}\right), \\ \frac{\partial^3 f(x, x_{\alpha})}{\partial x_{\alpha}^3} &= -\frac{1-2x_{\alpha}}{x_{\alpha}^2(1-x_{\alpha})^2}, \end{aligned} \quad (2.19)$$

it can be shown that the critical cluster radius,  $R_c$ , behaves as

$$\lim_{x \rightarrow x_{sp}} R_c \propto \lim_{x \rightarrow x_{\alpha}} \frac{1}{(x_{\alpha} - x)}. \quad (2.20)$$

In this derivation, the equation  $(\partial^2 f(x, x_{\alpha})/\partial x_{\alpha}^2)|_{x_{\alpha}=x_{sp}} = 0$  has been employed [15]. The dependence of the critical cluster size on supersaturation is illustrated in Fig. 2.6.

The results summarized above are reflected also in Figs. 2.3a-c. As evident from the figures, with an increase of the supersaturation (molar fraction in the ambient

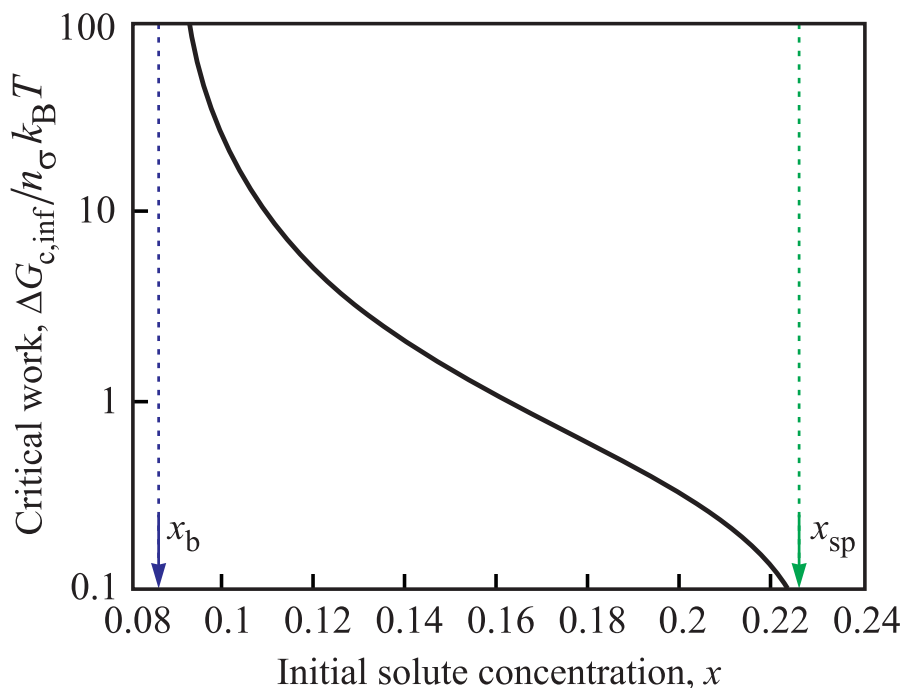


Fig. 2.5. Dependence of the minimum work of critical cluster formation,  $\Delta G_{c,\text{inf}}/(n_\sigma k_B T)$ , on the initial solute concentration,  $x$ , for infinite domains (specified by the abbreviation, inf) when changes of the state of the ambient solution due to cluster formation can be neglected.

phase) the nucleation barrier decreases, the location of the saddle point is shifted closer to the line of initial states,  $x_\alpha = x$ , and at the spinodal,  $x = x_{sp}$ , the position of the critical cluster tends to the composition of the ambient phase, i.e., the critical cluster is located in this limiting case on the line of initial states. Since, for the initial states corresponding to the spinodal curve, the condition  $x_\alpha \rightarrow x$  holds, for such states the work of critical cluster formation (determined via the generalized Gibbs' approach employed here) tends to zero.

For unstable initial states,  $x_{sp} < x \leq 0.5$ , the situation is different. Here the critical cluster has always a composition equal to the composition of the ambient phase (cf. Fig. 2.4 and [16]). The critical cluster size cannot be expressed here directly employing Eqs. (2.14) and (2.19), since for  $x_\alpha = x$  the relations

$$\left. \frac{\Delta G}{k_B T} \right|_{x_\alpha=x} = \left. \frac{\partial}{\partial x_\alpha} \left( \frac{\Delta G}{k_B T} \right) \right|_{x_\alpha=x} = \left. \frac{\partial}{\partial n_\alpha} \left( \frac{\Delta G}{k_B T} \right) \right|_{x_\alpha=x} = 0 \quad (2.21)$$

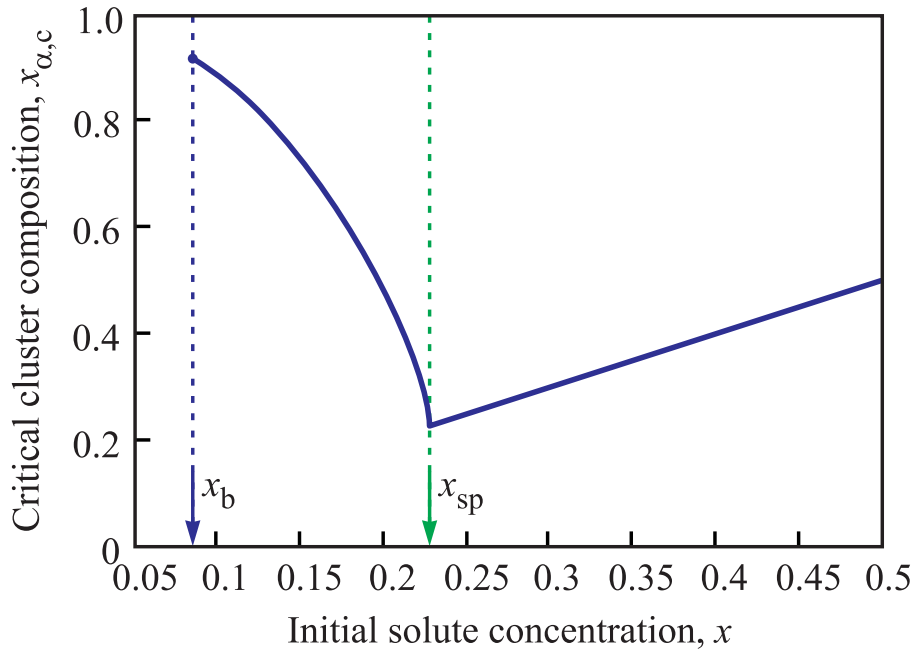


Fig. 2.6. Dependence of the critical cluster radius,  $R_{c,inf}/R_\sigma$ , on the initial solute concentration,  $x$ , for phase formation in an infinite domain at metastable ( $x_b < x < x_{sp}$ ) and unstable ( $x > x_{sp}$ ) initial states of the ambient solution.

hold independently of the value of  $n_\alpha$  in Eq. (2.9). In the definition of the critical cluster size for unstable initial states we have to rely thus on the second-order differential of  $\Delta G$  with respect to  $n_\alpha$  and  $x_\alpha$ . As can be proven easily, the second-order differential of  $\Delta G$  for states with  $x_\alpha = x$  is given by  $d^2\Delta G|_{x_\alpha=x} = (\partial^2\Delta G/\partial x_\alpha^2)|_{x_\alpha=x} dx_\alpha^2$ . The second-order derivative of  $\Delta G$  with respect to  $x_\alpha$  at  $x_\alpha = x$  can be expressed as

$$\frac{\partial^2}{\partial x_\alpha^2} \left( \frac{\Delta G}{k_B T} \right) \Big|_{x_\alpha=x} = 3n_\sigma^{1/3} n_\alpha^{2/3} \left\{ 1 - \left( \frac{n_\alpha}{n_{\alpha,c}} \right)^{1/3} \right\}, \quad (2.22)$$

where the notations

$$n_{\alpha,c}^{1/3} = \frac{3n_\sigma^{1/3}}{2K}, \quad K = -\frac{1}{2} \frac{\partial^2 f(x, x_\alpha)}{\partial x_\alpha^2} \Big|_{x_\alpha=x} = \frac{1}{2} \left[ 4 \left( \frac{T_c}{T} \right) - \frac{1}{x} - \frac{1}{1-x} \right] \quad (2.23)$$

are employed.

In the range of metastable initial states  $x_b < x < x_{sp}$ , the critical cluster

corresponds to a minimum of  $\Delta G(n_\alpha(x_\alpha), x_\alpha)$  with respect to the variations of the state of the cluster, i.e.,  $(d^2\Delta G/dx_\alpha^2) > 0$  holds [23]. For unstable initial states, states along the trajectory  $x_\alpha = x$  with  $\Delta G = 0$  correspond again to minima with respect to variations of the state parameters of the cluster phase at fixed values of the cluster sizes if the inequality  $(n_\alpha/n_{\alpha,c})^{1/3} < 1$  is fulfilled (cf. Eq. (2.22)). However, there exists a cluster size,  $n_{\alpha,c}$ , where the state along the line  $x = x_\alpha$  switches from a minimum to a maximum of  $\Delta G$  with respect to variations of the cluster composition at fixed values of the cluster sizes. Possible trajectories of evolution for  $n_\alpha \geq n_{\alpha,c}$  are shown by full curves with arrows in Figs. 2.3d-f.

Moreover, on Figs. 2.3 d-f, the solid curve,  $\Delta G = 0$ , divides regions with  $\Delta G \geq 0$  and  $\Delta G \leq 0$  as compared with the states corresponding to  $x_\alpha = x$ . In the first region (that is in the region with  $\partial^2\Delta G/\partial x_\alpha^2|_{x_\alpha=x} > 0$  or  $(n_\alpha/n_{\alpha,c}) < 1$ ) cluster composition changes lead to the growth of the Gibbs free energy, and the cluster is stable in such region. In the second region ( $\partial^2\Delta G/\partial x_\alpha^2|_{x_\alpha=x} < 0$  or  $(n_\alpha/n_{\alpha,c}) > 1$ ) any composition change (both increase and decrease of the concentration of the cluster concentration) results in a decrease of the Gibbs free energy. In such region, the cluster is unstable and the decomposition proceeds via growth of the concentration differences, i.e., according to the basic mechanism commonly assigned to spinodal decomposition. Thus, for  $x > x_{sp}$ , the system is stable for small clusters and unstable for clusters with a size  $n_\alpha > n_{\alpha,c}$ . So, changing the size of the clusters with compositions equal to the composition of the ambient phase, we arrive at a transition from metastable to unstable states and at  $n_\alpha = n_{\alpha,c}$  the minimum transforms into a maximum via a singular point of third order. Reminding the physical meaning of a critical cluster size as the lowest size of a cluster for which a spontaneous further growth in accordance with the thermodynamic evolution laws is possible,  $n_{\alpha,c}$  as defined via Eq. (2.23) is obviously an appropriate definition of the critical cluster size for unstable initial states.

In terms of the radius, we may express the critical cluster size in infinite domain as

$$R_{c,\text{inf}} = \frac{3R_\sigma}{2K}. \quad (2.24)$$

The parameter  $K$  is positive for values of  $x$  in the range of unstable initial states and tends to zero at the spinodal curve (cf. [15, 16]) resulting in a divergence of the critical cluster size for unstable initial states near the spinodal curve (cf. Fig. 2.6). The work of formation of such critical cluster is, in the range of unstable initial states of the ambient phase, always equal to zero (cf. Eq. (2.9)).

### 2.3.2. Kinetics versus thermodynamics in phase separation

In discussing the trajectories of evolution in phase separation processes, we assumed here in line with the commonly employed assumption that the evolution to the new phase proceeds via the saddle point of the thermodynamic potential surface. Ridge crossing as another possible channel of formation of the new phase [39–41] we believe to be of importance only in the vicinity of the spinodal curve [16] since otherwise the increase of the potential barrier required for ridge crossing as compared with the evolution via the saddle point overcompensates as a rule the advantages connected with the eventually easier realization of the kinetics of the process. Of course, the trajectories of evolution via the saddle point will depend on the kinetics and, for the model system considered, on the ratio of the partial diffusion coefficients of both components. The different paths of evolution of the critical clusters and their further growth in dependence on the ratio of the diffusion coefficients of both components are illustrated in Fig. 2.7.

For this purpose, we choose a volume of radius  $R$  in the center of some spherical domain (see Fig. 2.7, left side). This selected volume has initially the same

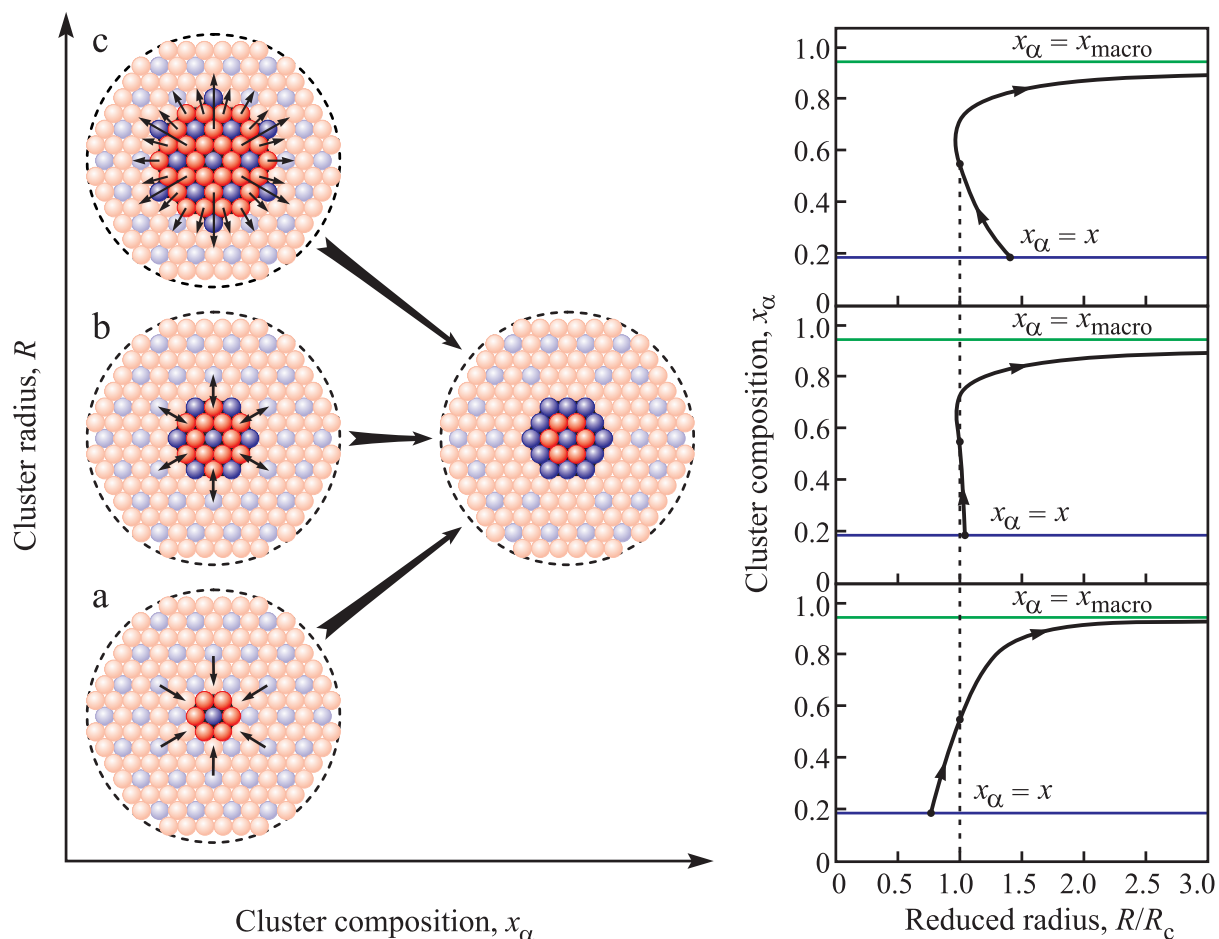


Fig. 2.7. Schematic illustration of trajectories of evolution in dependence on the ratio of the partial diffusion coefficients of the different components in the solution. At the right-hand side, the change of the composition of the clusters in dependence on reduced cluster sizes,  $R/R_c$ , is shown for the three different cases considered: a)  $D_2 \gg D_1$ , b)  $D_2 \cong D_1$ , c)  $D_2 \ll D_1$ .

composition as the ambient phase, therefore it is not a cluster yet. If atoms of the second component are incorporated into this volume, the concentration,  $x_\alpha$ , of this component in the cluster increases, its size increases, and it becomes a (super)critical nucleus of a new phase. Such scenario is realized (cf. [16]) when the mobility of the atoms of the second component is higher than for the atoms of the first sort (Fig. 2.7a). The dependence of concentration of the cluster on its radius is given on the right hand side.

In the opposite case, when the mobility of atoms of the first kind is higher, the formation of the critical cluster proceeds in such a way that atoms of the first kind

leave the region where the cluster will be formed. In such case, the concentration,  $x_\alpha$ , of the cluster increases but its size decreases (Fig. 2.7c). Again, the dependence of cluster composition on cluster size is shown on the right hand side. Once the critical cluster is formed in such process, its further growth is then determined by the motion of the second less mobile component, again. So, here we have the situation that growth processes will proceed with much smaller effective diffusion coefficients as the nucleation process. And, finally, in the case when atoms of the first kind in the cluster are replaced by atoms of the second one, i.e., when the mobilities of both components are nearly equal (or more precisely, if the relation  $D_1(1 - x) \cong D_2x$  holds, cf. Eq. (2.17)), the change of the composition of the cluster proceeds at nearly constant size (Fig. 2.7b). In all these cases, the critical cluster is the same (determined thermodynamically) but the trajectories of evolution differ (see also [16]) due to different ratios of the partial diffusion coefficients of the different components involved in the process of formation of the new phase.

## 2.4. Phase separation in finite domains

### 2.4.1. Thermodynamic analysis

It was shown in the preceding analysis that, neglecting depletion effects, the critical cluster size diverges in the vicinity of the spinodal curve (Fig. 2.6). Taking into account that phase separation processes in real systems proceed always in systems of finite size, the model of an infinite domain is not appropriate in a variety of cases already by this reason. In the further analysis, the effects of finite domain size on the phase separation processes are studied.

Similarly to Figs. 2.3, Figs. 2.8-2.11 give an impression about the shape of the Gibbs free energy surface  $\Delta G(n_{1\alpha}, n_{2\alpha})$  in dependence on the domain size,  $R_0$ , for different values of the initial solute concentration (Fig. 2.8:  $x = 0.15 < x_{sp}$ , Fig. 2.9:

$x = x_{sp} \approx 0.226$ , Fig. 2.10:  $x = 0.3 > x_{sp}$  and Fig. 2.11:  $x = 0.4 > x_{sp}$ ). As

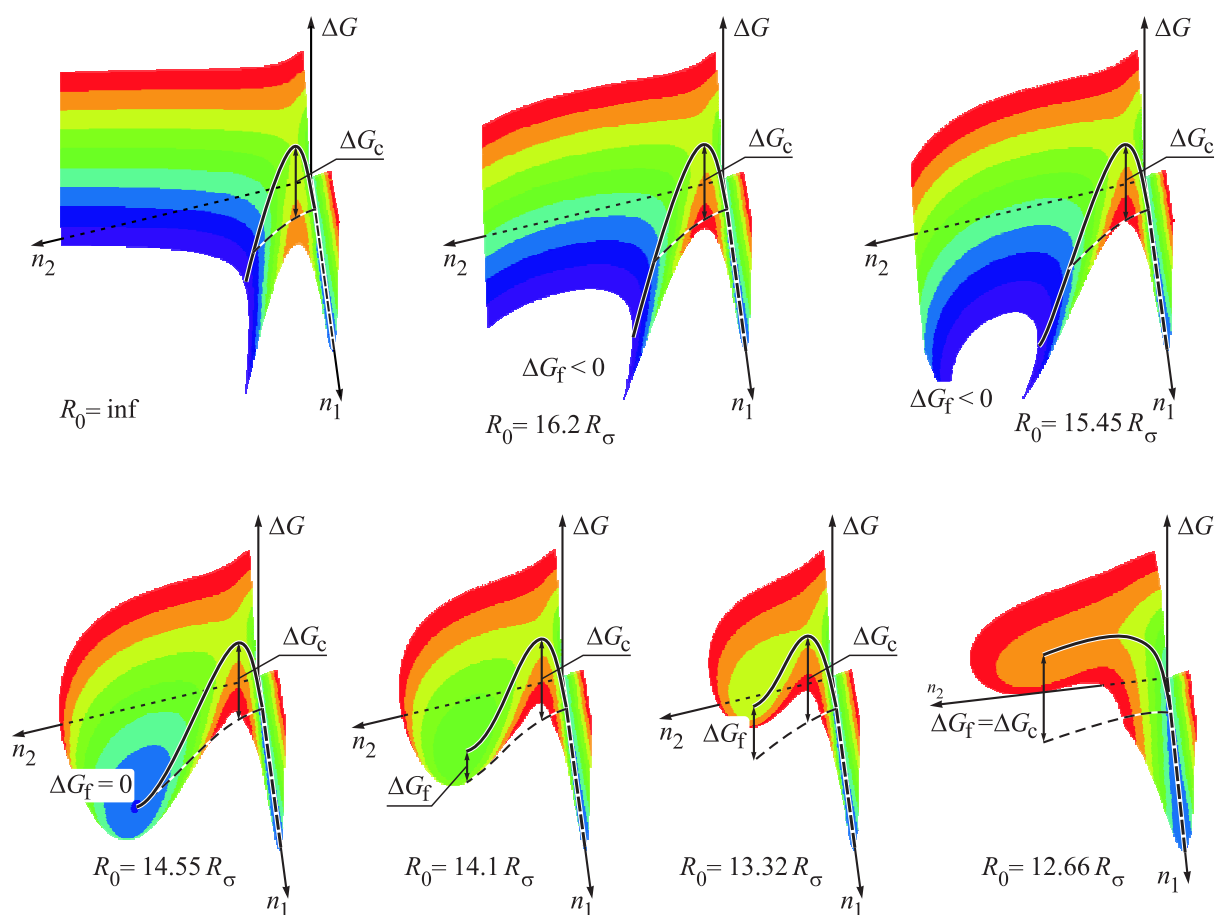


Fig. 2.8. Shape of the Gibbs free energy surface for  $x = 0.15$  and for different values of the domain size,  $R_0$ .

evident, at a given value of the supersaturation, the degree of instability of the system decreases with the decrease of the domain size. For example, for the case of an initial molar fraction equal to  $x = 0.15$  (Fig. 2.8), the critical cluster sizes,  $R_c$ , and the nucleation barrier,  $\Delta G_c$ , increase with the reduction of the size of the domain,  $R_0$ . The free energy difference,  $\Delta G_f$ , corresponding to a stable coexistence of a single cluster with radius,  $R_f$ , in the ambient phase noticeably grows, the size of this stable cluster,  $R_f$ , decreases considerably. The free energy difference,  $\Delta G_f$ , reaches a value equal to zero at  $R_0/R_\sigma = 14.55$ . At such system size, initial (homogeneous) and final (heterogeneous) states become equivalent from a thermodynamic point of view. With the further reduction of  $R_0$ ,  $\Delta G_f$  becomes positive, and for  $R_0/R_\sigma = 12.66$  the relation  $\Delta G_f = \Delta G_c$  holds and the transition to a two-phase system becomes

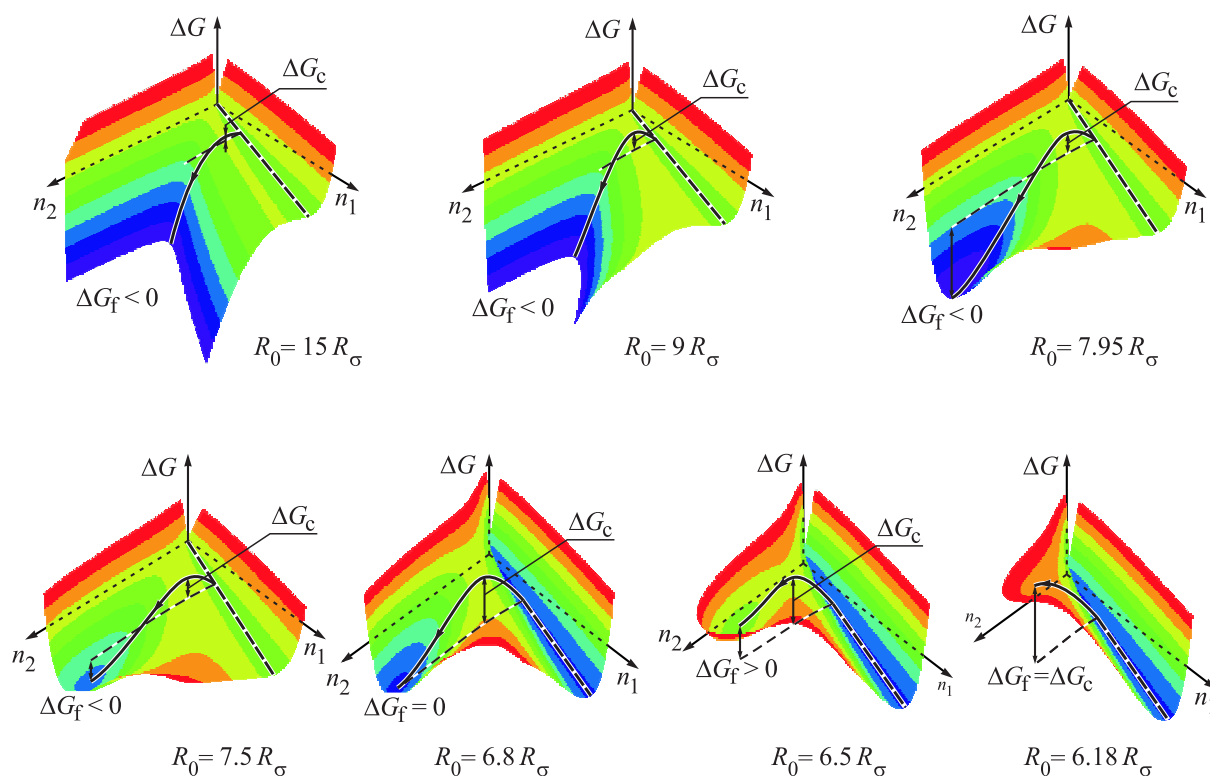


Fig. 2.9. Shape of the Gibbs free energy surface for  $x = x_{sp}$  and for different values of the domain size,  $R_0$ .

impossible due to finite-size effects.

For the considered supersaturation, in the range  $R_0/R_\sigma > 14.55$ , the initial state of the finite system is metastable. The final two-phase state is characterized by smaller values of the Gibbs free energy,  $\Delta G_f < 0$ , as compared with the homogeneous initial state. As a consequence, once a stable state of the cluster in the ambient phase has been formed, the reverse transition is, as a rule, highly improbable. For  $R_0/R_\sigma = 14.55$ , the initial state of the system is also a metastable state, however, now homogeneous and heterogeneous states are characterized by the same values of the Gibbs free energy, i.e.  $\Delta G_f = 0$ . By this reason, the heterogeneous state can be transferred by appropriate processes back to the homogeneous initial state. Thus the inequality

$$\Delta G_f \leq 0 \tag{2.25}$$

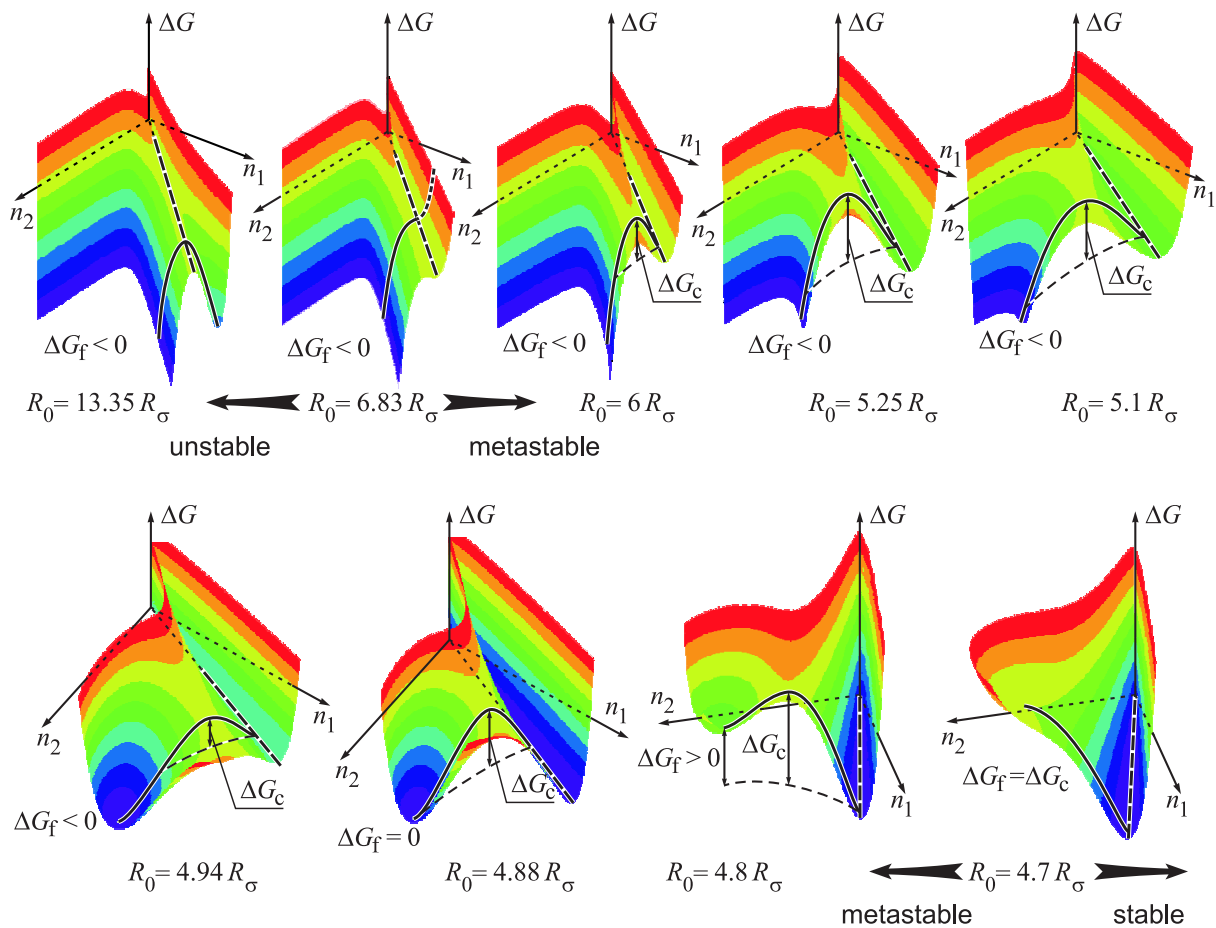


Fig. 2.10. Shape of the Gibbs free energy surface for  $x = 0.3$  and for different values of the domain size,  $R_0$ .

can be considered as the condition of metastability for the homogeneous initial state. Similar processes occur with even higher probability in the range  $12.66 < R_0/R_\sigma < 14.55$ . Here the initial state of the system is metastable, again, but the final state has larger values of Gibbs' free energy as compared with the homogeneous initial state, i.e.

$$\Delta G_c > \Delta G_f > 0 \tag{2.26}$$

holds. So, Eq. (2.26) is the condition of metastability for the heterogeneous state. And, finally, even if phase transformations may occur in a sufficiently large system, this is excluded for domain sizes  $R_0/R_\sigma < 12.66$ . For such system sizes, the system is to be considered here as stable.

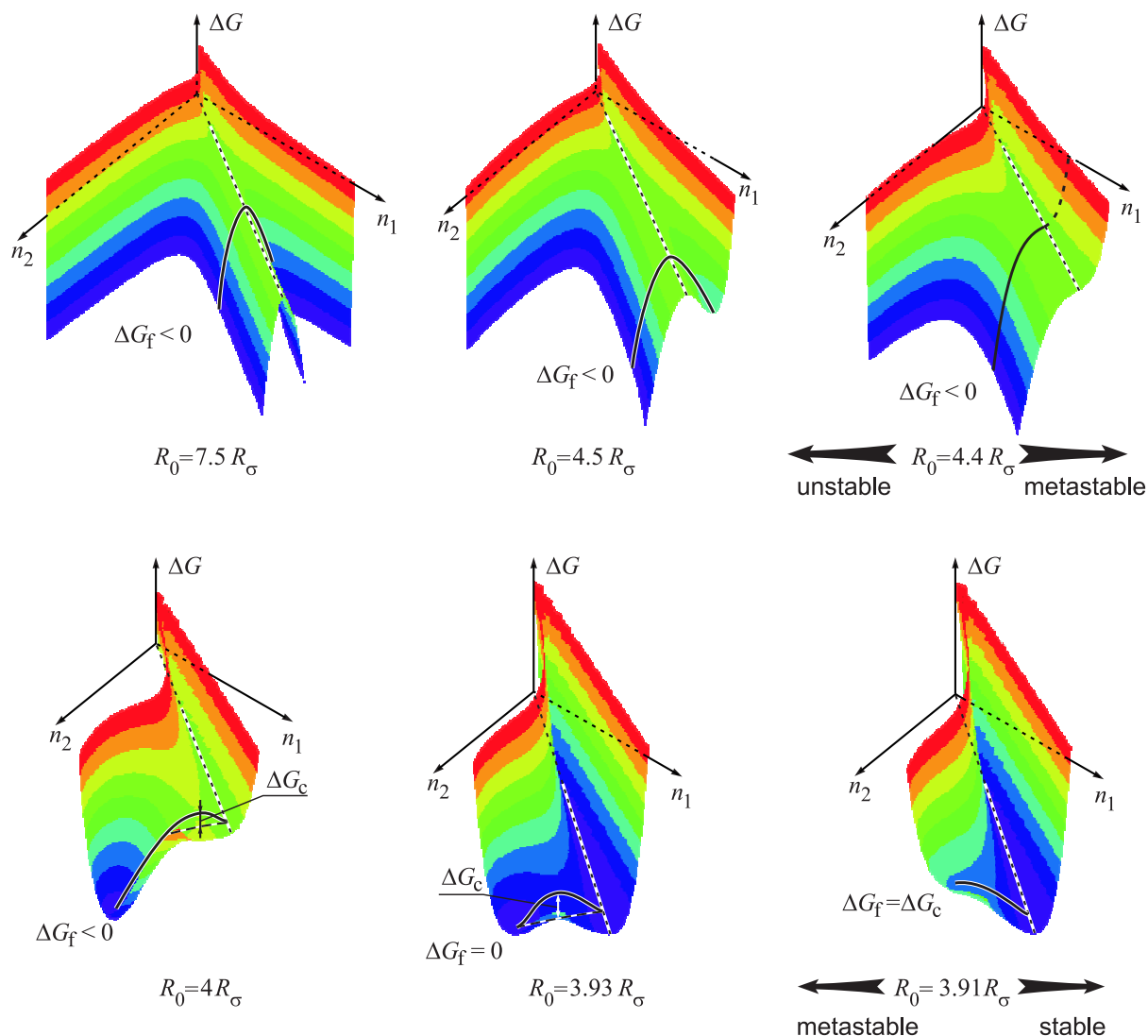


Fig. 2.11. Shape of the Gibbs free energy surface for  $x = 0.4$  and for different values of the domain size,  $R_0$ .

The results discussed here for a particular value of the initial supersaturation in the range of metastable (for infinite systems) initial states – i.e., increase of the critical cluster size,  $R_c$ , and the work of critical cluster formation,  $\Delta G_c$ , the increase of  $\Delta G_f$  and decrease of  $R_f$  – are general consequences of depletion effects in nucleation. They have been derived analytically in the framework of the classical Gibbs’ approach both for condensation in gases and phase formation in solid solutions earlier [24–27, 32–35]. It can be shown that the respective conclusions remain valid when the generalized Gibbs’ approach is employed for the description of the thermodynamics of cluster formation [42]. From a more general point of view, such dependencies can

be considered as consequences of the principle of le Chatelier-Brown [25,43].

However, as to our knowledge, so far the effect of finite size on the kinetics has not been studied for the case that the process starts from unstable initial states. This task will be performed in the subsequent analysis. Shapes of the Gibbs free energy surface  $\Delta G(n_{1\alpha}, n_{2\alpha})$  for  $x = x_{sp} \approx 0.226$  and for different values of the domain size,  $R_0$ , are presented on Fig. 2.9. The shapes of the free energy are qualitatively very similar to the respective results shown on Fig. 2.8.

The respective dependencies,  $\Delta G(n_{1\alpha}, n_{2\alpha})$ , for unstable initial states with  $x = 0.3$ , are shown on Fig. 2.10. In addition, the dependence of  $\Delta G$  along the evolution path are shown on Fig. 2.12 (here the path,  $s$ , is the distance in  $(n_{1\alpha}/n_\sigma, n_{2\alpha}/n_\sigma)$ -space, that is  $ds = (dn_{1\alpha}^2 + dn_{2\alpha}^2)^{1/2}/n_\sigma$  holds, and  $s > 0$  for  $x_\alpha > x$  and  $s < 0$  for  $x_\alpha < x$ ). For  $R_0/R_\sigma > 6.83$ , spinodal decomposition is a possible mode of evolution

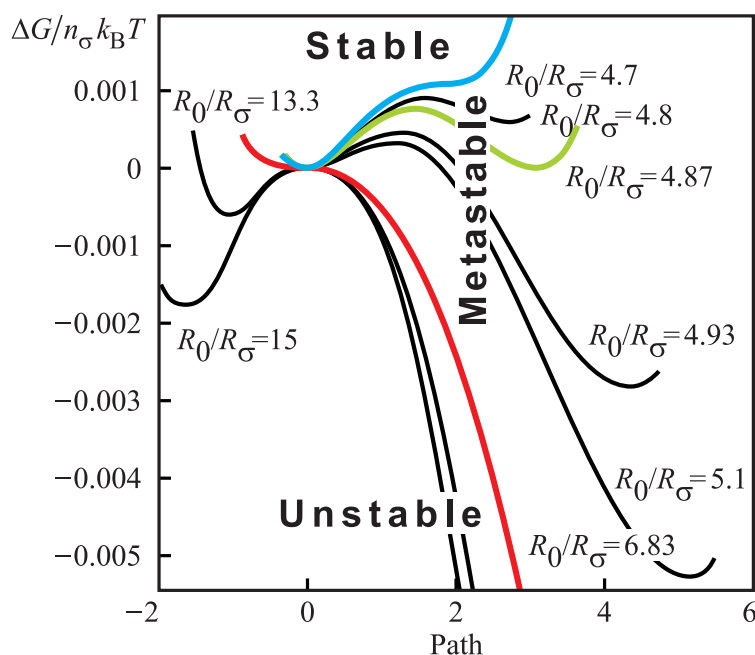


Fig. 2.12. Gibbs free energy along the preferred trajectory of evolution to the new phase for initial states of the ambient phase with  $x = 0.3$  and for different values of the domain size,  $R_0$ .

to the new phase. For low system sizes, here at  $R_0/R_\sigma < 6.83$ , a nucleation barrier arises and the system transforms to a metastable one. With the further reduction of the domain size the behavior of system is the same as for  $x \leq x_{sp}$ . For  $x = 0.4$ ,

the surface  $\Delta G(n_{1\alpha}, n_{2\alpha})$  is shown on Fig. 2.11. The shapes of the thermodynamic potential surfaces are similar to the case  $x = 0.3$ , only the characteristic values of the system size  $R_0$ , at which the transition from spinodal decomposition to nucleation occurs, are smaller.

Equation  $\Delta G_c(R_0, x) = \Delta G_f(R_0, x)$  defines the minimal domain size,  $R_{0,b}(x)$ , which allows nucleation in the initially homogeneous system, it defines the binodal depending on the domain size. Let us define as the next step the spinodal curve for the domain of finite size. Eq. (2.22) may be rewritten as

$$\left. \frac{\partial^2 \Delta G}{\partial x_\alpha^2} \right|_{x_\alpha=x} = 2K \left( \frac{R}{R_{c,\text{inf}}} \right)^2 \left\{ 1 - \frac{R}{R_{c,\text{inf}}} \left[ 1 - \left( \frac{R}{R_0} \right)^3 \right] \right\} \left[ 1 - \left( \frac{R}{R_0} \right)^3 \right]^{-2}, \quad (2.27)$$

and then Eq. (2.21), which determines critical size in spinodal region, takes the form

$$R_c^4 - R_c R_0^3 + R_0^3 R_{c,\text{inf}} = 0. \quad (2.28)$$

The equation has only one root for

$$R_0 = R_{0,sp}(x) = \frac{4^{4/3}}{3} R_{c,\text{inf}}(x) = R_\sigma \frac{2}{3} 4^{4/3} \left( 4 \frac{T_c}{T} - \frac{1}{x} - \frac{1}{1-x} \right)^{-1}, \quad (2.29)$$

and two real roots for  $R_0 > R_{0,sp}(x)$ , and at  $R_0 < R_{0,sp}(x)$  Eq. (26) does not have any roots. Consequently, the function  $R_{0,sp}(x)$  determines the minimal domain size  $R_{0,sp}(x)$ , which allows spinodal decomposition in the system, i.e., it defines the spinodal depending on the domain size.

Dependencies of minimal domain sizes  $R_{0,b}/R_\sigma$  and  $R_{0,sp}/R_\sigma$  on the initial solute concentration,  $x$ , are presented on Fig. 2.13. Metastable region is located between curves  $R_{0,b}(x)$  and  $R_{0,sp}(x)$ , unstable (spinodal) region is located to the right from  $R_{0,sp}(x)$ .

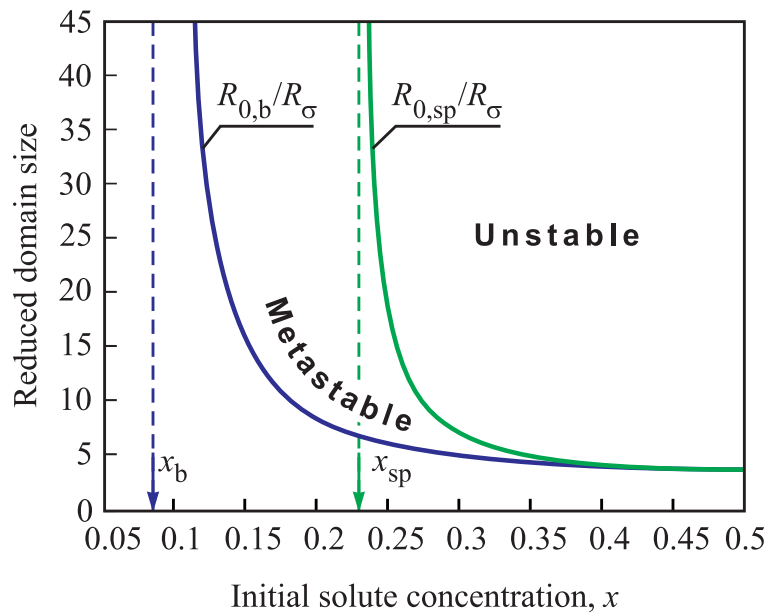


Fig. 2.13. Dependence of the reduced minimal domain size,  $R_{0,b}/R_{\sigma}$  and  $R_{0,sp}/R_{\sigma}$ , on the initial solute concentration,  $x$ .

The critical radius for the minimal domain size is determined by

$$R_{c,sp}(x) \equiv R_c(R_{0,sp}, x) = R_{\sigma} \frac{8}{3} \left( 4 \frac{T_c}{T} - \frac{1}{x} - \frac{1}{1-x} \right)^{-1}. \quad (2.30)$$

The dependence of the reduced critical radius  $R_c$  on the initial solute concentration  $x$  for different values of the domain size  $R_0$  is illustrated on Fig. 2.14. In the metastable region,  $R_c(x)$  is determined by Eqs. (2.13), in the unstable one, by the solution of Eq. (2.30). Critical radii corresponding to the minimal domain size for the metastable region  $R_{c,b}(x) \equiv R_c(R_{0,b}, x)$ , and for the unstable one,  $R_{c,sp}(x)$ , are shown on Fig. 2.14 by dashed-dotted and dotted curves, respectively. Note that in the unstable region two critical radii exist: the smaller one is determined by the balance between volume reduction and the increase of the thermodynamic potential due to surface formation (as for an infinite domain), the larger one is determined by the effect of changes of the state parameters (depletion effect). Indeed, we see that the larger value of  $R_c$  is comparable with the domain size,  $R_0$ .

Dependence of the minimum value of the work of critical cluster formation,  $\Delta G_c/n_{\sigma}k_B T$ , on the initial solute concentration,  $x$ , for different values of the domain

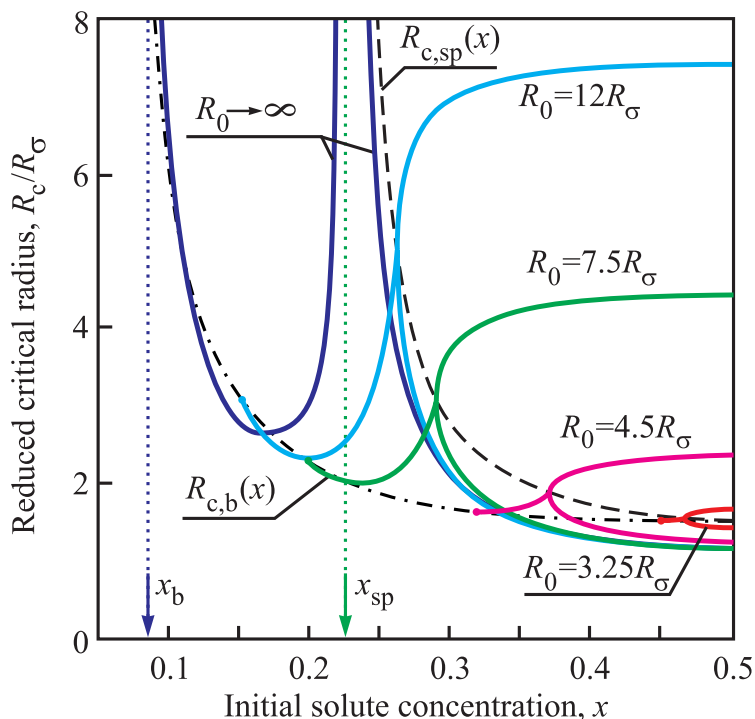


Fig. 2.14. Dependence of the reduced critical radius,  $R_c/R_\sigma$ , on the initial solute concentration,  $x$ , for different values of the domain size.

size,  $R_0$ , is shown on Fig. 2.15. In the region  $x < x_{sp}$ , with domain size reduction  $\Delta G_c$  increases insignificantly, while for  $x > x_{sp}$   $\Delta G_c = 0$  for  $R_0 \rightarrow \infty$ , and nonzero value of  $\Delta G_c$  arises only for finite values of  $R_0$ . Dependence of the composition of the critical cluster,  $x_{\alpha,c}$ , on the initial solute concentration  $x$ , for different values of the domain size,  $R_0$ , is shown on Fig. 2.16. We see that with growth of solute concentration  $x_{\alpha,c}$  decreases down to value  $x_{\alpha,c} = x$ , which corresponds to the unstable region.

## 2.4.2. Kinetics

Having performed the respective thermodynamic analysis, we will consider, now, the time evolution of the clusters in segregation processes in systems of finite size. We assume that the composition in a certain region of the ambient phase is

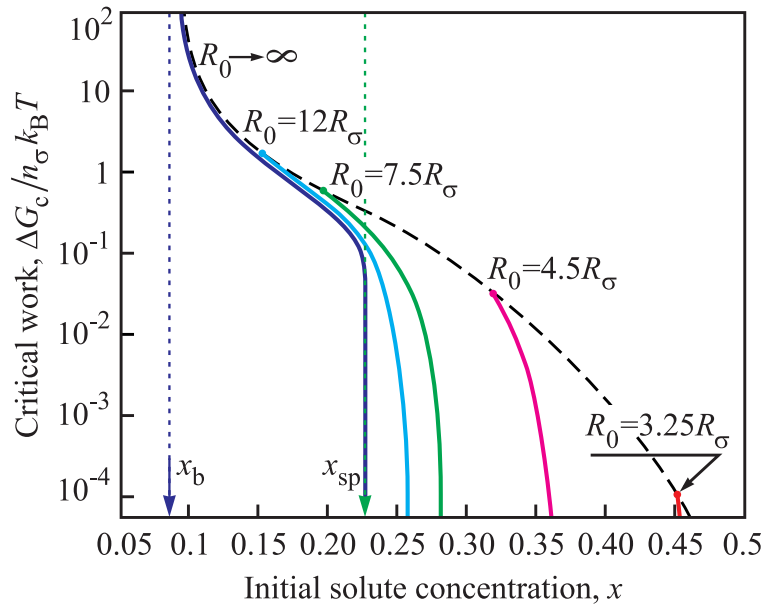


Fig. 2.15. Dependence of the minimum value of the work of critical cluster formation  $\Delta G_c/k_B T$  on the initial solute concentration,  $x$ , for different values of the domain size.

slightly shifted as compared with the composition of the matrix by a value  $\delta n_{i\alpha}$ , i.e.

$$n_{1\alpha} = n_{1\alpha,0} + \delta n_{1\alpha} , \quad n_{2\alpha} = n_{2\alpha,0} + \delta n_{2\alpha} . \tag{2.31}$$

It is assumed further that the growth is kinetically limited (i.e., we set  $u = 2/3$  in Eq. (2.18)) A substitution of Eqs. (2.31) into Eqs. (2.17) yields

$$\frac{d\delta n_{1\alpha}}{dt} = -D_1(1 - x_\beta)\Theta(n_{1\alpha}, n_{2\alpha})\frac{d\Delta G}{ds} \cos \varphi , \tag{2.32}$$

$$\frac{d\delta n_{2\alpha}}{dt} = -D_2x_\beta\Theta(n_{1\alpha}, n_{2\alpha})\frac{d\Delta G}{ds} \sin \varphi . \tag{2.33}$$

Here  $d\Delta G/ds$  is the absolute value of the gradient of the function  $\Delta G(n_{1\alpha}, n_{2\alpha})$  at values of  $x_\alpha$  near to  $x_\alpha = x$ ,  $\varphi$  is the angle between the direction of the gradient and

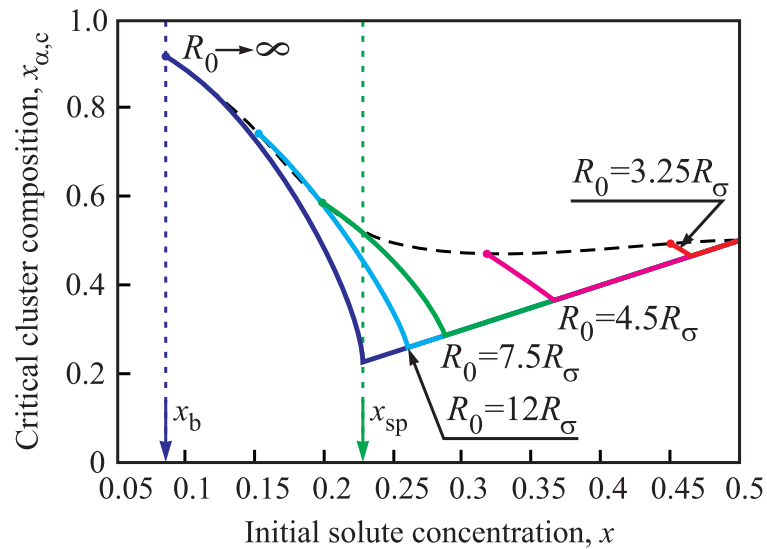


Fig. 2.16. Dependence of the composition of the critical cluster,  $x_{\alpha,c}$ , on the initial solute concentration  $x$ , for different values of the domain size.

the axis  $n_{1\alpha}$ . It is defined by the equation

$$\text{tg } \varphi = \frac{n_{2\alpha,0}}{n_{1\alpha,0} + n_{2\alpha,0}} = \frac{1 - x}{x} . \tag{2.34}$$

Dividing Eq. (2.33) by Eq. (2.32) and taking into account Eq. (2.34), we obtain

$$\delta n_{1\alpha} = -\frac{D_1}{D_2} \delta n_{2\alpha} . \tag{2.35}$$

Using the variable  $x_\alpha$  instead of  $\delta n_{2\alpha}$ ,

$$x_\alpha = \frac{n_{2\alpha}}{n_{1\alpha} + n_{2\alpha}} = \frac{n_{2\alpha,0} + \delta n_{2\alpha}}{n_{1\alpha,0} + n_{2\alpha,0} + \left(1 - \frac{D_1}{D_2}\right) \delta n_{2\alpha}} , \tag{2.36}$$

we get the equation

$$\frac{dx_\alpha}{dt} = \Theta_0 x (1 - x) \left(\frac{R_{c,\text{inf}}}{R}\right)^4 [xD_1 + (1 - x) D_2] \left(-\frac{\partial^2 \Delta G}{\partial x_\alpha^2} \Big|_{x=x_\alpha}\right) (x_\alpha - x) , \tag{2.37}$$

where  $R$  is initial cluster radius, and  $(\partial^2 \Delta G / \partial x_\alpha^2)|_{x=x_\alpha}$  is determined by Eq. (2.27). This linear equation has a solution of the form  $(x_\alpha - x) \sim e^{\gamma(R)t}$ , where the growth increment (or amplification factor)  $\gamma(R)$  is determined via

$$\gamma(R) = M \left( \frac{R_{c,\text{inf}}}{R} \right)^4 \left( - \frac{\partial^2 \Delta G}{\partial x_\alpha^2} \Big|_{x=x_\alpha} \right) \quad (2.38)$$

and

$$M = \Theta_0 x (1 - x) [x D_1 + (1 - x) D_2] \quad (2.39)$$

holds.

For finite systems with a domain size lower than some upper value  $R_{0m}$

$$R_0 \leq R_{0m} = 2R_{0,sp} = R_\sigma \frac{4^{7/3}}{3} \left( 4 \frac{T_c}{T} - \frac{1}{x} - \frac{1}{1-x} \right)^{-1}, \quad (2.40)$$

the function  $\gamma = \gamma(R)$  has a maximum. The value of the maximum increases with increasing domain size. Moreover, at  $R_0 \geq R_{0m}$  a second maximum of equal height arises. After this second maximum appeared, the height of the maxima does not vary any more with the further increase of the size of the domain (Fig. 2.17). The growth increment reaches the maximum value for a domain size equal to

$$R_{0,max}(R, x) = \begin{cases} \left( \frac{R}{R_\sigma} \right)^{4/3} \left( \frac{R}{R_\sigma} - \frac{3}{K} \right)^{-1/3} & \text{for } R > R_{\gamma,max} \\ R_{0m} & \text{for } R \leq R_{\gamma,max} \end{cases} \quad (2.41)$$

where  $R_{\gamma,max} = (8R_\sigma/3K)$ .

The dependence of the growth increment,  $\gamma(R)$ , on cluster radius for various fixed domain sizes,  $R_0$  (full curves), and for  $R_0 = R_{0,max}(R, x)$  (dashed curve) is shown on Fig. 2.17 for the case  $D_1 = D_2$  and  $x = 0.45$ , i.e., for macroscopically

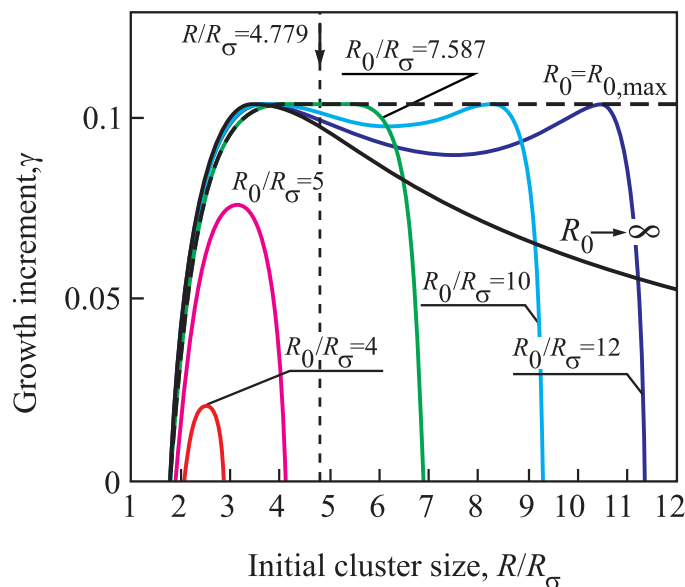


Fig. 2.17. Dependence of the growth increment on the cluster radius,  $R/R_\sigma$ , for various domain sizes (full curves) and for  $R_0 = R_{0,max}(R, x)$  (dashed curve) for  $x = 0.45$ .

unstable initial states.

Equation (2.38) looks similar to the expression for the growth increment in the classical Cahn-Hilliard theory of spinodal decomposition [9, 10]. Indeed, let us introduce a *wave vector* via  $k \equiv R_\sigma/R$ , then Eq. (2.38) gets the form

$$\gamma(k) = Mk^4 \left( - \frac{\partial^2 \Delta G}{\partial x_\alpha^2} \Big|_{x=x_\alpha} \right), \tag{2.42}$$

$$\frac{\partial^2 \Delta G}{\partial x_\alpha^2} \Big|_{x_\alpha=x} = \frac{2K}{k^2} \left\{ 1 - \frac{1}{k} \left[ 1 - \left( \frac{k_0}{k} \right)^3 \right] \right\} \left[ 1 - \left( \frac{k_0}{k} \right)^3 \right]^{-2}. \tag{2.43}$$

Employing these relations, on Fig. 2.18 the Cahn plots  $\gamma(k)/k^2$  vs  $k^2$  are shown for various fixed domain sizes,  $R_0$  (full curves), and for  $R_0 = R_{0,max}(R, x)$  (dashed curve), where the notation  $k_c = R_\sigma/R_c$  is used. On Fig. 2.19, the result for  $R_0 = R_{0,max}(R, x)$  is compared with experimental data for spinodal decomposition in the glass  $\text{SiO}_2\text{-}12.5 \text{ Na}_2\text{O}$  [44]. The Cahn-plot, obtained in this way, is different in its

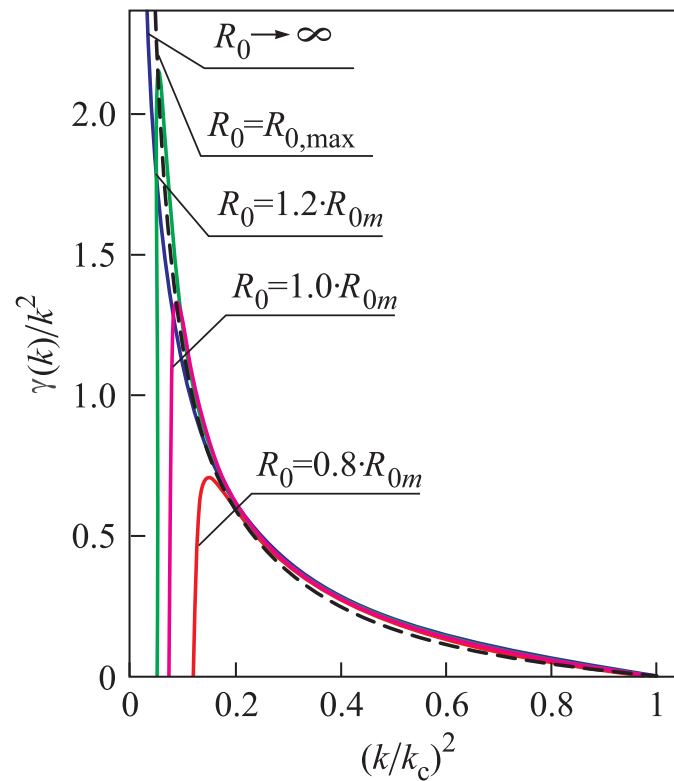


Fig. 2.18. Dependence of the ratio  $\gamma/k^2$  on  $k^2$  for various domain sizes (full curves) and for  $R_0 = R_{0,\max}(R, x)$  (dashed curve) for  $x = 0.45$ .

shape as compared with the linear classical dependence [9,10], it is in good agreement with the experimental curves shown for comparison. Thus, the linear analysis of Eqs. (2.32) and (2.33) allows us to determine the growth increment for spinodal decomposition (Eq. (2.42)) depending on supersaturation, cluster and domain sizes in a way giving a better agreement with experimental data as the classical theory.

The numerical solution of Eqs. (2.32) and (2.33) allows one not only to analyze the initial states of spinodal decomposition but to trace the whole process of evolution of the cluster. In doing so, we assume kinetic limited growth ( $u = 2/3$  in Eq. (2.18)) and set the temperature equal to  $T = 0.7T_c$ , again. Domain size and the initial cluster radius are chosen to correspond to the maximal growth increment, i.e.,  $R_0 = R_{0m}$  and  $R = R_{\gamma,\max}$  (see Eqs. (2.40) and (2.41)), the initial cluster composition is given by  $x_\alpha|_{t=0} = x(1 + \delta)$ .

Results of calculations of the cluster evolution for a regular solution with a molar fraction of the segregating component in the ambient phase equal to  $x = 0.45$

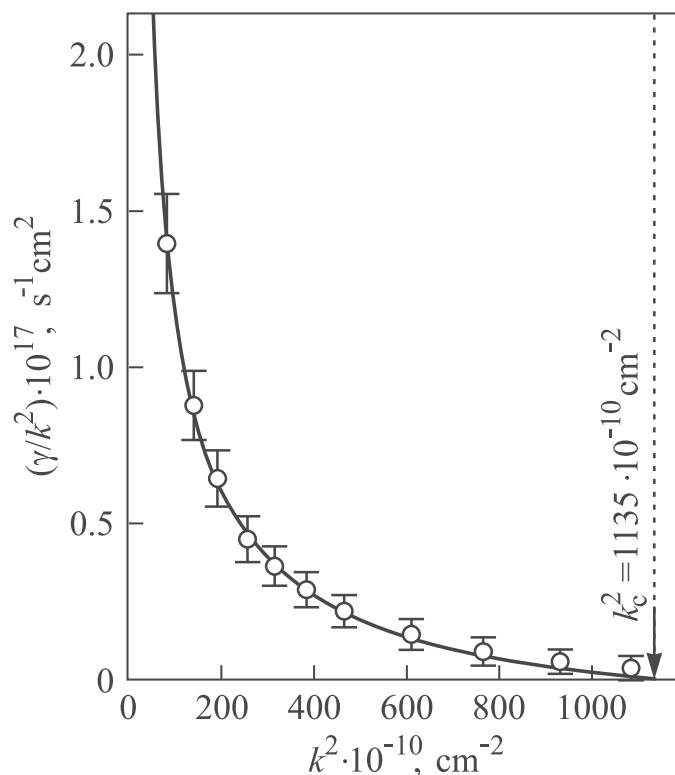


Fig. 2.19. Dependence of the ratio  $\gamma/k^2$  on  $k^2$ : result of calculation for  $R_0 = R_{0,\max}(R, x)$  for  $x = 0.45$ ; circles refer to experimental data for the glass  $\text{SiO}_2\text{-}12.5 \text{ Na}_2\text{O}$  at  $530 \text{ }^\circ\text{C}$  obtained by small-angle x-ray scattering [44].

and  $\delta = 0.01$  are presented on Figs. 2.20-2.23.

The shape of the Gibbs free energy surface and the trajectory of cluster evolution in the  $(n_{1\alpha}/n_\sigma, n_{2\alpha}/n_\sigma)$  space ( $n_\sigma$  is determined by Eq. (2.11)) are shown on Fig. 2.20 for different values of the partial diffusion coefficient  $D_1$  and  $D_2$  ((a)  $D_1/D_2 = 100$ , (b)  $D_1/D_2 = 1$ , (c)  $D_1/D_2 = 0.025$  and (d)  $D_1/D_2 = 0.001$ ; as earlier, we assume  $D_1 D_2 = \text{const.}$ ). The process starts in the point S and develops either increasing (path  $S \rightarrow F$ , curves (a), (b), (c), and (d)) or decreasing ( $S \rightarrow F'$ , curves (a'), (b'), (c') and (d')) the concentration of the second component. For  $x \neq 0.5$ , the minima of Gibbs free energy, the system may approach following the different pathes of evolution, have different depths (for  $x < 0.5$   $\Delta G_F < \Delta G_{F'}$ ). Preferred is the path  $S \rightarrow F$ , therefore further we consider only this version.

The dependencies of compositions of cluster and ambient phase both on time and on cluster radius are shown on Figs. 2.21 and 2.22, respectively (cf. also Fig. 2.7).

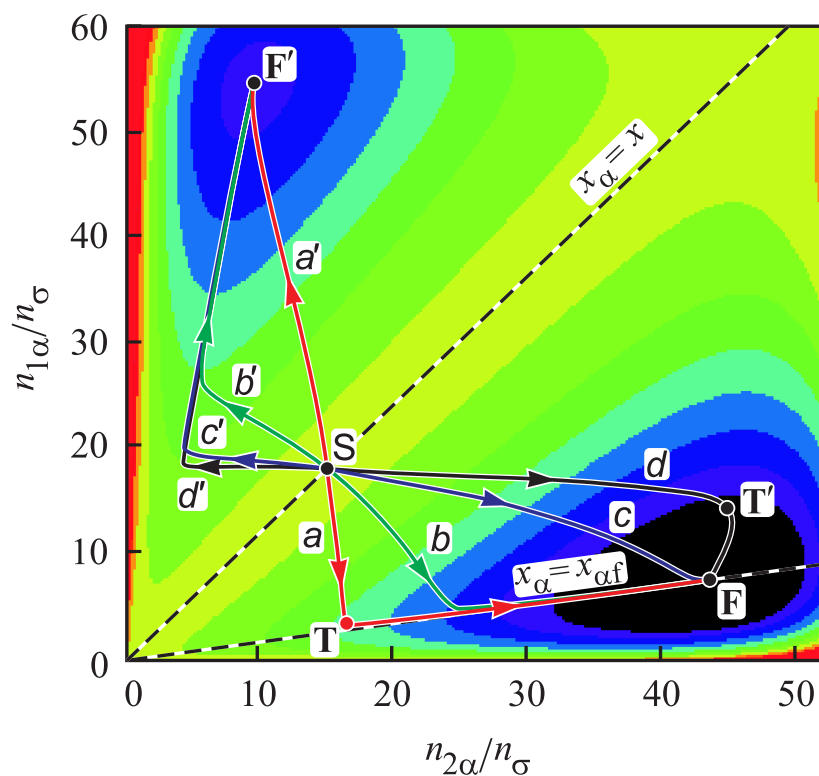


Fig. 2.20. Shape of the Gibbs free energy surface and trajectory of cluster evolution in the  $(n_{1\alpha}/n_c, n_{2\alpha}/n_c)$  space for a regular solution with a molar fraction of the segregating component in the ambient phase equal to  $x = 0.45$  for different values of  $D_1/D_2$ : a)  $D_1/D_2 = 100$ , b)  $D_1/D_2 = 1$ , c)  $D_1/D_2 = 0.025$  and d)  $D_1/D_2 = 0.001$ .

For the case of a quickly moving first component ( $D_1/D_2 = 100$ , curve (a)), the evolution along the path  $S \rightarrow T$  proceeds via emission of particles of the first component from the cluster. As the result, the cluster shrinks in size (see also Fig. 2.21b). After a time,  $\tau_{\alpha f}$ , the composition of the cluster almost reaches its final value,  $x_\alpha \approx x_{\alpha f} \approx 0.853$  (the point  $T_\alpha$  on Figs. 2.20 and 2.22, note also that this state corresponds to the minimum of Gibbs free energy). During the initial time interval,  $\tau < \tau_{\alpha f}$ , the compositions of cluster and ambient phase change approximately with equal rate. This rate can be determined by the analytical expressions Eq. (2.38) with good accuracy (dotted curves on Fig. 2.21). Once this stage of evolution is completed, the cluster begins to grow with approximately constant composition while the composition of the ambient phase continues to change. Since the condition of constancy of cluster composition requires attachment of atoms of both kinds in

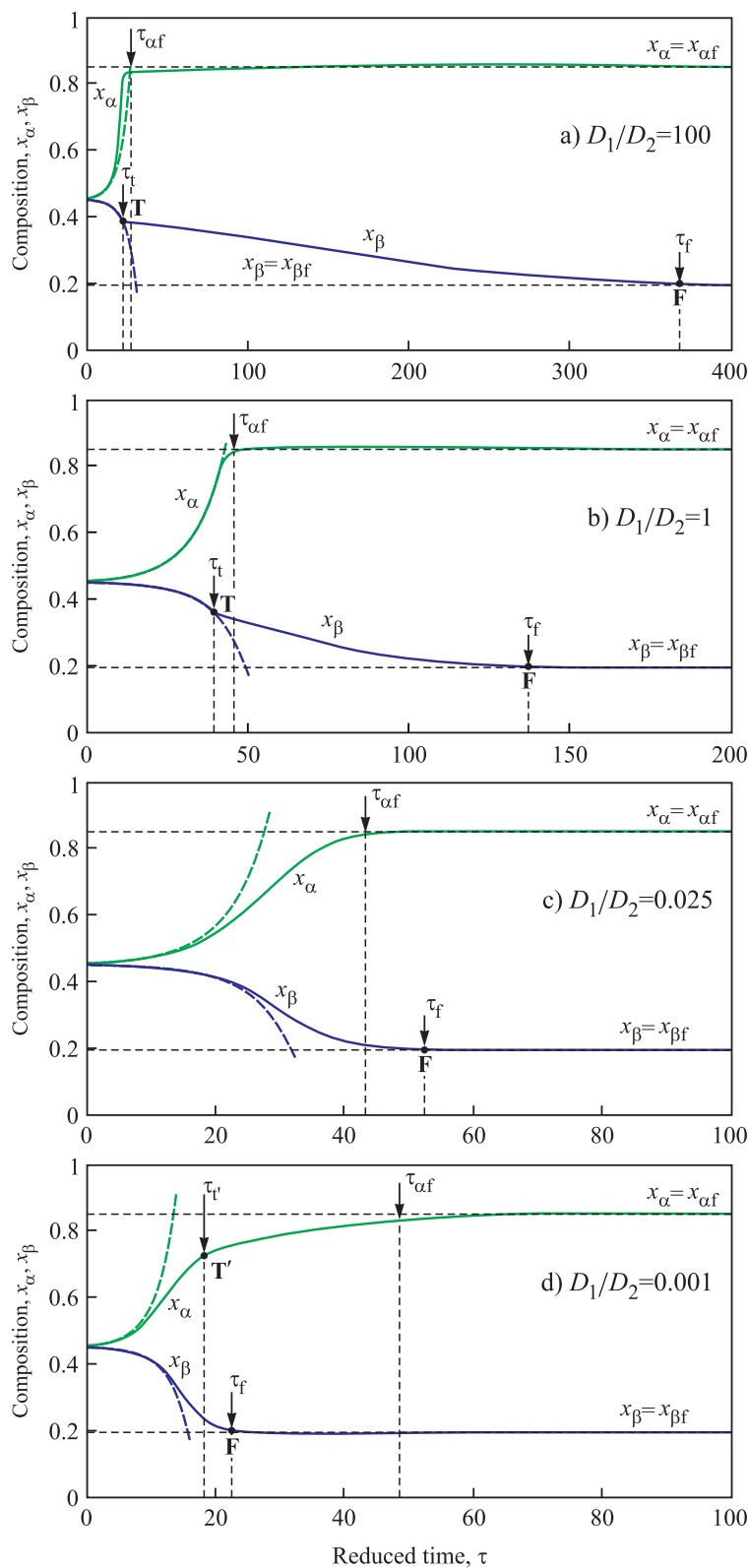


Fig. 2.21. Dependence of the compositions of the cluster,  $x_\alpha$ , and ambient phase,  $x_\beta$ , on time for different values of  $D_1/D_2$ : (a)  $D_1/D_2 = 100$ , (b)  $D_1/D_2 = 1$ , (c)  $D_1/D_2 = 0.025$  and (d)  $D_1/D_2 = 0.001$ .

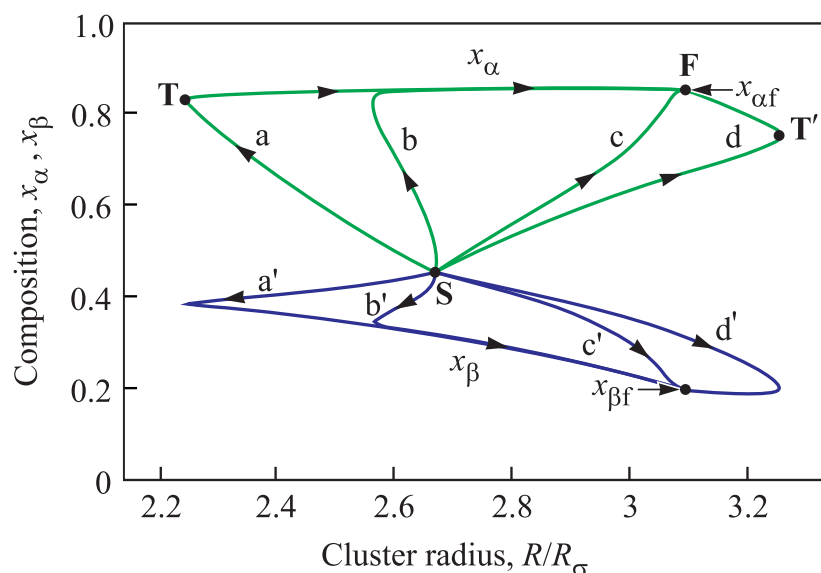


Fig. 2.22. Dependence of the compositions of the cluster,  $x_\alpha$ , and ambient phase,  $x_\beta$ , on the reduced cluster radius for different values of  $D_1/D_2$ : (a)  $D_1/D_2 = 100$ , (b)  $D_1/D_2 = 1$ , (c)  $D_1/D_2 = 0.025$  and (d)  $D_1/D_2 = 0.001$ .

a certain well-defined proportion, the rate of evolution along the path  $T \rightarrow F$  is limited by the rate of attachment of atoms of the slow second component (see Fig. 2.21c). In the time  $\tau_{\beta f}$ , the composition of the ambient phase reaches its final value,  $x_\beta \approx x_{\beta f} \approx 0.194$ .

For the case of nearly equal partial diffusion coefficients,  $D_2 = D_1$ , the evolution proceeds similarly with the difference that the cluster size changes only insignificantly at the initial stage of evolution,  $\tau < \tau_{\alpha f}$  (see Fig. 2.21b) and the time interval  $\tau_{\beta f}$  is considerably shorter as compared with the previous case. Such two-stage behavior is preserved in a wide interval of components mobility, actually only at  $D_1/D_2 \approx 0.025$  cluster size and concentration begin to change monotonically down to end (see Fig. 2.22, curves (c) and (c')).

At  $D_1 \ll D_2$ , the situation is to some extent opposite. Along the path  $S \rightarrow T'$ , the cluster grows quickly due to the incorporation of atoms of the second fast component. Then, after a time  $x_\beta \approx x_{\beta f}$ , the composition of the ambient phase has almost reached its final value  $x_\beta \approx x_{\beta f}$ , and a slow reduction of the cluster size due to emission of atoms of the first component is found along the path  $T' \rightarrow F$ .

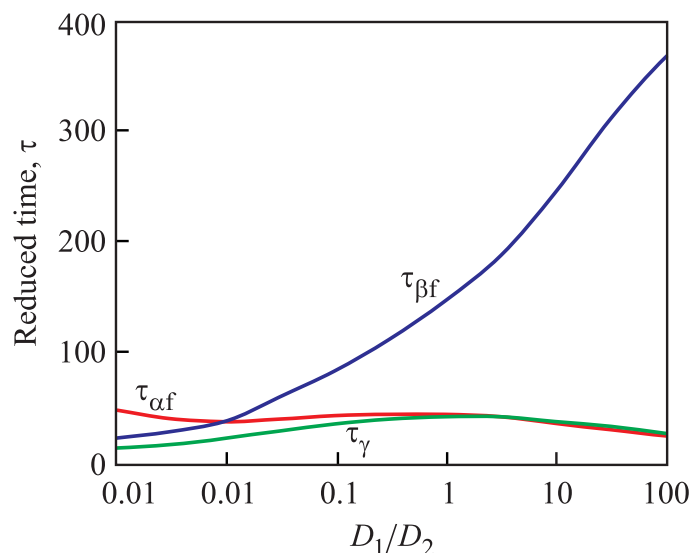


Fig. 2.23. Dependence of the characteristic times  $\tau_{\beta f}$ ,  $\tau_{\alpha f}$  and  $\tau_{\gamma}$  on the  $D_1/D_2$  ratio.

Fig. 2.23 shows the dependence on the  $(D_1/D_2)$ -ratio of the characteristic times of change of cluster composition,  $\tau_{\alpha f}$ , of ambient phase change,  $\tau_{\beta f}$ , and time  $\tau_{\gamma}$ . Latter parameter can be computed via the analytical expression, Eq. (2.38), resulting in

$$\tau_{\gamma} = \frac{1}{\gamma(R_{\gamma, \max})} \ln \left[ \frac{x_{\alpha f} - x}{x\delta} \right]. \quad (2.44)$$

The minimum time,  $\min(\tau_{\alpha f}, \tau_{\beta f})$ , of change of the composition of the cluster or the ambient phase differs only slightly from  $\tau_{\gamma}$ , while the full time of decomposition is determined by the maximum time  $\max(\tau_{\alpha f}, \tau_{\beta f})$ , which is twice as large as  $\tau_{\gamma}$  for  $D_1/D_2 \approx 0.01$ , and for  $D_1 \gg D_2$   $\tau_{\beta f}$  larger than  $\tau_{\alpha f}$  and  $\tau_{\gamma}$  by more than an order of magnitude.

### 2.4.3. Transition from independent cluster growth to coarsening

So far, we have considered phase separation in finite domains of size,  $R_0$ , considering the evolution of one cluster. However, the results of the analysis can

be employed more generally allowing one to derive important conclusions about the initial stages of phase separation processes for systems of arbitrarily large sizes. The model considered above actually represents the case of an infinite domain with an ensemble of identical clusters. The analysis of such systems has been shown to be very fruitful already in previous investigations of the kinetics of phase separation in solutions when the classical Gibbs' approach was employed for the thermodynamic description of the clusters and cluster ensembles [25,32–35]. The respective analyses are attempted to be generalized in future.

For a more detailed analysis of the kinetics of phase formation, the existence and evolution of the cluster size distributions has to be taken into consideration. Independent growth of clusters of nearly the same sizes is possible only at the initial stage of the process, and such distributions are unstable. Once the depletion effects begin to dominate, the  $\delta$ -shaped or Gaussian type distribution functions are inevitably widened and the system passes into the coalescence stage [37]. In the simplest way, this can be done by solving the equations of motion of the clusters numerically. Such approach has been performed in terms of the classical description of cluster formation and evolution by a variety of authors. Here we would like to show that these analyzes can be generalized by the mentioned approach accounting both for variations of cluster sizes and compositions. In order to illustrate these features, here we restrict the analysis to the evolution of cluster ensembles consisting only of few clusters.

Completing the analysis, we demonstrate that the transition to the competitive growth stage can be described adequately in terms of the approach employed here independently on whether the system starts the transformation from a metastable or unstable initial state. For this purposes, we consider the evolution of a system of three clusters in one domain. The clusters due not interact directly but only via consuming

particles from the ambient phase. The conservation law, Eq. (2.1), gets then the form

$$\begin{aligned}
 n_0 &= \sum_i \left( n_\alpha^{(i)} + n_\alpha^{(i)} \right) = \text{const.} , & (2.45) \\
 \sum_i \left( n_{1\alpha}^{(i)} + n_{2\alpha}^{(i)} \right) &= \sum_i \left[ n_{1\alpha}^{(i)}(0) + n_{2\alpha}^{(i)}(0) \right] = \text{const.} , \\
 \sum_i \left( n_{1\beta}^{(i)} + n_{2\beta}^{(i)} \right) &= \sum_i \left[ n_{1\beta}^{(i)}(0) + n_{2\beta}^{(i)}(0) \right] = \text{const.} , \\
 n_\alpha^{(i)} &= n_{1\alpha}^{(i)} + n_{2\alpha}^{(i)} , & n_\beta^{(i)} &= n_{1\beta}^{(i)} + n_{2\beta}^{(i)} ,
 \end{aligned}$$

where the indices  $i = 1, 2, 3$  specify the different clusters evolving in the system. The concentration of the second component in the ambient solution is given then by

$$x_\beta = \sum_i n_{2\beta}^{(i)} \left( \sum_i n_\beta^{(i)} \right)^{-1} , \quad (2.46)$$

and in the  $i$ -th cluster by

$$x_\alpha^{(i)} = \frac{n_{2\alpha}^{(i)}}{n_{1\alpha}^{(i)} + n_{2\alpha}^{(i)}} . \quad (2.47)$$

The evolution of the system is determined by the set of equations

$$\frac{dn_{1\alpha}^{(i)}}{dt} = -D_1(1 - x_\beta)\Theta \frac{d}{dn_{1\alpha}^{(i)}} \Delta G \left( \left\{ n_{1\alpha}^{(i)} \right\}, \left\{ n_{2\alpha}^{(i)} \right\} \right) , \quad (2.48)$$

$$\frac{dn_{2\alpha}^{(i)}}{dt} = -D_2 x_\beta \Theta \frac{d}{dn_{2\alpha}^{(i)}} \Delta G \left( \left\{ n_{1\alpha}^{(i)} \right\}, \left\{ n_{2\alpha}^{(i)} \right\} \right) , \quad (2.49)$$

where

$$\frac{1}{k_B T} \Delta G \left( \left\{ n_{1\alpha}^{(i)} \right\}, \left\{ n_{2\alpha}^{(i)} \right\} \right) = \frac{3}{2} n_\sigma^{1/3} \sum_i \left( n_\alpha^{(i)} \right)^{2/3} \left( x_\alpha^{(i)} - x_\beta \right)^2 \quad (2.50)$$

$$+ \sum_i n_\alpha^{(i)} f(x_\beta, x_\alpha^{(i)}) - n_0 f(x_\beta, x).$$

As before, the functions  $f(x_\beta, x_\alpha^{(i)})$  and  $f(x_\beta, x)$  are determined by Eq. (2.10), and  $n_\sigma$  by Eq. (2.11). Domain size and the initial cluster radii are assumed to be equal to the maximum growth increment, i.e.,  $R_0 = 3^{1/3} R_{0m}$  and  $R = R_{\gamma, \max}$  (see Eqs. (2.40) and (2.41)), the initial cluster compositions are chosen as  $x_{\alpha, i} = x(1 + \delta_i)$ , where  $\delta_1 = 0.004$ ,  $\delta_2 = 1.12 \cdot \delta_1$ ,  $\delta_3 = 1.2 \cdot \delta_1$  (thus, the first cluster has the lowest deviation from the initial composition, the second a larger and the third the highest one). The results of the computations are shown on Figs. 2.24 and 2.25.

On Fig. 2.24, a cross-section of the Gibbs free energy surface and the trajectory of evolution of the first cluster is given in the  $\left( n_{1\alpha}^{(1)}/n_\sigma, n_{2\alpha}^{(1)}/n_\sigma \right)$  space. On Fig. 2.25, the dependence of the compositions,  $x_\alpha^{(i)}$ , the radii,  $R^{(i)}$ , of the clusters ( $i = 1, 2, 3$ ), and the composition of ambient phase,  $x_\beta$ , are shown in dependence on time. For three clusters the phase space is six-dimensional, therefore we plot only its two-dimensional sections for the first cluster (which is dissolved as the first one) for different moments of time (as specified on the figure).

At the first stage of the process, for  $\tau < \tau_\alpha^{(i)}$  ( $\tau_\alpha^{(1)} \approx 135$ ,  $\tau_\alpha^{(2)} \approx 128$ , and  $\tau_\alpha^{(3)} \approx 122$ ), all three clusters evolve in an almost equal manner: the concentration of the second component grows, the sizes of the clusters decrease (see Fig. 2.24b). In the initial state, the Gibbs free energy has a shape characteristic for the instability region (see Figs. 2.24a and 2.20), but already at  $\tau = \tau_b \approx 120$  a saddle point evolves being a characteristic feature of metastable states (Fig. 2.24b). At  $\tau = \tau_\alpha^{(1)}$ , the concentration of the second component in the first cluster approaches the maximum value (see Fig. 2.24c, it corresponds to the path  $S \rightarrow T$  on Fig. 2.20). After that, the cluster begins to grow, and at  $\tau = \tau_c \approx 160$  it reaches the maximum size. The

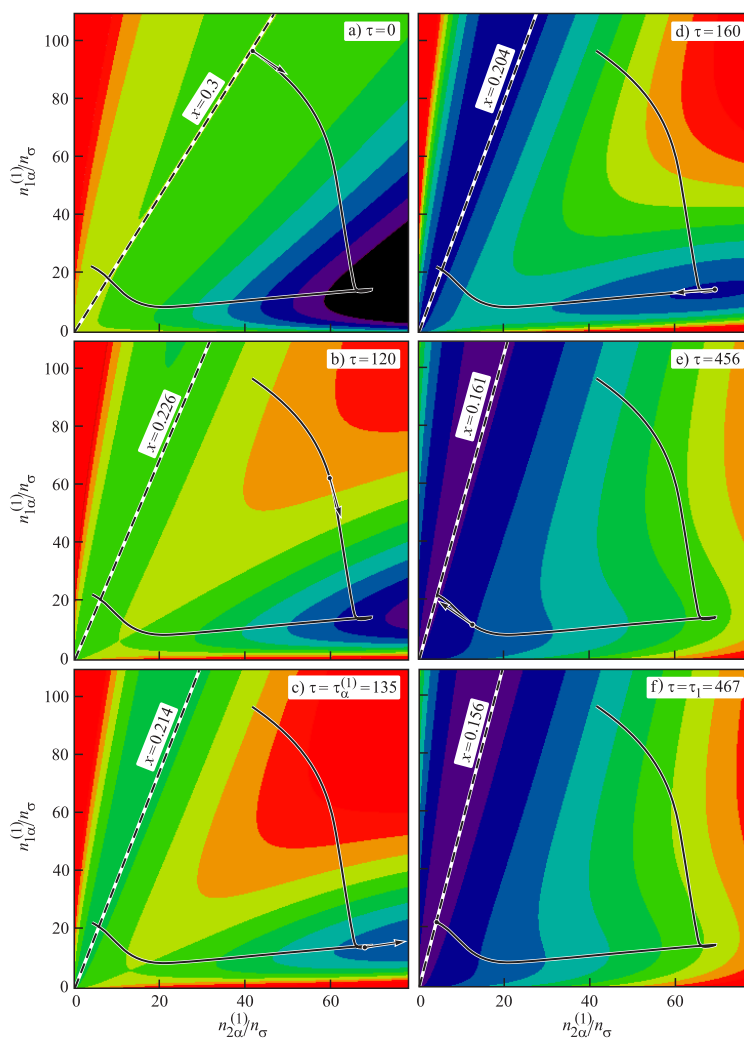


Fig. 2.24. Cross-section of the Gibbs free energy surface and trajectory of the first cluster evolution in the  $(n_{1\alpha}^{(1)}/n_c, n_{2\alpha}^{(1)}/n_c)$  space for a regular solution with a molar fraction of the segregating component in the ambient phase equal to  $x = 0.3$  for  $D_1/D_2 = 1$ .

Gibbs free energy reaches then a local minimum (see Fig. 2.24d). In the case of a single cluster, the process would have finished at such state, however, the second and the third clusters continue to consume atoms of the second component, lowering their concentration in the ambient phase. As the result of such depletion effects, the first cluster shrinks, the concentration of the second component decreases. This process corresponds to the beginning of dissolution of the first cluster. The process is completed in a time  $\tau_1 \approx 467$ , when the composition of the first cluster composition approaches the composition of the the ambient phase,  $x_\alpha^{(1)} = x_\beta$ . At this moment,

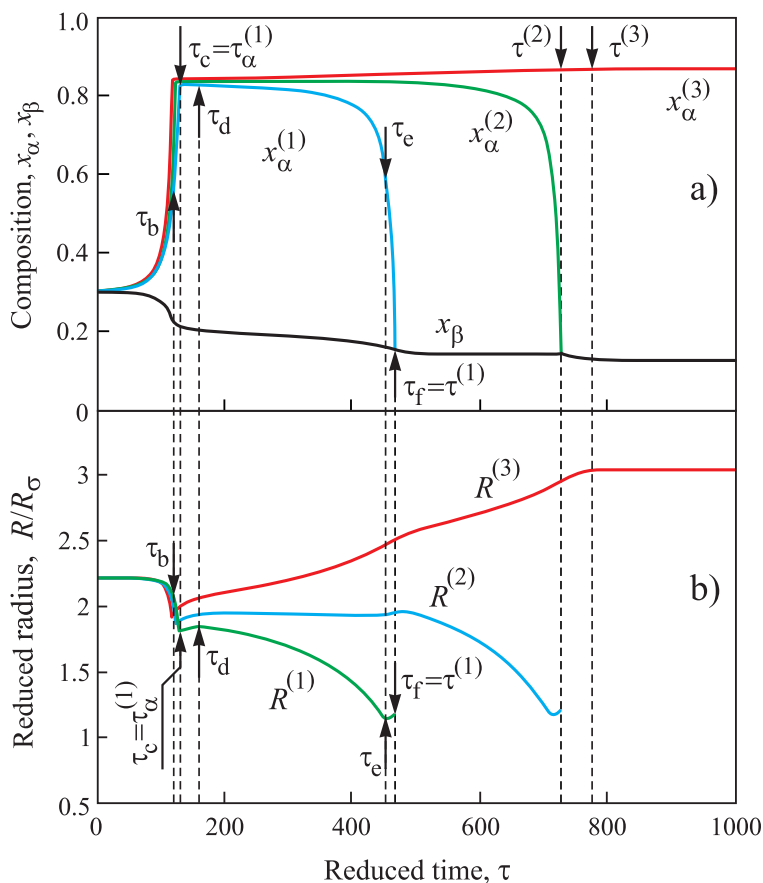


Fig. 2.25. Dependence of the compositions,  $x_\alpha^{(i)}$ , radiuses,  $R^{(i)}$ , of the clusters ( $i = 1, 2, 3$ ), and composition of ambient phase,  $x_\beta$ , on time.

the radius of the cluster remains finite (see Fig. 2.24b). The evolution of the second cluster proceeds similarly, and in time  $\tau_2 \approx 729$  it is dissolved. At  $\tau_3 \approx 937$  the process is finished and only one cluster remains in the domain.

### 2.5. Results and discussion

In the present paper, basic features of nucleation-growth and spinodal decomposition processes in solutions are analyzed within the framework of a thermodynamic cluster model based on the generalized Gibbs' approach. This approach allows one to determine the thermodynamic potentials of clusters and ensembles of clusters in the otherwise homogeneous ambient phase for thermodynamically well-defined (cf. [22,23]) non-equilibrium states of the considered

heterogeneous systems. Hereby the cluster, representing the density and/or composition fluctuations may change with time both in size and intensive state parameters. The thermodynamic analysis is employed further as the basis for the description of the kinetics of the decomposition processes.

The thermodynamic analysis of cluster formation is performed in dependence on supersaturation for metastable and unstable initial states and domains of infinite and finite sizes. For domains of infinite sizes, in particular, the parameters of the critical clusters – size, intensive state parameters, work of critical cluster formation – are determined for metastable initial states of the solutions. It is shown that – in the framework of the generalized Gibbs' approach – the notation of a critical cluster can be extended also to unstable initial states. Here the composition of the critical clusters is equal to the composition of the ambient phase and the work of critical cluster formation is equal to zero. The size of the critical clusters for unstable initial states behaves like the size of the regions with highest amplification of density/composition differences in the classical Cahn-Hilliard approach to the description of spinodal decomposition. As shown, moreover, there is no qualitative difference between nucleation and spinodal decomposition with respect to the basic mechanism of cluster evolution. Nucleation processes, starting from thermodynamically metastable initial states, proceed qualitatively widely similar as compared with processes of phase formation governed by spinodal decomposition. As it turns out further, the classical model of nucleation is not correct in application to phase formation in solutions (cf. also [14, 16]).

As an additional step, the effect of finite domain sizes on cluster formation is analyzed. It is shown, as a general consequence, that the degree of stability of the system to phase formation increases with decreasing system size due to depletion effects. In particular, the parameters of the critical clusters depend on system size. In addition, systems of finite size may be metastable or even stable even if the infinite samples are unstable. In this case the evolution of the system starts via spinodal

decomposition. Then, due to the growth of the clusters, the supersaturation decreases, and the system becomes metastable. Anyway, cluster growth continues. Finally, the supersaturation decreases to such extent that the dissolution of the clusters with smaller sizes becomes the prerequisite for the growth of the larger one, and the stage of coarsening starts [37]. Thus, the approach allows us to describe the evolution of the system from spinodal decomposition up to the coalescence stage accounting both for changes of the sizes and the intensive state parameters of the clusters in the course of this process. An analysis of experimental results on phase separation in solutions at high supersaturations is performed in terms of the generalized cluster model showing that the generalized cluster model allows us a more correct interpretation of the dynamics of phase separation as compared with this classical theory.

In our approach only the knowledge of macroscopic properties of the ambient and the newly evolving phases is required for the analysis of phase formation processes. By this reason, the approach presented here seems, to our opinion, to be preferable in the analysis of experimental results. The results of the analysis, as performed above, were obtained employing the model of regular solutions. They can be quantitatively modified by a more detailed account of the thermodynamic properties of the real system, by taking into consideration additional thermodynamic factors like special properties of domain boundaries or elastic stresses, which may be of importance in a number of cases, or by accounting for peculiarities of the process of diffusion not elaborated here. Nevertheless, we believe that the scenario outlined will be valid generally for processes of segregation in solid or liquid solutions. The application of the methods and results obtained to the interpretation of experimental data will be addressed in future publications. Another question is whether the results are applicable for other types of phase formation processes like, for example, condensation and boiling. This topic will be addressed in a forthcoming analysis.

## 2.6. Acknowledgments

The authors would like to express their gratitude to the Deutsche Forschungsgemeinschaft (DFG), to the Deutscher Akademischer Austauschdienst (DAAD) and the Science and Technology Center in the Ukraine (Project 1893) for financial support.

## References

1. M. Volmer, *Kinetik der Phasenbildung* (Steinkopff, Dresden, 1939).
2. Ya. I. Frenkel, *Kinetic Theory of Liquids* (Oxford University Press, Oxford, 1946).
3. K. Binder, Rep. Prog. Phys. **90**, 783 (1987).
4. V. P. Skripov and A. V. Skripov, Uspekhi Fiz. Nauk **128**, 193 (1979).
5. J. D. Gunton, M. San Miguel, and P. S. Sahni, *The Dynamics of First-Order Phase Transitions*, in: *Phase Transitions and Critical Phenomena*, vol. 8, edited by C. Domb and J. L. Lebowitz (Academic Press, London - New York, 1983).
6. J. W. P. Schmelzer (Ed.), *Nucleation Theory and Applications* (WILEY-VCH, Berlin-Weinheim, 2005).
7. V. P. Skripov and M. Z. Faizullin, *Crystal-Liquid-Gas Phase Transitions and Thermodynamic Similarity* (WILEY-VCH, Berlin-Weinheim, 2006).
8. V. G. Baidakov, *Explosive Boiling of Superheated Cryogenic Liquids* (WILEY-VCH, Berlin-Weinheim, 2007).
9. J. W. Cahn and J. E. Hilliard, J. Chem. Phys. **28**, 258 (1958); **31**, 688 (1959).
10. J. W. Cahn, Acta Met. **8**, 554 (1960).
11. J. W. Gibbs: *On the equilibrium of heterogeneous substances*, Transactions Connecticut Academy of Sciences **3**, 108 (1876); **16**, 343 (1878); J. W. Gibbs, The

- Collected Works, **vol. 1** (Longmans and Green, New York - London - Toronto, 1928).
12. J. D. van der Waals and Ph. Kohnstamm, *Lehrbuch der Thermodynamik* (Johann-Ambrosius-Barth Verlag, Leipzig und Amsterdam, 1908).
  13. J. S. Rowlinson, Translation of J. D. van der Waals' *The thermodynamic theory of capillarity under the hypothesis of a continuous variation of density*, *J. Stat. Phys.* **20**, 197 (1979); German version: J. D. van der Waals, *Z. Phys. Chemie* **13**, 657 (1893).
  14. J. W. P. Schmelzer, A. R. Gokhman, and V. M. Fokin, *J. Colloid Interface Science* **272**, 109 (2004).
  15. J. W. P. Schmelzer, J. Schmelzer Jr., and I. Gutzow, *J. Chem. Phys.* **112**, 3820 (2000).
  16. J. W. P. Schmelzer, A. S. Abyzov, and J. Möller, *J. Chem. Phys.* **121**, 6900 (2004).
  17. J. S. Langer, M. Bar-on, and H. D. Miller, *Phys. Rev. A* **11**, 1417 (1975).
  18. K. Binder: *Spinodal decomposition*. In: J. W. Cahn, P. Haase and R. J. Kramer (Eds.), *Materials Science and Technology*, vol. 5, *Phase Transformations in Materials*, Chapter 7, p. 405 ff (VCH, Weinheim, 1990).
  19. J. S. Langer: *An introduction to the kinetics of first-order phase transition*. In: G. Godreche (Ed.), *Solids far from equilibrium*, Ch. 3, p. 297 ff. (Cambridge University Press, Cambridge, 1992).
  20. K. Binder and D. Stauffer, *Advances in Physics* **25**, 343 (1976).
  21. M. Shah, O. Galkin, and P. G. Vekilov, *J. Chem. Phys.* **121**, 7505 (2004).
  22. J. W. P. Schmelzer, G. Sh. Boltachev, V. G. Baidakov: *Is Gibbs' thermodynamic theory of heterogeneous systems really perfect?* In: [6], pgs. 418-446.
  23. J. W. P. Schmelzer, G. Sh. Boltachev, V. G. Baidakov, *J. Chem. Phys.* **124**, 194502 (2006).
  24. H. Furukawa, *Phys. Rev. A.: Gen. Phys.* **28**, 1729 (1983).

25. H. Ulbricht, J. Schmelzer, R. Mahnke, and F. Schweitzer, *Thermodynamics of Finite Systems and the Kinetics of First-Order Phase Transitions* (Teubner, Leipzig, 1988).
26. J. Schmelzer and F. Schweitzer, *Z. Phys. Chemie (Leipzig)* **266**, 943 (1985); **270**, 5 (1989); **271**, 565 (1990).
27. F. Schweitzer and J. Schmelzer, *Rostocker Physikalische Manuskripte* **10**, 32 (1987); **12**, 61 (1988).
28. L. D. Gelb, K. E. Gubbins, R. Radhakrishnan, and M. Sliwinska-Bartkowiak, *Rep. Prog. Phys.* **62**, 1573 (1999).
29. D. Reguera and H. Reiss, *J. Chem. Phys.* **119**, 1533 (2003).
30. A. S. Shirinyan and A. M. Gusak, *Phil. Mag. A* **84**, 579 (2004).
31. A. V. Neimark and A. Vishnyakov, *J. Phys. Chem. B* **109**, 5962 (2005); **110**, 9403 (2006).
32. J. Schmelzer and H. Ulbricht, *J. Colloid Interface Science* **117**, 325 (1987); **128**, 104 (1989).
33. J. Schmelzer, *Phys. Stat. Solidi B* **161**, 123 (1990).
34. J. Schmelzer and I. Gutzow, *Z. Phys. Chemie (Leipzig)* **269**, 753 (1988).
35. J. Schmelzer, R. Pascova, and I. Gutzow, *Phys. Stat. Solidi A* **117**, 363 (1990).
36. R. Becker, *Ann. Phys.* **32**, 128 (1938).
37. I. M. Lifshitz and V. V. Slezov, *J. Phys. Chem. Solids* **19**, 35 (1961) and references cited therein.
38. J. W. Christian, in: R. W. Cahn (Ed.): *Physical Metallurgy* (North-Holland Publishers, Amsterdam, 1965, pgs. 227-346).
39. H. Trinkaus, *Phys. Rev. B* **27**, 7372 (1983).
40. M. Roskosz, M. J. Toplis, P. Besson, and P. Richet, *J. Non-Crystalline Solids* **351**, 1266 (2005).

41. M. Roskosz, M. J. Toplis, and P. Richet, *J. Non-Crystalline Solids* **352**, 180 (2006).
42. J. W. P. Schmelzer and A. S. Abyzov: *Generalized Gibbs' Thermodynamic Analysis of Cluster Formation in Confined Systems: General Results*, in preparation.
43. R. Kubo, *Thermodynamics* (North Holland, Amsterdam, 1968).
44. N. S. Andreev, G. G. Boiko, and N. A. Bokov, *J. Non-Cryst. Solids* **5**, 41 (1970).

## 2.7. Висновки до розділу 2

Результати досліджень, представлених у даному розділі, опубліковано в статті [2] (Додаток А. Список публікацій здобувача за темою дисертації). Серед основних результатів у якості висновків можна виділити наступні:

- Показано, що в узагальненому методі Гіббса з процеси нуклеації, починаючи з термодинамічно метастабільних початкових станів, протікають якісно значною мірою аналогічно процесу утворення нової фази за механізмом спінодального розпаду. Ця схожість особливо помітна, якщо розглядати *нестабільну* систему малого розміру. У цьому випадку еволюція системи починається за механізмом спінодального розпаду, але через зростання кластерів пересичення зменшується, система стає метастабільною. Нарешті, пересичення зменшується настільки, що розчинення кластерів з меншими розмірами стає необхідною умовою для зростання кластерів більшого розміру, і починається стадія коалесценції.

- Таким чином, узагальнений підхід Гіббса дозволяє описати еволюцію системи від спінодального розпаду до стадії коалесценції.

## РОЗДІЛ 3

### ЕВОЛЮЦІЯ РОЗПОДІЛУ КЛАСТЕРІВ ЗА РОЗМІРОМ У ПРОЦЕСАХ ЗАРОДЖЕННЯ-ЗРОСТАННЯ ТА СПІНОДАЛЬНОГО РОЗПАДУ В РЕГУЛЯРНОМУ РОЗЧИНІ

У першому та другому розділах аналіз процесу нуклеації було проведено методом найшвидшого спуску на гіперповерхні термодинамічного потенціалу, який дає тільки основний шлях еволюції кластера нової фази за розміром та складом. У третьому розділі проведено більш детальний аналіз за допомогою чисельного моделювання на основі кінетичної теорії нуклеації, термодинаміка формування кластерів аналізується на основі узагальненого методу Гіббса для моделі регулярного бінарного розчину. Проаналізована еволюція функції розподілу кластерів за розміром та складом як для метастабільних (нуклеація), так і для нестабільних (спінодальний розпад) початкових станів.

Journal of Non-Crystalline Solids 356 (2010) 2915–2922

#### Evolution of cluster size-distributions in nucleation-growth and spinodal decomposition processes in a regular solution

Alexander S. Abyzov<sup>a</sup>, Jörn W. P. Schmelzer<sup>b</sup>, Andriy A. Kovalchuk<sup>c</sup>,  
and Vitaly V. Slezov<sup>a</sup>

<sup>a</sup>National Science Center Kharkov Institute of Physics and Technology, Academician Street 1, 61108 Kharkov, Ukraine

<sup>b</sup>Institut für Physik der Universität Rostock, Universitätsplatz, 18051 Rostock, Germany

<sup>c</sup>B. Khmelnytsky National University, Department of Physics, 18031 Cherkasy, Ukraine

*Article history:*

Received 14 October 2009

Received in revised form 5 January 2010

*Keywords:*

Nucleation;

Spinodal decomposition;

Crystallization;

Melting

## ABSTRACT

Nucleation-growth and spinodal decomposition processes are two of the basic mechanisms first-order phase transitions – like condensation and boiling, segregation or crystallization and melting – may proceed. Their adequate theoretical description is essential in order to understand the basic mechanisms of self-structuring of matter at nano-scale dimensions. The basic features of evolution of cluster size-distribution are discussed in detail both for meta-stable (nucleation) and unstable (spinodal decomposition) initial states for a simple model of a binary mixture. The results are obtained by the numerical solution of a set of kinetic equations where the thermodynamics of cluster formation is formulated based on the generalized Gibbs' method. It is shown, that nucleation will not proceed, in general (especially in meta-stable initial states near to the spinodal curve), via the saddle point but in trajectories of evolution by-passing the saddle point. For systems in unstable initial states, spinodal decomposition can proceed similarly to nucleation forming clusters evolving to the new phase via the ridge of the thermodynamic potential hyper-surface. ©2010 Elsevier B.V. All rights reserved.

### 3.1. Introduction

In the preceding analysis of nucleation-growth processes in solutions performed by us [1–4], we always assumed, as it is generally done, that the flux of the clusters to the new phase passes the saddle point of the characteristic thermodynamic potential. Such scenario can be considered as appropriate for initial states near to the binodal curve, where the thermodynamic barrier to nucleation is relatively high and in the mean part of the meta-stable region, where the thermodynamic barrier is relatively low, but the critical radius is small as well. But near to the spinodal curve, the

thermodynamic barrier is low, the critical radius (computed via the generalized Gibbs approach or density functional computations) grows, again, and in order to evolve into the new phase via the saddle point very large clusters have to be formed. Such kind of evolution path is unfavorable from a kinetic point of view. In such situations, not the thermodynamic but the kinetic factors will govern the process, and the main flux to the new phase passes not the saddle but some ridge point of the thermodynamic potential, which corresponds to the smaller size of cluster. Such suggestion was formulated by us also in the already cited references [1–4] following earlier suggestions by other authors [5–11]. Here we will analyze these peculiarities in detail by solving directly a set of kinetic equations governing nucleation and growth processes employing the generalized Gibbs' approach for the description of the properties of sub-, critical and super-critical clusters.

### 3.2. Model system

We consider kinetic aspects of new phase formation in a binary solid or liquid solution. Since here we are mainly interested in the discussion of the basic principles and consequences of the newly developed generalized Gibbs' approach in application to phase separation, the solution is considered as a regular one representing one of the simplest models of a system consisting of two kinds of interacting molecules.

Cluster formation in a binary solution results from a redistribution of molecules. Following Gibbs' model approach, we consider a cluster as a spatially homogeneous part of the domain volume with a composition different from the ambient phase. Both size and composition of the cluster may vary in a wide range. As the dividing surface, separating the cluster from the ambient phase, in the thermodynamic description underlying the method of analysis, we always employ here the surface of tension [12–14]. In line with the basic assumptions underlying the model of regular solutions [15] and for simplicity of the notations, the volume per particle,  $\omega$ , is assumed to be

the same for both components and independent of composition ( $\omega_\alpha = \omega_\beta \equiv \omega$ , the subscript  $\alpha$  specifying the cluster, and  $\beta$ , the parameters of the ambient phase). Cluster radius,  $R$ , and particle number in a cluster,  $n_\alpha$ , are related then by the following simple expression

$$\frac{4\pi}{3}R^3 = n_\alpha\omega . \quad (3.1)$$

The change of the Gibbs free energy,  $\Delta G$ , connected with the formation of one cluster in the initially homogeneous ambient phase can be written in a commonly good approximation as [2, 16, 17]

$$\Delta G = \sigma A + \sum_j n_j (\mu_{j\alpha} - \mu_{j\beta}) . \quad (3.2)$$

The first term in the right hand side of Eq. (3.2) reflects cluster surface effects ( $\sigma$  is the interfacial tension, and  $A$  is the surface area of the cluster) and the second term cluster bulk contributions to the change of the Gibbs' free energy,  $n_j$  are the numbers of particles of the different components in the cluster,  $n_\alpha = n_1 + n_2$  (the subscript  $\alpha$  is omitted for  $n_1$  and  $n_2$  for convenience of the notations).

For binary regular solutions, the chemical potentials of the different components in the cluster,  $\mu_{j\alpha}$ , and ambient solution,  $\mu_{j\beta}$ , are given by [15]

$$\begin{aligned} \mu_{1\alpha} &= \mu_{1\alpha}^* + k_B T \ln(1 - x_\alpha) + \Omega x_\alpha^2 , \\ \mu_{2\alpha} &= \mu_{2\alpha}^* + k_B T \ln x_\alpha + \Omega (1 - x_\alpha)^2 , \\ \mu_{1\beta} &= \mu_{1\beta}^* + k_B T \ln(1 - x) + \Omega x^2 , \\ \mu_{2\beta} &= \mu_{2\beta}^* + k_B T \ln x + \Omega (1 - x)^2 , \end{aligned} \quad (3.3)$$

where  $k_B$  is the Boltzmann constant,  $T$  the absolute temperature,  $x_\alpha$  and  $x$  are the molar fractions of the second component in the cluster and the ambient phase,

respectively,

$$x_\alpha = \frac{n_2}{n_1 + n_2},$$

and  $\Omega$  is an interaction parameter describing specific properties of the considered system. The parameter,  $\Omega$ , can be expressed via the critical temperature,  $T_c$ , of the system (cf. also Fig. 3.1) as

$$T_c = \frac{\Omega}{2k_B}. \quad (3.4)$$

The surface tension between two macroscopic phases with compositions  $x_\alpha$  and  $x$ , respectively, is given, according to Becker ([15], see also [18]) by

$$\sigma = \tilde{\sigma} (x_\alpha - x)^2. \quad (3.5)$$

From Eqs. (3.2) – (3.5) we have

$$\frac{\Delta G(n_\alpha, x_\alpha)}{k_B T} = \frac{3}{2} n_\sigma^{1/3} n_\alpha^{2/3} (x_\alpha - x)^2 + n_\alpha f(x, x_\alpha), \quad (3.6)$$

where

$$f(x, x_\alpha) = (1 - x_\alpha) \left\{ \ln \frac{1 - x_\alpha}{1 - x} + 2 \frac{T_c}{T} (x_\alpha^2 - x^2) \right\} \\ + x_\alpha \left\{ \ln \frac{x_\alpha}{x} + 2 \frac{T_c}{T} [(1 - x_\alpha)^2 - (1 - x)^2] \right\} \quad (3.7)$$

holds and the scaling parameter,  $n_\sigma$ , for the particle number in the cluster is specified

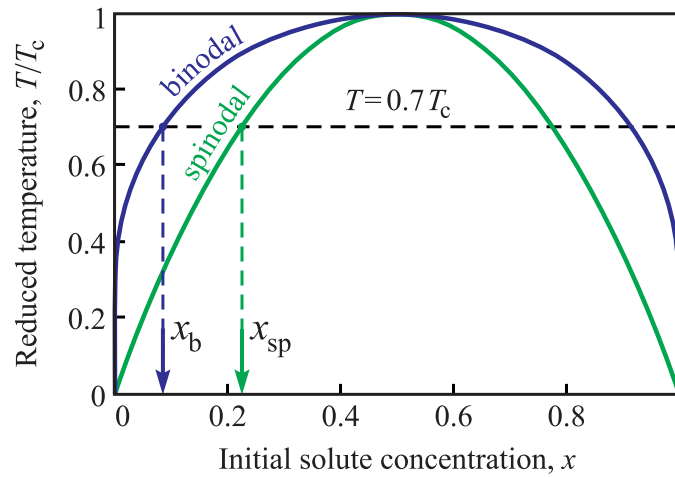


Fig. 3.1. Phase diagram of a binary regular solution with binodal and spinodal curves. The spinodal curve separates thermodynamically stable from thermodynamically unstable states of the homogeneous ambient phase. In the present analysis, we assume that the temperature is equal to  $T = 0.7T_c$  and vary the driving force of the phase transformation process by changing the initial composition of the ambient phase,  $x$ .

as

$$n_\sigma^{1/3} = \frac{2\tilde{\sigma}}{k_B T} \left( \frac{4\pi}{3} \right)^{1/3} \omega^{2/3} . \tag{3.8}$$

In addition, we introduce via Eqs. (3.1) and (3.8) also a scaling parameter,  $R_\sigma$ , for the cluster radius as

$$R_\sigma = \left( \frac{3n_\sigma\omega}{4\pi} \right)^{1/3} = \frac{2\tilde{\sigma}\omega}{k_B T} . \tag{3.9}$$

In the further analysis, we will always assume for an illustration of the results that the temperature in the system is equal to  $T = 0.7T_c$ . The concentration of the solute in the initially homogeneous system is varied in the range from  $x = x_b \cong 0.086$  (left branch of the binodal curve) to  $x = x_{sp} \cong 0.226$  (left branch of the spinodal curve) covering meta-stable initial states and  $x_{sp} < x \leq 0.5$  covering unstable initial states (see Fig. 3.1). Since the phase diagram of a regular solution is symmetric, we may restrict the analysis to initial states in the considered range

with initial concentrations,  $x \leq 0.5$ . A specification of further parameters like  $\tilde{\sigma}$  and  $\omega$  is not required, since we compute reduced characteristics, so that such system parameters enter the description only via the scaling quantities (see also [2]).

Above given equations allow us to determine the thermodynamic potential surface as a function of the number of particles,  $n_1$  and  $n_2$ , in the cluster. The results are shown for different values of the initial supersaturation in Fig. 3.2 both for meta-stable ((a)  $x = 0.17$ ) and unstable ((b)  $x = 0.3$ ) initial states. As far as we are interested mainly in the demonstration of the basic qualitative features, in Fig. 3.2 and similar ones, the numbers are omitted at the axes.

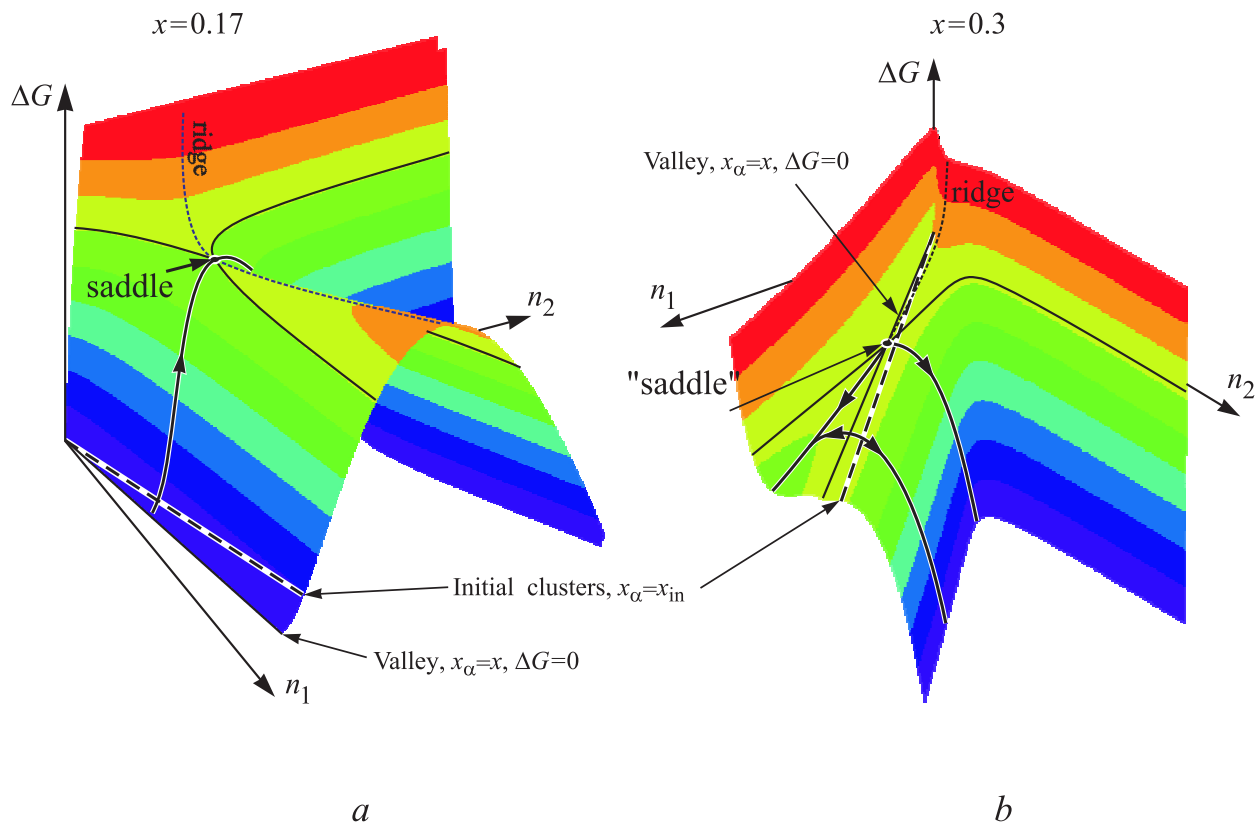


Fig. 3.2. Shape of the Gibbs free energy surface for meta-stable ( $x = 0.17$ , Fig. 3.2a) and unstable initial states ( $x = 0.3$ , Fig. 3.2b). As mentioned, the temperature is chosen equal to  $T/T_c = 0.7$  (for further details, see text).

For each of the meta-stable initial states, the thermodynamic potential surface has, in the vicinity of the critical cluster coordinates, a typical saddle-shape. The

position of this saddle-point is determined by the set of equations

$$\frac{\partial \Delta G(n_1, n_2)}{\partial n_1} = 0, \quad \frac{\partial \Delta G(n_1, n_2)}{\partial n_2} = 0. \quad (3.10)$$

In order to allow us a better understanding of the shape of the thermodynamic potential surface, contour lines through the saddle are included in the figures by full curves and the ridge position by dashed curves. The thick full curve with arrows describes the most probable trajectory of cluster evolution. It starts at some point along the dashed curve determined by the initial conditions  $x_\alpha = x_{in}$  (in the initial state the composition of the cluster is different from the ambient phase,  $x_{in} > x$ , the detailed explanation see below). Then it passes the saddle point and follows further the trajectory of macroscopic growth with an initial cluster size slightly above the critical size. As discussed in detail in [2], the trajectory of evolution from the initial state to the saddle point can be assumed to coincide, in general, with the path of cluster dissolution starting with initial states slightly below the critical cluster size. The most probable trajectory of evolution is determined thus for both regions by the macroscopic growth equations. For segregation in solutions, these equations can be written in the form

$$\frac{dn_1}{dt} = -D_1(1 - x_\beta)\Theta(n_1, n_2)\frac{d\Delta G}{dn_1}, \quad (3.11)$$

$$(3.12)$$

$$\frac{dn_2}{dt} = -D_2x\Theta(n_1, n_2)\frac{d\Delta G}{dn_2},$$

where  $D_1$  and  $D_2$  are the partial diffusion coefficients of the different components in the ambient phase, and the notation

$$\Theta(n_1, n_2) = \Theta_0 n_\alpha^\kappa \quad (3.13)$$

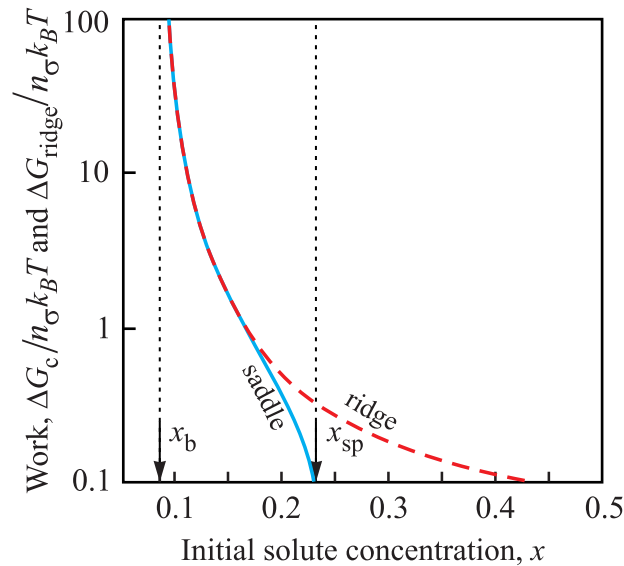


Fig. 3.3. Dependence of the minimum work of critical cluster formation,  $\Delta G_c / (n_\sigma k_B T)$ , and the minimum work of ridge cluster formation,  $\Delta G_{ridge} / (n_\sigma k_B T)$ , on the initial solute concentration,  $x$ .

is employed. The parameter  $\kappa$  has the value  $\kappa = 2/3$  for kinetic-limited growth, and  $\kappa = 1/3$  for diffusion-limited growth and  $\Theta_0$  is a parameter depending only on temperature (we set, as mentioned, the temperature equal to  $T = 0.7T_c$ ). As evident from above considerations and the structure of Eqs. (3.11), the path of cluster evolution depends on the partial diffusion coefficients of both components of the solution (see for the details [18]), however, qualitatively the picture remains always the same. On Fig. 3.2, the trajectories are shown for  $D_1 = D_2$ .

The analysis of Eqs. (3.10) shows [2, 16, 17] that the work of critical cluster formation decreases monotonically with increasing supersaturation and tends to zero at the spinodal curve (see Fig. 3.3, solid curve). The dependence of the critical cluster size,  $R_c$ , on supersaturation is illustrated in Fig. 3.4 (solid curve). We can see, that - computed in terms of the generalized Gibbs approach - near the spinodal curve the critical radius increases, and in order to evolve into the new phase via the saddle point very large clusters have to be formed which is unfavorable from a kinetic point of view. In such situations, we can predict, that not the thermodynamic but kinetic factors will govern the process, and the main flux to the new phase passes not the

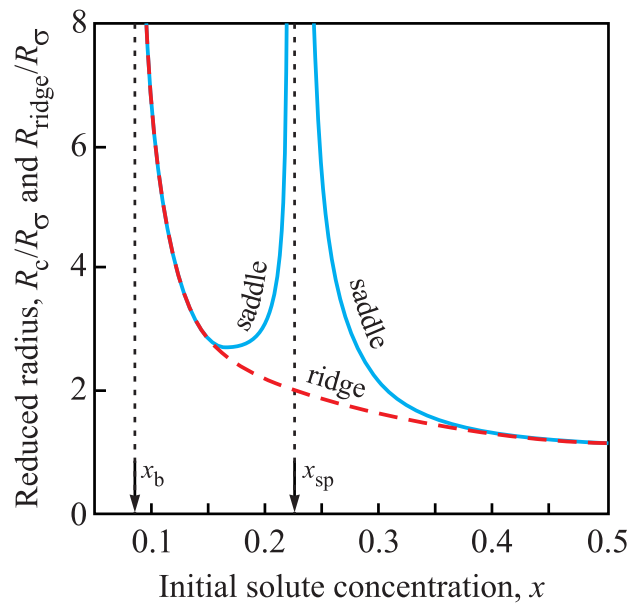


Fig. 3.4. Dependence of the critical cluster radius,  $R_c/R_\sigma$  (solid curve) and ridge crossing radius,  $R_{ridge}$  (dashed curve), on the initial solute concentration,  $x$ , for phase formation at meta-stable ( $x_b < x < x_{sp}$ ) and unstable ( $x > x_{sp}$ ) initial states of the ambient solution.

saddle but some ridge point of the thermodynamic potential, which corresponds to smaller sizes of the cluster. This expectation will be confirmed by the results of the numerical computations.

Having at our disposal the expression for the thermodynamic potential, we can now formulate the set (for any possible values of  $n_1$  and  $n_2$ ) of equations, which defines the evolution of the distribution function of clusters,  $f(n_1, n_2)$ :

$$\begin{aligned} \frac{\partial f(n_1, n_2)}{\partial t} = & \quad (3.14) \\ & = \omega_1^-(n_1 + 1, n_2) f(n_1 + 1, n_2) + \omega_1^+(n_1 - 1, n_2) f(n_1 - 1, n_2) + \\ & + \omega_2^-(n_1, n_2 + 1) f(n_1, n_2 + 1) + \omega_2^+(n_1, n_2 - 1) f(n_1, n_2 - 1) - \\ & - [\omega_1^+(n_1, n_2) + \omega_1^-(n_1, n_2) + \omega_2^+(n_1, n_2) + \omega_2^-(n_1, n_2)] f(n_1, n_2) . \end{aligned}$$

Here the kinetic coefficients  $\omega_{1(2)}^+$  have the meaning of the probability of incorporation into the cluster of atom of sort 1(2), and  $\omega_{1(2)}^-$  the probability of emission. These

kinetic coefficients are given by

$$\frac{\omega_1^-(n_1 + 1, n_2)}{\omega_1^+(n_1, n_2)} = \exp \left\{ \frac{\Delta g_1(n_1 + 1, n_2)}{k_B T} \right\}, \quad (3.15)$$

$$\frac{\omega_1^-(n_1, n_2)}{\omega_1^+(n_1, n_2)} = \exp \left\{ \frac{\Delta g_1(n_1, n_2)}{k_B T} \right\}, \quad (3.16)$$

$$\frac{\omega_2^-(n_1, n_2 + 1)}{\omega_2^+(n_1, n_2)} = \exp \left\{ \frac{\Delta g_2(n_1, n_2 + 1)}{k_B T} \right\}, \quad (3.17)$$

$$\frac{\omega_2^-(n_1, n_2)}{\omega_2^+(n_1, n_2)} = \exp \left\{ \frac{\Delta g_2(n_1, n_2)}{k_B T} \right\}, \quad (3.18)$$

$$\omega_1^+(n_1, n_2) = 4\pi D_1(1 - x)\omega^{-2/3}n^{1/3}, \quad (3.19)$$

$$\omega_2^+(n_1, n_2) = 4\pi D_2 x \omega^{-2/3}n^{2/3}, \quad (3.20)$$

where

$$\Delta g_1(n_1 + 1, n_2) = \Delta G(n_1 + 1, n_2) - \Delta G(n_1, n_2), \quad (3.21)$$

$$\Delta g_1(n_1, n_2) = \Delta G(n_1, n_2) - \Delta G(n_1 - 1, n_2), \quad (3.22)$$

$$\Delta g_2(n_1, n_2 + 1) = \Delta G(n_1, n_2 + 1) - \Delta G(n_1, n_2), \quad (3.23)$$

$$\Delta g_2(n_1, n_2) = \Delta G(n_1, n_2) - \Delta G(n_1, n_2 - 1). \quad (3.24)$$

Let us introduce, now, the new reduced variables

$$t' \equiv t \cdot 4\pi \sqrt{D_1 D_2} \omega^{-2/3} n_\sigma^{2/3}, \quad (3.25)$$

$$R' \equiv R/R_\sigma, \quad n'_{1,2} \equiv n_{1,2}/n_\sigma, \quad D'_{1,2} \equiv \frac{D_{1,2}}{\sqrt{D_1 D_2}}, \quad (3.26)$$

where  $R_\sigma$  and  $n_\sigma$  are defined via the Eqs. (3.9) and (3.8), respectively. We will omit the primes for convenience of the notations, and then Eq. (3.15) gets the form

$$\begin{aligned} \frac{\partial f(n_1, n_2)}{\partial t} = & \quad (3.27) \\ & = \omega_1^+(n_1, n_2) \left[ f(n_1 + 1, n_2) \exp \left\{ \frac{\Delta g_1(n_1 + 1, n_2)}{k_B T} \right\} - f(n_1, n_2) \right] \\ & + \omega_2^+(n_1, n_2) \left[ f(n_1, n_2 + 1) \exp \left\{ \frac{\Delta g_2(n_1, n_2 + 1)}{k_B T} \right\} - f(n_1, n_2) \right] \\ & - \omega_1^+(n_1 - 1, n_2) \left[ f(n_1, n_2) \exp \left\{ \frac{\Delta g_1(n_1, n_2)}{k_B T} \right\} - f(n_1 - 1, n_2) \right] \\ & - \omega_2^+(n_1, n_2 - 1) \left[ f(n_1, n_2) \exp \left\{ \frac{\Delta g_2(n_1, n_2)}{k_B T} \right\} - f(n_1, n_2 - 1) \right], \end{aligned}$$

where

$$\omega_1^+(n_1, n_2) = D_1(1 - x)n^{1/3}, \quad \omega_2^+(n_1, n_2) = D_2xn^{1/3}. \quad (3.28)$$

The total flux of clusters in the space  $(n_1, n_2)$  can be written in the form

$$\mathbf{J}(n_1, n_2, t) = \mathbf{J}_r(n_1, n_2, t) + \mathbf{J}_s(n_1, n_2, t), \quad (3.29)$$

where

$$J_{r,i}(n_1, n_2, t) = -\omega_i^+(n_1, n_2) \frac{f(n_1, n_2)}{k_B T} \frac{\partial \Delta G(n_1, n_2)}{\partial n_i} \quad (3.30)$$

is the regular part of the flux ( $i = 1, 2$ ), and

$$J_{s,i}(n_1, n_2, t) = -\omega_i^+(n_1, n_2) \frac{\partial f(n_1, n_2)}{\partial n_i} \quad (3.31)$$

is the fluctuational part of the flux.

Let us note that the formal use of the potential Eq. (3.2) with Eq. (3.28) leads to a non-physical result, that is, the clusters in the space  $(n_1, n_2)$  are floating towards the bigger sizes along the bottom of the valley,  $\Delta G = 0$ , corresponding to the initial concentration  $x$ . Therefore we can formally choose in any place of the initial phase the domain of the corresponding size, and because such “cluster” is not distinguished from the environment its formation work equals zero and therefore all these states are virtual. It is evident that the process of cluster formation can be influenced only by the domains with a concentration which is different from the initial one by some value, which is defined by the structures of the new and the initial phase. For example, if in the domain of the initial phase consisting of 1000 atoms of kind  $A$  one atom is replaced with the atom of kind  $B$  one gets a cluster with the concentration of atoms of kind  $B$ ,  $x_\alpha$ , equal to 0.001, if this domain consists of 50 atoms, one gets the concentration  $x_\alpha = 0.02$ , in the case of 100 atoms  $x_\alpha = 0.1$ . Obviously the first case is physically unrealistic, as opposed to the third and, probably, second cases, so one should put a limit where a cluster starts being considered as different from the environment.

In the further analysis, we set the limit in such a way that the initial cluster has a concentration,  $x_{in}$ , which is by 10% or more different from the initial one. For example, for the concentration of the initial phase  $x = 0.2$  the clusters have then a minimum concentration  $x \geq x_{in} = 0.22$  to be treated as a cluster of the new phase. Such an approach is approximate, because in the general case,  $x_{in}$  depends on the size of the cluster, and also the exact solution of this problem significantly depends on the properties of the specific materials and therefore is not considered in the present work. We do not take into account the fluctuations with  $x_\alpha < x$  as well, because for the case under consideration,  $x < 0.5$ , they will be significant only in the very unstable region, but in such case we need to take into account the law of conservation of matter which is not considered in the present work (we assume that the number of clusters and their sizes are sufficiently small so that the state of the ambient solution is not changed).

### 3.3. Results and discussion

Eq. (3.28) was solved numerically for particle numbers in the cluster in the range  $n_{1,2} = 1, 2, \dots, 100$ , the composition of the initial clusters was chosen as  $n_1(0) = 0, n_2(0) = 2$ , that is  $f(0, 2)|_{t=0} = 10^{10}$  and  $f(n_1, n_2)|_{t=0} = 0$  for  $n_2 \neq 2$ . The distribution function for the different moments of time,  $t = 100, 1000, 3000$ , and  $t > 10000$ , is presented on Figs. 3.5a-d, respectively. The molar fraction of the ambient phase was chosen here to be equal to  $x = 0.17$ , and the diffusion coefficients are supposed to obey the relation  $D_1 = D_2$ .

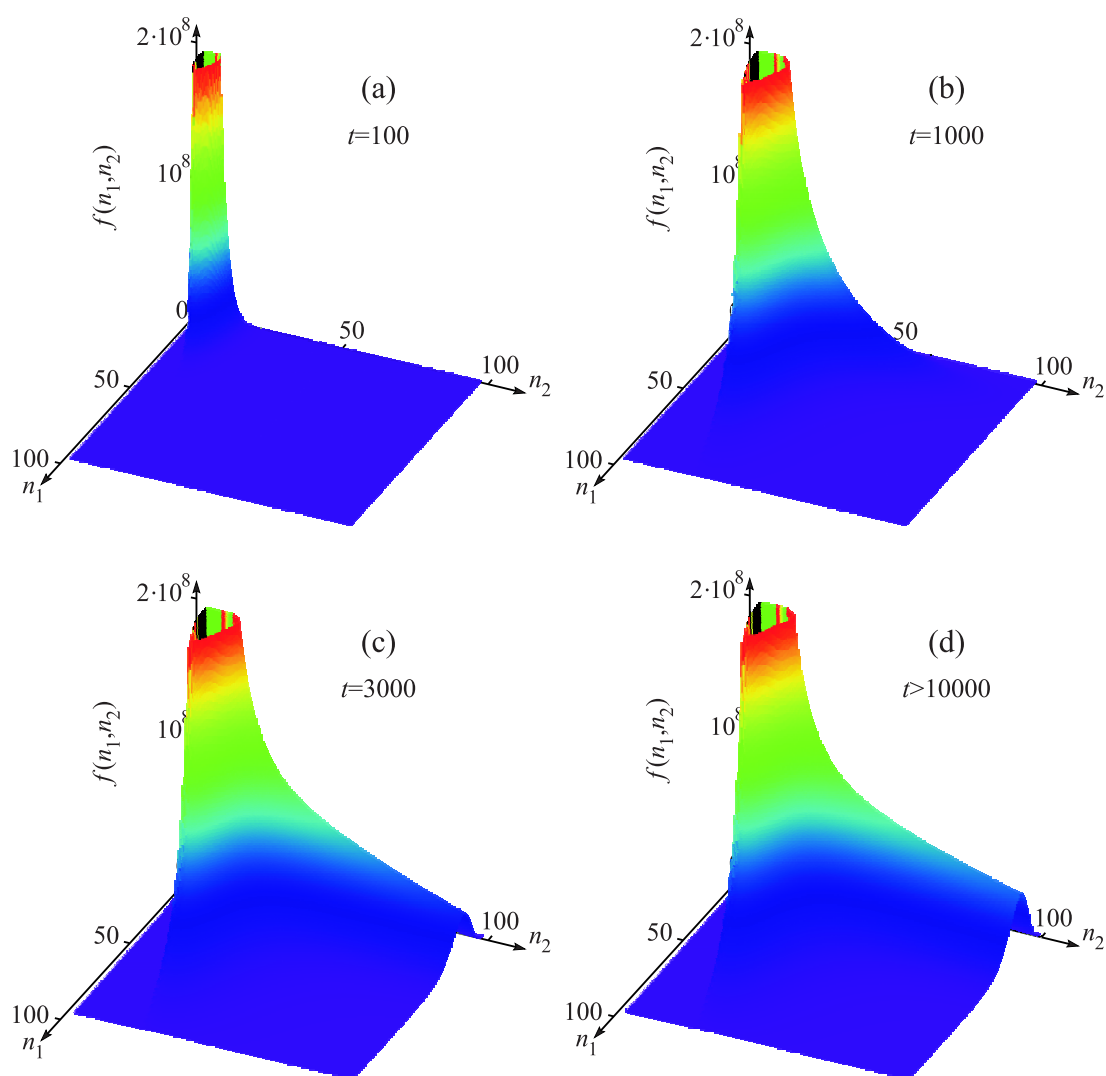


Fig. 3.5. Cluster distribution functions for different moments of time: a)  $t = 100$ , b)  $t = 1000$ , c)  $t = 3000$ , and d)  $t > 10000$ .

In Figs. 3.6a-d, the shape of the Gibbs free energy surface and the path of the cluster evolution is shown in the  $(n_1, n_2)$ -space for the molar fraction of the ambient phase equal to  $x = 0.13, 0.17, 0.21,$  and  $0.25,$  respectively. We set, as mentioned, the temperature equal to  $T = 0.7T_c.$  One can see, that at first the clusters in the

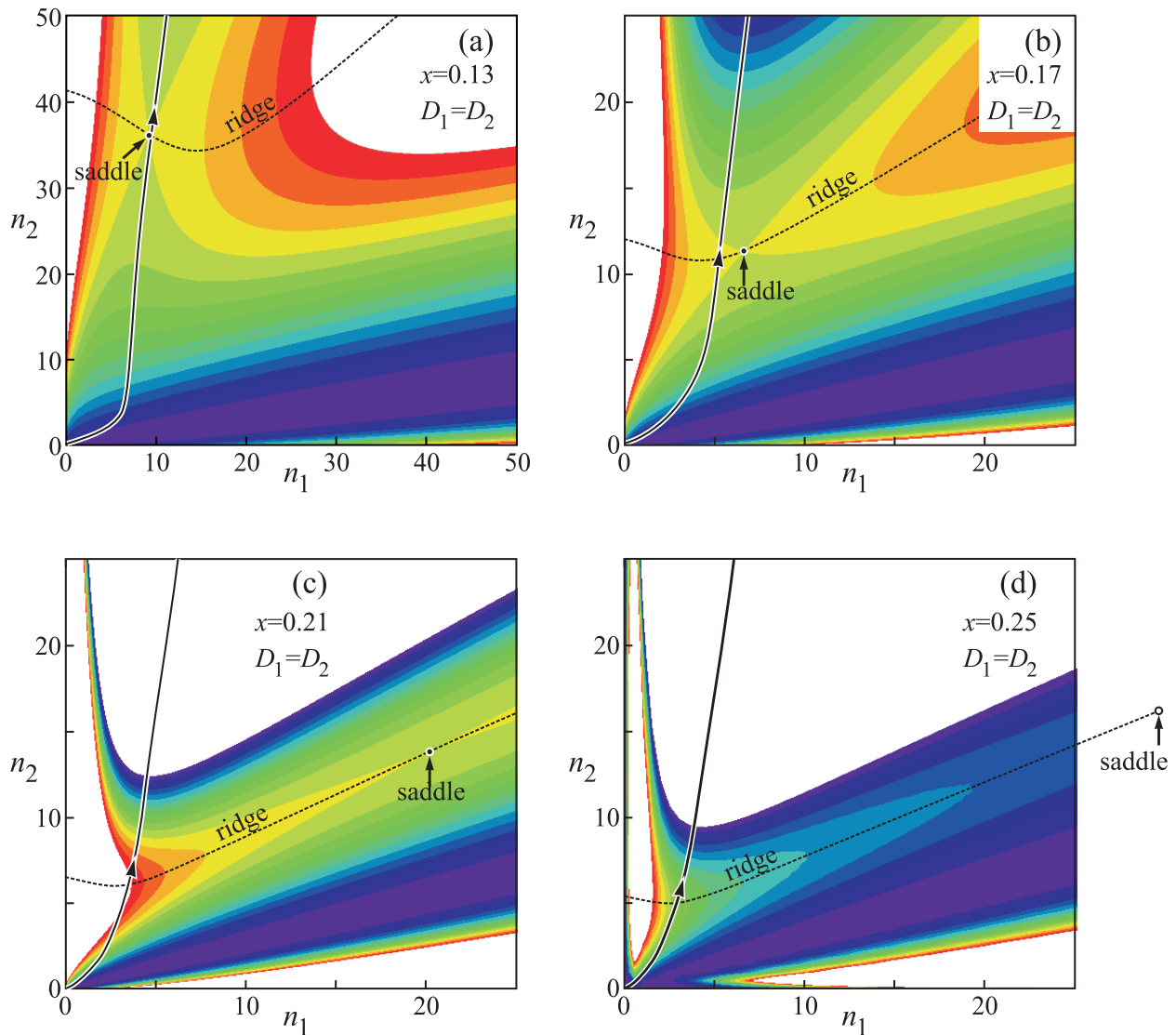


Fig. 3.6. Shape of the Gibbs free energy surface and schematic illustration of the trajectories of evolution for different values of the supersaturation: a)  $x = 0.13,$  b)  $x = 0.17,$  c)  $x = 0.21,$  and d)  $x = 0.25.$  In all cases, we have set here  $D_2 \cong D_1.$

space  $(n_1, n_2)$  are floating towards the bigger sizes along the bottom of the valley, the distribution function has a maximum at  $x \cong x_{in}.$  Such clusters can be considered as homo-phase fluctuations of the initial state. Then the nucleation process starts, and a maximum of the distribution function is formed, which corresponds to the new phase

(hetero-phase fluctuations). As it was mentioned before, we do not take into account here the law of conservation of matter, so after the time  $t \approx 10000$ , the process becomes a steady-state one.

On Fig. 3.6, the dashed line shows the position of the ridge of the Gibbs free energy surface, which is determined from the condition that the regular part of the flux of clusters,  $J_r = (\mathbf{J}_r \mathbf{S})$  ( $\mathbf{J}_r$  is defined by Eq. (3.30),  $\mathbf{S}$  is normal vector to the ridge), equals zero, and the solid line shows the maximum of the full flux of clusters Eq. (3.29). It can be seen, that in the case of small supersaturation ( $x = 0.13$ , Fig. 3.6a), the nucleation goes through the saddle point, but with increasing supersaturation ( $x = 0.17$ , Fig. 3.6b and  $x = 0.21$ , Fig. 3.6c) the point where the flux crosses the ridge (with a radius  $R_{ridge}$ ) more and more deviates from the saddle point, more precisely, the critical radius,  $R_c$ , which corresponds to the saddle point, increases to infinity at  $x = x_{sp}$ , while  $R_{ridge}$  decreases but insignificantly (see also Fig. 3.4, solid and dashed lines correspond to the  $R_c$  and  $R_{ridge}$ , respectively). Ridge crossing as another possible channel of formation of the new phase in the framework of classical nucleation theory has been considered for the first time by Trinkaus [5] and later in [6–11].

Let us note, that for unstable initial states the critical cluster has always a composition equal to the composition of the ambient phase, and the critical cluster corresponds to a cluster size where the state along the line  $x = x_\alpha$  switches from a minimum to a maximum of  $\Delta G$  with respect to variations of the cluster composition at fixed values of the cluster sizes. This critical point of third order differs from the usual saddle point of second order which determines nucleation in the metastable region but fulfils a similar role (for details see [1–4]). For  $R < R_c$ , cluster composition changes lead to the growth of the Gibbs free energy, and the cluster is stable in such region. For  $R > R_c$ , any composition change (both increase and decrease of the cluster concentration) results in a decrease of the Gibbs free energy. In such region, the cluster is unstable and the decomposition proceeds via growth of the concentration

differences, i.e., according to the basic mechanism commonly assigned to spinodal decomposition. Nevertheless, we can see that in the region of weakly unstable initial states ( $x = 0.25$ , Fig. 3.6d), the process evolves via a nucleation scenario passing the ridge of Gibbs free energy surface.

The cross-sections of the distribution function for  $t > 10000$ ,  $x = 0.17$ ,  $D_1 = D_2$  are presented in Figs. 3.7 for the ridge position and different numbers of atoms in the cluster (that is for  $n_1 + n_2 = \text{const.}$ ). One can see, that these cross sections for

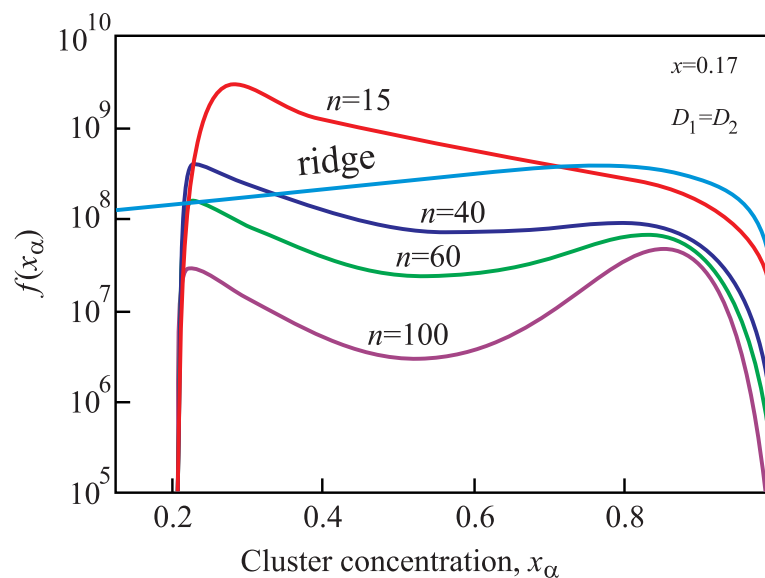


Fig. 3.7. Cross-sections of the distribution function for  $t > 10000$ ,  $x = 0.17$ ,  $D_1 = D_2$  for the ridge position and different number of atoms in the cluster (that is for  $n_1 + n_2 = \text{const.}$ ).

$n = \text{const.}$  have two maxima, the first, at small values of  $n$ , corresponds to homophase fluctuations of the initial state, the second one corresponds to the clusters of the new phase or hetero-phase fluctuations.

In Fig. 3.8 the flux via the ridge in dependence on the size of the ridge position (here expressed via  $n_1$ ) is shown, by a circle the position of the critical cluster is specified. It is evident that the maximum of the flux is located near to the critical cluster size only for relatively small and moderate initial super-saturations. In addition, we can conclude that the transition to the new phase for a moderate entrance into the

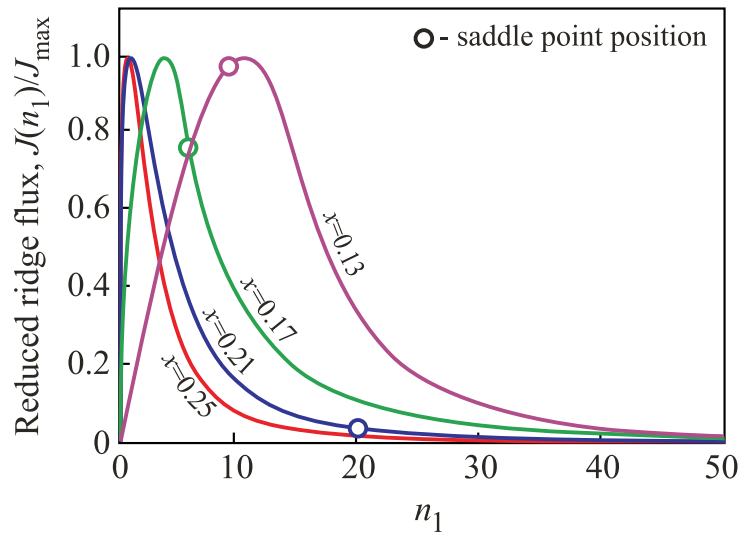


Fig. 3.8. Flux density via the ridge in dependence on the size of the ridge position (here expressed via  $n_1$ ), for different values of the supersaturation:  $x = 0.13$ ,  $x = 0.17$ ,  $x = 0.21$ , and  $x = 0.25$ . By a circle the position of the critical cluster is specified, in all cases, we have set here  $D_1 = D_2$ .

unstable region (which is usually associated with spinodal decomposition) occurs by a similar nucleation scenario. This happens because near to the spinodal curve the characteristic size of the Cahn-Hilliard instability region is large (see e.g. [2, 3, 19] and Fig. 3.4), and it is much easier for the system to overcome the small potential barrier by the nucleation scenario with the cluster of smaller size. Nevertheless this process being activated by its nature has, again, features considered conventionally as specific to spinodal decomposition, namely, during the evolution of the clusters their composition changes significantly.

Finally, in Fig. 3.9 the flux density via the ridge Eq. (3.29) in dependence on size of the ridge position is shown for  $x = 0.17$  and for different values of the  $(D_1/D_2)$ -ratio ( $D_1 D_2 = \text{const.}$ ). The dependence of the maximal value of flux density,  $J_{max}$ , and integral flux,  $J_{int}$ , via the ridge on the  $(D_1/D_2)$ -ratio is shown in Fig. 3.10a; and the dependence of the minimum work of ridge cluster formation,  $\Delta G_{ridge}/(n_\sigma k_B T)$  and the size of the ridge position (here expressed via  $n_{1,r}$ ), on the  $(D_1/D_2)$ -ratio is shown in Fig. 3.10b. Dashed lines show the minimum work of cluster formation and  $n_{1,c}$  is the value for the saddle point. In all cases, we have set

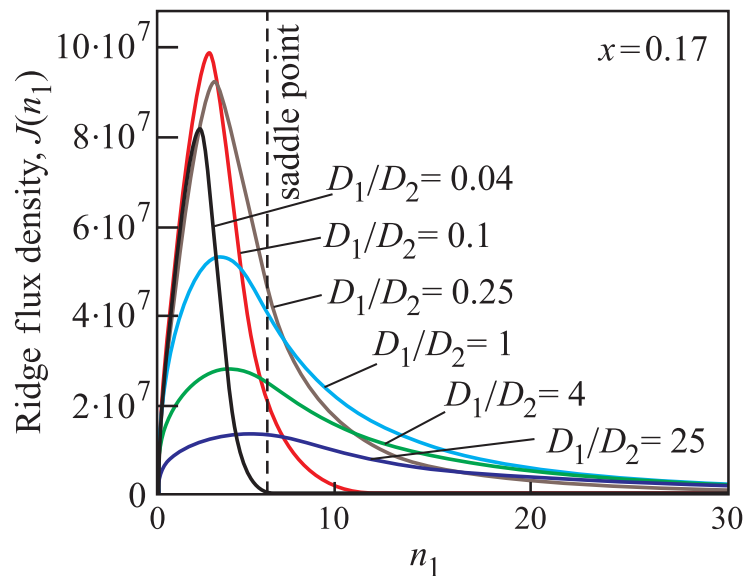


Fig. 3.9. Flux density via the ridge in dependence on the size of the ridge position (here expressed via  $n_1$ ), for different values of the  $(D_1/D_2)$ -ratio and  $x = 0.17$ .

here  $x = 0.17$ . We see, that for large  $(D_1/D_2)$ -ratios the process evolves passing the ridge of Gibbs free energy surface near to the saddle point, but with a decrease of the  $(D_1/D_2)$ -ratio the ridge crossing point,  $(n_{1,r}, n_{2,r})$ , more and more deviates from the saddle point  $(n_{1,c}, n_{2,c})$ , so that  $n_{2,r} \approx n_{2,c}$ , but  $n_{1,r} < n_{1,c}$  and decreases with a decrease of the  $(D_1/D_2)$ -ratio (see Fig. 3.10b). This happens because for a low mobility of the atoms of the first kind it is much easier for the system to overcome the relatively higher potential barrier, but with clusters consisting of a smaller number of particles  $n_1$  (see Fig. 3.10b). The maximal value of flux density,  $J_{max}$ , reaches a maximum at  $D_1/D_2 \approx 0.15$  and the integral flux,  $J_{int}$ , has a maximum at  $D_1/D_2 \approx 0.5$  (see Fig. 3.10a).

The discussed above results are obtained under the assumption that the number of the clusters is small and they do not influence the composition of the initial phase significantly, so the law of conservation of matter is not taken into account explicitly in computing the state of the ambient phase. Therefore, the results can be employed only for the description of the initial stages of the process. This comment is especially important when large super-saturations are considered, i.e., when the fast-growing clusters deplete the surrounding phase. Nevertheless the results obtained in the present

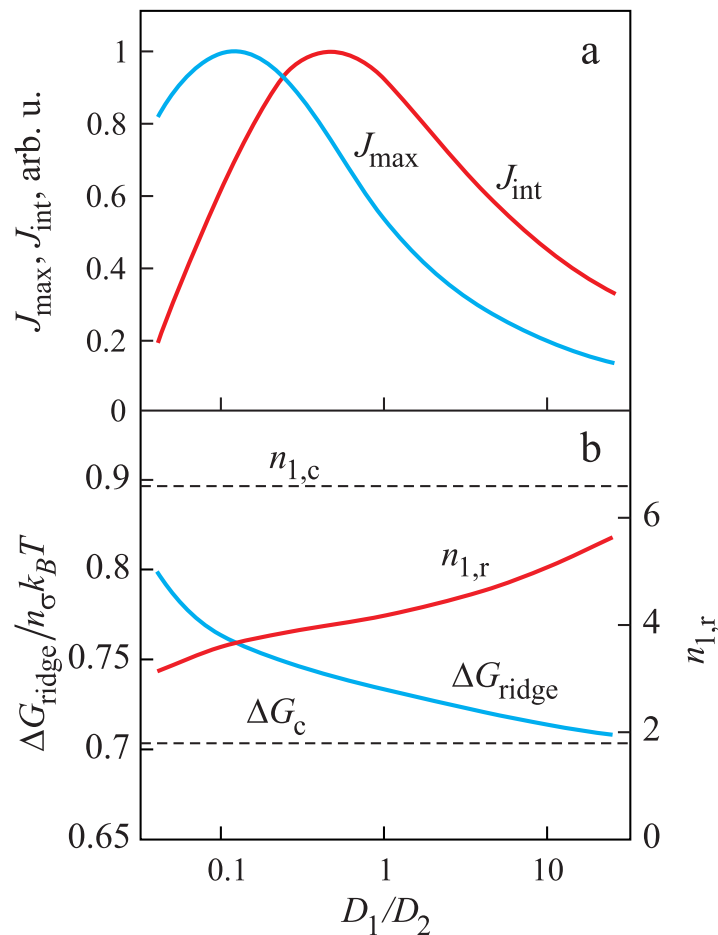


Fig. 3.10. a) Maximal value of flux density,  $J_{max}$ , and total flux,  $J_{tot}$ , via the ridge in dependence on the  $(D_1/D_2)$ -ratio; b) minimum work of ridge cluster formation,  $\Delta G_{ridge}/(n_{\sigma}k_B T)$  and the size of the ridge position (here expressed via  $n_{1,r}$ ), in dependence on the  $(D_1/D_2)$ -ratio. Dashed lines show the minimum work of cluster formation and  $n_{1,c}$  value for the saddle point. In all cases, we have set here  $x = 0.17$ .

work qualitatively agree with the conclusions we have obtained earlier, where it was also shown that taking depletion effect into account leads to the fact that in an unstable region the process may proceed via the common nucleation scenario [3]. Of course, it is more correct to calculate the kinetics of the process together with taking into account from the very beginning the depletion effect. It can also be shown that in such case the cluster distribution as a rule has a bimodal form, where the first maximum corresponds to the fluctuations of the initial phase concentration, and the second one corresponds to the clusters of the new growing phase. Both topics will be addressed in detail in future analyses.

### 3.4. Acknowledgments

The present research is supported by the Ministry of Education and Science of Ukraine (Project M/235-2009) and the International Bureau of the Federal Ministry of Education and Research of Germany (BMBF UKR 08/020). The authors also express their gratitude to the German Academic Exchange Service for the support of collaboration (DAAD Award A/08/01715) and travel grants. One of the authors (J. W. P. Schmelzer) acknowledges the discussions with Dr. Attila R. Imre, Budapest, performed in the framework of the common project EAI-2009/004 financed by the Hungarian Academy of Sciences.

### References

1. J. W. P. Schmelzer, A. R. Gokhman, V. M. Fokin, *J. Colloid Interface Science* **272**, 109 (2004).
2. J. W. P. Schmelzer, A. S. Abyzov, J. Möller, *J. Chem. Phys.* **121**, 6900 (2004).
3. A. S. Abyzov, J. W. P. Schmelzer, *J. Chem. Phys.* **127**, 114504 (2007).
4. J. W. P. Schmelzer and A. S. Abyzov, *J. Engineering Thermophysics* **16**, 119-129 (2007).
5. H. Trinkaus, *Phys. Rev.* **B 27**, 7372 (1983).
6. J.-S. Li, K. Nishioka, and I. L. Maksimov, *Phys. Rev.* **E 58**, 7580 (1998).
7. I. L. Maksimov, K. Nishioka, *Phys. Lett.* **A 264**, 51 (1999).
8. J.-S. Li, I. L. Maksimov, and G. Wilemski *Phys. Rev.* **E 61**, R4710 (2000).
9. I. L. Maksimov, M. Sanada, and K. Nishioka, *J. Chem. Phys.* **113**, 3323 (2000).
10. M. Roskosz, M. J. Toplis, P. Besson, and P. Richet, *J. Non-Crystalline Solids* **351**, 1266 (2005).

11. M. Roskosz, M. J. Toplis, and P. Richet, *J. Non-Crystalline Solids* **352**, 180 (2006).
12. J. W. Gibbs: *On the equilibrium of heterogeneous substances*, *Transactions Connecticut Academy of Sciences* **3**, 108 (1876); **16**, 343 (1878); J. W. Gibbs, *The Collected Works*, **vol. 1** (Longmans and Green, New York - London - Toronto, 1928).
13. J. W. P. Schmelzer, G. Sh. Boltachev, V. G. Baidakov: *Is Gibbs' thermodynamic theory of heterogeneous systems really perfect?* In: J. W. P. Schmelzer (Ed.), *Nucleation Theory and Applications* (WILEY-VCH, Berlin-Weinheim, 2005), pgs. 418-446.
14. J. W. P. Schmelzer, G. Sh. Boltachev, V. G. Baidakov, *J. Chem. Phys.* **124**, 194502 (2006).
15. R. Becker, *Ann. Phys.* **32**, 128 (1938).
16. J. W. P. Schmelzer, J. Schmelzer Jr., and I. Gutzow: *Reconciling Gibbs and van der Waals: a New Approach to Nucleation Theory*. In: *Nucleation Theory and Applications*, Eds.: J. W. P. Schmelzer, G. Röpke, V. B. Priezhev (JINR, Dubna, 1999), pgs. 237-267.
17. J. W. P. Schmelzer, J. Schmelzer Jr., and I. Gutzow, *J. Chem. Phys.* **112**, 3820 (2000).
18. J. W. Christian, in: R. W. Cahn (Ed.): *Physical Metallurgy* (North-Holland Publishers, Amsterdam, 1965, pgs. 227-346).
19. K. Binder, *Rep. Prog. Phys.* **90**, 783 (1987).

### 3.5. Висновки до розділу 3

Результати досліджень, представлених у даному розділі, опубліковано в статті [3] (Додаток А. Список публікацій здобувача за темою дисертації). Серед

основних результатів у якості висновків можна виділити наступні:

- Проведено детальний аналіз процесу нуклеації нової фази з за допомогою чисельного моделювання на основі кластерної динаміки, термодинаміка формування кластерів аналізується на основі узагальненого методу Гіббса для моделі регулярного бінарного розчину.
- Проаналізована еволюція функції розподілу кластерів за розміром та складом як для метастабільних (нуклеація), так і для нестабільних (спінодальний розпад) початкових станів.
- Проведено порівняння швидкості нуклеації основі узагальненого методу Гіббса і для класичної теорії. Показано, що вихід на квазістаціонарний режим нуклеації в узагальненому підході Гіббса відбувається повільніше, ніж в класичному випадку, але швидкість нуклеації помітно вище.
- Розраховано потік кластерів нової фази в просторі розмірів, показано, що у нестабільних початкових станах поблизу *класичної спінодалі* максимум потоку може проходити через гребінь гіперповерхні термодинамічного потенціалу, тобто утворення фаз може протікати через *активаційний бар'єр*, незважаючи на те, що у цьому випадку значення роботи формування критичного кластера, що відповідає сідловій точці термодинамічного потенціалу, дорівнює нулю.

## РОЗДІЛ 4

**КІНЕТИКА ПРОЦЕСІВ СЕГРЕГАЦІЇ У РОЗЧИНАХ: ЕВОЛЮЦІЯ  
ЧЕРЕЗ СІДЛОВУ ТОЧКУ АБО ЧЕРЕЗ ГРЕБІНЬ  
ТЕРМОДИНАМІЧНОГО ПОТЕНЦІАЛУ**

У четвертому розділі за допомогою чисельного моделювання на основі кластерної динаміки у бінарному регулярному розчині визначається найбільш вірогідний потік кластерів нової фази в просторі розмірів залежно від початкового пересичення.

Journal of Non-Crystalline Solids 384 (2014) 8–14

**Kinetics of segregation processes in solutions: Saddle point versus ridge crossing of the thermodynamic potential barrier**

Alexander S. Abyzov<sup>a</sup>, Jörn W. P. Schmelzer<sup>b</sup>

<sup>a</sup>*National Science Center Kharkov Institute of Physics and Technology, Academician Street 1, 61108 Kharkov, Ukraine*

<sup>b</sup>*Institut für Physik der Universität Rostock, Universitätsplatz, 18051 Rostock, Germany*

*Article history:*

Received 22 November 2012

Received in revised form 7 April 2013

*Classification codes:*

80: Crystallization

80.400: Nucleation

*Keywords:*

Nucleation;

General theory and computer simulations of nucleation;

General theory of phase transitions;

Thermodynamics of nucleation

**ABSTRACT**

Based on the solution of the set of kinetic equations, describing nucleation and growth in solutions, the most probable path of evolution of the cluster ensemble in nucleation and growth processes is specified in dependence on the initial supersaturation. Hereby, on one side, the classical Gibbs' approach is employed for the description of the thermodynamic properties of the

system (utilizing the capillarity approximation). As an alternative method, the classical Gibbs' method of description is replaced by the generalized Gibbs' approach. It is shown that significant deviations from the saddle point trajectory of evolution are found only if in the thermodynamics of cluster evolution the generalized Gibbs' approach is employed allowing one to account for and to determine changes of the state of the clusters in dependence on supersaturation and cluster size. In addition, the basic origin for the deviation of the most probable path of evolution from the path via the saddle point of the thermodynamic potential surface is specified.

©2013 Elsevier B.V. All rights reserved.

#### **4.1. Introduction**

In the analysis of nucleation-growth processes in glass-forming melts, it is commonly assumed that nucleation processes proceed along a trajectory passing the maximum or, more generally, the saddle point of the thermodynamic potential surface [1, 2]. Hereby the properties of the critical clusters are identified as a rule with the properties of the newly evolving macroscopic phases in line with Gibbs' classical theory of heterogeneous systems [3]. Extending Gibbs' classical theory to the description of heterogeneous systems in non-equilibrium states (for an overview, c.f. [4]), we have re-analyzed in two recent publications the process of segregation in solutions from thermodynamic [5] and kinetic [6] points of view by analytical methods and by solving numerically the set of kinetic equations describing nucleation and growth processes. Following earlier suggestions by other authors [7–13] it was shown, in particular, that for sufficiently large supersaturation the transition to the newly evolving phase does not proceed via the saddle but via a ridge of the thermodynamic potential barrier and that such switch in the choice of the preferential path of evolution to the new phase is of much more significance if the generalized Gibbs' approach is employed for the thermodynamic description of the cluster

ensemble evolving in the ambient solution.

This analysis is continued and developed in more detail in the present paper. Based on the solution of the set of kinetic equations, describing nucleation and growth in solutions, the most probable path of evolution is specified in dependence on the initial supersaturation (i.) if on one side the classical Gibbs’ approach is employed for the description of the thermodynamic properties of the system (utilizing the capillarity approximation), and on the other side, (ii.) if the classical Gibbs’ is replaced by the generalized Gibbs’ approach. In addition, (iii.) the basic origin for the deviation of the most probable path of evolution from the path via the saddle point is specified. The starting point of the analysis and the problem to be analyzed can be described as follows:

The critical cluster size,  $R_c$ , and the work of critical cluster formation,  $\Delta G_c$ , in dependence on the initial solute concentration,  $x$ , in the ambient phase can be represented, according to [5,6], in a form as shown in Fig. 4.1. While in the respective

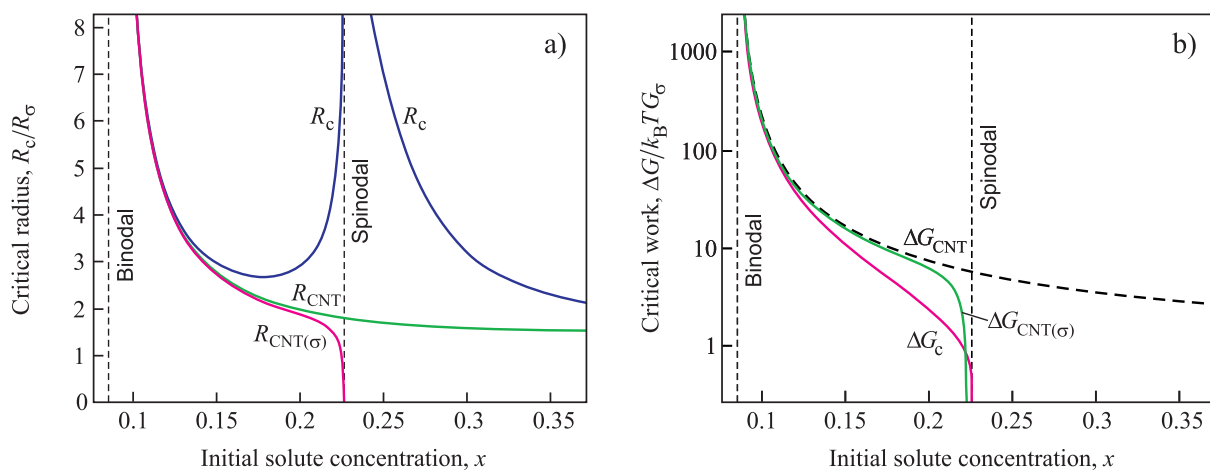


Fig. 4.1. Critical cluster size and work of critical cluster formation according to the classical (employing the capillarity approximations, dashed curve,  $R_{CNT(\sigma_\infty)}$ ,  $\Delta G_{CNT(\sigma_\infty)}$ ) and the generalized (full curve,  $R_c$ ,  $\Delta G_c$ ) Gibbs’ approaches (scaling parameters,  $R_\sigma$  and  $G_\sigma$ , for the cluster radius and the work of critical cluster formation are introduced via Eqs. (4.9) and (4.10)). If in the classical Gibbs’ approach a curvature dependence of the interfacial tension is introduced in such a way that the work of critical cluster formation tends to zero at the spinodal curve, then the critical cluster size approaches zero as well (dashed-dotted curve,  $R_{CNT(\sigma(R))}$ ,  $\Delta G_{CNT(\sigma(R))}$ )

dependencies obtained via the classical Gibbs' approach,  $R_{\text{CNT}(\sigma_\infty)}$  and  $\Delta G_{\text{CNT}(\sigma_\infty)}$ , (employing the capillarity approximation) no peculiarities occur in the vicinity of the spinodal curve, the critical cluster – computed via the generalized Gibbs' approach – diverges here and the work of critical cluster formation tends to zero remaining equal to zero also in the region of unstable initial states. Provided we introduce in the classical Gibbs' approach a curvature dependence of the interfacial tension in such a way that the work of critical cluster formation tends – as it should be the case – to zero at the spinodal, then the critical cluster size tends to zero at the spinodal in such approach as well (c.f. e.g. [14,15]). In the subsequent analysis we will not consider the latter case but employ the capillarity approximation as usually done in the classical theory of nucleation and growth. Note as well that in the framework of the generalized Gibbs' approach – in contrast to the classical Gibbs' method of description – a critical cluster size can be determined also for unstable initial states [5], it corresponds to the lower limit of the size of the region where spontaneous density or composition amplification may be realized according to the Cahn-Hilliard theory [16] of spinodal decomposition. So, the question we would like to address here is: Will the evolution of the system to the new phase proceed via some of the specified saddle points – determined either by the classical or generalized Gibbs' approaches – or will there occur deviations from the saddle-point trajectory of cluster evolution and, if this is the case, why.

In the analysis, we employ the methodology as outlined in detail in [5,6] and for the description of the thermodynamics the model of a binary regular solution. The method and the model are sketched here only briefly. The reader is referred for the respective details to above cited papers.

## 4.2. Brief description of the methodology and the model system

Cluster formation in a binary solution results from a redistribution of molecules in space. Following Gibbs' model approach, we consider a cluster as a spatially homogeneous part of the domain volume with a composition different from the ambient phase. As the dividing surface, separating the cluster from the ambient phase, in the thermodynamic description utilized in the analysis, we always employ here the surface of tension [3, 17]. In line with the basic assumptions underlying the model of binary regular solutions [18, 19] and for simplicity of the notations, the volume per particle,  $\omega$ , is assumed to be the same for both components and independent of composition ( $\omega_\alpha = \omega_\beta \equiv \omega = a^3$ , the subscript  $\alpha$  specifying the cluster, and  $\beta$ , the parameters of the ambient phase,  $a$  is an interatomic distance parameter). Cluster radius,  $R$ , and particle number in a cluster,  $n_\alpha$ , are related then by the following simple expression

$$\frac{4\pi}{3}R^3 = n_\alpha\omega = n_\alpha a^3. \quad (4.1)$$

The change of the Gibbs free energy,  $\Delta G$ , connected with the formation of one cluster in the initially homogeneous ambient phase can be written in a commonly good approximation as [20, 21]

$$\Delta G = \sigma A + \sum_j n_j (\mu_{j\alpha} - \mu_{j\beta}). \quad (4.2)$$

The first term in the right hand side of Eq. (4.2) reflects cluster surface effects ( $\sigma$  is the interfacial tension, and  $A$  is the surface area of the cluster) and the second term cluster bulk contributions to the change of the Gibbs' free energy,  $n_j$  are the numbers of particles of the different components in the cluster,  $n_\alpha = n_1 + n_2$  (the subscript  $\alpha$  is omitted for  $n_1$  and  $n_2$  for convenience of the notations).

For binary regular solutions, the chemical potentials of the different components in the cluster,  $\mu_{j\alpha}$ , and ambient solution,  $\mu_{j\beta}$ , are given by [19]

$$\begin{aligned}\mu_{1\alpha} &= \mu_{1\alpha}^* + k_B T \ln(1 - x_\alpha) + \Omega x_\alpha^2, \\ \mu_{2\alpha} &= \mu_{2\alpha}^* + k_B T \ln x_\alpha + \Omega (1 - x_\alpha)^2, \\ \mu_{1\beta} &= \mu_{1\beta}^* + k_B T \ln(1 - x) + \Omega x^2, \\ \mu_{2\beta} &= \mu_{2\beta}^* + k_B T \ln x + \Omega (1 - x)^2,\end{aligned}\quad (4.3)$$

where  $k_B$  is the Boltzmann constant,  $T$  the absolute temperature,  $x$  and  $x_\alpha = n_2 / (n_1 + n_2)$  are the molar fractions of the second component in the ambient phase and the cluster, respectively,  $\Omega = 2k_B T_c$  is an interaction parameter describing specific properties of the considered system, and  $T_c$  is the critical temperature of the system. The interfacial tension between two macroscopic phases with compositions  $x_\alpha$  and  $x$ , respectively, is given, according to Becker ([18], see also [19]) by

$$\sigma = \tilde{\sigma} (x_\alpha - x)^2. \quad (4.4)$$

From Eqs. (4.2) – (4.4) we have

$$\frac{\Delta G(n_\alpha, x_\alpha)}{k_B T} = \frac{3}{2} n_\sigma^{1/3} n_\alpha^{2/3} (x_\alpha - x)^2 + n_\alpha \psi(x, x_\alpha) + \Delta \psi(n, x, x_\alpha), \quad (4.5)$$

where

$$\begin{aligned}\psi(x, x_\alpha) &= (1 - x_\alpha) \left\{ \ln \frac{1 - x_\alpha}{1 - x} + 2 \frac{T_c}{T} (x_\alpha^2 - x^2) \right\} \\ &+ x_\alpha \left\{ \ln \frac{x_\alpha}{x} + 2 \frac{T_c}{T} [(1 - x_\alpha)^2 - (1 - x)^2] \right\}\end{aligned}\quad (4.6)$$

holds. In Eq. (4.5), a correction term

$$\Delta\psi(n, x, x_\alpha) = \begin{cases} \frac{\delta(n_\alpha - n_m)}{(x_\alpha - x)^2} & \text{for } n_\alpha > n_m, \\ 0 & \text{for } n_\alpha \leq n_m \end{cases} \quad (4.7)$$

is incorporated to remove the virtual clusters, that is the clusters with the same composition,  $x = x_\alpha$ , as the initial solution,  $n_m$  is the number of atoms in one structural unit of the solution (see also [6] for more details). Here the scaling parameter,  $n_\sigma$ , for the particle number in the cluster is specified as

$$n_\sigma^{1/3} = \frac{2\tilde{\sigma}a^2}{k_B T} \left( \frac{4\pi}{3} \right)^{1/3}. \quad (4.8)$$

In addition, we introduce via Eqs. (4.1) and (4.8) also scaling parameters,  $R_\sigma$ , for the cluster radius as

$$R_\sigma = a \left( \frac{3n_\sigma}{4\pi} \right)^{1/3} = a \frac{2\tilde{\sigma}a^2}{k_B T}, \quad (4.9)$$

and for the work of cluster formation,  $G_\sigma$ , as

$$G_\sigma = \frac{16\pi}{3} \left( \frac{\tilde{\sigma}a^2}{k_B T} \right)^3. \quad (4.10)$$

The reduced critical parameters,  $R_c/R_\sigma$ ,  $R_{CNT}/R_\sigma$ , and  $\Delta G_c/k_B T G_\sigma$ ,  $\Delta G_{CNT}/k_B T G_\sigma$ , do not depend on the interfacial tension,  $\sigma$  [21], and we will use these reduced variables ( $R/R_\sigma$  and  $\Delta G/k_B T G_\sigma$ ) for the presentation of our results.

In the analysis, we always assume for an illustration of the results that the temperature in the system is equal to  $T = 0.7T_c$ . The concentration of the solute in the initially homogeneous system is varied in the range from  $x = x_b \cong 0.086$  (left branch of the binodal curve) to  $x = x_{sp} \cong 0.226$  (left branch of the spinodal

curve) covering meta-stable initial states and  $x_{sp} < x \leq 0.5$  covering unstable initial states. Since the phase diagram of a regular solution is symmetric, we may restrict the analysis to initial states in the considered range with initial concentrations,  $x \leq 0.5$ .

Having at our disposal the expression for the thermodynamic potential, we can now formulate the set (for any possible values of  $n_1$  and  $n_2$ ) of equations, which defines the evolution of the distribution function of clusters,  $f(n_1, n_2)$ :

$$\begin{aligned} \frac{\partial f(n_1, n_2)}{\partial t} = & \quad (4.11) \\ & = \omega_1^-(n_1 + 1, n_2) f(n_1 + 1, n_2) + \omega_1^+(n_1 - 1, n_2) f(n_1 - 1, n_2) + \\ & + \omega_2^-(n_1, n_2 + 1) f(n_1, n_2 + 1) + \omega_2^+(n_1, n_2 - 1) f(n_1, n_2 - 1) - \\ & - [\omega_1^+(n_1, n_2) + \omega_1^-(n_1, n_2) + \omega_2^+(n_1, n_2) + \omega_2^-(n_1, n_2)] f(n_1, n_2) . \end{aligned}$$

Here the kinetic coefficients  $\omega_{1(2)}^+$  have the meaning of the probability of incorporation into the cluster of atom of sort 1(2), and  $\omega_{1(2)}^-$  is the probability of emission per unit time. These kinetic coefficients are given by

$$\begin{aligned} \frac{\omega_1^-(n_1 + 1, n_2)}{\omega_1^+(n_1, n_2)} &= \exp \left\{ \frac{\Delta g_1(n_1 + 1, n_2)}{k_B T} \right\} , & (4.12) \\ \frac{\omega_1^-(n_1, n_2)}{\omega_1^+(n_1, n_2)} &= \exp \left\{ \frac{\Delta g_1(n_1, n_2)}{k_B T} \right\} , \\ \frac{\omega_1^-(n_1, n_2)}{\omega_1^+(n_1, n_2)} &= \exp \left\{ \frac{\Delta g_1(n_1, n_2)}{k_B T} \right\} , \\ \frac{\omega_2^-(n_1, n_2)}{\omega_2^+(n_1, n_2)} &= \exp \left\{ \frac{\Delta g_2(n_1, n_2)}{k_B T} \right\} , \end{aligned}$$

$$\begin{aligned} \omega_1^+(n_1, n_2) &= 4\pi D_1(1 - x)a^{-2}n^{1/3} , & (4.13) \\ \omega_2^+(n_1, n_2) &= 4\pi D_2xa^{-2}n^{2/3} , \end{aligned}$$

where

$$\begin{aligned}
\Delta g_1(n_1 + 1, n_2) &= \Delta G(n_1 + 1, n_2) - \Delta G(n_1, n_2) , \\
\Delta g_1(n_1, n_2) &= \Delta G(n_1, n_2) - \Delta G(n_1 - 1, n_2) , \\
\Delta g_2(n_1, n_2 + 1) &= \Delta G(n_1, n_2 + 1) - \Delta G(n_1, n_2) , \\
\Delta g_2(n_1, n_2) &= \Delta G(n_1, n_2) - \Delta G(n_1, n_2 - 1) .
\end{aligned} \tag{4.14}$$

Let us introduce, now, the a dimensionless time scale via

$$t' \equiv t \frac{4\pi\sqrt{D_1 D_2}}{a^2} , \tag{4.15}$$

and dimensionless diffusivities as

$$D'_{1,2} \equiv \frac{D_{1,2}}{\sqrt{D_1 D_2}} . \tag{4.16}$$

We will omit further the primes for convenience of the notations, and then Eq. (4.12) gets the form

$$\begin{aligned}
\frac{\partial f(n_1, n_2)}{\partial t} &= \\
&= \omega_1^+(n_1, n_2) \left[ f(n_1 + 1, n_2) \exp \left\{ \frac{\Delta g_1(n_1 + 1, n_2)}{k_B T} \right\} - f(n_1, n_2) \right] \\
&+ \omega_2^+(n_1, n_2) \left[ f(n_1, n_2 + 1) \exp \left\{ \frac{\Delta g_2(n_1, n_2 + 1)}{k_B T} \right\} - f(n_1, n_2) \right] \\
&- \omega_1^+(n_1 - 1, n_2) \left[ f(n_1, n_2) \exp \left\{ \frac{\Delta g_1(n_1, n_2)}{k_B T} \right\} - f(n_1 - 1, n_2) \right] \\
&- \omega_2^+(n_1, n_2 - 1) \left[ f(n_1, n_2) \exp \left\{ \frac{\Delta g_2(n_1, n_2)}{k_B T} \right\} - f(n_1, n_2 - 1) \right] ,
\end{aligned} \tag{4.17}$$

where

$$\omega_1^+(n_1, n_2) = D_1(1-x)n^{1/3} , \quad \omega_2^+(n_1, n_2) = D_2 x n^{1/3} . \tag{4.18}$$

The total flux of clusters in the space  $(n_1, n_2)$  can be written in the form

$$\mathbf{J}(n_1, n_2, t) = \mathbf{J}_r(n_1, n_2, t) + \mathbf{J}_s(n_1, n_2, t) , \tag{4.19}$$

where

$$J_{r,i}(n_1, n_2, t) = -\omega_i^+(n_1, n_2) \frac{f(n_1, n_2)}{k_B T} \frac{\partial \Delta G(n_1, n_2)}{\partial n_i} \quad (4.20)$$

is the regular part of the flux ( $i = 1, 2$ ), and

$$J_{s,i}(n_1, n_2, t) = -\omega_i^+(n_1, n_2) \frac{\partial f(n_1, n_2)}{\partial n_i} \quad (4.21)$$

is the fluctuational part of the flux. By solving numerically this set of equations, we can now compute a variety of characteristics of the nucleation-growth process.

### 4.3. Results and discussion

The set of kinetic equations describing nucleation and growth processes Eqs. (4.17) has been solved numerically assigning the following values to the parameters  $a$  and  $T_c$ :  $a = 4.5 \cdot 10^{-10}$  m,  $T_c = 1400$  K. The computations were performed for different values of the interfacial tension being equal to  $\sigma = 0.014, 0.021, 0.028, 0.04, \text{ and } 0.055$  J/m<sup>2</sup>, respectively. These values of interfacial tension correspond to the respective values at states of equilibrium coexistence of both phases at planar interfaces, when  $x_\alpha = x_b^{\text{right}} = 1 - x_b$  and  $x = x_b$  hold. Eq. (4.4) yields

$$\tilde{\sigma} = \frac{\sigma}{(1 - 2x_b)^2}. \quad (4.22)$$

With Eq. (4.22), we arrive at the following set of values of  $\tilde{\sigma}$ :  $\tilde{\sigma} = 0.019, 0.03, 0.04, 0.06, 0.083$  J/m<sup>2</sup>. The scaling parameters (Eqs. (4.9) and (4.10)) get the values  $R_\sigma/a = 0.176, 0.236, 0.354, 0.532, 0.708$  and  $G_\sigma = 0.0114, 0.0275, 0.0929, 0.315, 0.743$ , respectively. The calculations were performed for particle numbers in the cluster in the range  $n_{1,2} = 1, 2, \dots, N$  ( $N$  was chosen in a range 200 ... 1600, depending on the interfacial tension, because the characteristic dimension,  $n_\sigma$ , grows according to Eq. (4.8) with  $\sigma$ ), the composition of the initial clusters was

chosen as  $n_1(0) = n_{1i}$ ,  $n_2(0) = 1$ , that is  $f(n_{1i}, 1)|_{t=0} = 3.7 \cdot 10^{28} n_m^{-1}$  (which corresponds to the interatomic distance  $a = 3 \cdot 10^{-10} \text{m}$ ) and  $f(n_1, n_2)|_{t=0} = 0$  for  $(n_1, n_2) \neq (n_{1i}, 1)$ . Here  $n_m = 1 + n_{1i}$ ,  $n_{1i}$  is equal to the integer part of  $(1 - x)/x$ . For the calculations in the framework of classical nucleation theory (CNT) the same set of kinetic equations, Eqs. (4.17), was used, but the interfacial tension was fixed, that is  $\sigma = \tilde{\sigma} (1 - 2x_b)^2$ , and in addition,  $\Delta\psi(n, x, x_\alpha) = 0$  was set in Eq. (4.5).

In Fig. 4.2, results of computations of the nucleation rate,  $J$ , are shown. It is illustrated how the steady-state nucleation rate is established in the system

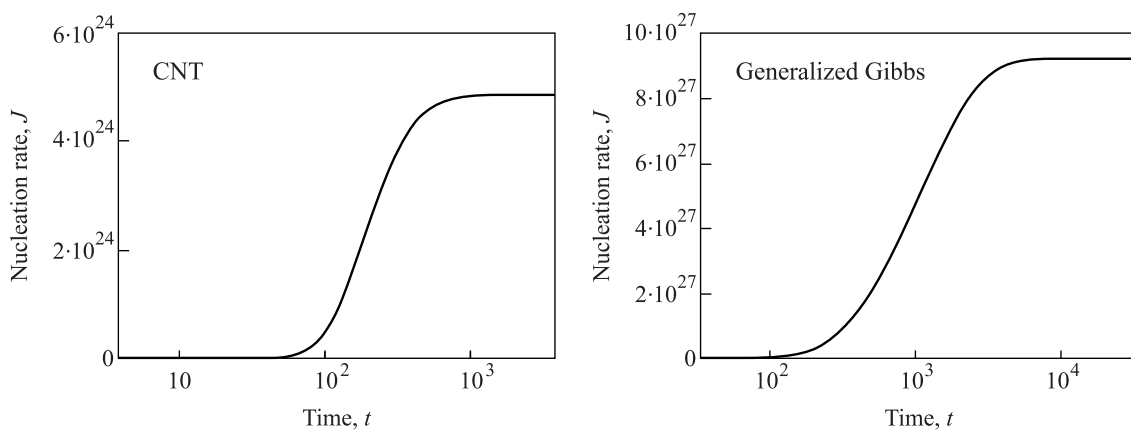


Fig. 4.2. Establishment of the steady-state nucleation rate as determined by the solution of the set of kinetic equations employing classical (left) and generalized (right) Gibbs' approaches for the description of the thermodynamics of cluster ensembles.

employing both the classical (top) and generalized (bottom) Gibbs' approaches for the description of the thermodynamic potential of an ensemble of clusters in the ambient phase. Hereby it is assumed that the state of the ambient phase is not changed, i.e., the volume fraction of the cluster phase is small. In agreement with general conclusions [22] we find for all computations performed including the one shown in Fig. 4.2 that CNT underestimates the nucleation rate. It is also evident from this figure, that the time-lag in nucleation – the characteristic time required to establish steady-state conditions – is smaller in CNT as compared to the estimates obtained utilizing the generalized Gibbs' approach. Employing the connection between time-lag in

nucleation and critical cluster size,  $\tau \propto n_c^{4/3-\kappa}$  (with  $\kappa = (2/3)$  for kinetic limited growth [23,24]) as obtained employing basic assumptions of CNT, this result could be eventually treated as a consequence that in the generalized Gibbs' approach the critical cluster size is larger as compared to the respective value obtained employing the classical Gibbs' approach (c.f. Fig. 4.1). However, the basic mechanism is here somewhat different: The time-lag in nucleation is smaller in CNT as compared to the estimates obtained via the generalized Gibbs' approach due to the fact, that in the evolution of the cluster ensemble, when described via the generalized Gibbs' approach, first homophase fluctuation type clusters [25] evolve (i.e., clusters with a composition near to  $x_\alpha = x$ , which have a small work of formation, c.f. Fig. 4.3). This process takes some time and increases the time-lag. So, here a more detailed

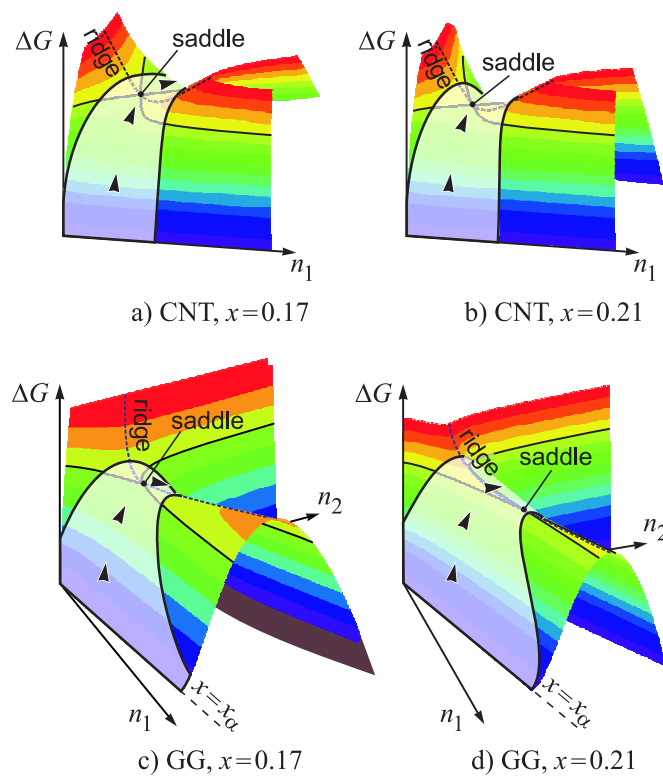


Fig. 4.3. The flux via the ridge of the thermodynamic potential surface: (a)-(b) In the classical Gibbs' approach, the flux is bounded to a narrow range near to the saddle point. In contrast, such picture is realized in the generalized Gibbs' description only for initial states near to the binodal curve (c.f. Fig. 3c,  $x = 0.17$ ). For initial states corresponding to a higher supersaturation (c.f. Fig. 3d,  $x = 0.21$ ), the flux via the ridge is found in a wide interval, and has a maximum not at the saddle point.

analysis is eventually required to give a final explanation to mentioned peculiarity.

Employing the classical Gibbs' method of description, the trajectory of evolution to the newly evolving phase proceeds always widely via the saddle point of the thermodynamic potential surface (the calculated difference of the position of maximum flux via the ridge from the saddle point is less than 0.05 percent when the cluster radii at the saddle point and of the ridge clusters are compared, see also Figs. 4.3a and b,  $x = 0.17, 0.21, \sigma = 0.028 \text{ J/m}^2$ ). In contrast, such picture – that the evolution to the new phase proceeds along a path near to the saddle point – is realized in the generalized Gibbs' description only for initial states near to the binodal curve (c.f. Fig. 4.3c,  $x = 0.17, \sigma = 0.028 \text{ J/m}^2$ ). For such parameters, when the supersaturation is low, the flux via the ridge is found in a narrow interval and has its maximum at the saddle point.

For initial states corresponding to a higher supersaturation (c.f. Fig. 4.3b,  $x = 0.21, \sigma = 0.028 \text{ J/m}^2$ ), the situation becomes a different one: A flux via the ridge is found in a wide interval, and has its maximum not at the saddle point but beyond it.

These results are further illustrated in more detail in Fig. 4.4 showing the dependence of the flux on cluster size along the ridge. Here  $R_j$  specifies the size of the ridge cluster with the maximum,  $J_{\max}$ , of the flux,  $R_j^-$  and  $R_j^+$  are the lower and upper values of the ridge clusters in between which an intensive flow into the direction of the new phase is observed (defined by  $J(R_j^-) = J(R_j^+) = J_{\max}/2$ ). For small values of the supersaturation, the flux is found in a narrow interval, and the parameters  $R_j^-$  and  $R_j^+$  are not so different from the parameter  $R_j$  corresponding to the ridge cluster of maximum flow (Fig. 4.4,  $x = 0.15$ ). With increasing supersaturation, the flux becomes significant in a broader range and is shifted to smaller cluster sizes (Fig. 4.4,  $x = 0.17$ ). The maximum of the width is reached near to the spinodal curve (Fig. 4.4,  $x = 0.225$ ). With an even further increase of the supersaturation, with values of  $x$  in the unstable region, the range of significant fluxes becomes more narrow, again (Fig. 4.4,  $x = 0.27$ ).

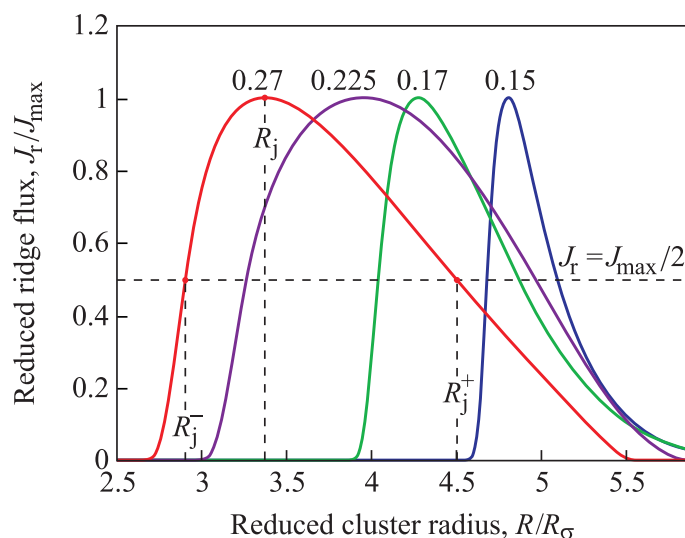


Fig. 4.4. Dependence of the flux via the ridge on the cluster size along the ridge for different supersaturations. Employing the classical method of description, widely independent on the initial supersaturation the flux is located near to the saddle with its maximum at the saddle point. Employing the generalized Gibbs' approach, latter scenario is realized for low supersaturation, only. For moderate and large supersaturations, the evolution to the new phase proceeds along a ridge path with a maximum value of the flux,  $R_j$ , not located at the saddle of the Gibbs' thermodynamic potential surface. Here  $R_j^-$  and  $R_j^+$  are the lower and upper values of the size along the ridge where intensive flow processes of clusters to the new phase are observed.

In Fig. 4.5, the region of intensive fluxes to the new phase is compared with the critical cluster sizes as obtained via classical and generalized Gibbs' approaches. For weakly and moderately metastable states, the ridge cluster radius of maximal flow,  $R_j$ , is equal to the critical size for the saddle point and decreases with an increase of the supersaturation. Near to the spinodal curve, where the critical size, corresponding to the saddle point, grows, the ridge critical radius decreases, similarly to the critical radius as computed via the classical Gibbs' approach and employed in classical nucleation theory.

Fig. 4.6 shows the dependence of the parameters of the critical clusters on supersaturation,  $x$ , for different values of the interfacial energies  $\sigma = 0.014, 0.021, 0.028, 0.04, \text{ and } 0.055 \text{ J/m}^2$ : Size (Fig. 4.6a), work of formation (Fig. 4.6b) and composition (Fig. 4.6c). The dependencies are shown always employing three

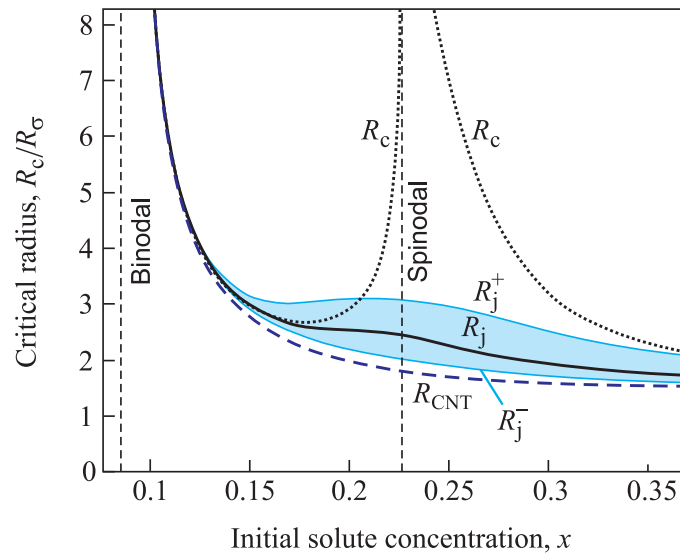


Fig. 4.5. Dependence of the ridge flux parameters  $R_j$  (location of the maximum of the flux, full curve),  $R_j^-$  and  $R_j^+$  (lower and upper values of the size along the ridge where intensive flow processes of clusters to the new phase are observed) on the initial solute concentration,  $x$ . Critical cluster sizes,  $R_c$ , for nucleation via the saddle point obtained via the generalized Gibbs' approach (dotted curve), and  $R_{CNT}$  for CNT (dashed curve) are shown for comparison.

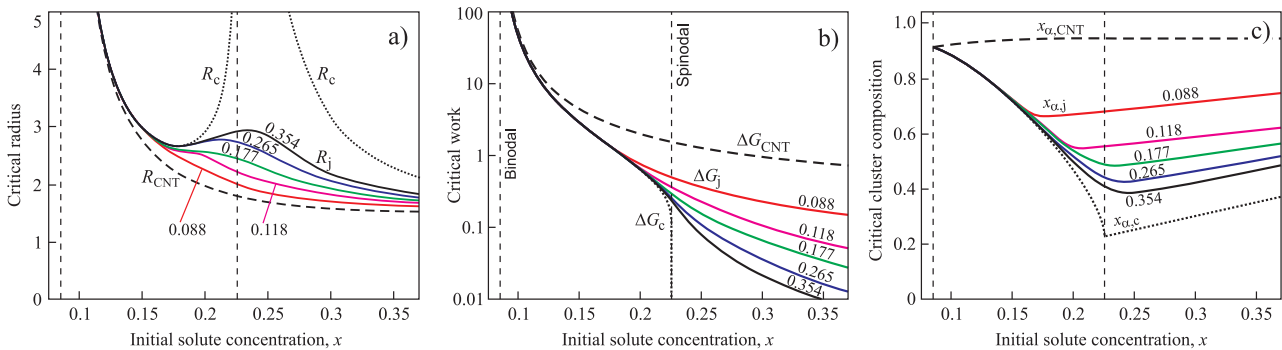


Fig. 4.6. Dependence of the parameters of critical clusters on the initial solute concentration,  $x$ , for different surface energies,  $\sigma = 0.014, 0.021, 0.028, 0.04,$  and  $0.055 \text{ J/m}^2$ , computed by three different approaches, classical nucleation theory (dashed lines), thermodynamical generalized Gibbs approach (nucleation proceeds via saddle point, dotted lines), and kinetic generalized Gibbs approach (nucleation can proceed via ridge, solid lines): (a) sizes ( $R_{CNT}/R_\sigma, R_c/R_\sigma,$  and  $R_j/R_\sigma$ ), (b) work of formation ( $\Delta G_{CNT}/k_B T G_\sigma, \Delta G_c/k_B T G_\sigma,$  and  $\Delta G_j/k_B T G_\sigma$ ) and (c) composition ( $x_{\alpha,CNT}, x_{\alpha,c},$  and  $x_{\alpha,j}$ ). Recall that for the reduced variables,  $R_c/R_\sigma$  and  $\Delta G_c/k_B T G_\sigma$ , and for composition,  $x_{\alpha,CNT}, x_{\alpha,c},$  the critical parameters for CNT and thermodynamical generalized Gibbs do not depend on the interfacial tension,  $\sigma$  [19].

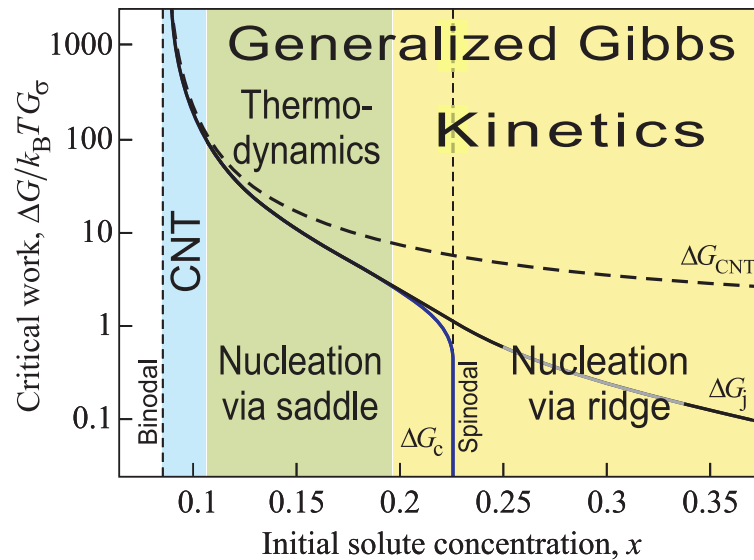


Fig. 4.7. Effective work of critical cluster formation and specification of the different ranges of validity of the approaches discussed

different approaches, classical nucleation theory (dashed lines), thermodynamical generalized Gibbs approach (nucleation proceeds via saddle point, dotted lines), and kinetic generalized Gibbs approach (nucleation can proceed via the ridge, solid lines) (recall that for the reduced variables,  $R/R_\sigma$  and  $\Delta G/k_B T G_\sigma$ , and for the cluster composition,  $x_\alpha$ , the critical parameters for CNT and thermodynamical generalized Gibbs' approach do not depend on the interfacial energy,  $\sigma$  [21]). We can see that the nucleation path according to the kinetic approach is located always between CNT and thermodynamical generalized Gibbs predictions. For large values of the interfacial tension, the evolution path is moved to the path as predicted by the thermodynamical generalized Gibbs' method (nucleation proceeds via saddle point), for low values of the interfacial tension the nucleation path is moved to the curves as expected from CNT.

In Fig. 4.7, the effective work of critical cluster formation – for the different trajectories of evolution of the cluster ensemble – is shown in dependence on supersaturation and it is specified which of the theoretical approaches is most suitable for the different ranges of the initial supersaturation. For weakly metastable states, CNT and generalized Gibbs lead to the same results and both methods are valid.

For moderately metastable states, CNT results in too high values of the work of critical cluster formation, and the thermodynamic analysis in the framework of the generalized Gibbs approach has to be applied. Here the evolution to the new phase proceeds via the saddle of the thermodynamic potential surface. In the metastable region near to the spinodal curve, nucleation proceeds via the ridge, but not via the saddle point, and only the kinetically based analysis of nucleation in the framework of generalized Gibbs approach is valid. This conclusion holds similarly in the region of thermodynamically unstable initial states in the vicinity of the spinodal curve.

Finally, we would like to analyze why the transition from a path of evolution via the saddle is switched with increasing supersaturation to evolution processes proceeding via the ridge of the thermodynamic potential surface. The origin of such kind of behavior is the following: As shown in detail in previous analysis (c.f. [4]), the mechanism of nucleation in solutions does not consist – as assumed in the classical picture – in the growth of the cluster in size with more or less given composition. In contrast, nucleation is characterized by an initial amplification of density fluctuations in a region of the ambient phase with a radius of the critical cluster size. The nucleation rate of clusters evolving via the saddle can be represented then consequently as being proportional to

$$J(R_c) \propto \Phi_c(R_c) = N(R_c) \exp\left(-\frac{W_c}{k_B T}\right) = \left(\frac{R_\sigma}{R_c}\right)^3 \exp\left(-\frac{\Delta G(R_c)}{k_B T}\right). \quad (4.23)$$

Here  $N(R_c)$  is proportional to the number of nucleation sites in the system when nucleation proceeds via the saddle of the thermodynamic potential surface.

With an increase of the supersaturation, the work of critical cluster formation via the saddle,  $\Delta G(R_c)$ , decreases and the exponential term increases. However, the pre-factor,  $1/R_c^3$ , in the expression of the steady-state nucleation rate overcompensates this effect as soon as  $R_c$  as determined via the generalized Gibbs' approach starts to increase with increasing supersaturation. By this reason, assuming that the process

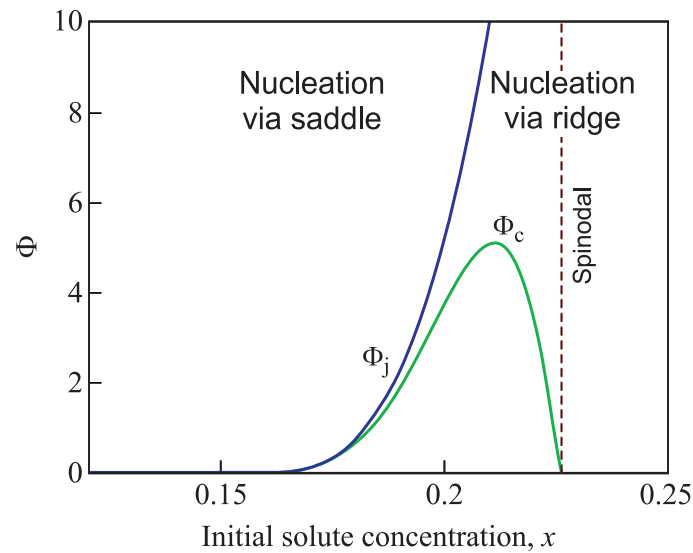


Fig. 4.8. Illustration of the origin of deviation of the most probable path of cluster evolution from the saddle point trajectory.

proceeds similarly via a ridge, the maximum ridge nucleation rate

$$J(R_j) \propto \Phi_j(R_j) = N(R_j) \exp\left(-\frac{W_c}{k_B T}\right) = \left(\frac{R_\sigma}{R_j}\right)^3 \exp\left(-\frac{\Delta G(R_j)}{k_B T}\right) \quad (4.24)$$

is larger and consequently this way of evolution represents the preferred trajectory of cluster formation and growth (Fig. 4.8).

The switch from the saddle point evolution path to ridge crossing allows the system to realize higher nucleation rates, and by this reason, higher rates of change of the characteristic thermodynamic potential. This switch in the preferred path of evolution can be considered in this way as a special realization of the principle of maximum entropy production (or here the Gibbs' free energy decrease) as formulated in [26] as a criterion of selection of the most probable among several possible reaction paths. The switch position,  $x_{sw}$ , can be estimated as the inflection point of  $J(R_c)$  as given by Eq. (4.23), i.e., as a root of the equation

$$\frac{\partial^2}{\partial x^2} \Phi(R_c) = 0. \quad (4.25)$$

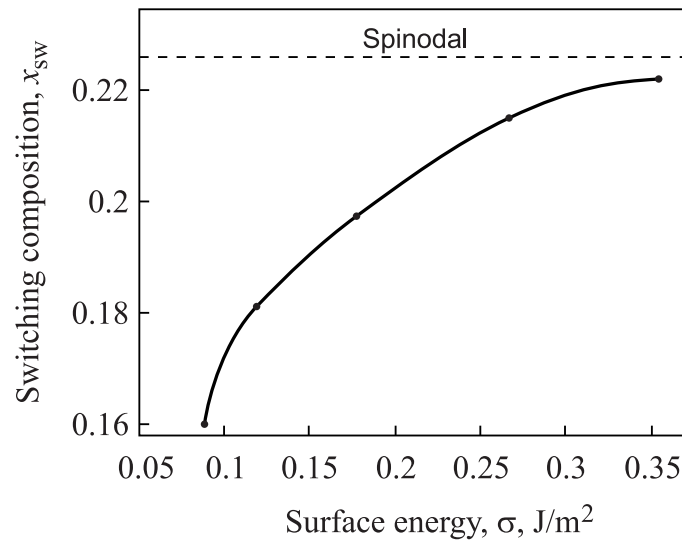


Fig. 4.9. Dependence of the composition of the switching point,  $x_{sw}$ , where ridge cluster passage starts to become dominating, on interfacial tension,  $\sigma$ .

The dependence of  $x_{sw}$  on interfacial tension,  $\sigma$ , determined via Eq. (4.25) is shown in Fig. 4.9. For low values of the interfacial tension switching occurs at moderate supersaturations, and the switching point shifts to the spinodal with growing values of  $\sigma$ .

#### 4.4. Conclusions

Employing the generalized Gibbs' approach, the work of critical nucleus formation in solutions is found generally to have lower values as compared with the result obtained by the classical Gibbs' approach when the capillarity approximation is employed. Therefore the nucleation rate computed via the generalized Gibbs' approach is, as a rule, considerably larger. These results are a consequence of the possible variations of bulk properties of the critical clusters accounted for and determined in the generalized Gibbs' approach. For small supersaturation, the results of the classical and generalized Gibbs' approaches lead to widely equivalent results. This is the range, where the classical Gibbs' method underlying classical nucleation

theory is directly applicable. For moderately metastable states, the thermodynamic analysis in the framework of the generalized Gibbs approach can be applied in order to determine the flux via the saddle point dominating here the nucleation process. However, for both metastable and unstable initial states near to the spinodal curve the evolution to the new phase can and will, as a rule, proceed not via the saddle point, but via the ridge of the appropriate thermodynamic potential relief. In this range of supersaturation, only the analysis of the kinetics of nucleation and growth based on the solution of the set of kinetic equations employing for the thermodynamic description the generalized Gibbs approach is valid. For low interfacial tension values, the process of nucleation proceeds visually similar to CNT – critical size and work of critical cluster formation are near to the values predicted by CNT. Nevertheless, the physical nature of the process is very different: in the framework of CNT, nucleation proceeds via the saddle point, but in the generalized Gibbs' approaches (i) the saddle point is as a rule located at another place, and (ii) nucleation proceeds via the ridge of the thermodynamic potential relief.

### **Acknowledgments**

The authors express their gratitude to the German funding agency Deutsche Forschungsgemeinschaft (DFG: SCHM 937/16-1) for financial support.

### **References**

1. I. S. Gutzow, J. W. P. Schmelzer, *The Vitreous State: Thermodynamics, Structure, Rheology, and Crystallization* (Springer, Berlin, 1995; 2nd enlarged edition, Springer, Weinheim, 2013 (in press)).
2. J. W. P. Schmelzer, *J. Non-Crystalline Solids* 354 (2008) 269; 356 (2010) 2901.

3. J. W. Gibbs: *On the equilibrium of heterogeneous substances*, Transactions Connecticut Academy of Sciences 3, 108 (1876); 16, 343 (1878); J. W. Gibbs, The Collected Works, vol. 1 (Longmans and Green, New York - London - Toronto, 1928).
4. J. W. P. Schmelzer, V. M. Fokin, A. S. Abyzov, E. D. Zanutto, I. Gutzow, International Journal of Applied Glass Science 1 (2010) 16.
5. A. S. Abyzov, J. W. P. Schmelzer, J. Chem. Phys. 127 (2007) 119.
6. A. S. Abyzov, J. W. P. Schmelzer, A. A. Kovalchuk, V. V. Slezov, J. Non-Crystalline Solids 356 (2010) 2915.
7. H. Trinkaus, Phys. Rev. B 27 (1983) 7372.
8. J.-S. Li, K. Nishioka, I. L. Maksimov, Phys. Rev. E 58 (1998) 7580.
9. I. L. Maksimov, K. Nishioka, Phys. Lett. A 264 (1999) 51.
10. J.-S. Li, I. L. Maksimov, G. Wilemski, Phys. Rev. E 61 (2000) R4710.
11. I. L. Maksimov, M. Sanada, K. Nishioka, J. Chem. Phys. 113 (2000) 3323.
12. M. Roskosz, M. J. Toplis, P. Besson, P. Richet, J. Non-Cryst. Solids 351 (2005) 1266.
13. M. Roskosz, M. J. Toplis, P. Richet, J. Non-Cryst. Solids 352 (2006) 180.
14. V. G. Baidakov, G. Sh. Boltachev, J. W. P. Schmelzer, J. Colloid Interface Science 231 (2000) 312 .
15. J. W. P. Schmelzer, V. G. Baidakov, J. Phys. Chem. 105 (2001) 11595.
16. J. W. Cahn, J. E. Hilliard, J. Chem. Phys. 28 (1958) 258; 31 (1959) 688.
17. J. W. P. Schmelzer, G. Sh. Boltachev, V. G. Baidakov: *Is Gibbs' thermodynamic theory of heterogeneous systems really perfect?* In: J. W. P. Schmelzer (Ed.), *Nucleation Theory and Applications* (WILEY-VCH, Berlin-Weinheim, 2005), pgs. 418-446.
18. R. Becker, Ann. Phys. 32 (1938) 128.

19. J. W. Christian, in: R. W. Cahn (Ed.): *Physical Metallurgy* (North-Holland Publishers, Amsterdam, 1965, pgs. 227-346).
20. J. W. P. Schmelzer, A. S. Abyzov, J. Möller, *J. Chem. Phys.* **121** (2004) 6900.
21. J. W. P. Schmelzer, J. Schmelzer Jr., and I. Gutzow, *J. Chem. Phys.* **112** (2000) 3820.
22. J. W. P. Schmelzer, G. Sh. Boltachev, V. G. Baidakov, *J. Chem. Phys.* **124** (2006) 194503.
23. V. V. Slezov, J. W. P. Schmelzer, *Kinetics of Nucleation - Growth Processes: The First Stages*. In: W. P. Schmelzer, G. Röpke, V. B. Priezhev (Editors): *Nucleation Theory and Applications, Workshop Proceedings 1997 - 1999*, Joint Institute for Nuclear Research Publishing Department, Dubna, Russia, 1999, pgs. 6 - 81.
24. V. V. Slezov, *Kinetics of First-Order Phase Transitions*, WILEY-VCH, Berlin-Weinheim, 2009.
25. Ya. I. Frenkel, Ya. I., *The Kinetic Theory of Liquids*, Oxford University Press, Oxford, 1946
26. A. M. Gusak, *Diffusion-Controlled Solid-State Reactions*, WILEY-VCH, Berlin-Weinheim, 2010.

#### 4.5. Висновки до розділу 4

Результати досліджень, представлених у даному розділі, опубліковано в статті [4] (Додаток А. Список публікацій здобувача за темою дисертації). Проведено детальний аналіз процесу нуклеації нової фази з за допомогою чисельного моделювання на основі кластерної динаміки, проаналізована еволюція функції розподілу кластерів за розміром та складом. Показано, що можна виділити три області залежно від ступеня нестабільності системи:

- У першій області, при малому значенні пересичення, результати класи-

чної теорії нуклеації на основі капілярного наближення та узагальненого методу Гіббса майже ідентичні, максимум потоку кластерів нової фази в просторі розмірів проходить через сідлову точку.

- В другій області, при більшому значенні пересичення, робота створення кластера нової фази помітно менша, ніж в класичній теорії нуклеації, що призводить до істотно більш високого значення швидкості нуклеації. Максимум потоку в просторі розмірів, як і в першій області, проходить переважно через сідло. У першій і другій областях можна використовувати для розрахунку швидкості нуклеації прості аналітичні вирази через активаційний бар'єр.

- У третій області, поблизу спінодалі, нуклеація відбуватиметься не через сідлову точку, але траєкторією, що проходить через гребінь гіперповерхні термодинамічного потенціалу. Розрахунок швидкості нуклеації у третій області можливий тільки на основі чисельного моделювання на основі кластерної динаміки.

## РОЗДІЛ 5

### УЗАГАЛЬНЕНИЙ МЕТОД ГІББСА ДЛЯ ГЕТЕРОГЕННОЇ НУКЛЕАЦІЇ

У п'ятому розділі досліджено гетерогенне зародження кластерів нової фази (конденсація та кипіння) на плоских твердих поверхнях з урахуванням зміни параметрів стану критичних кластерів (крапельок або бульбашок) залежно від пересичення в однокомпонентній рідині ван дер Ваальса. В узагальненому підході Гіббса об'ємні параметри кластера залежать від ступеня пересичення розчину, тому можна припустити, що при гетерогенній нуклеації на плоскій поверхні контактний кут також буде змінюватися і параметри критичного кластера будуть не такими, як у гомогенному випадку. Це основна ідея даного розділу.

THE JOURNAL OF CHEMICAL PHYSICS 138, 164504 (2013)

#### **Generalized Gibbs' approach in heterogeneous nucleation**

Alexander S. Abyzov<sup>1</sup> and Jörn W. P. Schmelzer<sup>2</sup>

<sup>1</sup>*National Science Center Kharkov Institute of Physics and Technology, Academician Street 1, 61108 Kharkov, Ukraine*

<sup>2</sup>*Institut für Physik der Universität Rostock, Universitätsplatz, 18051 Rostock, Germany*

(Received 21 February 2013; accepted 4 April 2013; published online 25 April 2013)

Heterogeneous nucleation (condensation and boiling) on planar solid surfaces is described taking into account changes of the state parameters of the critical clusters in dependence on supersaturation. The account of the variation of the state parameters of the cluster phase on nucleation is performed in the framework of the generalized Gibbs' approach. One-component van der Waals fluids are chosen as a model for the analysis of the basic qualitative

characteristics of the process. The analysis is performed for both hydrophobic and hydrophilic surfaces and similarities and differences between condensation and boiling processes are discussed for the two different cases. It is shown that, in the generalized Gibbs' approach, contact angle and catalytic factor for heterogeneous nucleation become dependent on the degree of metastability (undercooling or superheating) of the fluid. For the case of formation of a droplet in supersaturated vapor on a hydrophobic surface and bubble formation in a liquid on a hydrophilic surface the solid surface has only a minor influence on nucleation. In the alternative cases of condensation of a droplet on a hydrophilic surface and of bubble formation in a liquid on a hydrophobic surface, nucleation is significantly enhanced by the solid. Effectively, the existence of the solid surface results in a significant shift of the spinodal to lower supersaturations as compared with homogeneous nucleation. Qualitatively the same behavior is observed now near the new (solid surface induced) limits of instability of the fluid as compared with the behavior near to the spinodal curve in the case of homogeneous nucleation.

©2013 AIP Publishing LLC. [<http://dx.doi.org/10.1063/1.4802201>]

## 5.1. Introduction

In the interpretation of phase formation processes, two well-established thermodynamic approaches are presently widely employed going back to Gibbs [1] and van der Waals [2, 3]. Employing Gibbs' theory for the description of critical cluster formation it is, in addition, widely assumed in classical nucleation theory that the bulk properties of the clusters of the newly evolving phase are to a large extent similar to the properties of the respective macroscopic phases. As a second additional assumption it is frequently supposed that the specific interfacial energy or the surface (interfacial) tension is equal to the respective values for an equilibrium

coexistence of both phases at planar interfaces (capillarity approximation). While the first of these assumptions (similarity of the bulk properties of the critical clusters with the parameters of the respective macroscopic phases) is to a large degree a consequence of Gibbs' theory, the second assumption can be and is often released by introducing a curvature or size dependence of the surface tension or of the specific interfacial energy. Latter approach is used (and it is the only possibility in Gibbs' classical approach) in order to arrive at a better agreement between experimental data on nucleation rates and the theoretical predictions [4, 5]. In such approach, the surface tension serves to some extent (or fully) as a fit parameter in order to reconcile experiment and theory with respect to the value of the nucleation rate. However, such approach – employing the value of the specific interfacial energy as a fit parameter as it is done generally by necessity in the description of crystallization processes – may lead to other contradictions between theory and experiment and to internal problems in the theoretical description itself [6].

However, there exists an alternative method to improve the agreement between theory and experiment in the description of nucleation. Indeed, as it was shown for the first time by Cahn and Hilliard [7] applying the van der Waals' approach to the description of the kinetics of phase formation, the properties of the critical clusters may deviate significantly from the properties of the newly evolving macroscopic phases. This deviation of the bulk properties of the critical clusters from the properties of the macroscopic phases is not accounted for appropriately in Gibbs' theory. As shown by us in the last decade [8, 9], generalizing Gibbs' approach such possible changes of the bulk properties may be incorporated into the description allowing one to reconcile Gibbs' and van der Waals-type approaches in the description of nucleation. The mentioned generalization of Gibbs' approach consists basically in the formulation of the thermodynamic theory by extending it from the very beginning to the description of non-equilibrium states of clusters in the ambient phase. Only after this task has been resolved the theory is applied then to the description of the

properties of the clusters in nucleation and growth. The application of the generalized Gibbs' approach was shown to allow one a more correct description of nucleation as compared with the classical theory: (i.) for model systems the results are in agreement with density functional computations; (ii.) the approach allows one an adequate theoretical description of a variety of experimental data which had not found an adequate interpretation so far [10, 11].

The generalized Gibbs' approach was applied by us so far in detail to the description of condensation and boiling in one-component systems [12–14], boiling in multi-component liquids [15], segregation processes in solutions [8, 17–20] and crystallization of glass-forming melts [6, 10, 11]. Predictions of the generalized Gibbs' approach have been compared, at part, in these papers with results of van der Waals' density functional computations [14–16] and experiment (e.g. [6, 11, 12, 15]). However, in all these investigations we considered so far exclusively homogeneous nucleation processes. On the other hand, in a huge variety of processes of phase formation in nature, experiment and technological applications, the formation of the newly evolving phase does not proceed via homogeneous nucleation but by involving different types of heterogeneous nucleation cores [21–27]. These effects can be treated straightforwardly in terms of Gibbs' classical theory [4]. By this reason, a generalization of the approaches as developed employing the classical Gibbs' theory but accounting for – in terms of the generalized Gibbs' approach – for possible changes of the bulk state parameters of the critical clusters of the new phase can be expected to be possible in a straightforward way. In order to develop the theory in this direction, with the present paper we start a series of investigations to demonstrate how, in a similar way as in the classical treatment, heterogeneous nucleation can be treated in terms of the generalized Gibbs' approach. For the outline of the basis ideas and differences as compared to the treatment in terms of the classical Gibbs' approach, we start here the analysis with some of the simplest cases, the description of condensation and boiling at planar interfaces as performed – in the framework of

the classical treatment – e.g. by Volmer [21].

In brief, in the present article heterogeneous nucleation (condensation and boiling of one-component fluids) at planar solid interfaces is described in the framework of the generalized Gibbs' approach. The van der Waals' fluid [2, 28] is chosen as a model for the analysis of the basic qualitative characteristics of the process similarly as it was done in our previous analysis of homogeneous nucleation (condensation and boiling in one-component van der Waals' fluids) [12–14]. As in the latter case, in the analysis we account for the fact that the state parameters (which is density for a one-component system) of the newly evolving clusters and, in particular, the critical clusters (drops or bubbles) may deviate in their values considerably from the respective values of the macroscopic phases. This additional as compared to the classical picture variation of the bulk parameters affects also the surface parameters like surface tension and wetting angles and gives thus an additional contribution to the activity factor of the respective heterogeneous nucleation core with respect to nucleation. So, in order to determine the work of critical cluster formation the dependence of the surface parameters on the density of the critical nuclei (drops, bubbles) has to be determined. This program will be implemented here for four cases: bubble formation in superheated (stretched) liquids and droplet formation from the supersaturated (supercooled) vapor both for the cases of hydrophilic and hydrophobic planar interfaces. Similarities and differences between condensation and boiling processes are discussed as well.

The article is structured as follows: In Section 5.2, the van der Waals' equation of state is briefly discussed as far as required for the subsequent derivations, the location of binodal and spinodal curves are specified, and the general expressions are developed allowing us to determine the work of critical cluster formation for condensation and boiling at planar interfaces. In Section 5.3, the expressions for the contact angle and catalytic activity factor for critical droplet and bubble formation are computed. Combining the results obtained in Sections 5.2 and 5.3, in Section 5.4

heterogeneous condensation and boiling of a van der Waals gas on hydrophilic and hydrophobic planar surfaces is analyzed. A summary of the results, conclusions and of possible generalizations (Section 5.5) completes the paper.

## 5.2. Basic equations

### 5.2.1. Bulk properties of ambient and newly evolving phases, binodal and spinodal curves

To describe the bulk properties of the ambient and newly formed phases the van der Waals equation of state will be used. In dimensionless variables, this equation has the form [2, 28]

$$\Pi(\omega, \theta) = \frac{8\theta}{3\omega - 1} - \frac{3}{\omega^2}, \quad (5.1)$$

$$\Pi \equiv \frac{p}{p_c} \quad \omega \equiv \frac{v}{v_c}, \quad \theta \equiv \frac{T}{T_c}, \quad (5.2)$$

were  $v$ ,  $p$ , and  $T$  are the molar volume, pressure, and temperature, by  $v_c$ ,  $p_c$  and  $T_c$  the values of the same parameters in the critical point are denoted. The chemical potential of the van der Waals fluid can be written as [12]

$$\mu(\omega, \theta) = -\frac{8\theta}{3} \ln(3\omega - 1) + \frac{8\theta\omega}{3\omega - 1} - \frac{6}{\omega}. \quad (5.3)$$

The position of the spinodal, the border between the thermodynamically metastable and unstable states in the absence of heterogeneous nucleation centers (we will denote

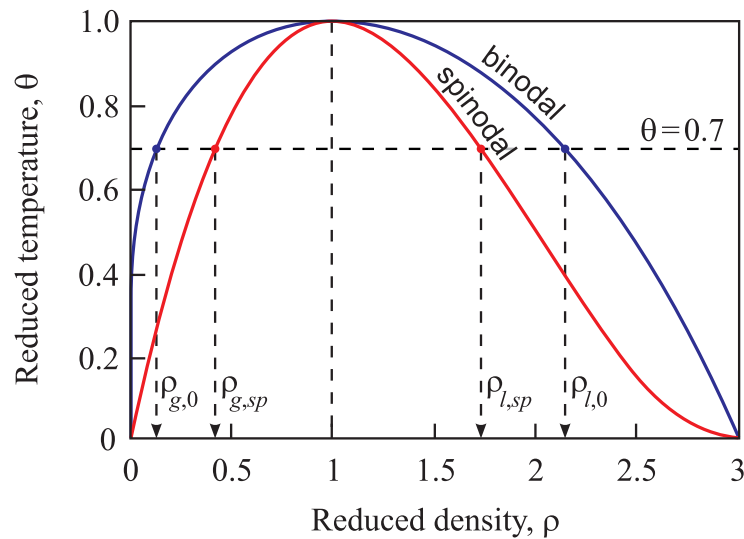


Fig. 5.1. Location of the binodal and spinodal curves for a van der Waals fluid. For an illustration of the results, we will perform here the computations for a value of the reduced temperature equal to  $\theta = 0.7$  (see also text).

it more specifically later also as "bulk spinodal"), is given by the equation

$$\frac{d}{d\omega}\Pi(\omega, \theta) = 0. \quad (5.4)$$

For any value of temperature below the critical temperature ( $\theta < \theta_c = 1$ ), Eq. (5.4) yields two solutions which coincide at the critical point. The location of the binodal curve is determined by the conditions of thermodynamic equilibrium of vapor (gas) and liquid at a planar interface (equality of pressure and chemical potential) that is, by the solution of the system of equations

$$\Pi(\omega_{gas}, \theta) = \Pi(\omega_{liq}, \theta), \quad \mu(\omega_{gas}, \theta) = \mu(\omega_{liq}, \theta). \quad (5.5)$$

Similarly to above discussed case, for any value of temperature in the range  $\theta < \theta_c = 1$ , Eq. (5.5) yields one solution for  $\omega_g$  and one for  $\omega_l$ . These two solutions coincide at the critical point, again. The binodal and spinodal curves are given in terms of reduced density,  $\rho = 1/\omega$ , in Fig. 5.1.

Numerical computations will be performed here assuming the reduced

temperature to be equal to  $\theta = 0.7$ . In such case, the values of the reduced volume at the binodal ( $\omega_b$ ) and spinodal ( $\omega_{sp}$ ) curves are equal to

$$\omega_b^{(left)} = 0.467, \quad \omega_b^{(right)} = 7.811, \quad (5.6)$$

$$\omega_{sp}^{(left)} = 0.579, \quad \omega_{sp}^{(right)} = 2.376. \quad (5.7)$$

Accordingly, the equilibrium densities of liquid ( $\rho_{l,0}$ ) and vapor ( $\rho_{g,0}$ ) are

$$\rho_{l,0} = \left(\omega_b^{(left)}\right)^{-1} = 2.14, \quad \rho_{g,0} = \left(\omega_b^{(right)}\right)^{-1} = 0.128, \quad (5.8)$$

and the densities at the liquid ( $\rho_{l,sp}$ ) and vapor branches ( $\rho_{g,sp}$ ) of the spinodal curve are

$$\rho_{l,sp} = \left(\omega_{sp}^{(left)}\right)^{-1} = 1.727, \quad \rho_{g,sp} = \left(\omega_{sp}^{(right)}\right)^{-1} = 0.421. \quad (5.9)$$

The non-equilibrium values of density of liquid and vapor will be denoted as  $\rho_l$  and  $\rho_g$ , respectively. An illustration of these notations and results is also given in Fig. 5.1.

### 5.2.2. Work of critical cluster formation: General expression

Suppose that the system is instantaneously transferred into a metastable state located in between the binodal and spinodal curves and that afterwards pressure and temperature are kept constant (later-on we will consider also initial states beyond these limits, i.e., unstable initial states in between both spinodal curves). As a first step in the description, we determine the parameters of the critical clusters (drop or bubble) formed on the planar solid surface.

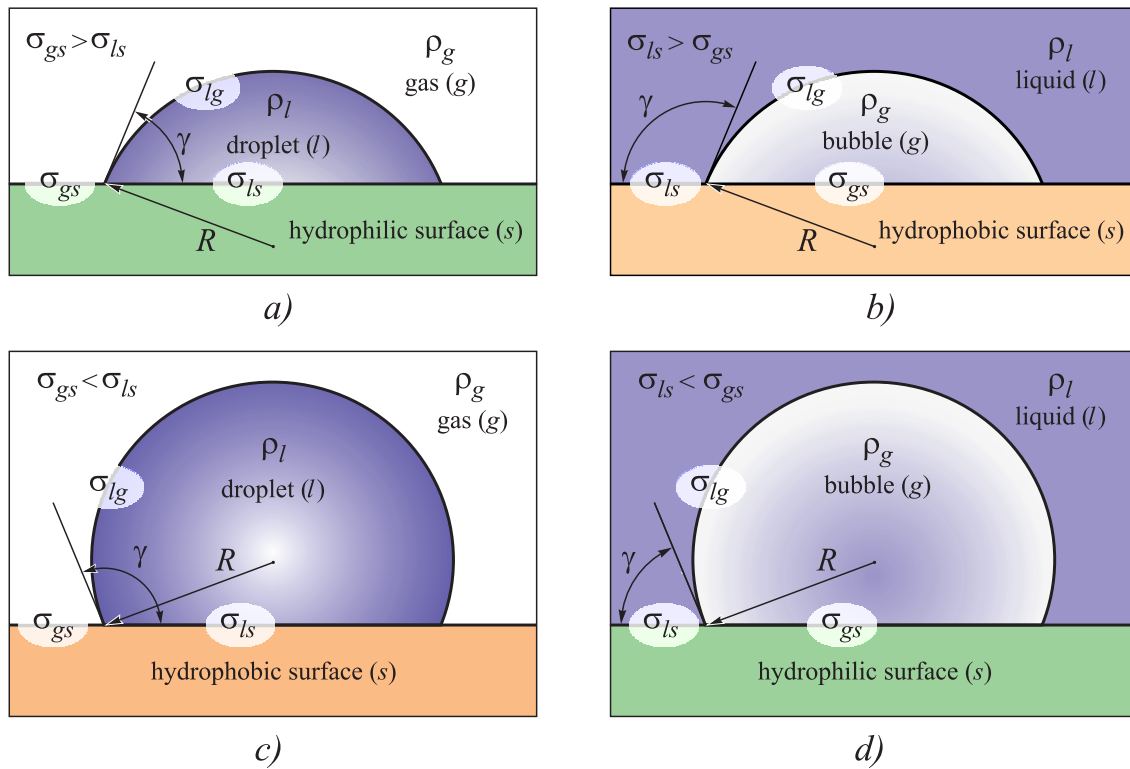


Fig. 5.2. Heterogeneous nucleation of a droplet (a, b) and a bubble (c, d) of radius  $R$  on hydrophilic (a, d) and hydrophobic (c, b) planar solid surfaces.

The expression for the change of the thermodynamic potential (the Gibbs' free energy,  $G$ ) for a one-component system due to the formation of a drop of the considered shape (segments of a sphere with a radius,  $R$ , cf. Fig. 5.2) in the vapor phase can be written both in the classical and generalized Gibbs' approaches then as [4, 9, 15, 21]

$$\Delta G = \sigma_{lg}A_{lg} + (\sigma_{ls} - \sigma_{gs})A_{ls} + (p - p_\alpha)V_\alpha + n_\alpha(\mu_\alpha - \mu_\beta), \quad (5.10)$$

and, for nucleation of a bubble in a liquid, as

$$\Delta G = \sigma_{lg}A_{lg} + (\sigma_{gs} - \sigma_{ls})A_{gs} + (p - p_\alpha)V_\alpha + n_\alpha(\mu_\alpha - \mu_\beta). \quad (5.11)$$

Here  $\sigma_{ls}$ ,  $\sigma_{gs}$  and  $\sigma_{lg}$  are the specific surface energies (surface tension) of the liquid-solid, vapor-solid and vapor-liquid interfaces, respectively,  $A_{ls}$ ,  $A_{gs}$  and  $A_{lg}$  are the

respective interfacial areas (see Fig. 5.2),  $n_\alpha$  is the number of particles (atoms, molecules) in the cluster. In both equations and furtheron, the index  $\alpha$  always denotes the parameters of the cluster (liquid phase in case of droplet formation or vapor phase in boiling), and the index  $\beta$  refers to ambient phase parameters (vapor or liquid, respectively). As independent variables, we use the radius,  $R$ , and the density of the cluster,  $\rho_g$  (bubble) and  $\rho_l$  (drop), respectively.

The bulk contributions,  $\Delta G_V$ , to the Gibbs' free energy change can be written for the case of formation of a droplet with a radius,  $R$ , and a contact angle,  $\gamma$  (cf. Fig. 5.2a and b), generally as [21]

$$\Delta G_V = (p - p_\alpha)V_\alpha + n_\alpha(\mu_\alpha - \mu_\beta) , \quad (5.12)$$

$$\Delta G_V = \frac{4\pi}{3}R^3\phi [(p - p_\alpha) + \rho_\alpha(\mu_\alpha - \mu_\beta)] ,$$

where  $\phi$  is determined via the contact angle,  $\gamma$ , as

$$\phi = \frac{1}{4} (2 - 3 \cos \gamma + (\cos \gamma)^3) = \frac{1}{4} (2 + \cos \gamma)(1 - \cos \gamma)^2 . \quad (5.13)$$

The surface contribution,  $\Delta G_S$ , to the Gibbs' free energy of cluster formation is given according to Eq. (5.10) as

$$\Delta G_S = \sigma_{lg}A_{lg} + (\sigma_{ls} - \sigma_{gs})A_{ls} , \quad (5.14)$$

$$\Delta G_S = 2\pi R^2(1 - \cos \gamma)\sigma_{lg} + \pi R^2(1 - \cos^2 \gamma)(\sigma_{ls} - \sigma_{gs}) .$$

The condition of mechanical equilibrium along the line of contact where three phases

meet is given by Young's equation [21]

$$\sigma_{gs} = \sigma_{ls} + \sigma_{lg} \cos \gamma . \quad (5.15)$$

Once this relation is fulfilled, we can write the surface contributions to the Gibbs' free energy as (cf. Eq. (5.13))

$$\Delta G_S = 4\pi R^2 \sigma_{lg} \left[ \frac{1}{4} (2 + \cos \gamma) (1 - \cos \gamma)^2 \right] = 4\pi R^2 \sigma_{lg} \phi . \quad (5.16)$$

Similarly to [4, 21], the work of droplet formation at heterogeneous nucleation on planar solid surfaces can be written finally as

$$\Delta G_{het} = \phi \left\{ \frac{4\pi}{3} R^3 ((p - p_\alpha) + \rho_\alpha (\mu_\alpha - \mu_\beta)) + 4\pi R^2 \sigma_{lg} \right\} \quad (5.17)$$

or

$$\Delta G_{het} = \phi \Delta G_{hom} . \quad (5.18)$$

This relation holds generally for any values of the radius of the surface of the cluster (bubble, drop) and any appropriate value of the contact angle,  $\gamma$ . Employing in addition the thermodynamic equilibrium conditions at the liquid-vapor interface, the parameter  $\phi$  becomes equal to the catalytic activity of a given nucleation site (planar surface in the case under consideration) with respect to nucleation. In the analysis of heterogeneous nucleation in the framework of the generalized Gibbs approach the factor  $\phi$  becomes dependent on the density of both liquid and vapor phases (see Sections 9.4 and 8.4 for the details). Similar considerations with identical results can be performed straightforwardly also for the case of boiling.

A detailed derivation of the expression for the work of cluster formation in the generalized Gibbs approach for homogeneous nucleation of a bubble in a liquid is

given in [12] and for a droplet in vapor in [13]. Employing the results obtained there, we can rewrite Eqs. (5.10)-(5.11) as

$$\frac{\Delta g(r, \rho_g, \rho_l, \theta)}{k_B T} = \phi(\rho_g, \rho_l) \left[ 3 (\rho_l - \rho_g)^\delta r^2 + 2f(\rho_g, \rho_l, \theta) r^3 \right], \quad (5.19)$$

where

$$\Delta g \equiv \frac{\Delta G}{\Omega_1}, \quad \Omega_1 = \frac{16\pi}{3} \frac{1}{p_c^2 k_B T_c \theta} \Theta^3(\theta), \quad (5.20)$$

$$r \equiv \frac{R}{R_\sigma}, \quad R_\sigma = \frac{2}{p_c} \Theta(\theta).$$

The factor  $\Theta(\theta)$  and the parameter  $\delta$  are determined by the chosen relation for the dependence of the surface tension on the state parameters of liquid and gas phases, they are determined by (see [12, 13] and Section 6.3.1 for details)

$$\sigma_{lg} = \Theta(\theta) (\rho_l - \rho_g)^\delta, \quad \delta = 2.5. \quad (5.21)$$

The expression for the work of critical cluster formation, Eq. (5.19), differs from the one describing homogeneous nucleation [12, 13] by the nucleation-activity factor,  $\phi(\rho_g, \rho_l)$ , which is equal to one in the case of homogeneous nucleation. It will be determined below (see Section 8.4) for the different cases under consideration. The expression in square brackets in Eq. (5.19) describes the work of cluster formation in homogeneous nucleation, the function  $f$  in the second term of this expression can be written for nucleation of a droplet in vapor [13] as

$$f(\rho_g, \rho_l, \theta) = \Pi(\rho_l, \theta) - \Pi(\rho_g, \theta) + \rho_l \left( \frac{\mu(\rho_g, \theta) - \mu(\rho_l, \theta)}{p_c v_c} \right), \quad (5.22)$$

and for the bubble formation in a liquid [12] as

$$f(\rho_g, \rho_l, \theta) = \Pi(\rho_g, \theta) - \Pi(\rho_l, \theta) + \rho_g \left( \frac{\mu(\rho_l, \theta) - \mu(\rho_g, \theta)}{p_c v_c} \right). \quad (5.23)$$

where (with  $\rho = \omega^{-1}$  and Eq. (5.3))

$$\mu(\rho, \theta) = -\frac{8\theta}{3} \ln \left( \frac{3}{\rho} - 1 \right) + \frac{8\theta}{3 - \rho} - 6\rho. \quad (5.24)$$

Critical cluster parameters, size ( $r_{cr}$ ), and density, ( $\rho_{cr}$ ), are determined by the solution of the system of equations

$$\frac{\partial \Delta g(r, \rho_g, \rho_l, \theta)}{\partial r} = 0, \quad \frac{\partial \Delta g(r, \rho_g, \rho_l, \theta)}{\partial \rho_{l(g)}} = 0. \quad (5.25)$$

In the second of latter equations, the derivative with respect to cluster density has to be taken with respect to the density of the drop,  $\rho_l$ , for nucleation of the droplet in vapor, respectively, with respect to the density of the bubble,  $\rho_g$ , for boiling. The system of equations, Eqs. (5.15), (5.19) and Eq. (5.25), determines the work of critical cluster formation at heterogeneous nucleation.

### 5.3. Contact angle and catalytic activity factor for nucleation at a planar surface

#### 5.3.1. Contact angle

In heterogeneous nucleation on a planar solid surface the work of cluster formation is affected considerably by the value of the contact angle [4, 21, 27]. In the terminology usually employed for water, if the contact angle has values less than  $90^\circ$ , the surface is denoted as hydrophilic, contact angles larger than  $90^\circ$  imply

that the surface is hydrophobic. This terminology we will employ here similarly for condensation and boiling of the considered van der Waals fluid. Since the contact angle can be computed via Young's equation, Eq. (5.15), as

$$\cos \gamma = \frac{\sigma_{gs} - \sigma_{ls}}{\sigma_{lg}}, \quad (5.26)$$

for a hydrophilic surface  $\sigma_{ls} < \sigma_{gs}$  holds while for a hydrophobic surface the inequality  $\sigma_{ls} > \sigma_{gs}$  is fulfilled. These different cases of nucleation are illustrated in Fig. 5.2 showing a droplet (Fig. 5.2a and b) and a bubble (Fig. 5.2c and d) on a hydrophilic (Fig. 5.2a and d) and hydrophobic (Fig. 5.2b and c) surfaces, respectively. These four different cases of heterogeneous nucleation we consider here in detail separately.

In the classical approach to heterogeneous nucleation, the bulk properties of the cluster phase and the ambient phase fluid are considered commonly as given and fixed and, by this reason, also the surface energy terms entering Eq. (5.15) can be treated as constants. By this reason, the contact angle is a constant as well. Accounting, in terms of the generalized Gibbs' approach, for changes of the bulk state parameters of the newly evolving phase leads to the consequence that the contact angle has to be determined as a function of these state parameters as well affecting then finally also the catalytic activity with respect to nucleation. By this reason, we first consider the problem of determining the contact angle in dependence on the state parameters of both ambient and newly evolving in the system phases.

According to Eq. (5.26) in order to determine the contact angle it is necessary to know the specific energy of the liquid-solid, vapor-solid and liquid-vapor interfaces for the case, when density of the ambient phase (by changing externally the supersaturation) varies in a range from the equilibrium value of the vapor density,  $\rho_{g,0}$ , to the equilibrium value of the liquid density,  $\rho_{l,0}$  (determined by Eq. (5.8)), and the density of the critical clusters varies accordingly in this range or takes over values even beyond it. In order to have an expression for the fluid-solid specific interfacial

energy, we proceed here as follows.

The specific energy of the solid-fluid interface,  $\sigma_{fs}$ , depends on the density of the fluid (vapor or liquid), which is in contact with the solid surface, and in the simplest (linear in the density of the fluid) approximation can be written as

$$\sigma_{fs}(\rho) = \frac{\sigma_{gs,0}(\rho_{l,0} - \rho) + \sigma_{ls,0}(\rho - \rho_{g,0})}{\rho_{l,0} - \rho_{g,0}}. \quad (5.27)$$

Here  $\sigma_{ls,0}$  and  $\sigma_{gs,0}$  are the specific energy of the liquid-solid and vapor-solid interfaces for the equilibrium states of the liquid and vapor, respectively. The corresponding parameters without index 0 refer to the current values of these quantities for an arbitrary value of the density of the fluid.

This equation can be obtained from the following considerations: First, we write down Taylor expansions of the fluid-solid specific interface energy,  $\sigma_{fs}(\rho)$ , both in the vicinity of the equilibrium density ( $\rho_{l,0}$ ) of the liquid,  $\sigma_{ls}(\rho)$ , and the vapor (with the equilibrium density,  $\rho_{g,0}$ ),  $\sigma_{gs}(\rho)$ ,

$$\begin{aligned} \sigma_{ls}(\rho) &= \sigma_{ls,0} + \left. \frac{\partial \sigma_{ls}}{\partial \rho} \right|_{\rho=\rho_{l,0}} (\rho - \rho_{l,0}), \\ \sigma_{gs}(\rho) &= \sigma_{gs,0} + \left. \frac{\partial \sigma_{gs}}{\partial \rho} \right|_{\rho=\rho_{g,0}} (\rho - \rho_{g,0}). \end{aligned} \quad (5.28)$$

In addition, we assume here linearity of the dependence of  $\sigma_{fs}(\rho)$  on density in the whole interval leading to

$$\left. \frac{\partial \sigma_{gs}}{\partial \rho} \right|_{\rho=\rho_{g,0}} = \left. \frac{\partial \sigma_{ls}}{\partial \rho} \right|_{\rho=\rho_{l,0}} = \frac{\sigma_{ls,0} - \sigma_{gs,0}}{\rho_{l,0} - \rho_{g,0}}. \quad (5.29)$$

A combination of Eqs. (5.28) and (5.29) results immediately in Eq. (5.27).

Eq. (5.27) yields then further

$$\sigma_{gs} - \sigma_{ls} = \sigma_{fs}(\rho_g) - \sigma_{fs}(\rho_l) = (\sigma_{gs,0} - \sigma_{ls,0}) \frac{\rho_l - \rho_g}{\rho_{l,0} - \rho_{g,0}}. \quad (5.30)$$

We can see from Eq. (5.30) that the difference  $(\sigma_{gs} - \sigma_{ls})$  is linear in  $(\rho_l - \rho_g)$ , positive for hydrophilic  $((\sigma_{gs,0} - \sigma_{ls,0}) > 0)$  and negative for hydrophobic  $((\sigma_{gs,0} - \sigma_{ls,0}) < 0)$  surfaces in accordance with above given definition. The difference in the signs of the mentioned specific surface energy terms is the main difference for the two types of surfaces which is reflected also in the different types of behavior in heterogeneous nucleation.

As a second parameter, we have to know the surface tension for liquid-vapor coexistence. As it is discussed in detail in [5, 14], the surface tension of the liquid-vapor interface,  $\sigma_{lg}$ , for the equilibrium coexistence of vapor and liquid is frequently found experimentally to be proportional to some power law with respect to the density differences of liquid and vapor. Extending this result to arbitrary values of the densities of liquid and gas as performed also in the analysis of homogeneous nucleation in [5, 14] with adequate results, we arrive at

$$\sigma_{lg} = \sigma_{lg,0} \left( \frac{\rho_l - \rho_g}{\rho_{l,0} - \rho_{g,0}} \right)^\delta, \quad \delta = 2.5. \quad (5.31)$$

Here  $\sigma_{lg,0}$  is the surface tension of the liquid-vapor interface for the equilibrium coexistence states of the liquid and vapor. In this notation, the coefficient  $\Theta$  in Eq. (5.21) takes the form

$$\Theta = \sigma_{lg,0} (\rho_{l,0} - \rho_{g,0})^{-\delta}. \quad (5.32)$$

Equation (5.26), accounting for Eqs. (5.30) and (5.31), yields

$$\cos \gamma(\rho_g, \rho_l) = \cos \gamma_0 \left( \frac{\rho_{l,0} - \rho_{g,0}}{\rho_l - \rho_g} \right)^{\delta-1}, \quad (5.33)$$

where

$$\cos \gamma_0 = \frac{\sigma_{gs,0} - \sigma_{ls,0}}{\sigma_{lg,0}} . \quad (5.34)$$

The first factor in Eq. (5.33),  $\cos \gamma_0$ , can be considered as some property of the solid surface with respect to the liquid under consideration, while the second factor in Eq. (5.34) depends on the density of the fluid (liquid or vapor). Thus, for the analysis of heterogeneous nucleation it is necessary to know the contact angle for the equilibrium values of the density of vapor and liquid,  $\gamma_0$ . For further calculations we choose this value as equal to  $\gamma_0 = 67^\circ$  for a hydrophilic surface and  $\gamma_0 = (180^\circ - 67^\circ) = 113^\circ$  for a hydrophobic one (as will be shown below, this option provides a certain symmetry between the processes of nucleation on hydrophilic and hydrophobic surfaces). With respect to this term, the situation is similar to the analysis as performed employing the classical Gibbs approach to the description of heterogeneous nucleation. Generalizing this result to take into consideration changes in the density of the fluid phase, we have here to account adequately also for the second term in Eq. (5.33).

### 5.3.2. Catalytic factor for nucleation: Limiting cases

A straightforward analysis of heterogeneous nucleation in terms of the generalized Gibbs' approach shows that – similarly to the classical treatment [21] – the work of critical cluster formation can be written in a form as given by Eq. (5.17), i.e. as  $\Delta G_{het} = \phi \Delta G_{hom}$ , where for the case of droplet formation the nucleation activity factor,  $\phi$ , has the form

$$\phi(\rho_g, \rho_l) = \frac{1}{4} (2 - 3 \cos \gamma + (\cos \gamma)^3) . \quad (5.35)$$

For the case of nucleation of a bubble in a liquid ( $\gamma \rightarrow \pi - \gamma$ ), we obtain

$$\phi(\rho_g, \rho_l) = \frac{1}{4} (2 + 3 \cos \gamma - (\cos \gamma)^3) . \quad (5.36)$$

The contact angles in Eqs. (5.35) and (5.36) are determined in our approach by Eq. (5.33) and not via Eq. (5.34) as it is the case in Volmer's classical and subsequently performed similar analysis. The first general problem we have to analyze consists in one particular feature of Eq. (5.33). It has real solutions only when the inequality

$$\rho_l - \rho_g \geq |\cos \gamma_0|^{1/(\delta-1)} (\rho_{l,0} - \rho_{g,0}) \quad (5.37)$$

is fulfilled. First we have to find out therefore which kind of behavior can be expected when Eq. (5.37) is not fulfilled.

As can be verified easily, in such cases the formation of a critically sized drop or bubble in contact with the solid is excluded. Indeed, in the limiting case when the contact angle approaches the boundaries of the interval, given by Eq. (5.37), for nucleation of a droplet on a hydrophobic surface and for the nucleation of a bubble on the hydrophilic surface, the contact angle approaches  $180^\circ$ . In other words, we have in this limit and beyond the situation that the droplet or bubble are separated from the surface. In such cases,  $\phi(\rho_g, \rho_l) = 1$  holds and heterogeneous nucleation is not more favorable as compared to homogeneous nucleation. For nucleation of a droplet on a hydrophilic surface and a bubble on a hydrophobic surface, the limiting value of the contact angle is equal to  $0^\circ$ , and the catalytic activity factor tends to zero,  $\phi(\rho_g, \rho_l) = 0$ . In other words, heterogeneous nucleation may proceed here not requiring the overcoming of a thermodynamic potential barrier, i.e., proceeds similar via a non-threshold mechanism of phase formation similar to the spinodal decomposition in unstable homogeneous states. The corresponding "crossover densities" of the liquid in the critical droplet,  $\rho_{lm}$ , and of the vapor in the critical bubble,  $\rho_{gm}$ , are given by the equations

$$\rho_{lm} = \rho_g + |\cos \gamma_0|^{1/(\delta-1)} (\rho_{l,0} - \rho_{g,0}) , \quad (5.38)$$

$$\rho_{gm} = \rho_l - |\cos \gamma_0|^{1/(\delta-1)} (\rho_{l,0} - \rho_{g,0}) . \quad (5.39)$$

Thus, a contact angle in the range  $0 < \theta < \pi$  can be observed only when  $\rho > \rho_{lm}$  at droplet nucleation and for  $\rho < \rho_{gm}$  at bubble nucleation.

We see that the factors affecting nucleation act in opposite directions, factors which stimulate nucleation of the droplets inhibit the nucleation of bubbles, and vice versa, in dependence on the type of solid surface. Thus, it follows that a change of the contact angle (deviations from its equilibrium value  $\gamma_0$ ), as computed here in terms of the generalized Gibbs' approach, reduces the work of formation of droplets of critical size on a hydrophilic surface and increases it on a hydrophobic one. For the nucleation of bubbles the situation is opposite: the work of critical nucleus increases with a change of the contact angle on a hydrophilic surface and decreases on a hydrophobic one.

## 5.4. Heterogeneous condensation on planar solid surfaces: Results

### 5.4.1. Vapor condensation on a hydrophilic surface

For a hydrophilic surface (assuming, as it was mentioned earlier that the classical (equilibrium) contact angle,  $\gamma_0$ , is taken equal to  $\gamma_0 = 67^\circ$ ), the analysis of Eqs. (5.19) and Eq. (5.35) leads to the conclusion that, for a moderate supersaturation (initial states located near to the binodal curve with the density  $\rho_{g,0} = 0.128$ ), the work of critical cluster (droplet) formation has a typical saddle shape in the  $(r, \rho)$ -space near to the state corresponding to the parameters of the critical cluster,  $(r_{cr}, \rho_{cr})$  (see Fig. 5.3a). In Fig. 5.3a, this kind of behavior is illustrated for a value of the reduced temperature equal to  $\theta = 0.7$  and an initial density of the vapor equal to  $\rho_g = 0.18$ .

Such kind of behavior is found with increasing density of the vapor up to an upper limiting value equal to  $\rho_{g,sh} = 0.191$  (which we denote as surface spinodal to distinguish it from the bulk spinodal which is determined by Eq. (5.9)) for the

chosen parameters ( $\theta = 0.7$ ,  $\gamma_0 = 67^\circ$ ). For larger values of the density of the vapor,  $\rho_g > \rho_{g,sh}$ , there is opened now a new path of evolution to the newly evolving liquid phase where no activation barrier has to be overcome. The critical cluster with the radius  $r_{cr}$  and a density  $\rho_{cr}$  corresponds in these cases to a work of critical cluster formation equal to zero. For droplet sizes larger than these critical cluster sizes, there exists a path of evolution where its further growth leads to a decrease of the Gibbs free energy. By this reason, we denote the respective cluster state also as critical cluster with a critical cluster radius despite its different physical meaning as compared to "normal" cases when the critical cluster corresponds to a maximum or a saddle point of the thermodynamic potential surface. These results are illustrated in Fig. 5.3b (path of evolution 1;  $\theta = 0.7$ ,  $\rho_g = 0.20$ ).

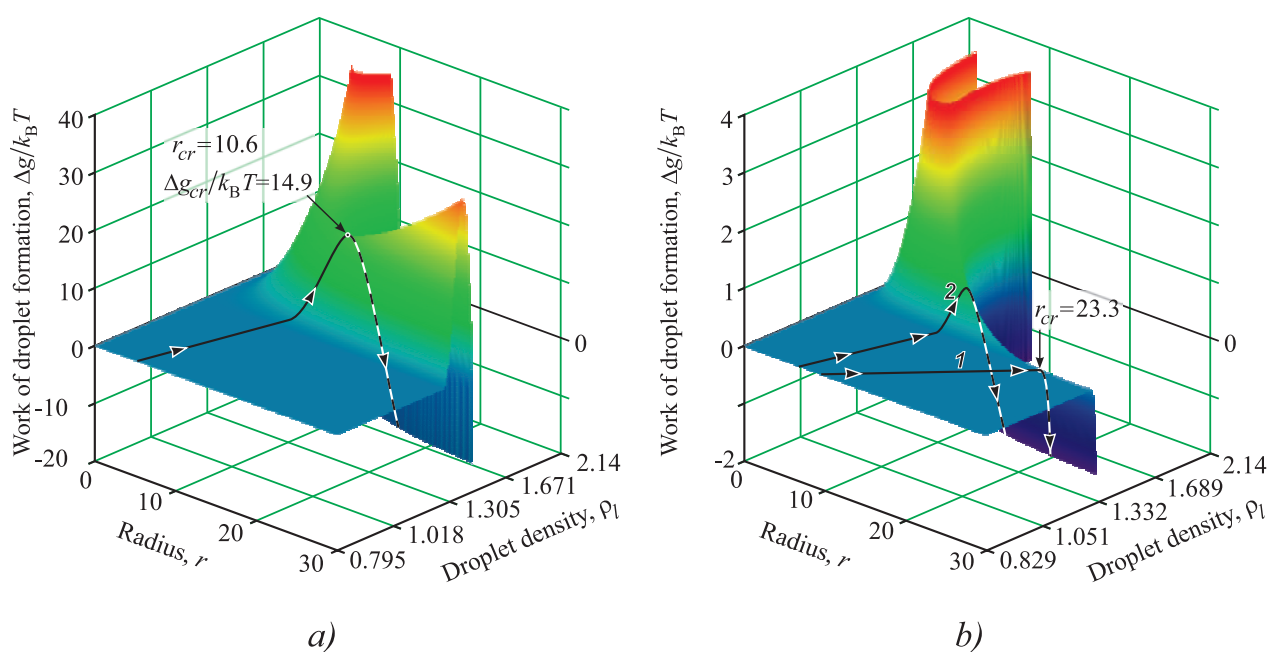


Fig. 5.3. Landscape of Gibbs free energy of droplet formation in dependence on the state parameters of the droplet for a metastable state with an initial density of the gas equal to  $\rho_g = 0.18$ . For such case, the thermodynamic landscape in the vicinity of the critical droplet size has a saddle-type shape (a). For values of the density of the gas higher than an upper limit,  $\rho_g > \rho_{g,sh}$ , e.g., for a value  $\rho_g = 0.20$ , an evolution path to the new phase is possible without overcoming of a thermodynamic potential barrier (b).

The limiting value of the density,  $\rho_{g,sh}$ , is determined by the solution of the equation

$$\rho_{lm}(\rho_{g,sh}) = \rho_{cr}(\rho_{g,sh}) , \quad (5.40)$$

where  $\rho_{lm}$  is given by Eq. (5.38) and  $\rho_{cr}$  is the solution of the system of equations Eqs. (5.25), i.e., the droplet density of the critical cluster (drop in the considered here case). The density of the critical cluster is equal to  $\rho_{lm}(\rho_g)$  for  $\rho_g > \rho_{g,sh}$ , and equal to  $\rho_{cr}(\rho_g)$  for  $\rho_g < \rho_{g,sh}$ . The parameters of the critical cluster in dependence on vapor density are illustrated in Fig. 5.4 ((a) density of the critical cluster, (b) critical droplet radius, (c) work of critical droplet formation). With an increase of the density of the vapor starting at initial states near the binodal curve, the density of the critical droplet decreases and reaches the density of the vapor at  $\rho_g = \rho_{g,sh}$ . With a

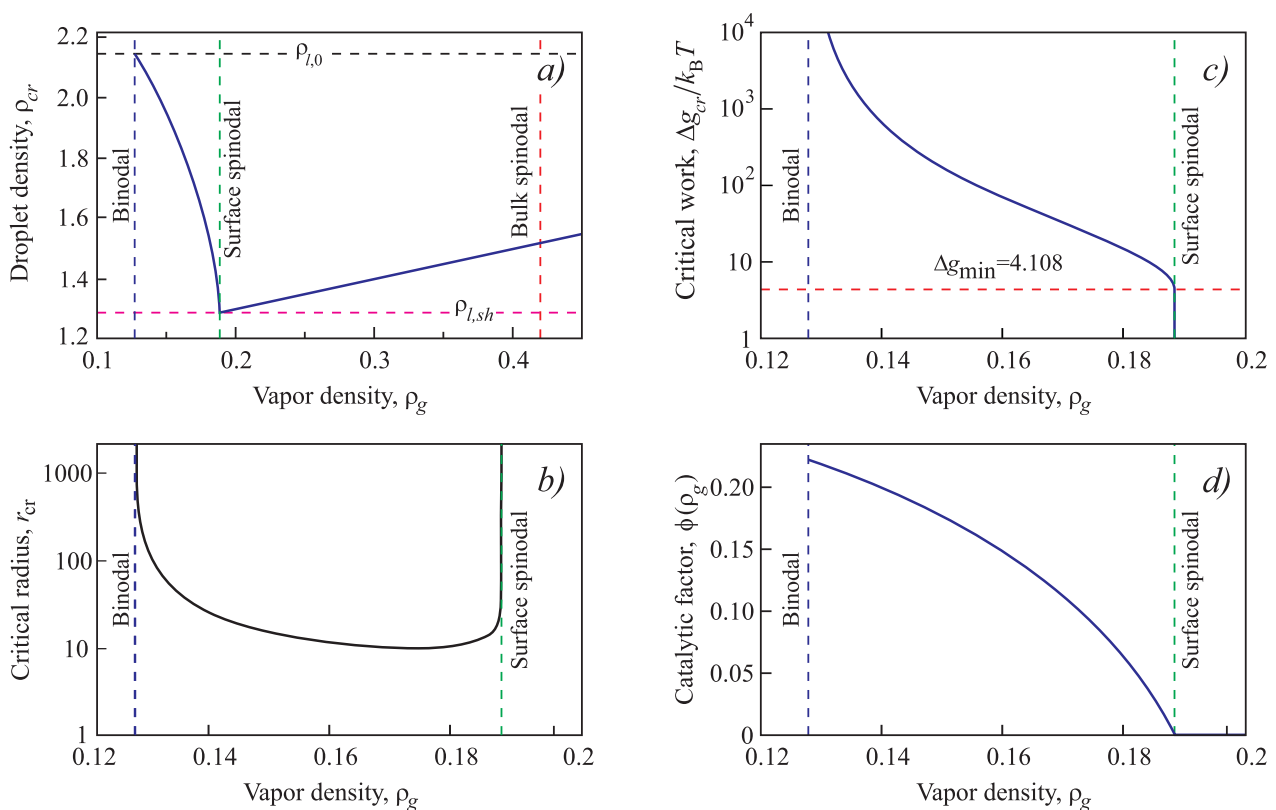


Fig. 5.4. Dependence of the parameters of the critical droplet on the density of the gas for vapor condensation on a hydrophilic planar solid surface: (a) density of critical droplet, (b) critical radius, (c) work of critical cluster formation, (d) catalytic activity factor.

further increase of the density of the vapor, the density of the critical droplet linearly grows with the density of the vapor (Fig. 5.4a and Eq. (5.38)). In agreement with the classical picture, the size of the critical droplet tends to infinity for initial states of the vapor in the vicinity of the binodal. With an increase of the density of the gas,  $\rho_g$ , the critical droplet size decrease first. However, in contrast to the classical picture, in the approach to the limiting value,  $\rho_g = \rho_{g,sh}$ , the critical cluster size starts to increase again and reaches infinity at  $\rho_g = \rho_{g,sh}$ . For even higher values of  $\rho_g$ , the critical cluster size decreases then again (Fig. 5.4b). Similarly, the work of critical droplet formation decreases monotonically from infinity (for initial states at the binodal curve) to a finite value  $\Delta g_{min}$  at  $\rho_g = \rho_{g,sh}$ . It becomes identically equal to zero at  $\rho_g > \rho_{g,sh}$  (Fig. 5.4c). Note also that at  $\rho_g = \rho_{g,sh}$  the work of a critical cluster formation has a discontinuity,  $\Delta g_{cr}/k_B T|_{\rho_g=\rho_{g,sh}} = \Delta g_{min}/k_B T = 4.108$ . However, at any values  $\rho_g > \rho_{g,sh}$  the work of critical cluster formation is identically equal to zero, i.e.,  $\Delta g_{cr} = 0|_{\rho_g>\rho_{g,sh}}$ . Fig. 5.4d shows dependence of the catalytic activity factor,  $\phi(\rho_g) = \phi(\rho_g, \rho_{lc}(\rho_g))$ , in the work of critical cluster formation, Eqs. (5.17) and (5.38), on vapor density. It decreases with increasing density of the gas and is equal to zero at  $\rho_g \geq \rho_{g,sh}$ .

A similar behavior as found here and illustrated in Figs. 5.3-5.4 was earlier also observed by us in the analysis of homogeneous condensation and boiling ([12–15], e.g. Figs. 1, 2, 5 in [14]) and of segregation processes in solutions in the absence of heterogeneous nucleation cores ([17, 18], e.g., Figs. 4-6 in [18]). In both cases, for homogeneous phase formation a similar behavior as obtained here in the approach to  $\rho_{sh}$  is found there in the approach of the classical spinodal curve (cf. Fig. 5.1). Consequently, we may conclude that the existence of heterogeneous nucleation cores may result effectively in a shift of the spinodal curve from the value computed thermodynamically for the homogeneous systems (as illustrated in Fig. 5.1) to a value affected in addition by the properties of the solid nucleation core ( $\rho_g = \rho_{g,sh}$ ). Therefore we can consider the range of gas densities,  $\rho_{l,0} < \rho_g < \rho_{g,sh}$ , with respect

to heterogeneous nucleation as the metastable region and the range  $\rho_g > \rho_{g,sh}$  as thermodynamically unstable states, the value  $\rho_g = \rho_{g,sh}$  is to be treated consequently as a part of the spinodal curve with respect to heterogeneous nucleation.

Summarizing briefly the results for the case under consideration, we can conclude: Employing the generalized Gibbs approach to condensation of a droplet in a supersaturated vapor on a hydrophilic surface leads effectively to a significant shift of the spinodal to lower supersaturations as compared to the case of homogeneous condensation. However, all basic features found for homogeneous nucleation like the divergence of the critical radius or the approach of zero values of the work of critical cluster formation near to the spinodal are retained in a qualitatively identical form.

#### 5.4.2. Vapor condensation on a hydrophobic surface

The computations for the description of heterogeneous nucleation on a hydrophobic surface can be performed similarly to the first case of condensation on a hydrophilic surface. The resulting from the computations dependencies of the parameters of the critical cluster on the vapor density for the case of nucleation on hydrophobic surface are shown in Fig. 5.5 ((a) density of the droplet of critical size, (b) critical radius of the drop, (c) work of critical droplet formation).

The analysis has been carried out for a value of the contact angle,  $\gamma_0$ , equal to  $\gamma_0 = 113^\circ$ . For  $\rho_{g,0} < \rho_g < \rho_{g,sh}$  (where  $\rho_{g,sh}$  is determined by Eq. (5.40), again), nucleation occurs heterogeneously, size and work of critical cluster formation are less than for the homogeneous case. However, for the considered case, the degree of activation of nucleation by the planar solid surface is much less expressed than for the hydrophilic case. This is seen from a comparison of full curves (representing heterogeneous nucleation) with the dashed lines showing the respective parameters of the critical droplet computed for the case of homogeneous nucleation (i.e. for  $\phi = 1$ ). With an increase of the vapor density, at some upper limiting value of the density of

the vapor, here  $\rho_{g,sh} = 0.254$ , nucleation becomes fully independent of the existence of the solid surface.

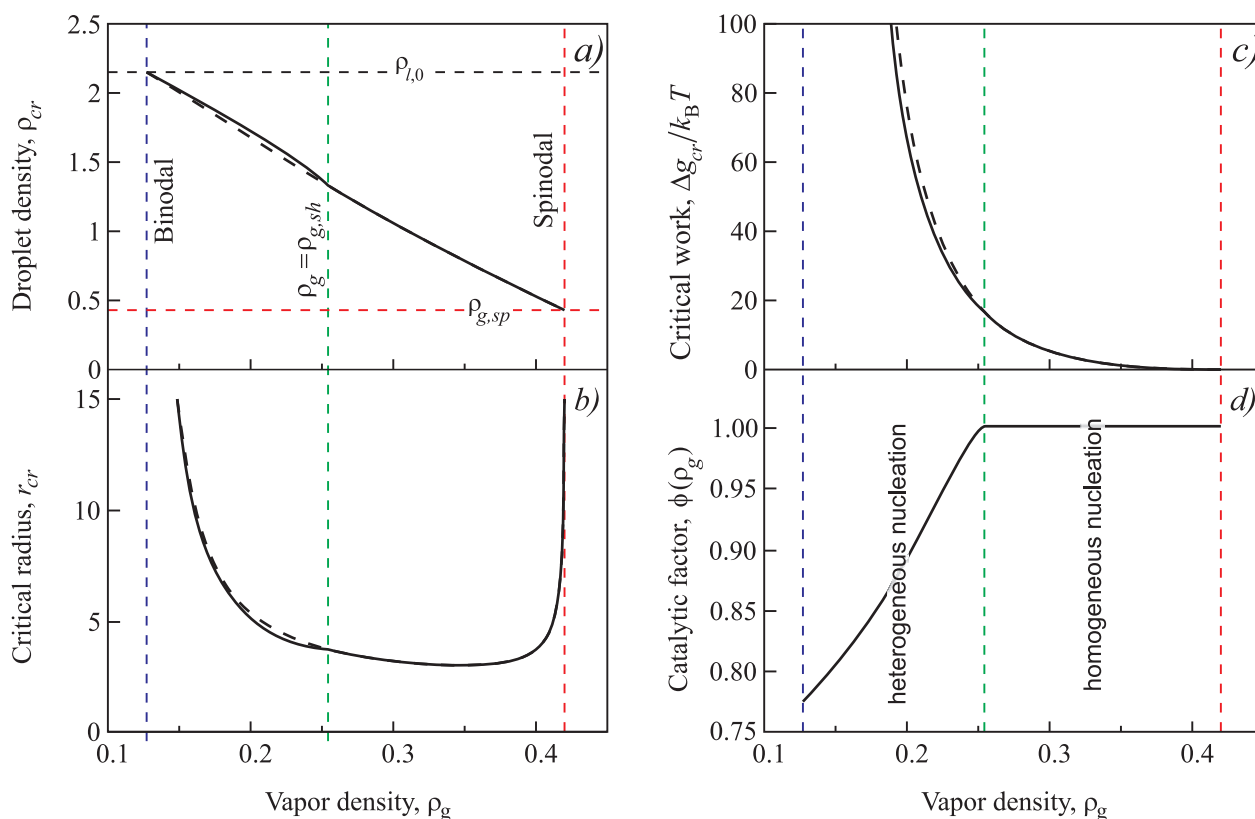


Fig. 5.5. Dependence of the parameters of the critical droplet on the density of the gas for vapor condensation on a hydrophobic planar solid surface: (a) density of critical droplet, (b) critical radius, (c) work of critical cluster formation, (d) catalytic activity factor. Dashed lines show the same dependencies for the case of homogeneous nucleation, i.e.,  $\phi(\rho_g, \rho_l) = 1$ .

Fig. 5.5d shows the dependence of the catalytic activity factor,  $\phi(\rho_g) = \phi(\rho_g, \rho_{lc}(\rho_g))$ , on the vapor density. It is less than one for  $\rho_g < \rho_{g,sh}$ . At  $\rho_g > \rho_{g,sh}$  the relation  $\phi = 1$  is generally fulfilled, i.e., all parameters of the critical cluster are the same as for homogeneous nucleation.

### 5.4.3. Boiling on a hydrophobic surface

For the case of boiling catalyzed by a planar solid interface, we can proceed similarly as in the case of condensation, however, now the density of the liquid,  $\rho_l$ , is varied (decreased). For a hydrophobic surface (assuming, again,  $\gamma_0 = 113^\circ$ ), an analysis of Eqs. (5.19) and (5.36) yields that in the interval between the binodal,  $\rho_{l,0} = 2.14$ , and some lower limiting density,  $\rho_{l,sh}$  (here  $\rho_{l,sh} = 2.01$ ), the Gibbs free energy in the space  $(r, \rho)$  near the critical point,  $(r_{cr}, \rho_{cr})$ , has a characteristic saddle-type shape (see Fig. 5.6a,  $\rho_l = 2.035$ ). For  $\rho \leq \rho_{l,sh}$ , there exists again a path of evolution with a zero value of the work of formation of the critical bubble (see Fig. 5.6b,  $\rho_l = 1.95$ ; curve 1). The limiting density of the liquid,  $\rho_{l,sh}$ , is determined

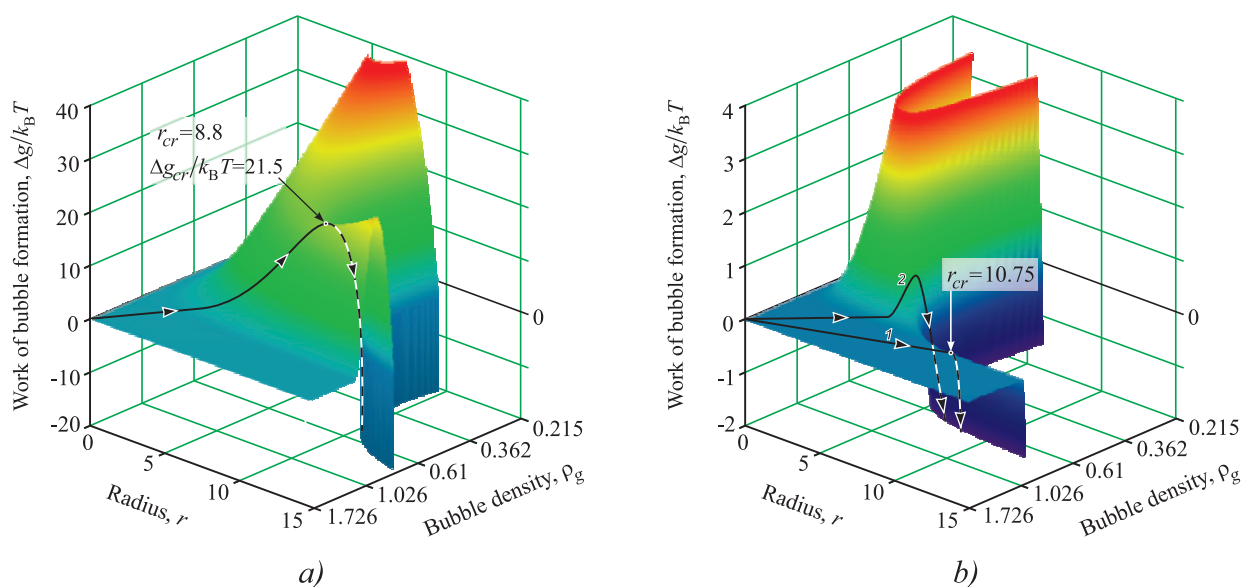


Fig. 5.6. Landscape of Gibbs free energy for boiling in dependence on the state parameters of the bubble starting from (a) a metastable,  $\rho_l = 2.035$ , and (b) an unstable initial state,  $\rho_l = 1.95$ . Path 1 in figure (b) shows the energetically favored path of evolution, curve 2 the real path.

by the solution of the equation

$$\rho_{gm}(\rho_{l,sh}) = \rho_{cr}(\rho_{l,sh}), \quad (5.41)$$

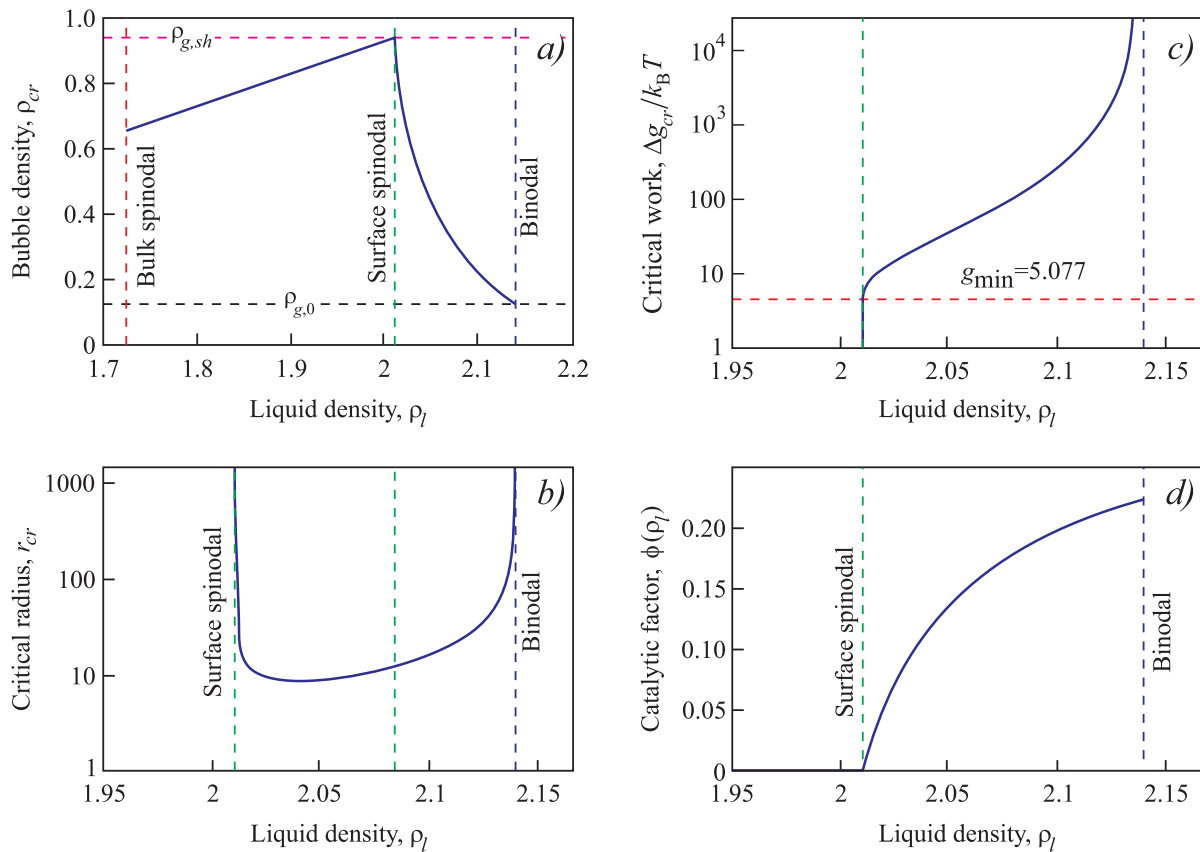


Fig. 5.7. Dependence of the parameters of the critical bubble on the density of the liquid gas for boiling on a hydrophobic planar solid surface: (a) density of the bubble of critical size, (b) critical bubble radius, (c) work of critical bubble formation, (d) catalytic activity factor.

where  $\rho_{gm}$  is determined by Eq. (5.39),  $\rho_{cr}$  is the the critical density of the bubble given by the solution of the system of equations, Eq. (5.25). The density of the critical bubble is equal to  $\rho_{gm}(\rho_l)$  at  $\rho_l < \rho_{l,sh}$ , and  $\rho_{cr}(\rho_l)$  at  $\rho_l > \rho_{l,sh}$ .

The dependence of the parameters of the critical bubble on the density of the liquid are shown in Fig. 5.7 ((a) bubble density, (b) radius, (c) work of critical bubble formation).

Fig. 5.7d shows the dependence of the catalytic activity factor,  $\phi(\rho_l) = \phi(\rho_{gc}(\rho_l), \rho_l)$ , on the density of the liquid. It is evident that Figs. 5.7 in essence are mirrored versions of Figs. 5.4. Consequently, the conclusions drawn in Section 6.4.1 with respect to vapor condensation on a hydrophilic surface are fully applicable for the considered in this subsection case of boiling on a hydrophobic surface.

#### 5.4.4. Boiling on hydrophilic surface

For a hydrophilic surface (assuming, again,  $\gamma_0 = 67^\circ$ ), the dependencies of the parameters of the critical bubble on the density of the liquid are shown in Fig. 5.8 ((a) density, critical bubble radius, work of critical bubble formation). Fig. 5.8d shows the dependence of the catalytic activity factor,  $\phi(\rho_l) = \phi(\rho_{gc}(\rho_l), \rho_l)$ , on the density of the liquid. By dashed lines, the respective parameters are given calculated for the case  $\phi = 1$ , i.e., for the case of homogeneous nucleation. We can see that the Figs. 5.8 are mirrored versions of Figs. 5.5, so that the conclusions derived in Section 6.4.2 with respect to vapor condensation on a hydrophobic surface are fully applicable to the case of boiling on hydrophilic surface considered in the present subsection.

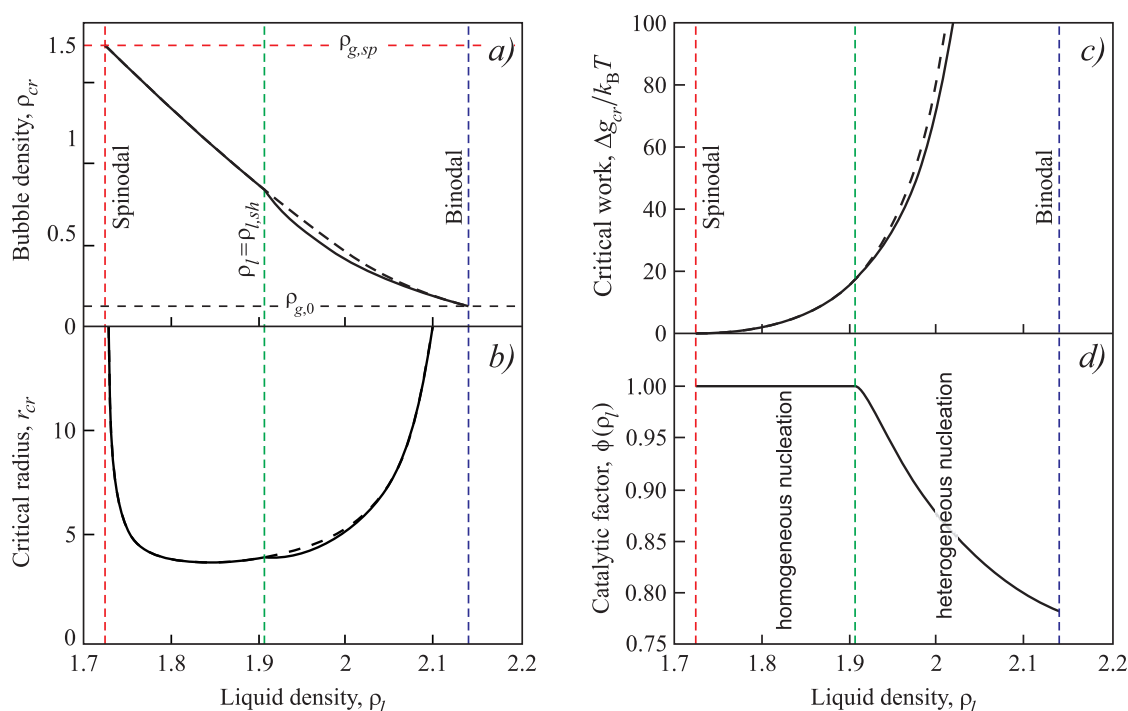


Fig. 5.8. Dependence of the parameters of the critical bubble on the density of the liquid gas for boiling on a hydrophilic planar solid surface: (a) density of the bubble of critical size, (b) critical bubble radius, (c) work of critical bubble formation, (d) catalytic activity factor. Dashed lines show the same dependencies for the case of homogeneous nucleation, i.e.,  $\phi(\rho_g, \rho_l) = 1$ .

### 5.4.5. Saddle-point versus ridge crossing

Let us finally briefly address also another point connected with the question to what extent the parameters of the critical clusters determine the evolution to the newly evolving phase. As discussed by us in detail for the case of (homogeneous) segregation in solutions [17–20] – employing the generalized Gibbs’ approach – the evolution to the new phase does not proceed necessarily via the the thermodynamically preferable trajectory (passage of the saddle point) shown here in Figs. 5.3a and 5.6a, respectively, in Figs. 5.3b and 5.6b by curves *1*. For kinetic reasons, it may be more appropriate for the system to select a trajectory of evolution where some potential barrier has to be overcome even if a path without overcoming such barrier does exist. A similar behavior is to be expected, of course, also for homogeneous condensation and boiling near to the classical spinodal and for heterogeneous nucleation, discussed here, near to the respective “heterogeneous” spinodal curves. For vapor condensation on a hydrophilic surface, the evolution to the new phase will not proceed, as a rule, via the saddle point (cf. Fig. 5.3b, curve *1*) but via the ridge of the thermodynamic potential surface (ridge crossing; cf. Fig. 5.3b, curve *2*). A similar behavior can be expected also for boiling on a hydrophobic surface (cf. Fig. 5.6b, curve *2*).

## 5.5. Discussion and conclusions

Employing the generalized Gibbs approach to the description of condensation of a droplet in a supersaturated vapor on a hydrophilic surface and to boiling of a liquid on a hydrophobic surface we arrive widely at the same result: as compared with homogeneous nucleation, a significant shift of the spinodal curve to lower supersaturation occurs caused by the existence of the planar solid interface. This result implies that the region of instability of the fluid is enlarged and the range of initially metastable states is reduced. Such features – observed already in application

of the generalized Gibbs' approach to homogeneous condensation and boiling and changing essentially the results obtained via the classical Gibbs' treatment – like the divergence of the critical radius in the approach of the spinodal and the possibility of nucleation passing not the saddle but the ridge of the thermodynamic potential surface analyzed in detail for homogeneous phase formation [17–20] are found here as well for the new boundary of metastability.

For the case of condensation of a droplet on a hydrophobic surface and boiling of liquid on a hydrophilic surface the catalytic activity factor,  $\phi$ , increases with increasing supersaturation, it reaches a value equal to one at a certain density of the ambient fluid phase ( $\rho_{g,sh}$  or  $\rho_{l,sh}$  for the cases of droplet or bubble nucleation, respectively). In this limiting case, all parameters of the critical cluster are the same as for homogeneous nucleation. At  $\rho_g < \rho_{g,sh}$  and  $\rho_l > \rho_{l,sh}$  heterogeneous nucleation occurs, the size and work of critical cluster formation are less than for the respective homogeneous case. For all these cases (condensation of a droplet on a hydrophobic surface and boiling of liquid on a hydrophilic surface), the account of changes of the contact angle leads to an increase of the catalytic factor in nucleation and to a lowering of the respective heterogeneous nucleation rate.

In order to develop the theory, in the present analysis Eqs. (5.30) and (5.31) have been employed in order to describe the effect of density changes of the fluid on phase formation. These equations can be modified if required as well as the relations for the bulk properties of the fluid, Eq. (5.3), in order to describe more correctly a given system of interest. Note, in particular, as well that the specific (linear) form of Eq. (5.30), employed here in the analysis, can be easily generalized not changing the basic results. For example, the same results are obtained when this dependence is monotonous – positive for the hydrophilic surface and negative – for hydrophobic, and has a linear expansion in the vicinity of equilibrium densities of liquid and vapor, respectively. Then instead of Eq. (5.30) we will have two separate equations, one for the condensation of liquid droplets from vapor phase and the second one for the

description of the boiling of the liquid.

In the present study, we have considered the simple case of nucleation on planar interfaces. The account of changes of the state parameters of the cluster phase on the nucleation activity – as discussed here in detail for planar surfaces – is believed to be of significance also in a variety of other cases of phase formation, for example, in a variety of solid-solid or liquid-solid phase transformations. They are expected to be of importance also in the analysis of the size-dependence of nucleation cores as analyzed first, employing the classical Gibbs' approach, by Krastanov [29] and Fletcher [30]. Another generalization of the present analysis could consist in the incorporation of line tension effects [31–33]. All these topics can be addressed employing the general methods as outlined in the present paper.

### Acknowledgments

The authors express their gratitude to the German funding agency Deutsche Forschungsgemeinschaft (DFG: SCHM 937/16-1) for financial support.

### References

1. J. W. Gibbs, *On the Equilibrium of Heterogeneous Substances*, Transactions Connecticut Academy of Sciences **3**, 108, 343 (1875–78); see also: J. W. Gibbs, *The Collected Works*, vol. 1 (Longmans, New York – London – Toronto, 1928).
2. J. D. van der Waals and Ph. Kohnstamm, *Lehrbuch der Thermodynamik* (Johann-Ambrosius-Barth Verlag, Leipzig und Amsterdam, 1908).
3. J. S. Rowlinson: Translation of J. D. van der Waals' *The thermodynamic theory of capillarity under the hypothesis of a continuous variation of density*. J. Stat. Phys. **20**, 197 (1979); German version: J. D. van der Waals, Z. Phys. Chem. **13**, 657 (1893).
4. I. Gutzow and J. W. P. Schmelzer, *The Vitreous State: Thermodynamics, Structure, Rheology, and Crystallization* (First edition: Springer, Berlin, 1995; Second edition: Springer, Heidelberg, 2013).

5. V. G. Baidakov, *Explosive Boiling of Superheated Cryogenic Liquids* (Wiley-VCH, Berlin-Weinheim, 2007).
6. V. M. Fokin, E. D. Zanotto, N. S. Yuritsyn, and J. W. P. Schmelzer, *J. Non-Crystalline Solids* **352**, 2681 (2006).
7. J. W. Cahn and J. E. Hilliard, *J. Chem. Phys.* **28**, 258 (1958); **31**, 688 (1959).
8. J. W. P. Schmelzer, J. Schmelzer Jr., and I. Gutzow, *J. Chem. Phys.* **112**, 3820 (2000).
9. J. W. P. Schmelzer, G. Sh. Boltachev, and V. G. Baidakov, *J. Chem. Phys.* **124**, 194503 (2006).
10. J. W. P. Schmelzer, A. R. Gokhman, and V. M. Fokin, *J. Colloid Interface Science* **272**, 109 (2004).
11. J. W. P. Schmelzer, V. M. Fokin, A. S. Abyzov, E. D. Zanotto, and I. Gutzow, *International Journal of Applied Glass Science* **1**, 16 (2010).
12. J. W. P. Schmelzer and J. Schmelzer Jr., *Atmospheric Research* **65**, 303 (2003).
13. J. W. P. Schmelzer and J. Schmelzer Jr., *J. Chem. Phys.* **114**, 5180 (2001).
14. J. W. P. Schmelzer and V. G. Baidakov, *J. Phys. Chem. B* **105**, 11595 (2001).
15. J. W. P. Schmelzer, V. G. Baidakov, and G. Sh. Boltachev, *J. Chemical Physics* **119**, 6166 (2003).
16. V. G. Baidakov, G. Sh. Boltachev, and J. W. P. Schmelzer, *J. Colloid Interface Science* **231**, 312 (2000).
17. J. W. P. Schmelzer, A. S. Abyzov, and J. Möller, *J. Chem. Phys.* **121**, 6900 (2004).
18. A. S. Abyzov and J. W. P. Schmelzer, *J. Chem. Phys.* **127**, 114504 (2007).
19. A. S. Abyzov, J.W.P. Schmelzer, A.A. Kovalchuk, and V.V. Slezov, *J. Non-Cryst. Solids* **356** (2010) 2915.
20. A. S. Abyzov and J. W. P. Schmelzer, *Kinetics of segregation processes in solutions: Saddle point versus ridge crossing of the thermodynamic potential barrier*, *J. Non-Crystalline Solids*, submitted.

21. M. Volmer, *Kinetik der Phasenbildung* (Th. Steinkopff, Dresden, Leipzig, 1939).
22. B. J. Mason, *The Physics of Clouds* (Clarendon Press, Oxford, 1957).
23. J. P. Hirth and G. M. Pound, *Condensation and Evaporation* (Pergamon Press, London, 1963).
24. F. M. Kuni, A. K. Shchekin, and A. P. Grinin, *Physics Uspekhi* **44**, 331 (2001).
25. A. Dobрева-Veleva, Ts. Vassilev, J. A. de Saja, M. A. Rodriguez, and I. Gutzow, *J. Non-Crystalline Solids* **253**, 99 (1999).
26. V. Guencheva, C. Rüssel, V. M. Fokin, and I. Gutzow, *Phys. Chem. Glasses: European J. Glass Science and Technology* **48**, 48 (2007).
27. O. Hellmuth, V. I. Khvorostyanov, J. A. Curry, A. K. Shchekin, J. W. P. Schmelzer, R. Feistel, Yu. S. Djikaev, and V. G. Baidakov, *Selected Aspects of Atmospheric Ice and Salt Crystallisation*. In: J. W. P. Schmelzer and O. Hellmuth (Editors), *Nucleation Theory and Applications-Special Issues: Review Series on Selected Topics of Atmospheric Sol Formation*, Volume 1 (Joint Institute for Nuclear Research Publishing Department, Dubna, Russian, 2013).
28. J. D. van der Waals, Thesis (Sijthoff, Leiden 1873; German translation: *Die Kontinuität des gasförmigen und flüssigen Zustandes* (Johann-Ambrosius Barth Publishers, Leipzig, 1881 (first edition); 1899-1900 (second edition))).
29. L. Krastanov, *Hydrologiya i Gidrologiya SSSR* (Moscow) **12**, 16 (1957) (in Russian)
30. N. H. Fletcher, *J. Chem. Phys.* **29**, 572 (1958); *The Physics of Rainclouds* (Cambridge University Press, Cambridge, 1962).
31. B. Widom, *J. Phys. Chem.* **99** 2803 (1995).
32. G. Navascues and P. Tarazona, *J. Chem. Phys.* **75**, 2441 (1981).
33. V. Talanquer and D. W. Oxtoby, *J. Chem. Phys.* **104**, 1483 (1996).

## 5.6. Висновки до розділу 5

Результати досліджень, представлених у даному розділі, опубліковано в статті [5] (Додаток А. Список публікацій здобувача за темою дисертації). Досліджено гетерогенне зародження кластерів нової фази на плоских твердих поверхнях з урахуванням зміни параметрів стану критичних кластерів залежно від пересичення в однокомпонентній рідині ван дер Ваальса. Серед основних результатів у якості висновків можна виділити наступні:

- Показано, що у випадку утворення крапельки в перенасиченій парі на гідрофобній поверхні та утворення бульбашок у рідині на гідрофільній поверхні ефект гетерогенності незначний.

- В альтернативних випадках конденсації крапельки на гідрофільній поверхні та утворення бульбашок у рідині на гідрофобній поверхні передбачено *ефект зменшення кута змочування*, і, таким чином, збільшення каталітичної активності поверхні і швидкості нуклеації.

- Розвинуто теоретичний опис цього ефекту у випадку утворення кластерів нової фази на поверхні з низькою (контактний кут більше  $90^\circ$ ) та високою змочуваністю (контактний кут менше  $90^\circ$ ), показано, що у цьому випадку існування твердої поверхні призводить до значного зміщення спінодалі до менших значень пересичення порівняно з гомогенною нуклеацією, тобто гетерогенна спінодаль наближається до бінодалі, а область метастабільності звужується за рахунок розширення області нестабільності.

## РОЗДІЛ 6

### ГЕТЕРОГЕННА НУКЛЕАЦІЯ В РОЗЧИНАХ: УЗАГАЛЬНЕНИЙ ПІДХІД ГІББСА

У шостому розділі досліджено гетерогенне зародження кластерів нової фази у регулярному бінарному розчині на плоских твердих поверхнях.

THE JOURNAL OF CHEMICAL PHYSICS 140, 244706 (2014)

#### **Heterogeneous nucleation in solutions: Generalized Gibbs' approach**

Alexander S. Abyzov<sup>1</sup> and Jörn W. P. Schmelzer<sup>2</sup>

<sup>1</sup>*National Science Center Kharkov Institute of Physics and Technology, Academician Street 1, 61108 Kharkov, Ukraine*

<sup>2</sup>*Institut für Physik der Universität Rostock, Universitätsplatz, 18051 Rostock, Germany*

(Received 28 April 2014; accepted 9 June 2014; published online 25 June 2014)

Heterogeneous nucleation in solutions on planar solid surfaces is modeled taking into account changes of the state parameters of the critical clusters in dependence on supersaturation. The account of the variation of the state parameters of the cluster phase on nucleation is performed in the framework of the generalized Gibbs' approach. A regular solution is chosen as a model for the analysis of the basic qualitative characteristics of the process. It is shown that, employing the generalized Gibbs approach, contact angle and catalytic activity factor for heterogeneous nucleation become dependent on the degree of metastability (supersaturation) of the solution. For the case of formation of a cluster in supersaturated solutions on a surface of low wettability (the macroscopic equilibrium contact angles being larger than  $90^\circ$ ) the solid surface has only a minor influence on nucleation. In the alternative case of high wettability (for macroscopic

equilibrium contact angles being less than  $90^\circ$ ) nucleation is significantly enhanced by the solid surface. Effectively, the existence of the solid surface results in a significant shift of the spinodal to lower supersaturations as compared with homogeneous nucleation. Qualitatively the same behavior is observed now near the new (solid surface induced) limits of instability of the solution as compared with the behavior near to the spinodal curve in the case of homogeneous nucleation. ©2014 AIP Publishing LLC. [<http://dx.doi.org/10.1063/1.4884395>]

## 6.1. Introduction

Nucleation of new-phase aggregates, the process of stochastic formation of clusters of a newly evolving phase exceeding some critical size, and their subsequent growth is one of the basic mechanisms of how first-order phase transitions may proceed. These nucleation processes may be catalyzed by solid particles or planar interfaces. Latter mentioned factors may result in a decrease of the so-called work of critical cluster formation, the thermodynamic barrier which has to be overcome by a new-phase aggregate to evolve to a viable nucleus capable of further deterministic growth.

In the classical theory of nucleation and growth processes heterogeneous nucleation is commonly treated – similarly to the theoretical analysis of homogeneous nucleation – by assuming that the state parameters of the critical clusters (bulk and surface properties) are widely identical to the respective parameters of the newly evolving macroscopic phase [1–5]. This approach is supported by the classical thermodynamic theory of cluster formation as developed by Gibbs [6]. However, in reality this assumption is as a rule not fulfilled [2, 7–9].

As shown in preceding papers [8–11], the classical Gibbs approach to the thermodynamic description of thermodynamically heterogeneous systems can be

generalized to account appropriately for possible deviations of the properties of critical clusters as compared to the properties of the respective macroscopic phases. This (as denoted by us) generalized Gibbs' approach was so far mainly employed to describe different cases of homogeneous nucleation, i.e., nucleation in the absence of heterogeneous nucleation cores. Problems of the theoretical description of heterogeneous nucleation in terms of the generalized Gibbs' approach were treated by us for the first time in detail in [12]. In this analysis, we considered condensation and boiling in one-components fluids in the presence of planar solid interfaces. As a model system, we analyzed these processes for one-component van der Waals fluids.

It was shown in this analysis that, accounting for changes of the bulk properties of the critical clusters in terms of the generalized Gibbs approach, contact angle and catalytic factor for heterogeneous nucleation become dependent on the degree of metastability of the ambient fluid. For the case of formation of a droplet in a supersaturated vapor on a hydrophobic surface (the macroscopic equilibrium contact angle being larger than  $90^\circ$ ) and bubble formation in a liquid on a surface of high wettability (the macroscopic equilibrium contact angle being less than  $90^\circ$ ) the solid surface has only a minor influence on nucleation. In the alternative cases of condensation of a droplet on a hydrophilic surface and of bubble formation in a liquid on a hydrophobic surface, nucleation is significantly enhanced by the presence of the solid. As it turns out [12], effectively, the existence of the solid planar interface results at otherwise identical conditions in a significant shift of the spinodal to lower supersaturations as compared with homogeneous nucleation.

In the present paper we further advance these theoretical studies and analyze heterogeneous nucleation in supersaturated solutions in the presence of planar solid interfaces. As the method of description, we employ again the generalized Gibbs approach. As a model system for the description of the properties of the system, a two-component regular solution [13, 14] is chosen similarly as it was done in our previous analysis of homogeneous nucleation in solutions [8, 15, 16]. The general

qualitative conclusions are widely independent on this particular choice of the model system. In addition, performing the analysis for the same model as done earlier for the study of homogeneous nucleation allows us to directly specify the effect of the considered heterogeneous nucleation sites on phase formation in solutions. The main difference in our approach as compared with previous studies consists, again, in the proper account of the fact that the state parameters of the newly evolving clusters and, in particular, of the critical clusters may deviate considerably from the respective values of the newly evolving macroscopic phases. We assume incompressibility of the solutions, by this reason the appropriate state parameter for the description of both ambient and newly evolving phase is the composition of the solution.

The accounted for in our analysis additional as compared to the classical picture variation of the bulk parameters of the clusters affects also their surface properties like surface tension and wetting angles and gives thus, again, an additional contribution to the catalytic activity factor of the considered heterogeneous nucleation core with respect to nucleation. Consequently, in order to determine the work of critical cluster formation the dependence of these interface parameters on the composition of the critical nuclei has to be specified. This program will be implemented here for two cases of cluster formation in supersaturated solutions, both for the cases of high wettability (the macroscopic contact angles have values less than  $90^\circ$ ) and low wettability (the macroscopic contact angles are larger than  $90^\circ$ ).

The present article is structured as follows: In Section 9.2, the equation of state of a regular solution is briefly discussed as far as required for the subsequent derivations. In addition, the location of binodal and spinodal curves are specified, and general relations are developed allowing us to determine the work of critical cluster formation at solid planar interfaces. In Section 9.4, the expressions for the contact angle and catalytic activity factor for critical cluster formation are evaluated. Combining the results obtained in Sections 9.2 and 9.4, in Section 8.4 heterogeneous nucleation in a regular solution on planar surfaces is analyzed. A summary of the

results, conclusions, and of possible extensions (Section 8.5) completes the paper.

## 6.2. Basic equations

### 6.2.1. Bulk properties of ambient and newly evolving phases, binodal and spinodal curves

Similarly to our previous analysis of homogeneous nucleation in solutions [8, 15, 16], we consider now phase formation in a binary solid or liquid regular solution catalyzed by the presence of a planar solid interface. Regular solutions can be described by the following expressions for the chemical potentials  $\mu_j$  of the two components in the solution [13, 14],

$$\mu_1 = \mu_1^* + k_B T \ln(1 - x) + \Omega x^2, \quad (6.1)$$

$$\mu_2 = \mu_2^* + k_B T \ln x + \Omega (1 - x)^2, \quad (6.2)$$

where  $k_B$  is the Boltzmann constant,  $T$  is the absolute temperature, and  $x$  is the molar fraction of the second component (we denote it further – to some extent arbitrarily – as the solute),  $\Omega = 2k_B T_c$  is an interaction parameter describing specific properties of the system under consideration, and  $T_c$  is the critical temperature of the system.

We assume that the external pressure is kept constant. In the  $(T, x)$ -phase diagram, the binodal and spinodal curves are given then by the relations

$$\ln \left( \frac{1 - x}{x} \right) = 2 \frac{T_c}{T} (1 - 2x), \quad (6.3)$$

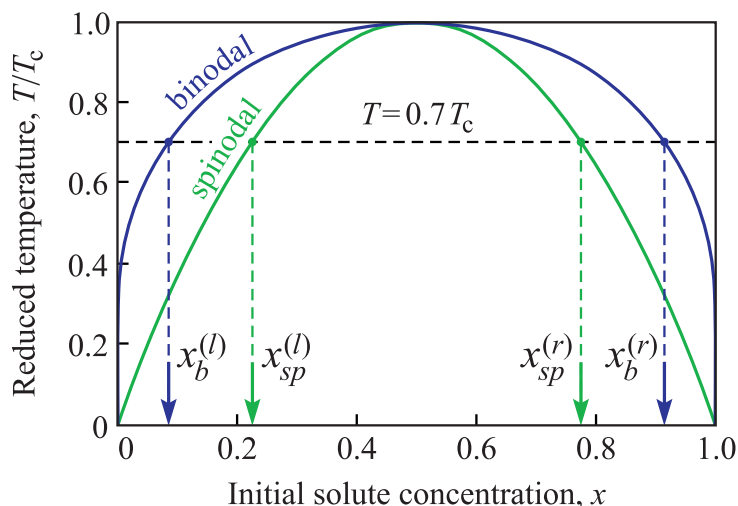


Fig. 6.1. Location of the binodal and spinodal curves for a regular solution. For an illustration of the results, we will perform here the computations for different values of the solute concentration,  $x$ , and a value of the reduced temperature equal to  $T/T_c = 0.7$ . The left-hand (marked by  $(l)$ ) and right-hand (marked by  $(r)$ ) side branches of the binodal ( $x_b^{(r)} = 1 - x_b^{(l)}$ ) and the spinodal ( $x_{sp}^{(r)} = 1 - x_{sp}^{(l)}$ ) curves are specified in the figure as well (see also text).

$$x(1-x) = 4 \frac{T}{T_c}. \quad (6.4)$$

The respective curves are shown in Fig. 6.1. They are symmetric with respect to  $x = 1/2$ . Thus, if for a given value of temperature the composition  $x$  refers to one of these curves, the composition  $(1-x)$  gives the location of the respective alternative branch.

Numerical computations will be performed here assuming the reduced temperature to be equal to  $T/T_c = 0.7$ . The left-hand side branches of the binodal,  $x_b^{(l)}$ , and the spinodal,  $x_{sp}^{(l)}$ , curves are located for this temperature at

$$x_b^{(l)} = 0.0857, \quad x_{sp}^{(l)} = 0.2261, \quad (6.5)$$

respectively. The respective right-hand side values of the molar fractions for the

binodal and spinodal curves are given by

$$x_b^{(r)} = 1 - x_b^{(l)} = 0.9143, \quad x_{sp}^{(r)} = 1 - x_{sp}^{(l)} = 0.7739. \quad (6.6)$$

An illustration of these notations and results is given in Fig. 6.1.

### 6.2.2. Work of critical cluster formation: General expression

Suppose that the system is instantaneously transferred into a metastable state located in between the left-hand side binodal and spinodal curves ( $x_b^{(l)} < x \lesssim x_{sp}^{(l)}$ ) and that afterwards composition and temperature are kept constant (later-on we will extend the analysis to initial concentrations on the right-hand side of the phase diagram as shown in Fig. 6.1, that is to the range  $x_{sp}^{(r)} \lesssim x < x_b^{(r)}$ ). As a first step in the description, we determine the parameters of the critical clusters formed on a planar solid interface in dependence on supersaturation (molar fraction of the solute,  $x$ ).

Cluster formation in a binary solution results from a redistribution of molecules in space. Following Gibbs' model approach [6], we consider a cluster as a spatially homogeneous part of the system with a composition different from the ambient phase. In the thermodynamic description we always employ the surface of tension [6, 10, 11] as the dividing surface, separating the cluster from the ambient phase. The expression for the change of the thermodynamic potential (the Gibbs free energy,  $G$ ) for a two-component system due to the formation of a cluster of the considered shape (segments of a sphere with a radius,  $R$ , and a contact angle,  $\gamma$  (c.f. Fig. 6.2)) in the ambient phase can be written both in the classical and generalized Gibbs' approaches then as [1–3, 12]

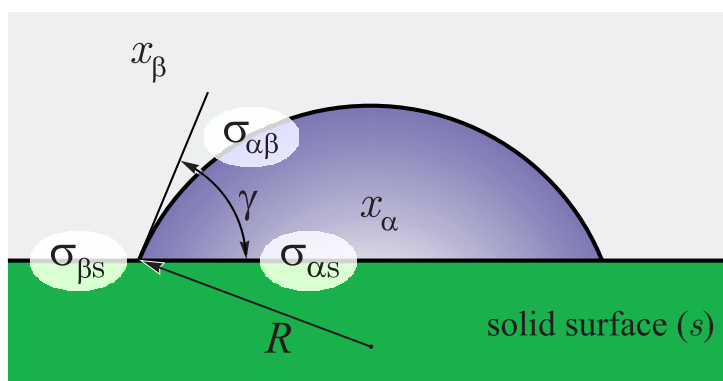


Fig. 6.2. Model employed in the analysis of heterogeneous nucleation of a cluster on a planar solid interface. Here  $R$  is the radius of curvature of the cap-shaped aggregate with composition  $x_\alpha$ ,  $x_\beta$  is the molar fraction of one of the components in the ambient solid or liquid solution,  $\gamma$  is the contact angle,  $\sigma_{\alpha\beta}$ ,  $\sigma_{\beta s}$ , and  $\sigma_{\alpha s}$  are the respective specific surface energies.

$$\Delta G = \sigma_{\alpha\beta} A_{\alpha\beta} + (\sigma_{\alpha s} - \sigma_{\beta s}) A_{\alpha s} + \sum_{j=1,2} n_j (\mu_{j\alpha} - \mu_{j\beta}) . \quad (6.7)$$

Here  $\sigma_{\alpha s}$ ,  $\sigma_{\beta s}$ , and  $\sigma_{\alpha\beta}$  are the specific surface energies (surface tension) of the cluster-solid, ambient phase-solid and cluster-ambient phase interfaces, respectively,  $A_{\alpha s}$  and  $A_{\alpha\beta}$  are the respective interfacial areas (see Fig. 6.2),  $n_\alpha = n_{1\alpha} + n_{2\alpha}$  is the number of particles (atoms, molecules) in the cluster,  $\mu_{j\alpha}$  and  $\mu_{j\beta}$  are the chemical potentials of the different components in the cluster and ambient phase, respectively (see Eqs. (6.1) and (6.2)). Here and further on, the index  $\alpha$  always denotes the parameters of the cluster, and the index  $\beta$  refers to ambient phase parameters. As independent variables for the specification of the state of the clusters, we use  $n_1$  and  $n_2$  (the subscript  $\alpha$  is omitted for  $n_1$  and  $n_2$  for convenience of the notations) or the radius,  $R$ , and the molar fraction of the second component in the cluster,  $x_\alpha = n_2 / (n_1 + n_2)$ .

In line with the basic assumptions underlying the model of binary regular solutions [13, 14] and for simplicity of the notations, the volume per particle,  $\omega$ , is assumed to be the same for both components and independent of composition ( $\omega_\alpha = \omega_\beta \equiv \omega = a^3$ ,  $a$  is an interatomic distance parameter). Cluster radius,  $R$  (more

precisely it is the radius of a segment of a sphere, but we will use the notation “cluster radius” for simplicity, again), and particle number in a cluster,  $n_\alpha$ , are related then by the following simple expression

$$\varphi \frac{4\pi}{3} R^3 = n_\alpha \omega = n_\alpha a^3, \quad (6.8)$$

where  $\varphi$  can be expressed via the contact angle,  $\gamma$ , as

$$\varphi = \frac{1}{4} (2 - 3 \cos \gamma + \cos^3 \gamma) = \frac{1}{4} (2 + \cos \gamma)(1 - \cos \gamma)^2. \quad (6.9)$$

The bulk contributions,  $\Delta G_V$ , to the Gibbs free energy change can be written for the case of formation of a cluster with a radius,  $R$ , and a contact angle,  $\gamma$  (c.f. Fig. 6.2), generally as [3, 15, 16]

$$\Delta G_V = \sum_{j=1,2} n_j (\mu_{j\alpha} - \mu_{j\beta}), \quad (6.10)$$

or, equivalently, as

$$\Delta G_V = -\varphi \left( \frac{4\pi}{3\omega} \right) R^3 \Delta\mu = \varphi \left( \frac{4\pi}{3\omega} \right) R^3 k_B T f, \quad \Delta\mu = -k_B T f. \quad (6.11)$$

In this relation, terms reflecting the effect of depletion of the ambient phase due to cluster formation are neglected. These terms are not relevant for the further derivations. The function  $f(x_\alpha, x)$  is given by the following relation

$$f(x_\alpha, x) = (1 - x_\alpha) \left\{ \ln \frac{1 - x_\alpha}{1 - x} + 2 \frac{T_c}{T} (x_\alpha^2 - x^2) \right\} + x_\alpha \left\{ \ln \frac{x_\alpha}{x} + 2 \frac{T_c}{T} [(1 - x_\alpha)^2 - (1 - x)^2] \right\}. \quad (6.12)$$

As evident from its definition (Eq. (6.11)), the function  $\Delta\mu \propto (-f(x_\alpha, x))$  has the

meaning of the thermodynamic driving force for cluster formation.

The dependence of the function  $f(x_\alpha, x)$  on the independent state variables  $x$  and  $x_\alpha$  is analyzed in detail in [8, 15, 16]. In particular, in Fig. 6.3(a) and (b) this function is shown in dependence on the composition of the cluster phase,  $x_\alpha$ , for different values of the supersaturation or the molar fraction of the segregating component,  $x$ , in the ambient phase. Note that, for any value of the composition,  $x$ , of the ambient solution, except for  $x = x_{sp}^{(l,r)}$ , the function  $f(x_\alpha)$  has one maximum and two minima. In the metastable range of composition of the ambient phase (c.f. Fig. 6.3(a)) in between left-hand side binodal and spinodal curves,  $x_b^{(l)} < x < x_{sp}^{(l)}$ , the first of these minima corresponds to the state of the ambient phase,  $x_\alpha = x$ , the second one,  $x_\alpha = x_B$ , to the minimum of the bulk contributions to the Gibbs free energy. This is the final macroscopic state of the segregating phase the cluster would evolve to for the given fixed value of the composition of the ambient phase,  $x$ . In the considered range of  $x$ -values,  $x_B$  is defined by the equation (c.f. Eqs. (6.11) and (6.12))

$$\left. \frac{\partial f(x_\alpha, x)}{\partial x_\alpha} \right|_{x=x_B} = 0. \quad (6.13)$$

At the spinodal,  $x = x_{sp}^{(l)}$ , the function  $f(x_\alpha)$  has an inflection point at  $x_\alpha = x$ . In the thermodynamically unstable range,  $x_{sp}^{(l)} < x < x_{sp}^{(r)}$ , the maximum of the function  $f(x_\alpha)$  corresponds to the state of the initial phase,  $x_\alpha = x$  (c.f. Fig. 6.3(b)). There exist now two values of the molar fraction of the cluster phase,  $x_\alpha = x_A$  and  $x_\alpha = x_B$ , for which the bulk contributions to the Gibbs free energy have a local minimum. These states are determined similarly to Eq. (6.13) by the relation

$$\left. \frac{\partial f(x_\alpha, x)}{\partial x_\alpha} \right|_{x=x_A \text{ or } x=x_B} = 0. \quad (6.14)$$

The dependencies of  $x_A$  and  $x_B$  on the initial composition,  $x$ , are shown in Fig. 6.3(c)

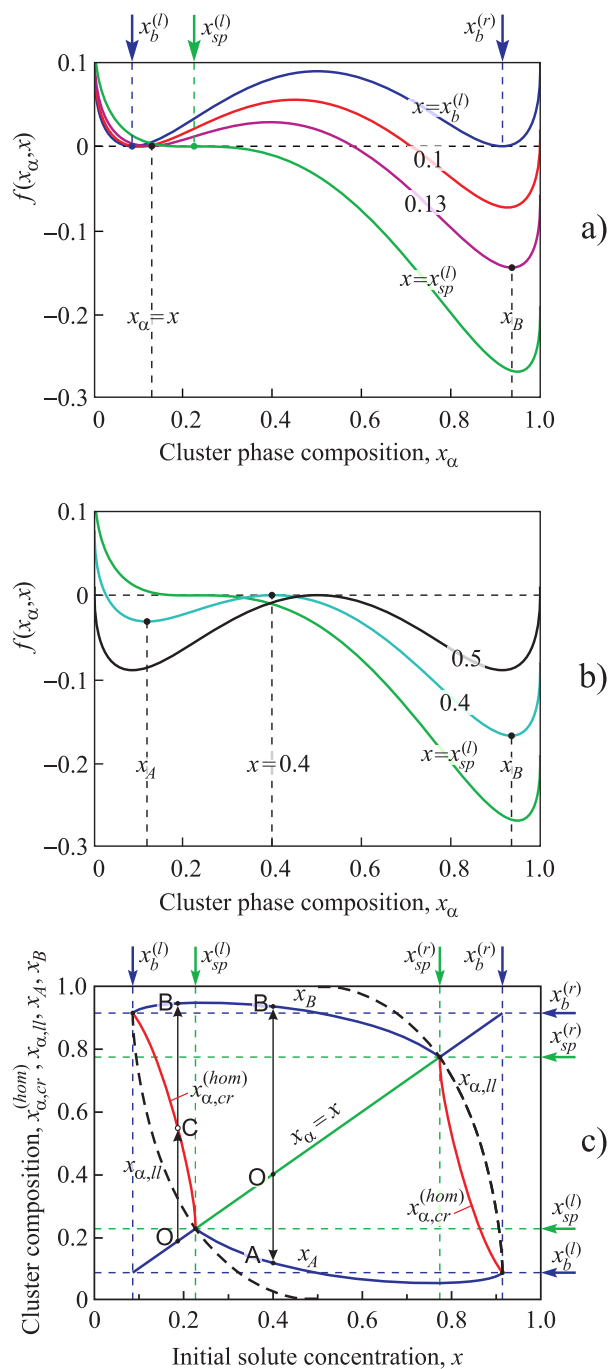


Fig. 6.3. Dependence of the function  $f(x_\alpha, x)$  on the composition of the cluster phase,  $x_\alpha$ , for different values of supersaturation or the molar fraction,  $x$ , of the segregating component in the ambient phase: a) in the thermodynamically metastable range,  $x_b^{(l)} < x < x_{sp}^{(l)}$ , b) in the unstable range,  $x_{sp}^{(l)} < x < x_{sp}^{(r)}$ . c) Composition of the critical clusters,  $x = x_{\alpha,cr}^{(hom)}$  (full red curves), its minimal value,  $x_{\alpha,ll}$  (dashed curve), and  $x_A, x_B$  (full blue curves) in dependence on initial supersaturation for the case of homogeneous nucleation in solutions.

in the whole range of possible initial compositions of the ambient solution. Let us note that all data are symmetric with respect to  $x = 1/2$  and  $x_\alpha = 1/2$ . By this reason, we analyze them in detail only for the range  $x \leq 1/2$ .

At given pressure and temperature macroscopic evolution processes in thermodynamic systems are accompanied by a decrease of the Gibbs free energy [19]. By this reason, the necessary condition for formation of aggregates of a new phase can be written as  $f(x_\alpha, x) < 0$  (the thermodynamic driving force for cluster formation has to be positive, in such case cluster evolution leads to a decrease of the bulk contributions to the Gibbs free energy). Consequently, for the metastable range of  $x$ -values the composition of the critical clusters has to exceed a lower limiting value,  $x_{\alpha, ll}$ , determined by the relation

$$f(x_{\alpha, ll}, x) = 0 \quad . \quad (6.15)$$

The dependence of  $x_{\alpha, ll}$  on the initial composition,  $x$ , is shown in Fig. 6.3(c) by dashed curves.

For comparison, the composition of the critical cluster,  $x_{\alpha, cr}^{(hom)}$ , in homogeneous nucleation (c.f. [8, 15, 16] and the subsequent discussion) is shown in Fig. 6.3(c) by full curves. Latter parameter is determined by the interplay between bulk and surface contributions to critical cluster properties. A possible path of evolution ( $O \rightarrow C \rightarrow B$ : arrows originating at the initial state and proceeding via the critical cluster composition to  $x_B$ ), starting from metastable initial states, is shown in Fig. 6.3(c). For the given value of the concentration of the ambient phase,  $x$ , the new phase attains first the composition of the critical cluster and then evolves to a state characterized by  $x_B$ . For metastable initial states, one path of evolution exists while for unstable initial states two such pathes are accessible proceeding into the direction of either  $x_A$  or  $x_B$ .

Generally, the relation  $x_{\alpha, ll} \leq x_{\alpha, cr}^{(hom)}$  holds. The inequality is reduced to the identity  $x_{\alpha, ll} = x_{\alpha, cr}^{(hom)}$  only for  $x = x_b^{(l)}$  and  $x = x_{sp}^{(l)}$ . In the latter of these special

cases, this particular value of the cluster composition,  $x_{\alpha, ll} = x_{\alpha, cr}^{(hom)}$ , determines the composition of a cluster which can be formed without the necessity of overcoming a potential barrier but, despite that, is capable of a further deterministic growth. As will be shown shortly, a similar situation may occur also in heterogeneous nucleation but for different values of the initial composition (less than  $x_{sp}^{(l)}$ ) as compared with the case of homogeneous nucleation (c.f. Eq. (6.46) and the discussion of it).

The surface contributions,  $\Delta G_S$ , to the Gibbs free energy of cluster formation are given according to Eq. (6.7) by

$$\Delta G_S = \sigma_{\alpha\beta} A_{\alpha\beta} + (\sigma_{\alpha s} - \sigma_{\beta s}) A_{\alpha s} , \quad (6.16)$$

or, equivalently, by

$$\Delta G_S = 2\pi R^2(1 - \cos \gamma)\sigma_{\alpha\beta} + \pi R^2(1 - \cos^2 \gamma)(\sigma_{\alpha s} - \sigma_{\beta s}) . \quad (6.17)$$

The condition of mechanical equilibrium along the line of contact where three phases meet is expressed by Young's equation (e.g. [1–5])

$$\sigma_{\beta s} = \sigma_{\alpha s} + \sigma_{\alpha\beta} \cos \gamma . \quad (6.18)$$

Once this relation is fulfilled, we can write the surface contributions to the Gibbs free energy as (c.f. Eq. (6.9))

$$\Delta G_S = 4\pi R^2 \sigma_{\alpha\beta} \left[ \frac{1}{4}(2 + \cos \gamma)(1 - \cos \gamma)^2 \right] = 4\pi R^2 \sigma_{\alpha\beta} \varphi . \quad (6.19)$$

Similarly to [2,3], the work of cluster formation at heterogeneous nucleation on planar

solid surfaces can be written finally as

$$\Delta G_{het} = \varphi \left\{ \frac{4\pi}{3\omega} R^3 \Delta\mu + 4\pi R^2 \sigma_{\alpha\beta} \right\} \quad (6.20)$$

or

$$\Delta G_{het} = \varphi(\gamma) \Delta G_{hom} . \quad (6.21)$$

This relation holds generally for any values of the radius,  $R$ , of the surface of the cluster and any appropriate value of the contact angle,  $\gamma$ . Employing in addition the thermodynamic equilibrium conditions at the cluster-ambient phase interface, the parameter  $\varphi$  becomes equal to the catalytic activity of a given nucleation site (planar solid interface in the case under consideration) with respect to nucleation.

A detailed derivation and discussion in terms of the generalized Gibbs approach of the expression for the work of cluster formation and, in particular, the work of critical cluster formation for homogeneous nucleation in a regular solution is given in [9, 15, 16]. Employing the notations introduced and the results obtained there, we can rewrite Eqs. (6.20)-(6.21) as

$$\frac{\Delta G(R, x_\alpha, x)}{k_B T} = \varphi(\gamma) \frac{4\pi}{3\omega} \left[ \frac{3}{2} R_\sigma R^2 (x_\alpha - x)^2 + R^3 f(x_\alpha, x) \right] , \quad (6.22)$$

where

$$R_\sigma = \frac{2\sigma_{\alpha\beta,0} a^3}{k_B T} \left( x_b^{(r)} - x_b^{(l)} \right)^{-2} . \quad (6.23)$$

Here the interfacial tension between two macroscopic phases with compositions  $x_\alpha$

and  $x$ , respectively, is expressed following Becker [13] (see also [14]) via

$$\sigma_{\alpha\beta} = \sigma_{\alpha\beta,0} \left( \frac{x_\alpha - x}{x_b^{(r)} - x_b^{(l)}} \right)^2 . \quad (6.24)$$

In Eq. (6.24),  $\sigma_{\alpha\beta,0}$  is the specific surface energy of the cluster-ambient phase interface for the case, when ambient and newly evolving phases are in equilibrium state (that is for  $x = x_b^{(l)}$  and  $x_\alpha = x_b^{(r)}$ ).

We further introduce reduced variables via the relations

$$r \equiv \frac{R}{R_\sigma} , \quad \Delta g \equiv \frac{\Delta G}{G_\sigma} , \quad (6.25)$$

$$G_\sigma = \frac{16\pi (\sigma_{\alpha\beta,0} a^2)^3}{3 (k_B T)^2} \left( x_b^{(r)} - x_b^{(l)} \right)^{-6} . \quad (6.26)$$

In these variables, Eq. (6.22) can be written in the form

$$\Delta g(r, x_\alpha, x) = \varphi(\gamma) \left[ 3r^2 (x_\alpha - x)^2 + 2r^3 f(x_\alpha, x) \right] . \quad (6.27)$$

The dependence of  $\Delta g$  on the value of the interfacial tension is reflected here by the term  $(x_\alpha - x)^2$ .

Critical cluster parameters, i.e. its size,  $r_{cr}$ , and composition,  $x_{cr}$ , are determined by the solution of the system of equations

$$\frac{\partial \Delta g(r, x_\alpha, x)}{\partial r} = 0 , \quad \frac{\partial \Delta g(r, x_\alpha, x)}{\partial x_\alpha} = 0 , \quad (6.28)$$

where  $\Delta g$  is given by Eq. (6.27). Substituting the respective values into Eq. (6.27), we may determine the work of critical cluster formation at heterogeneous nucleation. Note, however, that for a cluster of the considered shape (segments of a sphere) its

radius,  $R$  (or  $r$ ), is the radius of curvature of the cluster surface. Its value does not define unambiguously the number of atoms in the cluster (see Eq. (6.8)). By this reason, the numbers of atoms in the cluster,  $(n_1, n_2)$ , are more convenient variables as compared to the set  $(r, x_\alpha)$ .

Introducing similarly to the radius reduced particle numbers as

$$n'_1 \equiv \frac{n_1}{n_\sigma}, \quad n'_2 \equiv \frac{n_2}{n_\sigma}, \quad n_\sigma \equiv \frac{4\pi}{3} \left( \frac{R_\sigma}{a} \right)^3, \quad (6.29)$$

and omitting primes for simplicity of the notations, we can rewrite Eq. (6.27) as

$$\Delta g(n_1, n_2, x) = 3 [\varphi(\gamma)]^{1/3} n^{2/3} \left( \frac{n_2}{n} - x \right)^2 + 2nf(x, n_2/n), \quad (6.30)$$

where

$$n \equiv n_1 + n_2 = \varphi r^3 \quad (6.31)$$

is the reduced total number of atoms in the cluster. Similarly to Eq. (6.28), critical cluster parameters,  $(n_{1,cr}, n_{2,cr})$ , are determined by the solution of the system of equations

$$\frac{\partial \Delta g(n_1, n_2, x)}{\partial n_1} = 0, \quad \frac{\partial \Delta g(n_1, n_2, x)}{\partial n_2} = 0, \quad (6.32)$$

where  $\Delta g$  is now given by Eq. (6.30). With account of Eq. (6.25), the work of critical cluster formation,  $\Delta G_{cr}$ , is determined by Eq. (6.30) reducing it to a relation of the form  $(\Delta G_{cr}/G_\sigma) \equiv \Delta g_{cr}(x) = \Delta g(n_{1,cr}, n_{2,cr}, x)$ .

In heterogeneous nucleation on a planar solid surface the work of cluster formation is affected considerably by the value of the contact angle [2–4]. The expression for the work of critical cluster formation, Eq. (6.27), differs from the one describing homogeneous nucleation [15, 16] by the nucleation-activity factor,

$\varphi(\gamma)$ . This factor is equal to one in the case of homogeneous nucleation, its value in heterogeneous nucleation on planar interfaces determines, consequently, its nucleation activity. As evident from Eqs. (6.9) and (6.21), the nucleation activity is determined basically by the value of the contact angle,  $\gamma$ . In the analysis of heterogeneous nucleation in the framework of the generalized Gibbs approach, primarily the contact angle becomes dependent on the composition of both ambient and cluster phases and determines then the catalytic activity and, finally, the work of critical cluster formation in heterogeneous nucleation as will be shown now in Sections 9.4 and 8.4.

### **6.3. Contact angle in heterogeneous nucleation at a planar solid surface**

#### **6.3.1. Contact angle**

In the classical approach to heterogeneous nucleation, the bulk properties of the cluster phase are considered commonly as given and fixed and, by this reason, also the surface energy terms entering Young's equation, Eq. (6.18), can be treated as constants. By this reason, the contact angle is a constant as well. Accounting, in terms of the generalized Gibbs approach, for changes of the bulk state parameters of the cluster of the newly evolving phase leads to the consequence that the contact angle,  $\gamma$ , has to be determined as a function of these state parameters as well affecting then finally also the catalytic activity factor with respect to nucleation,  $\varphi(\gamma)$ . By this reason, we first consider here the problem of determining the contact angle in dependence on the state parameters of both ambient and newly evolving in the system phases.

For the case of high wettability the contact angle has values less than  $90^\circ$ , contact angles are larger than  $90^\circ$  for the case of low wettability. Since the contact

angle can be computed via Young's equation, Eq. (6.18), as

$$\cos \gamma = \frac{\sigma_{\beta s} - \sigma_{\alpha s}}{\sigma_{\alpha\beta}}, \quad (6.33)$$

for a high wettability  $\sigma_{\alpha s} < \sigma_{\beta s}$  holds while for a low wettability the inverse inequality  $\sigma_{\alpha s} > \sigma_{\beta s}$  is fulfilled. These two different cases of heterogeneous nucleation we consider here in detail separately. However, in order to proceed with this task, we have to specify first the specific surface energy of the solid-liquid interface.

### 6.3.2. Specific energy of the solid-liquid interface

According to Eq. (6.33) in order to determine the contact angle it is necessary to know the specific energy of the cluster-solid, ambient phase-solid and cluster-ambient phase interfaces. This knowledge is required for all compositions of the ambient and cluster phases varying in a range from the equilibrium value at the left binodal,  $x_b^{(l)}$ , to the equilibrium value at the right binodal,  $x_b^{(r)}$  (determined by Eq. (6.6)). Both of these phases we will denote as "fluids" for simplicity, but the results hold similarly also for segregation of a solid solution at a planar interface.

In order to have at our disposal an expression for the fluid-solid specific interfacial energy, we proceed here as follows. The specific energy of the fluid-solid interface,  $\sigma_{fs}$ , depends on the composition of the fluid (cluster or ambient phase), which is in contact with the solid surface, and in the simplest (linear in the composition of the fluid) approximation can be written as

$$\sigma_{fs}(x) = \frac{\sigma_{\beta s,0} (x_b^{(r)} - x) + \sigma_{\alpha s,0} (x - x_b^{(l)})}{x_b^{(r)} - x_b^{(l)}}. \quad (6.34)$$

Here  $\sigma_{\beta s,0}$  and  $\sigma_{\alpha s,0}$  are the specific energy of the ambient phase-solid and cluster-solid interfaces for the case, when ambient and newly evolving phases are in an equilibrium state (that is for  $x = x_b^{(l)}$  and  $x_\alpha = x_b^{(r)}$ ). The corresponding parameters without the subscript 0 refer to the current values of these quantities for an arbitrary value of the composition of the fluid (ambient phase or cluster).

This equation can be obtained from the following considerations: First, we write down Taylor expansions of the fluid-solid specific interface energy,  $\sigma_{fs}(x)$ , both in the vicinity of the equilibrium composition ( $x_b^{(r)}$ ) of the cluster,  $\sigma_{\alpha s}(x)$ , and the ambient phase (with the equilibrium composition,  $x_b^{(l)}$ ),  $\sigma_{\beta s}(x)$ ,

$$\sigma_{\alpha s}(x) = \sigma_{\alpha s,0} + \left. \frac{\partial \sigma_{fs}}{\partial x} \right|_{x=x_b^{(r)}} (x - x_b^{(r)}) , \quad (6.35)$$

$$\sigma_{\beta s}(x) = \sigma_{\beta s,0} + \left. \frac{\partial \sigma_{fs}}{\partial x} \right|_{x=x_b^{(l)}} (x - x_b^{(l)}) .$$

where

$$\sigma_{\alpha s,0} = \sigma_{fs}(x_b^{(r)}) , \quad \sigma_{\beta s,0} = \sigma_{fs}(x_b^{(l)}) . \quad (6.36)$$

In addition, we assume here linearity of the dependence of  $\sigma_{fs}(x)$  on composition  $x$  in the whole interval leading to

$$\left. \frac{\partial \sigma_{fs}}{\partial x} \right|_{x=x_b^{(l)}} = \left. \frac{\partial \sigma_{fs}}{\partial x} \right|_{x=x_b^{(r)}} = \frac{\sigma_{\alpha s,0} - \sigma_{\beta s,0}}{x_b^{(r)} - x_b^{(l)}} . \quad (6.37)$$

A combination of Eqs. (6.35) and (6.37) results immediately in Eq. (6.34). Eq. (6.37) yields then further

$$\sigma_{\beta s} - \sigma_{\alpha s} = \sigma_{fs}(x) - \sigma_{fs}(x_\alpha) = (\sigma_{\beta s,0} - \sigma_{\alpha s,0}) \left( \frac{x_\alpha - x}{x_b^{(r)} - x_b^{(l)}} \right) . \quad (6.38)$$

We can see from Eq. (6.38) that the difference  $(\sigma_{\beta s} - \sigma_{\alpha s})$  is linear in  $(x_\alpha - x)$ , positive for high wettability ( $\sigma_{\beta s,0} > \sigma_{\alpha s,0}$ ) and negative for low wettability ( $\sigma_{\beta s,0} < \sigma_{\alpha s,0}$ ) in accordance with above given definition. The difference in the signs of the mentioned specific surface energy terms is the main difference distinguishing the two types of solid surfaces. This difference is the basic origin of the different types of catalytic activity in heterogeneous nucleation.

### 6.3.3. Some first consequences

The surface tension for cluster-ambient phase coexistence is determined by Eq. (6.24). Equation (6.24), accounting for Eqs. (6.18), (6.38) and (6.33), yields

$$\cos \gamma(x, x_\alpha) = \cos \gamma_0 \left( \frac{x_b^{(r)} - x_b^{(l)}}{x_\alpha - x} \right), \quad (6.39)$$

where

$$\cos \gamma_0 = \frac{\sigma_{\beta s,0} - \sigma_{\alpha s,0}}{\sigma_{lg,0}}. \quad (6.40)$$

The first factor on the right-hand side of Eq. (6.39),  $\cos \gamma_0$ , can be considered as some given property of the solution (liquid or solid) under consideration in a macroscopic equilibrium state with the planar solid surface. Thus, for the analysis of heterogeneous nucleation it is necessary to know the contact angle,  $\gamma_0$ , for the case, when ambient and newly evolving phases are in a macroscopic equilibrium state. In the present study, we assign here to  $\gamma_0$  different values analyzing, on one hand, quantitative changes of the behavior in dependence on the value of  $\gamma_0$  and reflecting, on the other hand, the two considered qualitatively different cases of high and low wettability.

Employing the classical Gibbs approach, the contact angle is determined

exclusively by this first term  $\cos \gamma_0$  and determines in this classical approach the catalytic activity. The second factor in Eq. (6.39) depends on the composition of the both fluids (ambient and cluster phases). Generalizing the classical Gibbs approach to heterogeneous nucleation, this term accounts for changes in the composition of the cluster and the ambient phases, we have here to incorporate into the determination of the catalytic activity via Eqs. (6.9) and (6.39). Eq. (6.39) implies that, at

$$x_{\alpha,0} = \left( x_b^{(r)} - x_b^{(l)} \right) \cos \gamma_0 + x, \quad (6.41)$$

the contact angle is equal to  $\gamma = 0$ . At

$$x_{\alpha,\pi} = - \left( x_b^{(r)} - x_b^{(l)} \right) \cos \gamma_0 + x, \quad (6.42)$$

the contact angle is equal to  $\gamma = \pi$ .

In the ranges of values of the cluster compositions

$$x_\alpha < x_{\alpha,\pi}, \quad x_\alpha > x_{\alpha,0} \quad \text{at} \quad \gamma_0 < \frac{\pi}{2}, \quad (6.43)$$

$$x_\alpha < x_{\alpha,0}, \quad x_\alpha > x_{\alpha,\pi} \quad \text{at} \quad \gamma_0 > \frac{\pi}{2},$$

nucleation at a planar solid interface proceeds heterogeneously with cluster shapes as shown in Fig. 6.2. In the range

$$x < x_\alpha \leq x_{\alpha,0} \quad \text{at} \quad \gamma_0 < \frac{\pi}{2}, \quad (6.44)$$

$$x_{\alpha,0} \leq x_\alpha < x \quad \text{at} \quad \gamma_0 > \frac{\pi}{2},$$

the contact angle is equal to  $\gamma = 0$ . In this limit, we have perfect wetting,  $\varphi = 0$ , and the work of cluster formation Eq. (6.10) is determined here only by the bulk contribution defined by the thermodynamic driving force, Eq. (6.21). In the range

$$x_{\alpha,\pi} \leq x_{\alpha} < x \quad \text{at} \quad \gamma_0 < \frac{\pi}{2}, \quad (6.45)$$

$$x < x_{\alpha} \leq x_{\alpha,\pi} \quad \text{at} \quad \gamma_0 > \frac{\pi}{2},$$

the contact angle equals  $\gamma = \pi$ . For these clusters nucleation proceeds homogeneously, i.e. it becomes fully independent of the existence of the solid surface. For a macroscopic equilibrium contact angle equal to  $\gamma_0 = 90^\circ$  we get  $\varphi = 1/2$ . In this case, the cluster is a hemisphere, so it has a twice smaller size (volume) and free energy of cluster formation as compared to the case of homogeneous nucleation.

## 6.4. Nucleation activity and heterogeneous nucleation on planar solid interfaces: Results

### 6.4.1. Case of high wettability

For the case of high wettability, the analysis of Eqs. (6.9) and (6.27) leads to the conclusion that, for a moderate supersaturation (for initial states located in the central part of the interval  $x_b^{(l)} < x < x_{sp}^{(l)}$ ), the hypersurface modeling the work of cluster formation has a typical saddle shape in the  $(n_1, n_2)$ -space near to the state corresponding to the parameters of the critical cluster,  $(n_{1,cr}, n_{2,cr})$ .

As an example, such kind of behavior is shown on Fig. 6.4(a) for a macroscopic equilibrium contact angle equal to  $\gamma_0 = 90^\circ$  ( $T/T_c = 0.7$ ,  $x = 0.17$ ). The behavior is here quite similar to the case of homogeneous nucleation. In this case, i.e. for  $\gamma_0 = 90^\circ$  (Fig. 6.4(a)), the Gibbs potential profile corresponds to the one obtained

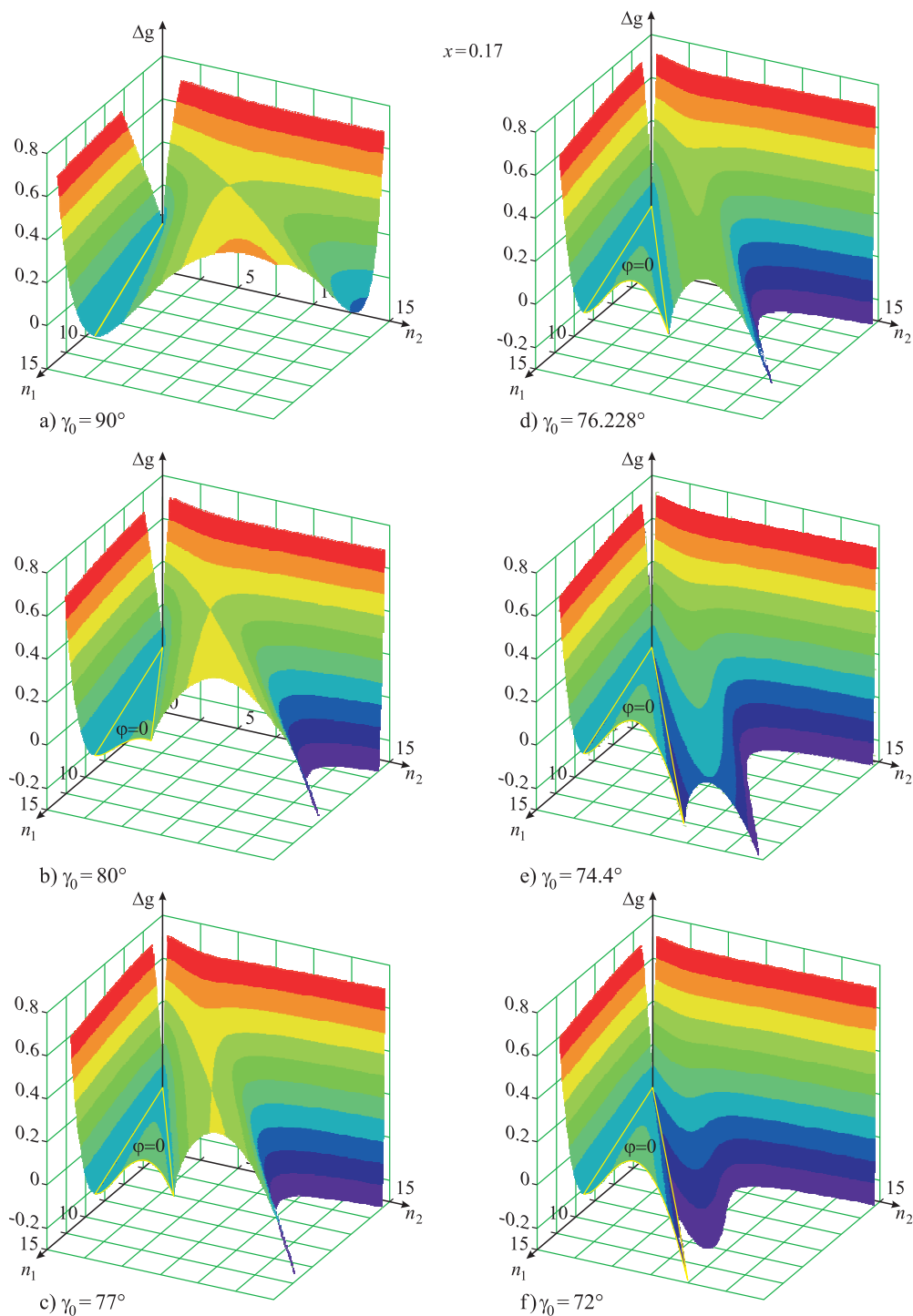


Fig. 6.4. Gibbs' free energy landscape of cluster formation for different values of the macroscopic equilibrium contact angle,  $\gamma_0$ : a)  $\gamma_0 = 90^\circ$ , b)  $\gamma_0 = 80^\circ$ , c)  $\gamma_0 = 77^\circ$ , d)  $\gamma_0 = 76.228^\circ$ , e)  $\gamma_0 = 74.4^\circ$ , f)  $\gamma_0 = 72^\circ$  at otherwise identical conditions. The reduced temperature is taken equal to  $T/T_c = 0.7$  in all these cases, the initial composition of the ambient phase is chosen equal to  $x = 0.17$ . The range with a value of the catalytic activity factor,  $\varphi$ , equal to zero is especially distinguished.

for the case of homogeneous nucleation multiplied by a factor of 0.5 (as the cluster is a hemisphere in the case under consideration, it has, as already mentioned, a twice smaller size and free energy of formation), with the valley at  $x_\alpha = x = 0.17$  and the saddle at the point corresponding to the critical cluster. Latter state is determined by the system of equations, Eqs. (6.32).

The situation changes significantly as compared to the case shown in Fig. 6.4(a) when  $\gamma_0$  decreases. This variation of the type of behavior is illustrated in Figs. 6.4(b-f), which show the Gibbs free energy surface of cluster formation for different values of the equilibrium contact angle ( b)  $\gamma_0 = 80^\circ$ , c)  $\gamma_0 = 77^\circ$ , d)  $\gamma_0 = 76.228^\circ$ , e)  $\gamma_0 = 74.4^\circ$ , f)  $\gamma_0 = 72^\circ$ ) at otherwise identical conditions. The reduced temperature is taken equal to  $T/T_c = 0.7$  in all these cases, the initial composition of the ambient phase is chosen equal to  $x = 0.17$ .

When the contact angle decreases, the work of critical cluster decreases as well, and a region with a cluster composition in the range  $x < x_\alpha < x_{\alpha,0}$  appears, where  $\varphi = 0$  holds. Such type of behavior is shown in Fig. 6.4(b) for a value of  $\gamma_0$  equal to  $\gamma_0 = 80^\circ$ . As discussed in the previous section, the boundary of this region, i.e., the value of  $x_{\alpha,0}$  is determined by Eqs. (6.41). This region with a value of the nucleation activity  $\varphi = 0$  expands with decreasing values of the parameter  $\gamma_0$  (Fig. 6.4(c-f)). In this range defined by  $\varphi = 0$ , the interfacial contributions to the Gibbs free energy are equal to zero. The work of cluster formation given by Eq. (6.10) is determined here exclusively by the bulk contribution defined by the thermodynamic driving force, Eq. (6.30) (note that in this case  $r \rightarrow \infty$  according to Eq. (6.31), see Fig. 6.6b as well).

In case the composition of the ambient phase approaches the value  $x = x_{ss}^{(hw)}(\gamma_0)$  (superscript *hw* means high wettability), the work of critical cluster formation at  $x_\alpha = x_{\alpha,0}$  becomes equal to zero (for the given value of  $x = 0.17$  it takes place at  $\gamma_0 = 76.228^\circ$ , see Fig. 6.4(d)). Here  $x_{ss}^{(hw)}(\gamma_0)$  is a root of the equation

$$x_{\alpha,0} \left( x_{ss}^{(hw)}(\gamma_0), \gamma_0 \right) = x_{\alpha,ll} \left( x_{ss}^{(hw)}(\gamma_0) \right), \quad (6.46)$$

where  $x_{\alpha,0}$  is determined by Eq. (6.41) and  $x_{\alpha,ll}$  by Eq. (6.15).

For even smaller values of the equilibrium contact angle, the evolution of the clusters with compositions close to  $x_{\alpha,0}$  can proceed without the necessity of overcoming of a potential barrier i.e. by a scenario of phase formation similar to spinodal decomposition (Figs. 6.4(e and f)). For these clusters with a composition  $x_{\alpha} \approx x_{\alpha,0}$ , the contact angle is very small or equal to zero (see Fig. 6.5 as well). In this limiting case, line tension effects may gain importance [20–22]. The range

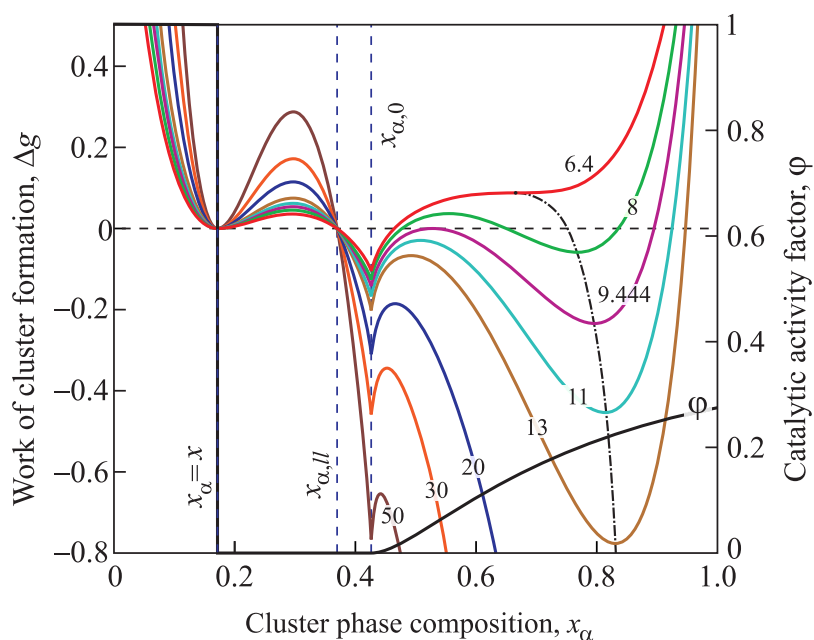


Fig. 6.5. Dependence  $\varphi(x_{\alpha})$  (right axis), and cross-sections of the Gibbs free energy surface,  $\Delta g(n, x_{\alpha})|_{n=\text{const}}$  (left axis), for different fixed values of  $n$  specified by the numbers at the respective curves (at  $x = 0.17$  and  $\gamma_0 = 72^\circ$ ).

$x_{\alpha,ll} < x_{\alpha} \leq x_{\alpha,0}$ , where the contact angles vanishes, represents perfect wetting [23, 24] In this composition range, clusters are more appropriately treated as flat islands and not as the spherical segments, which are formed in the range  $x_{\alpha} > x_{\alpha,0}$ . For the qualitative analysis of such clusters, the model used here is expected to remain valid, however, for a quantitative description of the nucleation behavior in this limit the model should be further advanced taking into account mentioned effects. However,

such task is beyond the scope of the present analysis, these effects will be analyzed in more detail in a future study.

Fig. 6.5 presents the dependence  $\varphi(x_\alpha)$  and the cross-sections of the Gibbs free energy surface,  $\Delta g(n, x_\alpha)|_{n=\text{const}}$ , for  $x = 0.17$ ,  $\gamma_0 = 72^\circ$  (which was shown in Fig. 6.4(f) as well), at different values of  $n$  given in the figure as numbers to the respective curves. As evident from the figure, there exist two minima of  $\Delta g$  along these cross sections. One of them is located at  $x = x_{\alpha,0}$ , it refers to the case of flat island formation ( $\varphi = 0$ ). The minimum work of flat island phase formation,  $\Delta g(n, x_{\alpha,0})$ , is determined by Eq. (6.30) at  $\varphi = 0$ , equal to

$$\Delta g(n, x_{\alpha,0}) = 2nf(x, x_{\alpha,0}) . \quad (6.47)$$

It is linear in  $n$  and decreases for the parameters under consideration. The dashed-dotted curve in Fig. 6.5 shows the position of the second minimum for clusters of spherical segments shape. With increasing cluster size the minimum deepens and the composition of the clusters tends to the value  $x_B$ , determined by Eq. (6.14).

The parameters of the critical cluster in dependence on initial supersaturation are illustrated in Fig. 6.6 [a) composition of the critical cluster  $x_{\alpha,cr}$ , b) critical cluster size,  $n_{cr}$ , c) work of critical cluster formation,  $\Delta g_{cr}$ ] for different values of the contact angle,  $\gamma_0$ , equal to  $\gamma_0 = 60^\circ, 70^\circ, 80^\circ, 90^\circ$ , and  $180^\circ$  (the latter one corresponds to the case of homogeneous nucleation). With an increase of the supersaturation starting at initial states near to the binodal curve, the concentration of the atoms of the second component in the critical cluster,  $x_{\alpha,cr}$ , decreases first and reaches its minimum,  $x_{\alpha,0}$  (the dotted curve in Fig. 6.6(a)), at  $x = x_{ss}^{(hw)}(\gamma_0)$ . With a subsequent further increase of the supersaturation,  $x_{\alpha,cr}$  grows linearly (see Eq. (6.41)).

In agreement with the classical picture, the size of the critical cluster tends to infinity for initial states of the ambient phase in the vicinity of the binodal, and with an increase of the supersaturation the critical size decreases first. However, in contrast to the classical picture, in the approach to the limiting value,  $x = x_{ss}^{(hw)}$ , the critical

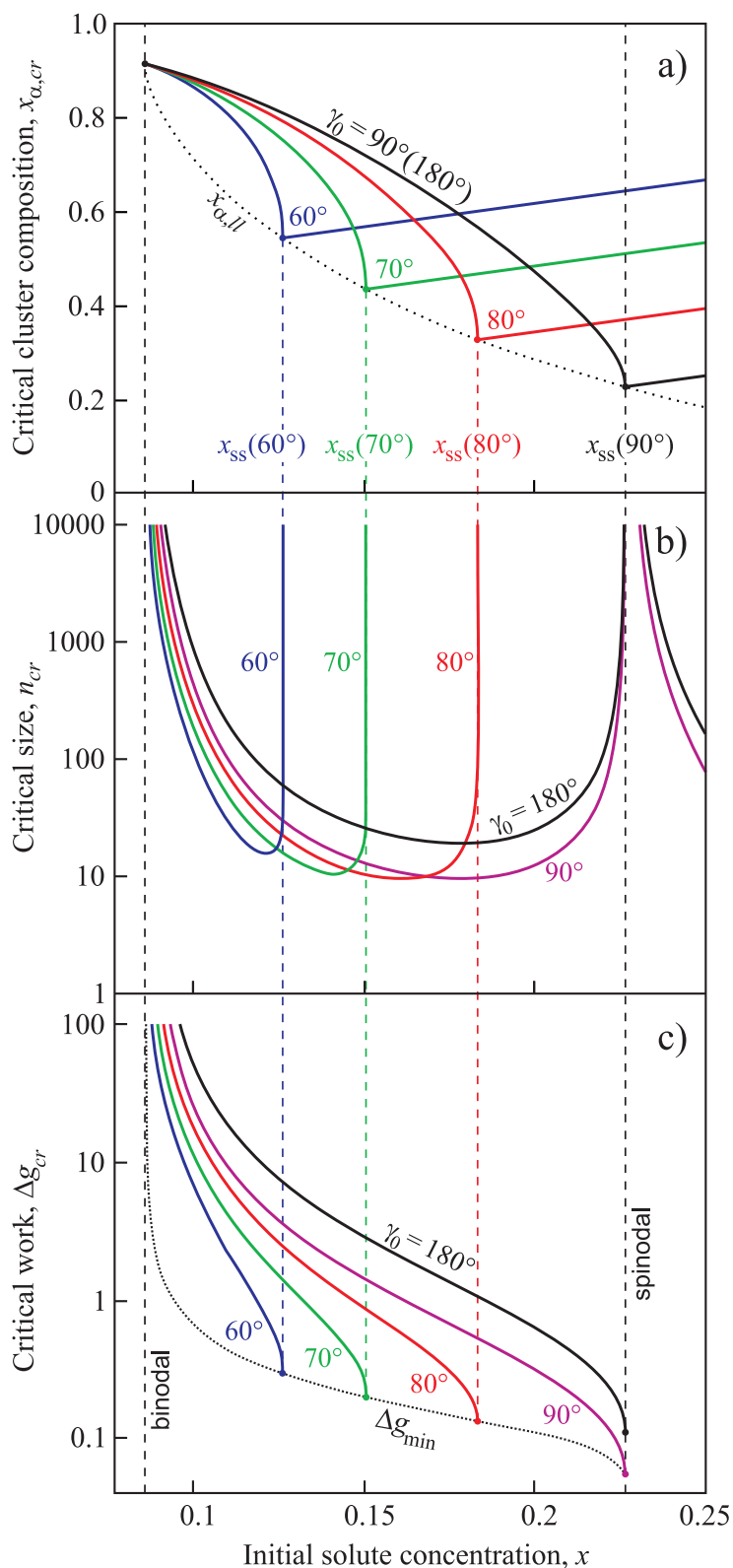


Fig. 6.6. The parameters of the critical cluster in dependence on initial supersaturation: a) composition  $x_{\alpha,cr}$ , b) critical cluster size  $n_{cr}$ , c) work of critical cluster formation,  $\Delta g_{cr}$ , for different values of the macroscopic equilibrium contact angle,  $\gamma_0 = 60^\circ, 70^\circ, 80^\circ, 90^\circ$ , and  $180^\circ$ .

cluster size starts to increase again and reaches infinity at  $x = x_{ss}^{(hw)}$ .

At  $x > x_{ss}^{(hw)}$ , a critical cluster in the classical sense does not exist. Thermodynamically cluster evolution starts at  $n = 0$  (or, in physical terms, from one structural unit) and proceeds via a valley at  $x = x_{\alpha,0}$  (see Figs. 6.4f and 6.5). This valley is separated from the final state (which is shown by the dashed-dotted curve in Fig. 6.5) by some barrier. Based on this picture, we can expect that the phase transition will proceed at such states in two-stages: first, by the formation of a flat island phase followed by the second stage, the formation of the final state phase with clusters of spherical segments shape. Details of such path of evolution can be derived based on the solution of an appropriate set of kinetic equations employing the generalized Gibbs approach for the thermodynamic description. In application to homogeneous nucleation, such approach was developed in [17, 18].

For the considered variations of the composition of the ambient phase, the work of critical cluster formation decreases monotonically from infinity (for initial states at the binodal curve) till, at  $x = x_{ss}^{(hw)}$ , it exhibits a discontinuity. It has a finite value  $\Delta g_{cr}(x_{ss}^{(hw)}) = \Delta g_{\min}$  (the dotted curve in Fig. 6.6(c)) at  $x = x_{ss}^{(hw)}$ , however, at any values  $x > x_{ss}^{(hw)}$  the work of critical cluster formation is identically equal to zero, i.e.,  $\Delta g_{cr}|_{x > x_{ss}^{(hw)}} = 0$ . The scenario of phase evolution for the thermodynamically unstable initial states in the range  $x_{sp}^{(l)} < x < x_{sp}^{(r)}$  will be analyzed in detail in Section 6.4.3. Note that the minimal values,  $x_{\alpha,0}$  and  $\Delta g_{\min}$ , shown by the dotted curves in Fig. 6.6(a and c), have no real physical meaning. They correspond to clusters of infinite size, which cannot be realized in the system. Instead of forming a very large (critical) cluster, for both metastable and unstable initial states near to the spinodal curve the evolution to the new phase will, as a rule, proceed via the ridge of the appropriate thermodynamic potential relief and not via the saddle point (see [17, 18] for details).

Note as well that heterogeneous nucleation at  $\gamma_0 = 90^\circ$  proceeds similarly to homogeneous nucleation characterized by  $\gamma_0 = 180^\circ$  [15, 16]. Indeed, in this case the contact angle does not depend on the cluster parameters (composition),  $\gamma =$

$\gamma_0 = 90^\circ$  (see Eq. (6.39)). In this case, clusters formed at the planar interface have a hemispherical shape. This is also the reason for why the dependencies  $x_{\alpha,cr}(x)$  are identical for both heterogeneous and homogeneous cases, but the work of critical cluster formation and its size,  $n_{cr}$ , are by a factor of 1/2 smaller than for homogeneous nucleation.

A similar behavior, as found here and illustrated, in particular, in Figs. 6.4 and 6.6, was observed earlier by us in the analysis of condensation and boiling at planar interfaces (c.f. Figs. 3 and 4 in [12]) and in the analysis of homogeneous nucleation in solutions [15, 16]. So, similarly to [12], we may conclude that the existence of heterogeneous nucleation cores may result effectively in a shift of the spinodal curve from the value for homogeneous systems ( $x = x_{sp}^{(l)}$  as illustrated in Fig. 6.1) to a value  $x = x_{ss}^{(hw)} \leq x_{sp}^{(l)}$  affected in addition by the properties of the solid nucleation core. Therefore we can consider the range of supersaturations,  $x_b^{(l)} < x < x_{ss}^{(hw)}$ , with respect to heterogeneous nucleation as the metastable region and the composition range  $x > x_{ss}^{(hw)}$  as thermodynamically unstable states. The value of the composition of the ambient phase  $x = x_{ss}^{(hw)}$  is to be treated consequently as a part of the spinodal curve with respect to heterogeneous nucleation. Full spinodal curves  $x_{ss}^{(hw)}(T)$  are presented in the left part of Fig. 6.10 for different values of the macroscopic equilibrium contact angle,  $\gamma_0 = 60^\circ, 70^\circ, 80^\circ$ , and  $90^\circ$ .

Summarizing briefly the results for the case under consideration, we arrive at the following consequences: Employing the generalized Gibbs approach to nucleation of a new phase in a supersaturated regular solution on a surface of high wettability it is concluded that the existence of the planar solid interface leads effectively to a significant shift of the spinodal to lower supersaturations as compared to the case of homogeneous nucleation. However, all basic features found for homogeneous nucleation like the divergence of the critical cluster radius or the approach of zero values of the work of critical cluster formation near to the spinodal curve are retained in a qualitatively identical form.

### 6.4.2. Case of low wettability

The computations for the description of heterogeneous nucleation for the case of low wettability can be performed similarly to the first case of phase formation on a highly wettable surface. The resulting from the computations dependencies of the parameters of the critical cluster on the initial supersaturation for the case of low wettability are shown in Fig. 6.7 [a) composition of the critical cluster, b) particle number in the critical clusters, c) work of critical cluster formation]. The analysis has been carried out, again, for different values of the macroscopic equilibrium contact angle,  $\gamma_0$ , equal to  $\gamma_0 = 90^\circ, 100^\circ, 110^\circ, 120^\circ$ , and for homogeneous nucleation,  $\gamma_0 = 180^\circ$ . For  $x_b^{(l)} < x < x_{ss}^{(lw)}$ , where the boundary of heterogeneous nucleation,  $x_{ss}^{(lw)}$ , is determined similarly to Eq. (6.46) as a root of the equation

$$x_{\alpha,\pi} \left( x_{ss}^{(lw)}(\gamma_0), \gamma_0 \right) = x_{\alpha,cr}^{(hom)} \left( x_{ss}^{(lw)}(\gamma_0) \right), \quad (6.48)$$

nucleation occurs heterogeneously, size and work of critical cluster formation are less than for the homogeneous case (here  $x_{\alpha,\pi}$  is determined by Eq. (6.42), and  $x_{\alpha,cr}^{(hom)}$  is the composition of the critical cluster in homogeneous nucleation [8, 15, 16], i.e. for  $\varphi = 1$ , superscript  $lw$  means low wettability). However, for the considered case, the degree of activation of nucleation by the planar solid surface is much less expressed than for the case of high wettability. This is seen from a comparison of full curves (representing heterogeneous nucleation) with the dashed lines showing the respective parameters of the critical cluster computed for the case of homogeneous nucleation (i.e. for  $\gamma_0 = 180^\circ$ ). With an increase of the supersaturation, at some upper limiting value of the composition of the ambient phase,  $x_{ss}^{(lw)}(\gamma_0)$ , nucleation becomes fully independent of the existence of the solid surface. Dependencies  $x_{ss}^{(lw)}(T)$  are presented in the right part ( $x > 0.5$ ) of Fig. 6.10 for different values of the contact angle,  $\gamma_0 = 90^\circ, 100^\circ, 110^\circ$ , and  $120^\circ$ , for the range  $x < 0.5$  it is needed only to replace  $x$  by  $(1 - x)$  (see Section 6.4.4 for more details).

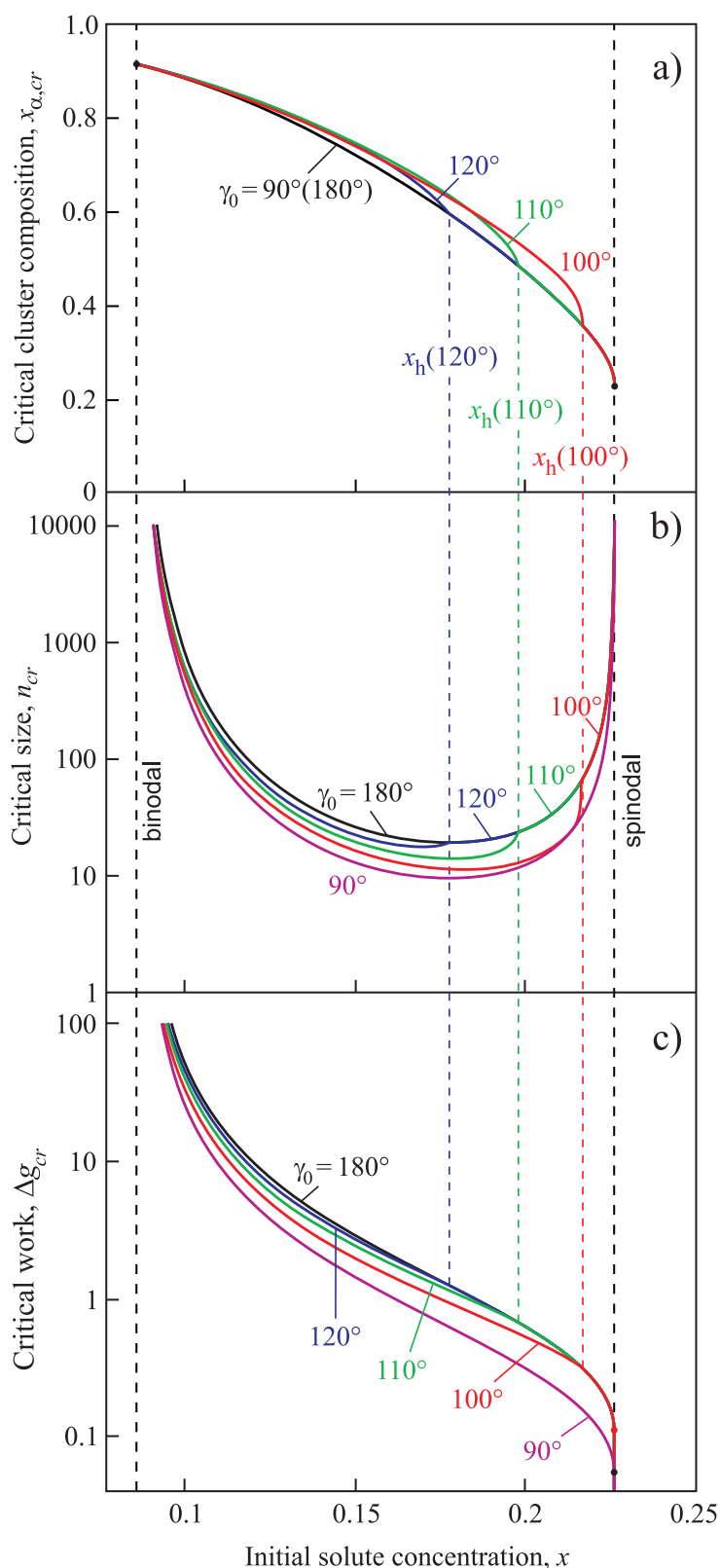


Fig. 6.7. Parameters of the critical cluster in dependence on initial supersaturation for the case of low wettability: a) composition of the critical cluster  $x_{\alpha,cr}$ , b) critical cluster size  $n_{cr}$ , c) work of critical cluster formation,  $\Delta g_{cr}$ , for different values of the contact angle,  $\gamma_0 = 90^\circ, 100^\circ, 110^\circ, 120^\circ, \text{ and } 180^\circ$ .

### 6.4.3. Segregation in thermodynamically unstable initial states

In the unstable region,  $x_{sp}^{(l)} < x < x_{sp}^{(r)}$ , in the case of homogeneous nucleation ( $\gamma_0 = 180^\circ$ ) and for heterogeneous nucleation at  $\gamma_0 = 90^\circ$ , the surface modeling the work of cluster formation in vicinity of the critical cluster state has a very particular shape corresponding to a third-order saddle point. Clusters with a composition  $x_\alpha = x$  are stable against variation of its composition ( $\partial^2 \Delta g / \partial x_\alpha^2 < 0$ ) for  $n < n_{cr}$  and unstable ( $\partial^2 \Delta g / \partial x_\alpha^2 > 0$ ) for  $n > n_{cr}$ . This particular critical size parameter,  $n_{cr}$ , is determined here by the equation

$$\left. \frac{\partial^2 \Delta g (n_{cr}, x_\alpha)}{\partial x_\alpha^2} \right|_{x_\alpha=x} = 0. \quad (6.49)$$

Note that the work of formation of such particular aggregates – unlike to the case of critical cluster formation in metastable initial states – is equal to zero (its origin is discussed in detail in [16, 17]).

The Gibbs potential profile for a macroscopic equilibrium contact angle equal to  $\gamma_0 = 90^\circ$  is shown on Fig. 6.8(a) for  $x = 0.5$  and on Fig. 6.8(b) for  $x = 0.35$ . Cluster evolution proceeds here first in the vicinity of the line  $O \rightarrow C$ , and then via the path  $C \rightarrow A$  or  $C \rightarrow B$ , approaching finally either the composition  $x_\alpha = x_B$  or  $x_\alpha = x_A$ , respectively ( $x_{A,B}$  are determined by Eq. (6.14)). The thermodynamic potential relief for  $x = 0.5$  is symmetric with respect to the change  $n_1 \leftrightarrow n_2$ , and the path  $O \rightarrow C \rightarrow A$  is equivalent to the path  $O \rightarrow C \rightarrow B$ . For  $x = 0.35$  symmetry breaking takes place, and the path  $O \rightarrow C \rightarrow B$  becomes thermodynamically more favorable as compared to  $O \rightarrow C \rightarrow A$ . Note that the states with  $\gamma_0 = 90^\circ$  are degenerated. Really, at  $\gamma_0 = 90^\circ$  the catalytic factor is always equal to  $\varphi = 1/2$  for any cluster (see Eq. (6.9)), but Eq. (6.40) has a discontinuity at  $x_\alpha = x$ , and  $\varphi$  changes from 0 to 1 at small variation of  $x_\alpha$  in the vicinity of  $x$ . This is the reason why for  $\gamma_0 \neq 90^\circ$  the Gibbs potential profile changes significantly, and the critical cluster size vanishes (see Fig. 6.8(c,d)).

For the case of high wettability ( $\gamma_0 = 88^\circ$ , Fig. 6.8(c)), at the thermodynamically preferred path  $O \rightarrow B$  the work of cluster formation decreases with cluster size. Initially along this path the cluster composition equals  $x_\alpha = x_{\alpha,0} > x$  (where  $x_{\alpha,0}$  is determined by Eq. (6.41)), and with an increase of cluster size it approaches the composition  $x_\alpha = x_B$ . The path of cluster evolution  $O \rightarrow C \rightarrow A$  becomes here more difficult, since the critical size is doubled due to the growth of the catalytical factor from  $\varphi = 0.5$  to  $\varphi = 1$ .

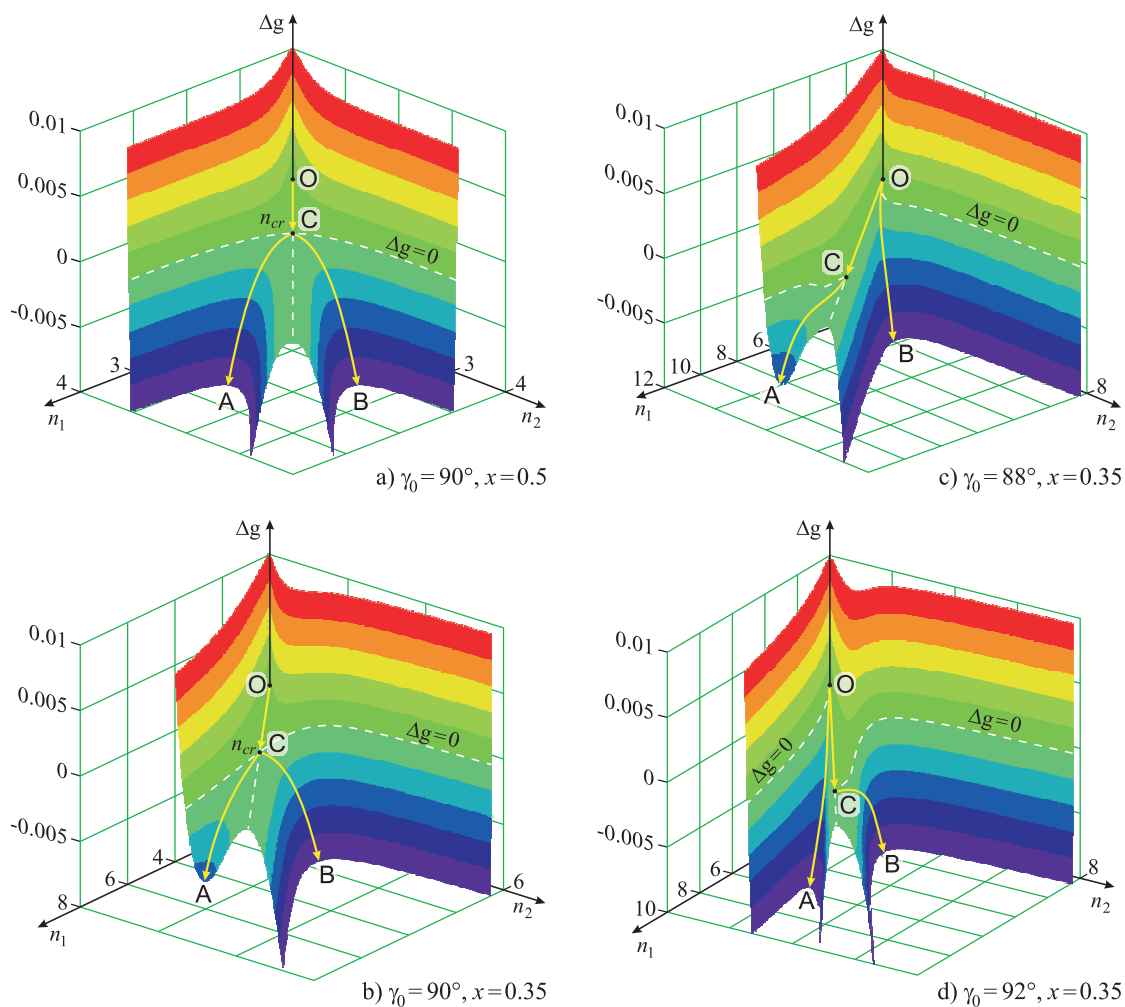


Fig. 6.8. Gibbs' free energy landscape of cluster formation for different values of the macroscopic equilibrium contact angle,  $\gamma_0$ : a)  $\gamma_0 = 90^\circ$ , b)  $\gamma_0 = 80^\circ$ , c)  $\gamma_0 = 100^\circ$ , at otherwise identical conditions. The reduced temperature is taken equal to  $T/T_c = 0.7$  in all these cases, the initial composition of the ambient phase is chosen equal to  $x = 0.35$ .

For the case of low wettability ( $\gamma_0 = 92^\circ$ , Fig. 6.8(d)), the path  $O \rightarrow A$  is

preferred at  $x_\alpha = x_{\alpha,0} < x$  approaching the final composition  $x_\alpha = x_A$ . The path of cluster evolution  $O \rightarrow C \rightarrow A$  becomes more difficult, since the critical size is doubled (as compared to the case  $\gamma_0 = 90^\circ$ ) due to the growth of the catalytical factor from  $\varphi = 0.5$  to  $\varphi = 1$ . Fig. 6.9(a) presents the dependence  $\varphi(x_\alpha)$  and the cross-sections of the Gibbs free energy surface,  $\Delta g(n, x_\alpha)|_{n=\text{const}}$ , for the low wettability case ( $x = 0.35$ ,  $\gamma_0 = 100^\circ$ ), at different values of  $n$  given in the figure as numbers to the respective curves. At  $n < 4.71$  the function  $\Delta g(x_\alpha)$  has only one minimum, at

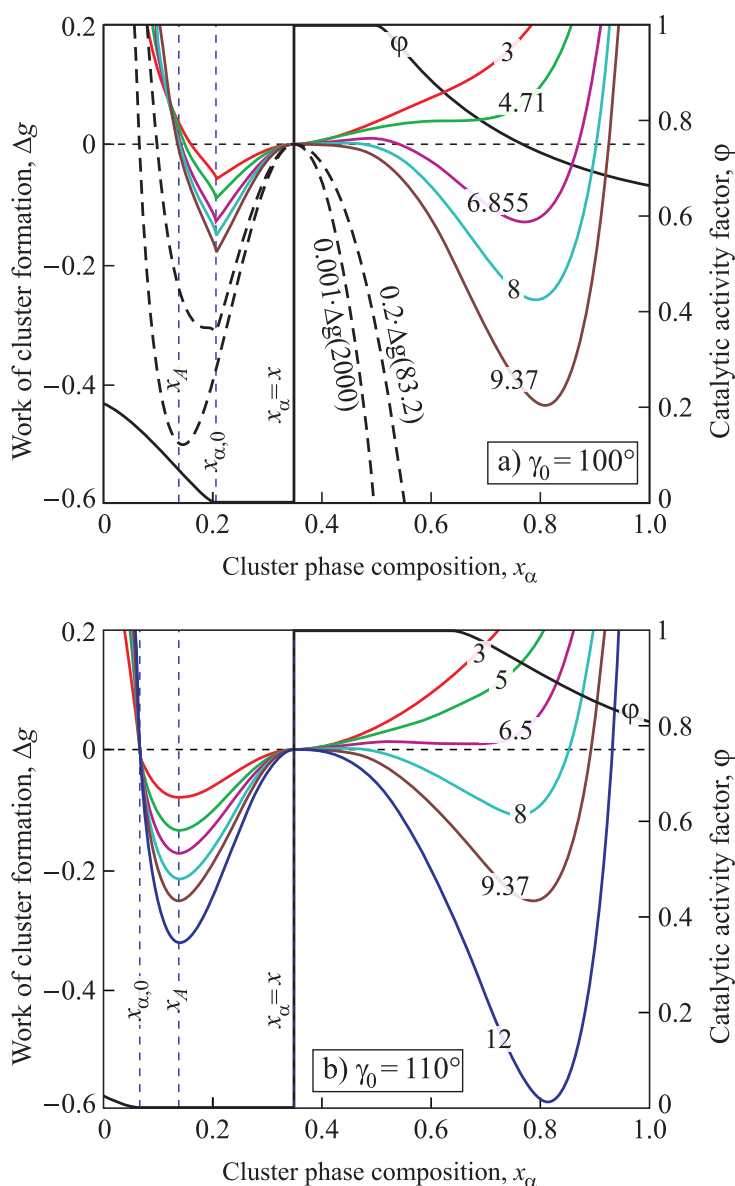


Fig. 6.9. Dependence  $\varphi(x_\alpha)$  (right axis), and cross-sections of the Gibbs free energy surface,  $\Delta g(n, x_\alpha)|_{n=\text{const}}$  (left axis), for different fixed values of  $n$  specified by the numbers at the respective curves (at  $x = 0.35$  and a)  $\gamma_0 = 100^\circ$ , b)  $\gamma_0 = 110^\circ$ ).

$x_\alpha = x_{\alpha,0}$ , for  $n > 4.71$  a second minimum appears, at  $n > 6.855$  it becomes deeper than the first one. At large values of  $n$ , i.e. at  $n > 83.2$ , near to the first minimum appears a new one, which tends to the final state composition  $x_\alpha = x_B$  at high  $n$  (see the dashed curves in Fig. 6.9(a)). For  $\gamma_0 > \gamma_A$ , where  $\gamma_A(x)$  is determined by the intersection of the  $x_A(x)$  and  $x_{\alpha,0}(x)$  lines, that is by the root of the equation

$$x_{\alpha,0}(x, \gamma_A) = x_A(x), \quad (6.50)$$

the inequality  $x_{\alpha,0} < x_A$  is valid, and in the range  $x_\alpha < x$  only one minimum exists,  $x_\alpha = x_A$  (see Fig. 6.9(b)).

Consequently, in thermodynamically unstable initial states the work of critical cluster formation is always equal to zero, but there are two critical sizes, which correspond to different modes of evolution. For the first mode, the critical size is equal to zero, corresponding to a cluster composition  $x_{\alpha,cr} = x_{\alpha,0}$ , for the second one the critical size is determined by Eq. (6.49), and  $x_{\alpha,cr} = x$  holds. The critical cluster parameters, composition and size, are shown in Fig. 6.10 for different contact angles.

For the case of high wettability ( $\gamma_0 < 90^\circ$ ), the critical size  $n_{cr} = 0$  for the “favorable” mode with increasing concentration,  $x_\alpha \rightarrow x_B$ , and  $n_{cr} > 0$  for the “unfavorable” mode with decreasing concentration,  $x_\alpha \rightarrow x_A$ . For the low wettability case ( $\gamma_0 > 90^\circ$ ) an opposite behavior is found:  $n_{cr} > 0$  for the “favorite” mode with increasing concentration,  $x_\alpha \rightarrow x_B$ , and  $n_{cr} = 0$  for the “unfavorable” mode with decreasing concentration,  $x_\alpha \rightarrow x_A$ : latter mode will have more possibilities to advance. Nevertheless, as it was mentioned already, thermodynamics yields only a qualitative description of such processes. A more detailed analysis has to be based on the solution of the set of kinetic equations employing the generalized Gibbs approach for the thermodynamic description, as it was performed in [17, 18] for homogeneous nucleation.

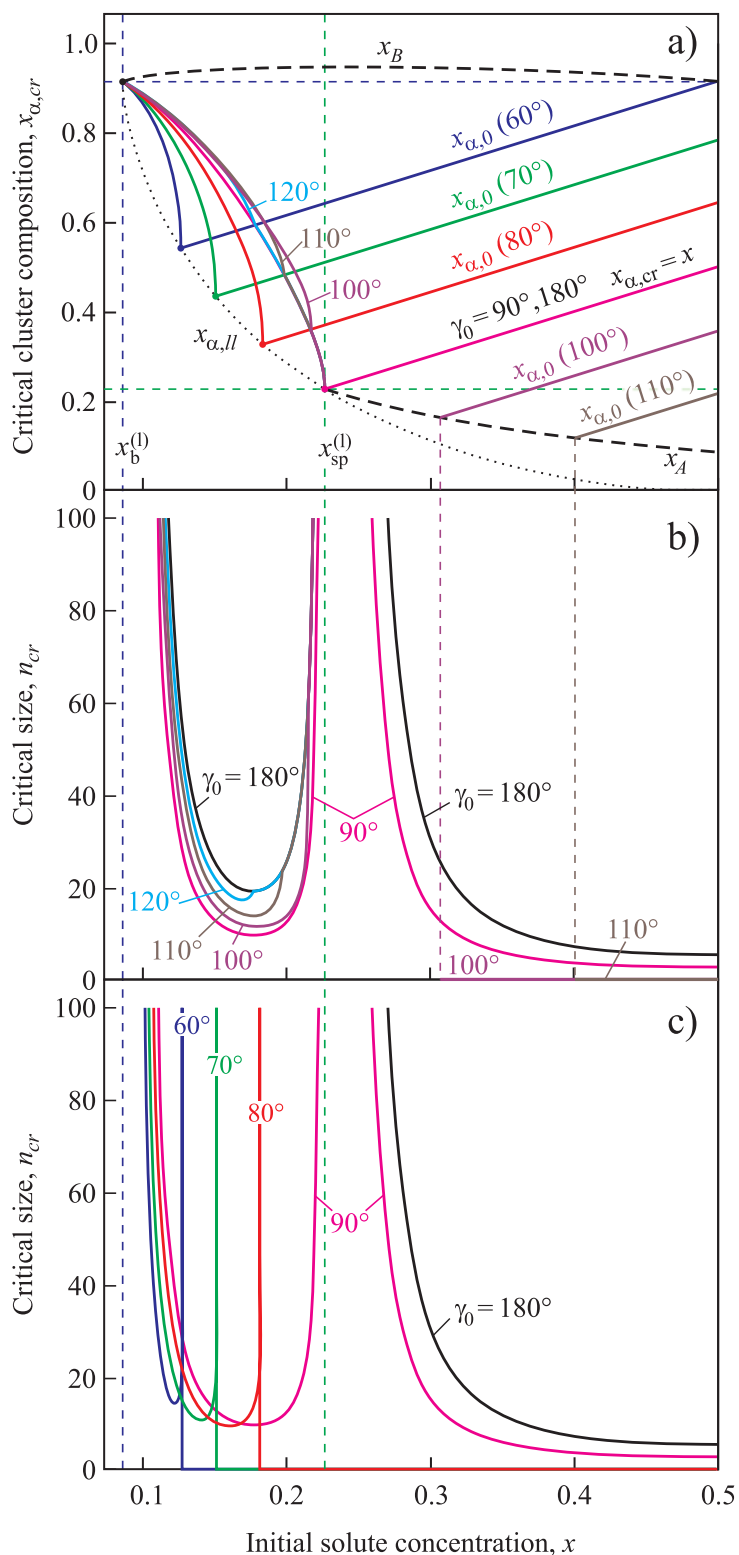


Fig. 6.10. Parameters of the critical cluster in dependence on initial supersaturation: a) composition of the critical cluster  $x_{\alpha,cr}$ , b) critical cluster size  $n_{cr}$  for the case of low wettability ( $\gamma_0 = 90^\circ, 100^\circ, 110^\circ, 120^\circ$ , and  $180^\circ$ ), c) critical cluster size  $n_{cr}$  for the case of high wettability ( $\gamma_0 = 60^\circ, 70^\circ, 80^\circ, 90^\circ$ ).

#### 6.4.4. Alternative case: Segregation at solute concentrations $x > 0.5$

The choice of the independent variable in the description of the solutions under consideration is arbitrary. By this reason, the process of formation of a new phase cluster, wherein the concentration of the second component,  $x$ , increases from a value in the range  $x_b^{(l)} < x < x_{sp}^{(l)}$  to  $x_b^{(r)}$ , can be interpreted as the formation of the cluster in which the concentration of the first component decreases from a value in the range  $x_{sp}^{(r)} < x < x_b^{(r)}$  to the value  $x_b^{(l)}$ . Considering also that the equation of state for binary regular solutions is symmetric with respect to  $x = 1/2$  (see Fig. 6.1), one is attempted to suppose that the segregation behavior in such solution with the composition, for example,  $x = 0.8$ , will be similar to that at  $x = 0.2$ , and to describe such a process it is needed only to replace  $x$  by  $1 - x$  (and, correspondingly,  $x_b^{(l)} \rightarrow 1 - x_b^{(l)} = x_b^{(r)}$  and  $x_{sp}^{(l)} \rightarrow 1 - x_{sp}^{(l)} = x_{sp}^{(r)}$ ).

However, this symmetry is broken when a catalytic surface appears. Indeed, if at  $x < 0.5$  the equilibrium contact angle is determined by Eq. (6.40), where  $\sigma_{\alpha s,0}$  and  $\sigma_{\beta s,0}$  are determined by Eq. (6.37), i.e., at the left and right binodal, respectively, then for  $x > 0.5$  the binodal molar fractions have to be interchanged in their places in the equation i.e.  $x_b^{(l)} \leftrightarrow x_b^{(r)}$ . By this reason, Eq. (6.40) takes form

$$\cos \gamma_0 = \frac{\sigma_{\alpha s,0} - \sigma_{\beta s,0}}{\sigma_{lg,0}}. \quad (6.51)$$

Thus, the cosine of the contact angle changes its sign to the opposite one and  $\gamma_0 \rightarrow 180 - \gamma_0$ , so if for  $x < 0.5$  the surface was of high wettability, then for  $x > 0.5$  it becomes a poorly wettable one and vice versa. This asymmetry is demonstrated in Figs. 6.11 and 6.12.

Fig. 6.11 presents the location of the binodal and spinodal curves, dependencies of the heterogeneous interface induced spinodal,  $x_{ss}^{(hw)}$ , and of the heterogeneous nucleation border,  $x_{ss}^{(lw)}$ , for different values of the contact angle, (1)  $\gamma_0 = 90^\circ$ , (2)  $\gamma_0 = 80^\circ(100^\circ)$ , (3)  $\gamma_0 = 70^\circ(110^\circ)$ , (4)  $\gamma_0 = 60^\circ(120^\circ)$ , the contact angle values

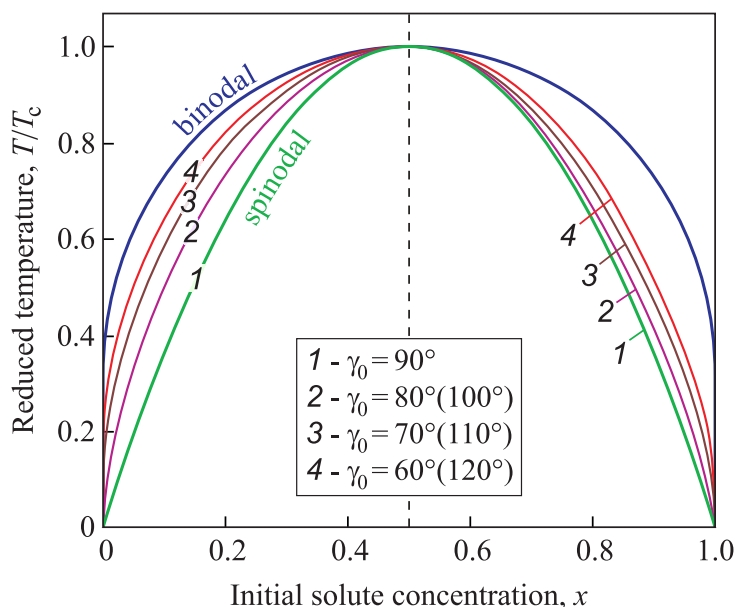


Fig. 6.11. Location of the binodal and spinodal curves, dependencies of the heterogeneous interface induced spinodal,  $x_{ss}^{(hw)}$ , and of the heterogeneous nucleation border,  $x_{ss}^{(lw)}$ , for different values of the contact angle, (1)  $\gamma_0 = 180^\circ$ , (2)  $\gamma_0 = 90^\circ$ , (3)  $\gamma_0 = 80^\circ(100^\circ)$ , (4)  $\gamma_0 = 70^\circ(110^\circ)$ , (5)  $\gamma_0 = 60^\circ(120^\circ)$  (see text for details).

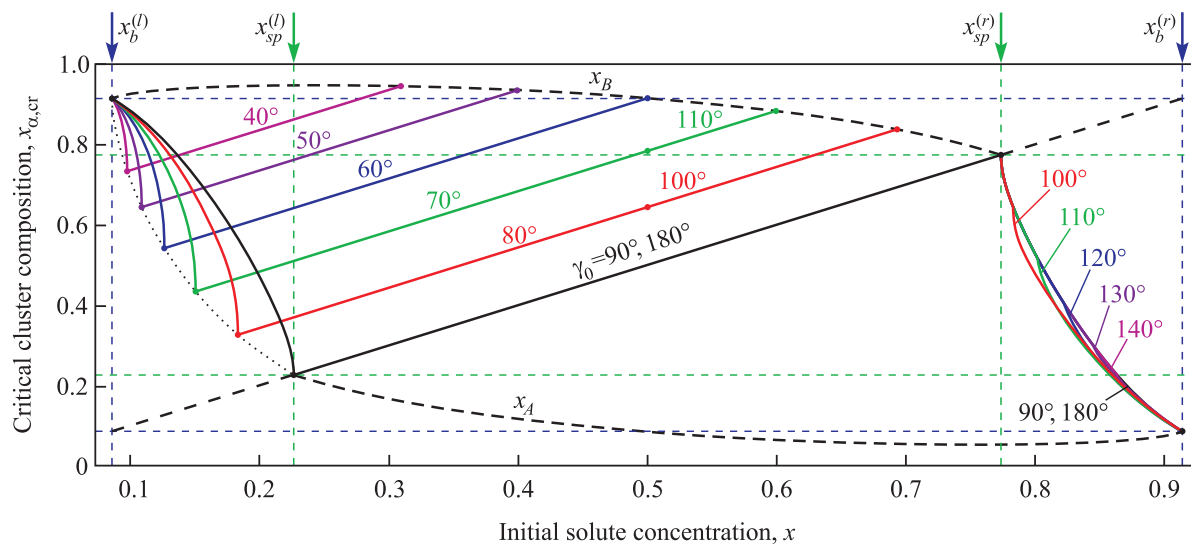


Fig. 6.12. The dependence of the composition of the critical clusters,  $x_{\alpha,cr}$ , in the whole range of possible initial compositions of the ambient solution, for different values of the specific interfacial energy. The curves for the contact angle values  $\gamma_0 = 40^\circ, 50^\circ, 60^\circ, 70^\circ, 80^\circ$ , which for  $x < 0.5$  correspond to the case of the high wettability, at  $x > 0.5$  correspond to the case of the low wettability with the contact angle values  $\gamma_0 = 140^\circ, 130^\circ, 120^\circ, 110^\circ, 100^\circ$ , respectively.

are given for  $x < 0.5$  ( $x > 0.5$ ), respectively. Fig. 6.12 shows the dependence of the composition of the critical clusters in the whole range of possible initial compositions of the ambient solution, for different values of the specific interfacial energy, the curves for the contact angle values  $\gamma_0 = 40^\circ, 50^\circ, 60^\circ, 70^\circ, 80^\circ$ , which for  $x < 0.5$  correspond to the case of the high wettability, at  $x > 0.5$  correspond to the case of the low wettability with the contact angle values  $\gamma_0 = 140^\circ, 130^\circ, 120^\circ, 110^\circ, 100^\circ$ , respectively, and  $T/T_c = 0.7$  holds as before. As we can see, Fig. 6.12 is actually a compilation of Figs. 6.6(a) and 6.7(a). Work of formation and size of the critical clusters can be obtained similarly.

#### 6.4.5. Effect on the steady-state nucleation rate

Employing the notations introduced in the present paper, the steady-state nucleation rate (see, e.g., [1, 2]) can be written as

$$J = J_0 \exp\left(-\frac{\Delta g_{cr} G_\sigma}{k_B T}\right). \quad (6.52)$$

The pre-exponential term,  $J_0$ , is proportional to the number of heterogeneous nucleation cores per unit surface times the characteristic vibration frequency. The scaling factor,  $G_\sigma$ , in the exponent is determined by Eq. (6.26).

Fig. 6.13 presents a comparison of the reduced nucleation rates,  $J/J_0$ , as determined via the generalized Gibbs approach (solid curves) and the classical Gibbs approach utilizing, in addition, the capillarity approximation (dashed curves) for different values of the contact angle,  $\gamma_0 = 60^\circ, 70^\circ, 80^\circ$ , and  $90^\circ$ . The calculations were performed for  $T_c = 1143$  K,  $T = 0.7T_c$  and  $a = 3.65 \cdot 10^{-10}$  m,  $\sigma_{\alpha\beta,0} = 0.08$  J/m<sup>2</sup>, for such parameters  $G_\sigma = 61.6 k_B T$  and  $R_\sigma = 3.087 a$ . As we can see, nucleation rates determined according to the generalized Gibbs' approach increase with supersaturation and reach its maximal value,  $J_0$ , at  $x \geq x_{ss}^{(hw)}(\gamma_0)$ .

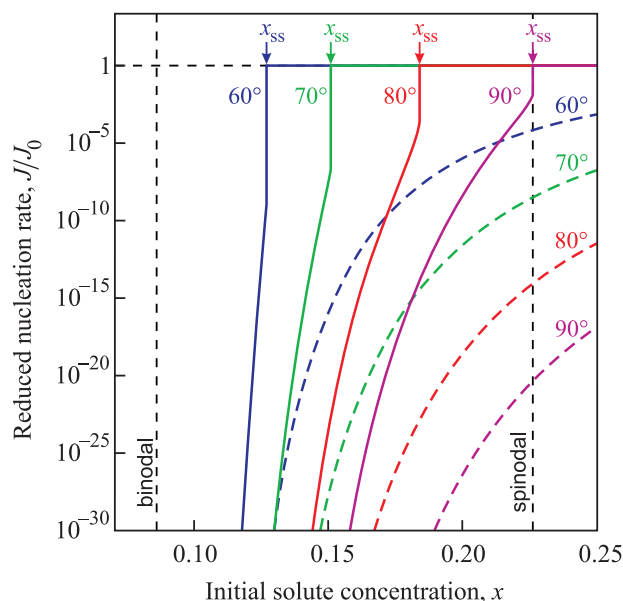


Fig. 6.13. Comparison of the reduced nucleation rates,  $J/J_0$ , as determined via the generalized Gibbs' approach (solid curves) and the classical Gibbs' approach utilizing, in addition, the capillarity approximation (dashed curves) for different values of the contact angle,  $\gamma_0 = 60^\circ, 70^\circ, 80^\circ$ , and  $90^\circ$ .

The classical nucleation rates are significantly less for all values of the macroscopic equilibrium contact angle.

## 6.5. Discussion and conclusions

Employing the generalized Gibbs approach to the description of segregation in a binary regular solution in the presence of a planar interface we arrive widely at the same result as obtained for heterogeneous nucleation for a one-component van der Waals fluid [12]: as compared with homogeneous nucleation, a significant shift of the spinodal curve to lower supersaturations occurs caused by the existence of the high wettable planar solid interface. This result implies that the region of instability of the fluid is enlarged and the range of initially metastable states is reduced. Such features – observed already in application of the generalized Gibbs approach to homogeneous condensation and boiling and changing essentially the

results obtained via the classical Gibbs treatment – like the divergence of the critical radius in the approach of the spinodal and the possibility of nucleation passing not the saddle but the ridge of the thermodynamic potential surface analyzed in detail for homogeneous phase formation [8, 13, 17, 18, 25] are found here as well for the new boundary of metastability. Similarly to condensation and boiling the present results can be extended straightforwardly to account for finite size effects in the catalytic activity of heterogeneous nucleation cores [26, 27]. The respective generalization of the present results to account for such finite size effects will be presented in future contributions.

### Acknowledgments

The authors express their gratitude to the German funding agency Deutsche Forschungsgemeinschaft (DFG: SCHM 937/16-1) and the Heisenberg-Landau Program of the BMBF Germany for financial support.

### References

1. K. F. Kelton and A. L. Greer, *Nucleation in Condensed Matter: Applications in Materials and Biology* (Elsevier, Amsterdam, 2010).
2. I. S. Gutzow and J. W. P. Schmelzer, *The Vitreous State: Thermodynamics, Structure, Rheology, and Crystallization* (First edition: Springer, Berlin, 1995; Second edition: Springer, Heidelberg, 2013).
3. M. Volmer, *Kinetik der Phasenbildung* (Th. Steinkopff, Dresden, Leipzig, 1939).
4. O. Hellmuth, V. I. Khvorostyanov, J. A. Curry, A. K. Shchekin, J. W. P. Schmelzer, R. Feistel, Yu. S. Djikaev, and V. G. Baidakov, *Selected Aspects of Atmospheric Ice and Salt Crystallisation*. In: J. W. P. Schmelzer and O. Hellmuth (Editors),

*Nucleation Theory and Applications-Special Issues: Review Series on Selected Topics of Atmospheric Sol Formation*, Volume 1 (Joint Institute for Nuclear Research Publishing Department, Dubna, Russia, 2013; ISBN 978-5-9530-0349-0).

5. E. U. Bormashenko, *Wetting of Real Surfaces* (de Gruyter, Berlin, 2013).
6. J. W. Gibbs: *On the equilibrium of heterogeneous substances*, Transactions Connecticut Academy of Sciences **3**, 108 (1876); **16**, 343 (1878); J. W. Gibbs, *The Collected Works*, vol. 1, Thermodynamics (Longmans and Green, New York - London - Toronto, 1928).
7. J. W. Cahn and J. E. Hilliard, J. Chem. Phys. **28**, 258 (1958); **31**, 688 (1959).
8. J. W. P. Schmelzer, J. Schmelzer Jr., and I. Gutzow, J. Chem. Phys. **112**, 3820 (2000).
9. J. W. P. Schmelzer, A. R. Gokhman, and V. M. Fokin, J. Colloid Interface Science **272** (2004) 109.
10. J. W. P. Schmelzer, G. Sh. Boltachev, and V. G. Baidakov, J. Chem. Phys. **124**, 194503 (2006).
11. J. W. P. Schmelzer, G. Sh. Boltachev, and V. G. Baidakov, *Is Gibbs' thermodynamic theory of heterogeneous systems really perfect?* In: J. W. P. Schmelzer (Ed.), *Nucleation Theory and Applications* (WILEY-VCH, Berlin-Weinheim, 2005, pgs. 418-446).
12. A. S. Abyzov and J. W. P. Schmelzer, J. Chem. Phys. **138**, 164504 (2013).
13. R. Becker, *Annalen der Physik* **32**, 128 (1938).
14. J. W. Christian, in: R. W. Cahn (Ed.): *Physical Metallurgy* (North-Holland Publishers, Amsterdam, 1965, pgs. 227-346).
15. J. W. P. Schmelzer, A. S. Abyzov, and J. Möller, J. Chem. Phys. **121**, 6900 (2004).
16. A. S. Abyzov and J. W. P. Schmelzer, J. Chem. Phys. **127**, 119 (2007).

17. A. S. Abyzov, J. W. P. Schmelzer, A. A. Kovalchuk, and V. V. Slezov, *J. Non-Crystalline Solids* **356**, 2915 (2010).
18. A. S. Abyzov and J. W. P. Schmelzer, *J. Non-Crystalline Solids* **384**, 8 (2014).
19. R. Kubo, *Thermodynamics* (North-Holland-Publishing Company, Amsterdam, 1968).
20. B. Widom, *J. Phys. Chemistry* **99**, 2803 (1995).
21. G. Navascues and P. Tarazona, *J. Chem. Phys.* **75**, 2441 (1981).
22. V. Talanquer and D. W. Oxtoby, *J. Chem. Phys.* **104**, 1483 (1996).
23. J. W. Cahn, *J. Chem. Phys.* **66**, 3667 (1977).
24. P. G. de Gennes, *Reviews of Modern Physics* **57**, 827 (1985).
25. J. W. P. Schmelzer and A. S. Abyzov, *J. Chem. Phys.* **134**, 054511 (2011).
26. L. Krastanov, *Gidrologiya i Meteorologiya SSSR (Moscow)* **12**, 16 (1957) (in Russian).
27. N. H. Fletcher, *J. Chem. Phys.* **29**, 572 (1958); *The Physics of Rainclouds* (Cambridge University Press, Cambridge, 1962).

## 6.6. Висновки до розділу 6

Результати досліджень, представлених у даному розділі, опубліковано в статті [6] (Додаток А. Список публікацій здобувача за темою дисертації). Досліджено гетерогенне зародження кластерів нової фази у регулярному бінарному розчині на плоских твердих поверхнях. Серед основних результатів у якості висновків можна виділити наступні:

- Показано, що контактний кут та каталітичний фактор для гетерогенної нуклеації стають залежними від ступеня метастабільності (пересичення) розчину.

- У випадку утворення кластерів нової фази на поверхні з низькою змочуваністю (контактний кут більше  $90^\circ$ ) каталітична активність твердої поверхні мала.

- В альтернативному випадку високої змочуваності (контактний кут менше  $90^\circ$ ) інтенсивність зародження значно посилюється твердою поверхнею.

- Таким чином, у цьому випадку, як і у рідині ван дер Ваальса (яку було проаналізовано в попередньому розділі), гетерогенна спінодаль наближається до бінодалі, а область метастабільності звужується за рахунок розширення області нестабільності.

## РОЗДІЛ 7

**ГЕТЕРОГЕННА НУКЛЕАЦІЯ НА ДЕФЕКТНИХ ПОВЕРХНЯХ:  
УЗАГАЛЬНЕНИЙ ПІДХІД ГІББСА**

У цьому розділі досліджено гетерогенне зародження (конденсація) крапель рідини з пари (газу) на дефектній твердій поверхні в моделі флюїду ван дер Ваальса, як поверхневий дефект обрана конічна пора.

THE JOURNAL OF CHEMICAL PHYSICS 138, 164504 (2013)

**Heterogeneous nucleation on rough surfaces: Generalized Gibbs' approach**

Alexander S. Abyzov<sup>1</sup>, Jörn W. P. Schmelzer<sup>2</sup> and Leonid N. Davydov<sup>1</sup>

<sup>1</sup>*National Science Center Kharkov Institute of Physics and Technology, Academician Street 1, 61108 Kharkov, Ukraine*

<sup>2</sup>*Institut für Physik der Universität Rostock, Albert-Einstein-Strasse 23-25, 18059 Rostock, Germany*

(Received 26 September 2017; accepted 9 November 2017; published online 7 December 2017)

Heterogeneous nucleation (condensation) of liquid droplets from vapor (gas) on a defective solid surface is considered. The vapor is described by the van der Waals equation of state. The dependence of nucleating droplet parameters on droplet size is accounted for within the generalized Gibbs approach. As a surface defect, a conic void is taken. This choice allows us to simplify the analysis and at the same time to follow the main aspects of the influence of the surface roughness on the nucleation process. Similarly to condensation on ideal planar surfaces, contact angle and catalytic factor for heterogeneous nucleation on a rough surface depend on the degree of vapor overcooling. In case of droplet formation on a hydrophilic surface of a conic void the nucleation rate considerably increases in comparison with the condensation on a planar interface. In fact, the presence of a defect on the hydrophilic surface leads to a considerable shift of the spinodal towards

lower supersaturation in comparison with heterogeneous nucleation on a planar interface. With the decrease in the void cone angle the heterogeneous spinodal approaches the binodal, and the region of metastability is diminished at the expense of the instability region. *Published by AIP Publishing.*  
<https://doi.org/10.1063/1.5006631>

## 7.1. Introduction

Processes of formation of a new phase are of great scientific and technological importance. The starting stage of this process is the nucleation of microvolumes of a new phase. It may proceed both homogeneously and heterogeneously.

Homogeneous nucleation takes place under special conditions when any catalysing foreign surfaces are absent in the sample where the phase formation proceeds. In practice these conditions are rarely met and homogeneous nucleation is supplemented by heterogeneous nucleation. In particular, at low supersaturation, nucleation takes place predominately at the external surfaces or on surfaces of the existing in media solid phase inclusions (e.g. nanoparticles) and should be considered as heterogeneous.

The effect of foreign, respectively, internal surfaces and its wettability on nucleation are the topic of many papers dealing with heterogeneous nucleation (see, e.g. [1]). The first analyses in this direction dealt with planar surfaces [2–4]. They were supplemented by extensions accounting for the value and sign (positive or negative) of the surface curvature [5–7] with application to nucleation, in particular, on aerosol particles [7,8]. Simultaneously it was realized that a uniform flat substrate is not a good approximation to practical conditions. Solid surfaces are always more or less rough. Such surface structures may be modelled by assuming surface cavities of particular shape and size. The possibility that embryos may nucleate in such surface cavities was first pointed out by Volmer in 1939 [9] and studied by many others,

e.g. [10–13].

Generally, for the interpretation of processes of formation of a new phase two conventional thermodynamic approaches are widely applied developed by Gibbs [14] and van der Waals [15, 16], respectively. Applying Gibbs theory to the description of critical cluster formation in the classical theory of nucleation, one assumes in line with Gibbs theory that the bulk properties of new phase clusters are widely similar to the properties of the corresponding macroscopic phases. Another condition which is frequently supposed to be fulfilled is that the specific surface energy (or surface tension) is the same as for the flat boundary under equilibrium between both phases (capillary approximation). If the first supposition (the similarity of bulk properties of critical clusters to the corresponding macroscopic phases) is intrinsically a corollary of Gibbs theory, the latter one can be replaced by the introduction of the dependence of the surface tension on the interphase surface curvature or on the cluster size as also suggested already by Gibbs. This approach is used commonly in classical nucleation theory to achieve a better agreement between the theoretical predictions and the experimentally measured rate of cluster formation [17, 18]. In such approach the surface tension value is used as the only possible fitting parameter for improving conformity of the theory with the experiment. However, the application of the surface tension as the only fitting parameter in the description of the new phase nucleation (as it usually done) can result in other inconsistencies between the theory and experiment, and may also lead to intrinsic problems in the theoretical description itself [19].

Going beyond the application of the size dependence of the surface tension, there exists an alternative method to improve the correlation of theory and experiment in the description of the newly evolving phase. Indeed, as was shown for the first time by Cahn and Hilliard [20, 21], when applying the van der Waals approach to the description of the phase formation kinetics, one may find that properties of critical clusters differ considerably from the properties of the evolving macroscopic phase. Such deviations of bulk properties of critical clusters from the macroscopic phase

properties cannot be properly accounted for in Gibbs' classical theory. However, as we have shown in the last decade [22,23], such deviation of bulk properties can be accounted for performing a generalization of Gibbs' description. This generalization allows one "to reconcile" the approaches of Gibbs and van der Waals in the description of nucleation.

The mentioned generalization of the Gibbs approach demanded the development of the thermodynamic description of non-equilibrium states of clusters in a surrounding medium. Such approach was applied by us then to the description of properties of clusters in processes of nucleation and growth in various applications [24,25]. As shown in these analyses, the generalized Gibbs approach allowed us to describe nucleation more correctly as compared to the classical theory, namely: (1) for model systems the results are in agreement with the calculations by density functional methods and computer simulation (e.g. molecular dynamics); (2) the generalized approach gives an adequate theoretical interpretation of various experimental data, which was difficult, if not impossible, to achieve in the classical theory of nucleation [24,25].

The generalized Gibbs approach is applicable both for the description of homogeneous and heterogeneous nucleation. With respect to the latter problems, the generalized Gibbs approach was applied so far to the description of condensation and boiling in van der Waals liquids [26] and new phase nucleation in a regular solution [27], restricting the considerations of heterogeneous nucleation so far to phase formation on a flat rigid smooth interface.

However, in a huge variety of nucleation processes in nature, in experiment, and in technological applications the formation of the evolving phase takes place at various heterogeneous nucleation centers and at surface defects [28–33]. Aiming at a further development of the theory of heterogeneous nucleation, the present paper starts the research on the application of the generalized Gibbs approach to heterogeneous nucleation at surface imperfections.

In particular, we concentrate below on the heterogeneous nucleation of a liquid drop in a supersaturated vapor (gas) in a conic cavity employing the generalized Gibbs approach. The van der Waals equation [15, 34] is chosen as a model for the analysis of principal quantitative characteristics of the heterogeneous process considered, similarly as it was performed for homogeneous nucleation [26]. In the analysis we account appropriately for the fact that the state parameters of new phase clusters (for a one-component system it is the density) can differ considerably from those for the corresponding macroscopic phase. In such approach, beyond the parameters involved in the classical treatment, an additional parameter must appear accounting for its effects on the surface tension and wetting angles and, thus, on the catalytic activity of the surface. Therefore, for the correct determination of the work of formation of the critical cluster the dependence of surface tension and wetting angle on the density of a critical size droplet has to be established.

The article is structured as follows: In Section 7.2, briefly, as far as it is necessary for the following analysis, the van der Waals equation of state is discussed, the binodal and spinodal curves are determined, the general expression for the work of formation of the critical cluster in a conic void on a hydrophilic rigid surface is obtained, as well as the expressions for the contact angle and factor of catalytic activity for critical size droplets are found. In Section 7.3 the heterogeneous condensation of the van der Waals gas on a hydrophilic rigid surface is analyzed. The paper is completed with Section 7.4 containing a brief summary of results, conclusions and possible generalizations.

## **7.2. Work of the formation of a critical cluster in the generalized Gibbs approach**

For the description of the bulk properties of the ambient and evolving phases we use the van der Waals equation of state. In dimensionless variables this equation

reads [15, 34]

$$\Pi(\omega, \theta) = \frac{8\theta}{3\omega - 1} - \frac{3}{\omega^2}, \quad (7.1)$$

$$\Pi \equiv \frac{p}{p_c}, \quad \omega \equiv \frac{v}{v_c}, \quad \theta \equiv \frac{T}{T_c}, \quad (7.2)$$

where  $v$ ,  $p$  and  $T$  are molar volume, pressure, and temperature,  $v_c$ ,  $p_c$  and  $T_c$  are the same parameters in the critical point. The chemical potential of van der Waals gas (normalized to  $p_c v_c$ ) can be written as [35, 36]

$$\mu(\omega, \theta) = -\frac{8\theta}{3} \ln(3\omega - 1) + \frac{8\theta\omega}{3\omega - 1} - \frac{6}{\omega}. \quad (7.3)$$

The spinodal curve in phase space defines the boundary between thermodynamically metastable and unstable states. In the absence of the centers of heterogeneous nucleation it is defined by the equation (we will name it further as a “bulk spinodal”),

$$\frac{d}{d\omega} \Pi(\omega, \theta) = 0. \quad (7.4)$$

At any temperature below the critical one ( $\theta < \theta_c = 1$ ), Eq. (7.4) has two solutions which merge in the critical point.

The position of the binodal curve is defined by the condition of thermodynamic equilibrium between vapor (gas) and liquid on a planar interface (equality of pressure and chemical potential); thus, the binodal is defined by the solution of the following set of equations

$$\Pi(\omega_{gas}, \theta) = \Pi(\omega_{liq}, \theta), \quad \mu(\omega_{gas}, \theta) = \mu(\omega_{liq}, \theta). \quad (7.5)$$

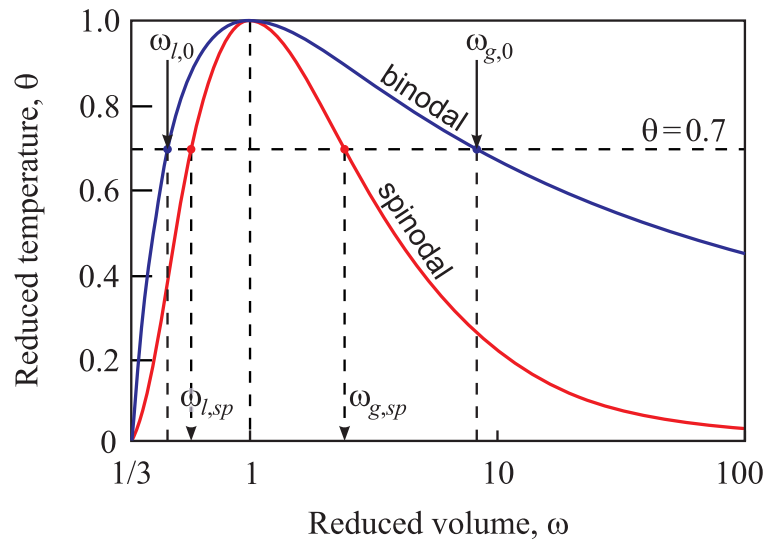


Fig. 7.1. Spinodal and binodal curves for the van der Waals gas. As an example the curves are shown for a reduced temperature equal  $\theta = 0.7$  (for the notations, see text).

In the temperature range  $\theta < \theta_c = 1$  Eqs. (7.5) have two solutions describing the state of the gas and the liquid. Like for the spinodal, these two solutions merge in the critical point. Spinodal and binodal curves are shown in dimensionless variables  $\theta$  and  $\rho = 1/\omega$  in Fig. 7.1.

To provide an illustration the calculations were carried out for a temperature  $\theta = 0.7$ . The corresponding dimensionless volumes on binodal,  $\omega_b$ , and spinodal,  $\omega_{sp}$ , curves are

$$\omega_{l,0} = 0.467, \quad \omega_{g,0} = 7.811, \quad (7.6)$$

$$\omega_{l,sp} = 0.579, \quad \omega_{g,sp} = 2.376. \quad (7.7)$$

Respectively, the equilibrium densities of liquid,  $\rho_{l,0}$ , and vapor,  $\rho_{g,0}$ , on the binodal possess the values

$$\rho_{l,0} = (\omega_{l,0})^{-1} = 2.14, \quad \rho_{g,0} = (\omega_{g,0})^{-1} = 0.128, \quad (7.8)$$

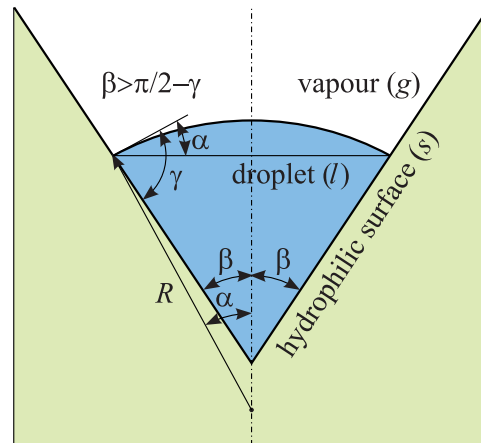


Fig. 7.2. Heterogeneous nucleation of a droplet in a conic void on a hydrophilic rigid surface.

and the densities of liquid,  $\rho_{l,sp}$ , and vapor,  $\rho_{g,sp}$ , on the spinodal are

$$\rho_{l,sp} = (\omega_{l,sp})^{-1} = 1.727, \quad \rho_{g,sp} = (\omega_{g,sp})^{-1} = 0.421. \quad (7.9)$$

Current values of liquid and vapor densities we will denote, respectively, as  $\rho_l$  and  $\rho_g$ .

Let us assume that the gas is instantly transferred to a metastable state in a region between the binodal and spinodal and after that the pressure and temperature are kept constant (below we consider also unstable initial states, i.e. the states between the left and right branches of the spinodal curve, Fig. 7.1). After such transition the vapor (gas) is supersaturated and nucleation of liquid droplets may proceed. Considering heterogeneous nucleation on a rough surface we analyze here as an example nucleation of a critical droplet in a conic void on a hydrophilic rigid surface (Fig. 7.2). Note, that in the terminology used for the description of processes in water, the surface is called as hydrophilic if the contact angle is less than  $90^\circ$ , and hydrophobic if the contact corner is larger than  $90^\circ$ . We will use this terminology for condensation processes in a van der Waals gas also.

As a first step in this analysis, we define the parameters of a critical size droplet created in a conic void on a hydrophilic rigid surface (Fig. 7.2).

The change of the thermodynamic potential (Gibbs' free energy,  $G$ ) for a one-component system due to the formation of a droplet of the considered shape (Fig. 7.2) in the vapor phase both in classical, and in generalized Gibbs's approaches can be written as [17,23,27]

$$\Delta G = \sigma_{lg} A_{lg} + (\sigma_{ls} - \sigma_{gs}) A_{ls} + (p_g - p_l) V_l + n_l (\mu_l - \mu_g) . \quad (7.10)$$

Here  $\sigma_{ls}$ ,  $\sigma_{gs}$ , and  $\sigma_{lg}$ , are the specific surface energies (surface tension) between liquid and solid, vapor and solid, and vapor and liquid, respectively (Fig. 7.3);  $A_{ls}$ ,  $A_{gs}$ , and  $A_{lg}$ , are the areas of the corresponding interfaces, and  $n_l$  is the number of particles (atoms, molecules) in the new phase cluster. In the above equations and below the index  $l$  always specifies the parameters of a cluster (liquid droplet), and the index  $g$  the surrounding vapor (gas). As independent variables the density of the liquid droplet  $\rho_l$  and the radius  $R$  of its surface are commonly used.

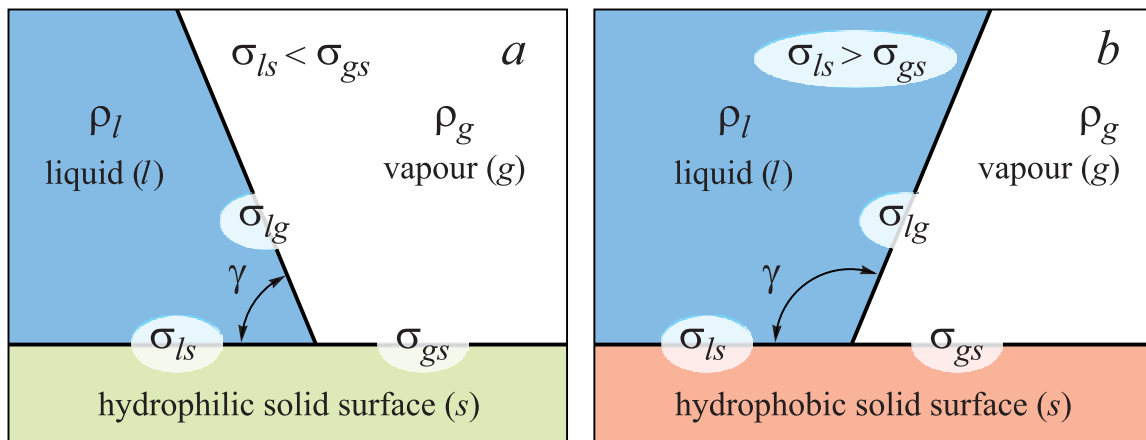


Fig. 7.3. Definition of contact angle for (a) hydrophilic and (b) hydrophobic surfaces.

The bulk contribution  $\Delta G_v$  to the change of the Gibbs free energy for the case of formation of a droplet with a radius  $R$  and a contact angle  $\gamma$  (see the Fig. 7.2) can be presented in the form [26]

$$\Delta G_V = (p_g - p_l) V_l + n_l (\mu_l - \mu_g) = \frac{4\pi}{3} R^3 \varphi [(p_g - p_l) + \rho_l (\mu_l - \mu_g)] . \quad (7.11)$$

Here the factor of catalytic activity,  $\varphi$ , is determined by contact angle  $\gamma$  and cone angle  $\beta$  as

$$\begin{aligned}\varphi &= \frac{1}{4} (2 - 3 \cos \alpha + \cos^3 \alpha + \operatorname{ctg} \beta \sin^3 \alpha), \\ \alpha &= \gamma + \beta - \frac{\pi}{2}.\end{aligned}\quad (7.12)$$

The surface contribution  $\Delta G_S$  to the change of the Gibbs free energy in cluster formation is defined, according to Eq. (7.10), as

$$\begin{aligned}\Delta G_S &= \\ &= \sigma_{lg} A_{lg} + (\sigma_{ls} - \sigma_{gs}) A_{ls} = 2\pi R^2 (1 - \cos \alpha) \sigma_{lg} + \pi R^2 \frac{1 - \cos^2 \alpha}{\sin \beta} (\sigma_{ls} - \sigma_{gs}).\end{aligned}\quad (7.13)$$

For small enough cone angles,  $\beta < \frac{\pi}{2} - \gamma$  (for hydrophilic surfaces  $\gamma < \frac{\pi}{2}$ ), the droplet surface becomes concave and the surface term in free energy becomes negative. In this case a droplet may arise in undersaturated vapor as well. We consider below only the case  $\beta \geq \frac{\pi}{2} - \gamma$ , presented in Fig. 7.2.

The requirement of mechanical balance on the contact line of all three phases is defined by the Young equation [26] (Fig. 7.3)

$$\sigma_{gs} = \sigma_{ls} + \sigma_{lg} \cos \gamma. \quad (7.14)$$

Assuming this requirement satisfied and accounting for Eq. (7.12), it is possible to write down a surface term in Gibbs free energy in the following form

$$\Delta G_S = 4\pi R^2 \sigma_{lg} \left[ \frac{1 - \cos \alpha}{2} - \frac{\cos \gamma (1 - \cos^2 \alpha)}{4 \sin \beta} \right] = 4\pi R^2 \sigma_{lg} \varphi. \quad (7.15)$$

Therefore, similarly to [17, 26], the work of a droplet formation at the heterogeneous

nucleation in a cone void can be written as

$$\Delta G_{het} = \varphi \left\{ \frac{4\pi}{3} R^3 ((p - p_l) + \rho_l (\mu_l - \mu_g)) + 4\pi R^2 \sigma_{lg} \right\}, \quad (7.16)$$

or

$$\Delta G_{het} = \varphi \Delta G_{hom}. \quad (7.17)$$

This relation is satisfied for any value of the radius of the cluster (droplet) surface and for any admissible values of the contact angle  $\gamma$ . Deviations from nucleation on planar interfaces are connected exclusively with the term  $\sin \beta$ , equal to unity for planar surfaces. In the analysis of heterogeneous nucleation within the generalized Gibbs approach, the factor  $\varphi$  becomes dependent on liquid and vapor density already for condensation on planar interfaces. The respective effect in conic voids is amplified by smaller values of  $\sin \beta$  affecting also the value of the angle  $\alpha$  for the critical clusters.

In order to determine the parameters of the critical cluster, we can rewrite Eq. (7.16) in the following form [26]

$$\frac{\Delta g(r, \rho_g, \rho_l)}{k_B T} = \varphi(\rho_g, \rho_l) \left[ 3(\rho_l - \rho_g)^\delta r^2 + 2f(\rho_g, \rho_l) r^3 \right], \quad (7.18)$$

where

$$\Delta g \equiv \frac{\Delta G}{\Omega_1}, \quad \Omega_1 = \frac{16\pi}{3} \frac{1}{p_c^2 k_B T_c \theta} \Theta^3(\theta), \quad (7.19)$$

$$r \equiv \frac{R}{R_\sigma}, \quad R_\sigma = \frac{2}{p_c} \Theta(\theta).$$

The factor  $\Theta(\theta)$  and the parameter  $\delta$  are determined from the dependence of the

surface tension on the state parameters of liquid and vapor phases (see [26]):

$$\sigma_{lg} = \Theta(\theta) (\rho_l - \rho_g)^\delta, \quad \delta = 2.5. \quad (7.20)$$

The function  $f$  in the second term in Eq. (7.18) can be written in the form [26]

$$f(\rho_g, \rho_l) = \Pi(\rho_l, \theta) - \Pi(\rho_g, \theta) + \rho_l \left( \frac{\mu(\rho_g, \theta) - \mu(\rho_l, \theta)}{p_c v_c} \right), \quad (7.21)$$

where (with the account of Eq. (7.3) and  $\rho = \omega^{-1}$ )

$$\mu(\rho) = -\frac{8\theta}{3} \ln \left( \frac{3}{\rho} - 1 \right) + \frac{8\theta}{3-\rho} - 6\rho. \quad (7.22)$$

In agreement with Eqs. (7.16) and (7.17), the expression for the work of cluster formation (7.18) differs from that for homogeneous nucleation due to the presence of the catalytic activity factor  $\varphi$ . This factor equals unity in case of homogeneous nucleation (the factor  $\varphi(\rho_g, \rho_l)$  as a function of  $\rho_g$  and  $\rho_l$  will be specified below). Expression in square brackets in Eq. (7.18) describes the work of formation of a droplet in the process of homogeneous nucleation.

Note that in the studied case of the droplet nucleated at a surface defect (a conic void) using of the curvature radius as an independent parameter presents difficulties because for hydrophilic surface at  $\beta \rightarrow \frac{\pi}{2} - \gamma$  the outside surface of the droplet become flat and the curvature radius tends to infinity while the droplet volume remains finite. Therefore, instead of curvature radius we will use the normalized number of particles (atoms, molecules) in the droplet,

$$n \equiv \frac{n_l}{n_\sigma} = \varphi r^3, \quad n_\sigma = \frac{4\pi}{3} \left( \frac{R_\sigma}{a} \right)^3, \quad (7.23)$$

where  $r$  and  $R_\sigma$  are defined in Eq. (7.19) and  $a$  is a mean interatomic distance. In

this case Eq. (7.18) takes the form

$$\frac{\Delta g(n, \rho_g, \rho_l)}{k_B T} = 3 [\varphi(\rho_g, \rho_l)]^{1/3} n^{2/3} (\rho_l - \rho_g)^\delta + 2nf(\rho_g, \rho_l). \quad (7.24)$$

Parameters of the critical cluster (its size  $n_{cr}$ , and density  $\rho_{cr}$ ) are determined by the solution of the set of equations

$$\frac{\partial \Delta g(r, \rho_g, \rho_l, \theta)}{\partial r} = 0, \quad \frac{\partial \Delta g(r, \rho_g, \rho_l, \theta)}{\partial \rho_l} = 0. \quad (7.25)$$

This set of equations, Eqs.(7.25), together with Eqs. (7.14) and (7.18) defines also the work of formation of the critical cluster in heterogeneous nucleation.

At heterogeneous nucleation the work of formation of the critical size cluster essentially depends on the value of the contact angle [17,28,33], which, according to Young's equation (7.14), is defined as

$$\cos \gamma = \frac{\sigma_{gs} - \sigma_{ls}}{\sigma_{lg}}. \quad (7.26)$$

Therefore for a hydrophilic surface the inequality  $\sigma_{ls} < \sigma_{gs}$ , is fulfilled, and for a hydrophobic one  $\sigma_{ls} > \sigma_{gs}$  (see Fig. 7.3). In the present analysis we consider only nucleation on hydrophilic surfaces, where the catalyzing effect of the surface on droplet nucleation is much more significant.

In the classical approach to heterogeneous nucleation the bulk parameters of a cluster and surrounding media are generally considered as certain fixed characteristics (see, e.g. [37]). In this case the cluster surface energy (7.15) depends only on the size of the cluster surface, the same as for the homogeneous nucleation. For this reason the contact angle in the classical approach is also fixed. In contrast, in the generalized Gibbs approach the assumption of changes in bulk parameters of the new phase cluster results in the dependence of the contact angle on these parameters and considerably affects the catalytic activity of the surface. Therefore, as the next step we determine

the dependence of the contact angle on gas temperature and state parameters of the new phase [26].

According to Eq. (7.26) for the determination of the contact angle it is necessary to know the specific energies of liquid-solid, vapor-solid, and liquid-vapor interfaces for the cases, when the medium density changes (owing to the change in overcooling of vapor) in a range from equilibrium vapor density,  $\rho_{g,0}$ , to equilibrium liquid density,  $\rho_{l,0}$  (Eq. (7.8)). Accordingly, the density of the critical cluster changes in the same range.

The specific energy of the fluid-solid interphase  $\sigma_{fs}$ , depends on fluid density (we will use the term "fluid" for the medium described by the van der Waals equation as a general name of gas and liquid) which is in contact to a solid surface, and in the simplest approach (linear on density) it can be written down in a form

$$\sigma_{fs}(\rho) = \frac{\sigma_{gs,0}(\rho_{l,0} - \rho) + \sigma_{ls,0}(\rho - \rho_{g,0})}{\rho_{l,0} - \rho_{g,0}} . \quad (7.27)$$

Here  $\sigma_{ls,0}$  and  $\sigma_{gs,0}$  are the specific energies of liquid-solid and vapor-solid surfaces for equilibrium conditions of liquid and vapor, respectively. The corresponding parameters without index 0 refer to current values of these quantities at any density of the fluids.

This equation can be obtained in the following way: interface energy of a fluid in contact with a solid,  $\sigma_{fs}(\rho)$ , can be expanded in a Taylor series in the vicinity of the equilibrium densities of liquid  $\rho_{l,0}$ , and gas  $\rho_{g,0}$ :

$$\begin{aligned} \sigma_{fs}(\rho) &= \sigma_{ls,0} + \left. \frac{\partial \sigma_{ls}}{\partial \rho} \right|_{\rho=\rho_{l,0}} (\rho - \rho_{l,0}) , \\ \sigma_{fs}(\rho) &= \sigma_{gs,0} + \left. \frac{\partial \sigma_{gs}}{\partial \rho} \right|_{\rho=\rho_{g,0}} (\rho - \rho_{g,0}) . \end{aligned} \quad (7.28)$$

Besides, we will assume a linear dependence  $\sigma_{fs}(\rho)$  on density in the whole studied

range, so

$$\left. \frac{\partial \sigma_{gs}}{\partial \rho} \right|_{\rho=\rho_{g,0}} = \left. \frac{\partial \sigma_{ls}}{\partial \rho} \right|_{\rho=\rho_{l,0}} = \frac{\sigma_{ls,0} - \sigma_{gs,0}}{\rho_{l,0} - \rho_{g,0}} . \quad (7.29)$$

Substituting Eq. (7.28) into Eq. (7.29) we obtain Eq.(7.27), from which it follows

$$\sigma_{gs} - \sigma_{ls} = \sigma_{fs}(\rho_g) - \sigma_{fs}(\rho_l) = (\sigma_{gs,0} - \sigma_{ls,0}) \frac{\rho_l - \rho_g}{\rho_{l,0} - \rho_{g,0}} . \quad (7.30)$$

From Eq. (7.30) we see that the difference  $\sigma_{gs} - \sigma_{ls}$  is linear with respect to  $\rho_l - \rho_g$  and is positive for hydrophilic ( $\sigma_{gs,0} - \sigma_{ls,0} > 0$ ) and negative for hydrophobic ( $\sigma_{gs,0} - \sigma_{ls,0} < 0$ ) surfaces according to the definition given above. This main distinction determines different behavior of the heterogeneous nucleation for these two types of surfaces.

As it was studied in detail in [18], the surface energy of vapor-liquid,  $\sigma_{lg}$  at equilibrium coexistence of vapor and liquid is proportional to certain power of the difference between liquid and vapor densities. Extending this result to any values of liquid and gas densities, we obtain

$$\sigma_{lg} = \sigma_{lg,0} \left( \frac{\rho_l - \rho_g}{\rho_{l,0} - \rho_{g,0}} \right)^\delta, \quad \delta = 2.5 . \quad (7.31)$$

Here  $\sigma_{lg,0}$  is the surface tension of the liquid-vapor interface at equilibrium coexistence of liquid and vapor. In these notations the factor  $\Theta$  in Eq. (7.20) becomes

$$\Theta = \sigma_{lg,0} (\rho_{l,0} - \rho_{g,0})^{-\delta} . \quad (7.32)$$

Equation (7.26) with the account of Eqs. (7.30) and (7.31) gives

$$\cos \gamma(\rho_g, \rho_l) = \cos \gamma_0 \left( \frac{\rho_{l,0} - \rho_{g,0}}{\rho_l - \rho_g} \right)^{\delta-1}, \quad (7.33)$$

where

$$\cos\gamma_0 = \frac{\sigma_{gs,0} - \sigma_{ls,0}}{\sigma_{lg,0}}. \quad (7.34)$$

The first factor in Eq. (7.33),  $\cos\gamma_0$ , can be considered as a characteristic of the liquid surface while the second one depends on fluid density (liquid or vapor). Thus, for the analysis of heterogeneous nucleation in the considered linear approach (Eq. (7.29)) it is sufficient to know only the contact angle for the equilibrium condition of liquid and its vapor,  $\gamma_0$ . For illustration the calculations below will be carried out for a hydrophilic surface with  $\gamma_0 = 67^\circ$ . Note that the first factor in Eq. (7.33) is the same as in the classical description of the heterogeneous nucleation, while the second factor appears as the result of the generalization of Gibbs' approach.

In the case of droplet nucleation on a hydrophilic surface under consideration the angle  $\alpha$ , defining the factor of catalytic activity (7.12), will be greater than zero only at  $\rho_l > \rho_{lm}$  where

$$\rho_{lm} = \rho_g + (\rho_{l,0} - \rho_{g,0}) \left| \frac{\cos\gamma_0}{\sin\beta} \right|^{\frac{1}{\delta-1}}. \quad (7.35)$$

At smaller liquid droplet density the contact angle  $\alpha$  turns out to be equal to zero and the factor of catalytic activity also becomes equal to zero  $\varphi(\rho_g, \rho_l) = 0$ . That is, at  $\rho_l < \rho_{lm}$  the formation of a new phase can occur spontaneously, without any barrier, like spinodal decomposition of an unstable homogeneous system.

We see that in terms of the generalized Gibbs' approach the account of variations of the contact angle (deviations from the equilibrium value  $\gamma_0$ ) due to the changes in the droplet density, leads to the decrease (under certain conditions tending to zero) of the work of formation of the critical size droplet on the hydrophilic surface.

### 7.3. Vapor condensation on a hydrophilic surface

An analysis of Eq. (7.18) for a planar interface ( $\beta=90^\circ$ ) and a conic void ( $\beta=60^\circ$ ), reveals that at a certain moderate (initial supersaturation close to the binodal curve,  $\rho_{g,0}=0.128$ ) a profile of the Gibbs free energy in the  $(r,\rho)$ -space near to the critical cluster has a characteristic saddle-shaped form (Fig. 7.4a, c;  $\theta=0.7$ ;  $\rho_g=0.17$ ).

Such behavior of the system is characteristic for vapor densities up to the value  $\rho_{g,sh}$  situated on a curve which we will call “surface spinodal” in contrast to bulk spinodal, defined by Eq. (7.9), for the chosen calculation parameters ( $\theta=0.7$ ,  $\gamma_0=67^\circ$ )  $\rho_{g,sh}=0.191$  at  $\beta=90^\circ$  and  $\rho_{g,sh}=0.178$  at  $\beta=60^\circ$ .

For large densities,  $\rho_g > \rho_{g,sh}$ , there is a path of evolution to the new phase without activation barrier (Fig. 7.4b, d,  $\theta=0.7$ ,  $\rho_g=0.205$ ).

The critical density  $\rho_{g,sh}$  is determined from the solution of the following equation

$$\rho_{lm}(\rho_{g,sh}) = \rho_{cr}(\rho_{g,sh}) \quad , \quad (7.36)$$

where  $\rho_{lm}$  is defined by Eq. (7.35),  $\rho_{cr}$  is the liquid density in a droplet of the critical size determined as the solution of Eqs. (7.25). The density of the critical droplet is equal to  $\rho_{lm}(\rho_g)$  at  $\rho_g > \rho_{g,sh}$  and  $\rho_{cr}(\rho_g)$  at  $\rho_g < \rho_{g,sh}$ . Parameters of the critical droplet as functions of the vapor density are presented in Fig. 7.5 (a – droplet density; b – critical size, c – work of formation and d – catalytic factor for  $\beta=90^\circ$  and  $\beta=60^\circ$ ). With the increase of vapor density starting on the binodal curve, the critical droplet density decreases down to  $\rho_l = \rho_{cr}(\rho_{g,sh})$  (Fig. 7.5a).

Similar to the classical picture, the size of the critical droplet tends to infinity close to the binodal; the increase in vapor density,  $\rho_g$ , decreases the critical size, and at  $\rho_g \geq \rho_{g,sh}$  the critical size equals zero (Fig. 7.5b). Note, however, that the curvature radius of the droplet goes to infinity with the increase in vapor density to the value

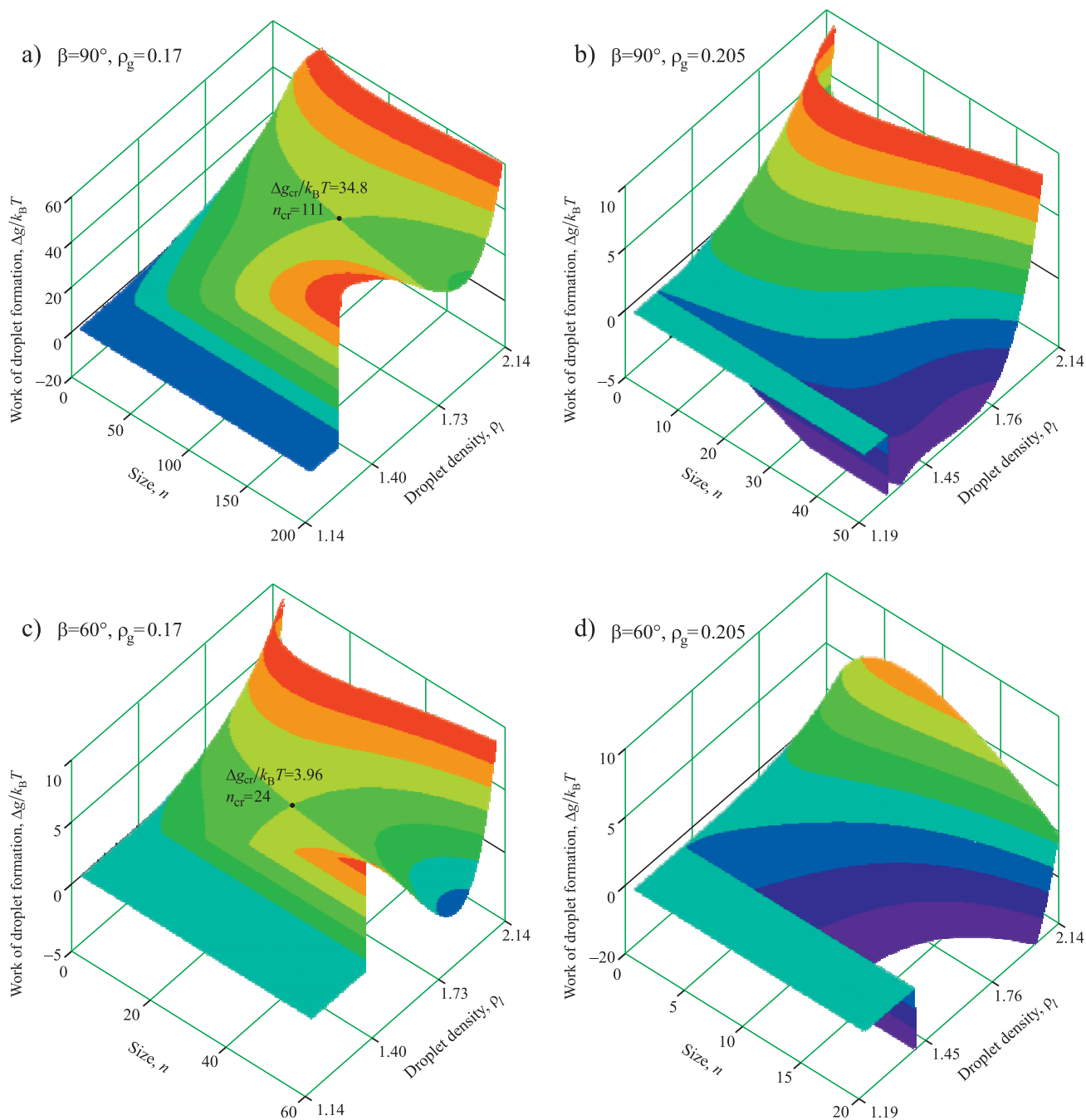


Fig. 7.4. (a, b) Profiles of Gibbs free energy of droplet formation on a planar interface ( $\beta= 90^\circ$ ) and (c, d) in a conic void ( $\beta= 60^\circ$ ) in dependence on state parameters. (a, c) metastable conditions with initial density of vapor  $\rho_g= 0.17$ ; (b, d) unstable conditions with  $\rho_g= 0.205$ .

$\rho_g = \rho_{g,sh}$  and the gas-liquid interface becomes flat as it has to be the case according to density functional computations [20,21] and the generalized Gibbs approach [17, 22,23,26,27]. The work of formation of the critical cluster decreases from infinity on binodal to zero at  $\rho_g = \rho_{g,sh}$  (Fig. 7.5c). Fig. 7.5d shows the dependence of the catalytic factor on vapor density,  $\varphi(\rho_g) = \varphi(\rho_g, \rho_{cr}(\rho_g))$ , (see Eqs. (7.16) and (7.25)). We see that it decreases steadily, reaching zero at  $\rho_g = \rho_{g,sh}$ . Note that at  $\rho_g > \rho_{g,sh}$  the concept of critical parameters of a droplet has no physical sense any more because the critical size is equal to zero.

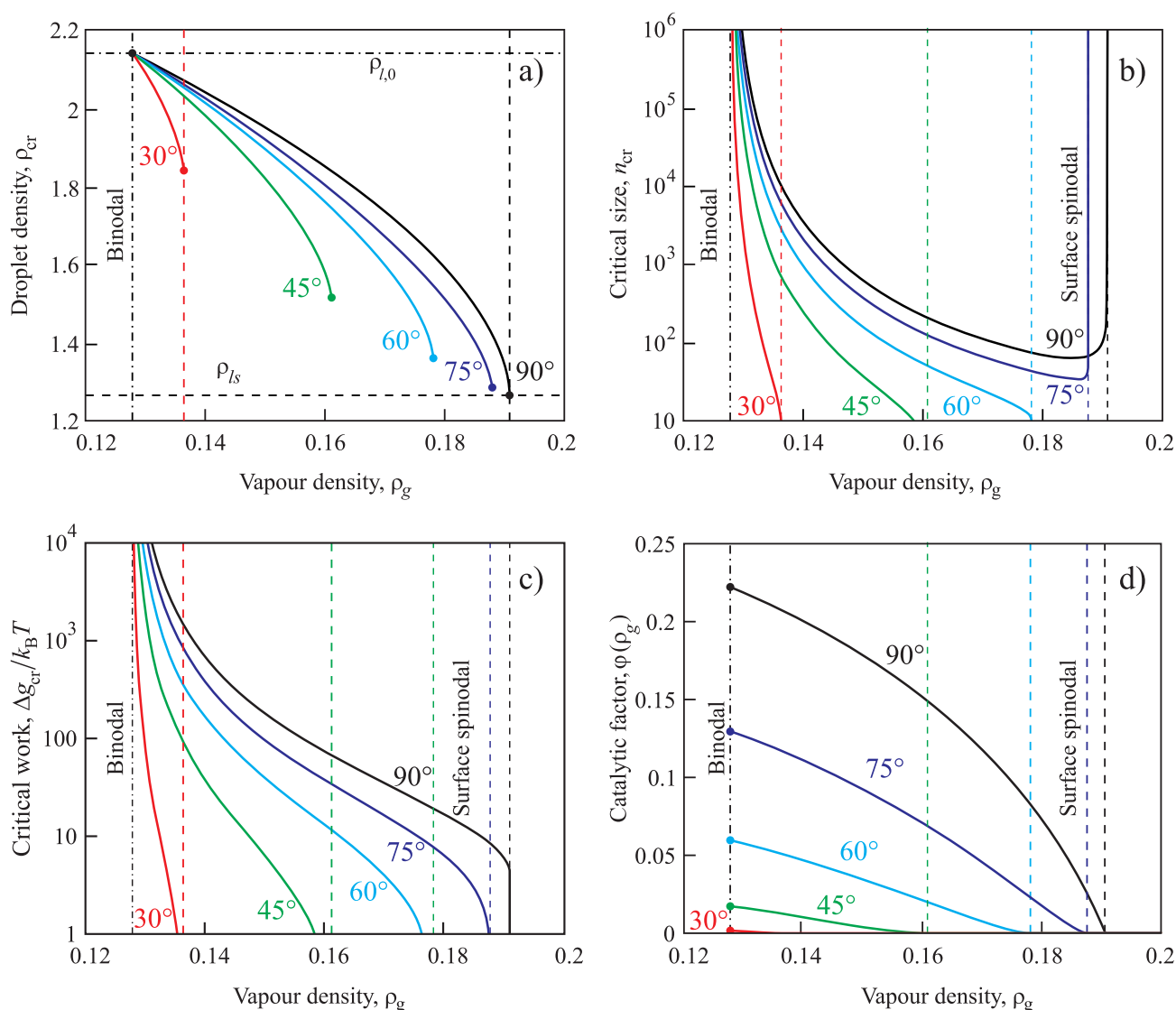


Fig. 7.5. Dependence of critical droplet parameters on vapor density for condensation on a hydrophilic surface: (a) density, (b) critical size, (c) work of formation, (d) catalytic factor for  $\beta = 90^\circ, 75^\circ, 60^\circ, 45^\circ,$  and  $30^\circ$ .

A behavior similar to the one obtained above at the approach to  $\rho_{sh}$  (Fig. 7.5), was observed also in the analysis of heterogeneous nucleation at a planar interface at processes of the condensation and boiling [26] and segregation in solutions [27]. Therefore, one can conclude that the presence of the heterogeneous nucleation centers leads to the shift of the spinodal from its values calculated thermodynamically for a homogeneous system (Fig. 7.1) to the value  $\rho_g = \rho_{g,sh}$  which depends on the properties of the nucleation centers. In the case under consideration of a cone-shaped void the value  $\rho_{g,sh}$  decreases with the decrease of the cone angle  $\beta$  to  $\rho_{g,0}$  at  $\beta = \pi/2 - \gamma_0$  (Fig. 7.6). Consequently, a system state can be considered in the range  $\rho_{g,0} < \rho_g < \rho_{g,sh}$  as metastable with respect to heterogeneous nucleation, and at  $\rho_g > \rho_{g,sh}$  as thermodynamically unstable (see Fig. 7.7). The gas density value  $\rho_g = \rho_{g,sh}$  can be viewed as belonging to the spinodal curve for heterogeneous nucleation.

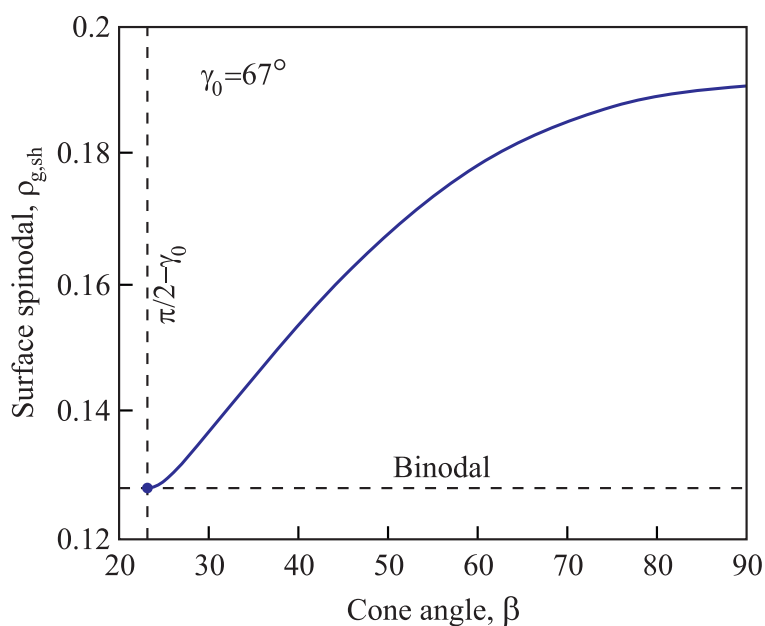


Fig. 7.6. Dependence of the heterogeneous surface spinodal  $\rho_{g,sh}$  on the cone angle  $\beta$ .

Thus, the account of the dependence of the contact angle on the liquid density in an evolving droplet in the generalized Gibbs model actually leads to an appreciable shift of the spinodal in the direction of smaller supersaturations. The shifting magnitude depends on the cone angle  $\beta$  of the droplet. At the displaced

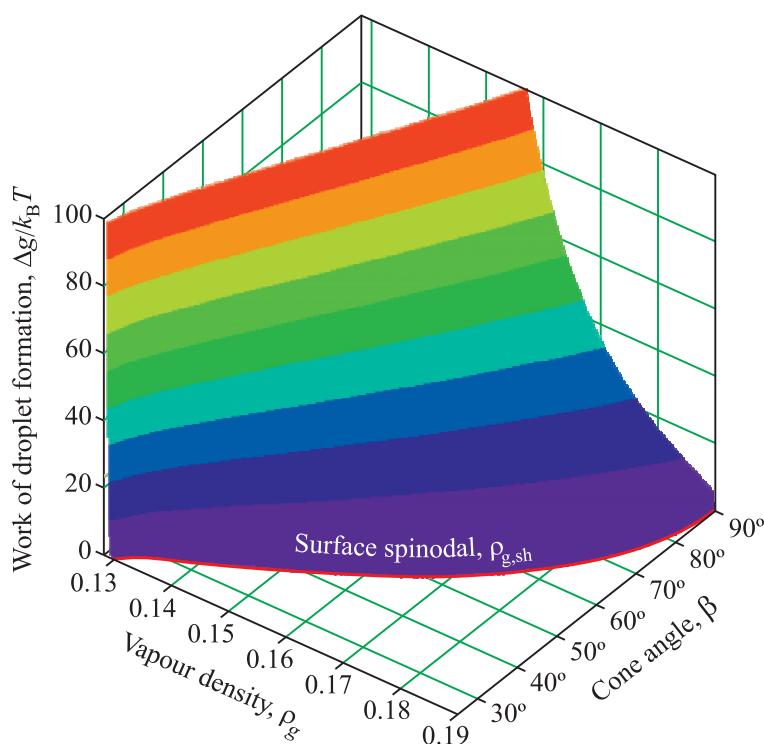


Fig. 7.7. Dependence of work of critical droplet formation on vapor density and cone angle for condensation on the hydrophilic surface.

spinodal curve the work of critical cluster formation turns, as it should be, to zero.

#### 7.4. Conclusion

The generalized Gibbs approach makes it possible to account for the dependence of a contact angle of the nucleating cluster on its density. In the case of liquid nucleation from vapor on a hydrophilic surface of a cone-shaped void such account leads to the shift of the spinodal towards smaller values of metastability (in comparison with homogeneous nucleation). As the cone angle decreases the heterogeneous spinodal comes nearer to the binodal, the area of metastability is narrowed, and the area of instability is extended.

Only a simple case of liquid droplet nucleation from supersaturated vapor in a conic void was studied above. However, the influence of the change of state

parameters of a new phase cluster on intensity of the nucleation as observed here can be expected to occur on surface defects of various form, i.e., on cracks, spherical voids, and also for a case of boiling of liquids. These problems, as well as applications of more realistic equations of state applied for specific liquid or gas media [38, 39], can be considered on the basis of the general approach formulated above.

## References

1. E.Yu. Bormashenko, *Physics of Wetting*, De Gruyter Textbook, 2017, 232 p.
2. M. Volmer, *Zeitschrift für Elektrochemie* **35**, 555-561 (1929).
3. D. Turnbull, *Acta Metallurgica* **1**, 8-14 (1953).
4. J.W. Christian, *The Theory of Transformations in Metals and Alloys*, Part I, Ch.10, The Classical Theory of Nucleation, Pergamon Press, 2002, p. 422-479.
5. N.H. Fletcher, Size Effect in Heterogeneous Nucleation, *Journal of Chemical Physics* **29** (3) (1958) 572-576.
6. M. Qian, Heterogeneous nucleation on potent spherical substrates during solidification, *Acta Materialia* **55** (2007) 943-953.
7. M. Lazaridis, M. Kulmala, A. Laaksonen, Binary heterogeneous nucleation of a water-sulphuric acid system: The effect of hydrate interaction, *J. Aerosol Sci.* **22** (7) (1991) 823-830.
8. M. Lazaridis, The effects of surface diffusion and line tension on the mechanism of heterogeneous nucleation. *J. Coll. Interface Sci.* **155** (2) (1993) 386-391.
9. M. Volmer. *Kinetik der Phasenbildung*, Th. Steinkopff, Dresden and Leipzig, 1939.
10. D. Turnbull, Kinetics of Heterogeneous Nucleation, *J. Chem. Physics.* **18** (2) (1950) 198-203.

11. P. Griffith, J.D. Wallis, The role of surface conditions in nucleate boiling, Chemical Engineering Progress Symposium Series, no. 30, v. 56 (1960) 49-63.
12. M. Lazaridis, O. Hov, K. Eleftheriadis, Heterogeneous nucleation on rough surfaces: implications to atmospheric aerosols, Atmospheric Research 55 (2000) 103-113.
13. Bin Yang, J.H. Perepezko, J.W.P. Schmelzer, Yulai Gao, and Ch. Schick, Dependence of crystal nucleation on prior liquid overheating by differential fast scanning calorimeter, J. Chem. Physics 140, 104513 (2014).
14. J.W. Gibbs, *On the Equilibrium of Heterogeneous Substances*, Transactions Connecticut Academy of Sciences 3 (1874-1878) 108-248 & 343-524; see also: J.W. Gibbs, *The Collected Works*, vol. 1, Longmans, New York – London & Toronto (1928).
15. J.D. van der Waals and Ph. Kohnstamm, *Lehrbuch der Thermodynamik*, Johann-Ambrosius-Barth Verlag, Leipzig und Amsterdam, 1908.
16. J.S. Rowlinson, Translation of J.D. van der Waals, The thermodynamic theory of capillarity under the hypothesis of a continuous variation of density, J. Stat. Phys. 20 (1979) 197-244.
17. I. Gutzow and J.W.P. Schmelzer, *The Vitreous State: Thermodynamics, Structure, Rheology, and Crystallization*, 1st edition, Springer, Berlin, 1995; 2d edition: Springer, Heidelberg, 2013.
18. V.G. Baidakov, *Explosive Boiling of Superheated Cryogenic Liquids*, Wiley-VCH, Berlin-Weinheim, 2007.
19. V. M. Fokin, E.D. Zanutto, N.S. Yuritsyn, and J.W.P. Schmelzer, Homogeneous crystal nucleation in silicate glasses: A 40 year perspective, J. Non-Cryst. Solids 352 (2006) 2681-2714.
20. J.W. Cahn and J.E. Hilliard, Free energy of a non-uniform system I. Interfacial energy, J. Chem. Phys. 28 (1958) 258-267.

21. J.W. Cahn and J.E. Hilliard, Nucleation in a Two-Component Incompressible Fluid, *Chem. Phys.* 31 (1959) 688-699.
22. J.W.P. Schmelzer, J. Schmelzer Jr., and I. Gutzow, Reconciling Gibbs and van der Waals: A new approach to nucleation theory, *J. Chem. Phys.* 112 (2000) 3820-3831.
23. J.W.P. Schmelzer, G.Sh. Boltachev, and V.G. Baidakov, Classical and generalized Gibbs' approaches and the work of critical cluster formation in nucleation theory, *J. Chem. Phys.* 124 (2006) 194503.
24. J.W.P. Schmelzer, A.R. Gokhman, and V.M. Fokin, Dynamics of first-order phase transitions in multicomponent systems: a new theoretical approach, *J. Colloid Interface Science* 272 (2004) 109-133.
25. J.W.P. Schmelzer, V.M. Fokin, A.S. Abyzov, E.D. Zanotto, and I.Gutzow, How do crystals form and grow in glass-forming liquids: Ostwald's rule of stages and beyond, *International Journal of Applied Glass Science* 1 (2010) 16-26.
26. A.S. Abyzov, J.W.P. Schmelzer, Generalized Gibbs' approach in heterogeneous nucleation, *J. Chem. Physics* 138 (2013) 164504.
27. A.S. Abyzov, J.W.P. Schmelzer, Generalized Gibbs' approach in heterogeneous nucleation in regular solution, *J. Chem. Physics* 140 (2014) 244706.
28. J.L. McCormick and J.W. Westwater, *Chem. Eng. Sci.* 20 (1965) 1021-1036.
29. Wei Xu, Zhong Lan, Benli Peng, Rongfu Wen and Xuehu Ma, Heterogeneous nucleation capability of conical microstructures for water droplets, *RSC Adv.* 5 (2015) 812-818.
30. F.M. Kuni, A.K. Shchekin, A.P. Grinin. Theory of heterogeneous nucleation for vapor undergoing a gradual metastable state formation, *Physics-Uspekhi* 44 (2001) 331-370.
31. Jianguo Lia, Yawei Liub, Guangfeng Jianga and Xianren Zhang, Vapour-to-liquid nucleation in cone pores, *Molecular Simulation* 42 (2016) 1-8.

32. E. Ruckenstein and G.O. Berim, Kinetics of heterogeneous nucleation on a rough surface: nucleation of a liquid phase in nanocavities, *J. Colloid Interface Sci.* 351 (2010) 277-282.
33. O. Hellmuth, V.I. Khvorostyanov, J.A. Curry, A.K. Shchekin, J.W.P. Schmelzer, R. Feistel, Yu.S. Djikaev, and V.G. Baidakov, Selected Aspects of Atmospheric Ice and Salt Crystallisation. In: *Nucleation Theory and Applications-Special Issues: Review Series on Selected Topics of Atmospheric Sol Formation, Vol. 1*, edited by J.W.P. Schmelzer and O. Hellmuth (Editors), Joint Institute for Nuclear Research Publishing Department, Dubna, Russia, 2013.
34. J.D. van der Waals, Over de Continuïteit van den Gasen, Thesis, Sijthoff, Leiden 1873; German translation: *Die Kontinuität des gasförmigen und flüssigen Zustandes*, Johann-Ambrosius Barth Publishers, Leipzig, 1881 (1st Edition); 1899-1900 (2d Edition).
35. J.W.P. Schmelzer and J. Schmelzer Jr., Kinetics of bubble formation and the tensile strength of liquids, *Atmospheric Research* 65 (2003) 303-324.
36. J.W.P. Schmelzer and J. Schmelzer Jr., Kinetics of condensation of gases: A new approach, *J. Chem. Phys.* 114 (2001) 5180-5193.
37. K. Kelton, A. Greer. *Nucleation in Condensed Matter, Applications in Materials and Biology*, Vol. 15, Pergamon (2010).
38. A.R. Imre, A.S. Abyzov, I.F. Barna, and J.W.P. Schmelzer, Homogeneous bubble nucleation limit of mercury under the normal working conditions of the planned European spallation neutron source, *Eur. Phys. J. B* 79 (2011) 107-113.
39. A.S. Abyzov, J.W.P. Schmelzer, L.N. Davydov, V.V. Slezov, Homogeneous bubble nucleation limit of lead, *Problems of atomic science and technology*, N 1. Series: Nuclear Physics Investigations 57 (2012) 283-287.

## 7.5. Висновки до розділу 7

Результати досліджень, представлених у даному розділі, опубліковано в статті [7] (Додаток А. Список публікацій здобувача за темою дисертації). Досліджено гетерогенне зародження крапель рідини з пари (газу) на дефектній твердій поверхні в моделі газу ван дер Ваальса. Серед основних результатів у якості висновків можна виділити наступні:

- Показано, що контактний кут та каталітичний фактор для зародження на дефектній поверхні залежать від ступеня переохолодження пари. У разі утворення крапель на гідрофільній поверхні кінчної пори швидкість зародження значно збільшується порівняно з конденсацією на планарній поверхні.

- Наявність дефекту на гідрофільній поверхні призводить до значного зсуву спінодалі порівняно з гетерогенним зародженням на планарній поверхні: зі зменшенням кута конуса пори гетерогенна спінодаль наближається до бінодалі, і область метастабільності звужується за рахунок розширення області нестабільності.

- Існує граничний кут конуса пори, менше якого формування нової фази проходить безбар'єрно.

## РОЗДІЛ 8

### ГЕТЕРОГЕННА НУКЛЕАЦІЯ У РОЗЧИНАХ НА ДЕФЕКТНИХ ТВЕРДИХ ПОВЕРХНЯХ: УЗАГАЛЬНЕНИЙ ПІДХІД ГІББСА

У восьмому розділі досліджена гетерогенна нуклеація кластерів нової фази в *регулярному бінарному розчині* на дефектній твердій поверхні, як і в попередньому розділі, як дефект поверхні обрана конічна пора. Розрахована швидкість нуклеації кластера нової фази у залежності від кута конуса пори і ступеня пересичення розчину.

*entropy*

### Heterogeneous Nucleation in Solutions on Rough Solid Surfaces: Generalized Gibbs Approach

**Alexander S. Abyzov<sup>1</sup>, Leonid N. Davydov<sup>1\*</sup> and Jörn W. P. Schmelzer<sup>2</sup>**

<sup>1</sup>National Science Center Kharkov Institute of Physics and Technology, Academician Street 1, 61108 Kharkov, Ukraine

<sup>2</sup>Institut für Physik der Universität Rostock, Albert-Einstein-Strasse 23-25, 18059 Rostock, Germany

\*Correspondence: ldavydov@kipt.kharkov.ua; Fax: +38-057-349-1058

(Received: 19 July 2019; Accepted: 7 August 2019; Published: 9 August 2019)

**Abstract:** Heterogeneous nucleation of new phase clusters on a rough solid surface is studied. The ambient phase is considered to be a regular supersaturated solution. In contrast to existing studies of the same problem, the possible difference between the state parameters of the critical cluster and the corresponding parameters of a newly formed macroscopic phase is accounted for. This account is performed within the framework of the generalized Gibbs approach. Surface imperfections are chosen in the form of cones. The model allows us to simplify the analysis but also to obtain the basic results concerning the defect influence on the nucleation

process. It is shown that the catalytic activity factor for nucleation of the cone depends both on the cone angle and the supersaturation in the solution determining the state parameters of the critical clusters. Both factors considerably affect the work of critical cluster formation. In addition, they may even lead to a shift of the spinodal curve. In particular, in the case of good wettability (macroscopic contact angle is less than  $90^\circ$ ) the presence of surface imperfections results in a significant shifting of the spinodal towards lower values of the supersaturation as compared with heterogeneous nucleation on a planar solid surface. With the decrease of the cone pore angle, the heterogeneous spinodal is located nearer to the binodal, and the metastability range is narrowed, increasing the range of states where the solution is thermodynamically unstable.

**Keywords:** heterogeneous nucleation; kinetic theory; rough surface; gibbs theory; surface tension

**PACS:** 64.60.Bd General theory of phase transitions; 64.60.Q Nucleation in phase transitions; 82.60.Nh Thermodynamics of nucleation; 68.35.Md Surface energy of surfaces and interfaces; 64.60.an Phase transitions in finite-size systems; 68.35.Md Thermodynamic properties of surfaces and interfaces.

## 8.1. Introduction

The nucleation of new phase clusters can be catalyzed by solid or liquid particles dissolved in the ambient phase, by planar Surfaces, and, in particular, by defects of such surfaces. In all these cases of heterogeneous nucleation the thermodynamic barrier – the work of formation of the critical cluster which must be overcome for a nucleus for consequent deterministic growth – is reduced as

compared to homogeneous nucleation when the surface or particles dissolved in the ambient phase are absent. Such effects are intensively studied in the framework of classical nucleation theory [1–6]. However, the classical theory of nucleation (both homogeneous, and heterogeneous) commonly relies on the assumption that the state parameters of the critical cluster are widely identical to the corresponding parameters of the macroscopic phase to be formed. However, in practice this assumption, as a rule, is not met [7–10]. The significance of such changes of the state parameters of the critical clusters in heterogeneous nucleation was demonstrated by us for the first time in Refs. [11–13]. In [11, 12], we studied such processes for condensation and boiling on planar interfaces, in [13], we considered condensation and boiling on rough interfaces. This analysis is extended here considering heterogeneous nucleation in solutions catalyzed by rough solid interfaces.

In detail, in the present paper a theoretical analysis of heterogeneous nucleation in a binary regular solution on a rough solid surface is conducted employing the generalized Gibbs approach. The main difference of the proposed approach from theoretical treatments performed so far consists, as already noted above, is in the consistent account of the difference between the state parameters of the critical cluster and the corresponding parameters of the macroscopic phase to be formed. Surface imperfections are chosen in form of cones that allows us to simplify the analysis and at the same time to obtain the main results of the defect influence on the nucleation process. The general qualitative conclusions do not depend widely on the specific model employed for the description.

The thermodynamic analysis of nucleation in terms of the generalized Gibbs approach supplies us with the work of formation of the aggregates of the newly evolving phase in dependence on size and shape. This dependence we analyze here. The knowledge of such dependence is a precondition for modeling the kinetics of both nucleation and growth processes. In nucleation and growth, the clusters may change both their shape and size and both parameters may even fluctuate. However,

this analysis refers to a different topic and will be addressed in a future study.

## 8.2. Basic Equations

We consider the formation of a new phase cluster on a rough rigid surface. For the description of the bulk properties of the ambient and the newly formed phases we use the model of a binary solid or liquid regular solution. The chemical potentials  $\mu_j$  of each of the two components ( $j = 1, 2$ ) of a regular solution can be written in the form [14]

$$\mu_1 = \mu_1^* + k_B T \ln(1 - x) + \Omega x^2, \quad (8.1)$$

$$\mu_2 = \mu_2^* + k_B T \ln x + \Omega(1 - x)^2, \quad (8.2)$$

where  $k_B$  is the Boltzmann constant,  $T$  is the absolute temperature,  $x$  and  $(1 - x)$  are the molar fractions of the second and first components, correspondingly (for unambiguity we consider the solvent as the first component and the dissolved substance as the second component),  $\Omega = 2k_B T_c$  is the interaction parameter describing specific properties of the considered system, and  $T_c$  is the critical temperature of the system.

In thermodynamics, the binodal curve is the locus of phase states (in  $(T, x)$ -diagram) where two distinct phases may coexist in equilibrium. This coexistence curve is defined by the condition at which the chemical potentials of solution components are equal in each phase. The extremum of the binodal curve in temperature is known as a critical point. At this point, the binodal curve coincides with the extremum of the spinodal curve. The spinodal curve in its turn is the locus of the phase states where the system's local stability with respect to small fluctuations is

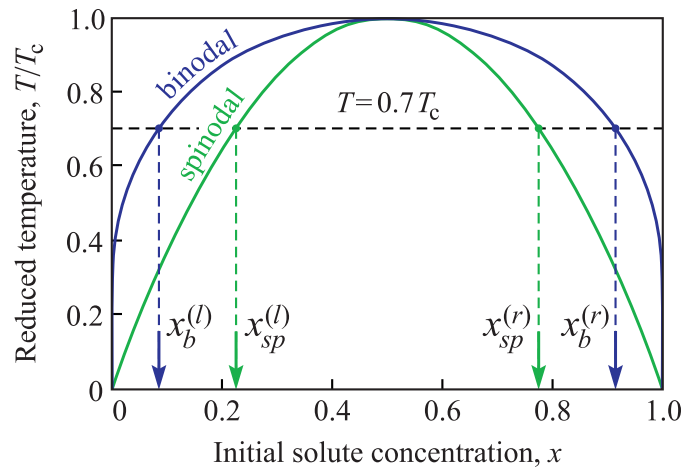


Fig. 8.1. Binodal (dark blue) and spinodal (green) curves as functions of the composition of a regular solution. The left and right binodal ( $x_b^{(l)}, x_b^{(r)}$ ) and spinodal ( $x_{sp}^{(l)}, x_{sp}^{(r)}$ ) values are shown for temperature  $T = 0.7T_c$ .

broken and is defined by the condition that the second derivative of Gibbs free energy (with respect to concentration  $x$ ) is zero. Therefore, in our case at constant external pressure the positions of the binodal and spinodal on the phase diagram  $(T, x)$  are determined by the following equations,

$$\ln \left( \frac{1-x}{x} \right) = 2 \frac{T_c}{T} (1-2x), \tag{8.3}$$

$$x(1-x) = \frac{T}{4T_c}. \tag{8.4}$$

They are shown in Figure 8.1.

The values of the left binodal ( $x_b^{(l)}$ ) and spinodal ( $x_{sp}^{(l)}$ ) branches, calculated at temperature  $T = 0.7T_c$ , are, correspondingly

$$x_b^{(l)} = 0.1857, \quad x_{sp}^{(l)} = 0.2261. \tag{8.5}$$

Both curves are symmetric with respect to  $x = 1/2$ ; therefore, the correspondi-

ng values for the right-hand side branches are

$$x_b^{(r)} = 1 - x_b^{(l)} = 0.9143, \quad x_{sp}^{(r)} = 1 - x_{sp}^{(l)} = 0.7739. \quad (8.6)$$

These values are especially distinguished in Figure 8.1.

Let us assume that due to the change in temperature or composition, the system is transferred into a metastable state somewhere between left binodal and spinodal ( $x_b^{(l)} < x < x_{sp}^{(l)}$ , see Figure 8.1). After this sudden transfer, temperature and composition are maintained unchanged. For this system first we define the parameters of the critical cluster nucleated in a conic pore depending on the created supersaturation (i.e., the molar concentration of the dissolved substance,  $x$ ). We remind that as an example of surface imperfections we choose a conic pore. This approach allows us to simplify the analysis and at the same time to receive main results of the defect influence on the nucleation process.

In a binary solution a new phase will be nucleated as a result of the redistribution of molecules (atoms) in space. Following Gibbs model [6], we consider a new phase cluster as a spatially homogeneous part of the system with a composition, however, different from the ambient phase. The boundary is modeled by a mathematical surface of zero thickness with a corresponding value of the tension surface [1, 6, 12]. The change of the thermodynamic potential (Gibbs free energy  $G$ ) of the binary system owing to the creation of a cluster in form of a spherical cone with the radius  $R$  in a conic pore (Figure 8.2) can be given by [1–3, 11]

$$\Delta G = \sigma_{\alpha\beta} A_{\alpha\beta} + (\sigma_{\alpha s} - \sigma_{\beta s}) A_{\alpha s} + \sum_{j=1,2} n_j (\mu_{j\alpha} - \mu_{j\beta}). \quad (8.7)$$

Here specific interphase energies (surface tensions) of the corresponding boundaries are denoted as:  $\sigma_{\alpha s}$  (cluster ( $\alpha$ )-pore ( $s$ )),  $\sigma_{\beta s}$  (outer solution ( $\beta$ )-pore ( $s$ )), and  $\sigma_{\alpha\beta}$  (cluster ( $\alpha$ )-outer solution ( $\beta$ )). Next,  $A_{\alpha s}$  and  $A_{\alpha\beta}$  are the

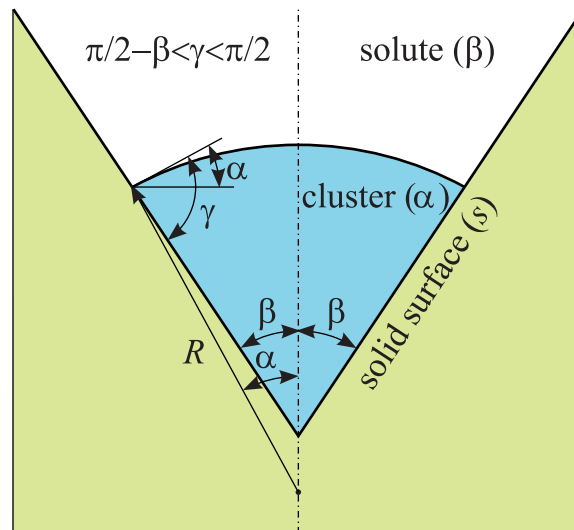


Fig. 8.2. Model used in the analysis of heterogeneous nucleation of a new phase cluster in a conic pore. Here  $R$  is the curvature radius of the cluster outer surface,  $\gamma$  is the contact angle, and  $2\beta$  is the cone angle.

boundary surface area between the cluster and pore, and the outer solution, correspondingly (Figure 8.2),  $\mu_{j\alpha}$  and  $\mu_{j\beta}$  are the chemical potentials of both components ( $j = 1, 2$ ) in the cluster and outside it (see Equations (8.1) and (8.2)). The indices  $\alpha$  and  $\beta$  denote the parameters of the cluster and the ambient phase, accordingly. For the description of the cluster state the numbers of atoms of a kind 1 and 2 are used as independent variables,  $n_1$  and  $n_2$  (the index  $\alpha$  in  $n_1$  and  $n_2$  is omitted to simplify the notations). The total number of atoms in a cluster is  $n_\alpha = n_1 + n_2$ .

For simplification, similarly to [10, 12], the particle volume  $\omega$  is supposed not to depend on composition ( $\omega_\alpha = \omega_\beta \equiv \omega = a^3$ , where  $a$  is the interatomic distance).

The radius of curvature,  $R$ , of the spherical cone (for simplicity we will name it “cluster radius”) is determined by the number of particles in the cluster,  $n_\alpha$ , via

$$\varphi \frac{4\pi}{3} R^3 = n_\alpha \omega = n_\alpha a^3, \tag{8.8}$$

where  $\varphi$  is expressed through the contact angle,  $\gamma$ , and the cone angle,  $2\beta$ , as

$$\varphi = \frac{1}{3}(2 - 3 \cos \alpha + \cos^3 \alpha + \text{ctg } \beta \sin^3 \alpha), \quad \alpha = \gamma + \beta - \frac{\pi}{2}. \tag{8.9}$$

The change in Gibbs free energy due to cluster creation is determined in correspondence with Equation (8.7) as [2,3,11]

$$\Delta G = \Delta G_V + \Delta G_S, \quad (8.10)$$

$$\Delta G_V = -\varphi \left( \frac{4\pi}{3\omega} \right) R^3 \Delta\mu = \varphi \left( \frac{4\pi}{3\omega} \right) R^3 k_B T f, \quad \Delta\mu = -k_B T f, \quad (8.11)$$

$$\Delta G_S = 2\pi R^2 (1 - \cos \alpha) \sigma_{\alpha\beta} + \pi R^2 \frac{1 - \cos^2 \alpha}{\sin \beta} (\sigma_{\alpha s} - \sigma_{\beta s}). \quad (8.12)$$

For a wettable surface ( $\gamma < \pi/2$ ) at low cone angle of  $\beta < \pi/2 - \gamma$  the cluster outer surface becomes concave, the contribution of the surface component in the work of its formation becomes negative, and the cluster can start to grow in the range  $x > x_b$  at any initial size. However, this conclusion is correct only for a conic pore which has a sufficiently large depth. Indeed, when the cluster grows up to a flat surface surrounding the pore its surface becomes convex, and, actually, one must consider nucleation on a flat surface [12]. If a pore is not deep, the cluster does not succeed to grow up to a critical size, and the effect of the pore decreases. This particular case is beyond the scope of the present work, therefore we shall limit ourselves here to the range of angles  $\beta > \pi/2 - \gamma$  (see Figure 8.2).

In the derivation of Equation (8.11) we have neglected possible modifications of the solution composition caused by the nucleation process. This effect is not essential at an early stage of nucleation for sufficiently large systems. An analysis of the effect of such changes in systems of small sizes is given in [10,15]. At such conditions, the function  $f(x_\alpha, x)$  in Equation (8.11) has the meaning of the thermodynamic driving

force of cluster formation. It is determined by the relation [2, 3, 11],

$$f(x_\alpha, x) = (1 - x_\alpha) \left\{ \ln \frac{1 - x_\alpha}{1 - x} + 2 \frac{T_c}{T} (x_\alpha^2 - x^2) \right\} + x_\alpha \left\{ \ln \frac{x_\alpha}{x} + 2 \frac{T_c}{T} [(1 - x_\alpha)^2 - (1 - x)^2] \right\} . \tag{8.13}$$

The dependence of function  $f(x_\alpha, x)$  on cluster composition,  $x_\alpha$ , for different values of the supersaturations,  $x$ , is shown in Figure 8.3.

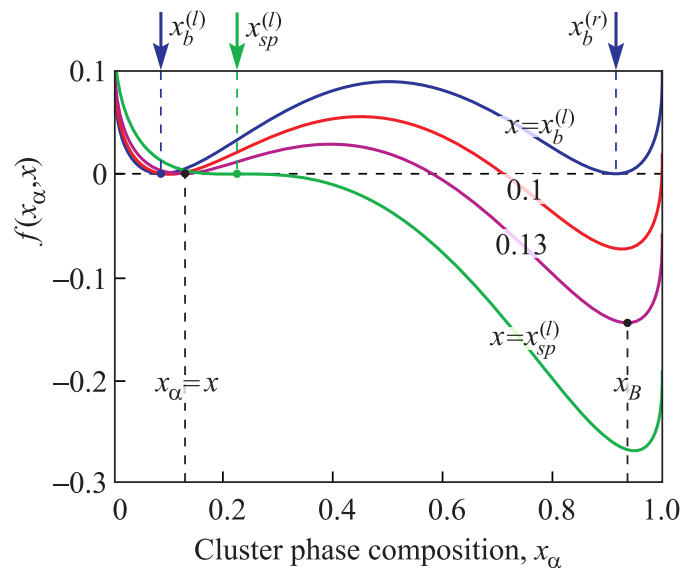


Fig. 8.3. Dependence of the function  $f(x_\alpha, x)$  on cluster composition,  $x_\alpha$ , at different supersaturations  $x = x_b^{(l)}$ , 0.1, 0.13,  $x_{sp}^{(l)}$  in the region of metastability  $x_b^{(l)} < x < x_{sp}^{(l)}$  of the ambient solution.

The regions of metastability are in composition ranges  $x_b^{(l)} < x < x_{sp}^{(l)}$  (between the left branches of the binodal and spinodal) and  $x_{sp}^{(r)} < x < x_b^{(r)}$  (between the right branches of the spinodal and binodal). The function  $f(x_\alpha)$  has one maximum and two minima (for  $x \neq x_{sp}^{(l,r)}$ ). The first minimum,  $x_\alpha = x$ , corresponds to the state of the ambient phase. The second minimum,  $x_\alpha = x_B$ , corresponds to the final macroscopic state of the precipitating phase, to which a cluster evolves at fixed composition of the surrounding solution,  $x$ . It is determined by the minimum of the bulk contribution to

the Gibbs free energy (Figure 8.3),

$$\left. \frac{\partial f(x_\alpha, x)}{\partial x_\alpha} \right|_{x=x_B} = 0. \quad (8.14)$$

At the spinodal,  $x = x_{sp}^{(l)}$ , the function  $f(x_\alpha)$  has an inflection point corresponding to  $x_\alpha = x$ ,  $\left. \frac{\partial^2 f(x_\alpha, x)}{\partial x_\alpha^2} \right|_{x_\alpha=x} = 0$ . The range  $x_{sp}^{(r)} < x < x_{sp}^{(l)}$  is thermodynamically unstable. The maximum of the function  $f(x_\alpha)$  in this region corresponds to the initial state,  $x_\alpha = x$ , there are also two local minima of the function  $f(x_\alpha)$  at  $x_\alpha = x_A < x$  and  $x_\alpha = x_B > x$ . Similar to Equation (8.14) they are determined by the equation

$$\left. \frac{\partial f(x_\alpha, x)}{\partial x_\alpha} \right|_{x=x_A \text{ or } x=x_B} = 0. \quad (8.15)$$

Figure 8.4 illustrates the dependence of the concentrations  $x_A$  and  $x_B$  on the initial composition  $x$  of the surrounding solution in the whole possible range of compositions. Taking into account the symmetry with respect to the substitution  $x \leftrightarrow 1 - x$ , we consider only initial states with a composition  $x \leq 1/2$ .

At any given pressure and temperature, the thermodynamic driving force for cluster formation should be positive, i.e.,  $f(x_\alpha, x) < 0$  (the bulk contribution to Gibbs free energy is decreased in this case [11]). This condition holds for

$$x_\alpha < x_{\alpha, ll}, \quad (8.16)$$

where  $x_{\alpha, ll}$  is the solution of the equation

$$f(x_{\alpha, ll}, x) = 0. \quad (8.17)$$

The function  $x_{\alpha, ll}(x)$  is represented in Figure 8.4 by a dashed line, and the

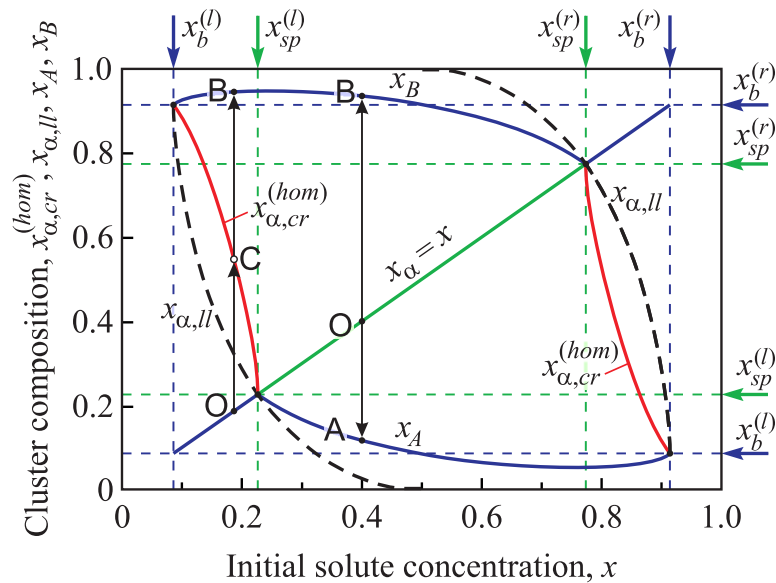


Fig. 8.4. Composition  $x_{\alpha,cr}^{(hom)}$  of the critical cluster (red lines), its minimum value  $x_{\alpha,ll}$  (dotted line), and concentrations  $x_A$ ,  $x_B$  (continuous dark blue lines) in dependence on the initial composition,  $x$ , of the solution. These results refer to the case of homogeneous nucleation.

composition of the critical cluster for homogeneous nucleation  $x_{\alpha,cr}^{(hom)}$  is shown by a solid line. The evolution of an initially metastable state proceeds along the following path:  $O \rightarrow C \rightarrow B$ . It starts at the initial state  $x_{\alpha} = x$  and propagates through a critical cluster (C) to  $x_B$ . For an initially unstable state two variants of evolution are possible, first  $O \rightarrow A$ , with a decrease of the cluster concentration to  $x_A$ , and second  $O \rightarrow B$ , with an increase in the concentration up to  $x_B$ . Generally, the inequality  $x_{\alpha,ll} \leq x_{\alpha,cr}^{(hom)}$  holds, it goes over to an equality only at  $x = x_b^{(l)}$  and  $x = x_{sp}^{(l)}$ . In the latter case, when  $x_{\alpha,ll} = x_{\alpha,cr}^{(hom)}$ , the cluster can evolve without overcoming a potential barrier. This process corresponds to spinodal decomposition. As will be shown below, at heterogeneous nucleation in a conic pore a similar situation can arise even at appreciably smaller supersaturations  $x < x_{sp}^{(l)}$ .

The Young equation determines the mechanical equilibrium at the contact line of three phases [1–5]

$$\sigma_{\beta s} = \sigma_{\alpha s} + \sigma_{\alpha\beta} \cos \gamma . \tag{8.18}$$

Assuming that this condition is fulfilled and taking into account Equation (8.9) we obtain from Equation (8.12) the interfacial contribution of a new phase cluster to the Gibbs free energy as

$$\Delta G_S = 4\pi R^2 \sigma_{\alpha\beta} \left[ \frac{1 - \cos \alpha}{2} - \frac{\cos \gamma (1 - \cos^2 \alpha)}{4 \sin \beta} \right] = 4\pi R^2 \sigma_{\alpha\beta} \varphi . \quad (8.19)$$

Thus, the work of cluster formation at heterogeneous nucleation in a conic pore can be written as

$$\Delta G_{\text{het}} = \varphi \Delta G_{\text{hom}} , \quad (8.20)$$

where

$$\frac{\Delta G_{\text{hom}}}{k_B T} = \frac{4\pi}{3\omega} \left[ \frac{3}{2} R_\sigma R^2 (x_\alpha - x)^2 + R^3 f(x_\alpha, x) \right] , \quad (8.21)$$

$$R_\sigma = \frac{2\sigma_{\alpha\beta,0} a^3}{k_B T} (x_b^{(r)} - x_b^{(l)})^{-2} , \quad (8.22)$$

and the catalytic factor  $\varphi$  is determined by Equation (8.9). Equations (8.19)–(8.21) are fulfilled at all possible values of the cone pore angle  $\beta$ , contact angle  $\gamma$ , and radius  $R$  (note, however, that here we do not consider the case of a concave outer surface of the cluster, when  $R < 0$ ). Equation (8.19) is similar to that obtained for heterogeneous nucleation on a smooth planar surface [11] and differs only by the factor  $\sin \beta$  (which equals unity for a flat surface, when  $\beta = 90^\circ$ ). The catalytic factor  $\varphi$  within the framework of the generalized Gibbs approach becomes dependent not only on the angles  $\gamma$  and  $\beta$ , but also on the compositions of the initial phase and the critical cluster. The specific interfacial energy between two phases with compositions  $x_\alpha$  and

$x$ , can be expressed according to Becker [14] (see also [16]) as

$$\sigma_{\alpha\beta} = \sigma_{\alpha\beta,0} \left( \frac{x_{\alpha} - x}{x_b^{(r)} - x_b^{(l)}} \right)^2. \quad (8.23)$$

Here  $\sigma_{\alpha\beta,0}$  is the respective value, when a new phase cluster and the solution surrounding it are in equilibrium, i.e.,  $x = x_b^{(l)}$  and  $x = x_b^{(r)}$ .

For further analysis it is convenient to introduce the dimensionless variables

$$r \equiv \frac{R}{R_{\sigma}}, \quad \Delta g \equiv \frac{\Delta G}{G_{\sigma}}, \quad (8.24)$$

$$G_{\sigma} = \frac{16\pi (\sigma_{\alpha\beta,0} a^2)^3}{3 (k_B T)^2} (x_b^{(r)} - x_b^{(l)})^{-6}. \quad (8.25)$$

In these variables Equation (8.20) takes the form

$$\Delta g(r, x_{\alpha}) = \varphi(\gamma, \beta) [3r^2(x_{\alpha} - x)^2 + 2r^3 f(x_{\alpha}, x)]. \quad (8.26)$$

As already was noted above,  $R$  is the radius of the cluster surface contacting with the ambient solution, and it can have positive, infinite, and negative values. Therefore, it is more convenient to use as independent variables for the description of the cluster state the numbers of atoms in the cluster  $(n_1, n_2)$  instead of  $(r, x)$ . Also is convenient to normalize these quantities to  $n_{\sigma}$  as

$$n'_1 \equiv \frac{n_1}{n_{\sigma}}, \quad n'_2 \equiv \frac{n_2}{n_{\sigma}}, \quad n_{\sigma} \equiv \frac{4\pi}{3} \left( \frac{R_{\sigma}}{a} \right)^3. \quad (8.27)$$

To simplify the notations we omit primes, then Equation (8.26) takes the form

$$\Delta g(n_1, n_2, x) = 3[\varphi(\gamma, \beta)]^{\frac{1}{3}} n_{\sigma}^{\frac{2}{3}} \left( \frac{n_2}{n} - x \right)^2 + 2nf \left( x, \frac{n_2}{n} \right), \quad (8.28)$$

where  $n \equiv n_1 + n_2 = \varphi r^3$ . The parameters of the critical cluster,  $(n_{1,cr}, n_{2,cr})$ , are determined by a solution of the set of equations

$$\frac{\partial \Delta g(n_1, n_2, x)}{\partial n_1} = 0, \quad \frac{\partial \Delta g(n_1, n_2, x)}{\partial n_2} = 0. \quad (8.29)$$

The work of formation of the critical cluster is determined by

$$\left( \frac{\Delta G_{cr}}{G_\sigma} \right) \equiv \Delta g_{cr}(x) = \Delta g(n_{1,cr}, n_{2,cr}, x). \quad (8.30)$$

Above relations are the basic for the subsequent analysis of surface roughness on the properties of critical clusters in heterogeneous nucleation on rough surfaces. This analysis we will start with the discussion of the contact angle.

### 8.3. Determination of the Contact Angle

In classical nucleation theory the parameters of a cluster are taken to be widely equal to the properties of the newly evolving macroscopic phase. By this reason, the values of the specific surface energies in Young's equation, Equation (8.18), are constants for some given values of pressure and temperature. Consequently, the contact angle is also constant. In the generalized Gibbs approach, parameters of a new phase cluster are functions of the supersaturation, therefore the contact angle  $\gamma$  and, consequently, the catalytic factor  $\varphi(\gamma, \beta)$  also depend on supersaturation.

For the case when the surface tension of the cluster boundary with the pore surfaces is less than that between solutions and the same surfaces ( $\sigma_{\alpha s} < \sigma_{\beta s}$ ), and the contact angle determined by Young Equation (8.18), as

$$\cos \gamma = \frac{\sigma_{\beta s} - \sigma_{\alpha s}}{\sigma_{\alpha \beta}}, \quad (8.31)$$

is less than  $90^\circ$ , the surface is well wettable (Figure 8.5a). Otherwise,  $\sigma_{\alpha s} > \sigma_{\beta s}$ ,

the contact angle is larger than 90°, the surface is badly wettable (Figure 8.5b). In the present work we consider only the first case, when wettability is good and the influence of surface defects becomes most apparent.

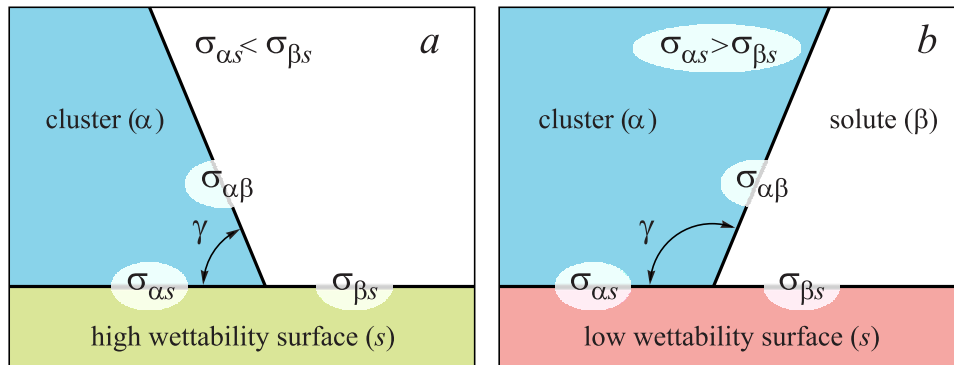


Fig. 8.5. Contact angle  $\gamma$  for well (a) and badly (b) wettable surfaces. The corresponding specific interface energies are  $\sigma_{\alpha\beta}$ ,  $\sigma_{\beta s}$ , and  $\sigma_{\alpha s}$ .

For the determination of the contact angle one must know the specific interfacial energies of all boundaries as functions of the cluster and surrounding solution compositions (for unification of the notations we shall use the term “fluid” both for cluster and solution and denote it with a subindex “f”) in the whole range from the left binodal,  $x_b^{(l)}$ , up to the right binodal,  $x_b^{(r)}$ . It is easy to show that in a simple linear approximation the specific interfacial energy of the fluid-surface interphase can be expressed as (details see [13])

$$\sigma_{fs}(\rho) = \frac{\sigma_{\beta s,0}(x_b^{(r)} - x) + \sigma_{\alpha s,0}(x - x_b^{(l)})}{x_b^{(r)} - x_b^{(l)}}. \tag{8.32}$$

Here, as above (see Eq. (8.23)), the index “0” relates to the case, when a new phase cluster and surrounding solution are in equilibrium, i.e.,  $x = x_b^{(l)}$  and  $x_\alpha = x_b^{(r)}$ , and the quantities without index “0” denote parameters for current composition (cluster or solution). From Equation (8.32) it follows that

$$\sigma_{\beta s} - \sigma_{\alpha s} = \sigma_{fs}(x) - \sigma_{fs}(x_\alpha) = (\sigma_{\beta s,0} - \sigma_{\alpha s,0}) \left( \frac{x_\alpha - x}{x_b^{(r)} - x_b^{(l)}} \right). \tag{8.33}$$

It is evident that the difference  $(\sigma_{\beta s} - \sigma_{\alpha s})$  is a linear function of  $(x_\alpha - x)$ . It is

positive when  $\sigma_{\beta s,0} > \sigma_{\alpha s,0}$  (good wetting) and is negative when  $\sigma_{\beta s,0} < \sigma_{\alpha s,0}$  (bad wetting) in correspondence with above-stated definition. This difference determines the degree of catalytic activity of the solid surface at heterogeneous nucleation.

From Equation (8.23) with allowance for Equations (8.31) and (8.33) we obtain an expression determining the contact angle  $\gamma$  as a function of the compositions of the cluster,  $x_\alpha$ , and of the surrounding solution,  $x$ ,

$$\cos \gamma(x, x_\alpha) = \cos \gamma_0 \left( \frac{x_b^{(r)} - x_b^{(l)}}{x_\alpha - x} \right), \quad (8.34)$$

where

$$\cos \gamma_0 = \frac{(\sigma_{\beta s,0} - \sigma_{\alpha s,0})}{\sigma_{\alpha\beta,0}}. \quad (8.35)$$

Thus, for the further analysis there is no need in the knowledge of the specific interfacial energies; it merely required to know the equilibrium contact angle  $\gamma_0$ .

In the considered case of cluster nucleation on a well-wettable surface the angle  $\alpha$ , defining the catalytic activity factor Equation (8.9), has values larger zero only when  $x_\alpha < x_{\alpha,0}$  where  $x_{\alpha,0}$  is determined by the equation

$$x_{\alpha,0} = (x_b^{(r)} - x_b^{(l)}) \frac{\cos \gamma_0}{\cos(\pi/2 - \beta)} + x. \quad (8.36)$$

Intersection of the plots  $x_{\alpha,0}(x)$  and  $x_{\alpha,ll}(x)$  (see Equations (8.16) and (8.17) and Figure 8.6) determines the position of the spinodal  $x_{sh}$  for heterogeneous nucleation

$$x_{\alpha,0}(x_{sh}) = x_{\alpha,ll}(x_{sh}). \quad (8.37)$$

At  $x > x_{sh}$  the catalytic activity factor equals zero,  $\varphi(\gamma, \beta) = 0$ , i.e., in this case the nucleation of a new phase cluster in a pore proceeds in a mode when the energy barrier is absent, like spinodal decomposition of the unstable homogeneous system. Figure 8.7 presents the dependence of the heterogeneous spinodal position

$x_{sh}$  on cone angle  $\beta$  and contact angle  $\gamma_0$ .

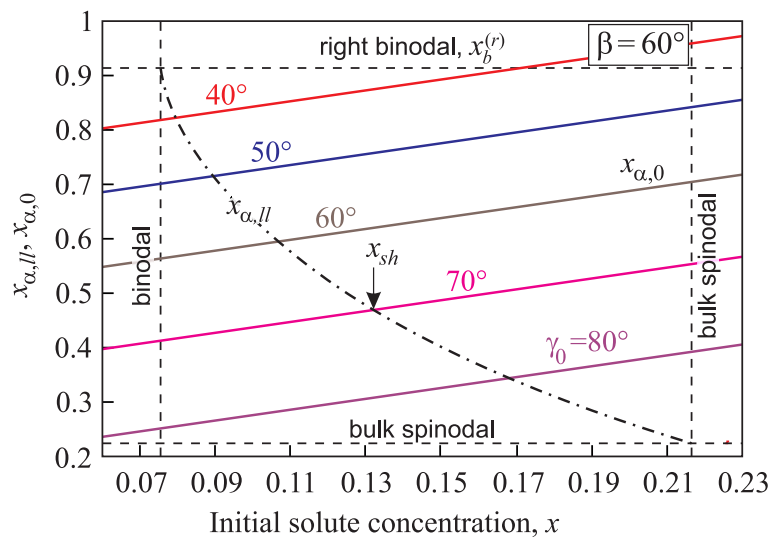


Fig. 8.6. Dependence of function  $f(x_\alpha, x)$  on cluster composition  $x_\alpha$  at different supersaturations  $x = x_b^{(l)}$ , 0.1, 0.13,  $x_{sp}^{(l)}$  in the region of metastability  $x_b^{(l)} < x < x_{sp}^{(l)}$ .

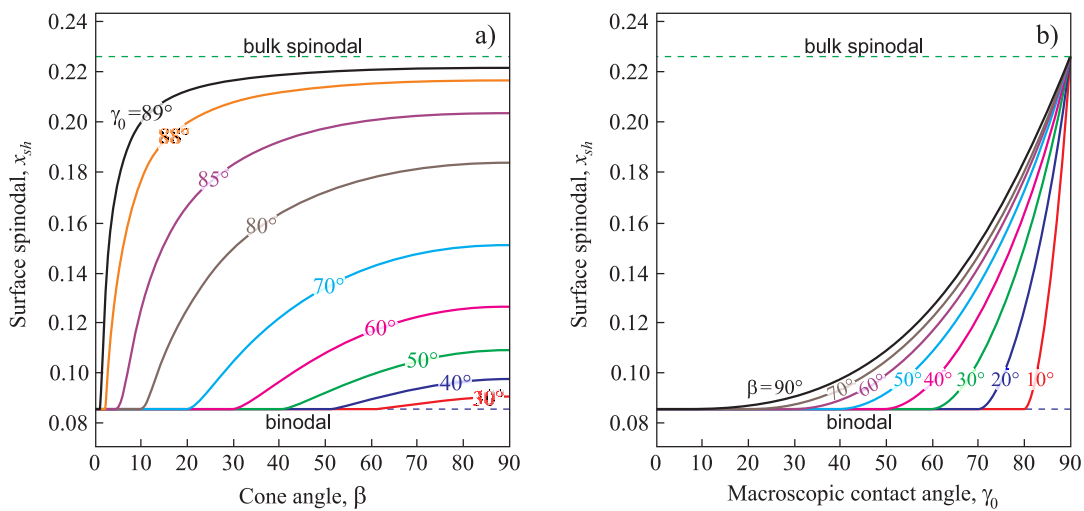


Fig. 8.7. Dependence of the spinodal position  $x_{sh}$  for heterogeneous nucleation on cone angle,  $\beta$ , (left) and equilibrium contact angle,  $\gamma_0$  (right).

Is evident that the spinodal for heterogeneous nucleation is located nearer to the binodal as both the pore cone angle  $\beta$  (Figure 8.7a) and the macroscopic contact angle  $\gamma_0$  (Figure 8.7b) yield its shift to decreasing values of  $x$ . If the equilibrium contact angle is equal to  $\gamma_0 = 90^\circ$ , the heterogeneous spinodal coincides with the macroscopic one, i.e.,  $x_{sh} = x_{sp}^{(l)}$ , like in the case of the homogeneous nucleation.

### 8.4. Heterogeneous Nucleation in a Conic Pore: Results

For a metastable state of the initial solution,  $x_b^{(l)} < x < x_{sp}^{(l)}$ , the work of critical cluster formation in the space  $(n_1, n_2)$  has characteristic saddle points properties near to the parameters of the critical cluster,  $(n_{1,cr}, n_{2,cr})$ . The surface is shown in Figure 8.8 for the case of nucleation of a new phase cluster in a pore with an angle  $\beta = 60^\circ$  and for an equilibrium contact angle  $\gamma_0 = 60^\circ$  and at the composition of the ambient phase equal to  $x = 0.15$ . The “valley” at  $x_\alpha = x = 0.15$  corresponds to the initial state, and the saddle point to the critical cluster. Its parameters are determined by Equations (8.29). In the course of its growth, the new phase cluster passes through a saddle point. Finally, its composition tends to an equilibrium value nearly equal to the respective value on the right binodal  $x_\alpha \rightarrow x_b^{(r)} \approx 0.91$ .

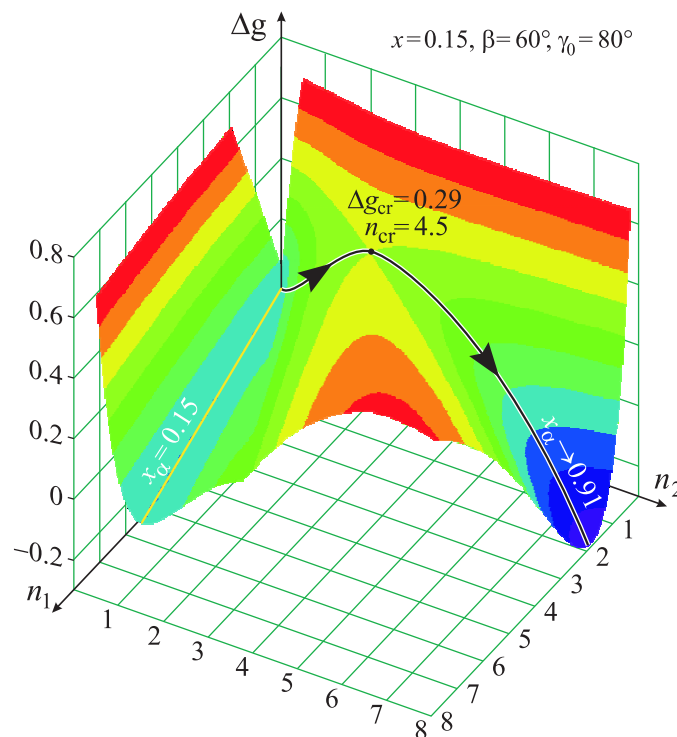


Fig. 8.8. Shape of the Gibbs free energy of cluster formation in a metastable regular solution with  $x = 0.15$  ( $x < x_{sh} \approx 0.178$ ) in a conic pore with the angle  $\beta = 60^\circ$ . The equilibrium contact angle is chosen equal to  $\gamma_0 = 80^\circ$ .

The composition of a critical cluster,  $x_{\alpha,cr}$ , is shown in Figures 8.9 and 8.10 in dependence on the initial supersaturation for the case of nucleation in a conic pore with various angles  $\beta = 40^\circ, 50^\circ, 60^\circ, 70^\circ, 80^\circ, 90^\circ$  and two different values

of the equilibrium contact angle  $\gamma_0 = 60^\circ$  (Figure 8.9) and  $\gamma_0 = 80^\circ$  (Figure 8.10). With an increase of the supersaturation from an initial value close to the binodal the concentration of the second component in the critical cluster,  $x_{\alpha,cr}$ , decreases down to the minimum value  $x_{\alpha,0}$  at  $x = x_{sh}(\gamma_0)$  (Figures 8.9 and 8.10). If the supersaturation increases further,  $x_{\alpha,cr}$  grows linearly (see Equation (8.36) and Figure 8.6).

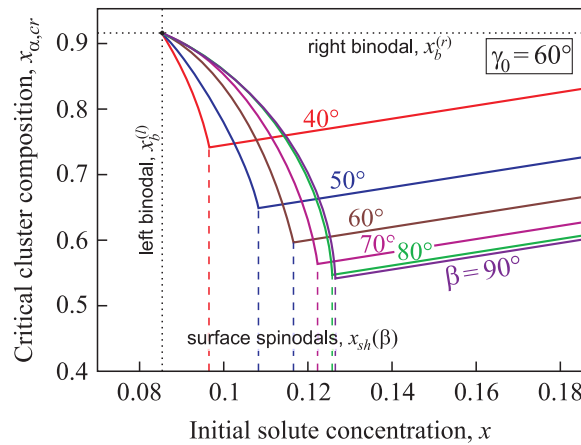


Fig. 8.9. Composition of the critical cluster,  $x_{\alpha,cr}$ , in dependence on supersaturation for nucleation in a conic pore with various angles  $\beta = 40^\circ, 50^\circ, 60^\circ, 70^\circ, 80^\circ,$  and  $90^\circ$ . The equilibrium contact angle is chosen equal to  $\gamma_0 = 60^\circ$ .

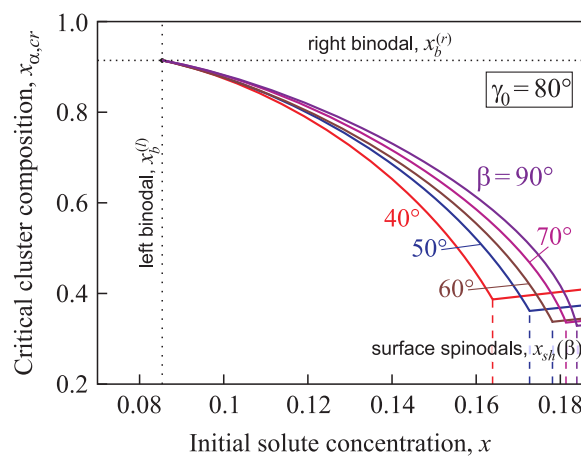


Fig. 8.10. Composition of the critical cluster,  $x_{\alpha,cr}$ , in dependence on supersaturation for nucleation in conic pores with various angles  $\beta = 40^\circ, 50^\circ, 60^\circ, 70^\circ, 80^\circ,$  and  $90^\circ$ . Here the equilibrium contact angle is chosen equal to  $\gamma_0 = 80^\circ$ .

According to the classical nucleation theory the size of a critical cluster tends to infinity for initial phase composition approaching the binodal. With an increase of the supersaturation grows the critical cluster size decreases. At  $x > x_{sh}$ , the critical

size in its classical interpretation does not exist anymore because cluster growth can proceed without overcoming a thermodynamic potential barrier starting from  $n = 0$  (or, in a more precise formulation, starting with one structural unit). However, in terms of the generalized Gibbs approach, in contrast to the classical theory and in agreement with density functional computations [7,8], this decrease in size may be followed by an increase with a further increase of the supersaturation (Figures 8.11 and 8.12). Consequently, the transition from metastable to thermodynamically unstable states proceeds here in a quite different way. As one consequence it follows that near to the spinodal the formation of critical clusters will, in general, not proceed via the saddle point of the thermodynamic potential surface but via a ridge point (for details see [17,18]).

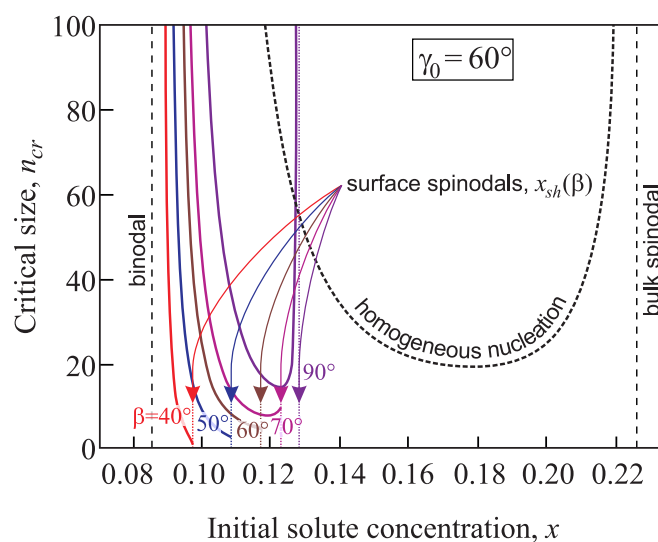


Fig. 8.11. Critical cluster size,  $n_{cr}$ , as a function of the concentration for nucleation in conic pores with different angles  $\beta = 40^\circ$ ,  $50^\circ$ ,  $60^\circ$ ,  $70^\circ$ , and  $90^\circ$ . The equilibrium contact angle is taken as  $\gamma_0 = 60^\circ$ . For comparison, the dashed line shows the dependence  $n_{cr}(x)$  for homogeneous nucleation.

For the equilibrium contact angle  $\gamma_0 = 60^\circ$  and small values of the cone pore angles  $\beta = 40^\circ$ ,  $50^\circ$ ,  $60^\circ$ , along with the increase of the supersaturation the critical cluster size decreases monotonically from infinity at the binodal up to values of  $x$  at the spinodal for heterogeneous nucleation  $x = x_{sh}$  (Figure 8.11). Then it exhibits a discontinuity and becomes equal to zero at further increase of the supersaturation. For

planar solids surfaces  $\beta = 90^\circ$ , the decrease of the critical cluster size with increasing supersaturation is followed by its further increase. This increase is then also followed by a similar discontinuity at  $x = x_{sh}$ .

When the equilibrium contact angle equals  $\gamma_0 = 80^\circ$  and the cone pore angle has values in the range  $\beta = 40^\circ \dots 90^\circ$  the dependence of the critical cluster size on supersaturation is non-monotonic: first  $n_{cr}$  decreases from infinity at the binodal, then the decrease is followed by its growth up to  $x = x_{sh}$ , and for  $x \geq x_{sh}$  the critical cluster size becomes equal to zero (Figure 8.12).

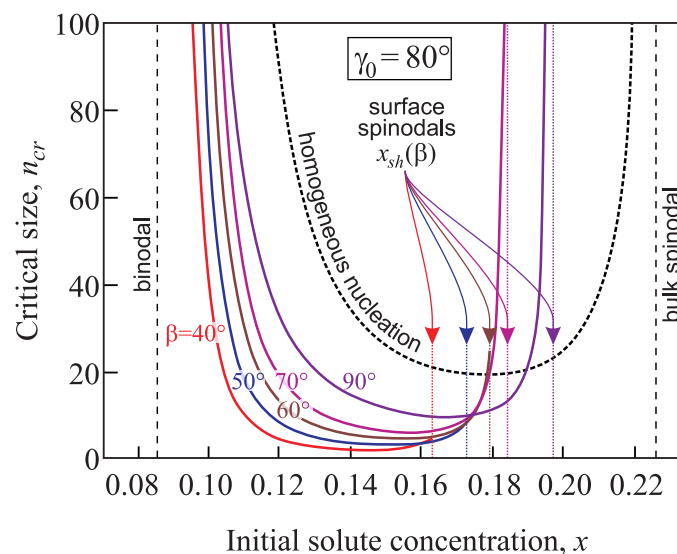


Fig. 8.12. Critical cluster size,  $n_{cr}$ , as a function of the concentration for nucleation in conic pores with different angles  $\beta = 40^\circ, 50^\circ, 60^\circ, 70^\circ,$  and  $90^\circ$ . Here the equilibrium contact angle is taken equal to  $\gamma_0 = 80^\circ$ . For comparison, the dashed line shows the dependence  $n_{cr}(x)$  for homogeneous nucleation.

Figures 8.13 and 8.14 illustrate the normalized work of formation of a critical cluster,  $\Delta g_{cr} = (\Delta G_{cr}/G_\sigma)$ , in dependence on supersaturation for nucleation in conic pores with various angles  $\beta = 40^\circ, 50^\circ, 60^\circ, 70^\circ, 80^\circ,$  and  $90^\circ$ , the equilibrium contact angle is  $\gamma_0 = 60^\circ$  (Figure 8.13) and  $\gamma_0 = 80^\circ$  (Figure 8.14). The work of formation of a cluster decreases from infinity at the binodal, and for  $x \geq x_{sh}$  it becomes equal to zero. The less the cone pore angle  $\beta$  and the contact angle  $\gamma_0$  are, the faster the work of a critical cluster formation decreases.

The work of critical cluster formation determines widely the steady-state

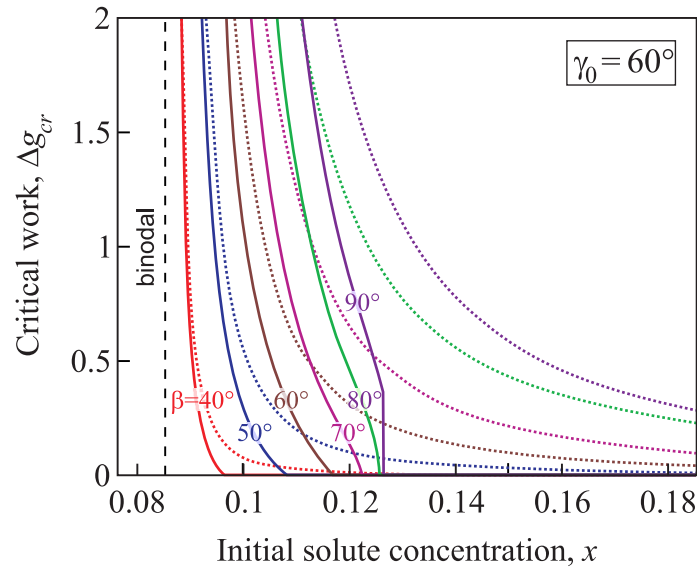


Fig. 8.13. Normalized work of formation of a critical cluster,  $\Delta g_{cr}$ , as function of the concentration for nucleation in conic pores with various angles  $\beta = 40^\circ, 50^\circ, 60^\circ, 70^\circ, 80^\circ,$  and  $90^\circ$ ; the equilibrium contact angle is  $\gamma_0 = 60^\circ$ . For a comparison, the dotted lines show the function  $\Delta g_{cr}(x)$  calculated via the classical nucleation theory for conic pores.

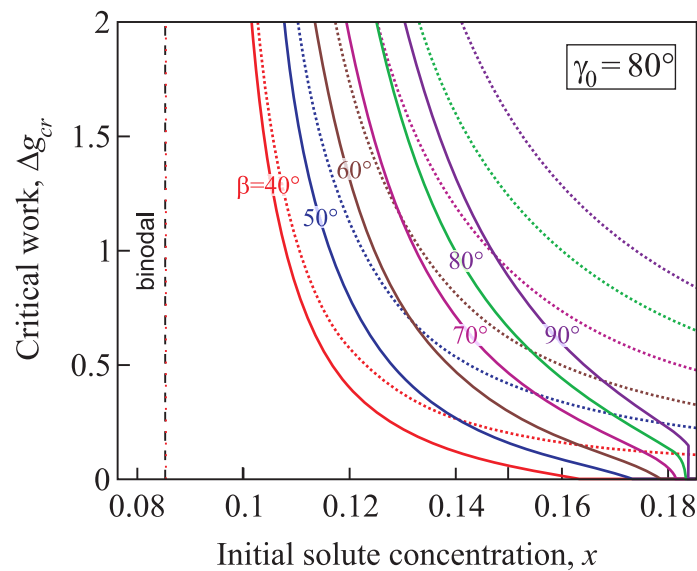


Fig. 8.14. Normalized work of formation of a critical cluster,  $\Delta g_{cr}$ , as function of the concentration for nucleation in conic pores with various angles  $\beta = 40^\circ, 50^\circ, 60^\circ, 70^\circ, 80^\circ,$  and  $90^\circ$ ; the equilibrium contact angle is  $\gamma_0 = 80^\circ$ . For comparison, the dotted lines show the function  $\Delta g_{cr}(x)$  calculated via the classical nucleation theory for conic pores.

nucleation rate,  $J$ . It can be expressed generally as (see, for example [1,4])

$$J = J_0 \exp\left(-\frac{\Delta g_{cr} G_\sigma}{k_B T}\right). \tag{8.38}$$

The pre-exponential factor,  $J_0$ , is determined by the diffusion coefficients of the solution and by the number of possible nucleation centers per unit area. The quantity  $G_\sigma$  is determined by Equation (8.25).

Figures 8.15 and 8.16 supply us with a comparison of the normalized nucleation rates,  $J/J_0$ , in conic pores with various angles  $\beta = 40^\circ, 50^\circ, 60^\circ, 70^\circ,$  and  $90^\circ$  determined within the generalized (solid lines) and via the classical Gibbs (dotted line) approaches in the case of good wettability ( $\gamma_0 = 60^\circ$  and  $80^\circ$ ). The calculations were performed for a temperature  $T = 0.7T_c$  with  $T_c = 1143$  K and the parameters  $G_\sigma = 61.6 k_B T$  and  $R_\sigma = 3.087a$  with  $a = 3.65 \times 10^{-10}$  m. The nucleation rate calculated via the generalized Gibbs approach is much higher than the results obtained via the classical theory. With the increase of the supersaturation it reaches the maximum value,  $J_0$ , at  $x \geq x_{sh}(\gamma_0, \beta)$ .

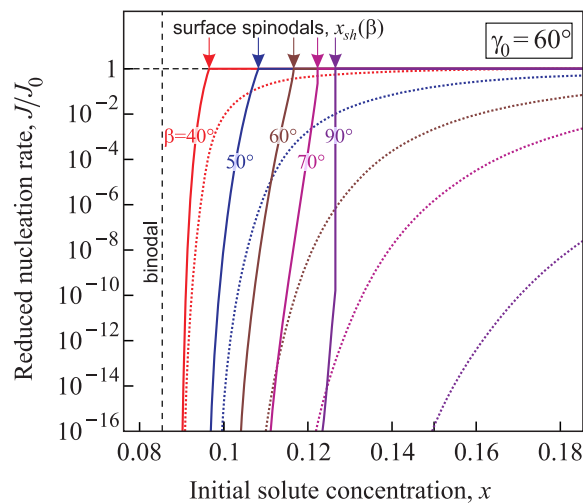


Fig. 8.15. Comparison of the normalized steady-state nucleation rates,  $J/J_0$ , computed via the generalized Gibbs approach (solid lines) and using classical nucleation theory (dotted line) in conic pores with various angles  $\beta = 40^\circ, 50^\circ, 60^\circ, 70^\circ,$  and  $90^\circ$ . The equilibrium contact angle is taken as  $\gamma_0 = 60^\circ$ .

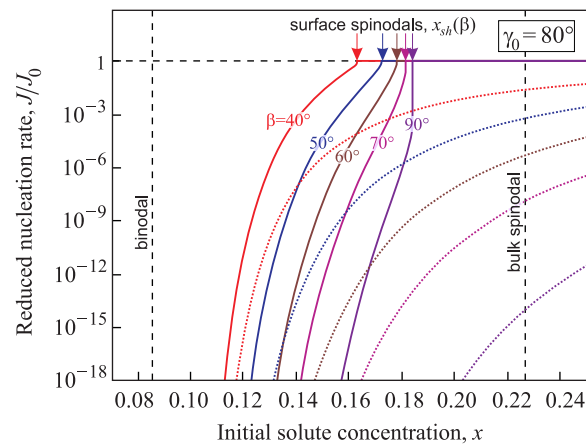


Fig. 8.16. Comparison of the normalized nucleation rates,  $J/J_0$ , determined via the generalized Gibbs approach (solid lines) and in terms of the classical nucleation theory (dotted lines) in conic pores with various angles  $\beta = 40^\circ, 50^\circ, 60^\circ, 70^\circ$ , and  $90^\circ$ . The equilibrium contact angle is taken here  $\gamma_0 = 80^\circ$ .

## 8.5. Conclusions

The generalized Gibbs approach applied to the description of the precipitation in a binary regular solution on a rough solid surface (conic pore) results as a whole in similar conclusions as obtained by us earlier in the analysis of heterogeneous nucleation in a one-component van der Waals liquid [13]: the presence of heterogeneous nucleation centers can effectively result in a shift of the spinodal from the value  $x = x_{sp}^{(l)}$ , as shown in Figure 8.7, to smaller values of the concentration,  $x = x_{sh} \leq x_{sp}^{(l)}$ . Therefore, the concentration range  $x_b^{(l)} < x < x_{sh}$  of the initial solution we can consider as metastable with respect to heterogeneous nucleation, and the concentration range  $x > x_{sh}$  as thermodynamically unstable. This result has the consequence that the range of metastable states decreases at the expense of an increase of the instability region, resulting in intensification of the nucleation rate. This effect became stronger with a decrease of the cone angle of the pore and the equilibrium contact angle. In line with the general result obtained in [19] for the case of homogeneous nucleation, also in heterogeneous nucleation the generalized Gibbs approach yields lower values of the work of critical cluster formation and higher values of the steady-state nucleation rates as compared to the results obtained via

Gibbs classical treatment.

Actually, the surface roughness is not uniform. In frame of the studied approach the roughness state of a surface may differ in depth of the cones and their cone angles. Its account may be approximated as a spread in these parameters within some model distribution. As can be seen from the comparison of plots in Figure 8.7 the differences in cone angle do influence the cluster critical size and with it the nucleation probability. The lesser the cone angle is the more important is the role of heterogeneous nucleation. In addition, the dependence of the nucleation rate on cone parameters is exponential. It means that the nucleation preferentially proceeds in pores with the lowest cone angle. The cone depth may also influence the nucleation when it is too low to form a viable cluster in it. This situation can happen on rather smooth surfaces. As it follows from Figure 8.7 more influential is the change of the equilibrium contact angle but it is rather the case of different surface materials, say composites or metamaterials.

**Author Contributions:** The authors equally contributed to the present paper. A.S.Abyzov wrote the paper. All three authors have read and approved the final manuscript.

**Funding:** This research received no external funding.

**Conflicts of Interest:** The authors declare no conflict of interest.

## References

1. Kelton, K.F.; Greer, A.L. *Nucleation in Condensed Matter: Applications in Materials and Biology*; Elsevier: Amsterdam, The Netherlands, 2010.
2. Gutzow, I.S.; Schmelzer, J.W.P. *The Vitreous State: Thermodynamics, Structure, Rheology, and Crystallization*, 1st ed., Springer: Berlin, Germany, 1995. (2nd enlarged edition, Springer: Heidelberg, Germany, 2013).
3. Volmer, M. *Kinetik der Phasenbildung*; English Translation: Kinetics of Phase

- Formation; Th. Steinkopff: Dresden & Leipzig, Germany, 1939.
4. Hellmuth, O.; Khvorostyanov, V.I.; Curry, J.A.; Shchekin, A.K.; Schmelzer, J.W.P.; Feistel, R.; Djikaev, Y.S.; Baidakov, V.G. Selected Aspects of Atmospheric Ice and Salt Crystallisation. In *Nucleation Theory and Applications-Special Issues: Review Series on Selected Topics of Atmospheric Sol Formation*; Schmelzer, J.W.P., Hellmuth, O., Eds.; Joint Institute for Nuclear Research Publishing Department: Dubna, Russia, 2013; Volume 1, ISBN 978-5-9530-0349-0.
  5. Bormashenko, E.U. *Wetting of Real Surfaces*; de Gruyter: Berlin, Germany, 2013.
  6. Gibbs, J.W. On the equilibrium of heterogeneous substances. *Transactions Connecticut Academy of Sciences*. **1874-1878**, 3, 108-248 & 343-524; see also: Gibbs, J.W. *The Collected Works, Vol. 1. Thermodynamics*; Longmans and Green: New York, NY, USA; London, UK; Toronto, ON, Canada, 1928.
  7. Cahn, J.W.; Hilliard, J.E. Free energy of a non-uniform system I. Interfacial energy. *J. Chem. Phys.* **1958**, 28, 258–267.
  8. Cahn, J.W.; Hilliard, J.E. Nucleation in a two-component incompressible fluid. *J. Chem. Phys.* **1959**, 31, 688–699.
  9. Schmelzer, J.W.P.; Abyzov, A.S.; Möller, J. Nucleation versus spinodal decomposition in phase formation processes in multicomponent solutions. *J. Chem. Phys.* **2004**, 121, 6900–6917.
  10. Abyzov, A.S.; Schmelzer, J.W.P. Nucleation versus spinodal decomposition in confined binary solutions. *J. Chem. Phys.* **2007**, 127, 114504.
  11. Abyzov, A.S.; Schmelzer, J.W.P. Generalized Gibbs approach in heterogeneous nucleation. *J. Chem. Phys.* **2013**, 138, 164504.
  12. Abyzov, A.S.; Schmelzer, J.W.P. Heterogeneous nucleation in solutions: Generalized Gibbs' approach. *J. Chem. Phys.* **2014**, 140, 244706.

13. Aabyzov, S.; Schmelzer, J.W.P.; Davydov, L.N. Heterogeneous nucleation on rough surfaces: Generalized Gibbs' approach. *J. Chem. Phys.* **2017**, *147*, 214705.
14. Becker, R. Die Keimbildung bei der Ausscheidung in metallischem Mischkristallen (Engl. Translation: Nucleation in segregation processes of metallic solid solutions). *Annalen der Physik* **1938**, *32*, 128–140.
15. Schmelzer, J.W.P.; Aabyzov, A.S. Thermodynamic Analysis of Nucleation in Confined Space: Generalized Gibbs' Approach. *J. Chem. Phys.* **2011**, *134*, 054511.
16. Christian, J.W. *Physical Metallurgy*; Cahn, R.W., Ed.; North-Holland Publishers: Amsterdam, The Netherlands, 1965; pp. 227–346.
17. Aabyzov, A.S.; Schmelzer, J.W.P.; Kovalchuk, A.A.; Slezov, V.V. Evolution of Cluster Size-Distributions in Nucleation-Growth and Spinodal Decomposition Processes in a Regular Solution. *J. Non-Cryst. Solids* **2010**, *356*, 2915–2922.
18. Aabyzov, A.S.; Schmelzer, J.W.P. Kinetics of segregation processes in solutions: Saddle point versus ridge crossing of the thermodynamic potential barrier. *J. Non-Cryst. Solids* **2014**, *384*, 8–14.
19. Schmelzer, J.W.P.; Boltachev, G.S.; Baidakov, V.G. Classical and generalized Gibbs approaches and the work of critical cluster formation in nucleation theory. *J. Chem. Phys.* **2006**, *124*, 194503.

©2019 by the authors. Licensee MDPI, Basel, Switzerland. This article is an open access article distributed under the terms and conditions of the Creative Commons Attribution (CC BY) license (<http://creativecommons.org/licenses/by/4.0/>).

## 8.6. Висновки до розділу 8

Результати досліджень, представлених у даному розділі, опубліковано в статті [8] (Додаток А. Список публікацій здобувача за темою дисертації).

Досліджена гетерогенна нуклеація кластерів нової фази в регулярному бінарному розчині на дефектній твердій поверхні. Серед основних результатів у якості висновків можна виділити наступні:

- Вплив дефектів поверхні проявляється також, як і для газу ван дер Ваальса, тобто

- 1) наявність дефекту призводить до значного зсуву спінодалі порівняно з гетерогенним зародженням на планарній поверхні: зі зменшенням кута конуса пори гетерогенна спінодаль наближається до бінодалі, і область метастабільності звужується за рахунок розширення області нестабільності;

- 2) існує граничний кут конуса пори, менше якого формування нової фази проходить безбар'єрно.

- Розрахована швидкість нуклеації кластера нової фази у залежності від кута конуса пори і ступеня пересичення розчину.

## РОЗДІЛ 9

**МЕЖА ГОМОГЕННОЇ НУКЛЕАЦІЇ БУЛЬБАШОК РТУТІ ЗА  
НОРМАЛЬНИХ УМОВ РОБОТИ ЗАПЛАНОВАНОГО  
ЄВРОПЕЙСЬКОГО ДЖЕРЕЛА НЕЙТРОНІВ, ЩО ПРАЦЮЄ НА  
РЕАКЦІЇ СКОЛЮВАННЯ**

У дев'ятому розділі теоретично досліджено процес закипання ртуті у імпульсних джерелах нейтронів, що працюють на реакції сколювання (Spallation Neutron Source). При адсорбуванні протонного пучка ртуть піддається великим термічним ударам та ударам тиску. Ці локальні зміни стану ртуті можуть спричинити утворення в рідині нестабільних бульбашок, які можуть пошкодити при їх кавітації конструкційні матеріали (стінка труби).

Eur. Phys. J. B 79, 107–113 (2011)

DOI: 10.1140/epjb/e2010-10700-1

**Homogeneous bubble nucleation limit of mercury  
under the normal working conditions of the planned European  
spallation neutron source**

A.R. Imre<sup>1</sup> A.S. Abyzov<sup>2</sup>, I.F. Barna<sup>1</sup> and J.W.P. Schmelzer<sup>3,4</sup>

<sup>1</sup>KFKI Atomic Energy Research Institute, 1525 Budapest, POB 49, Hungary

<sup>2</sup>National Science Center Kharkov Institute of Physics and Technology, Academician Street 1, 61108 Kharkov, Ukraine

<sup>3</sup>Bogoliubov Laboratory of Theoretical Physics, Joint Institute for Nuclear Research, ul. Joliot-Curie 6, 141980 Dubna, Russia

<sup>4</sup>Institut für Physik der Universität Rostock, Albert-Einstein-Strasse 23-25, 18059 Rostock, Germany

Received 13 September 2010 / Received in final form 3 November 2010

Published online 21 December 2010 – © EDP Sciences, Società Italiana di Fisica, Springer-Verlag 2010

**Abstract.** In spallation neutron sources, liquid mercury, upon adsorbing the proton beam, is exhibited to large thermal and pressure shocks. These local changes in the state of mercury can cause the formation of unstable bubbles

in the liquid, which can damage at their collapse the enclosing the liquid solid material. While there are methods to deal with the pressure shock, the local temperature shock cannot be avoided. In our paper we calculated the work of the critical cluster formation (for mercury micro-bubbles) together with the rate of their formation (nucleation rate). It is shown that the homogeneous nucleation rates are very low at the considered process conditions even after adsorbing several proton pulses, therefore, the probability of temperature induced homogeneous bubble nucleation is negligible.

## 9.1. Introduction

Irradiating liquid metals (usually mercury) with proton beams is one of the best known methods to produce highintensity, multi-purpose neutron beams. This method has been used in various existing facilities and it is planned to be employed in the European spallation source (ESS), too. Unfortunately upon adsorbing the high-intensity proton beam in the liquid the neutrons are not the only particles emitted; an unavoidable heat and pressure wave will be emitted simultaneously from the adsorption region. The increase of the temperature and (in the negative period of the pressure wave) the decrease of the pressure can cause cavitation in the liquid. The metal vapor bubbles then will flow with the liquid and upon reaching high pressure and low temperature regions, they will collapse, causing eventually some severe damage in nearby solid structures. This phenomenon is known as cavitation erosion and one of the main factors which (due to pitting and weight loss) significantly may shorten the lifetime of structural materials. To our present knowledge, four mercury targets are needed at the Oak Ridge spallation neutron source (SNS) at 1 mW power per year. Therefore to avoid cavitation is one of the main challenges of the design of the spallation source target [1–7].

It should be mentioned here that, along the methods to minimize cavitation

itself, there are two other ways to minimize the damage. One of them consist in the various ways of surface treatments (plasma nitriding, plasma carbonizing, etc.), which makes the surface more resistant to the damaging pressure wave emitted by the collapsing bubble [8,9]. The other one is the addition of helium micro-bubbles, which is a proven way to soften up and to reduce the damage by absorbing the expansion of liquid mercury and mitigating the pressure waves [8–12]. Considering this method as a successful one to deal with the pressure-drop induced cavitation, in our paper we focused our attention mainly on the temperature increase induced cavitation and allowed only small pressure changes to occur (down to  $-5$  bar). Our main aim is to find out whether the conditions discussed here are able to cause cavitation or not. We approached the problem in three steps. In the first step (Sect. 2), we calculated the phase equilibrium properties, the stability limit and various other properties of mercury by using a slightly modified version of the equation of state proposed by Redlich and Kwong [13], Morita et al. [14–16]. In the next step (Sect. 3), we made an estimation for the magnitude of pressure and temperature changes by using single and repeated proton pulses. In the final step (Sect. 4), we calculated the work of critical bubble formation in mercury as well as the rate of homogeneous nucleation in the pressure-temperature range defined according to the results of the previous section. The paper is completed by a short summary and discussion (Sect. 5).

## 9.2. Model system

### 9.2.1. Location of binodal and spinodal curves

For the description of mercury (Hg) in both the liquid and gas phases, we will apply a slightly modified thermal equation of state as compared to the expression proposed by Morita et al. (see [13, 14], and, in particular, Eq. (15) in [15])

$$p = \frac{RT}{K(T)(v - b)} - \frac{a(T)}{v(v + c)}, \quad (9.1)$$

$$a(T) = a_c \left( \frac{T}{T_c} \right)^n \quad \text{at} \quad T \leq T_c, \quad (9.2)$$

where  $R = 8.314 \text{ J} \cdot \text{mol}^{-1}$  is the universal gas constant,  $p$  is pressure,  $v$  is molar volume,  $T$  is temperature,  $a_c$ ,  $b$ ,  $c$  and  $n$  are the model parameters specific for the substance considered,  $T_c$  is critical temperature. The correction coefficient  $K(T)$  is dependent on temperature only, it was introduced in the repulsive term instead of the parameter  $x_d$ , which is a function of  $T$  and  $p$  (see [16], in such case Eq. (9.1) becomes an equation for definition of  $p(v, T)$ , and has no analytical solution).

We employ further dimensionless variables

$$\Pi = \frac{p}{p_c}, \quad \omega = \frac{v}{v_c}, \quad \theta = \frac{T}{T_c}, \quad (9.3)$$

where  $v_c$  is the molar volume,  $p_c$  the pressure both at the critical point with the critical temperature,  $T_c$ . These parameters can be determined from Eq. (9.1) in the common way via

$$\left( \frac{\partial p}{\partial v} \right)_T = \left( \frac{\partial^2 p}{\partial v^2} \right)_T = 0 \quad \text{at} \quad T = T_c. \quad (9.4)$$

The equation of state in reduced variables is given by

$$\Pi(\theta, \omega) = \frac{\theta}{\chi_c(\theta)(\omega - \beta)} - \frac{\alpha(\theta)}{\omega(\omega + \delta)}. \quad (9.5)$$

Here

$$\chi_c(\theta) = \frac{p_c v_c}{RT_c} K(\theta) \quad (9.6)$$

is the reduced critical compressibility, and

$$K(\theta) = 1.106697 - 0.106697 \cdot \exp\left(\frac{\theta - 1}{0.17026}\right), \quad (9.7)$$

$$\alpha(\theta) = \frac{a_c \theta^n}{p_c v_c^2} = \alpha \theta^n, \quad \beta = \frac{b}{v_c}, \quad \xi = \frac{c}{v_c}. \quad (9.8)$$

According to [15] we have then

$$\alpha = 2.5272, \quad \beta = 0.3952, \quad \xi = -0.16567, \quad n = -0.0284127. \quad (9.9)$$

From Eqs. (9.1) and (9.4) we get [15]

$$v_c = 1.797 \cdot 10^{-4} \text{ m}^3/\text{kg}, \quad \rho_c = 5566 \text{ kg/m}^3, \quad (9.10)$$

$$p_c = 158 \cdot 10^6 \text{ Pa}, \quad T_c = 1762 \text{ K}.$$

The location of the classical spinodal curve can be found via the determination of the extrema of the thermal equation of state,  $\Pi(\theta, \omega)$  (Eq. (9.5)) considering the temperature  $\theta$  as constant. By taking the derivative of  $\Pi(\theta, \omega)$  with respect to  $\omega$ , we obtain from equation (9.5) the result

$$\frac{\partial}{\partial \omega} \Pi(\theta, \omega) = \frac{\alpha(\theta)(2\omega + \xi)}{\omega^2(\omega + \xi)^2} - \frac{\theta}{\chi_c(\omega - \beta)^2} = 0. \quad (9.11)$$

For  $\theta < 1$ , this equation has two positive solutions  $\omega_{\text{sp}}^{(\text{left})}$  and  $\omega_{\text{sp}}^{(\text{right})}$  for  $\omega$  corresponding to the specific volumes of the both macrophases at the spinodal curves (or at the limits of metastability).

Similarly, the binodal curves give for  $\theta \leq 1$  the values of the specific volumes of the liquid and the gas phases coexisting in thermal equilibrium at a planar interface. From the left branch of the binodal curve, we get the specific volume of the liquid phase ( $\omega_l^{(\text{eq})}(\theta) = \omega_b^{(\text{left})}(\theta)$ ), from the right branch of the binodal curve, we obtain the specific volume of the gas ( $\omega_g^{(\text{eq})}(\theta) = \omega_b^{(\text{right})}(\theta)$ ). For  $\theta = 1$ , both solutions coincide in the critical point ( $\omega_l^{(\text{eq})} = \omega_g^{(\text{eq})} = \omega_c = 1$ ), again. Consequently, in order to determine the specific volumes of the liquid and the gas at some given temperature in the range  $\theta \leq 1$ , we have to specify the location of the binodal curve.

The location of the binodal curve may be determined from the necessary thermodynamic equilibrium conditions (for planar interfaces) – equality of pressure and chemical potentials – via the solution of the set of equations

$$\Pi_l(\omega_l, \theta) = \Pi_g(\omega_g, \theta) , \quad \mu_l(\omega_l, \theta) = \mu_g(\omega_g, \theta) . \quad (9.12)$$

Here by  $\mu$  the chemical potential of the atoms or molecules in the liquid ( $l$ ) and the gas ( $g$ ) are denoted. Having at our disposal already the equation for the reduced pressure (c.f. Eq. (9.5)), we have now to determine in addition the chemical potential in dependence on pressure and temperature (see Sect. 2.2).

Isotherms for mercury Eq. (9.5) for different values of the reduced temperature  $\theta = 0.4, 0.65, 0.8, 0.891$  and  $0.92$  are shown in Fig. 9.1, dashed and dashed-dotted curves present binodal and spinodal, correspondingly. One can see, that there are two classes of isotherms: for the first one ( $\theta \geq \theta_s$ )  $p \geq 0$ , and for the second class ( $\theta < \theta_s$ ) pressure may be both positive and negative. Only in this temperature range, cavitation

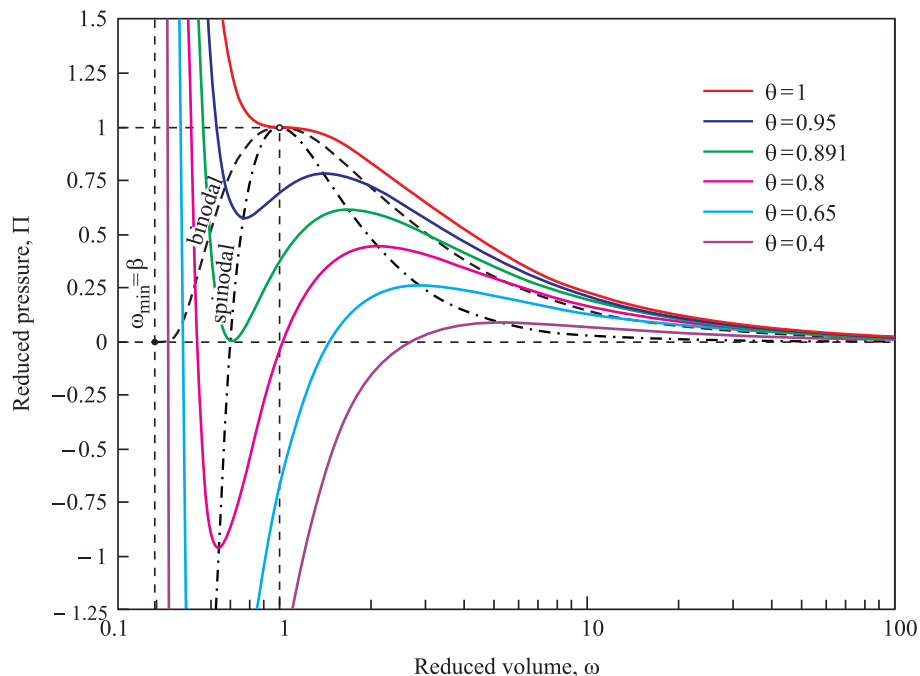


Fig. 9.1. (Color online) Isotherms of mercury as described via equation (9.5) for different values of the reduced temperature, from  $\theta = 0.4$  (bottom curve) to  $\theta = 1$  (upper curve).

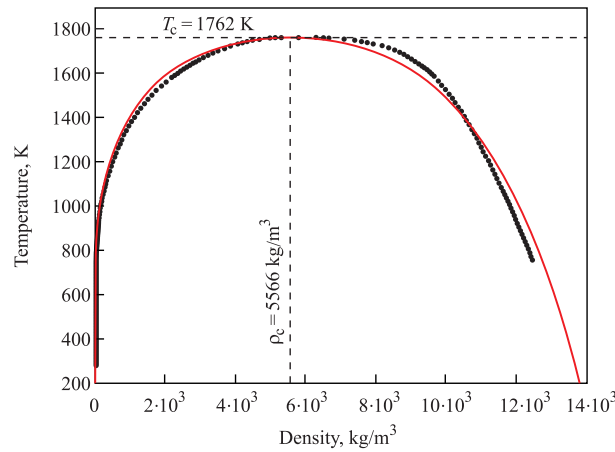


Fig. 9.2. (Color online) Comparison of experimental data (according to [17, 18]) for the vapor-liquid coexistence properties of mercury with the theoretical results (full curve determined via Eq.(9.5)) obtained in this work.

processes may occur. The parameter  $\theta_s$  is determined via the equation

$$\Pi_l(\omega_{sp}(\theta_s), \theta_s) = 0, \tag{9.13}$$

for mercury  $\theta_s \approx 0.891$  and  $T_s \equiv T_c \theta_s \approx 1570$  K. A comparison of experimental data [17, 18] for the vapor-liquid coexistence properties of mercury with results obtained in this work are shown in Fig. 9.2 and Fig. 9.3 for  $T$ ,  $\rho$  and  $p$ ,  $T^{-1}$  variables, respectively.

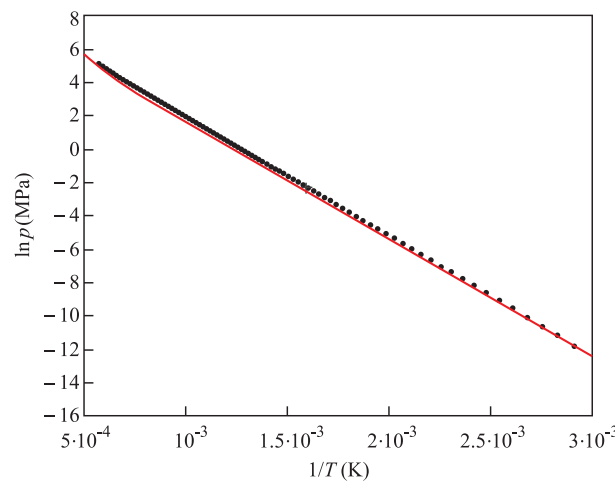


Fig. 9.3. (Color online) Comparison of experimental vapor pressure for mercury (according to [17, 18]) with theoretical results (full curve determined via Eq.(9.5)).

### 9.2.2. Determination of the chemical potential and the interfacial tension

For isothermal processes, the change of the Helmholtz free energy,  $F$ , may be expressed as

$$dF = -pdV + \mu dn . \quad (9.14)$$

Here  $V$  is the volume of the system and  $n$  the number of moles in it. For a given fixed mole number,  $n$ , of the substance ( $n = \text{constant}$ ), we have, in particular,

$$d\varphi_n = -pdv , \quad \varphi_n = \frac{F}{n} , \quad v = \frac{V}{n} , \quad (9.15)$$

or, in reduced variables,

$$d \left( \frac{\varphi_n}{p_c v_c} \right) = -\Pi d\omega . \quad (9.16)$$

Employing in the integration of Eq. (9.16) the equation of the state, Eq. (9.5), we obtain

$$\left( \frac{\varphi_n}{p_c v_c} \right) = - \left[ \frac{\alpha(\theta)}{\xi} \ln \left( 1 + \frac{\xi}{\omega} \right) + \frac{\theta}{\chi_c(\theta)} \ln(\omega - \beta) \right] . \quad (9.17)$$

Alternatively, the change of the Helmholtz free energy – provided the volume  $V$  is fixed – is given at constant temperature by

$$dF = \mu dn . \quad (9.18)$$

From Eq. (9.18), we arrive at

$$d\varphi_v = -\frac{\mu}{v^2} dv , \quad \varphi_v = \frac{F}{V} . \quad (9.19)$$

On the other side, the functions  $\varphi_n$  and  $\varphi_v$  are connected by

$$F = \varphi_n n = \varphi_v V, \quad \varphi_v = \frac{\varphi_n}{v}. \quad (9.20)$$

With Eq. (9.17), we have then

$$\varphi_v = \frac{p_c}{\omega} \left[ \frac{\alpha(\theta)}{\xi} \ln \left( 1 + \frac{\xi}{\omega} \right) + \frac{\theta}{\chi_c(\theta)} \ln(\omega - \beta) \right]. \quad (9.21)$$

With Eqs. (9.19) and (9.21), the expression for the chemical potential of a HLM can be obtained then via

$$\mu = -v^2 \frac{\partial \varphi_v}{\partial v} = -v_c \omega^2 \frac{\partial \varphi_v}{\partial \omega}. \quad (9.22)$$

This relation yields

$$\frac{\mu}{p_c v_c} = - \left[ \frac{\alpha(\theta)}{\omega + \xi} + \frac{\theta \omega}{\chi_c(\theta)(\omega - \beta)} + \frac{\alpha(\theta)}{\xi} \ln \left( 1 + \frac{\xi}{\omega} \right) + \frac{\theta \ln(\omega - \beta)}{\chi_c(\theta)} \right]. \quad (9.23)$$

In addition to the bulk properties of the system under consideration, we have to know the value  $\sigma$  of the surface tension for a coexistence of both phases at planar interfaces in dependence on the parameters describing the state of both phases. The following form was chosen for our calculation [19–22])

$$\sigma(\omega_g, \omega_l, \theta) = \Theta(\theta) \left[ \frac{1}{\omega_l} - \frac{1}{\omega_g} \right]^\delta, \quad \delta = 2.5, \quad (9.24)$$

where

$$\Theta(\theta) = A \left[ \frac{1}{\omega_b^{(\text{left})}} - \frac{1}{\omega_b^{(\text{right})}} \right]^{n-\delta}, \quad (9.25)$$

and  $A$  and  $n$  are constant parameters. Comparison of Eqs. (9.24) and (9.25) with experimental data [23]

$$\sigma(T) = 0.5446544 - 0.000204917 \cdot T \quad (9.26)$$

(here the temperature is given in Kelvin and the surface tension in  $\text{J}/\text{m}^2$ ) at  $\omega_1 = \omega_b^{(\text{left})}$  and  $\omega_g = \omega_b^{(\text{right})}$  yields

$$A = 0.033253 \text{ J}/\text{m}^2, \quad n = 3. \quad (9.27)$$

In Fig. 9.4 dependence of the surface tension on temperature is shown, solid curve presents Eq. (9.24) at  $\omega_1 = \omega_b^{(\text{left})}$ ,  $\omega_g = \omega_b^{(\text{right})}$ , and dashed curve – Eq. (9.26).

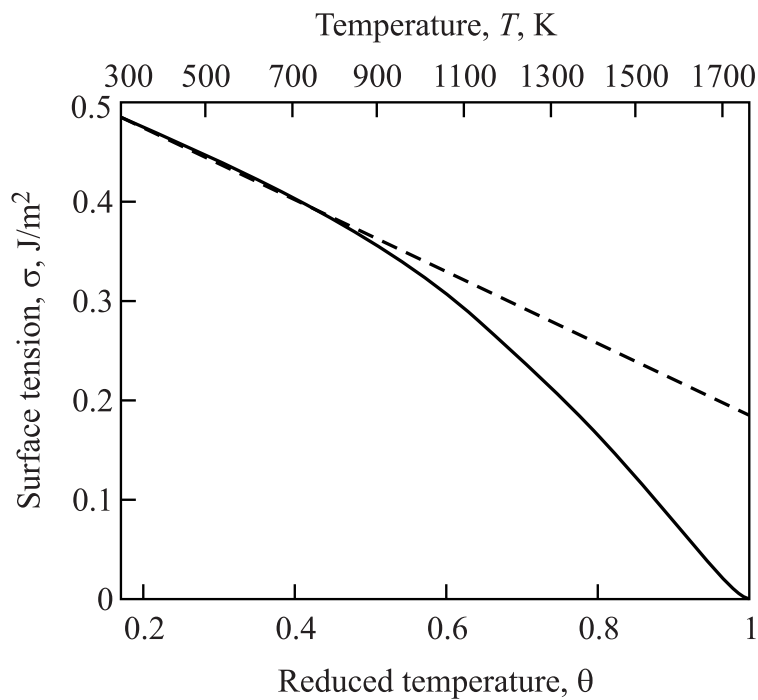


Fig. 9.4. Dependence of the surface tension on temperature, solid curve presents Eq. (9.24) at  $\omega_1 = \omega_b^{(\text{left})}$ ,  $\omega_g = \omega_b^{(\text{right})}$ , and dashed curve – Eq. (9.26)

### 9.3. Determination of the pressure and temperature change after proton adsorption

For the determination of the pressure and temperature change, a “one dimensional six-equation two-fluid model” was employed, which is capable to describe transient-like pressure waves and quick evaporation or condensation which is proportional to cavitation caused by energetic proton interaction in mercury target [24]. The method was developed to describe the sudden and drastic steam condensation, called water hammer [25, 26].

The model contains six first-order partial-differential equations which describe one-dimensional surface-averaged mass, momentum and energy conservation laws for both phases. A special numerical procedure ensures that shock-waves can be described without any numerical dispersion. With two major modifications this model can be applied to investigate the thermo-hydraulic properties of the planned mercury target in the european spallation source (ESS). These modifications are the following: the equation of state namely the density and the internal energy of both mercury phases should be known in a broad range of pressure (1 Pa to 100 MPa) and temperature (273 K to 1000 K). As a second point the interaction of the high energy proton beam with mercury has to be included. This is a much simpler task because we may consider that about 50energy is absorbed as a 2 ms long heat shock square pulse, giving a new source term in the energy equation of the liquid phase. The ESS mercury target station is modeled as a 18 m long closed loop which is bent in three dimensions and the pipe diameter is 15 cm. We consider that 150 kJ heat is absorbed in a 10 cm long pipe, this is approximately the width of the proton pulse. Calculation shows that such a single pulse heats up the mercury with about 40–44 K, assuming that the initial temperature was between 293–373 K (i.e. within the normal working range of the spallation source). In the calculations, low velocities 0.5–4 m/s, low initial pressure 1–4 bar and low initial temperature (below 374 K) were assumed. To our knowledge the existing Japanese Spallation Neutron Source Hg loop is about 15

m long, with a diameter of 15 cm, the flow velocity of Hg is 0.7 m/s and the pressure is approximately equal to 1 bar.

Concerning the pressure change, the model is able to estimate the positive part, but at the negative region (where most of the low temperature cavitation is expected to happen [27]), a stability problem aroused. Therefore we focused our calculation to the heat shock and, at present, neglected the pressure change. Preliminary calculation yielded a few bar changes [24], in agreement with the results of Ida [28], therefore the latter calculations were performed in the  $-5$  to 10 bar range. We should mention here, that other models predicted much larger pressure changes (even hundreds of bars) [29, 30] both in the positive and negative pressure region.

Also the effects of repeated pulses were checked. The calculations were performed with a 2 ms square pulse train where the delay time was 20 ms which is similar to a 16 Hz repetition rate. We started with a flow system with initial  $p = 4$  bar,  $T_{initial} = 353$  K and initial flow velocity  $v = 4$  m/s. We found that the temperature jumps are more or less additive which means that after the beginning of the third pulse the temperature was about 430 K.

#### 9.4. Determination of the work of critical cluster formation

Let us assume, now, that the system is brought suddenly into a metastable state located between spinodal curve and binodal curve at the liquid branch of the equation of state. Then, by nucleation and growth processes, bubbles may appear spontaneously in the liquid and a phase separation takes place [31]. Based on the relations outlined above, we will determine now the parameters of the critical clusters governing bubble nucleation in dependence on the state parameters, pressure and temperature.

We start with the general expression for the change of the thermodynamic

potential

$$\Delta G = \sigma A + (p_\beta - p_\alpha)V_\alpha + \sum_j n_{j\alpha}(\mu_{j\alpha} - \mu_{j\beta}), \quad (9.28)$$

Here the subscript  $\alpha$  specifies the parameters of the cluster (bubble) phase while  $\beta$  refers to the ambient liquid phase. This relation holds as long as the state of the liquid remains unchanged by the formation of one bubble. For a one-component system, this expression is reduced to

$$\Delta G = \sigma A + (p_\beta - p_\alpha)V_\alpha + n_\alpha(\mu_\alpha - \mu_\beta). \quad (9.29)$$

As independent variables, we selected the radius of the bubble,  $r$ , and the molar volume of the gas phase in the bubble. Similarly to [19,32,33], we arrive then at

$$\frac{\Delta g(r, \omega_g, \omega_l, \theta)}{k_B T} = 3 \left( \frac{1}{\omega_l} - \frac{1}{\omega_g} \right)^\delta r^2 + 2f(\omega_g, \omega_l, \theta) r^3, \quad (9.30)$$

where the following notations have been introduced:

$$f(\omega_g, \omega_l, \theta) = \Pi(\omega_g, \theta) - \Pi(\omega_l, \theta) + \frac{1}{\omega_g} \left( \frac{\mu(\omega_l, \theta) - \mu(\omega_g, \theta)}{p_c v_c} \right), \quad (9.31)$$

$$g \equiv \frac{G}{\Omega_1}, \quad \Omega_1 = \frac{16\pi}{3} \frac{1}{p_c^2 k_B T_c \theta} \Theta(\theta)^3, \quad (9.32)$$

$$r \equiv \frac{R}{R_\sigma}, \quad R_\sigma = \frac{2}{p_c} \Theta(\theta). \quad (9.33)$$

The dependence of the scaling parameters  $\Omega_1$  and  $R_\sigma$  on the reduced temperature is shown in Figure 9.5.

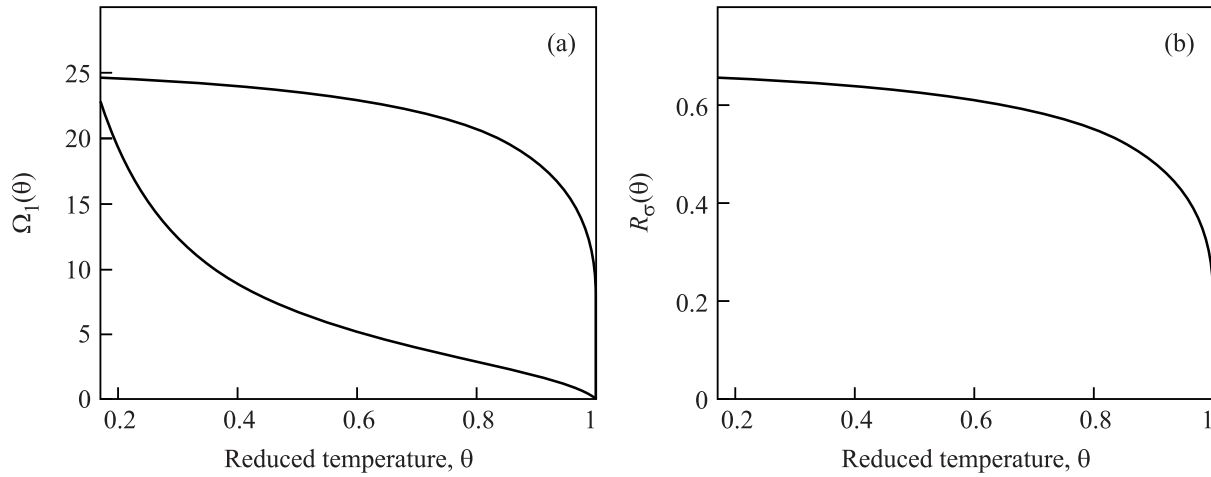


Fig. 9.5. Dependence of the scaling parameters  $\Omega_1$  and  $R_\sigma$  on the reduced temperature,  $\theta$ .

The Gibbs free energy surface for the metastable initial state has a typical saddle shape near to the configuration corresponding to a bubble of critical size (see Fig. 9.6,  $\theta = 0.92$ ,  $\omega_1 = 0.65$ ) in the space of critical radius-molar volume and work of cluster formation. The critical point position is determined by the set of equations

$$\frac{\partial \Delta g(r, \omega_g, \omega_1, \theta)}{\partial r} = 0, \quad \frac{\partial \Delta g(r, \omega_g, \omega_1, \theta)}{\partial \omega_g} = 0. \quad (9.34)$$

The dependence of the critical cluster parameters on the initial molar volume of liquid,  $\omega_1$ , are shown in Figs. 9.7–9.10, for different values of temperature,  $\theta = 0.17, 0.5, 0.7, 0.8, 0.891$  and  $0.92$ . The positions of the binodal curves are given then by  $\omega_b^{(\text{left})} = 0.409, 0.45, 0.494, 0.531, 0.589, 0.62$ , and  $\omega_b^{(\text{right})} = 1.663 \cdot 10^8, 90.5, 11.606, 5.634, 3.043, 2.475$ , the respective parts of the spinodal curves are located at  $\omega_{\text{sp}}^{(\text{left})} = 0.452, 0.528, 0.59, 0.634, 0.696, 0.726$ , and  $\omega_{\text{sp}}^{(\text{right})} = 13.609, 4.04, 2.584, 2.087, 1.679, 1.547$ , correspondingly.

The dependence of the work of formation and radius of the critical cluster on temperature for the practically significant cases  $p = -5, 0, 1, 2, 5$  and  $10$  Bar. is presented in Fig. 9.10. In Fig 9.11 dependence of the nucleation rates on temperature for the same values of pressure are shown (the value of pre-exponential factor  $J_0 =$

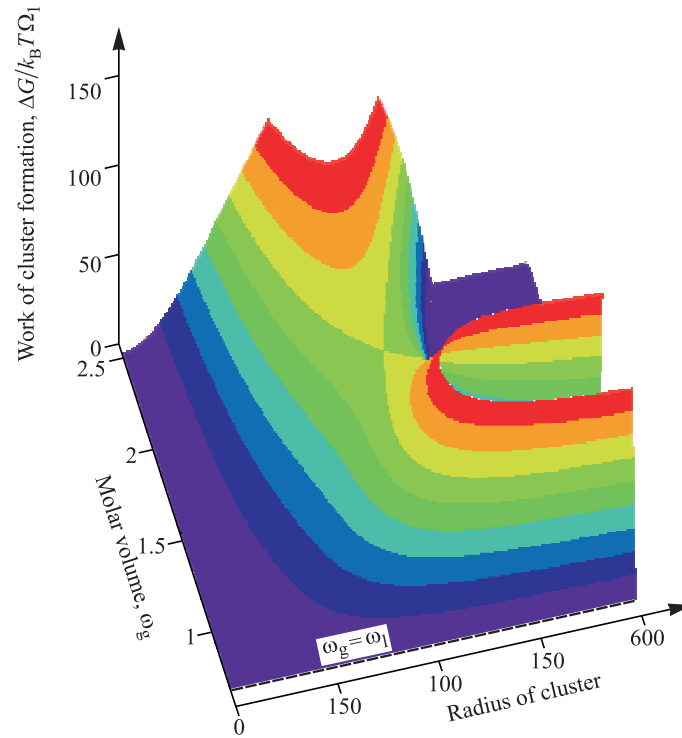


Fig. 9.6. (Color online) Gibbs free energy surface for metastable initial state,  $\theta = 0.92$ ,  $\omega_1 = 0.65$ .

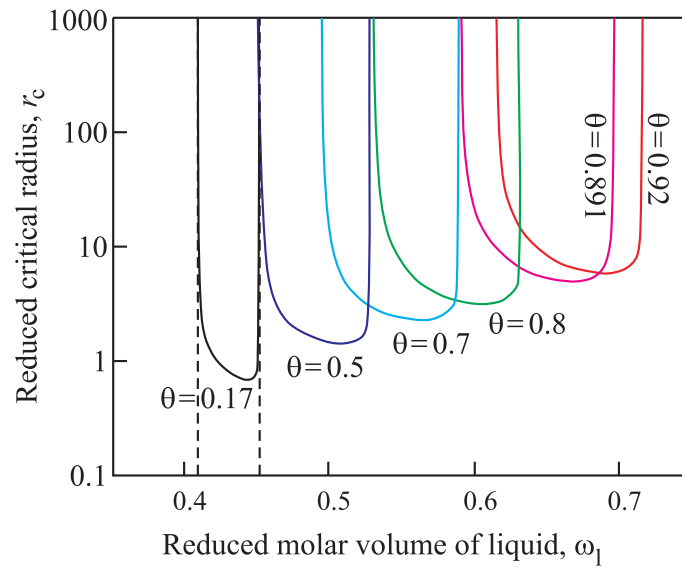


Fig. 9.7. (Color online) Dependence of the critical cluster radius,  $r_c = R_c/R_\sigma$ , on the initial molar volume of liquid,  $\omega_1$ , for different values of temperature,  $\theta = 0.17, 0.5, 0.7, 0.8, 0.891$  and  $0.92$ .

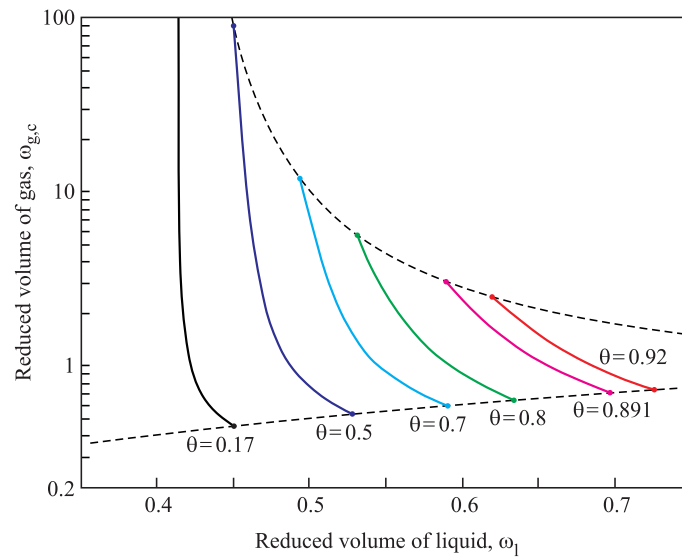


Fig. 9.8. (Color online) Dependence of the gas molar volume in critical bubble,  $\omega_{g,c}$ , on the initial molar volume of liquid,  $\omega_1$ , for different values of temperature,  $\theta = 0.17, 0.5, 0.7, 0.8, 0.891$  and  $0.92$ .

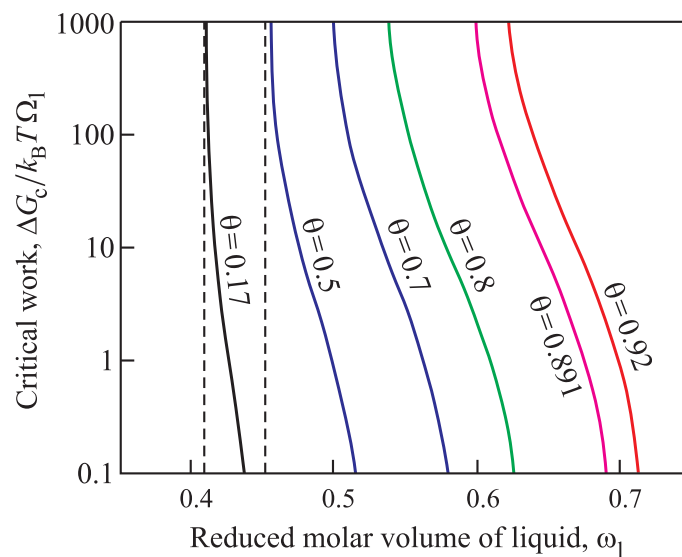


Fig. 9.9. (Color online) Dependence of the work of critical cluster formation,  $\Delta G_c / k_B T \Omega_1$ , on the initial molar volume of liquid,  $\omega_1$ , for different values of temperature,  $\theta = 0.17, 0.5, 0.7, 0.8, 0.891$  and  $0.92$ .

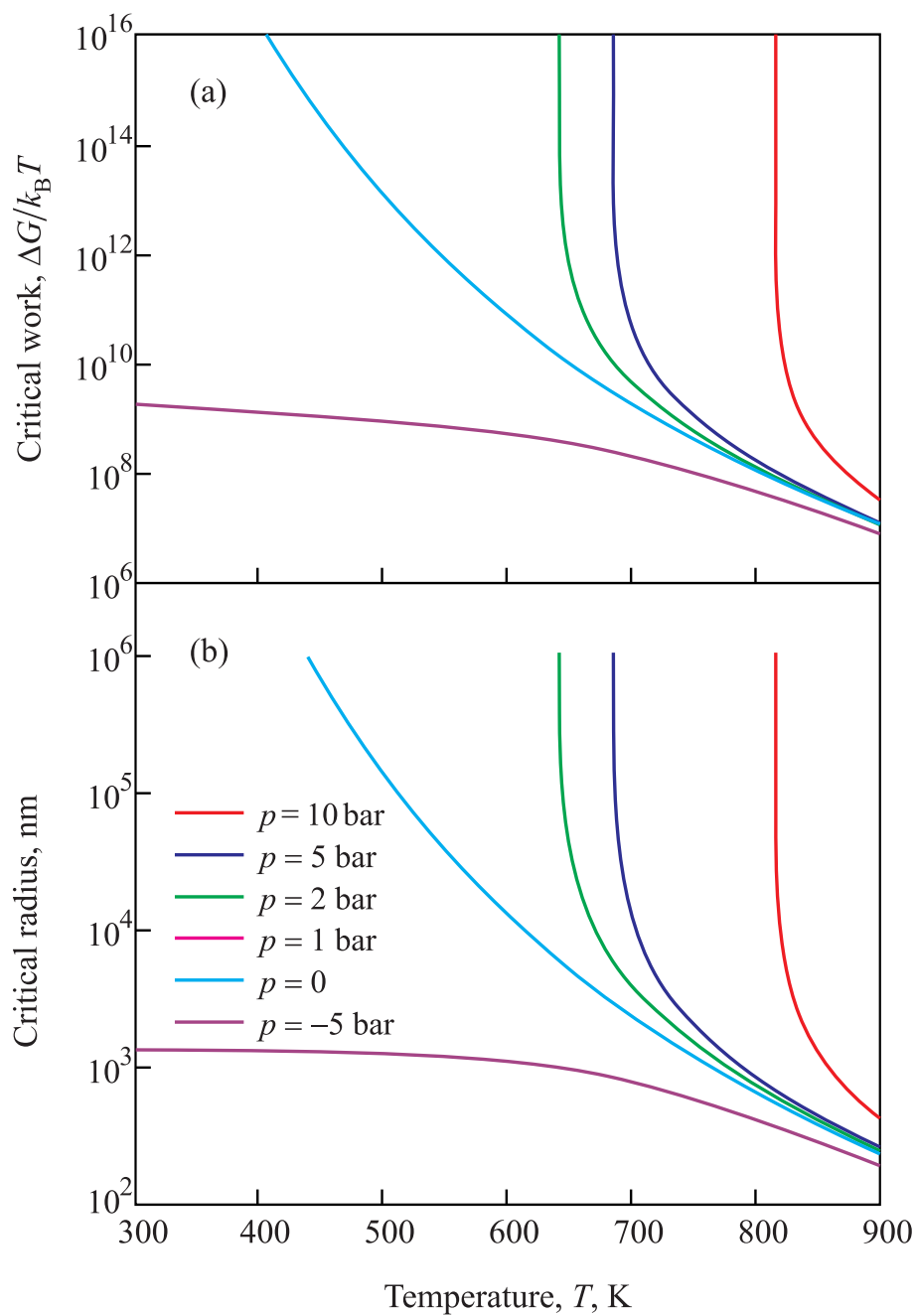


Fig. 9.10. (Color online) Dependence of the work of critical cluster formation,  $\Delta G_c/k_B T$  (a), and of the critical cluster radius (b) on temperature for  $p = -5, 0, 1, 2, 5$  and  $10$  Bar.

$10^{41} \text{s}^{-1} \text{m}^{-3}$  have been used for the calculation). One can see, that in such case

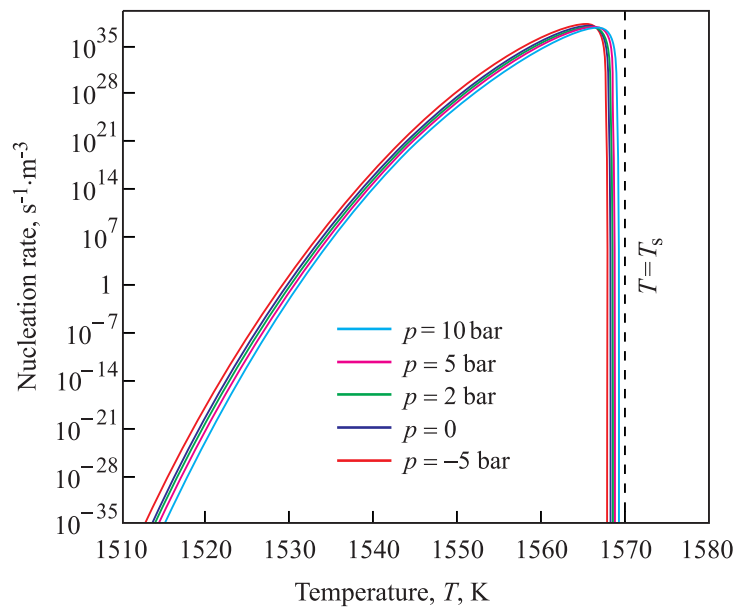


Fig. 9.11. (Color online) Dependence of the nucleation rate on temperature for  $p = -5, 0, 1, 2, 5$  and  $10$  Bar.

nucleation is possible only at very high temperatures, near  $T_s \approx 1570$  K. One can observe as well that concerning a 20 cm diameter sphere (region of proton adsorption) and 2 ms time span, one can expect 1 or more nucleation events above 1530.5 K. We arrive in this way at the conclusion that at the conditions analyzed intensive formation of supercritical bubbles by homogeneous nucleation is included. However, heterogeneous nucleation induced by different kinds of nucleation cores dissolved in liquid mercury may occur, of course, also at lower temperatures.

## 9.5. Conclusions

In spallation neutron sources, liquid mercury is the subject of large thermal and pressure shocks (including negative pressures) upon adsorbing the proton beam. Increased temperature and negative pressure can result in the formation of unstable bubbles which can cause cavitation erosion of the structural material, shortening the

life-time of the equipment and contaminating the liquid mercury with tiny steel pieces. Therefore it is crucial to avoid or minimize bubble nucleation. While pressure shock can be softened by adding helium micro-bubbles to the mercury, there is no way to deal with the thermal shock (i.e. local heating is not possible in the middle of the liquid mercury). Therefore our calculation focused on the calculation of the degree of temperature increase, the work of critical cluster formation (i.e. the nucleus of a macroscopic bubble) and the nucleation rate. It has been shown that after repeated proton pulses the temperature can be increased with a few hundred K, but the nucleation rate is so low that the possibility of homogeneous nucleation (i.e. bubble formation in the pure mercury) is highly improbable, even when the pressure gets values below the vapor pressure.

The authors express their gratitude to the Hungarian Academy of Sciences for financial support in the framework of the common Hungary-Russia/Dubna project EAI-2009/004 and DFFD of Ukraine for partial financial support in the framework of the common Ukraine-Byelorussia project F29.2/019, contract Number FP7 GA n° 202247 “NeutronSourceESS”.

## References

1. M. Futukawa, H. Kogawa, H. Rino, H. Date, H. Takeshi, *Int. J. Impact Eng.* **28**, 123 (2003)
2. B.W. Riemer, J.R. Haines, J.D. Hunn, D.C. Lousteau, T.J. McManamy, C.C. Tsai, *J. Nucl. Mat.* **92**, 318 (2003)
3. H. Date, M. Futakawa, *Int. J. Impact Eng.* **32**, 118 (2005).
4. N.J. Nicholas, P.V. Chitnis, R.G. Holt, R.A. Roy, R.O. Cleveland, B. Riemer, M. Wendel, *J. Acoust. Soc. Am.* **127**, 2231 (2010).
5. D.A. McClintock, P.D. Ferguson, L.K. Mansur, *J. Nucl. Mat.* **398**, 73 (2010)

6. J.R. Haines, B.W. Riemer, D.K. Felde, J.D. Hunn, S.J. Pawel, C.C. Tsai, *J. Nucl. Mat.* **343**, 58 (2005)
7. S.J. Pawel, L.K. Mansur, *J. Nucl. Mat.* **398**, 180 (2010)
8. T. Naoe, I. Masato, M. Futukawa, *Nucl. Inst. Meth. Phys. Res. A* **586**, 382 (2008)
9. T. Naoe, M. Futukawa, T. Shoubu, T. Wakui, H. Kogawa, H. Takeuchi, M. Kawai, *J. Nucl. Sci. Technol.* **45**, 698 (2008)
10. R.P. Taleyarkhan, F. Moraga, *Nucl. Eng. Des.* **207**, 181 (2001)
11. M. Futukawa, H.T. Kogawa, S. Hasegawa, T. Naoe, I. Masato, K. Haga, T. Wakui, N. Tanaka, Y. Mashumoto, Y. Ikeda, *J. Nucl. Sci. Technol.* **45**, 1041 (2008)
12. K. Okita, S. Takagi, Y.T. Matsumoto, *JFST* **3**, 116 (2008)
13. O. Redlich, J.N.S. Kwong, *Chem. Rev.* **44**, 233 (1949)
14. K. Morita, W. Maschek, M. Flad, Y. Tobita, H. Yamano, *J. Nucl. Sci. Technol.* **43**, 526 (2006)
15. K. Morita, V. Sobolev, M. Flad, *J. Nucl. Mat.* **362**, 227 (2007)
16. K. Morita, E.A. Fischer, *Nucl. Eng. Des.* **183**, 177 (1998)
17. N.B. Vargaftik, Y.K. Vinogradov, V.S. Yargin, *Handbook of Physical Properties of Liquid and Gases*, 3rd edn. (Begell House, New York, 1996)
18. W. Goetzlaff, doctoral thesis, Philips-Universität Marburg, Germany, 1988
19. J.W.P. Schmelzer, J. Schmelzer Jr., *J. Chem. Phys.* **114**, 5180 (2001)
20. J.D. van der Waals, Ph. Kohnstamm, *Lehrbuch der Thermodynamik* (Johann-Ambrosius-Barth Verlag, Leipzig und Amsterdam, 1908)
21. K. Binder, Spinodal Decomposition, in *Materials Science and Technology*, edited by R.W. Cahn, P. Haasen, E.J. Kramer (VCH, Weinheim, 1991), Vol. 5, p. 405
22. D.B. Macleod, *Trans. Faraday Soc.* **19**, 38 (1923)
23. J.J. Jasper, *Phys. Chem. Ref. Data* **1**, 841 (1972)
24. I.F. Barna, A.R. Imre, L. Rosta, F. Mezei, *Eur. Phys. J. B* **66**, 419 (2008)

25. I. Tiselj, S. Petelin, Trans. ASME J. Fluids Eng. **120**, 363 (1998)
26. I.F. Barna, A.R. Imre, G. Baranyai, Gy. Ezsöl, Nucl. Eng. Des. **240**, 146 (2010)
27. *Liquids Under Negative Pressure*, edited by A.R. Imre, H.J. Maris, P.R. Williams, NATO Science Series (Kluwer, 2002)
28. M. Ida, T. Naoe, M. Futukawa, Phys. Rev. E **75**, 046304 (2007)
29. B.W. Riemer, J. Nucl. Mat. **343**, 81 (2005)
30. S. Ishikura, H. Kogawa, M. Futakawa, K. Kikuchi, R. Hino, C. Arakawa, J. Nucl. Mat. **318**, 113 (2003)
31. V.P. Skripov, *Metastable Liquids* (Nauka, Moscow, 1972; Wiley, New York, 1974)
32. J.W.P. Schmelzer, J. Schmelzer Jr., Atm. Res. **65**, 303 (2003)
33. A.S. Abyzov, J.W.P. Schmelzer, J. Chem. Phys. **127**, 114504 (2007)

## 9.6. Висновки до розділу 9

Результати досліджень, представлених у даному розділі, опубліковано в статті [9] (Додаток А. Список публікацій здобувача за темою дисертації). Теоретично досліджено процес закипання ртуті у імпульсних джерелах нейтронів, що працюють на реакції сколювання (Spallation Neutron Source). Серед основних результатів у якості висновків можна виділити наступні:

- Обчислена робота формування критичних кластерів (мікробульбашок пари ртуті) та швидкість їх зародження в залежності від тиску і температури.
- Показано, що швидкість гомогенного зародження дуже низька при розглянутих умовах процесу навіть після адсорбції декількох імпульсів протонів, тому ймовірність кавітаційних процесів незначна.

## РОЗДІЛ 10

### ТЕОРІЯ УТВОРЕННЯ ПОРИ В РОЗТЯГНУТОМУ СКЛІ: УЗАГАЛЬНЕНИЙ ПІДХІД ГІББСА

У десятому розділі проведено теоретичний аналіз процесу зародження пори у малих зразках переохолодженої діопсидної рідини у процесі кристалізації поверхневого шару зразка на основі узагальненого методу Гіббса. Через невідповідність густини кристалічної та рідкої фаз зростання кристалічного шару на поверхні зразка призводить до рівномірного розтягування інкапсульованої рідини і, подібно до кавітації в простих рідинах, до зародження однієї пори. Аналіз цього процесу з точки зору класичної теорії нуклеації дає якісно правильний результат, однак кількісно теоретичні оцінки та експериментальні дані відрізняються.

Journal of Non-Crystalline Solids 357 (2011) 3474–3479

#### Theory of pore formation in glass under tensile stress: Generalized Gibbs approach

Alexander S. Abyzov<sup>a</sup>, Jörn W. P. Schmelzer<sup>b</sup>, Vladimir M. Fokin<sup>c</sup>

<sup>a</sup>National Science Center Kharkov Institute of Physics and Technology, Academician Street 1, 61108 Kharkov, Ukraine

<sup>b</sup>Institut für Physik der Universität Rostock, Universitätsplatz, 18051 Rostock, Germany

<sup>c</sup>Vavilov State Optical Institute, 193 171 St. Petersburg, Russia

*Article history:*

Received 4 February 2011

Received in revised form 13 June 2011

Available online 15 July 2011

*Keywords:*

Glass;

Crystallization;

Stress;

Nucleation

#### ABSTRACT

A theoretical analysis is performed of the process of nucleation of a pore in small samples of an under-cooled diopside liquid, enclosed by a solid

crystalline surface layer growing from the melt. Due to the density misfit of the crystal and liquid phases the growth of the crystalline layer leads to a uniform stretching of the encapsulated liquid. After reaching some critical values, the resulting tensile stress results in nucleation of a single pore. Nucleation of the pore is followed by its rapid growth, which decreases considerably the magnitude of elastic stresses and therefore eliminates the pre-condition for nucleation. This process has been analyzed earlier in terms of classical nucleation theory leading to a qualitatively correct interpretation. However, quantitatively, theoretical estimates performed in the framework of classical nucleation theory and experimental data differ. It is shown here that the generalized Gibbs approach results in a more adequate quantitatively correct description of the process of pore nucleation.

©2011 Elsevier B.V. All rights reserved.

## 10.1. Introduction

According to Abyzov, Fokin et al. [1–3](c.f. also [4–6]), there is abundant evidence of formation of pores in crystallization processes of small samples of under-cooled glass-forming melts, when the samples crystallize from the outer boundaries. The basic model of the mechanism of pore formation has already been developed [1–3]. Due to the density misfit of the crystal phase and under-cooled melt the growth of the crystalline layer leads to a uniform stretching of the encapsulated liquid and, similar to cavitation in simple liquids, to nucleation of a single pore (see Figs. 1 and 2). In accordance with the principle of le Chatelier-Braun, the pore is formed to compensate, at least partially, the elastic strains caused by the density difference between glass and crystal phases. Pore formation is followed by rapid growth, which diminishes considerably the magnitude of elastic tensile stresses and therefore eliminates the pre-condition for nucleation of further pores. Such scenario is quite general because the densities of most glasses differ from those of their isochemical crystals. By this reason, the effects studied are of great technological significance for

glass-ceramic development and sinter-crystallization processes [1–6]). In the present analysis, diopside glass has been used as a model system for the detailed study of these processes because its density is significantly less than that of the crystal, which increases the effect of elastic tensile stresses (see details given in [2]).

In a preceding paper, we performed the first theoretical analysis of pore nucleation in such samples in terms of classical nucleation theory (CNT) employing the classical Gibbs approach to the thermodynamic description of heterogeneous systems [2]. As it is shown in this earlier work the proposed basic mechanism – i.e. homogeneous formation of pores due to tensile stresses – works qualitatively well, however, quantitatively, classical theory overestimates the work of critical pore formation by a factor of the order of two. In the present contribution, it is demonstrated that the generalized Gibbs approach provides a more adequate description of the process of pore nucleation as compared to classical nucleation theory and allows us to interpret pore formation in the considered elastically stretched liquids even in a quantitatively correct way, i.e. as cavitation-like processes caused by elastic stresses.

## 10.2. Experimental data and their analysis

Samples of diopside glass in the form of small cubes, side  $a$  approximately 2, 3 or 4 mm, were heat-treated at  $T = 870^\circ\text{C}$  for different times,  $t$ . After a given period of time, the samples were quenched to room temperature. Then the top and bottom surfaces of the cubes were removed by grinding and polishing to study their interior and to measure the crystalline layer thickness. Optical microscopy and  $X$ -ray analysis were employed to identify the crystalline phases (see [2] for details). The heat-treatment temperature is lower than the melting temperature,  $T_m = 1392^\circ\text{C}$ , but is much higher than the standard glass transition temperature,  $T_g = 720^\circ\text{C}$ , so diopside crystals may form and they do it at the surface of the cubic samples (see, e.g. [7]). This process is illustrated in Fig. 10.1. Note that at the beginning of the nucleation-growth

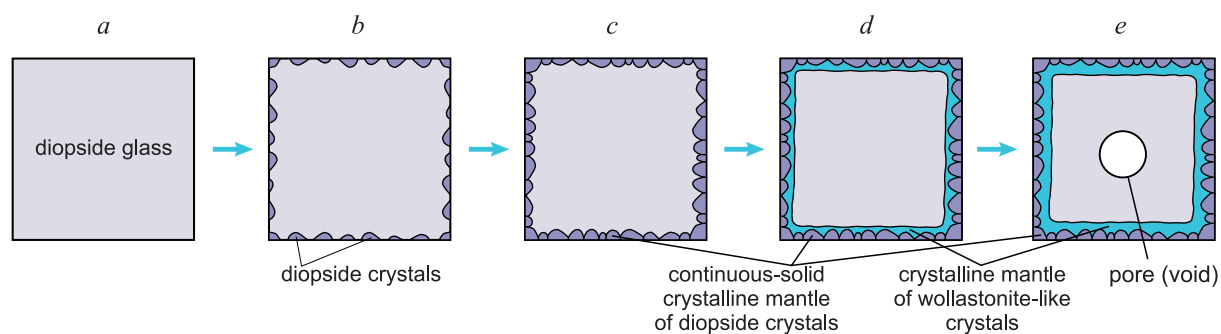


Fig. 10.1. Sketch of experimental results [2] showing the switch of the crystallizing phase in dependence on the width of the crystalline layer and stress induced pore formation: a) cubic sample of diopside glass; b) formation of diopside crystals at the surface of the sample; c) formation of a continuous solid crystalline layer; d) formation of a wollastonite-like crystalline layer; e) growth of the wollastonite-like phase and pore formation.

process diopside crystals do not develop a continuous solid crystalline mantle on the sample surface. In the early stages (Fig. 10.1b) there are gaps between the diopside crystallites, and only after some time has elapsed, due to the coalescence resulting from the growth of the initially separated small diopside crystals, a continuous solid crystalline layer is formed. This crystalline layer, like a nutshell, does not allow the stresses to relax fully and elastic stress energy – due to volume differences of the initial liquid and evolving crystal phase – accumulates with the further increase of the width of the layer in such stretched system. As a first response to the increase of the magnitude of elastic stresses the system exhibits a “switching” of the crystallization process from formation of diopside ( $1\text{CaO}\cdot 1\text{MgO}\cdot 2\text{SiO}_2$ ) to a wollastonite-like phase (see Fig. 10.1d). Latter phase has a composition of diopside but has a structure similar to wollastonite ( $\text{CaO}\cdot\text{SiO}_2$ , triclinic, for more details see [2]). The reason of such switch can be interpreted as a consequence of the fact that crystallisation of the wollastonite-like phase produces smaller values of elastic stress energy as compared to the formation of diopside. The density of the wollastonite-like phase is considerably lower than that of the diopside crystals (densities of diopside crystals and the melt are  $3.278 \times 10^3$  and  $2.84 \times 10^3 \text{ kg/m}^3$  [8], and density of wollastonite-like crystals is  $3.042 \times 10^3 \text{ kg/m}^3$  [2]). Consequently, the density misfit of the wollastonite-like

crystal phase and the diopside melt is lower and the resulting elastic stress effect in the crystallization process is smaller as compared to diopside crystal formation. Thus, we may suggest in agreement with experimental data [2] that – due to evolving tensile stresses – the formation and growth of diopside crystals terminates almost immediately after completion of formation of a continuous diopside crystalline layer. The average thickness of the diopside crystalline layer depends mainly on the typical distance between the diopside crystals formed independently in the initial stage of crystallization or, equivalently, on the number of crystallites formed in the crystalline layer. Taking into account that nucleation of diopside crystals is heterogeneous and occurs on some active centres (surface defects) [7], its number density depends only on the kind of surface [9].

In the course of subsequent development of the wollastonite-like crystalline layer, the remaining internal parts of the samples become uniformly stretched (see Fig. 10.1d and [1] for more details). As a result, like in cavitation processes in liquids, pores may spontaneously evolve (see Figs. 10.1e and 10.2). The origin of

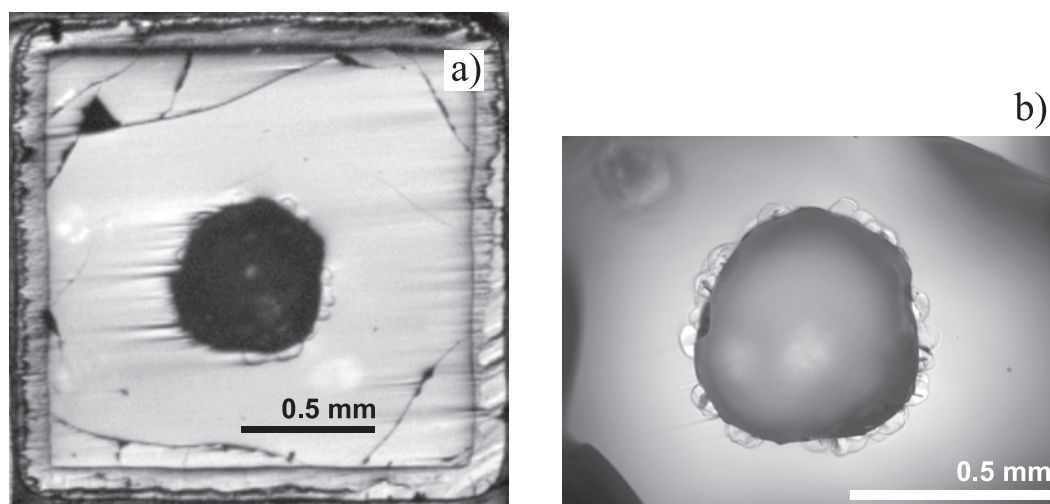


Fig. 10.2. Reflected (a) and transmitted (b) light optical micrographs of diopside glass sample of size  $2 \times 2 \times 2 \text{ mm}^3$  heat-treated at  $870^\circ\text{C}$  for 200 min [2] (the cracks on the sample appeared due to the preparation of the cross section needed to test the inner part of cubic sample).

pore nucleation is the elastic stress energy due to misfit of crystalline and ambient phase, again. Note, that for all experiments with annealing times  $t > t^*$  (when pores

have been formed), the size of the pores in the samples was almost the same, as it is shown in Fig. 10.2, and pores of intermediate sizes are not registered, which proves our assumption of very rapid, similar to cavitation processes, pore growth. Once a first pore is formed, as a rule, a second pore does not appear, since rapid growth of the first pore eliminates the elastic tensile stresses widely. As a consequence of this peculiarity, the main characteristic of the nucleation process considered is the waiting time for the appearance of the first pore,  $t^*$ , similar to crystallization of metal droplets [10, 11] or boiling of liquids [12]. Note that sometimes crystals are forming at the internal surface of the pore (see Fig. 10.2a), but this process takes place at the late stage of pore growth, and therefore cannot affect the considered here nucleation process.

In the analysis of experimental data on pore formation, a dimensionless parameter, the reduced thickness of the layer,  $X$ , was employed. This parameter characterises the size of the non-crystallised fraction of the cubes under consideration and is defined as

$$X = \frac{a - 2H}{a} . \quad (10.1)$$

where  $H$  is thickness of the crystalline layer. For a sample of size  $2 \times 2 \times 2 \text{ mm}^3$ , the measured dependence of  $X$  on annealing time is shown in Fig. 10.3, black triangles represent the experiments which finished without a pore, white ones – the experiments with pore formation. Pores were always formed at some well-defined finite values  $t = t^*$  and  $X = X^*$  (see [2] for more details).

The next step is to interpret these experimental results theoretically. As it was shown in our preceding works [1–3] the value of the thickness of the crystalline layer  $H$  basically determines the degree of development of elastic stresses in a finite system of the considered geometry. In this way,  $X^*$  and  $t^*$  are also the basic parameters to be employed in the theoretical description of pore formation and the comparison of experiment and theory.

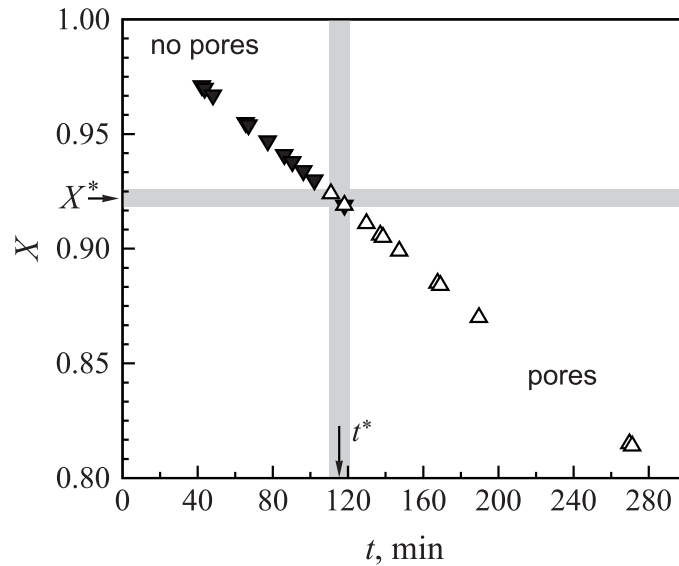


Fig. 10.3. Dependence of the measured values of  $X$  on annealing time,  $t$ , for diopside glass samples of size  $2 \times 2 \times 2 \text{ mm}^3$  heat-treated at  $870^\circ\text{C}$ . White and black triangles represent the experiments which finished with and without pore formation. Grey bands divide regions without ( $t < t^*$ ,  $X > X^*$ ) and with ( $t > t^*$ ,  $X < X^*$ ) pore formation.

### 10.3. Theory of pore formation

#### 10.3.1. Equation of state for stretched diopside glass

In order to apply the generalized Gibbs approach to the description of nucleation, the thermal equation of state of the system has to be known. Lacking respective data, we employ here the van der Waals equation of state for the diopside melt [13, 14], the thermal equation of state of the system where the process of nucleation takes place has to be known. Lacking suitable data, we employ the reduced form of the van der Waals equation of state [15–17] for the specification of the thermal equation of state of the diopside melt

$$\Pi(\omega) = \frac{8\theta}{3\left(\omega - \frac{1}{3}\right)} - \frac{3}{\omega^2}, \tag{10.2}$$

$$\Pi = \frac{p}{p_c}, \quad \omega = \frac{v}{v_c}, \quad \theta = \frac{T}{T_c}. \tag{10.3}$$

Here  $p$  is the pressure,  $v$  the specific volume,  $T$  the temperature, while  $p_c$ ,  $v_c$ , and  $T_c$  refer to the critical point. These critical parameters can be determined via density,  $\rho$ , Young's modulus,  $E$ , and bulk thermal expansion coefficient,  $\beta$ ,

$$\rho(\theta) = \frac{\rho_c}{\omega(\theta)}, \quad E(\theta) = \frac{p}{\Delta L/L_0} = -\omega p_c \left( \frac{d\omega}{d\Pi} \right)^{-1}, \quad \beta(\theta) = \frac{1}{\omega T_c} \frac{d\omega}{d\theta}. \quad (10.4)$$

For diopside glass [8] ( $\rho_0 = 2.84 \text{ kg/m}^3$ ,  $E_0 = 10^{11} \text{ J/m}^3$  for  $T = 20^\circ\text{C}$  and  $\beta = 11.73 \cdot 10^{-5} \text{ K}^{-1}$  for  $T = 870^\circ\text{C}$ ), the solution of the system of equations yields

$$p_c = 102 \text{ MPa}, \quad \rho_c = 971 \text{ kg/m}^3, \quad v_c = 1.03 \cdot 10^{-3} \text{ m}^3, \quad T_c = 3590 \text{ K}. \quad (10.5)$$

The chemical potential of the molecules in a van der Waals fluid can be written generally as [13]

$$\frac{\mu}{p_c v_c} = -\frac{8\theta}{3} \ln(3\omega - 1) + \frac{8\theta\omega}{3\omega - 1} - \frac{6}{\omega} + \chi(\theta). \quad (10.6)$$

Here  $\chi(\theta)$  is some well-defined function only of temperature.

Here we consider pore formation processes proceeding via nucleation and growth. Such processes occur for homogeneous initial states of the system (diopside melt) located in the region between binodal (the boundary between stable and metastable regions) and spinodal (the boundary between metastable and unstable regions) curves. To be definite, all further calculations will be performed here for a temperature  $T = 870^\circ\text{C}$  that corresponds to a reduced temperature,  $\theta = 0.318$ . In this particular case, the position of the binodal curves is given by  $\omega_b^{(\text{left})} = 0.373$ , and  $\omega_b^{(\text{right})} = 1663$ , the respective parts of the spinodal curves are located at  $\omega_{\text{sp}}^{(\text{left})} = 0.445$ , and  $\omega_{\text{sp}}^{(\text{right})} = 6.343$ , correspondingly. Thus, we consider initial states located between the left hand side branches of the spinodal and binodal curves, respectively, i.e., initial states in the range  $\omega_b^{(\text{left})} < \omega < \omega_{\text{sp}}^{(\text{left})}$ , that correspond to the interval of tensile stresses  $p_{\text{sp}} < p < p_b$  ( $p_{\text{sp}} \approx -769 \text{ MPa}$ ,  $p_b \approx -0.06 \text{ MPa}$ ).

Isotherms for the diopside melt according to Eq. (10.6) for different values of the reduced temperature  $\theta = 0.318, 0.6, 0.84, 1$  are shown in Fig. 10.4, dashed green and blue curves present binodal and spinodal curves, correspondingly.

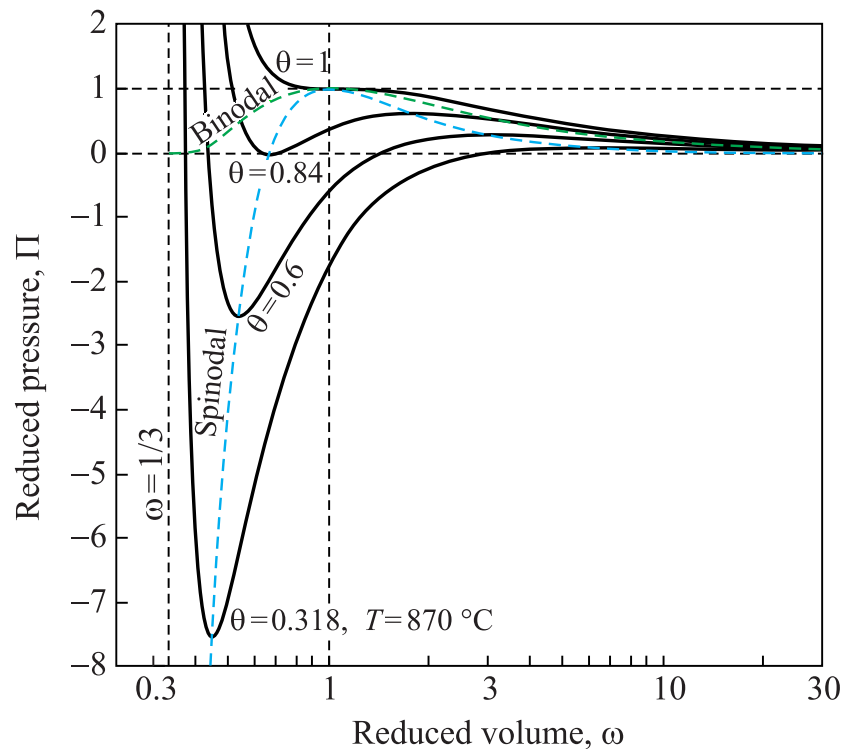


Fig. 10.4. van der Waals's isotherms adopted for the description of the diopside melt for different values of the reduced temperature  $\theta = 0.318, 0.6, 0.84$ . First value,  $\theta = 0.318$ , corresponds to the temperature in the experiment [2], the last three curves are placed just for reference.

One can see, that there are two classes of isotherms: for the first one ( $\theta \geq \theta_s$ ),  $p \geq 0$ , and for the second class ( $\theta < \theta_s$ ), the pressure may be both positive and negative. Only in this temperature range, melt can exist in a stretched state. The parameter  $\theta_s$  is determined via the equation

$$\Pi_l(\omega_{sp}(\theta_s), \theta_s) = 0, \quad (10.7)$$

which yields  $\theta_s \approx 0.844$  and  $T_s \equiv T_c \theta_s \approx 3029$  K. Let us note, that the parameters  $T_c$  and  $T_s$  are rather formal here, because diopside melt can decompose partially at high temperatures, but they are employed only for the definition of the

equation of state, which is used in the physically realistic range of temperatures and pressures.

### 10.3.2. Determination of the work of critical pore formation and of the nucleation rate

In order to determine the work of critical pore formation, governing the nucleation process, both the thermodynamic driving force for nucleation and the value of the surface tension has to be known. For the surface tension we choose here an equation of the form [13, 14]

$$\sigma(\omega_g, \omega_m, \theta) = \Theta(\theta) \left( \frac{1}{\omega_m} - \frac{1}{\omega_g} \right)^\delta, \quad \delta = 2. \quad (10.8)$$

where  $\omega_g$  is a specific volume of the gas in the pore,  $\omega_m$  is a specific volume of the melt, the function  $\Theta(\theta)$  is defined via

$$\Theta(\theta) = A \left( \frac{1}{\omega_b^{(\text{left})}} - \frac{1}{\omega_b^{(\text{right})}} \right)^{4-\delta}. \quad (10.9)$$

Here  $A = 0.0333 \text{ J/m}^2$ , which corresponds to the experimental value of the specific surface energy,  $\sigma = 0.377 \text{ J/m}^2$  [8].

Similarly to [13, 14], the basic equations employed for the determination of the work,  $\Delta G$ , of formation of a pore of radius  $R$  in the generalized Gibbs approach read

$$\frac{\Delta g(r, \omega_g, \omega_m, \theta)}{k_B T} = 3 \left( \frac{1}{\omega_m} - \frac{1}{\omega_g} \right)^\delta r^2 + 2f(\omega_g, \omega_m, \theta)r^3, \quad (10.10)$$

$$f(\omega_g, \omega_m, \theta) = \Pi(\omega_g, \theta) - \Pi(\omega_m, \theta) + \frac{1}{\omega_g} \frac{\mu(\omega_m, \theta) - \mu(\omega_g, \theta)}{p_c v_c}, \quad (10.11)$$

where the driving force of pore formation,  $\Delta g$ , and the critical pore size,  $r$ , in

dimensionless form are employed. In detail, the following notations have been used

$$\Delta g \equiv \frac{\Delta G}{\Omega_1}, \quad \Omega_1 = \frac{16\pi}{3} \frac{1}{p_c^2 k_B \theta T_c} \Theta(\theta)^3, \quad (10.12)$$

$$r \equiv \frac{R}{R_\sigma}, \quad R_\sigma = \frac{2}{p_c} \Theta(\theta). \quad (10.13)$$

The dependencies of the scaling factors  $\Omega_1$  and  $R_\sigma$  on temperature are shown in Fig. 10.5. For the chosen temperature,  $T = 870^\circ\text{C}$ , their values are equal to  $\Omega_1 = 14.665$  and  $R_\sigma = 1.027$  nm. These values are specified in the figure by dashed curves. These parameters tend to zero at  $T = T_c$ , but this limiting case is far beyond the physically interesting temperature interval between the glass transition temperature,  $T_g$ , and melting point,  $T_m$ . So, the analysis can be performed similarly with similar results also for other temperatures within the range  $T_g < T < T_m$ .

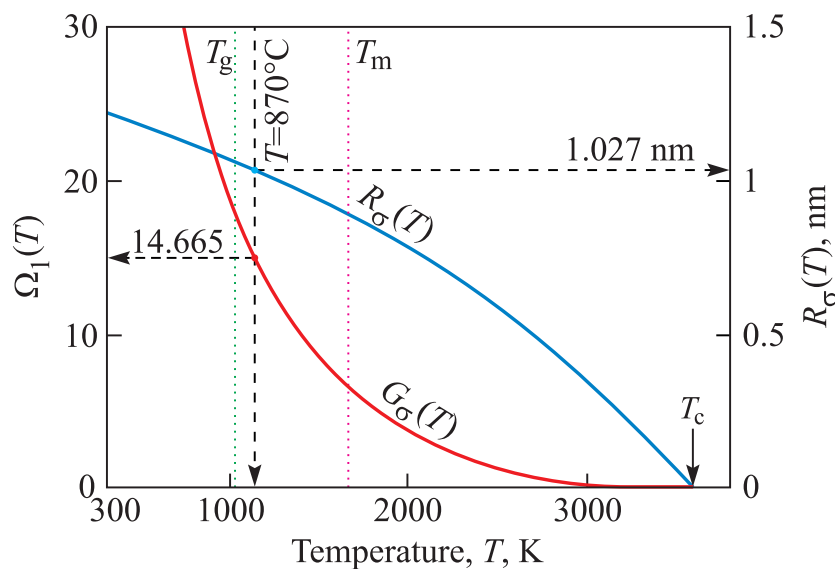


Fig. 10.5. Dependencies of the scaling factors,  $\Omega_1$  (left) and  $R_\sigma$  (right), on temperature.

The Gibbs free energy surface for the metastable initial state has a typical saddle shape at the critical point (see Fig 10.6). The saddle point position – supplying us with the work of formation and the size of the critical pore – is determined by the set

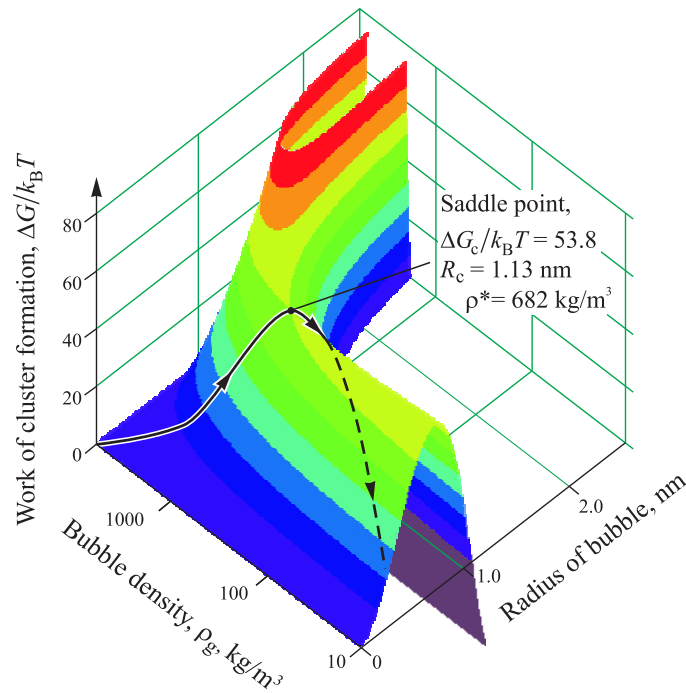


Fig. 10.6. Dependence of work of bubble formation,  $\Delta G/k_B T$ , on the radius of the bubble and the gas density in the bubble.

of equations

$$\frac{\partial \Delta g(r, \omega_g, \omega_m, \theta)}{\partial r} = 0, \quad \frac{\partial \Delta g(r, \omega_g, \omega_m, \theta)}{\partial \omega_g} = 0. \tag{10.14}$$

The dependencies of work of formation, size and gas density in the critical pore on negative pressure are shown in Figs. 10.7,a-c. The red curves correspond to the generalized Gibbs approach, while green curves refer to computations performed in the framework of CNT [12,14,18]. Once the work of critical pore formation is known, the following equation can be employed for the determination of the rate of nucleation,  $J$ , of pores [19]

$$J = J_0 \frac{h}{4l^3} \frac{1}{\eta} \exp\left(-\frac{\Delta G_c}{k_B T}\right). \tag{10.15}$$

$$\eta(T) = 10^{-4.27 + \frac{3961.2}{T-750.9}} \text{ [Pa s] }, \tag{10.16}$$

Here  $h$  is Planck’s constant,  $l \approx 2 \cdot 10^{-10}$  m is the size parameter of the diffusing building molecules, which is equivalent to the jump distance or the lattice parameter – parameters usually used in such kinetic analyses (see, e.g. [20, 21]), and  $\eta(T)$  is the viscosity of the melt [20], for the heat-treatment temperature  $T = 1143$  K  $\eta = 6.74 \times 10^5$  Pa s.

Some uncertainty in the definition of the pre-exponential term,  $J_0$ , will not strongly affect the nucleation rate, the value  $J_0 = 10^{41} \text{ s}^{-1}\text{m}^{-3}$  has been used for the calculation [22]. In Fig. 10.9, dependencies of the nucleation rates for generalized Gibbs approach (red line) and CNT (green line) on pressure for the same values of temperature are shown. Utilizing Eq. (10.15), the following equation can be written then for the number of pores nucleated in the stretched melt in a period of time,  $t$ ,

$$N(t) = \int_0^t J(t')V(t')dt', \quad (10.17)$$

where  $V$  is the volume of the stretched melt. Since the negative pressure  $p$  determines, to

a large extent, the thermodynamic barrier for nucleation (see Fig. 10.7a), its increase with increasing thickness,  $H$ , of the crystalline layer leads to a strong increase of the

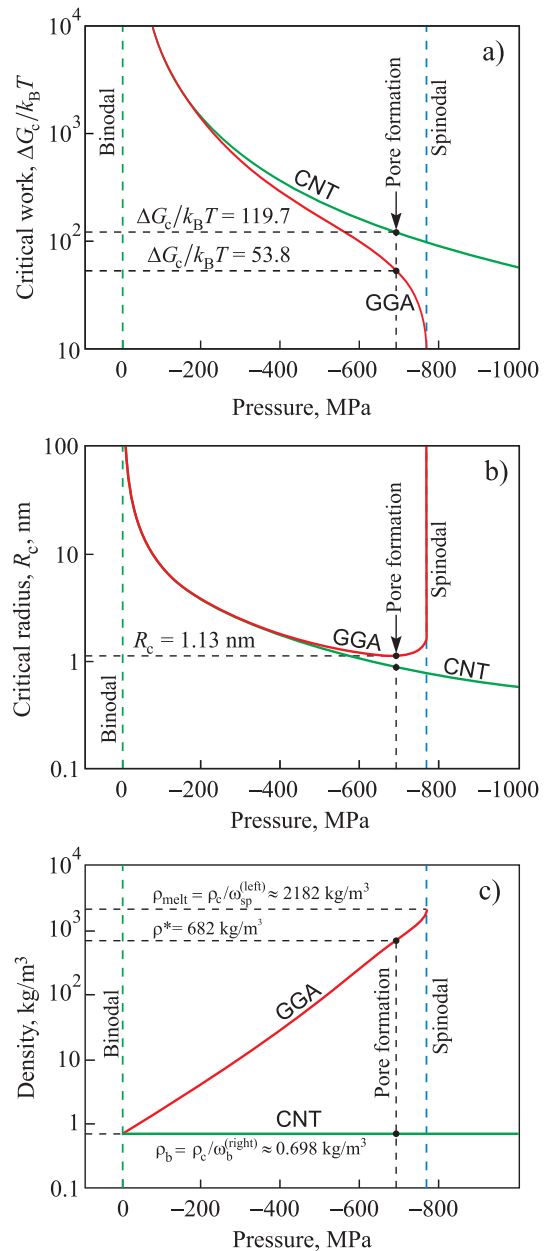


Fig. 10.7. a) Work of the critical bubble formation,  $\Delta G_c/k_B T$ , as a function of negative pressure; b) Radius of the critical bubble,  $R_c$ , as a function of negative pressure; c) Gas density in the critical bubble as a function of negative pressure.

nucleation rate with heat-treatment time,  $t$ , while  $V$  weakly decreases.

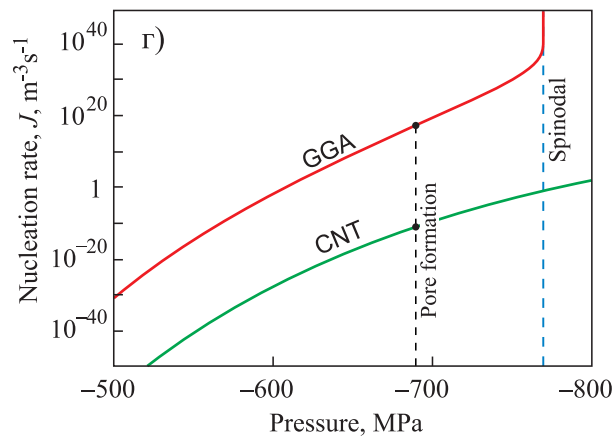


Fig. 10.8. Nucleation rate,  $J$ , as a function of negative pressure (red lines – generalized Gibbs approach, green line – CNT).

As it was already noted, generally, only one pore appears in a stretched melt since its fast growth eliminates the negative pressure and terminates further nucleation. The first pore is formed at a time  $t = t^*$  defined by

$$N(t^*) = 1. \quad (10.18)$$

Here  $t^*$  corresponds to the critical value of  $X^*$  to be compared with the results as detected in experiment

$$X^* = \frac{a - 2Ut^*}{a}, \quad (10.19)$$

where  $U = 0.672 \mu\text{m/s}$  is the growth rate of the crystalline layer [2].

To estimate the nucleation rate and then to perform the calculations by Eqs. (10.15)–(10.18), one needs to know the dependence of the negative pressure,  $p$ , on the position of crystal-melt interface,  $X$ . As was noted in [2], at the beginning the diopside crystals practically do not participate in the melt stretching, and only at the moment of formation of continuous the diopside layer, it could stretch the melt, and a switch to the wollastonite-like phase occurs (see Fig. 10.1). Therefore the

thickness of the diopside crystal layer was considered as independent of the size of the sample.

For the computations of the evolving elastic fields, we considered a sample of spherical size (see [1] for details). Fig. 10.9 (blue line) shows the results of these calculations versus  $r_a = R_a/R_s$  for a radius of the sphere estimated as  $R_s = a/2$  (here  $R_s$  is the radius of the spherical sample and  $R_a$  is radius of the amorphous core). After approaching some critical value of pressure,  $p^*$ , that corresponds to  $X^*$  i.e.

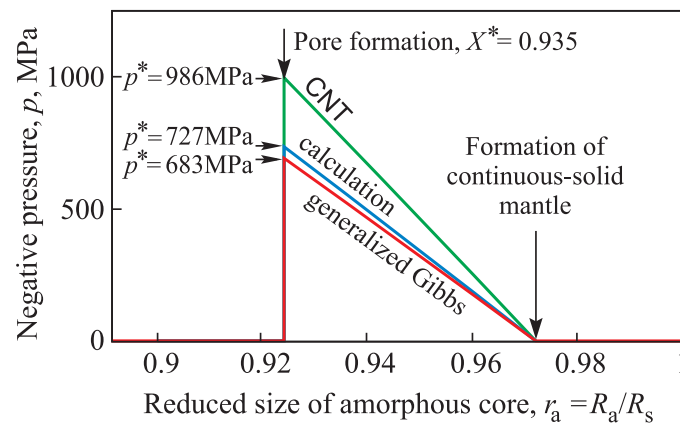


Fig. 10.9. Dependence of the negative pressure on reduced size of amorphous core. Red line – dependence  $p(X)$  as it is needed for nucleation of a pore according to the generalized Gibbs approach, green line – according to CNT, blue line – calculation of  $p(X)$  [1].

formation of the pore, negative pressure drops rapidly. Taking into account Eq. (10.19) one can rewrite the condition of pore formation Eq. (10.18) as  $N(X^*) = 1$ .

A comparison between the predictions of the value of  $X^*$  via CNT and experiment shows that CNT overestimates the work of critical bubble formation (see [2] for details), and, vice versa, the generalized Gibbs approach slightly underestimates the work of critical bubble formation, that is a pore is created at a lower value of negative pressure. In order to arrive at a satisfactory agreement of experimental values of  $X^*$  with theoretical predictions, for CNT we have to increase the negative pressure by a factor 1.356 (green line in Fig. 10.7), and for generalized Gibbs approach we have to reduce the negative pressure by a factor 0.939 (red line in Fig. 10.7). Such reduction of the theoretically estimated pressure can be easily

explained by the difference in the shapes of the samples studied theoretically [1] and experimentally [2].

Fig. 10.10 shows the dependence of  $X^*$  on the volume of sample, circles show experimental data, the curve is calculated by Eqs. (10.15)–(10.19). The thickness of the diopside crystal layer,  $X_{d/w}$ , was used here as a fit parameter, the best result is obtained for a value  $X_{d/w} = 27.1 \mu\text{m}$ , which is in good agreement with the experimental data [2].

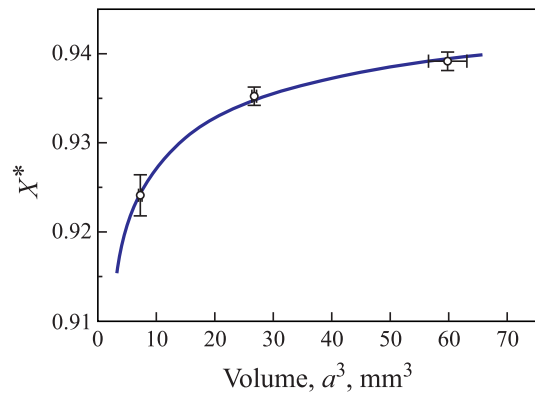


Fig. 10.10. Dependence of  $X^*$  on the volume of the sample. Circles show experimental data, the curve is calculated by Eqs. (10.15)–(10.19).

#### 10.4. Summary of results and discussion

The generalized Gibbs approach leads to much smaller values of the work of critical bubble formation ( $\Delta G_c = 56.8 k_B T$ ), as compared to CNT, being nearly identical to the value required to predict the experimental results quantitatively exactly. The result obtained via CNT ( $\Delta G_c = 121.9 k_B T$ , see Fig. 10.7a) is much higher leading to a huge difference of the values of the steady-state nucleation rates obtained via the two different methods (Fig. 10.7d). So, the generalized Gibbs approach provides a more adequate description of the process of pore nucleation as compared with the classical nucleation theory and allows one also in a quantitatively correct way to interpret pore formation in the considered elastically stretched liquids as cavitation-like processes caused by elastic stresses.

Note that our theoretical analysis was performed for spherical geometry, but the experiments were performed on cubic samples. The difference in the shapes of the samples studied theoretically and experimentally is expected to be origin for the remaining quantitative deviation of theoretical and experimental results. In order to

verify this assumption, now we perform similar experiments for samples of different shapes (spheres and thin plates) for a more precise comparison of the results.

### **10.5. Conclusions**

The switch of surface crystallization of diopside melts from diopside crystals to a wollastonite-like crystalline phase and pore formation in the glass-forming diopside melt can be qualitatively and quantitatively described as the result of elastic stresses caused by crystallization. In contrast to CNT, the generalized Gibbs approach has shown to be capable of giving not only a qualitative but even a quantitatively correct interpretation of this process. In this way, phase switch and pore formation due to crystallization is a general phenomenon which has to be taken properly into account in any processes like sintering, fabrication of glass-ceramic materials involving partial crystallization of glass powders.

### **Acknowledgment**

The authors would like to express their gratitude to the Deutscher Akademischer Austauschdienst (DAAD) for financial support.

### **References**

1. A. S. Abyzov, J. W. P. Schmelzer, and V. M. Fokin, *J. Non-Crystalline Solids* 356, p. 1670 (2010).
2. V. M. Fokin, A. S. Abyzov, J. W. P. Schmelzer, and E. D. Zanotto, *J. Non-Crystalline Solids* 356, p. 1679 (2010).

3. A.S. Abyzov, J.W.P. Schmelzer, V.M. Fokin, in: J.W.P. Schmelzer, G. Röpke, V.B. Priezhev (Eds.), *Nucleation Theory and Applications*, Joint Institute for Nuclear Research Publishing Department, Dubna, Russia, 2008, p. 379.
4. A. Karamanov and M. Pelino, *J. European Ceramic Society* 26 (2006) 2511.
5. A. Karamanov and M. Pelino, *J. European Ceramic Society* 26 (2006) 2519.
6. A. Karamanov and M. Pelino, *J. European Ceramic Society* 28 (2008) 555.
7. E.D. Zanutto, *J. Non-Cryst. Solids* 130 (1991) 217.
8. Sciglass database. <http://www.esm-software.com/sciglass>.
9. R. Möller, E.D. Zanutto, V.M. Fokin, *J. Non-Cryst. Solids* 274 (2000) 208.
10. V.P. Skripov, V.P. Koverda, *Spontaneous Crystallization of Super-cooled Liquids*, Nauka, Moscow, 1984 (in Russian).
11. B. Yang, Y.L. Gao, C.D. Zou, Q.J. Zhai, A.S. Abyzov, E. Zhuravlev, J.W.P. Schmelzer, C. Schick, *Appl. Phys. A: Mater. Sci. Process* 104 (1) (2011) 189.
12. V.P. Skripov, *Metastable liquids*, Wiley, New York, 1974.
13. J.W.P. Schmelzer, J. Schmelzer Jr., *J. Chem. Phys.* 114 (2001) 5180.
14. J.W.P. Schmelzer, J. Schmelzer Jr., *J. Atmos. Res.* 65 (2003) 303.
15. J.D. van der Waals, Thesis. Leiden (1873).
16. J.D. van der Waals, *Die Kontinuität des gasförmigen und flüssigen Zustandes*, 2nd ed. Johann-Ambrosius-Barth Verlag, Leipzig, 1899–1900.
17. J.D. van der Waals, Ph. Kohnstamm, *Lehrbuch der Thermodynamik*, Johann-Ambrosius-Barth Verlag, Leipzig und Amsterdam, 1908.
18. J.W.P. Schmelzer, J. Schmelzer Jr., in: J.W.P. Schmelzer, G. Röpke, V.B. Priezhev (Eds.), *Nucleation Theory and Applications*, Joint Institute for Nuclear Research Publishing Department, Dubna, Russia, 2002, p. 88.
19. E. D. Zanutto, V. M. Fokin, *Phil. Trans. R. Soc. Lond. A* 361, p. 591 (2003).

20. M. L. F. Nascimento, E. B. Ferreira, and E. D. Zanotto, *J. Chem. Phys.* 121, p. 8924 (2004).
21. J.W.P. Schmelzer, *J. Non-Cryst. Solids* 356 (2010) 2901.
22. J.W. Christian, *The Theory of Transformations in Metals and Alloys. Part I*, Pergamon Press, Oxford, 1981.

### 10.6. Висновки до розділу 10

Результати досліджень, представлених у даному розділі, опубліковано в статті [10] (Додаток А. Список публікацій здобувача за темою дисертації). Проведено теоретичний аналіз процесу зародження пори у малих зразках переохолодженої діопсидної рідини у процесі кристалізації поверхневого шару зразка. Через невідповідність густини кристалічної та рідкої фаз зростання кристалічного шару на поверхні зразка призводить до рівномірного розтягування інкапсульованої рідини і, подібно до кавітації в простих рідинах, до зародження однієї пори. Серед основних результатів у якості висновків можна виділити наступні:

- Обчислена робота формування пори критичного розміру в залежності від негативного тиску та час очікування першого критичного зародка (пори) в процесі зростання кристалічного шару на поверхні зразка.
- Показано, що узагальнений підхід Гіббса приводить до кількісно правильного опису процесу зародження пори у переохолодженої діопсидної рідини і дозволив пояснити походження внутрішньогранулярних пір, що утворюються при спіканні кераміки.

## ВИСНОВКИ

У дисертаційній роботі побудована нова теорія нуклеації, *узагальнений метод Гіббса*, яка, на відміну від класичної теорії нуклеації, дає можливість аналізу процесу утворення нової фази не тільки поблизу бінодалі, але також у нестабільному початковому стані поблизу *класичної спінодалі*. Основні результати дисертаційної роботи сформульовані в наступних пунктах.

1. Показано, що нуклеація, тобто перша стадія формування кластерів нової фази, починаючи з метастабільних початкових станів виявляє властивості, що нагадують спінодальний розпад, хоча наявність активаційного бар'єра відрізняє процес нуклеації від класичного спінодального розпаду.

2. Показано, що утворення фаз у нестабільних початкових станах поблизу *класичної спінодалі* може протікати через *активаційний бар'єр*, незважаючи на те, що у цьому випадку значення роботи формування критичного кластера, що відповідає сідловій точці термодинамічного потенціалу, дорівнює нулю;.

3. Досліджена *гетерогенна нуклеація* на планарній твердій поверхні у моделі однокомпонентної рідини ван дер Ваальса. Показано, що контактний кут змочування і каталітичний фактор (фактор зменшення роботи утворення кластера нової фази критичного розміру на твердої поверхні) гетерогенної нуклеації стають залежними від ступеня метастабільності (переохолодження або перегрівання) рідини. У випадку утворення крапельки в перенасиченій парі на гідрофобній поверхні та утворення бульбашок у рідині на гідрофільній поверхні ефект гетерогенності незначний. В альтернативних випадках конденсації крапельки на гідрофільній поверхні та утворення бульбашок у рідині на гідрофобній поверхні *контактний кута змочування* зменшується, каталітична активність поверхні збільшується, і, таким чином, нуклеація посилюється. Фактично, у цьому випадку існування твердої поверхні призводить до значного

зміщення спінодалі до менших значень пересичення порівняно з гомогенною нуклеацією, тобто гетерогенна спінодаль наближається до бінодалі, а *область метастабільності звужується* за рахунок розширення області нестійкості.

4. Вперше досліджена *гетерогенна нуклеація* на планарній твердій поверхні у моделі регулярного бінарного розчину. *Показано*, що у випадку утворення кластерів нової фази на поверхні з низькою змочуваністю (контактний кут більше  $90^\circ$ ) каталітична активність твердої поверхні мала. В альтернативному випадку високої змочуваності (контактний кут менше  $90^\circ$ ) інтенсивність нуклеації значно посилюється твердою поверхнею. Таким чином, у цьому випадку, як і у рідині ван дер Ваальса, гетерогенна спінодаль наближається до бінодалі, а область метастабільності звужується за рахунок розширення області нестійкості.

5. Розглянуто ефекти *гетерогенної нуклеації на конічній пори* у моделі однокомпонентної рідини ван дер Ваальса та у моделі регулярного бінарного розчину. *Показано*, що контактний кут та каталітичний фактор для нуклеації на дефектній поверхні залежать від ступеня метастабільності (переохолодження, перегрівання або пересичення розчину). У разі утворення кластерів нової фази на гідрофільній поверхні конічної пори швидкість нуклеації значно збільшується в порівнянні з випадком планарній поверхні. Наявність дефекту на гідрофільній поверхні призводить до значного зсуву спінодалі – зі зменшенням кута конуса пори гетерогенна спінодаль наближається до бінодалі, і область метастабільності звужується за рахунок розширення області нестійкості. *Показано*, що існує *граничний кут конуса пори*, менш якого формування нової фази проходить безбар'єрно.

6. Теоретично досліджено процес закипання рідкої ртуті у імпульсних джерелах нейтронів, що працюють на реакції сколювання (Spallation Neutron Source), при адсорбуванні протонного пучка; обчислена робота формування критичних кластерів (мікробульбашок пари ртуті) та швидкість їх зародження.

*Показано*, що швидкість гомогенного зародження дуже низька при розглянутих умовах процесу навіть після адсорбції декількох імпульсів протонів, тому ймовірність кавітаційних процесів незначна.

7. Проведено теоретичний аналіз процесу зародження пори у малих зразках переохолодженої діюксидної рідини у процесі кристалізації поверхневого шару зразка. Обчислена робота формування пори критичного розміру в залежності від негативного тиску та час очікування першого критичного зародка (пори) в процесі зростання кристалічного шару на поверхні зразка. Аналіз цього процесу з точки зору класичної теорії нуклеації дає якісно правильний результат, однак кількісно теоретичні оцінки та експериментальні дані відрізняються. Показано, що *узагальнений підхід Гіббса призводить до кількісно правильного опису* процесу зародження пори у переохолодженої діюксидної рідини, що дозволяє пояснити походження внутрішньогранулярних пір, що утворюються при спіканні кераміки.

Таким чином, усі поставлені завдання виконані, і мета дисертаційної роботи досягнута.

Результати досліджень доповнюють і розширюють наявні уявлення про механізми фазових переходів першого роду. Вони визначають кінетику процесів самоструктурування речовини від нанорозмірних до галактичних розмірів із широким спектром застосувань як у фундаментальних, так і в прикладних дослідженнях (фізика, астрономія, хімія, біологія, метеорологія, медицина, матеріалознавство) та технології – конденсація та кипіння, сегрегація у твердих та рідких розчинах, або кристалізація та плавлення. Дослідження, проведені в дисертації, є актуальними та мають як фундаментальне, так і прикладне значення.

## Подяки

На закінчення хочу висловити подяку моєму науковому консультанту, доктору фізико-математичних наук, професору, академіку НАН України Олександрові Степановичу Бакаю за дуже стимулюючу підтримку, допомогу в роботі над дисертацією, обговорення проблем сучасної теоретичної фізики, теорії нуклеації та фізики твердого тіла.

Також висловлюю подяку своїм постійним співавторам, Йорну Шмельцеру (Jörn W. P. Schmelzer, Germany), Леоніду Миколайовичу Давидову та Володимирі Михайловичу Фокіну за плідну співпрацю, участь в постановці наукових проблем та обговоренні результатів.

Я щиро вдячний всім співробітникам Інституту теоретичної фізики імені О. І. Ахієзера за унікальну творчу атмосферу.

## ДОДАТОК А

## СПИСОК ПУБЛІКАЦІЙ ЗДОБУВАЧА ЗА ТЕМОЮ ДИСЕРТАЦІЇ

**Наукові праці, в яких опубліковані основні наукові результати дисертації:**

1. Schmelzer J., Abyzov A. S. and Möller J. Nucleation versus spinodal decomposition in phase formation processes in multicomponent solutions. *J. Chem. Physics*. 2004. Vol. 121. P. 6900-6917. [Квартиль Q1](#) (2004).
2. Abyzov A. S., Schmelzer J. Nucleation versus spinodal decomposition in confined binary solutions. *J. Chem. Physics*. 2007. Vol. 127. P. 114504. [Квартиль Q1](#) (2007).
3. Abyzov A. S., Schmelzer J., Kovalchuk A. A. and Slezov V. V. Evolution of cluster size-distributions in nucleation-growth and spinodal decomposition processes in a regular solution. *J. Non-Cryst. Solids*. 2010. Vol. 356. P. 2915-2955. [Квартиль Q1-Q2](#) (2010).
4. Abyzov A. S., Schmelzer J. Kinetics of segregation processes in solutions: Saddle point versus ridge crossing of the thermodynamic potential barrier. *J. Non-Cryst. Solids*. 2014. Vol. 384. P. 8-14. [Квартиль Q1-Q2](#) (2014).
5. Abyzov A. S., Schmelzer J. Generalized Gibbs' approach in heterogeneous nucleation. *J. Chem. Physics*. 2013. Vol. 138, P. 164504. [Квартиль Q1](#) (2013).
6. Abyzov A. S., Schmelzer J. Heterogeneous nucleation in solutions: Generalized Gibbs' approach. *J. Chem. Physics*. 2014. Vol. 140. P. 244706. [Квартиль Q1](#) (2014).
7. Abyzov A. S., Schmelzer J. and Davydov L. N. Heterogeneous nucleation on rough surfaces: Generalized Gibbs' approach. *J. Chem. Physics*. 2017. Vol. 147. P. 214705. [Квартиль Q1](#) (2017).
8. Abyzov A. S., Davydov L. N. and Schmelzer J. Heterogeneous nucleation in solutions on rough solid surfaces: Generalized Gibbs Approach. *Entropy*. 2019.

Vol. 21. P. 782. [Квартиль Q2](#) (2019).

9. Imre A. R., Abyzov A. S., Barna I. F. and Schmelzer J. Homogeneous bubble nucleation limit of mercury under the normal working conditions of the planned European Spallation Neutron Source. *Eur. Phys. J. B.* 2011. Vol. 79. P. 101-113. [Квартиль Q1](#) (2011).

10. Abyzov A. S., Schmelzer J. and Fokin V. M. Theory of pore formation in glass under tensile stress: Generalized Gibbs approach. *J. Non-Cryst. Solids.* 2011. Vol. 357. P. 3474–3479. [Квартиль Q1-Q2](#) (2011).

**Наукові праці, які засвідчують апробацію матеріалів дисертації:**

11. Abyzov A. S., Schmelzer J. Nucleation versus spinodal decomposition in confined binary solutions. *17th International Conference “Nucleation and Atmospheric Aerosols”*: Book of abstracts (August 13-17, 2007, National University of Ireland. Editors C. D. O’Dowd and P. Wagner). Galway, Ireland, 2007. P. 278-281.

12. Abyzov A. S., Kovalchuk A. A., Schmelzer J., Slezov V. V. Evolution of cluster size distributions in phase formation processes in multi-component solutions: nucleation and spinodal decomposition. *XIIIth Research Workshop Nucleation Theory and Applications* (JINR, April 1 – 30, 2009). Dubna, Russia, 2009.

13. Abyzov A. S., Schmelzer J., Kovalchuk A. A. and Slezov V. V. Evolution of cluster size-distributions in nucleation and spinodal decomposition in regular solutions. *9-th International Symposium on Crystallization in Glasses and Liquids* (September 10 – 13, 2009, Foz do Iguacu, PR). Brazil, 2009.

14. Abyzov A. S., Schmelzer J. Kinetics of Segregation Processes: Classical versus generalized Gibbs approaches. *XVIth Research Workshop Nucleation Theory and Applications* (JINR, April 1 – 30, 2012). Dubna, Russia, 2012.

15. Abyzov A. S., Schmelzer J. Kinetics of segregation processes: Classical versus generalized Gibbs approaches. *Diffusion and diffusional phase transformations (DSSR-2012)* (1-7 June, 2012). Cherkassy, Ukraine, 2012.

16. Abyzov A. S., Schmelzer J. Kinetics of nucleation: Classical versus generalized Gibbs approaches. *11th Lahnwitzseminar on Calorimetry 2012 in Rostock.*

Germany, 2012.

17. Schmelzer J., Abyzov A. S. Some comments on the thermodynamic analysis of nucleation in confined spaces. *Crystallization 2012. 10th International Symposium on Crystallization in Glasses and Liquids* (September 23 – 26, 2012). Goslar, Germany, 2012.

18. Abyzov A. S., Schmelzer J. Kinetics of segregation processes: Classical versus generalized Gibbs approaches. *Crystallization 2012. 10th International Symposium on Crystallization in Glasses and Liquids* (September 23 – 26, 2012). Goslar, Germany, 2012.

19. Abyzov A. S., Schmelzer J. Generalized Gibbs's approach in heterogeneous nucleation. *XVIIth Research Workshop Nucleation Theory and Applications* (JINR, April 1 – 30, 2013). Dubna, Russia, 2013.

20. Schmelzer J., Abyzov A. S. Kinetics of phase transitions: some new results. *Polymer Group Seminar, University of Rostock, Institute of Physics* (February 12). Rostock, Germany, 2013.

21. Abyzov A. S., Schmelzer J. Generalized Gibbs' approach in nucleation: Application to heterogeneous nucleation. *The Eighth International Conference on Material Technologies and Modeling (MMT-2014)* (Ariel University. July 28 - August 01, 2014) Ariel, Israel, 2014.

22. Schmelzer J., Abyzov A. S. Generalized Gibbs approach in nucleation: Basic ideas and results. *The Eighth International Conference on Material Technologies and Modeling (MMT-2014)* (Ariel University. July 28 - August 01, 2014) Ariel, Israel, 2014.

**Наукові праці, які додатково відображають наукові результати дисертації:**

23. Schmelzer J., Slezov V. V. and Abyzov A. S. A new method of determination of the coefficients of emission in nucleation theory. *Nucleation Theory*

*and Applications* (Editor J. Schmelzer, Wiley-VCH). 2006. P. 39-73.

24. Schmelzer J., Abyzov A. S. Generalized Gibbs' Approach to the thermodynamics of heterogeneous systems and the kinetics of first-order phase transitions. *J. Engineering Thermophysics*. 2007. Vol. 16. P. 119-129.

25. Schmelzer J., Abyzov A. S. Thermodynamic analysis of nucleation in confined space: Generalized Gibbs approach. *J. Chem. Physics*. 2011. Vol. 134. P. 054511. [Квартиль Q1](#) (2011).

26. Schmelzer J., Abyzov A. S. Comment on "Minimum free-energy pathway of nucleation" [J. Chem. Phys. 135, 134508 (2011)] *J. Chem. Physics*. 2012. Vol. 136. P. 107101. [Квартиль Q1](#) (2011).

27. Schmelzer J., Abyzov A. S. Comments on the thermodynamic analysis of nucleation in confined space. *J. Non-Cryst. Solids*. 2014. Vol. 384. P. 2-7. [Квартиль Q1-Q2](#) (2014).

28. Schmelzer J., Fokin V. M., Abyzov A. S., Zanotto E. and Gutzow I. S. How do crystals form and grow in glass-forming liquids: Ostwald's rule of stages and beyond. *Int. J. Appl. Glass Sci.* 2010. Vol. 1. P. 16-26. [Квартиль Q2](#) (2011).

29. Schmelzer J., Abyzov A. S. Crystallization of glass-forming liquids: Thermodynamic driving force. *J. Non-Cryst. Solids*. 2016. Vol. 449. P. 41-49. [Квартиль Q1-Q2](#) (2016).

30. Schmelzer J., Abyzov A. S. How do crystals nucleate and grow: Ostwald's rule of stages and beyond. *Thermal Physics and Thermal Analysis* (Editors: J. Šesták, P. Hubík, J. Mareš, Springer). 2017. P. 195-211.

31. Schmelzer J., Abyzov A. S. Crystallization of glass-forming melts: New answers to old questions. *J. Non-Cryst. Solids*. 2018. Vol. 501. P. 11-20. [Квартиль Q1-Q2](#) (2018).

32. Fokin V. M., Karamanov A., Abyzov A. S., Schmelzer J. and Zanotto E. D. Stress-induced pore formation and phase selection in a crystallizing stretched glass. *Glass. Selected Properties and Crystallization* (Editor J. Schmelzer, De Gruyter).

2014. P. 441–479.

33. Abyzov A. S., Schmelzer J., Davydov L. N. and Slezov V. V. Homogeneous bubble nucleation limit of lead. *Problems of atomic science and technology. Series: Nuclear Physics Investigations*. 2012. Vol. 57. P. 283-287. Квартиль Q3 (2012).